

CHEMICAL AND STRUCTURAL STUDIES OF SUBSTITUTED TRANSITION

METAL CARBONYL COMPLEXES

by

Gillian Wendy Harris

A Thesis Submitted to the Faculty of Science,  
University of the Witwatersrand, Johannesburg,  
for the Degree of Doctor of Philosophy.

November 1984

ABSTRACT

Catalytic routes were employed to prepare isonitrile (RNC) and phosphine ( $PR_3$ ) substituted derivatives of monomeric and dimeric transition metal carbonyl complexes, representative new derivatives being characterized by single crystal X-ray crystallography.

Isonitrile derivatives of ( $\eta^5$ -Arene)Cr(CO) $_3$  and ( $\eta^5$ -C $_5$ H $_5$ )-Mn(CO) $_3$  were synthesized by catalysed substitution reactions, catalysts being [( $\eta^5$ -C $_5$ H $_5$ )(CO) $_2$ ] $_2$  and/or PdO. The structures of two of the new derivatives, ( $\eta^5$ -C $_5$ H $_5$ CC $_2$ Me)Cr(CO) $_2$ (CNBu $^t$ ), and ( $\eta^5$ -C $_5$ H $_5$ )Mn(CO) $_2$ (CNBu $^t$ ), were determined by X-ray crystallography, and stereochemical information obtained used in explaining anomalous IR spectra of these complexes.

X-ray crystallography was employed to establish the substitution geometry of the di-isonitrile derivative of iron pentacarbonyl, Fe(CO) $_5$ (CNMe) $_2$ . The molecular structure was unable to account for anomalies in the IR spectrum.

A chemical and structural study was undertaken of isonitrile and phosphine derivatives of Re $_2$ (CO) $_{10}$ . The use of PdO to catalyse the reaction between Re $_2$ (CO) $_{10}$  and RNC enabled the facile syntheses of the isonitrile derivatives Re $_2$ (CO) $_{10-n}$ (CNR) $_n$  (n = 1-4). These new derivatives were fully characterized by IR,  $^1$ H NMR and mass spectroscopy. X-ray crystallography established the structures of a series of representative compounds, Re $_2$ (CO) $_9$ (CNBu $^t$ ), Re $_2$ (CO) $_8$ (CNC $_6$ H $_3$ Me $_2$ -2,6) $_2$ , Re $_2$ (CO) $_7$ (CNMe) $_3$  and Re $_2$ (CO) $_6$ (CNC $_6$ H $_3$ Me $_2$ -2,6) $_4$ . The structures of two analogous manganese carbonyl isonitrile derivatives, Mn $_2$ (CO) $_8$ (CNBu $^t$ ) $_2$  and Mn $_2$ (CO) $_6$ (CNC $_6$ H $_3$ Me $_2$ -2,6) $_4$ , were also investigated by X-ray crystallography. Differences observed in the IR and  $^1$ H NMR spectra of the di-isonitrile derivatives of rhenium and manganese carbonyl could be explained in terms of the observed molecular structures. The stereochemistry of the mono- to tetra-isonitrile substituted derivatives are discussed in terms of electronic and steric factors.

Attempts were made to extend the Pd-catalysed carbonyl substitution reaction of Re $_2$ (CO) $_{10}$  to phosphine ligands. Although the catalysed reaction with  $PR_3$  is much less facile than with RNC, this route was successfully employed in the synthesis of mono- and

di-substituted phosphine derivatives,  $\text{Re}_2(\text{CO})_{10-n}(\text{PR}_3)_n$  ( $n = 1, 2$ ). The X-ray crystal structure of diax $[\text{Re}_2(\text{CO})_8(\text{PMe}_2\text{Ph})_2]$  was determined. A correlation was established between IR spectral data and substitution geometry for  $\text{M}_2(\text{CO})_8(\text{L})_2$  ( $\text{M} = \text{Re}, \text{Mn}$ ) complexes.

This study demonstrated the synthetic utility of transition metal-catalyzed routes to substituted metal carbonyl derivatives. X-ray crystallography was shown to be a powerful tool in the rationalization, in terms of structure, of certain observed properties of these complexes.

DECLARATION

I hereby declare that the work presented in this thesis was carried out exclusively by myself under the supervision of Professor J.C.A. Booyens and Dr. N.J. Coville.

This thesis has never been submitted for a degree in any other university.

*G.W. Harris*  
*G.W. Harris*

G.W. Harris

1 November 1984



ACKNOWLEDGEMENTS

I should like to express my sincere thanks to the following:-

- . Professor J.C.A. Boeyens and Dr. N.J. Coville, my supervisors, for their guidance and enthusiasm.
- . Professor G.J. Kruger, for advice on crystallographic problems in Professor Boeyens' absence.
- . Mr. J. Albain, for the collection of the X-ray data.
- . Mr. D.C. Levensis, for assistance with computing problems.
- . Dr. M.O. Albers, for helpful advice on certain synthetic aspects, and for running the FTIR spectra.
- . Dr. P.R. Boshoff, for running the mass spectra.
- . Professor I.S. Butler, and Mr. P.D. Harvey, of McGill University, Montreal, for communicating the results of their Raman studies on the  $\text{Re}_2(\text{CO})_{10-n}(\text{CNR})_n$  ( $n = 1-4$ ) complexes prepared as part of this work.
- . Mrs. A. Maritz, for typing this thesis.
- . Mrs. M. Crabb and Mrs. R. Hillier, for the labelling of the ORTEP diagrams.

Finally, I wish to acknowledge the financial support from the University of the Witwatersrand, and the South African Council for Scientific and Industrial Research.

In addition, I should like to express my gratitude to

- . Mr. M.I.J. Manesf, of Birbeck College, University of London, for use of the SMPMS program.
  - . Drs. D.S. Moss, R.A. Palmer and B.J. Howlin, of Birkbeck College, University of London, for advice on crystallographic and computing problems.
- and Professor. T.L. Blundell, of Birkbeck College, for the use of the College Computing facilities.

PREFACE

It is not for nothing that the scholar invented the Ph.D. thesis as his principal contribution to literary form. The Ph.D. thesis is the perfect image of his world. It is work done for the sake of doing work - perfectly conscientious, perfectly laborious, perfectly irresponsible.

- Archibald MacLeish  
(The Irresponsibles)

TABLE OF CONTENTS

|   |       |
|---|-------|
| ACKNOWLEDGEMENTS  | v     |
| LIST OF TABLES  | xix   |
| LIST OF FIGURES   | xxv   |
| LIST OF ABBREVIATIONS AND SYMBOLS   | xxxii |
| I. Introduction   | 1     |
| II Catalytic Synthesis and characterization of Isonitrile Derivatives of $(\eta^6\text{Arene})\text{Cr}(\text{CO})_3$   | 5     |
| 2.1 Introduction  | 5     |
| 2.2 Result  | 7     |
| 2.2.1 Reaction of $(\eta^6\text{Arene})\text{Cr}(\text{CO})_3$ complexes with isocyanides   | 7     |
| 2.2.2 Reaction of $(\eta^6\text{C}_6\text{H}_5(\text{O}_2\text{Me})\text{Cr}(\text{CO})_3$ with 2,6-Me <sub>2</sub> C <sub>6</sub> H <sub>3</sub> NC, in the presence of Iron Dimer Catalysts   | 8     |
| 2.2.3 Formation of by-products of the type $\text{Cr}(\text{CO})_{6-n}(\text{CNC}_6\text{H}_3\text{Me}_2-2,6)_n$ (n = 3,4) in the reaction of $(\eta^6\text{C}_6\text{H}_5\text{CO}_2\text{Me})\text{Cr}(\text{CO})_3$ with 2,6-Me <sub>2</sub> C <sub>6</sub> H <sub>3</sub> NC  | 10    |
| 2.3 Spectroscopic properties of $(\eta^6\text{Arene})\text{Cr}(\text{CO})_2^-(\text{CNR})$ complexes  | 11    |
| 2.3.1 Infra Red   | 11    |
| 2.3.2 Proton Nuclear Magnetic Resonance   | 11    |
| 2.3.3 Mass Spectrum of $(\eta^6\text{C}_6\text{H}_5\text{CO}_2\text{Me})\text{Cr}(\text{CO})_2^-(\text{CNBu}^t)$  | 11    |
| 2.4 Experimental  | 14    |
| 2.4.1 The catalysed synthesis of $[(\eta^6\text{C}_6\text{H}_5\text{X})\text{Cr}(\text{CO})_2^-(\text{CNR})]$ (X = H, O <sub>2</sub> , Me; R = Bu <sup>t</sup> , 2,6-Me <sub>2</sub> C <sub>6</sub> H <sub>3</sub> )  | 14    |
| 2.4.2 Reaction of $(\eta^6\text{C}_6\text{H}_5\text{CO}_2\text{Me})\text{Cr}(\text{CO})_3$ with 2,6-Me <sub>2</sub> C <sub>6</sub> H <sub>3</sub> NC, with catalyst $[\text{CpFe}(\text{L})_2]$ (Cp = C <sub>5</sub> H <sub>5</sub> , C <sub>5</sub> H <sub>4</sub> CO <sub>2</sub> Me, C <sub>5</sub> Me <sub>5</sub> ; L = CO; Cp = C <sub>5</sub> H <sub>5</sub> , L = 2,6-Me <sub>2</sub> C <sub>6</sub> H <sub>3</sub> NC) and co-catalyst PdO | 14    |
| 2.4.3 Preparation of $[(\text{C}_5\text{H}_4\text{CO}_2\text{Me})\text{Fe}(\text{CO})_2]_2$   | 15    |
| 2.4.4 Reaction of $[(\text{C}_5\text{H}_4\text{CO}_2\text{Me})\text{Fe}(\text{CO})_2]_2$ with <sup>t</sup> BUNC (1:1 Ratio)   | 15    |

|     |       |   |    |
|-----|-------|---|----|
|     | 2.4.5 | Reaction of $[(C_5H_4CO_2Me)Fe(CO)_2]_2$<br>with $tBuNC$ (1:2 Ratio)                  | 16 |
| III |       | The Modification of $(\eta^6-C_6H_5CO_2Me)Cr(CO)_3$ by<br>Ligands L                   | 19 |
|     | 3.1   | Introduction  | 19 |
|     | 3.2   | The Structure of $(\eta^6-C_6H_5CO_2Me)Cr(CO)_3$                                      | 19 |
|     | 3.2.1 | Ligand geometry   | 20 |
|     | 3.2.2 | Conformation  | 20 |
|     | 3.2.3 | Cr-C bond lengths   | 23 |
|     | 3.2.4 | Ring C-C bond lengths   | 23 |
|     | 3.2.5 | Planarity of Ring   | 23 |
|     | 3.2.6 | Cr-C-O bond angles  | 24 |
|     | 3.2.9 | Packing considerations  | 24 |
|     | 3.3   | The structural effect of substitution of CO<br>by Ligand L                            | 24 |
|     | 3.3.1 | Ligand geometry   | 24 |
|     | 3.3.2 | Conformation  | 25 |
|     | 3.3.3 | Influence of electronic nature of L<br>on Cr-C bond lengths                           | 25 |
|     | 3.3.4 | Ring C-C bond lengths   | 25 |
|     | 3.3.5 | Planarity of Ring   | 25 |
|     | 3.3.6 | Cr-C-C and Cr-C-R bond angles<br>(L = CR)   | 26 |
|     | 3.3.7 | Packing, and Steric Factors   | 26 |
|     | 3.4   | X-ray Crystallographic Studies of $(\eta^6-C_6H_5-$<br>$CO_2Me)Cr(CO)_2L$ complexes   | 27 |
|     | 3.4.1 | OC-Cr-CO and OC-Cr-L angles   | 27 |
|     | 3.4.2 | Conformation; An exception  | 27 |
|     | 3.4.3 | Trends in Cr-C bond lengths   | 31 |
|     | 3.4.4 | Ring C-C bond lengths   | 31 |
|     | 3.4.5 | Ring planarity and bending of $CO_2Me$<br>group                                       | 31 |
|     | 3.4.6 | Cr-C-O and Cr-C-L bond angles (L = CR)  | 32 |
|     | 3.4.7 | Conformation of ligand L  | 32 |
|     | 3.5   | Conclusion  | 32 |
| IV  |       | The Crystal and Molecular Structure of $(\eta^6-C_6H_5CO_2Me)-$<br>$Cr(CO)_2(CNBU^t)$ | 33 |
|     | 4.1   | Introduction  | 33 |

|       |   |    |
|-------|---|----|
| 4.2   | Discussion of the Structure of ( $\eta^5\text{C}_5\text{H}_5\text{CO}_2\text{Me}$ )-<br>$\text{Cr}(\text{CO})_2(\text{CNBu}^t)$   | 33 |
| 4.2.1 | OC-Cr-CO and OC-Cr-CN angles  | 40 |
| 4.2.2 | Conformation  | 40 |
| 4.2.3 | Cr-C bond lengths   | 40 |
| 4.2.4 | Ring C-C bond lengths   | 41 |
| 4.2.5 | Ring planarity and bending of $\text{CO}_2\text{ME}$<br>group   | 41 |
| 4.2.6 | Cr-C-CO and Cr-C-N bond angles  | 42 |
| 4.2.7 | Conformation of the $\text{CNBu}^t$ ligand  | 42 |
| 4.3   | Unusual Structural Features of ( $\eta^5\text{C}_5\text{H}_5\text{CO}_2\text{Me}$ )-<br>$\text{Cr}(\text{CO})_2(\text{CNBu}^t)$   | 42 |
| 4.3.1 | Staggered Conformation  | 42 |
| 4.3.2 | Position of $^t\text{BuNC}$ vis-à-vis $\text{CO}_2\text{Me}$  | 42 |
| 4.3.3 | Bending of the $^t\text{BuNC}$ ligand   | 43 |
| 4.3.4 | Intra- and Inter-molecular Interactions   | 43 |
| 4.4   | Experimental  | 43 |
| 4.4.1 | Data collection   | 43 |
| 4.4.2 | Structure Solution and Refinement   | 44 |
| V     | Catalytic Synthesis and Characterization of Isonitrile<br>Derivatives of ( $\eta^5\text{C}_5\text{H}_5$ ) $\text{Mn}(\text{CO})_3$  | 48 |
| 5.1   | Introduction  | 48 |
| 5.2   | Results and Discussion  | 49 |
| 5.2.1 | PdO-catalyzed reaction of ( $\eta^5\text{C}_5\text{H}_5$ )-<br>$\text{Mn}(\text{CO})_3$ with isocyanides  | 49 |
| 5.2.2 | Characterization of ( $\eta^5\text{C}_5\text{H}_5$ ) $\text{Mn}(\text{CO})_2$ -<br>(CNR) products   | 49 |
|       | (a) Infrared  | 49 |
|       | (b) Proton Nuclear Magnetic Resonance   | 50 |
|       | (c) Mass spectrum of ( $\eta^5\text{C}_5\text{H}_5$ )-<br>$\text{Mn}(\text{CO})_2(\text{CNBu}^t)$   | 50 |
| 5.3   | Experimental - preparation of ( $\eta^5\text{C}_5\text{H}_5$ ) $\text{Mn}(\text{CO})_2$ -<br>(CNR), (R = $\text{Bu}^t$ , $\text{C}_6\text{H}_5\text{CH}_2$ , $\text{C}_6\text{H}_{11}$ , $\text{C}_6\text{H}_3\text{Me}_2$ -2,6,<br>Me) | 50 |
| VI    | The Modification of ( $\eta^5\text{C}_5\text{H}_5$ ) $\text{Mn}(\text{CO})_3$ by Ligands L  | 54 |
| 6.1   | Introduction  | 54 |
| 6.2   | The Structure of ( $\eta^5\text{C}_5\text{H}_5$ ) $\text{Mn}(\text{CO})_3$  | 54 |

|      |       |  |    |
|------|-------|--|----|
|      | 6.2.1 | Ligand geometry and conformation   | 54 |
|      | 6.2.2 | Conformation   | 55 |
|      | 6.2.3 | Mn-C-ring and Mn-CO bond lengths   | 55 |
|      | 6.2.4 | Ring planarity and C-C bond lengths  | 55 |
|      | 6.2.5 | Mn-C-O bond angles   | 55 |
|      | 6.2.6 | Packing considerations   | 55 |
|      | 6.3   | X-ray Crystallographic Studies of $(\eta^5\text{-C}_5\text{H}_5)\text{-Mn}(\text{CO})_2\text{L}$ complexes   | 57 |
|      | 6.3.1 | OC-Mn-CO and OC-Mn-L angles  | 57 |
|      | 6.3.2 | Molecular Conformation   | 57 |
|      | 6.3.2 | Mn-C-ring and Mn-CO bond lengths   | 58 |
|      | 6.3.4 | Ring C-C bond lengths  | 58 |
|      | 6.3.5 | Mn-C-O bond angles   | 62 |
|      | 6.3.6 | Packing and Steric Factors   | 62 |
|      | 6.4   | Conclusion   | 63 |
| VII  |       | The Crystal and Molecular Structure of $(\eta^5\text{-C}_5\text{H}_5)\text{Mn}(\text{CO})_2(\text{CNBu}^t)$  | 64 |
|      | 7.1   | Introduction   | 64 |
|      | 7.2   | Discussion of the Structure of $(\eta^5\text{-C}_5\text{H}_5)\text{Mn}(\text{CO})_2(\text{CNBu}^t)$  | 64 |
|      | 7.2.1 | OC-Mn-CO and OC-Mn-CN angles   | 64 |
|      | 7.2.2 | Molecular Conformation   | 64 |
|      | 7.2.3 | Mn-C bond lengths  | 71 |
|      | 7.2.4 | Ring planarity and C-C bond lengths  | 71 |
|      | 7.2.5 | M-C-O and M-C-N bond angles  | 71 |
|      | 7.2.6 | Conformation of the CNBu <sup>t</sup> ligand   | 72 |
|      | 7.2.7 | Packing  | 72 |
|      | 7.3   | Experimental   | 73 |
|      | 7.3.1 | Data collection  | 73 |
|      | 7.3.2 | Structure Solution and Refinement  | 73 |
| VIII |       | Anomalous Infra Red Spectra of $(\eta^5\text{-C}_5\text{H}_5)\text{Cr}(\text{CO})_2\text{-}(\text{CNR})$ and $(\eta^5\text{-C}_5\text{H}_5)\text{Mn}(\text{CO})_2(\text{CNR})$ complexes           | 78 |
|      | 8.1   | Introduction   | 78 |
|      | 8.2   | IR spectral studies of $(\eta^5\text{-C}_5\text{H}_5)\text{Cr}(\text{CO})_2\text{-}(\text{CNBu}^t)$ and $(\eta^5\text{-C}_5\text{H}_5)\text{Mn}(\text{CO})_2(\text{CNBu}^t)$ in different solvents | 79 |

|       |  |     |
|-------|--|-----|
| 8.3   | Structural data on $(\eta^5\text{-C}_5\text{H}_5\text{CO}_2\text{Me})\text{Cr}(\text{CO})_2(\text{CNBu}^t)$ and $(\eta^5\text{-C}_5\text{H}_5)\text{Mn}(\text{CO})_2(\text{CNBu}^t)$ from X-ray Crystallographic Studies | 81  |
| 8.4   | Structural data on $(\eta^5\text{-C}_5\text{H}_5)\text{Ru}(\text{CNBu}^t)_2\text{I}$ from an X-ray Crystallographic study  | 87  |
| 8.5   | The solid state IR spectrum and crystal structure of $(\eta^5\text{-C}_5\text{H}_5\text{CO}_2\text{Me})\text{Cr}(\text{CO})_2(\text{CMe}_2\text{C}_5\text{H}_3\text{Me}_2-2,6)$  | 87  |
| 8.6   | Possible explanations for the anomalous IR data  | 88  |
| 8.6.1 | Conformers in solution   | 88  |
| 8.6.2 | Solid state effects  | 89  |
| 8.6.3 | Lowering of molecular symmetry by bent isonitrile  | 90  |
| 8.7   | Conclusion   | 90  |
| IX    | The Geometry of $\text{Fe}(\text{CO})_{5-n}(\text{L})_n$ ( $n = 1, 2$ ) Structures, and the Crystal and Molecular Structure of $\text{Fe}(\text{CO})_3(\text{CNMe})_2$   | 91  |
| 9.1   | Introduction   | 91  |
| 9.2   | The Geometry of $\text{Fe}(\text{CO})_4\text{L}$ structures  | 92  |
| 9.2.1 | Axial versus Equatorial Site Preference of L   | 92  |
| 9.2.2 | Distortions to the <i>tpb</i> geometry   | 93  |
| 9.2.3 | Fe-CO bond length trends   | 98  |
| 9.2.4 | Fe-C-O bond angles   | 99  |
| 9.3   | The Geometry of $\text{Fe}(\text{CO})_3(\text{L})_2$ Structures  | 100 |
| 9.3.1 | Geometry, <i>tpb</i> , distorted <i>tpb</i> , <i>spy</i>   | 100 |
| 9.3.2 | Ligand site preferences - <i>ax-ax</i> , <i>ax-eq</i> , <i>eq-eq</i>   | 101 |
| 9.3.3 | Fe-CO bond length trends   | 105 |
| 9.3.4 | Re-C-O bond angles   | 106 |
| 9.4   | The Crystal and Molecular Structure of $\text{Fe}(\text{CO})_3(\text{CNMe})_2$   | 107 |
| 9.4.1 | Anomalous Infra Red Data   | 107 |
| 9.4.2 | Discussion of the Structure  | 108 |

|         |   |     |
|---------|---|-----|
| 9.5     | Experimental  | 113 |
| 9.5.1   | Data Collection   | 113 |
| 9.5.2   | Structure Solution and Refinement   | 113 |
| X       | Derivatives of dirhenium decacarbonyl - a survey of the Literature  | 118 |
| 10.1    | Introduction  | 118 |
| 10.2    | Reactions of $\text{Re}_2(\text{CO})_{10}$ with phosphines (and arsines)  | 120 |
| 10.2.1  | Thermal reactions   | 121 |
| 10.2.2  | Photochemical reactions   | 122 |
| 10.2.3  | Amine-oxide assisted reactions  | 123 |
| 10.2.4  | Comment on product formulations   | 123 |
| 10.3    | The reaction of $\text{Re}_2(\text{CO})_{10}$ with $^{13}\text{CO}$   | 123 |
| 10.4    | Photochemical reaction of $\text{Re}_2(\text{CO})_{10}$ with isonitriles  | 124 |
| 10.5    | Amine-oxide assisted reaction of $\text{Re}_2(\text{CO})_{10}$ with nitriles  | 124 |
| 10.6    | Photochemical reactions of $\text{Re}_2(\text{CO})_{10}$ with olefins   | 125 |
| 10.6.1  | The photochemical reaction of $\text{Re}_2(\text{CO})_{10}$ with olefins in hexane solution                                     | 125 |
| 10.6.2  | The photochemical reaction of $\text{Re}_2(\text{CO})_{10}$ with 1,3-butadiene  | 126 |
| 10.6.3  | The photochemical reaction of $\text{Re}_2(\text{CO})_{10}$ with 1,3,5-cycloheptatriene   | 131 |
| 10.6.4  | The photochemical reactions of $\text{Re}_2(\text{CO})_{10}$ with 1-alkenes and 2-alkenes and further reactions of the products | 131 |
| 10.7    | Photochemical reaction of $\text{Re}_2(\text{CO})_{10}$ with $\text{R}_2\text{SiH}_2$   | 138 |
| 10.8    | The photochemical reaction of $\text{Re}_2(\text{CO})_{10}$ with $\text{H}_2$   | 138 |
| 10.9    | Photochemical reaction of $\text{Re}_2(\text{CO})_{10}$ with water  | 138 |
| 10.10   | N-donor ligand derivatives of $\text{Re}_2(\text{CO})_{10}$   | 139 |
| 10.10.1 | Trimethylamine-N-oxide-induced reactions of $\text{Re}_2(\text{CO})_{10}$ with N-donor ligands                                  | 139 |



|         |  |     |
|---------|--|-----|
| 10.10.2 | Photolytic reactions of $\text{Re}_2(\text{CO})_{10-n}L_n$ ( $n = 1, 2$ , $L = \text{N-donor ligand}$ )                          | 140 |
| 10.10.3 | Preparation of $(\mu\text{-H})\text{Re}_2(\text{CO})_8(\mu\text{-NC}_5\text{H}_4)$ , and subsequent reactions with donor ligands | 140 |
|         | (a) Thermal reactions with ligand L  | 140 |
|         | (b) Reaction with $\text{Me}_2\text{NO}$ in the presence of ligand L   | 141 |
|         | (c) Photochemical reactions with ligand L  | 141 |
| 10.10.4 | Preparation of bis-N-donor-ligand derivatives of $\text{Re}_2(\text{CO})_{10}$   | 141 |
| 10.11   | Dirhenium carbonyl carbene complexes   | 142 |
| 10.12   | Thermal reaction of $\text{Re}_2(\text{CO})_{10}$ with acetylenes  | 143 |
| 10.13   | Formation of $[\text{cis-Re}_2(\text{CO})_9(\text{CHO})]^-$ from $\text{Re}_2(\text{CO})_{10}$                                   | 143 |
| 10.14   | Formation of $\text{Et}_4\text{N}^+[\text{cis-Re}_2(\text{CO})_9\text{H}]^-$ from $\text{Re}_2(\text{CO})_{10}$                  | 145 |
| 10.15   | Quaternary Ammonium Borohydride reductions of $\text{Re}_2(\text{CO})_{10}$  | 145 |
| 10.16   | Conclusion   | 145 |
| XI      | Catalytic Synthesis and Characterization of Isonitrile Derivatives of Dirhenium Decacarbonyl                                     | 147 |
| 11.1    | Introduction   | 147 |
| 11.2    | Catalyst Testing   | 148 |
| 11.3    | PdO-catalysed reaction of $\text{Re}_2(\text{CO})_{10}$ with isonitriles   | 151 |
| 11.4    | Characterization of the dirhenium carbonyl isonitrile derivatives  | 155 |
| 11.4.1  | Infra Red Spectroscopy   | 155 |
| 11.4.2  | Proton Nuclear Magnetic Resonance Spectroscopy   | 164 |
| 11.4.3  | Raman Spectroscopy   | 165 |
| 11.4.4  | Mass Spectroscopy  | 169 |
|         | (a) Mass spectrum of $\text{Re}_2(\text{CO})_9(\text{CNBu}^t)$   | 169 |
|         | (b) Mass spectrum of $\text{Mn}_2(\text{CO})_8(\text{CNBu}^t)_2$   | 174 |
|         | (c) Mass spectrum of $\text{Re}_2(\text{CO})_9(\text{C}_6\text{H}_5\text{Me}_2-2,6)_2$   | 173 |

|        |  |     |
|--------|--|-----|
| 11.5   | Mechanism of the reaction of $M_2(CO)_{10}$ ( $M = Re, Mn$ ) with isonitriles  | 184 |
| 11.5.1 | Mechanism of the PdO-catalysed reaction between $Re_2(CO)_{10}$ and $Bu^tNC$ to give $Re_2(CO)_9(CNBu^t)-^{13}CO$ labelling study            | 184 |
| 11.5.2 | Kinetic studies of the reaction of $M_2(CO)_{10}$ ( $M = Mn, Re$ ) with $Bu^tNC$   | 184 |
| 11.6   | Experimental   | 185 |
| 11.6.1 | Catalyst testing   | 185 |
| 11.6.2 | PdO-catalysed synthesis of $Re_2(CO)_{10-n}(CNR)_n$ ( $n = 1-3$ , $R = Bu^t, C_6H_5CH_2, C_6H_{11}$ ; $n = 1-4$ , $R = 2,6-Me_2C_6H_3, Me$ ) | 186 |
| 11.6.3 | PdO-catalysed synthesis of $Re_2(CO)_8^-(CNBu^t)(CNC_6H_3Me_2-2,6)$  | 186 |
| 11.6.4 | PdO-catalysed reaction of $Re_2(CO)_{10}$ and $Re_2(^{13}CO)_{10}$ with $Bu^tNC$ (1:1:2 ratio)   | 186 |
| XII    | The Modification of $Re_2(CO)_{10}$ by Ligands L   | 188 |
| 12.1   | Introduction   | 188 |
| 12.1   | The Structure of $Re_2(CO)_{10}$   | 188 |
| 12.2.1 | The Re-Re bond length  | 189 |
| 12.2.2 | The Re-CO bond lengths   | 191 |
| 12.2.3 | Molecular Conformation   | 192 |
| 12.2.4 | OC-Re-CO bond angles   | 193 |
| 12.2.5 | Re-C-O bond angles   | 194 |
| 12.2.6 | Packing  | 195 |
| 12.3   | Ringing the changes: the effects of ligand substitution on molecular geometry  | 195 |
| 12.3.1 | The Re-Re bond length  | 195 |
| (a)    | Bond order   | 195 |
| (b)    | Electronic nature of ligands   | 197 |
| (c)    | Steric factors   | 198 |
| (d)    | Bridging ligands   | 198 |
| 12.3.2 | The Re-CO bond lengths   | 199 |
| 12.3.3 | Molecular Conformation   | 200 |
| 12.3.4 | Re-CO bond angles  | 200 |
| 12.3.5 | Re-C-O bond angles   | 200 |

|      |   |     |
|------|---|-----|
|      | 12.3.6 Packing  | 200 |
| XIII | X-ray Crystallographic Studies of Dirhenium<br>Decacarbonyl Derivatives - a Survey of the<br>Literature   | 202 |
|      | 13.1 Introduction   | 202 |
|      | 13.2 Literature Structures  | 203 |
|      | 13.2.1 Structures without bridging ligands  | 203 |
|      | (a) Mono-substitution: $eq-Re_2^-$<br>$(CO)_9(L)$ , $L = CH(OMe)$ ; $C(OR)-$<br>$(SiPh_3)$ ; $R = Me, Et$   | 203 |
|      | (b) Di-substitution: 1,2-ax,eq-<br>$Re_2(CO)_8[C(OEt)(SiPh_3)]_2$   | 206 |
|      | 13.2.2 Structures with bridging ligands   | 208 |
|      | (a) A bridging olefin - $Re_2(CO)_8^-$<br>$[\mu-(\eta^2, \eta^2-C_4H_6)]$   | 208 |
|      | (b) A bridging carbene - $Re_2(CO)_8^-$<br>$[\mu-(\eta^1, \eta^3-CH=CMe_2)]$  | 208 |
|      | (c) $Re_2(CO)_8(\mu-NC_5H_4)(\mu-H)$ and $Re_2-$<br>$(CO)_7(ONMe_3)(\mu-NC_5H_4)(\mu-H)$  | 208 |
|      | (d) $Re_2(CO)_8[\mu-SiPh_2]_2$ , $Re_2(CO)_8(H)_2-$<br>$[\mu-SiPh_2]$ , $Re_2(CO)_7(H)_2[\mu-SiEt_2]_2$<br>and $Re_2(CO)_6(H)_4[\mu-SiEt_2]_2$                | 209 |
|      | (e) $Re_2(CO)_8[\mu-C(OMe)(C_6H_4Me-p)]_2$  | 211 |
|      | (f) $(CO)_4Re(\mu-C(SiPh_3)CO(OEt)Re(CO)_3-$<br>$[C(OEt)(SiPh_3)]$ - a carbonyl-<br>ligand bonded derivative of 1,2-<br>ax,eq- $Re_2(CO)_8[C(OEt)(SiPh_3)]_2$ | 211 |
|      | (g) $Re_2(CO)_8[\mu-(C(SiPh_3)(CO))](\mu-H)$ ,<br>and $Re_2(CO)_8[\mu-(CPh)](\mu-Br)$   | 211 |
|      | (h) $Re_2(CO)_8(\mu-H)_2$ - nn Re-Re double<br>bond?  | 212 |
|      | (i) An $Re_2(CO)_8(\mu-H)_2$ derivative -<br>$Re_2(CO)_8(\mu-H)_2[\mu-Ph_2PCH_2PPh_2]$  | 213 |
|      | (j) $Re_2(CO)_8(\mu-H)(\mu-NCHMe)[\mu-Ph_2P-$<br>$CH_2PPh_2]$ - a derivative of $Re_2-$<br>$(CO)_6(\mu-H)_2[\mu-Ph_2PCH_2PPh_2]$                              | 214 |

|        |   |     |
|--------|---|-----|
|        | (k) $\text{Re}_2(\text{CO})_6(\mu\text{-H})(\mu\text{-OH})[\mu\text{-Ph}_2\text{PCH}_2\text{-PPh}_2]$ - a formal derivative of                                    |     |
|        | $\text{Re}_2(\text{CO})_6(\mu\text{-H})_2(\mu\text{-Ph}_2\text{PCH}_2\text{PPh}_2)$   | 214 |
|        | (l) $[\text{Re}_2(\text{CO})_4(\text{PhCCPh})_3(\text{CNCH}_2\text{SO}_2\text{C}_6\text{H}_4\text{-Me-p})_2]$ , and $[\text{Re}_2(\text{CO})_4(\text{PhCCPh})_4]$ | 215 |
| 13.3   | Assessment  | 216 |
| 13.3.1 | The Re-Re bond length   | 216 |
| 13.3.2 | The Re-CO bond lengths  | 217 |
| 13.3.3 | Molecular Conformation  | 217 |
| 13.3.4 | OC-Re-CO bond angles  | 217 |
| 13.3.5 | Re-C-O bond angles  | 217 |
| 13.3.6 | Packing   | 217 |
| XIV    | X-ray Crystallographic studies of isonitrile derivatives of $\text{M}_2(\text{CO})_{10}$ (M = Re, Mn)   | 218 |
| 14.1   | Introduction  | 218 |
| 14.2   | X-ray Crystallographic  | 220 |
| 14.2.1 | Structure of $\text{M}(\text{CNBu}^t)$ (I)  | 220 |
| 14.2.2 | Structure of $\text{Re}_2(\text{CNC}_6\text{H}_3\text{Me}_2\text{-2,6})_2$ (II)   | 223 |
| 14.2.3 | Structure of $\text{Mn}_2(\text{CO})_8(\text{CNBu}^t)_2$ (V)  | 228 |
| 14.2.4 | Structure of $\text{Re}_2(\text{CO})_7(\text{CNMe})_3$ (III)  | 228 |
| 14.2.5 | Structure of $\text{Re}_2(\text{CO})_6(\text{CNC}_6\text{H}_3\text{Me}_2\text{-2,6})_4$ (IV)  | 238 |
| 14.2.6 | Structure of $\text{Mn}_2(\text{CO})_6(\text{CNC}_6\text{H}_3\text{Me}_2\text{-2,6})_4$ (VI)  | 243 |
| 14.3   | Structural Trends   | 243 |
| 14.3.1 | The M-M bond length   | 252 |
| 14.3.2 | The M-CO bond lengths   | 252 |
| 14.3.3 | Molecular Conformation  | 254 |
| 14.3.4 | C-M-C and M-M-Ceq bond angles   | 256 |
| 14.3.5 | M-C-O, M-C-N and M-N-C bond angles  | 256 |
| 14.3.6 | Packing   | 259 |
| 14.4   | Relating structure to chemical reactivity   | 261 |
| 14.5   | Experimental  | 262 |
| 14.5.1 | Data collection   | 262 |
| 14.5.2 | Structure solution and refinement   | 263 |
| 14.5.3 | Refinement problems with $\text{Mn}_2(\text{CO})_6\text{-CNC}_6\text{H}_3\text{Me}_2\text{-2,6})_4$ (VI)  | 267 |

|         |  |     |
|---------|--|-----|
| XV      | The Reaction between dirhenium decacarbonyl and phosphine ligands  | 280 |
| 15A.    | Introduction   | 280 |
| 15B     | Discussion of the IR spectral data of $\text{Re}_2(\text{CO})_{10-n}(\text{PR}_3)_n$ ( $n = 1-4$ ) complexes   | 280 |
| 15B.1   | Introduction   | 280 |
| 15B.2   | $\text{Re}_2(\text{CO})_9(\text{PR}_3)$ complexes  | 282 |
| 15B.3   | $\text{Re}_2(\text{CO})_8(\text{PR}_3)_2$ complexes  | 288 |
| 15B.4   | $\text{Re}_2(\text{CO})_7(\text{PR}_3)_3$ complexes  | 293 |
| 15B.5   | $\text{Re}_2(\text{CO})_6(\text{PR}_3)_4$ complexes  | 296 |
| 15B.6   | Conclusion   | 296 |
| 15C     | A Survey of Kinetic and Mechanistic Studies  | 297 |
| 15D.1   | Synthesis and characterization of $\text{Re}_2(\text{CO})_{10-n}(\text{PR}_3)_n$ ( $n = 1,2$ ) derivatives   | 303 |
| 15D.2   | Experimental   | 313 |
| 15D.2.1 | Synthesis of $\text{Re}_2(\text{CO})_{10-n}(\text{PR}_3)_n$ ( $n = 1,2$ ) from the reaction of $\text{Re}_2(\text{CO})_{10}$ and $\text{PR}_3$ in the presence of Pd-catalysts                             | 313 |
| 15D.2.2 | Synthesis of $\text{Re}_2(\text{CO})_{10-n}(\text{PR}_3)_n$ ( $n = 1,2$ ) by the $\text{NMe}_3\text{U}$ -assisted reaction of $\text{Re}_2(\text{CO})_{10}$ with $\text{PR}_3$ in $\text{CH}_2\text{Cl}_2$ | 313 |
| 15D.2.3 | Preparation of an isomer of $\text{Re}_2(\text{CO})_8(\text{PMe}_2\text{Ph})_2$  | 313 |
| 15D.2.4 | Preparation of an isomer of $\text{Re}_2(\text{CO})_8(\text{PMePh}_2)_2$   | 314 |
| 15E     | The Crystal and Molecular Structure of <u>di</u> ax- $[\text{Re}_2(\text{CO})_8(\text{PMe}_2\text{Ph})_2]$   | 314 |
| 15E.1   | Introduction   | 314 |
| 15E.2   | Discussion of related $\text{Mn}_2(\text{CO})_{10-n}(\text{PR}_3)_n$ ( $n = 1,2$ ) structures  | 315 |
| 15E.3   | Discussion of the structure of <u>di</u> ax- $[\text{Re}_2(\text{CO})_8(\text{PMe}_2\text{Ph})_2]$   | 316 |
| 15E.3.1 | Di axial phosphine substitution  | 316 |
| 15E.3.2 | The Re-Re, Re-P and Re-CO bond lengths   | 320 |

|            |   |     |
|------------|---|-----|
| 15E.3.3    | Molecular Conformation  | 324 |
| 15E.3.4    | P-Re-CO, OC-Re-CO and Re-Re-CO bond angles                          | 324 |
| 15E.3.5    | Re-C-O bond angles  | 327 |
| 15E.3.6    | Packing   | 327 |
| 15E.4      | Experimental  | 328 |
| 15E.4.1    | Data collection   | 328 |
| 15E.4.2    | Structure solution and refinement                                   | 330 |
| XVI        | Conclusion  | 334 |
| Appendix A | The Sources of Chemicals used in this study                         | 337 |
|            | (A) General Chemicals   | 337 |
|            | (B) Catalysts   | 337 |
|            | (C) Other Sources   | 337 |
| Appendix B | General Experimental Details  | 339 |
|            | (a) Synthetic Methods   | 339 |
|            | (b) Solvents  | 339 |
|            | (c) Instrumentation   | 339 |
|            | (d) X-ray data collection   | 340 |
|            | (e) Crystallographic Computing Programs                             | 340 |
|            | (f) Crystallographic R-indices                                      | 341 |
| Appendix C | Torsional Angles for the $M_2(CO)_{10-n}(L)_n$ Structures           | 342 |
|            | (I) $Re_2(CO)_9(CNBU^+)$  | 343 |
|            | (II) $Re_2(CO)_8(CNC_6H_3Me_2-2,6)_2$                               | 343 |
|            | (III) $Re_2(CO)_7(CNMe)_3$  | 344 |
|            | (IV) $Re_2(CO)_6(CNC_6H_3Me_2-2,6)_4$                               | 344 |
|            | (V) $Mn_2(CO)_8(CNBU^+)_2$  | 345 |
|            | (VI) $Mn_2(CO)_6(CNC_6H_3Me_2-2,6)_4$                               | 345 |
|            | (VII) $di\mu[Re_2(CO)_8(PMe_2Ph)_2]$                                | 345 |
| Appendix D | Structure Factor Tables -<br>Bound as a separate volume (105 pages) |     |
|            | List of contents  | 347 |
| Appendix E | List of Publications  | 348 |
| Appendix F | Molecular Mechanics Calculations                                    | 349 |
| References |   | 350 |

LIST OF TABLES

|  | <u>PAGE</u> |
|--|-------------|
| Table 2.1 : Spectroscopic data for the ( $\eta^6$ -Arene)Cr-(CO) <sub>2</sub> (CNR) complexes  | 12          |
| Table 2.2 : Analytical data for the ( $\eta^6$ -Arene)Cr(CO) <sub>2</sub> -(CNR) complexes   | 17          |
| Table 2.3 : Spectroscopic data for the Cr(CO) <sub>6-n</sub> -(CNC <sub>6</sub> H <sub>3</sub> Me <sub>2-2,5</sub> ) <sub>n</sub> (n = 3,4) complexes  | 17          |
| Table 2.4 : Analytical data for [(C <sub>5</sub> H <sub>4</sub> CO <sub>2</sub> Me)Fe(CO) <sub>2</sub> ] <sub>2</sub> and derivatives  | 18          |
| Table 2.5 : Spectroscopic data for [(C <sub>5</sub> H <sub>4</sub> CO <sub>2</sub> Me)Fe(CO) <sub>2</sub> ] <sub>2</sub> and derivatives   | 18          |
| Table 3.1 : X-ray Crystal Structures of ( $\eta^6$ -C <sub>6</sub> H <sub>5</sub> CO <sub>2</sub> Me)-Cr(CO) <sub>2</sub> L complexes  | 28          |
| Table 3.2 : Principal geometric characteristics of ( $\eta^6$ -C <sub>6</sub> H <sub>5</sub> CO <sub>2</sub> Me)Cr(CO) <sub>2</sub> L complexes  | 29          |
| Table 4.1 : Bond lengths for ( $\eta^6$ -C <sub>6</sub> H <sub>5</sub> CO <sub>2</sub> Me)Cr(CO) <sub>2</sub> -(CNBu <sup>t</sup> )  | 36          |
| Table 4.2 : Bond angles for ( $\eta^6$ -C <sub>6</sub> H <sub>5</sub> CO <sub>2</sub> Me)Cr(CO) <sub>2</sub> -(CNBu <sup>t</sup> )   | 36          |
| Table 4.3 : Bond parameters involving hydrogen atoms for ( $\eta^6$ -C <sub>6</sub> H <sub>5</sub> CO <sub>2</sub> Me)Cr(CO) <sub>2</sub> (CNBu <sup>t</sup> )                                       | 37          |
| Table 4.4 : Deviations of atoms from the plane defined by the six C-atoms of the arene ring in ( $\eta^6$ -C <sub>6</sub> H <sub>5</sub> CO <sub>2</sub> Me)Cr(CO) <sub>2</sub> (CNBu <sup>t</sup> ) | 37          |
| Table 4.5 : Principal geometric characteristics of ( $\eta^6$ -C <sub>6</sub> H <sub>5</sub> CO <sub>2</sub> Me)Cr(CO) <sub>2</sub> (CNBu <sup>t</sup> )   | 39          |
| Table 4.6 : Crystal data and details of structural analysis for ( $\eta^6$ -C <sub>6</sub> H <sub>5</sub> CO <sub>2</sub> Me)Cr(CO) <sub>2</sub> (CNBu <sup>t</sup> )                                | 45          |
| Table 4.7 : Fractional Atomic Co-ordinates for ( $\eta^6$ -C <sub>6</sub> H <sub>5</sub> CO <sub>2</sub> Me)Cr(CO) <sub>2</sub> (CNBu <sup>t</sup> )   | 46          |
| Table 4.8 : Anisotropic Thermal Parameters for the non-hydrogen atoms of ( $\eta^6$ -C <sub>6</sub> H <sub>5</sub> CO <sub>2</sub> Me)Cr(CO) <sub>2</sub> -(CNBu <sup>t</sup> )                      | 47          |

|   | <u>PAGE</u> |
|---|-------------|
| Table 5.1 : Analytical data for the $(\eta^5\text{-C}_5\text{H}_5)\text{Mn}(\text{CO})_2^-$<br>(CNR) complexes  | 51          |
| Table 5.2 : Spectroscopic data for the $(\eta^5\text{-C}_5\text{H}_5)\text{Mn}-$<br>$(\text{CO})_2$ (CNR) complexes   | 52          |
| Table 6.1 : X-ray Crystal structures of $(\eta^5\text{-C}_5\text{H}_5)\text{Mn}-$<br>$(\text{CO})_2\text{L}$ complexes  | 59          |
| Table 6.2 : Principal geometric characteristics of<br>$(\eta^5\text{-C}_5\text{H}_5)\text{Mn}(\text{CO})_2\text{L}$ complexes   | 60          |
| Table 7.1 : Bond lengths for $(\eta^5\text{-C}_5\text{H}_5)\text{Mn}(\text{CO})_2(\text{CNBu}^t)$   | 67          |
| Table 7.2 : Bond angles for $(\eta^5\text{-C}_5\text{H}_5)\text{Mn}(\text{CO})_2(\text{CNBu}^t)$  | 67          |
| Table 7.3 : Bond parameters involving hydrogen atoms<br>for $(\eta^5\text{-C}_5\text{H}_5)\text{Mn}(\text{CO})_2(\text{CNBu}^t)$  | 68          |
| Table 7.4 : Deviations of atoms from the plane<br>defined by the 5 C-atoms of the cyclo-<br>pentadienyl ring of $(\eta^5\text{-C}_5\text{H}_5)\text{Mn}(\text{CO})_2^-$<br>(CNBu <sup>t</sup> ) | 69          |
| Table 7.5 : Principal geometric characteristics of<br>$(\eta^5\text{-C}_5\text{H}_5)\text{Mn}(\text{CO})_2(\text{CNBu}^t)$  | 70          |
| Table 7.6 : Crystal data and details of structural<br>analysis for $(\eta^5\text{-C}_5\text{H}_5)\text{Mn}(\text{CO})_2(\text{CNBu}^t)$   | 75          |
| Table 7.7 : Fractional atomic co-ordinates for<br>$(\eta^5\text{-C}_5\text{H}_5)\text{Mn}(\text{CO})_2(\text{CNBu}^t)$  | 76          |
| Table 7.8 : Anisotropic thermal parameters for the non-<br>hydrogen atoms of $(\eta^5\text{-C}_5\text{H}_5)\text{Mn}(\text{CO})_2(\text{CNBu}^t)$   | 77          |
| Table 8.1 : IR spectral study of $\{(\eta^5\text{-C}_5\text{H}_5\text{CO}_2\text{Me})\text{Cr}(\text{CO})_2^-$<br>(CNBu <sup>t</sup> ) in different solvents                                    | 82          |
| Table 8.2 : IR spectral study of $(\text{C}_5\text{H}_5)\text{Mn}(\text{CO})_2(\text{CNBu}^t)$<br>in different solvents   | 83          |
| Table 9.1 : X-ray Crystal Structures of $\text{Fe}(\text{CO})_4\text{L}$<br>Complexes   | 94          |
| Table 9.2 : Geometric data for the ax-l- $\text{Fe}(\text{CO})_4$ tbp<br>structures   | 96          |
| Table 9.3 : X-ray Crystal Structures of $\text{Fe}(\text{CO})_3\text{LL}'$<br>Structures  | 102         |
| Table 9.4 : Geometric data for $\text{Fe}(\text{CO})_3\text{LL}'$ Structures  | 103         |
| Table 9.5 : Bond lengths for $\text{Fe}(\text{CO})_3(\text{CNMe})_2$  | 112         |



|               | <u>PAGE</u>   |
|---------------|---|
| Table 9.6 :   | Bond angles for $\text{Fe}(\text{CO})_3(\text{CNMe})_2$ 112   |
| Table 9.7 :   | Crystal data and details of structural analysis for $\text{Fe}(\text{CO})_3(\text{CNMe})_2$ 115   |
| Table 9.8(a): | Fractional atomic co-ordinates for the non-hydrogen atoms of $\text{Fe}(\text{CO})_3(\text{CNMe})_2$ 116  |
| Table 9.8(b): | Fractional atomic co-ordinates and isotropic temperature factors for the hydrogen atoms of $\text{Fe}(\text{CO})_3(\text{CNMe})_2$ 116  |
| Table 9.9 :   | Anisotropic temperature factors for the non-hydrogen atoms of $\text{Fe}(\text{CO})_3(\text{CNMe})_2$ 117   |
| Table 10.1 :  | Re-Re bonded dimeric products from the photochemical reaction of $\text{Re}_2(\text{CO})_{10}$ and olefins in hexane solution 128   |
| Table 11.1 :  | Effect of potential catalysts on the reaction $\text{Re}_2(\text{CO})_{10} + \text{Bu}^t\text{NC} \longrightarrow \text{Re}_2(\text{CO})_9(\text{CNBu}^t) + \text{CO}$ 150            |
| Table 11.2 :  | Reaction conditions and product yields for the PdO catalysed syntheses of the complexes $\text{Re}_2(\text{CO})_{10-n}(\text{CNR})_n$ ( $n = 1-4$ ) 153                               |
| Table 11.3 :  | Reaction times at 55°C for the uncatalysed and PdO-catalysed reaction $\text{Re}_2(\text{CO})_{10} + \text{RNC} \longrightarrow \text{Re}_2(\text{CO})_9(\text{CNR}) + \text{CO}$ 154 |
| Table 11.4 :  | Analytical data for the $\text{Re}_2(\text{CO})_{10-n}(\text{CNR})_n$ ( $n = 1-4$ ) complexes 156   |
| Table 11.5 :  | Infra Red Data of the complexes $\text{Re}_2(\text{CO})_{10-n}(\text{CNR})_n$ ( $n = 1-4$ ) 157   |
| Table 11.6 :  | $^1\text{H}$ NMR data of the complexes $\text{Re}_2(\text{CO})_{10-n}(\text{CNR})_n$ ( $n = 1-4$ ) 166  |
| Table 11.7 :  | Mass spectral data for $\text{Re}_2(\text{CO})_9(\text{CNBu}^t)$ 170  |
| Table 11.8 :  | Mass spectral data for $\text{Mn}_2(\text{CO})_8(\text{CNBu}^t)_2$ 175  |
| Table 11.9 :  | Mass spectral data for the complex $[\text{Re}(\text{CO})_4(\text{CNC}_6\text{H}_3\text{Me}_2-2,6)]_2$ 180  |
| Table 13.1 :  | X-ray Crystal Structures of dirhenium decacarbonyl derivatives, with a direct Re-Re bond 204  |

|               |   |     |
|---------------|---|-----|
| Table 13.2 :  | Average values of the Re-Re-C bond angles for the sq-Re <sub>2</sub> (CO) <sub>9</sub> (Carbene) structures (i) - (iii)   | 207 |
| Table 14.1 :  | Bond lengths for Re <sub>2</sub> (CO) <sub>9</sub> (CNBu <sup>t</sup> )(I)  | 226 |
| Table 14.2 :  | Bond angles for Re <sub>2</sub> (CO) <sub>9</sub> (CNBu <sup>t</sup> )(I)   | 227 |
| Table 14.3 :  | Bond lengths for Re <sub>2</sub> (CO) <sub>8</sub> (CNC <sub>6</sub> H <sub>3</sub> Me <sub>2</sub> -2,6) <sub>2</sub> (II)   | 231 |
| Table 14.4 :  | Bond angles for Re <sub>2</sub> (CO) <sub>8</sub> (CNC <sub>6</sub> H <sub>3</sub> Me <sub>2</sub> -2,6) <sub>2</sub> (II)  | 232 |
| Table 14.5 :  | Bond lengths for Mn <sub>2</sub> (CO) <sub>8</sub> (CNBu <sup>t</sup> ) <sub>2</sub> (V)  | 235 |
| Table 14.6 :  | Bond angles for Mn <sub>2</sub> (CO) <sub>8</sub> (CNBu <sup>t</sup> ) <sub>2</sub> (V)   | 236 |
| Table 14.7 :  | Bond lengths for Re <sub>2</sub> (CO) <sub>7</sub> (CNMe) <sub>3</sub> (III)  | 241 |
| Table 14.8 :  | Bond angles for Re <sub>2</sub> (CO) <sub>7</sub> (CNMe) <sub>3</sub> (III)   | 242 |
| Table 14.9 :  | Bond lengths for Re <sub>2</sub> (CO) <sub>6</sub> (CNC <sub>6</sub> H <sub>3</sub> Me <sub>2</sub> -2,6) <sub>4</sub> (IV)   | 246 |
| Table 14.10 : | Bond angles for Re <sub>2</sub> (CO) <sub>6</sub> (CNC <sub>6</sub> H <sub>3</sub> Me <sub>2</sub> -2,6) <sub>4</sub> (IV)  | 249 |
| Table 14.11 : | Bond lengths for Mn <sub>2</sub> (CO) <sub>6</sub> (CNC <sub>6</sub> H <sub>3</sub> Me <sub>2</sub> -2,6) <sub>4</sub> (IV)   | 250 |
| Table 14.12 : | Bond angles for Mn <sub>2</sub> (CO) <sub>6</sub> (CNC <sub>6</sub> H <sub>3</sub> Me <sub>2</sub> -2,6) <sub>4</sub> (IV)  | 251 |
| Table 14.13 : | Metal-metal bond length data for the complexes M <sub>2</sub> (CO) <sub>10</sub> (CNR) <sub>n</sub> (a) M = Re, n = 0-4; (b) M = Mn, n = 0,2,4                                  | 253 |
| Table 14.14 : | Average M-C bond length data for the complexes M <sub>2</sub> (CO) <sub>10</sub> (CNR) <sub>n</sub> (a) M = Re, n = 0-4; (b) M = Mn, n = 0,2,4                                  | 255 |
| Table 14.15 : | Average M-M-C bond angle data for the complexes M <sub>2</sub> (CO) <sub>10-n</sub> (CNR) <sub>n</sub> (a) M = Re, n = 0-4; (b) M = Mn, n = 0,2,4                               | 257 |
| Table 14.16 : | Average cis C-M-C bond angle data for the complexes M <sub>2</sub> (CO) <sub>10-n</sub> (CNR) <sub>n</sub> (a) M = Re, n = 0-4; (b) M = Mn, n = 0,2,4                           | 258 |
| Table 14.17 : | Average bond data for the M-C-O, M-C-N and C-N-C bond angles of the complexes M <sub>2</sub> (CO) <sub>10-n</sub> (CNR) <sub>n</sub> (a) M = Re, n = 0-4; (b) M = Mn, n = 0,2,4 | 260 |

|                  | <u>PAGE</u>   |     |
|------------------|---|-----|
| Table 14.18 :    | Crystal data and details of structure analyses for the $\text{Re}_2(\text{CO})_{10-n}(\text{CNR})_n$ ( $n = 1-4$ ) complexes (I - IV)                         | 264 |
| Table 14.19 :    | Crystal data and details of structure analyses for the $\text{Mn}_2(\text{CO})_{10-n}(\text{CNR})_n$ ( $n = 2,4$ ) complexes (V,VI)                           | 256 |
| Table 14.20 :    | Final atomic co-ordinates, and isotropic temperature factors of the C-atoms, for $\text{Re}_2(\text{CO})_9(\text{CNBu}^t)$ (I)                                | 268 |
| Table 14.21 :    | Final atomic co-ordinates, and isotropic temperature factors of the C-atoms, for $\text{Re}_2(\text{CO})_8(\text{CNC}_6\text{H}_3\text{Me}_2-2,6)_2$ (II)     | 269 |
| Table 14.22 :    | Final atomic co-ordinates, and isotropic temperature factors of the C-atoms, for $\text{Re}_2(\text{CO})_7(\text{CNMe})_3$ (III)                              | 271 |
| Table 14.23 :    | Final atomic co-ordinates, and isotropic temperature factors of the C-atoms, for $\text{Re}_2(\text{CO})_6(\text{CNC}_6\text{H}_3\text{Me}_2-2,6)_4$ (IV)     | 272 |
| Table 14.24(a) : | Final atomic co-ordinates of the non-H atoms for $\text{Mn}_2(\text{CO})_8(\text{CNBu}^t)_2$ (V)  | 273 |
| Table 14.24(b) : | Final atomic co-ordinates and isotropic temperature factors of the Hydrogen atoms, for $\text{Mn}_2(\text{CO})_8(\text{CNBu}^t)_2$ (V)                        | 274 |
| Table 14.25 :    | Final atomic co-ordinates, and isotropic temperature factors of the non-C atoms, for $\text{Mn}_2(\text{CO})_6(\text{CNC}_6\text{H}_3\text{Me}_2-2,6)_4$ (VI) | 275 |
| Table 14.26 :    | Anisotropic temperature factors for the non-C atoms of $\text{Re}_2(\text{CO})_9(\text{CNBu}^t)$ (I)  | 276 |
| Table 14.27 :    | Anisotropic temperature factors for the non-C atoms of $\text{Re}_2(\text{CO})_8(\text{CNC}_6\text{H}_3\text{Me}_2-2,6)_2$ (II)                               | 276 |
| Table 14.28 :    | Anisotropic temperature factors for the non-C atoms of $\text{Re}_2(\text{CO})_7(\text{CNMe})_3$ (III)  | 277 |
| Table 14.29 :    | Anisotropic temperature factors for the non-C atoms of $\text{Re}_2(\text{CO})_6(\text{CNC}_6\text{H}_3\text{Me}_2-2,6)_4$ (IV)                               | 277 |

|               | <u>PAGE</u>   |     |
|---------------|---|-----|
| Table 14.30 : | Anisotropic temperature factors for the non-H atoms of $Mn_2(CO)_8(CNBU^t)_2(V)$  | 278 |
| Table 14.31 : | Anisotropic temperature factors for the non-C atoms of $Mn_2(CO)_6(CNC_6H_3Me_2-2,6)_4(VI)$                               | 279 |
| Table 15.1 :  | IR spectral data of $M_2(CO)_8(L)$ ( $M = Mn, Re$ ; $L = AsR_3, PR_3$ ) complexes   | 285 |
| Table 15.2 :  | IR spectral data of $M_2(CO)_8(L)_2$ ( $M = Mn, Re$ ; $L = AsR_3, PR_3$ ) complexes                                       | 287 |
| Table 15.3 :  | IR spectral data of $Re_2(CO)_7(PR_3)_3$ complexes  | 295 |
| Table 15.4 :  | Correlation between IR data and molecular geometry for $M_2(CO)_8(L)_2$ complexes   | 298 |
| Table 15.5 :  | Details of catalytic syntheses of $Re_2(CO)_{10-n}(PR_3)_n$ ( $n = 1,2$ ) complexes                                       | 305 |
| Table 15.6 :  | IR spectral data for the $Re_2(CO)_{10-n}(PR_3)_n$ ( $n = 1,2$ ) derivatives  | 306 |
| Table 15.7 :  | IR spectral data for the $CfRe(CO)_3(PR_3)_2$ complexes   | 306 |
| Table 15.8 :  | Crystal data and selected bond parameters for $Mn_2(CO)_{10-n}(PR_3)_n$ structures ( $n = 1,2$ )                          | 317 |
| Table 15.9 :  | Bond lengths for $diax[Re_2(CO)_8(PMe_2Ph)_2]$ (VII)  | 321 |
| Table 15.10 : | Bond angles for $diax[Re_2(CO)_8(PMe_2Ph)_2]$ (VII)   | 322 |
| Table 15.11 : | Average bond length and bond angle data for $diax[Re_2(CO)_8(PMe_2Ph)_2]$ (VII)   | 323 |
| Table 15.12 : | Least squares planes for phenyl rings in $diax[Re_2(CO)_8(PMe_2Ph)_2]$ (VII)  | 329 |
| Table 15.13 : | Crystal data and details of structure analysis for $diax[Re_2(CO)_8(PMe_2Ph)_2]$ (VII)                                    | 331 |
| Table 15.14 : | Final atomic co-ordinates and isotropic temperature factors for the C and O atoms, of $diax[Re_2(CO)_8(PMe_2Ph)_2]$ (VII) | 332 |
| Table 15.15 : | Anisotropic temperature factors for the Re and P atoms of $diax[Re_2(CO)_8(PMe_2Ph)_2]$ (VII)                             | 332 |

| <u>LIST OF FIGURES</u>  | <u>PAGE</u> |
|---|-------------|
| Figure 2.1 : Fragmentation pattern for $[(\eta^6\text{-Arene})\text{-Cr}(\text{CO})_2(\text{CNBu}^t)]$  | 13          |
| Figure 3.1 : The three possible conformations for $(\text{C}_6\text{H}_5\text{R})\text{Cr}(\text{CO})_3$ : I. Staggered, IIa. anti-eclipsed, and IIb. syn-eclipsed                              | 21          |
| Figure 3.2 : Two sets of three hybrid orbitals of $\text{Cr}(\text{CO})_3$ : (a) empty, (b) filled  | 21          |
| Figure 3.3.a: Ring polarization with electron-accepting substituent A results in the anti-eclipsed conformation IIa for $(\text{C}_6\text{H}_5\text{A})\text{Cr}(\text{CO})_3$                  | 22          |
| Figure 3.3.b: Ring polarization with electron-donating substituent D results in the syn-eclipsed conformation IIb for $(\text{C}_6\text{H}_5\text{D})\text{Cr}(\text{CO})_3$                    | 22          |
| Figure 3.4 : Anti-eclipsed conformation of $(\eta^6\text{-C}_6\text{H}_5\text{CO}_2\text{-Me})\text{Cr}(\text{CO})_2\text{L}$ complex, viewed down ligand tripod onto arene ring                | 30          |
| Figure 3.5 : Unusual staggered conformation of the $(\eta^6\text{-C}_6\text{H}_5\text{CO}_2\text{Me})\text{Cr}(\text{CO})_2(\text{CNCOPh})$ molecule, viewed down ligand tripod onto arene ring | 30          |
| Figure 4.1 : An ORTEP view of the $(\eta^6\text{-C}_6\text{H}_5\text{CO}_2\text{Me})\text{Cr}(\text{CO})_2\text{-CNBu}^t$ molecule, showing the numbering system                                | 34          |
| Figure 4.2 : An ORTEP view of the unit cell of $(\eta^6\text{-C}_6\text{H}_5\text{CO}_2\text{Me})\text{Cr}(\text{CO})_2(\text{CNBu}^t)$ , looking down the c-axis                               | 35          |
| Figure 4.3 : Conformation of the $(\eta^6\text{-C}_6\text{H}_5\text{CO}_2\text{Me})\text{Cr}(\text{CO})_2\text{-}(\text{CNBu}^t)$ molecule, viewed down ligand tripod onto arene ring           | 41          |
| Figure 5.1 : Fragmentation pattern for $(\eta^5\text{-C}_5\text{H}_5)\text{Mn}(\text{CO})_2(\text{CNBu}^t)$   | 53          |
| Figure 6.1 : Conformation of $(\eta^5\text{-C}_5\text{H}_5)\text{Mn}(\text{CO})_3$ , looking down onto the $(\text{C}_5\text{H}_5)$ ring  | 56          |
| Figure 6.2 : Ring C-C bond lengths in $(\eta^5\text{-C}_5\text{H}_5)\text{Mn}(\text{CO})_3$   | 56          |

|               | <u>PAGE</u>   |     |
|---------------|---|-----|
| Figure 6.3 :  | Ring C-C bond length in $(\eta^5\text{-C}_5\text{H}_5)\text{Mn}(\text{CO})_2(\text{CMe})$   | 63  |
| Figure 7.1 :  | ORTEP view of the $(\eta^5\text{-C}_5\text{H}_5)\text{Mn}(\text{CO})_2(\text{CNBu}^t)$ molecule, showing the numbering system   | 65  |
| Figure 7.2 :  | ORTEP view of the unit cell of $(\eta^5\text{-C}_5\text{H}_5)\text{Mn}(\text{CO})_2(\text{CNBu}^t)$ , looking down the b-axis   | 66  |
| Figure 7.3 :  | Ring C-C bond lengths in $(\eta^5\text{-C}_5\text{H}_5)\text{Mn}(\text{CO})_2(\text{CNBu}^t)$   | 72  |
| Figure 8.1 :  | Solid state IR spectra (KBr) of $(\eta^6\text{-C}_6\text{H}_5\text{-CO}_2\text{Me})\text{Cr}(\text{CO})_2(\text{CNR})$ (a) $\text{R} = \text{C}_6\text{H}_3\text{Me}_2\text{-}2,6$ , (b) $\text{R} = \text{Bu}^t$   | 80  |
| Figure 8.2 :  | Sideways ORTEP view of the $(\eta^6\text{-C}_6\text{H}_5\text{CO}_2\text{Me})\text{-Cr}(\text{CO})_2(\text{CNBu}^t)$ molecule   | 84  |
| Figure 8.3 :  | Sideways ORTEP view of the $(\eta^5\text{-C}_5\text{H}_5)\text{Mn}(\text{CO})_2(\text{CNBu}^t)$ molecule  | 85  |
| Figure 8.4 :  | Diagram illustrating the conformation of the $\text{CNBu}^t$ ligand in $(\eta^6\text{-C}_6\text{H}_5\text{CO}_2\text{Me})\text{-Cr}(\text{CO})_2(\text{CNBu}^t)$ ((a) and (c)) and $(\eta^5\text{-C}_5\text{H}_5)\text{Mn}(\text{CO})_2(\text{CNBu}^t)$ ((b) and (d)) | 86  |
| Figure 9.1 :  | An ORTEP view of the $\text{Fe}(\text{CO})_3(\text{CNMe})_2$ molecule, showing the numbering system used  | 110 |
| Figure 9.2 :  | An ORTEP view of the unit cell of $\text{Fe}(\text{CO})_3(\text{CNMe})_2$ looking down the b-axis   | 111 |
| Figure 10.1 : | Possible Re-Re bonded dimeric olefin derivatives of $\text{Re}_2(\text{CO})_{10}$ (a) octa-carbonyl- $\mu$ -olefinyl- $\mu$ -hydride-dirhenium, (b) <i>enneacarbonyl-<math>\eta</math>-olefin-dirhenium</i>   | 127 |
| Figure 10.2 : | Re-Re bonded dimeric products of $\text{Re}_2(\text{CO})_{10}$ with olefins in hexane solution  | 128 |
| Figure 10.3 : | Re-Re bonded dimeric products from the photochemical reactions of $\text{Re}_2(\text{CO})_{10}$ with 1,3 butadiene  | 132 |
| Figure 10.4 : | Re-Re bonded dimeric products from the photochemical reaction of $\text{Re}_2(\text{CO})_{10}$ with 1,3,5-cycloheptatriene  | 132 |

|                  | <u>PAGE</u>   |     |
|------------------|---|-----|
| Figure 10.5 :    | Products from photolysis reactions of $Re_2(CO)_{10}$ with 1-alkenes and 2-alkenes  | 133 |
| Figure 10.6 :    | Dipolar addition product, $(\mu-H)(\mu-CH=CH_2)-Re_2(CO)_8(PMe_3)$  | 133 |
| Figure 10.7 :    | Darhenium carbonyl $(\mu$ -carbene) derivatives   | 137 |
| Figure 10.8 :    | Products of reaction of $(\mu-H)(\mu$ -trans- $CH=CHMe)Re_2(CO)_8$ with acetylene   | 137 |
| Figure 10.9 :    | Possible dipolar addition products, $(\mu-H)(\mu-C=CPh)Re_2(CO)_8(PMe_3)$   | 137 |
| Figure 10.10 :   | The two isomers of 1,2-ax,eq- $Re_2(CO)_8-[C(OEt)SiPh_3][C(OEt)C_6H_4Me]$   | 144 |
| Figure 11.1 :    | Synthetic routes to the mixed-isonitrile derivative, $Re_2(CO)_8(CNBu^t)(CNC_6H_3Me_2-2,6)$   | 154 |
| Figure 11.2 :    | IR spectra of (a) eq- $Re_2(CO)_8(CNBu^t)$ and (b) ax- $Mn_2(CO)_9(PMe_2Ph)$  | 158 |
| Figure 11.3(a) : | FTIR spectrum of 1,2-dieq- $Re_2(CO)_8-(CNC_6H_3Me_2-2,6)_2$  | 161 |
| Figure 11.3(b) : | FTIR spectrum of 1,1-cis-dieq- $Re_2(CO)_8-(CNBu^t)_2$  | 162 |
| Figure 11.4 :    | Plot of $\delta(CH_x)$ ( $x = 2,3$ ) vs $n(RNC)$ for the $Re_2(CO)_{10-n}(CNR)_n$ ( $n = 1-4$ ) complexes                                   | 167 |
| Figure 11.5 :    | Newman projection of the possible cis-equatorial conformational isomers of $M_2(CO)_7(CNR)_3$ ( $M = Re, Mn$ ), as viewed down the M-M bond | 168 |
| Figure 11.6 :    | Isomers of $Mn_2(CO)_8(CNBu^t)_2$ (A) 1,1-cis-dieq, and (B) 1,2-dieq  | 168 |
| Figure 11.7(a) : | Dimeric fragmentation pattern for $Re_2(CO)_9(CNBu^t)$  | 172 |
| Figure 11.7(b) : | Monomeric fragmentation pattern for $Re_2(CO)_9(CNBu^t)$  | 173 |
| Figure 11.8(a) : | Dimeric fragmentation pattern for $Mn_2(CO)_8(CNBu^t)_2$  | 177 |

|  | <u>PAGE</u> |
|--|-------------|
| Figure 11.8(b): Monomeric fragmentation pattern for $Mn_2(CO)_8(CNBu^t)_2$   | 178         |
| Figure 11.9(b): Dimeric fragmentation pattern for $[Re(CO)_4(CNC_6H_3Me_2-2,6)]_2$   | 182         |
| Figure 11.9(b): Monomeric fragmentation path for $[Re(CO)_4(CNC_6H_3Me_2-2,6)]_2$  | 183         |
| Figure 13.1 : Schematic representation of the structure of $(CO)_4Re[\mu-C(SiPh_3)CO(OEt)]Re(C(OEt)(SiPh_3)]$              | 212         |
| Figure 14.1 : The two possible structures of $Re_2(CO)_9(CNR)$ (Ia) equatorial substitution, (Ib) axial substitution       | 221         |
| Figure 14.2 : Newman projections of possible conformations of $M_2(CO)_9(CNR)_2$ (M = Re, Mn), as viewed down the M-M axis | 221         |
| Figure 14.3 : Newman projections of possible conformations of $Re_2(CO)_7(CNR)_3$ , as viewed down the Re-Re axis          | 222         |
| Figure 14.4 : Newman projections of possible conformations of $M_2(CO)_8(CNR)_4$ (M = Re, Mn), as viewed down the M-M axis | 222         |
| Figure 14.5 : ORTEP view of the $Re_2(CO)_9(CNBu^t)$ molecule (I), showing the numbering system used                       | 224         |
| Figure 14.6 : ORTEP view of the unit cell of $Re_2(CO)_9(CNBu^t)$ (I), looking down the $b$ -axis                          | 225         |
| Figure 14.7 : ORTEP view of the $Re_2(CO)_8(CNC_6H_3Me_2-2,6)_2$ molecule (II) showing the numbering system used           | 229         |
| Figure 14.8 : ORTEP view of the unit cell of $Re_2(CO)_8(CNC_6H_3Me_2-2,6)_2$ (II), looking down the $b$ -axis             | 230         |
| Figure 14.9 : ORTEP view of the $Mn_2(CO)_8(CNBu^t)_2$ molecule (V), showing the numbering system used                     | 233         |



|   | <u>PAGE</u> |
|---|-------------|
| Figure 14.10: ORTEP view of the unit cell of $Mn_2-$<br>$(CO)_6(CNBU^t)_2(V)$ , looking down the $b$ -axis                    | 234         |
| Figure 14.11: ORTEP view of the $Re_2(CO)_7(CNMe)_3$<br>molecule (III), showing the numbering<br>system used                  | 239         |
| Figure 14.12: ORTEP view of the unit cell of $Re_2(CO)_7-$<br>$(CNMe)_3(III)$ , looking down the $b$ -axis                    | 240         |
| Figure 14.13: ORTEP view of the $Re_2(CO)_6(CNC_6H_3Me_2-$<br>$2,6)_4$ molecule (IV), showing the numbering<br>system used    | 244         |
| Figure 14.14: ORTEP view of the unit cell of $Re_2(CO)_6-$<br>$(CNC_6H_3Me_2-2,6)_4(IV)$ , looking down the<br>$b$ -axis      | 245         |
| Figure 14.15: ORTEP view of the $Mn_2(CO)_6(CNC_6H_3Me_2-$<br>$2,6)_4$ molecule (VI), showing the<br>numbering system used    | 248         |
| Figure 14.16: ORTEP view of the unit cell of $Mn_2(CO)_6-$<br>$(CNC_6H_3Me_2-2,6)_4(VI)$ , looking down the<br>$b$ -axis      | 249         |
| Figure 15.1 : Possible isomers for $M_2(CO)_9(L)$ complexes   | 284         |
| Figure 15.2 : Possible isomers for $M_2(CO)_8(L)_2$<br>complexes  | 286         |
| Figure 15.3 : Possible isomers for $1,2,2-M_2(CO)_7-$<br>$(L)_3$ complexes  | 294         |
| Figure 15.4 : Schematic representation of the mechanism<br>for the formation of <u>diax</u> - $Re_2(CO)_8(PR_3)_2$<br>(IIA)   | 310         |
| Figure 15.5 : ORTEP view of the <u>diax</u> - $Re_2(CO)_8(PMe_2Ph)_2$<br>molecule (VII), showing the numbering<br>system used | 318         |
| Figure 15.6 : ORTEP view of the unit cell of <u>diax</u> -<br>$[Re_2(CO)_8(PMe_2Ph)_2](VII)$ , looking down<br>the $b$ -axis  | 319         |
| Figure 15.7 : Newman projection of <u>diax</u> - $Re_2(CO)_8-$<br>$(PMe_2Ph)_2$ looking down the Re(1)-Re(2)<br>bond          | 325         |

|               |  |     |
|---------------|--|-----|
| Figure 15.8 : | Newman projections of $\text{diox}[\text{Re}_2(\text{CO})_8-$<br>$(\text{PMe}_2\text{Ph})_2]$ , showing conformation of<br>phosphine groups relative to eq carbonyl<br>ligands | 325 |
| (a)           | Newman projection of $\text{diox}[\text{Re}_2(\text{CO})_8-$<br>$(\text{PMe}_2\text{Ph})_2]$ , looking down the P(1)-<br>Re(1)-Re(2)-P(2) axis                                 | 325 |
| (b)           | Newman projection of $\text{ax}[\text{Re}(\text{CO})_4-$<br>$(\text{PMe}_2\text{Ph})]$ fragments   | 326 |
| (i)           | looking down the P(1)-Re(1)<br>bond  | 326 |
| (ii)          | looking down the Re(2)-P(2)<br>bond  | 326 |

LIST OF ABBREVIATIONS AND SYMBOLS

|        |  |
|--------|--|
| IR     | infra red  |
| NMR    | nuclear magnetic resonance                                   |
| UV     | ultra violet   |
| MS     | mass spectroscopy  |
| TLC    | thin layer chromatography                                    |
| FT     | Fourier Transform  |
| MO     | Molecular Orbital  |
| Mr     | molecular weight   |
| Dc     | calculated density   |
| U      | unit cell volume ( $\text{\AA}^3$ )                          |
| $\mu$  | linear absorption co-efficient ( $\text{cm}^{-1}$ )          |
| s.o.f. | site occupancy factor  |
| mp     | melting point  |
| $\nu$  | frequency ( $\text{cm}^{-1}$ )                               |
| M      | metal atom   |
| L      | ligand   |
| R      | alkyl or aryl group  |
| X      | arene ring substituent, or halogen atom                      |
| /C     | activated carbon support                                     |
| RNC    | isonitrile   |
| TEABH  | tetraethylammonium borohydride                               |
| THF    | tetrahydrofuran  |
| TMS    | tetramethylsilane  |
| py     | pyridine   |
| phen   | phenanthroline   |
| biquin | biquinoline  |
| bipy   | bipyridyl  |
| xylyl  | 2,6-dimethylphenyl ( $2,6\text{-Me}_2\text{C}_6\text{H}_3$ ) |
| Me     | methyl   |
| Et     | ethyl  |
| Pr     | propyl   |
| Bu     | butyl  |
| Ph     | phenyl   |
| Cp     | cyclopentadienyl   |

|     |                      |
|-----|----------------------|
| n   | normal               |
| i   | iso                  |
| t   | tertiary             |
| o   | ortho                |
| m   | meta                 |
| p   | para                 |
| tbp | trigonal bipyramidal |
| spy | square pyramidal     |
| ax  | axial                |
| eq  | equatorial           |
| ap  | apical               |
| bs  | basal                |

With reference to IR spectra:-

|    |          |
|----|----------|
| s  | strong   |
| m  | medium   |
| w  | weak     |
| sh | shoulder |
| sp | sharp    |
| br | broad    |
| v  | very     |

With reference to NMR spectra:-

|   |           |
|---|-----------|
| s | singlet   |
| d | doublet   |
| t | triplet   |
| m | multiplet |

With reference to symmetry:-

|   |                    |
|---|--------------------|
| m | mirror (plane)     |
| i | centre of symmetry |

I. INTRODUCTION

Organometallic chemistry is dominated by the chemistry of metal carbonyl complexes. Due to the catalytic potential of such complexes, the study of their chemical and physical properties continues to be an area of active interest. One important reaction type relating to metal carbonyl complexes is the carbonyl substitution reaction. However, carbonyl substitution reactions of transition metal carbonyl complexes are often difficult to achieve, and owing to the lack of facile synthetic methods of bringing about such reactions, substituted transition metal carbonyl complexes are not always accessible for further chemical and structural studies.

Some years ago a facile process to induce CO substitution of transition metal carbonyl complexes by ligands in the presence of catalysts was discovered in these laboratories. Use of this catalytic route enables substituted metal carbonyl derivatives to be prepared under mild thermal conditions. This thesis in part presents further attempts at exploring the potential of this reaction type, using specifically isonitrile (RNC) as a probe ligand.

The isonitrile ligand is potentially an extremely useful ligand for investigating the effect of ligand substitution on transition metal carbonyl complexes. Electronically, RNC is very similar to CO, the two ligands being isoelectronic. Further, the steric bulk of the isonitrile ligands is generally not as great as to be an impediment to multiple substitution of metal carbonyl complexes.

Catalysts for the reaction of transition metal carbonyl complexes with isonitriles that were investigated in this study include supported metals eg. Pd/C, Pd/CaCO<sub>3</sub>, metals, and metal oxides, and the iron dimer  $[(\eta^5\text{-C}_5\text{R}_5)\text{Fe}(\text{CO})_2]_2$  (R = H, Me) with PdO as co-catalyst. Such catalytic synthetic methods have indeed provided access to isonitrile-substituted transition metal carbonyl complexes, and spectroscopic and crystallographic studies of these novel products have been undertaken.

In particular X-ray crystallographic studies were undertaken on representative metal carbonyl isonitrile derivatives,

- (i) to determine the substitution geometry,
- (ii) to investigate the effect of ligand substitution on molecular structure
- and (iii) to enable a correlation to be established between IR spectral data and substitution geometry.

These studies have provided the basis for the bulk of the material contained in this thesis.

The systems investigated in this study are  $(\eta^6\text{Arene})\text{Cr}(\text{CO})_3/\text{RNC}$ ,  $(\eta^5\text{C}_5\text{H}_5)\text{Mn}(\text{CO})_3/\text{RNC}$ ,  $\text{Fe}(\text{CO})_5/\text{RNC}$ , and  $\text{M}_2(\text{CO})_{10}/\text{L}$ ,  $\text{M} = \text{Re}, \text{Mn}, \text{L} = \text{RNC}, \text{PR}_3$ . In chs. II and V respectively, the catalytic syntheses of  $(\eta^6\text{Arene})\text{Cr}(\text{CO})_2(\text{CNR})$  and  $(\eta^5\text{C}_5\text{H}_5)\text{Mn}(\text{CO})_2(\text{CNR})$  derivatives are described. Chs. III and VI respectively give brief surveys of the  $(\eta^5\text{C}_5\text{H}_5\text{CO}_2\text{Me})\text{-Cr}(\text{CO})_2\text{L}$  and  $(\eta^5\text{C}_5\text{H}_5)\text{Mn}(\text{CO})_2\text{L}$  complexes for which X-ray crystal structures have been reported in the literature, while Chs. IV and VII respectively describe the X-ray crystal and molecular structures of the two representative isonitrile derivatives,  $(\eta^5\text{C}_5\text{H}_5\text{CO}_2\text{Me})\text{Cr}(\text{CO})_2(\text{CNBu}^t)$  and  $(\eta^5\text{C}_5\text{H}_5)\text{Mn}(\text{CO})_2(\text{CNBu}^t)$ . Finally, ch. VIII discusses the anomalous IR data for the  $(\eta^6\text{Arene})\text{Cr}(\text{CO})_2(\text{CNR})$  and  $(\eta^5\text{C}_5\text{H}_5)\text{Mn}(\text{CO})_2(\text{CNR})$  derivatives.

In ch. IX, a brief literature survey of  $\text{Fe}(\text{CO})_{5-n}(\text{L})_n$  ( $n = 0-2$ ) complexes for which a crystal structure has been reported is given. Against this background, the X-ray crystal and molecular structure of  $\text{Fe}(\text{CO})_3(\text{CNMe})_2$  is discussed. This structure was primarily undertaken in an attempt to explain the anomalous IR data of  $\text{Fe}(\text{CO})_3(\text{CNR})_2$  complexes. This aspect is discussed.

The remaining Chs. (X-XV) are concerned with the detailed chemical and structural study undertaken of  $\text{Re}_2(\text{CO})_{10-n}(\text{L})_n$  ( $\text{L} = \text{CNR}, n = 1-4; \text{L} = \text{PR}_3, n = 1,2$ ) complexes. To place this study in perspective, a literature

survey of derivatives of  $\text{Re}_2(\text{CO})_{10}$  is presented in Ch. X. Further, a survey of X-ray crystallographic studies of dirhenium decacarbonyl derivatives reported in the literature, is given in ch. XIII.

Chs. XI and XIV are concerned with the  $\text{Re}_2(\text{CO})_{10}/\text{RNC}$  system. Ch. XI describes the catalytic synthesis of  $\text{Re}_2(\text{CO})_{10-n}(\text{CNR})_n$  ( $n = 1-4$ ) derivatives, and discusses the chemical and spectroscopic properties of these complexes.

To set the stage for the X-ray crystal studies, the structural modification of  $\text{Re}_2(\text{CO})_{10}$  by ligands L is discussed in ch. XII in terms of the electronic and/or steric nature of L, relative to that of CO. The results of the X-ray crystal and molecular structures of a series of  $\text{Re}_2(\text{CO})_{10-n}(\text{CNR})_n$  ( $n = 1-4$ ) complexes are then discussed in ch. XIV. The isonitrile-derivatives studied in ch. XIV are  $\text{Re}_2(\text{CO})_9(\text{CNBu}^t)$ ,  $\text{Re}_2(\text{CO})_8(\text{CNC}_6\text{H}_3\text{Me}_2-2,6)_2$ ,  $\text{Re}_2(\text{CO})_7(\text{CNMe})_3$  and  $\text{Re}_2(\text{CO})_6(\text{CNC}_6\text{H}_3\text{Me}_2-2,6)_4$ . The X-ray structures of the related manganese complexes,  $\text{Mn}_2(\text{CO})_8(\text{CNBu}^t)_2$  and  $\text{Mn}_2(\text{CO})_6(\text{CNC}_6\text{H}_3\text{Me}_2-2,6)_4$ , are also presented in ch. XIV.

Ch. XV, which is divided into subsections (A-E) deals with the  $\text{Re}_2(\text{CO})_{10}/\text{PR}_3$  system. The introductory Section 15A outlines the content of the subsequent sections. Section 15B discusses the IR spectral data reported in the literature for compounds of the type  $\text{M}_2(\text{CO})_{10-n}(\text{PR}_3)_n$  ( $\text{M} = \text{Re}, \text{Mn}$ ,  $n = 1-4$ ). In particular, the correlation between IR data and molecular geometry is investigated. A summary of the kinetic and mechanistic studies on the reaction of  $\text{Re}_2(\text{CO})_{10}$  with phosphine ligands, which has been extensively investigated by several groups, is given in Section 15C. An extension of the catalytic methods to phosphine ligands is covered in Section 15D, where the synthesis and characterization of  $\text{Re}_2(\text{CO})_{10-n}(\text{PR}_3)_n$  ( $n = 1,2$ ) derivatives is described. The formation of geometric isomers of  $\text{Re}_2(\text{CO})_8(\text{PR}_3)_2$  is discussed in terms of synthetic routes and the steric bulk of the phosphine ligand. The X-ray crystal and molecular structure of  $\text{diax}[\text{Re}_2(\text{CO})_8(\text{PMe}_2\text{Ph})_2]$  is presented in Section 15E.

Finally, ch. XVI, the Conclusion, sums up the foregoing work, and gives a brief assessment of what has been achieved. Suggestions for further work related to this study are made.

Appendix A lists the sources of chemicals used in this study. In Appendix B, general experimental details are given, relating to (a) synthetic methods, (b) solvents, (c) instrumentation, (d) X-ray data collection, (e) Crystallographic Computing Programs used, and (f) definition of the Crystallographic R-indices. Appendix C gives the torsional angles for the  $M_2(\text{CO})_{10-n}(\text{CNR})_n$  ( $M = \text{Re}$ ,  $n = 1-4$ ,  $M = \text{Mn}$ ,  $n = 2,4$ ) structures of ch. XIV and for  $d_{\text{max}}\text{-}[\text{Re}_2(\text{CO})_8(\text{PMe}_2\text{Ph})_2]$  (Section 15E). A listing of the Structure Factor Tables for all the ten X-ray crystal structures is to be found in Appendix D, bound as a separate volume.

The literature surveys (which include X-ray structural data accessed from the Cambridge Crystallographic Data Base) presented in this thesis are considered complete up until December 1983, but mention has been made of pertinent publications that have appeared in 1984.



II. CATALYTIC SYNTHESIS AND CHARACTERIZATION OF ISONITRILE DERIVATIVES OF ( $\eta^6$ -ARENE)Cr(CO)<sub>3</sub>

2.1 Introduction

Interest in complexes of the type ( $\eta^6$ -Arene)Cr(CO)<sub>3</sub> has been stimulated by the demonstrated ability of such compounds to catalyze reactions such as the hydrogenation of olefins.<sup>1</sup> Replacement of a CO group by other ligand: L such as phosphines, arsines, stibines and isonitriles, significantly affects the catalytic properties of the ( $\eta^6$ -Arene)Cr(CO)<sub>2</sub>L complexes.<sup>2</sup> Consequently there is an interest in routes to such substituted complexes.

In an attempt to combine the advantages of homogeneous and heterogeneous catalysts, an ( $\eta^6$ -C<sub>6</sub>H<sub>5</sub>CO<sub>2</sub>Me)Cr(CO)<sub>2</sub> moiety has been bound to a polymer support through an isonitrile functionality.<sup>3</sup> Hence there is an interest in such isonitrile-substituted complexes.

Use has been made of arene chromium carbonyl complexes in organic chemistry. Arene chromium dicarbonyl chelates (synthesized photochemically<sup>4a</sup>) have been used to prepare chiral amines in good yields.<sup>4b</sup> The Cr(CO)<sub>2</sub>L unit (L = CO, CS, PR<sub>3</sub>) has been shown to increase reactivity, enhance selectivity, or protect the substituents of complexed arene rings with respect to alkylation.<sup>5</sup> The arene ligand can be removed by refluxing (Arene)Cr(CO)<sub>3</sub> with py,<sup>6</sup> and the [(py)<sub>3</sub>Cr(CO)<sub>3</sub>] generated can be recycled to prepare (Arene)Cr(CO)<sub>3</sub> complexes (*vide infra*). The replacement of L = C<sub>6</sub>H<sub>4</sub>Me<sub>2</sub>-p from L Cr(CO)<sub>3</sub> by C<sub>6</sub>H<sub>6</sub> is catalyzed by L'Cr(CO)<sub>3</sub> (L' = C<sub>6</sub>Me<sub>6</sub>) without L' replacement. Arene tricarbonyl complexes, obtained by the reaction of Arene and Cr(CO)<sub>6</sub> (*vide infra*), react with nucleophiles to form adducts and subsequently treated with trifluoroacetic acid under carbon monoxide, give substituted cyclohexadienes or, after oxidation, substituted arenes and Cr(CO)<sub>6</sub>, thereby providing a route to such dienes and arenes in a cyclic process.<sup>7</sup>

Although most simple arenes react with Cr(CO)<sub>6</sub> to give ( $\eta^6$ -Arene)Cr(CO)<sub>3</sub> complexes,<sup>8</sup> the reaction is slow, the removal of high-boiling solvents or excess arene from the

product may be difficult, and a complex apparatus<sup>10</sup> is required to prevent sublimation of  $\text{Cr}(\text{CO})_6$  from the reaction vessel. These problems have been overcome by the reported "solvent-assisted" reaction between  $\text{Cr}(\text{CO})_6$  and a variety of arenes, in a dibutyl ether-tetrahydrofuran (THF) solvent mix,<sup>11</sup> thereby making  $(\eta^6\text{-Arene})\text{Cr}(\text{CO})_3$  complexes easily accessible for further studies. Another reported successful synthetic method employs the reaction in refluxing dioxane of the arene and  $[(\text{NH}_3)_3\text{Cr}(\text{CO})_3]$ ,<sup>12</sup> which does not cause sublimation problems, thereby eliminating the need for special apparatus or solvents. In a similar method,  $[(\text{py})_3\text{Cr}(\text{CO})_3]$  is reacted with arene in the presence of boron trifluoride diethyl ether in boiling ether.<sup>6, 13</sup>

Replacement of CO in  $(\eta^6\text{-Arene})\text{Cr}(\text{CO})_3$  complexes by an isonitrile ligand, RNC, to give  $(\eta^6\text{-Arene})\text{Cr}(\text{CO})_2(\text{CNR})$  derivatives, has been achieved by direct<sup>14</sup> or indirect<sup>15, 16</sup> (involving photolysis of  $(\eta^6\text{-Arene})\text{Cr}(\text{CO})_3$  with KUN, to give  $\text{K}^+[(\eta^6\text{-Arene})\text{Cr}(\text{CO})_2(\text{CN})]^-$ , followed by reaction with RNC) photochemical methods. Photochemical methods have been employed to prepare chiral  $(\eta^6\text{-Arene})\text{Cr}(\text{CO})(\text{CNR})(\text{PR}_3)$ <sup>15</sup> and  $(\eta^6\text{-Arene})\text{Cr}(\text{CO})(\text{CS})(\text{PR}_3)$ <sup>17</sup> complexes. Direct substitution of an  $(\eta^6\text{-Arene})\text{Cr}(\text{CO})_3$  complex with  $\text{P}(\text{OEt})_3$  has been achieved by electrochemical techniques<sup>18</sup> (reported since this work was completed). However, no thermal synthesis of  $(\eta^6\text{-Arene})\text{Cr}(\text{CO})_2(\text{CNR})$  complexes is known. Further, thermochemical studies<sup>19</sup> have shown that under typical thermal reaction conditions required to induce Cr-CO bond cleavage, displacement of the arene ring from the  $\text{Cr}(\text{CO})_3$  moiety by ligand(s) L, becomes a competing process, leading to reactant decomposition, or formation of  $\text{Cr}(\text{CO})_3\text{L}_n$  ( $n = 1, 3$ ) complexes.

Hence a catalyst was sought to bring about the substitution of CO by RNC in  $(\eta^6\text{-Arene})\text{Cr}(\text{CO})_3$  complexes, under mild thermal conditions. To function effectively, the requirement of such a catalyst would be the ability to lower the activation energy for the Cr-CO bond cleavage process, without also reducing that of the competing Cr-

Arene displacement reaction. The iron dimer,  $[(\eta^5\text{-C}_5\text{H}_5)\text{Fe}(\text{CO})_2]_2$ , in the presence of suitable donor ligands (e.g.  $\text{PR}_3$ , RNC), is known to catalyse the replacement of CO ligands on transition metal complexes.<sup>10, 11</sup> Further,  $[(\eta^5\text{-C}_5\text{H}_5)\text{Fe}(\text{CO})_2]_2$ , together with co-catalysts such as PdO,  $\text{PtO}_2$ , Pd/C or Pd/ $\text{CaCO}_3$ , has been shown to successfully catalyse reactions between metal carbonyls and isonitriles.<sup>12</sup>

The reaction of  $(\eta^5\text{-C}_5\text{H}_5\text{X})\text{Cr}(\text{CO})_3$  (X = H, Cl,  $\text{CO}_2\text{Me}$ , Me) with isonitriles RNC (R =  $\text{Bu}^t$ , 2,6- $\text{Me}_2\text{C}_6\text{H}_3$ ), using as catalysts compounds of the type  $[\text{CpFe}(\text{CO})_2]_2$  (Cp =  $\text{C}_5\text{H}_5$ ,  $\text{C}_5\text{H}_4\text{CO}_2\text{Me}$ ,  $\text{C}_5\text{Me}_5$ ), together with PdO co-catalyst, were studied in order to explore the potential of this synthetic route. Variation of the arene substituent X allows the effect on the reaction of electron-donating or withdrawing properties to be investigated.

## 2.2 Results and Discussion

### 2.2.1 Reaction of $(\eta^5\text{-Arene})\text{Cr}(\text{CO})_3$ complexes with isonitriles

The reaction between  $(\eta^5\text{-C}_5\text{H}_5\text{X})\text{Cr}(\text{CO})_3$  (X = H, Cl,  $\text{CO}_2\text{Me}$ , Me) and RNC (R =  $\text{Bu}^t$ , 2,6- $\text{Me}_2\text{C}_6\text{H}_3$ ) in refluxing degassed heptane is catalysed by the iron dimer,  $[(\eta^5\text{-C}_5\text{Me}_5)\text{Fe}(\text{CO})_2]_2$ , and co-catalyst PdO, to yield the required substitution product,  $(\eta^5\text{-C}_5\text{H}_5\text{X})\text{Cr}(\text{CO})\text{CNR}$ , in moderate to good yields. In the absence of catalyst, or in the presence of  $[(\eta^5\text{-C}_5\text{Me}_5)\text{Fe}(\text{CO})_2]_2$  or PdO separately, less than 5% product formation was observed by IR spectroscopy even after long reaction times (6 h).

Reactions were slower with 2,6- $\text{Me}_2\text{C}_6\text{H}_3\text{NC}$  than with  $\text{tBuNC}$  [e.g.  $(\eta^5\text{-C}_5\text{H}_5\text{CO}_2\text{Me})\text{Cr}(\text{CO})_2(\text{CNC}_6\text{H}_3\text{Me}_2-2,6)$ , 80% yield, 6 h, cf.  $(\eta^5\text{-C}_5\text{H}_5\text{CO}_2\text{Me})\text{Cr}(\text{CO})_2(\text{CNBu}^t)$ , 90% yield, 1.5 min.] For both isonitrile ligands, reaction times were dependent on the substituent X of the co-ordinated arene ring. As expected, reaction time was found to increase with arenes with electron-releasing X-groups [e.g.  $(\eta^5\text{-C}_5\text{H}_5\text{CO}_2\text{Me})\text{Cr}(\text{CO})_2(\text{CNC}_6\text{H}_3\text{Me}_2-2,6)$ , 80% yield, 6 h, cf.  $(\eta^5\text{-C}_5\text{H}_5\text{Me})\text{Cr}(\text{CO})_2(\text{CNC}_6\text{H}_3\text{Me}_2-2,6)$ , 80% yield, 18 h]. This trend is in keeping with the increased metal-CO bond strength, reflected, for instance in the  $\nu(\text{CO})$  stretching frequencies of the starting materials (e.g. IR(hexane):  $(\eta^5\text{-C}_5\text{H}_5\text{CO}_2\text{Me})\text{Cr}(\text{CO})_3$ : 1991

and 1928  $\text{cm}^{-1}$ ;  $(\eta^5\text{C}_5\text{H}_5)\text{Cr}(\text{CO})_3$ : 1983 and 1915  $\text{cm}^{-1}$ ; and  $(\eta^5\text{C}_5\text{H}_5\text{Me})\text{Cr}(\text{CO})_3$ : 1975 and 1906  $\text{cm}^{-1}$ .

With the electron-withdrawing ring substituent  $X = \text{CO}_2\text{Me}$ , the consequent weakening of the  $\text{Cr}-(\eta^5\text{Arene})$  bond<sup>19</sup> allows the arene ring to be eliminated during the reaction of  $(\eta^5\text{C}_5\text{H}_5\text{CO}_2\text{Me})\text{Cr}(\text{CO})_3$  with 2,6- $\text{Me}_2\text{C}_6\text{H}_3\text{NC}$ , resulting in the formation of products of the type  $\text{Cr}(\text{CO})_{6-n}(\text{CNC}_6\text{H}_3\text{Me}_2-2,6)_n$  ( $n = 3,4$ ) (vide infra). This is not observed with the electron-donating ring substituent  $X = \text{Me}$ , where the  $\text{Cr}-(\eta^5\text{Arene})$  bond is stronger.<sup>19</sup>

#### 2.2.2 Reaction of $(\eta^5\text{C}_5\text{H}_5\text{CO}_2\text{Me})\text{Cr}(\text{CO})_3$ with 2,6- $\text{Me}_2\text{C}_6\text{H}_3\text{NC}$ in the Presence of Iron Dimer Catalysts

The reaction between  $(\eta^5\text{C}_5\text{H}_5\text{CO}_2\text{Me})\text{Cr}(\text{CO})_3$  and 2,6- $\text{Me}_2\text{C}_6\text{H}_3\text{NC}$ , was investigated in the presence of iron dimer catalysts. The most efficient catalyst was found to be an  $(\eta^5\text{C}_5\text{Me}_5/\text{Fe}(\text{CO})_2)_2/\text{PdO}$  mixture (vide infra).

Although the unsubstituted iron dimer  $[(\eta^5\text{C}_5\text{H}_5)\text{Fe}(\text{CO})_2]_2$ , together with PdO, catalyses the reaction, under the reaction conditions the iron dimer itself rapidly undergoes CO substitution to  $[(\eta^5\text{C}_5\text{H}_5)\text{Fe}(\text{CNC}_6\text{H}_3\text{Me}_2-2,6)_2]_2$ .<sup>21</sup> The modification of the iron dimer catalyst can readily be detected during the reaction by IR spectroscopy. Further, PdO is a poor catalyst for the reaction (2.1)<sup>22</sup>  $[(\eta^5\text{C}_5\text{H}_5)\text{Fe}(\text{CO})_2]_2 + n\text{RNC} \rightarrow [(\eta^5\text{C}_5\text{H}_5)_2\text{Fe}_2(\text{CO})_{4-n}(\text{CNR})_n] + n\text{CO}$  ( $n = 1,2$ ) (2.1) and is thus not responsible for the substitution reaction observed. Hence the addition of either  $[(\eta^5\text{C}_5\text{H}_5)\text{Fe}(\text{CO})_2]_2$  or  $[(\eta^5\text{C}_5\text{H}_5)\text{Fe}(\text{CNC}_6\text{H}_3\text{Me}_2-2,6)_2]_2$  (independently synthesized<sup>21</sup>) to reaction mixtures of  $[(\eta^5\text{C}_5\text{H}_5\text{CO}_2\text{Me})\text{Cr}(\text{CO})_3$  and  $\text{CNC}_6\text{H}_3\text{Me}_2-2,6$ , resulted in the same rate of formation of  $(\eta^5\text{C}_5\text{H}_5\text{CO}_2\text{Me})\text{Cr}(\text{CO})_2(\text{CNC}_6\text{H}_3\text{Me}_2-2,6)$ , as determined by IR spectroscopy. (ca. 15% product formation was observed for both reactions after 8 h).

The ring-substituted iron dimer,  $[(\eta^5\text{C}_5\text{H}_4\text{CO}_2\text{Me})\text{Fe}(\text{CO})_2]_2$ , with PdO, was also tried as a catalyst for this reaction, but IR data indicated that although initially product substitution was more rapid than with  $[(\eta^5\text{C}_5\text{H}_5)\text{Fe}(\text{CO})_2]_2/\text{PdO}$  catalyst, the reaction rates soon inverted, and

after ca. 3 h, the reaction with  $[(\eta^5\text{-C}_5\text{H}_4\text{CO}_2\text{Me})\text{Fe}(\text{CO})_2]_2/\text{PdO}$  as catalyst ceased. This result can be explained in terms of the increased ability of the  $[(\eta^5\text{-C}_5\text{H}_4\text{CO}_2\text{Me})\text{Fe}(\text{CO})_2]_2$  complex to undergo CO substitution since electron-withdrawing groups on the ring enhance the substitution reaction.<sup>23</sup> Consistent with this proposal are the results of the reaction between  $[(\eta^5\text{-C}_5\text{H}_4\text{CO}_2\text{Me})\text{Fe}(\text{CO})_2]_2$  and  ${}^t\text{BuNC}$ . (vide infra)

In refluxing benzene, a 1:2 reaction between  $[(\eta^5\text{-C}_5\text{H}_4\text{CO}_2\text{Me})\text{Fe}(\text{CO})_2]_2$  and  ${}^t\text{BuNC}$  rapidly (<15 min) gave  $[(\eta^5\text{-C}_5\text{H}_4\text{CO}_2\text{Me})_2\text{Fe}_2(\text{CO})_3(\text{CNBu}^t)]$ , and more slowly,  $[(\eta^5\text{-C}_5\text{H}_4\text{CO}_2\text{Me})\text{Fe}(\text{CO})(\text{CNBu}^t)]_2$  (50% isolated yield, 4 h.). A 1:1 reaction between  $[(\eta^5\text{-C}_5\text{H}_4\text{CO}_2\text{Me})\text{Fe}(\text{CO})_2]_2$  and  ${}^t\text{BuNC}$  in refluxing benzene gave predominately  $[(\eta^5\text{-C}_5\text{H}_4\text{CO}_2\text{Me})_2\text{Fe}_2(\text{CO})_3(\text{CNBu}^t)]$ , and some  $[(\eta^5\text{-C}_5\text{H}_4\text{CO}_2\text{Me})\text{Fe}(\text{CO})(\text{CNBu}^t)]_2$ , indicative of the facile nature of multiple CO substitution. (These new iron dimer derivatives have been completely characterized, and the pertinent analytical and spectral data are reported in Section 2.4.4.) By contrast, the reaction between  $[(\eta^5\text{-C}_5\text{H}_5)\text{Fe}(\text{CO})_2]_2$  and  ${}^t\text{BuNC}$  under identical reaction conditions, gives only  $[(\eta^5\text{-C}_5\text{H}_5)_2\text{Fe}_2(\text{CO})_3(\text{CNBu}^t)]$ , in near quantitative yield,<sup>24</sup> and trace amounts (<2%) of  $[(\eta^5\text{-C}_5\text{H}_5)\text{Fe}(\text{CO})(\text{CNBu}^t)]_2$ .<sup>25</sup> Under our reaction conditions (i.e. large excess of RNC), it can be anticipated that multiple CO substitution of  $[(\eta^5\text{-C}_5\text{H}_4\text{CO}_2\text{Me})\text{Fe}(\text{CO})_2]_2$  by RNC eventually occurs, presumably leading to catalyst deactivation.

To avoid this problem of catalyst substitution, the use as a catalyst of the pentamethyl derivative,  $[(\eta^5\text{-C}_5\text{Me}_5)\text{Fe}(\text{CO})_2]_2$ , was investigated. Owing to the electron-donating nature of the methyl substituents on the cyclopentadienyl ring, this dimer is inert to CO substitution.<sup>21</sup> A  $[(\eta^5\text{-C}_5\text{Me}_5)\text{Fe}(\text{CO})_2]_2/\text{PdO}$  mixture was found to be a convenient, though not highly active catalyst for the substitution of  $(\eta^5\text{-C}_5\text{H}_5\text{CO}_2\text{Me})\text{Cr}(\text{CO})_3$  with  $\text{CNC}_6\text{H}_3\text{Me}_2\text{-2,6}$ , and this catalytic method was employed in the synthesis of other  $(\eta^5\text{-Arene})\text{Cr}(\text{CO})_2$  (CNR) derivatives (vide supra). Further, it was possible to isolate the unsubstituted dimer catalyst,  $[(\eta^5\text{-C}_5\text{Me}_5)\text{Fe}(\text{CO})_2]_2$ ,

at the end of the reaction, thereby confirming the above hypothesis.

2.2.3 Formation of by-products of the type  $Cr(CO)_{6-n}$  ( $C_6H_3Me_2-2,6$ ) ( $n = 3,4$ ) in the reaction of  $(\eta^6-C_6H_5CO_2Me)Cr(CO)_3$  with 2,6- $Me_2C_6H_3NC$

A feature of the (catalysed) reaction between  $(\eta^6-C_6H_5CO_2Me)Cr(CO)_3$  and 2,6- $Me_2C_6H_3NC$  was the formation of products resulting from the cleavage of the  $(\eta^6-Arene)-Cr$  bond. In the  $[(\eta^5-Me_5)Fe(CO)_2]_2/PdO$  catalysed reaction between  $(\eta^6-C_6H_5CO_2Me)Cr(CO)_3$  and 2,6- $Me_2C_6H_3NC$ ,  $C_6H_5CO_2Me$ , together with complexes of the type  $[Cr(CO)_{6-n}(C_6H_3Me_2-2,6)_n]$  ( $n = 3,4$ ) were isolated (total yield of ring-cleavage by-products ca. 5%) from the reaction mixture by column chromatography, in addition to the major substitution product,  $(\eta^6-C_6H_5CO_2Me)Cr(CO)_2(C_6H_3Me_2-2,6)$  (70% yield, 6 h). The by-products  $[Cr(CO)_{6-n}(C_6H_3Me_2-2,6)_n]$  ( $n = 3,4$ ) were characterized by independent synthesis from  $[Cr(CO)_6]$  and 2,6- $Me_2C_6H_3NC$  in the presence of PdO as catalyst.<sup>14</sup> (Pertinent IR and NMR spectral data for these complexes are given in Section 2.4.2.)

The electron withdrawing  $CO_2Me$  arene ring substituent results in a weakening of the  $Cr-(\eta^6-Arene)$  bond,<sup>15</sup> and the consequent displacement of the arene ring in the side reaction (2.2)  $(C_6H_5CO_2CH_3)Cr(CO)_3 + 3(2,6-Me_2C_6H_3NC) + [Cr(CO)_3(C_6H_3Me_2-2,6)_3] + C_6H_5CO_2Me$  (2.2). The tetra-substituted derivative,  $[Cr(CO)_2(C_6H_3Me_2-2,6)_4]$ , is however unexpected and could arise from two potential pathways:— (a) displacement of the arene ligand to give  $[Cr(CO)_3(C_6H_3Me_2-2,6)_3]$  (Reaction (2.2)), followed by catalytic displacement of CO to give  $[Cr(CO)_2(C_6H_3Me_2-2,6)_4]$ ,<sup>16</sup> or (b) formation of  $[(\eta^6-C_6H_5CO_2Me)Cr(CO)_2(C_6H_3Me_2-2,6)]$ , followed by displacement of the arene ring by isonitrile.

A blank reaction between  $(\eta^6-C_6H_5CO_2Me)Cr(CO)_3$  and 2,6- $Me_2C_6H_3NC$ , in the absence of catalyst, indicated that ca. 5%  $[(\eta^6-C_6H_5CO_2Me)Cr(CO)_2(C_6H_3Me_2-2,6)]$ , as well as ca. 15% ring cleavage products had formed in 6 h, as detected by IR spectroscopy. This suggests that the major, if not exclusive pathway to formation of the  $[Cr(CO)_{6-n}]$

(CNC<sub>6</sub>H<sub>3</sub>Me<sub>2</sub>-2,6)<sub>n</sub>] (n = 3,4) derivatives is via a thermal non-catalytic route. Further, the reaction between [(n<sup>6</sup>C<sub>6</sub>H<sub>3</sub>CO<sub>2</sub>Me)Cr(CO)<sub>2</sub>(CNC<sub>6</sub>H<sub>3</sub>Me<sub>2</sub>-2,6)] and 2,6-Me<sub>2</sub>C<sub>6</sub>H<sub>3</sub>NC in both the absence (no reaction) and presence of catalyst (<1% ring cleavage) under similar reaction conditions rules out the possibility that the ring-cleavage derivatives are formed in secondary reactions via the decomposition of the product. The significant feature of the above experiments is the finding that catalytic cleavage of an (n<sup>6</sup>-Arene)-Cr bond does not take place under our reaction conditions.

### 2.3 Spectroscopic properties of (n<sup>6</sup>-Arene)Cr(CO)<sub>2</sub>(CNR) complexes

#### 2.3.1 Infra Red

The IR data (Table 2.1) for the (n<sup>6</sup>-Arene)Cr(CO)<sub>2</sub>(CNR) complexes show anomalous behaviour. Whereas two ν(CO) and one ν(NC) stretching frequencies are predicted, two ν(CO) and two ν(NC) absorption were observed in both solution and the solid state (except for (n<sup>6</sup>-C<sub>6</sub>H<sub>3</sub>CO<sub>2</sub>Me)Cr(CO)<sub>2</sub>(CNC<sub>6</sub>H<sub>3</sub>Me<sub>2</sub>-2,6), which has one ν(NC) and two ν(CO) bands in solution, and one ν(NC) and three ν(CO) bands in the solid state). This phenomenon will be discussed in Chapter VIII.

#### 2.3.2 Proton Nuclear Magnetic Resonance

The <sup>1</sup>H NMR data (Table 2.1) for the (n<sup>6</sup>-Arene)Cr(CO)<sub>2</sub>(CNR) complexes gave the expected resonances (number, position).

#### 2.3.3 Mass Spectrum of (n<sup>6</sup>-C<sub>6</sub>H<sub>3</sub>CO<sub>2</sub>Me)Cr(CO)<sub>2</sub>(CNBu<sup>t</sup>)

Mass spectra gave fragments consistent with the structural formulation proposed. A typical example is shown in Fig. 2.1, which indicates the fragmentation pattern (together with peak intensities and metastable peaks) for the mass spectrum of (n<sup>6</sup>-C<sub>6</sub>H<sub>3</sub>CO<sub>2</sub>Me)Cr(CO)<sub>2</sub>(CNBu<sup>t</sup>). The fragmentation pattern is in agreement with that reported for related complexes.<sup>13a</sup> The loss of the CO ligands precedes loss of <sup>t</sup>BuNC, indicative of the stronger σ-donor ability of <sup>t</sup>BuNC than CO. The <sup>t</sup>Bu-group is lost before the CN linkage.<sup>17</sup> The arene ligand is the last to be lost.

Table 2.1: Spectroscopic data for the ( $\eta^6$ -Arene)Cr(CO)<sub>2</sub>(CNR) complexes

| Complex   | IR (cm <sup>-1</sup> ) <sup>a</sup> |                  | <sup>1</sup> H NMR (ppm) <sup>b</sup> |   |                                       |                        |
|---|-------------------------------------|------------------|---------------------------------------|---|---------------------------------------|------------------------|
|   | $\nu(\text{NC})$                    | $\nu(\text{CO})$ | RNC(Me)                               | RNC(C <sub>6</sub> H <sub>5</sub> ) / Arene(Me) | Arene(C <sub>6</sub> H <sub>5</sub> ) |                        |
| ( $\eta^6$ -C <sub>6</sub> H <sub>5</sub> Me)Cr(CO) <sub>2</sub> (CNBu <sup>t</sup> )   | 2038, 2002                          | 1921, 1883       | 1.39                                  | -   | 2.09                                  | 4.99                   |
| ( $\eta^6$ -C <sub>6</sub> H <sub>5</sub> )Cr(CO) <sub>2</sub> (CNBu <sup>t</sup> )   | 2046, 2028                          | 1942, 1894       | 1.38                                  | -   | -                                     | 5.43                   |
| ( $\eta^6$ -C <sub>6</sub> H <sub>5</sub> Ct)Cr(CO) <sub>2</sub> (CNBu <sup>t</sup> )   | 2095, 2060                          | 1933, 1893       | 1.42                                  | -   | -                                     | 5.01, 5.05             |
| ( $\eta^6$ -C <sub>6</sub> H <sub>5</sub> CO <sub>2</sub> Me)Cr(CO) <sub>2</sub> (CNBu <sup>t</sup> ) <sup>c, d</sup>                                   | 2102, 2060                          | 1937, 1894       | 1.40                                  | -   | 3.83                                  | 4.99-5.78 <sup>e</sup> |
| ( $\eta^6$ -C <sub>6</sub> H <sub>5</sub> Me)Cr(CO) <sub>2</sub> (CNC <sub>6</sub> H <sub>3</sub> Me <sub>2</sub> -2,6)                                 | 2050, 2010                          | 1916, 1888       | 2.17                                  | 6.83  | 2.38                                  | 4.97                   |
| ( $\eta^6$ -C <sub>6</sub> H <sub>5</sub> )Cr(CO) <sub>2</sub> (CNC <sub>6</sub> H <sub>3</sub> Me <sub>2</sub> -2,6)                                   | 2040, 1992                          | 1916, 1874       | 2.37                                  | 7.00  | -                                     | 5.12                   |
| ( $\eta^6$ -C <sub>6</sub> H <sub>5</sub> CO <sub>2</sub> Me)Cr(CO) <sub>2</sub> (CNC <sub>6</sub> H <sub>3</sub> Me <sub>2</sub> -2,6) <sup>f, g</sup> | 2060                                | 1938, 1902       | 2.37                                  | 6.63  | 3.81                                  | 5.02-5.98 <sup>e</sup> |

<sup>a</sup> Recorded in hexane

<sup>b</sup> Recorded in CDCl<sub>3</sub> relative to TMS

<sup>c</sup>  $\nu(\text{COOMe}) = 1720 \text{ cm}^{-1}$

<sup>d</sup> IR(KBr),  $\nu(\text{NC})$ : 2090, 2060 (sh);  $\nu(\text{CO})$ : 1908, 1856,  $\nu(\text{COOMe})$ : 1700 cm<sup>-1</sup>

<sup>e</sup> Multiplet

<sup>f</sup>  $\nu(\text{COOMe}) = 1725 \text{ cm}^{-1}$

<sup>g</sup> IR(KBr),  $\nu(\text{NC})$ : 2070;  $\nu(\text{CO})$ : 1904, 1855, 1840;  $\nu(\text{COOMe})$ : 1715 cm<sup>-1</sup>



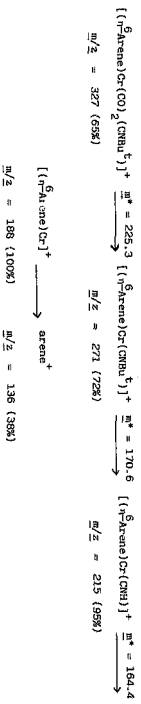


FIGURE 2.1 Fragmentation pattern for  $[(\text{C}_6\text{H}_5\text{Arzene})\text{Cr}(\text{CO})_2(\text{C}_6\text{H}_5\text{C}_6\text{H}_5)]^+$ . Fragments and intensity data refer to the samples with  $\text{C}_6\text{H}_5\text{Arzene} = \text{C}_6\text{H}_5\text{C}_6\text{H}_5\text{CO}_2\text{Me}$ . The spectrum was recorded at 48°C and all fragments with  $\underline{m/z} < 110$  are not reported.

## 2.4 Experimental

### 2.4.1 The catalysed synthesis of $\{(n^6\text{-C}_6\text{H}_5\text{X})\text{Cr}(\text{CO})_2(\text{CNR})\}$ $(\text{X} = \text{H}, \text{Cl}, \text{CO}_2\text{Me}, \text{Me}; \text{R} = \text{Bu}^t, 2,6\text{-Me}_2\text{C}_6\text{H}_3)$

$(n^6\text{-C}_6\text{H}_5\text{CO}_2\text{CH}_3)\text{Cr}(\text{CO})_3$  and  $(n^6\text{-C}_6\text{H}_5\text{Cl})\text{Cr}(\text{CO})_3$  were prepared by the method of Mahaffy and Pauson.<sup>11a</sup>

$\{(n^6\text{-C}_6\text{H}_5\text{X})\text{Cr}(\text{CO})_2\}$  (1.00 mmol), catalyst  $[(n^5\text{-C}_5\text{Me}_5\text{Fe}(\text{CO})_2)_2]$  (20 mg) and co-catalyst PdO (20 mg), and 2,6-Me<sub>2</sub>C<sub>6</sub>H<sub>3</sub>NC (1.3 mmol), or <sup>t</sup>BuNC (1.1 mmol), were combined in freshly distilled heptane (15 ml) the mixture was heated at reflux (100°C), and the reaction was monitored by TLC (silica; eluent : hexane-diethyl ether (30%)) and IR spectroscopy (2200-1700cm<sup>-1</sup> region). On completion of the reaction (or when no further changes were apparent (R = Bu<sup>t</sup>), or after 18 h (R = 2,6-Me<sub>2</sub>C<sub>6</sub>H<sub>3</sub>)), the reaction mixture was allowed to cool and the product isolated by column chromatography (2 cm x 40 cm column, silica ; gradient elution with hexane-diethyl ether mixtures). The column was run, and the product collected, under nitrogen, using deoxygenated eluent solutions, as the products tend to be air-sensitive, especially in solution. Recrystallization from dichloromethane-hexane solution gave the required product as yellow or orange crystalline material. (Table 2.2). Product yields were generally >80%. Even in the solid state, the  $(n^6\text{-C}_6\text{H}_5)\text{Cr}(\text{CO})_2(\text{CNR})$  derivatives decomposed on exposure to air, as evidenced by the change in colour from yellow to lime green.

### 2.4.2 Reaction of $(n^6\text{-C}_6\text{H}_5\text{CO}_2\text{Me})\text{Cr}(\text{CO})_3$ with 2,6-Me<sub>2</sub>C<sub>6</sub>H<sub>3</sub>NC, with catalyst $[\text{CpFe}(\text{L})_2]$ (Cp = C<sub>5</sub>H<sub>5</sub>, C<sub>5</sub>H<sub>4</sub>CO<sub>2</sub>Me, C<sub>5</sub>Me<sub>4</sub>; L = CO; Cp = C<sub>5</sub>H<sub>5</sub>, L = 2,6-Me<sub>2</sub>C<sub>6</sub>H<sub>3</sub>NC), and co-catalyst PdO

$(n^6\text{-C}_6\text{H}_5\text{CO}_2\text{Me})\text{Cr}(\text{CO})_3$  (1.00 mmol), catalyst  $[\text{CpFe}(\text{L})_2]$  (20 mg) and co-catalyst PdO (20 mg), and 2,6-Me<sub>2</sub>C<sub>6</sub>H<sub>3</sub>NC (1.3 mmol), were combined in freshly distilled heptane (15 ml), the mixture was heated at reflux (100°C), and the reaction was monitored by IR spectroscopy and TLC (as above). On completion of the reaction, or when no further changes were apparent, column chromatography (as above) was used to

isolate the product(s), which were purified by recrystallization from dichloromethane-hexane solutions. In addition to the main substitution product,  $(\eta^6\text{C}_6\text{H}_5\text{CO}_2\text{Me})\text{Cr}(\text{CO})_2^-$  ( $\text{C}_6\text{H}_5\text{CO}_2\text{Me}$ -2,6), arene-ring displacement products of the type  $\text{Cr}(\text{CO})_{6-n}(\text{CNC}_6\text{H}_3\text{Me}_2-2,6)_n$  ( $n = 3,4$ ), were obtained. These products were characterized by IR and  $^1\text{H}$  NMR spectroscopy (Table 2.3).

#### 2.4.3 Preparation of $[(\text{C}_5\text{H}_4\text{CO}_2\text{Me})\text{Fe}(\text{CO})_2]_2$

$\text{C}_5\text{H}_4\text{CO}_2\text{Me}$  was synthesized from  $\text{C}_6\text{H}_5\text{CO}_2\text{Me}$ , according to the method of Peters.<sup>18</sup>

A mixture of  $[\text{Fe}(\text{CO})_5]$  (8 ml, 0.06 mol), octane (100 ml), and  $\text{C}_5\text{H}_4\text{CO}_2\text{Me}$  (3 g, 0.024 mol), was degassed and the reaction mixture refluxed (120°C) under argon for 24 h. The mixture was cooled in ice, prior to filtering, and yielded 1.7 g (32%) of deep purple product. Cleavage with  $\text{I}_2$  yielded  $(\text{C}_5\text{H}_4\text{CO}_2\text{Me})\text{Fe}(\text{CO})_2\text{I}$  as a black crystalline material. Analytical and spectral data for these compounds are given in Tables 2.4 and 2.5 respectively.

#### 2.4.4 Reaction of $[(\text{C}_5\text{H}_4\text{CO}_2\text{Me})\text{Fe}(\text{CO})_2]_2$ with $^t\text{BuNC}$ (1:1 Ratio)

$[(\text{C}_5\text{H}_4\text{CO}_2\text{Me})\text{Fe}(\text{CO})_2]_2$  (0.47 g, 1.00 mmol) was dissolved in benzene (20 ml), and to this was added  $^t\text{BuNC}$  (130  $\mu\text{l}$ , 1.2 mmol). The solution was then brought to reflux (80°C). The reaction was monitored by TLC (silica; eluent: benzene-diethyl ether (20%)). The reaction was allowed to proceed for 3 h, during which time TLC indicated the formation of three products, with Rf-values of 0.34, 0.60 and 0.75 (trace). The products were separated by column chromatography (2 cm x 40 cm column, silica; eluent: benzene - diethyl ether (20%)), and purified by filtration and recrystallization from benzene-hexane solution. The lower brown band (Rf 0.60) yielded the monosubstituted maroon complex  $[(\text{C}_5\text{H}_4\text{CO}_2\text{Me})_2\text{Fe}_2(\text{CO})_3(\text{CNBu}^t)]$  (70%), while the upper green band (Rf 0.37) gave disubstituted  $[(\text{C}_5\text{H}_4\text{CO}_2\text{Me})\text{Fe}(\text{CO})(\text{CNBu}^t)]_2$  (< 10%), as a bottle green solid. Analytical and spectral data for these complexes are given in Tables 2.4 and 2.5 respectively. The trace product (Rf 0.75)

was present in insufficient amount to be isolated.

2.4.5 Reaction of  $[(C_5H_4CO_2Me)Fe(CO)_2]_2$  with  $tBuNC$  (1:2 Ratio)

$[(C_5H_4CO_2Me)Fe(CO)_2]_2$  (0.47g, 1.00 mmol) was dissolved in benzene (20 ml), and to this was added  $tBuNC$  (112  $\mu$ l, 1.00 mmol). The solution was then brought to reflux (80°C). The reaction was monitored by IR spectroscopy. The formation of the monosubstituted  $[(C_5H_4CO_2Me)_2Fe_2(CO)_3(CNBu^t)]$  was judged to be complete after 15 min. Further  $tBuNC$  (150  $\mu$ l, 1.53 mmol) was added. The progress of the reaction was monitored by TLC (as above). The reaction was allowed to proceed for 4 h, but complete conversion to the disubstituted product had not occurred in this time. The reaction was stopped and the solvent removed in vacuo. The products were separated by column chromatography (see above) and purified by recrystallization from benzene-hexane solution. The lower brown band (Rf 0.60) yielded maroon  $[(C_5H_4CO_2Me)_2Fe_2(CO)_3(CNBu^t)]$  (< 5%). The upper green band (Rf 0.41) gave 0.28g (50%) of green  $[(C_5H_4CO_2Me)Fe(CO)(CNBu^t)]_2$ . (See Tables 2.4 and 2.5). The trace product (Rf 0.75) was not collected.

TABLE 2.2: Analytical data for the  $(\eta^6\text{Phene})\text{Cr}(\text{CO})_2$  (Cm) complexes

| Complex  | Colour | mp (°C) | Elemental analysis<br>(Found (calcd. ) (%) ) |            |            |
|--|--------|---------|--|------------|------------|
|  |        |         | C  | H          | N          |
| $(\eta^6\text{-C}_6\text{H}_5\text{Me})\text{Cr}(\text{CO})_2$ (CmBu <sup>+</sup> )  | yellow | 77-78   | 59.5(59.4)                                   | 5.82(6.01) | 4.92(4.94) |
| $(\eta^6\text{-C}_6\text{H}_5\text{C}_3)\text{Cr}(\text{CO})_2$ (CmBu <sup>+</sup> )   | yellow | 86-88   | 51.4(51.4)                                   | 4.08(4.61) | 4.63(4.61) |
| $(\eta^6\text{-C}_6\text{H}_5\text{CO}_2\text{Me})\text{Cr}(\text{CO})_2$ (CmBu <sup>+</sup> )                                   | red    | 84-85   | 54.8(55.0)                                   | 5.19(5.20) | 4.35(4.28) |
| $(\eta^6\text{-C}_6\text{H}_5\text{Me})\text{Cr}(\text{CO})_2$ (CmC <sub>6</sub> H <sub>3</sub> Me <sub>2</sub> -2,6)            | orange | 99-100  | 66.1(65.2)                                   | 5.26(5.17) | 5.10(4.23) |
| $(\eta^6\text{-C}_6\text{H}_5\text{CO}_2\text{Me})\text{Cr}(\text{CO})_2$ (CmC <sub>6</sub> H <sub>3</sub> Me <sub>2</sub> -2,6) | red    | 73      | 60.4(60.8)                                   | 4.58(4.57) | 3.80(3.73) |

TABLE 2.3: Spectroscopic data for the  $\text{Cr}(\text{CO})_{6-n}(\text{CmC}_6\text{H}_3\text{Me}_2-2,6)_n$  ( $n = 3,4$ ) complexes

| Complex  | $\overline{\text{IR}}$ (cm <sup>-1</sup> ) <sup>a</sup> |                  | $^1\text{H NMR}$ (ppm) <sup>b</sup>       |   |  |
|--|---|------------------|---|---|--|
|  | $\nu(\text{C}=\text{C})$                                | $\nu(\text{CO})$ | $\text{C}_6\text{H}_3(\text{CH}_2)_2-2,6$ | $\text{C}_6\text{H}_3(\text{CH}_3)_2-2,6$ |  |
| $\text{Cr}(\text{CO})_3$ (CmC <sub>6</sub> H <sub>3</sub> Me <sub>2</sub> -2,6) <sub>3</sub> | 2134(w), 2060(w)  | 1954(2), 1904(s) | 2.23(s)                                   | 6.69, 6.68(d)                             |  |
| $\text{Cr}(\text{CO})_2$ (CmC <sub>6</sub> H <sub>3</sub> Me <sub>2</sub> -2,6) <sub>4</sub> | 2125(w), 2050(s), 1899(s), 1875(sh)                     |                  | 2.39,                                     | 6.74, 6.72(d)                             |  |
|  |   |                  | 1.304(s)                                  | 2.34(d)                                   |  |

<sup>a</sup> Recorded in CHCl<sub>3</sub>

<sup>b</sup> Recorded in C<sub>6</sub>D<sub>6</sub> relative to TMS

TABLE 2.4: Analytical data for  $[(C_5H_4CO_2Me)Fe(CO)_2]_2$  and derivatives

| Complex                                  | Colour       | mp(°C) | Elemental analysis |            |            |            |
|--|--------------|--------|--------------------|------------|------------|------------|
|  |              |        | C                  | H          | N          | I          |
|  |              |        | Found              | Calcd.     | (%)        |            |
| $[(C_5H_4CO_2Me)Fe(CO)_2]_2$             | purple       | >330   | 46.4(46.0)         | 2.94(3.00) | -          | -          |
| $(C_5H_4CO_2Me)Fe(CO)_2$                 | black        | 75-76  | 30.4(29.4)         | 2.05(1.95) | -          | 35.5(35.1) |
| $[(C_5H_4CO_2Me)_2Fe_2(CO)_3(CNBu^t)_1]$ | maroon       | 70-71  | 50.4(50.3)         | 4.55(4.41) | 2.60(2.67) | -          |
| $[(C_5H_4CO_2Me)Fe(CO)(CNBu^t)]_2$       | bottle green | >330   | 54.9(53.8)         | 5.84(5.56) | 4.36(4.33) | -          |

TABLE 2.5: Spectroscopic data for  $[(C_5H_4CO_2Me)Fe(CO)_2]_2$  and derivatives

| Complex                                  | IR (cm <sup>-1</sup> ) <sup>a</sup> |                  |                 | <sup>1</sup> H NMR (ppm) <sup>b</sup> |                                  |   |   |
|--|-------------------------------------|------------------|-----------------|---------------------------------------|----------------------------------|---|---|
|  | v(NC)                               | v(CO)(terminal)  | v(CO)(bridging) | v(COO)Me                              | C(CH <sub>3</sub> ) <sub>3</sub> | C <sub>5</sub> H <sub>4</sub> CO <sub>2</sub> CH <sub>3</sub> | C <sub>5</sub> H <sub>4</sub> CO <sub>2</sub> CH <sub>3</sub> |
| $[(C_5H_4CO_2Me)Fe(CO)_2]_2$             | -                                   | 2012(s), 1974(m) | 1790(s)         | 1720(m)                               | -                                | 3.80(s)   | 4.35 and 4.90(m)  |
| $(C_5H_4CO_2Me)Fe(CO)_2$                 | -                                   | 2052(s), 2012(s) | -               | 1730(m)                               | -                                | 3.24(s)   | 3.79 and 5.00(m)  |
| $[(C_5H_4CO_2Me)_2Fe_2(CO)_3(CNBu^t)_1]$ | 2136(m)                             | 1964(m)          | 1760(s)         | 1713(m)                               | 0.79(s)                          | 3.70(s)   | 4.46 and 5.04(m)  |
| $[(C_5H_4CO_2Me)Fe^+(CO)(CNBu^t)]_2$     | 2120(m), 2000(w)                    | -                | 1754(s)         | 1720(m)                               | 0.94(s)                          | 3.80(s)   | 4.41 and 5.10(m)  |

a Recorded in CH<sub>2</sub>Cl<sub>2</sub>

b Recorded on C<sub>6</sub>D<sub>6</sub>, relative to TMS

III. THE MODIFICATION OF  $(\eta^6\text{-C}_6\text{H}_5\text{CO}_2\text{Me})\text{Cr}(\text{CO})_3$  BY LIGANDS L

3.1 Introduction

A typical example of a half-sandwich metal carbonyl compound is  $(\eta^6\text{-C}_6\text{H}_5)\text{Cr}(\text{CO})_3$ . The crystal and molecular structure (at 78°K) of this complex has been determined by Rees and Coppens<sup>18</sup> using X-ray and neutron diffraction techniques. The molecule exhibits a "piano-stool" arrangement of the  $(\eta^6\text{-Arene})$  and the  $\text{Cr}(\text{CO})_3$  unit, with the conformation of the carbonyl ligands with respect to the carbon atoms of the Arene ring staggered.

Considerable interest has been shown in complexes of the type  $(\eta^6\text{-Arene})\text{Cr}(\text{CO})_3$ , owing to the catalytic potential of such compounds.<sup>1,2</sup> It is possible to modify the chemistry of  $(\text{Arene})\text{Cr}(\text{CO})_3$  in two ways:-

- (i) by varying the arene ligand  
or (ii) by the substitution of CO by ligand L (eg. RNC, CS, PR<sub>3</sub>). Further, if the  $(\eta^6\text{-C}_6\text{H}_6)$  ring is replaced by a ring containing an electron-withdrawing group, eg.  $\eta^6\text{-C}_6\text{H}_5\text{CO}_2\text{Me}$ , the stability of the complex (to air oxidation) increases,<sup>13c</sup> making such substituted derivatives more accessible for study.

The complex  $(\eta^6\text{-C}_6\text{H}_5\text{CO}_2\text{Me})\text{Cr}(\text{CO})_3$ ,<sup>14</sup> and a wide range of ligand substituted derivatives,  $(\eta^6\text{-C}_6\text{H}_5\text{CO}_2\text{Me})\text{Cr}(\text{CO})_2\text{L}$ , have been previously investigated by X-ray crystallographic techniques.<sup>14, 15-17</sup> Unlike the unsubstituted  $(\eta^6\text{-C}_6\text{H}_6)\text{Cr}(\text{CO})_3$ , the parent compound  $(\eta^6\text{-C}_6\text{H}_5\text{CO}_2\text{Me})\text{Cr}(\text{CO})_3$  adopts an eclipsed conformation of the carbonyl ligands with respect to the C-atoms of the arene ring, as do most of the  $(\eta^6\text{-C}_6\text{H}_5\text{CO}_2\text{Me})\text{-Cr}(\text{CO})_2\text{L}$  derivatives. This, and the effect of the ligand L on molecular structure, can be rationalized in terms of electronic effects.

3.2 The Structure of  $(\eta^6\text{-C}_6\text{H}_5\text{CO}_2\text{Me})\text{Cr}(\text{CO})_3$

The crystal and molecular structure of  $(\eta^6\text{-C}_6\text{H}_5\text{CO}_2\text{Me})\text{Cr}(\text{CO})_3$  was first determined by Carter, McPhail and Sim<sup>18a</sup> in 1967 (R-value of 14.1%) and in 1976 redetermined by Saillard and

Grandjean<sup>13b</sup> (R-value of 3.4%), improving the accuracy of bond parameter data.

### 3.2.1 Ligand geometry

The ( $\eta^6\text{-C}_6\text{H}_5\text{CO}_2\text{Me}$ )Cr(CO)<sub>3</sub> molecule has the typical "piano-stool" geometry, with the three OC-Cr-CO angles being equal within experimental error (av. 88.2(1)°).

### 3.2.2 Conformation

There are three possible conformations for a mono-substituted arene complex of the type ( $\text{C}_6\text{H}_5\text{R}$ )Cr(CO)<sub>3</sub> (Fig. 3.1), viz. staggered (I), anti-eclipsed (IIa), i.e. ortho and para C-atoms of ring eclipsed, and syn-eclipsed (IIb), i.e. C-atom bearing substituent R, and meta C-atoms of ring eclipsed

From electronic considerations,<sup>13-16</sup> it is possible to predict the most favourable conformation for a given ( $\eta^6\text{-C}_6\text{H}_5\text{R}$ )Cr(CO)<sub>3</sub> complex. According to the hybridization model, the Cr(CO)<sub>3</sub> unit has three filled hybrid orbitals collinear with the Cr-CO bonds and three empty hybrids, directed in an octahedral arrangement, with the empty hybrids staggering the Cr-CO bonds (Fig. 3.2). The Cr(CO)<sub>3</sub> group will orient itself such that the empty set of hybrid orbitals (a) are pointed towards regions of high electron density, and the filled set of hybrid orbitals (b) towards regions of low electron density on the arene ring. The charge distribution on the arene ring is dependent on the electronic nature of the ring substituent R. Case a: If R is an electron-acceptor A, the Cr(CO)<sub>3</sub> group will orient itself with the empty trio of orbitals (a) pointing towards the electron rich ipso and meta positions, and the filled trio of orbitals (b) towards the electron deficient ortho and para positions, giving the anti-eclipsed conformation (IIa). (Fig. 3.3a). Case b: If R is an electron-donor D, the Cr(CO)<sub>3</sub> group will orient itself with the empty trio of orbitals (a) pointing towards the electron rich ortho and para positions, and the filled trio of orbitals (b) towards the electron deficient ipso and meta positions, giving the syn-eclipsed conformation (IIb) (Fig. 3.3b).



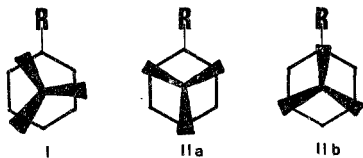


Figure 3.1 The three possible conformations for  $(C_6H_5R)-Cr(CO)_3$ : I. staggered, IIa. anti-eclipsed, and IIb. syn-eclipsed.

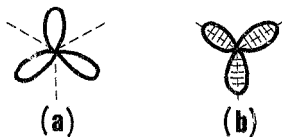


Figure 3.2 Two sets of three hybrid orbitals of  $Cr(CO)_3$ : (a) empty, (b) filled.

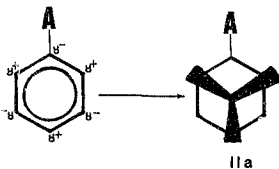


Figure 3.3a Ring polarization with electron-accepting substituent A results in the anti-eclipsed conformation IIa for  $(C_6H_5A)Cr(CO)_3$

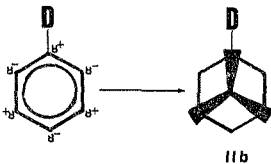


Figure 3.3b Ring polarization with electron-donating substituent D results in the syn-eclipsed conformation IIb for  $(C_6H_5D)Cr(CO)_3$

Hence for  $(\eta^6\text{C}_6\text{H}_5\text{R})\text{Cr}(\text{CO})_3$  complexes, electron-withdrawing R-groups favour the anti-eclipsed conformation (IIa), and electron-releasing R-groups the syn-eclipsed conformation (IIb). However, steric factors may favour a staggered conformation (I), especially if bulky groups are present.<sup>22,28</sup> Further, since the rotation barrier in many  $(\eta^6\text{C}_6\text{H}_5\text{R})\text{Cr}(\text{CO})_3$  complexes is not expected to be very large if the R-group is neither strongly electron-withdrawing or -releasing,<sup>27</sup> packing forces may be the determining factor in the conformation adopted in the solid state.

In the case of  $(\eta^6\text{C}_6\text{H}_5\text{CO}_2\text{Me})\text{Cr}(\text{CO})_3$ , since the  $\text{CO}_2\text{Me}$  group is an electron-withdrawing, the anti-eclipsed conformation in which the substituent resides on a non-eclipsed position would be expected. This is indeed the conformation found in the crystal.<sup>28</sup>

### 3.2.3 Cr-C bond lengths

The  $\nu$  values for the Cr-CO and Cr-C-ring bond lengths are  $1.842(3)\text{\AA}$  and  $2.217(3)\text{\AA}$  respectively. The distance between the chromium atom and the centre of gravity of the arene ring, Cr-Arene, is  $1.7144(4)\text{\AA}$ .<sup>28b</sup>

### 3.2.4 Ring C-C bond lengths

In the unsubstituted complex,  $(\eta^6\text{C}_6\text{H}_6)\text{Cr}(\text{CO})_3$ , which has a staggered conformation, there is a lowering of the benzene-ring symmetry from  $D_{3h}$  to  $C_{3v}$ ; the C-C bonds of the arene ring alternate in length, with the three non-eclipsed C-C bonds (av.  $1.406(1)\text{\AA}$ ) shorter than the three eclipsed C-C bonds (av.  $1.423(1)\text{\AA}$ ).<sup>29</sup> This effect has been rationalized in terms of Molecular Orbital (MO) Theory, which demonstrates that the observed bond lengths correlate well with electron overlap populations.<sup>29,30</sup>

However, in the eclipsed  $(\eta^6\text{C}_6\text{H}_5\text{CO}_2\text{Me})\text{Cr}(\text{CO})_3$  molecule, the C-C bonds of the arene ring are uniform within the error limits (av.  $1.407(4)\text{\AA}$ ).<sup>28b</sup>

### 3.2.5 Planarity of Ring

The arene ring in  $(\eta^6\text{C}_6\text{H}_5\text{CO}_2\text{Me})\text{Cr}(\text{CO})_3$  is essentially planar.<sup>28b</sup> In the case of  $(\eta^6\text{C}_6\text{H}_5)\text{Cr}(\text{CO})_3$ , the ring H-atoms

are displaced an av. of  $0.03\text{\AA}$  from the plane of the benzene ring towards the Cr-atom.<sup>29</sup> This slight bending of the hydrogen atoms towards the metal atom has been ascribed to better metal-ring orbital overlap.<sup>30</sup> This effect is not apparent in  $(\eta^6\text{-C}_6\text{H}_5\text{CO}_2\text{Me})\text{Cr}(\text{CO})_3$ , but the  $\alpha$ -C-atom of the substituent is bent  $0.010(3)\text{\AA}$  towards the Cr-atom.<sup>11b</sup>

### 3.2.6. Cr-C-O bond angles

In  $\text{M}(\text{CO})_n$  ( $n = 2, 3, 4$ ) groups, the M-C-O fragments are expected to be bent (ca.  $5^\circ$  deviation from linearity) due to the different occupation of the two anti-bonding  $\pi^*$  orbitals on a carbonyl ligand.<sup>31</sup> The carbonyl ligands in  $(\eta^6\text{-C}_6\text{H}_5\text{CO}_2\text{Me})\text{Cr}(\text{CO})_3$  are slightly bent, with Cr-C-O angles ranging from  $178.0$  to  $179.3^\circ$  (av.  $178.8(3)^\circ$ ).<sup>11b</sup> The slight difference in Cr-C-O angles within the  $\text{Cr}(\text{CO})_3$  group (although equal within experimental error) could be due to crystal packing forces, or to the influence of other groups within the molecule which lower the symmetry of the  $\text{M}(\text{CO})_3$  group from  $\text{C}_{3v}$ .<sup>32</sup>

### 3.2.7 Packing considerations

$(\eta^6\text{-C}_6\text{H}_5\text{CO}_2\text{Me})\text{Cr}(\text{CO})_3$  crystallizes in the triclinic centrosymmetric space group  $\text{C}_i^1$ , with four molecules in the unit cell. The molecules pack with the arene rings parallel, the separation between the adjacent benzene planes of  $3.38\text{\AA}$  being very close to the graphite distance of  $3.35\text{\AA}$ .<sup>11a</sup> There are no unusually short non-bonded contacts, but intermolecular repulsions could result in minor deviations from the ideal geometry.

## 3.3 The structural effect of substitution of CO by ligand L

The electronic nature of the ligand L, relative to CO, may result in structural changes in the  $(\eta^6\text{-C}_6\text{H}_5\text{CO}_2\text{Me})\text{Cr}(\text{CO})_2\text{L}$ . With bulky L groups, steric factors may also be important.

### 3.3.1 Ligand geometry

Although the "piano-stool" arrangement is retained, the OC-Cr-CO angle may differ significantly from the OC-Cr-L angles. If L is a better  $\pi$ -acceptor than CO, an increase in the OC-Cr-CO angle, and a diminution of the OC-Cr-L angles is expected.<sup>33</sup>

### 3.3.2 Conformation

Since the electronic preference for a conformation is governed by the electronic nature of the arene substituent, the ligand substituted derivatives  $(\eta^5\text{-C}_6\text{H}_5\text{CO}_2\text{Me})\text{Cr}(\text{CO})_2\text{L}$  would be expected to have the same conformation as the parent molecule  $(\eta^5\text{-C}_6\text{H}_5\text{CO}_2\text{Me})\text{Cr}(\text{CO})_3$ , viz. anti-eclipsed (IIa).

However, as mentioned previously, where the barrier to ring rotation is not large, packing forces may determine the molecular conformation in the crystal.<sup>37</sup>

Exceptions to the predicted conformation may also be caused by steric factors,<sup>38</sup> particularly if the L group is bulky. A staggered conformation may better accommodate a sterically demanding L group, by minimizing intramolecular repulsive interactions.

### 3.3.3 Influence of electronic nature of L on Cr-C bond lengths

The electronic nature of the ligand L, relative to CO, effects the Cr-C bond lengths in  $(\eta^5\text{-C}_6\text{H}_5\text{CO}_2\text{Me})\text{Cr}(\text{CO})_2\text{L}$ . Specifically, if the ligand L is a stronger ligand than CO, i.e. stronger  $\sigma$ -donor and  $\pi$ -acceptor properties than CO, a shortening of the Cr-CR (L = CR) bond (relative to the Cr-CO bond lengths in  $(\eta^5\text{-C}_6\text{H}_5\text{CO}_2\text{Me})\text{Cr}(\text{CO})_3$ ) is expected, with a concomitant lengthening of the Cr-CO bonds, and of the Cr-C ring bond lengths, and the Cr-arene distance, relative to these Cr-C distances in  $(\eta^5\text{-C}_6\text{H}_5\text{CO}_2\text{Me})\text{Cr}(\text{CO})_3$ . However, with a ligand L which is a poorer  $\pi$ -acceptor than CO, the inverse trends in Cr-C bond lengths are expected.<sup>39</sup>

### 3.3.4 Ring C-C bond lengths

The ring C-C bonds are expected to be uniform, as in  $(\eta^5\text{-C}_6\text{H}_5\text{CO}_2\text{Me})\text{Cr}(\text{CO})_3$ . Small differences may result from differences in the polarization of the electron density of specific carbon atoms of the ring by the  $\text{Cr}(\text{CO})_2\text{L}$  group itself.<sup>37</sup> The  $[\text{Cr}(\text{CO})_3]$  unit has been shown to exert an electron-withdrawing effect upon arene rings which is approximately equal to that of the nitro group.<sup>41</sup>

### 3.3.5 Planarity of Ring

The arene ring is expected to be essentially planar, as for  $(\eta^5\text{-C}_6\text{H}_5\text{CO}_2\text{Me})\text{Cr}(\text{CO})_3$ . The ring substituent may bend

slightly towards the Cr-atom, as in  $(\eta^6\text{-C}_6\text{H}_5\text{CO}_2\text{Me})\text{Cr}(\text{CO})_3$ , or may bend away from the Cr-atom. A bending away from the Cr-atom may be in an attempt to minimize repulsive intramolecular interactions. The bending of the ring substituent may also be influenced by intermolecular interactions. Steric factors are likely to be more dominant with bulky ligands L.

### 3.3.6 Cr-C-O and Cr-C-R bond angles (L = CR)

Non-linearity of Cr-C-O fragments is expected for  $\text{Cr}(\text{CO})_2$  groups, as for  $\text{Cr}(\text{CO})_3$  groups.<sup>19</sup> Linearity would only be expected for  $\text{M}(\text{CO})$ . This applies also to other ligands such as CNR, NO. Different Cr-C-O angles within the  $\text{Cr}(\text{CO})_2$  group (often equal within experimental error) could be due to crystal packing forces, or to the influence of other groups within the molecule which lower the symmetry. Steric constraints and crystal packing forces may cause the Cr-C-R (L = CR) angle to deviate from linearity.

### 3.3.7 Packing, and Steric factors

Packing considerations could be important in determining the overall conformation of the molecule. Packing forces may also be responsible for small deviations from ideal geometry within the molecule.

For a ligand of the type  $\text{L} = \text{CRR}'$ , the magnitude and direction of the bending of the ligand (i.e. the deviation of the C-R-R' angle from linearity, and whether the R' group bends in towards the two CO groups, or outwards away from the carbonyls), is probably determined largely by intramolecular and intermolecular interactions, and the influence of crystal packing forces. Steric factors are likely to be particularly dominant in determining the ligand conformation when there is no very strong electronic conformation preference, e.g. for isocyanide ligands, L = CNR, MO calculations indicate<sup>21</sup> that the energy difference between the linear (C-N-R = 180°) and slightly bent (C-N-R = 167-171°) conformations is small, although the linear conformation is slightly more stable electronically. Here steric factors may dominate, especially with bulky R-groups.

3.4 X-ray Crystallographic Studies of  $(\eta^6\text{-C}_6\text{H}_5\text{CO}_2\text{Me})\text{Cr}(\text{CO})_2\text{L}$  complexes

The  $(\eta^6\text{-C}_6\text{H}_5\text{CO}_2\text{Me})\text{Cr}(\text{CO})_2\text{L}$  complexes for which X-ray crystal and molecular structures have been reported in the literature are listed in Table 3.1. Note that the compound  $(\eta^6\text{-C}_6\text{H}_5\text{CO}_2\text{Me})\text{-Cr}(\text{CO})_2(\text{CNCOC}_6\text{H}_5)$  has two crystal morphologies, a triclinic form (A), and a monoclinic form (B), both of which, however, have very similar molecular structure.<sup>14</sup>

Table 3.2 summarizes the principal geometric characteristics of the above complexes. Trends and special features will be discussed.

The electronic nature of the ligand L is an important factor influencing molecular geometry, through the  $\sigma$ -donor and  $\pi$ -acceptor properties of L relative to CO. For the ligands L of interest, the order of increasing  $\sigma$ -donor strength is  $\text{CSe} > \text{CS} > \text{CNR} > \text{CNCOR} > \text{CO}$ , and of increasing  $\pi$ -acceptor ability is  $\text{CSe} > \text{CS} > \text{CNCOR} > \text{CO} > \text{CN}^+ > \text{PR}_3$ .<sup>14, 15, 16</sup> However, the  $\text{PF}_3$  ligand does not fall into the  $\text{PR}_3$  class with  $\text{PPh}_3$ , being a stronger  $\pi$ -acceptor than  $\text{CO}$ .<sup>14</sup>

3.4.1 OC-Cr-CO and OC-Cr-L angles

All the  $(\eta^6\text{-C}_6\text{H}_5\text{CO}_2\text{Me})\text{Cr}(\text{CO})_2\text{L}$  complexes have the usual "piano-stool" geometry. The order of increasing OC-Cr-CO angle, and decreasing av. OC-Cr-L angle for ligands L, relative to the av. OC-Cr-CO angle in  $(\eta^6\text{-C}_6\text{H}_5\text{CO}_2\text{Me})\text{Cr}(\text{CO})_3$  of  $88.2(1)^\circ$ , is  $\text{PPh}_3, \text{CO}, \text{PF}_3, \text{CS}, \text{CSe}$ , which parallels the order of increasing  $\pi$ -acceptor ability.

3.4.2 Conformation: An exception

The complexes  $(\eta^6\text{-C}_6\text{H}_5\text{CO}_2\text{Me})\text{Cr}(\text{CO})_2\text{L}$  (L =  $\text{PPh}_3, \text{CO}, \text{CS}, \text{CSe}$ ), all have the anti-eclipsed conformation as expected, with small angles of eclipse at the ortho and para positions (Fig 3.4). However, for L =  $\text{PF}_3$ , the angles of eclipse are large (av.  $18.1^\circ$ )<sup>14</sup> and the conformation can be described as "off-anti-eclipsed."

With the exception of L =  $\text{PPh}_3$ , the ligand L (L =  $\text{CSe}, \text{CS}, \text{PF}_3$ ) occupies the ortho position with the angle of eclipse ( $\alpha$ ) (Fig 3.4), where L has moved away from the  $\text{CO}_2\text{Me}$

TABLE 3.1: X-ray Crystal Structures of  $(\eta^6\text{-C}_6\text{H}_5\text{CO}_2\text{Me})\text{Cr}(\text{CO})_2\text{L}$  complexes

| <u>Complex</u>   | <u>Space Group, Z</u>               | <u>Reference</u> |
|--|-------------------------------------|------------------|
| $(\eta^6\text{-C}_6\text{H}_5\text{CO}_2\text{Me})\text{Cr}(\text{CO})_3$                | $\text{C}\bar{1}$ , 4               | 30               |
| $(\eta^6\text{-C}_6\text{H}_5\text{CO}_2\text{Me})\text{Cr}(\text{CO})_2\text{CS}$       | $\text{P}\bar{1}$ , 2               | 31               |
| $(\eta^6\text{-C}_6\text{H}_5\text{CO}_2\text{Me})\text{Cr}(\text{CO})_2\text{CSe}$      | $\text{P}\bar{1}$ , 2               | 32               |
| $(\eta^6\text{-C}_6\text{H}_5\text{CO}_2\text{Me})\text{Cr}(\text{CO})_2\text{PPh}_3$    | $\text{P}2_1/\text{n}$ , 4          | 33               |
| $(\eta^6\text{-C}_6\text{H}_5\text{CO}_2\text{Me})\text{Cr}(\text{CO})_2\text{PF}_3$     | $\text{P}\bar{1}$ , 2               | 34               |
| $(\eta^6\text{-C}_6\text{H}_5\text{CO}_2\text{Me})\text{Cr}(\text{CO})_2(\text{CNCOPh})$ | $\text{P}\bar{1}$ , 2 (Form A)      | 16               |
|  | $\text{P}2_1/\text{c}$ , 4 (Form B) |                  |



TABLE 3.2: Principal geometric characteristics (distances, Å; Angles, °) of  $(\eta^6\text{-C}_6\text{H}_5\text{CO}_2\text{Me})\text{Cr}(\text{CO})_2\text{L}$  complexes

| L   | P Ph <sub>3</sub>     | CNCOPh       | CO                    | rF <sub>3</sub>   | CS            | CSe           |
|---|-----------------------|--------------|-----------------------|-------------------|---------------|---------------|
| Conformation                                | Anti-eclipsed         | Staggered    | Anti-eclipsed         | Off-anti-eclipsed | Anti-eclipsed | Anti-eclipsed |
| Angles of <sup>a</sup><br>eclipse. a,b,c    |                       | -            | 4.3,4.9,4.2           | 17.6,17.7,19.0    | 0,6.0,1.5     | 1.7,5.4,2.5   |
| Ring planarity                              | Planar                | Planar       | Planar                | Planar            | Planar        | Planar        |
| Deviation of $\alpha\text{-C}$ <sup>b</sup> | <sup>c</sup>          | <sup>c</sup> | +0.010(3)             | +0.083(11)        | +0.037(3)     | 0°            |
| av Ring C-C                                 | 1.399(5)              | <sup>c</sup> | 1.407(4)              | 1.399(15)         | 1.401(4)      | 1.40(2)       |
| Cr-Arene                                    | 1.695(1) <sup>d</sup> | <sup>c</sup> | 1.714(1)              | 1.698(2)          | 1.730(1)      | 1.742(1)      |
| av Cr-C ring                                | 2.198(4)              | <sup>c</sup> | 2.217(2)              | 2.201(10)         | 2.226(2)      | 2.232(11)     |
| av Cr-CO                                    | 1.823(4)              | <sup>c</sup> | 1.842(3) <sup>e</sup> | 1.833(11)         | 1.848(3)      | 1.862(11)     |
| Cr-L  | 2.337(1)              | 1.85(1)      |                       | 2.132(3)          | 1.797(2)      | 1.786(11)     |
| OC-Cr-CO                                    | 85.3(1)               | <sup>c</sup> | 88.7(1) <sup>e</sup>  | 89.4(5)           | 90.9(1)       | 91.0(6)       |
| av OC-Cr-L                                  | 90.1(1) <sup>d</sup>  | <sup>c</sup> |                       | 88.6(5)           | 85.7(1)       | 84.9(5)       |
| av Cr-C-O                                   | 176.6(3) <sup>d</sup> | <sup>c</sup> | 176.8(3) <sup>e</sup> | 177.7(7)          | 176.9(2)      | 177.1(7)      |
| Cr-C-R <sup>f</sup>                         | -                     | 178.8(9)     |                       | -                 | 178.0(2)      | 179.0(7)      |

<sup>a</sup> See Fig 3.4

<sup>b</sup> Deviation of  $\alpha\text{-C}$  of  $\text{-CO}_2\text{Me}$  from mean plane of arene ring; + indicates towards Cr atom, - away from Cr atom

<sup>c</sup> Not quoted in reference

<sup>d</sup> Ref. 34

<sup>e</sup> av value for the three CO ligands

<sup>f</sup> Applicable for ligand type L = CR

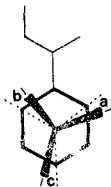


Figure 3.4 Anti-eclipsed conformation of  $(\eta^6\text{-C}_6\text{H}_5\text{CO}_2\text{Me})\text{Cr}(\text{CO})_2\text{L}$  complex, viewed down ligand tripod onto arene ring, showing angles of eclipse, a, b and c, at ortho positions and para C-atom respectively

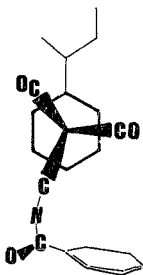


Figure 3.5 Unusual staggered conformation of the  $(\eta^6\text{-C}_6\text{H}_5\text{CO}_2\text{Me})\text{Cr}(\text{CO})_2(\text{CNCOPh})$  molecules, viewed down ligand tripod onto arene ring. (Both A and B forms the same structurally).

substituent, presumably for steric reasons. This could also account for the larger angle of eclipse (a) of 17.6° observed for L = PF<sub>3</sub>. However, for L = PPh<sub>3</sub>, the PPh<sub>3</sub> ligand occupies the ortho position with angle of eclipse (b).

There is one exception: the ( $\eta^6\text{-C}_6\text{H}_5\text{CO}_2\text{Me}$ )Cr(CO)<sub>2</sub>(CNCOPh) molecule has a staggered conformation (in both A and B forms) (Fig 3.5). Further, the relation of the ligand tripod to the arene substituent differs from all the other structures; if viewed down the ligand tripod onto the arene ring, the -OMe group points to the right, and not to the left, as is usual. (Fig 3.5, cf. Fig 3.4). The CNCOC<sub>6</sub>H<sub>5</sub> group is anti-parallel to the CO<sub>2</sub>Me substituent. Steric considerations could be responsible for the overall conformation, and crystal packing forces probably also play a role.

#### 3.4.3 Trends in Cr-C bond lengths

For the complexes ( $\eta^6\text{-C}_6\text{H}_5\text{CO}_2\text{Me}$ )Cr(CO)<sub>2</sub>L, (L = CSe, CS, PF<sub>3</sub>, PPh<sub>3</sub>, CO), the order of increasing Cr-CO bond length and of increasing Cr-C-ring and Cr-arene distances, is PPh<sub>3</sub>, PF<sub>3</sub>, CO, CS, CSe, which is the same as the order of increasing  $\pi$ -acceptor strength of the ligands L. This is also reflected in the Cr-CR (L = CR, R = Se, S, O, NCOPh) bond lengths CNCOPh < CO < CS < CSe. Note that the Cr-PF<sub>3</sub> bond (2.132(3)Å) is considerably shorter than the Cr-PPh<sub>3</sub> bond (2.337(1)Å), indicating that the PF<sub>3</sub> ligand, unlike PPh<sub>3</sub>, is a good  $\pi$ -acceptor.<sup>14</sup>

#### 3.4.4 Ring C-C bond lengths

The ring C-C bond lengths are consistent within a structure, and from structure to structure (ca. 1.40Å).

#### 3.4.5 Ring planarity and bending of CO<sub>2</sub>Me group

In all cases, the arene ring is planar, with the  $\alpha$ -C atom of the CO<sub>2</sub>Me group either planar with the ring (L = CSe), or bending in slightly towards the Cr-atom (L = CS, PF<sub>3</sub>, CO).

3.4.6 Cr-C-O and Cr-C-R bond angles (L = CR)

For all the complexes, the Cr-C-O angles deviate slightly for linearity (ca.  $177^\circ$ ), as expected. The Cr-C-R angles (L = CR, R = Se, S, NCOPh), are also slightly bent ( $178 - 179^\circ$ ).

3.4.7 Conformation of the ligand L

In the complex  $(\eta^6\text{-C}_6\text{H}_5\text{CO}_2\text{Me})\text{Cr}(\text{CO})_2(\text{CNCOPh})$ ,<sup>16</sup> the isonitrile ligand is bent, with a C-N-C angle of  $168(1)^\circ$ . This probably reflects steric and packing requirements.

3.5 Conclusion

From the foregoing analyses, it is apparent that structural variations in  $(\eta^6\text{-C}_6\text{H}_5\text{CO}_2\text{Me})\text{Cr}(\text{CO})_2\text{L}$  derivatives, relative to the parent  $(\eta^6\text{-C}_6\text{H}_5\text{CO}_2\text{Me})\text{Cr}(\text{CO})_3$ , may be rationalized by considering the influence of the electronic nature of the ligand L, relative to CO.

However, steric factors and the role of crystal packing forces should not be ignored, and these may account for exceptions encountered, as well as small deviations from ideal geometry.

IV. THE CRYSTAL AND MOLECULAR STRUCTURE OF  $(n^6\text{-C}_6\text{H}_5\text{CO}_2\text{Me})\text{Cr}(\text{CO})_2(\text{CNBu}^t)$

4.1 Introduction

An X-ray crystal study of  $(n^6\text{-C}_6\text{H}_5\text{CO}_2\text{Me})\text{Cr}(\text{CO})_2(\text{CNBu}^t)$ , was undertaken as part of an investigation into the anomalous IR spectra exhibited by certain complexes of this type. It was hoped that the X-ray study might provide a structural basis for the rationalization of the anomalous IR data. The IR spectra in relation to the structure, will be discussed separately in Chapter VIII.

$(n^6\text{-C}_6\text{H}_5\text{CO}_2\text{Me})\text{Cr}(\text{CO})_2(\text{CNBu}^t)$  crystallizes in the triclinic centrosymmetric space group  $P\bar{1}$ , with two molecules in the unit cell. Fig. 4.2 shows a view of the unit cell looking down the c-axis. A view of the molecule, looking down the ligand tripod onto the arene ring is shown in Fig. 4.1, together with the numbering system used in the analysis.

Bond lengths and bond angles, and bond parameters involving hydrogen atoms, are given in Table 4.1, 4.2 and 4.3 respectively. Table 4.4 lists the deviations ( $\bar{R}$ ) of the atoms from the mean plane through the ring C-atoms (C(1)-C(6)).

4.2 Discussion of the Structure of  $(n^6\text{-C}_6\text{H}_5\text{CO}_2\text{Me})\text{Cr}(\text{CO})_2(\text{CNBu}^t)$

The structure of the  $(n^6\text{-C}_6\text{H}_5\text{CO}_2\text{Me})\text{Cr}(\text{CO})_2(\text{CNBu}^t)$  molecule will be discussed in relation to the structures of related  $(n^6\text{-C}_6\text{H}_5\text{CO}_2\text{Me})\text{Cr}(\text{CO})_2\text{L}$  complexes (Table 3.2), following the scheme of analysis previously employed. Any irregularities observed will be examined in greater detail, and possible causes considered (section 4.3). The principal geometric characteristics of  $(n^6\text{-C}_6\text{H}_5\text{CO}_2\text{Me})\text{Cr}(\text{CO})_2(\text{CNBu}^t)$  are summarized in Table 4.5

Since the electronic nature of the ligand L has an important influence on structure, it should be noted that the  $\text{CNBu}^t$  ligand is a better  $\sigma$ -donor and a poorer  $\pi$ -acceptor than CO, but a better  $\pi$ -acceptor than  $\text{PR}_3$ .<sup>4,5a</sup>

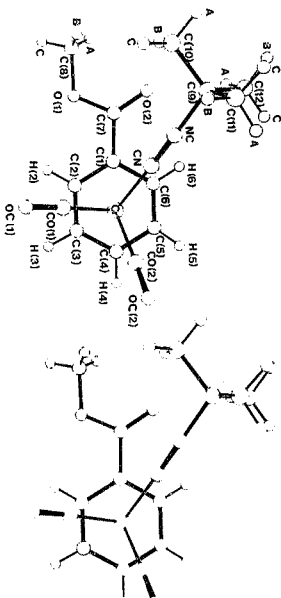


Figure 4.1 An ORTEP view of the [η<sup>5</sup>-C<sub>5</sub>H<sub>5</sub>CO<sub>2</sub>Me)Cr(CO)<sub>2</sub>(CNBu<sup>-</sup>) molecule, showing the numbering system

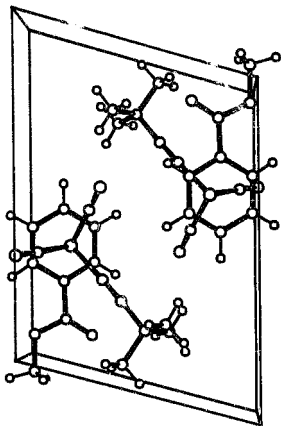


Figure 4.2 An ORTEP<sup>22</sup> view of the unit cell of  $(C_{10}H_{10}O_2Me)_2(Cr(CO)_2(CNBU^+))$ , looking down the c-axis

TABLE 4.1: Bond lengths (Å) for  $(\eta^6\text{-C}_6\text{H}_5\text{CO}_2\text{Me})\text{Cr}(\text{CO})_2(\text{CNBu}^t)$ 

|           |          |             |          |
|-----------|----------|-------------|----------|
| Cr-C(1)   | 2.190(4) | C(1)-C(2)   | 1.410(7) |
| Cr-C(2)   | 2.198(4) | C(2)-C(3)   | 1.405(8) |
| Cr-C(3)   | 2.207(5) | C(3)-C(4)   | 1.404(7) |
| Cr-C(4)   | 2.190(5) | C(4)-C(5)   | 1.407(9) |
| Cr-C(5)   | 2.224(5) | C(5)-C(6)   | 1.381(7) |
| Cr-C(6)   | 2.212(5) | C(6)-C(1)   | 1.420(6) |
| Cr-CO(1)  | 1.827(4) | CO(1)-OC(1) | 1.159(5) |
| Cr-CO(2)  | 1.838(3) | CO(2)-OC(2) | 1.157(4) |
| Cr-CN     | 1.940(5) | CN-NC       | 1.155(6) |
| C(1)-C(7) | 1.486(7) | NC-C(9)     | 1.451(8) |
| C(7)-O(1) | 1.346(5) | C(9)-C(10)  | 1.524(6) |
| C(7)-O(2) | 1.201(6) | C(9)-C(11)  | 1.512(8) |
| O(1)-C(8) | 1.448(6) | C(9)-C(12)  | 1.523(6) |

TABLE 4.2: Bond angles (°) for  $(\eta^6\text{-C}_6\text{H}_5\text{CO}_2\text{Me})\text{Cr}(\text{CO})_2(\text{CNBu}^t)$ 

|                  |          |                |          |
|------------------|----------|----------------|----------|
| Cr-CO(1)-OC(1)   | 178.3(3) | CO(1)-Cr-CO(2) | 86.2(2)  |
| Cr-CO(2)-OC(2)   | 177.9(3) | CO(1)-Cr-CN    | 90.7(2)  |
| Cr-CN-NC         | 177.3(4) | CO(2)-Cr-CN    | 90.2(2)  |
| NC-CN-C(9)       | 166.8(4) | C(1)-Cr-CO(1)  | 112.7(1) |
| CN-C(9)-C(10)    | 106.9(4) | C(2)-Cr-CO(1)  | 89.0(2)  |
| CN-C(9)-C(11)    | 107.1(4) | C(3)-Cr-CO(1)  | 93.4(2)  |
| CN-C(9)-C(12)    | 108.4(4) | C(4)-Cr-CO(1)  | 122.1(2) |
| C(10)-C(9)-C(11) | 111.9(5) | C(5)-Cr-CO(1)  | 159.0(2) |
| C(11)-C(9)-C(12) | 112.2(4) | C(6)-Cr-CO(1)  | 150.1(1) |
| C(12)-C(9)-C(10) | 110.1(4) | C(1)-Cr-CO(2)  | 161.1(2) |
| C(6)-C(1)-C(2)   | 119.2(4) | C(2)-Cr-CO(2)  | 149.1(2) |
| C(1)-C(2)-C(3)   | 119.8(4) | C(3)-Cr-CO(2)  | 112.6(2) |
| C(2)-C(3)-C(4)   | 120.0(5) | C(4)-Cr-CO(2)  | 89.7(2)  |
| C(3)-C(4)-C(5)   | 120.1(5) | C(5)-Cr-CO(2)  | 95.2(2)  |
| C(4)-C(5)-C(6)   | 119.9(4) | C(6)-Cr-CO(2)  | 123.6(2) |
| C(5)-C(6)-C(1)   | 120.7(5) | C(1)-Cr-CN     | 90.3(2)  |
| C(7)-C(1)-C(2)   | 122.7(4) | C(2)-Cr-       | 120.4(2) |
| C(7)-C(1)-C(6)   | 118.1(4) | C(3)-Cr-CN     | 157.0(2) |
| C(1)-C(7)-O(2)   | 124.6(4) | C(4)-Cr-CN     | 147.1(2) |
| C(1)-C(7)-O(1)   | 112.0(4) | C(5)-Cr-CN     | 110.2(2) |
| O(1)-C(7)-O(2)   | 123.4(4) | C(6)-Cr-CN     | 86.5(2)  |
| C(7)-O(1)-C(8)   | 115.3(4) | C(1)-Cr-C(2)   | 37.5(2)  |
| Cr-C(1)-C(2)     | 71.6(2)  | C(1)-Cr-C(3)   | 67.3(2)  |
| Cr-C(1)-C(6)     | 72.0(2)  | C(1)-Cr-C(4)   | 79.8(2)  |
| Cr-C(2)-C(1)     | 70.9(2)  | C(1)-Cr-C(5)   | 67.0(2)  |
| Cr-C(2)-C(3)     | 71.7(3)  | C(1)-Cr-C(6)   | 37.6(1)  |
| Cr-C(3)-C(2)     | 71.1(3)  | C(2)-Cr-C(3)   | 37.2(2)  |
| Cr-C(3)-C(4)     | 70.7(3)  | C(2)-Cr-C(4)   | 67.4(2)  |
| Cr-C(4)-C(3)     | 72.0(3)  | C(2)-Cr        | 79.1(2)  |
| Cr-C(4)-C(5)     | 72.7(3)  | C(2)-          | 67.2(2)  |
| Cr-C(5)-C(4)     | 70.1(3)  | C(3)-Cr        | 37.2(2)  |
| Cr-C(5)-C(6)     | 71.4(3)  | C(3)-Cr        | 66.7(2)  |
| Cr-C(6)-C(5)     | 72.3(3)  | C(3)-Cr-C(6)   | 78.7(2)  |
| Cr-C(6)-C(1)     | 70.3(3)  | C(4)-Cr-C(5)   | 37.2(2)  |
| Cr-C(1)-C(7)     | 127.3(3) | C(4)-Cr-C(6)   | 66.5(2)  |
|                  |          | C(5)-Cr-C(6)   | 36.3(2)  |



TABLE 4.3: Bond parameters involving hydrogen atoms for  
 $(\eta^6\text{C}_6\text{H}_5\text{CO}_2\text{Me})\text{Cr}(\text{CO})_2(\text{CNBu}^t)$

| a) Bond lengths (Å) |         |                   |         |
|---------------------|---------|-------------------|---------|
| C(2)-H(2)           | 0.97(4) | C(10)-H(10A)      | 0.97(5) |
| C(3)-H(3)           | 0.99(5) | C(10)-H(10B)      | 0.94(4) |
| C(4)-H(4)           | 0.98(4) | C(10)-H(10C)      | 1.07(4) |
| C(5)-H(5)           | 0.99(4) | C(11)-H(11A)      | 0.98(5) |
| C(6)-H(6)           | 0.96(5) | C(11)-H(11B)      | 0.97(4) |
| C(8)-H(8A)          | 0.95(5) | C(11)-H(11C)      | 0.95(4) |
| C(8)-H(8B)          | 0.91(4) | C(12)-H(12A)      | 1.00(4) |
| C(8)-H(8C)          | 1.03(4) | C(12)-H(12B)      | 0.96(5) |
|                     |         | C(12)-H(12C)      | 0.94(4) |
| b) Bond angles (°)  |         |                   |         |
| C(1)-C(2)-H(2)      | 118(3)  | Cr-C(2)-H(2)      | 124(2)  |
| C(3)-C(2)-H(2)      | 122(3)  | Cr-C(3)-H(3)      | 125(2)  |
| C(2)-C(3)-H(3)      | 117(2)  | Cr-C(4)-H(4)      | 129(2)  |
| C(4)-C(3)-H(3)      | 123(2)  | Cr-C(5)-H(5)      | 131(2)  |
| C(3)-C(4)-H(4)      | 119(2)  | Cr-C(6)-H(6)      | 131(2)  |
| C(5)-C(4)-H(4)      | 121(2)  | O(1)-C(8)-H(8A)   | 110(3)  |
| C(4)-C(5)-H(5)      | 121(3)  | O(1)-C(8)-H(8B)   | 110(3)  |
| C(6)-C(5)-H(5)      | 119(3)  | C(1)-C(8)-H(8C)   | 105(3)  |
| C(5)-C(6)-H(6)      | 121(2)  | C(9)-C(10)-H(10A) | 104(2)  |
| C(1)-C(6)-H(6)      | 119(2)  | C(9)-C(10)-H(10B) | 108(2)  |
| H(10A)-C(10)-H(10B) | 104(4)  | C(9)-C(10)-H(10C) | 110(2)  |
| H(10B)-C(10)-H(10C) | 119(3)  | C(9)-C(11)-H(11A) | 111(2)  |
| H(10C)-C(10)-H(10A) | 111(3)  | C(9)-C(11)-H(11B) | 109(4)  |
| H(11A)-C(11)-H(11B) | 105(4)  | C(9)-C(11)-H(11C) | 111(3)  |
| H(11B)-C(11)-H(11C) | 111(3)  | C(9)-C(12)-H(12A) | 112(2)  |
| H(11C)-C(11)-H(11A) | 109(4)  | C(9)-C(12)-H(12B) | 106(2)  |
| H(12A)-C(12)-H(12B) | 114(4)  | C(9)-C(12)-H(12C) | 112(2)  |
| H(12B)-C(12)-H(12C) | 105(4)  | H(8A)-C(8)-H(8B)  | 116(4)  |
| H(12C)-C(12)-H(12A) | 108(4)  | H(8B)-C(8)-H(8C)  | 118(3)  |
|                     |         | H(8C)-C(8)-H(8A)  | 96(3)   |

TABLE 4.4: Deviations (Å) of atoms from the plane defined by the six C-atoms (C(1)-C(6)) of the arene ring<sup>a</sup> in  $(\eta^6\text{C}_6\text{H}_5\text{CO}_2\text{Me})\text{Cr}(\text{CO})_2(\text{CNBu}^t)$

| Atom | Deviation from Plane (Å) |
|------|--------------------------|
| Cr   | 1.6975                   |
| C(1) | 0.0147                   |
| C(2) | -0.0046                  |
| C(3) | -0.0132                  |
| C(4) | 0.0209                   |
| C(5) | -0.0107                  |

TABLE 4.4 (Continued)

| <u>Atom</u>     | <u>Deviation from Plane (Å)</u> <sup>o</sup> |
|-----------------|--|
| C(6)            | -0.0071                                      |
| H(2)            | 0.0905                                       |
| H(3)            | 0.0572                                       |
| H(4)            | 0.0468                                       |
| H(5)            | -0.0285                                      |
| H(6)            | -0.0387                                      |
| C(7)            | 0.0787                                       |
| O(1)            | 0.0621                                       |
| O(2)            | 0.1447                                       |
| O(3)            | 0.1376                                       |
| H(8A)           | -0.5468                                      |
| H(8B)           | 0.9869                                       |
| H(8C)           | -0.2454                                      |
| CO(1)           | 2.7746                                       |
| CO(2)           | 2.8316                                       |
| OC(1)           | 2.4511                                       |
| OC(2)           | 3.5666                                       |
| CN <sup>a</sup> | 2.7731                                       |
| NC              | 3.3754                                       |
| C(9)            | 3.8288                                       |
| C(10)           | 3.8186                                       |
| C(11)           | 2.8604                                       |
| C(12)           | 5.2473                                       |
| H(10A)          | 4.0513                                       |
| H(10B)          | 2.9222                                       |
| H(10C)          | 4.5484                                       |
| H(11A)          | 3.0944                                       |
| H(11B)          | 1.9744                                       |
| H(11C)          | 2.8500                                       |
| H(12A)          | 4.8888                                       |
| H(12B)          | 4.661  |
| H(12C)          | 5.2949                                       |

<sup>a</sup> Equation of the plane defined by C(1)-C(6):

$$0.0478x + 1.1172y + 6.5952z = 1.6293$$

TABLE 4.4 (Continued)

| <u>Atom</u> | <u>Deviation from Plane (Å)</u> <sup>o</sup> |
|-------------|--|
| C(6)        | -0.0071                                      |
| H(2)        | 0.0905                                       |
| H(3)        | 0.0572                                       |
| H(4)        | 0.0468                                       |
| H(5)        | -0.0285                                      |
| H(6)        | -0.0387                                      |
| C(7)        | 0.0787                                       |
| O(1)        | 0.0621                                       |
| O(2)        | 0.1447                                       |
| C(8)        | 0.1376                                       |
| H(8A)       | -0.5468                                      |
| H(8B)       | 0.9869                                       |
| H(8C)       | -0.2454                                      |
| CO(1)       | 2.7746                                       |
| CO(2)       | 2.8316                                       |
| OC(1)       | 3.4511                                       |
| OC(2)       | 3.5666                                       |
| CN'         | 2.7731                                       |
| NC          | 3.3754                                       |
| C(9)        | 3.8288                                       |
| C(10)       | 3.8186                                       |
| C(11)       | 2.8604                                       |
| C(12)       | 5.2473                                       |
| H(10A)      | 4.0513                                       |
| H(10B)      | 2.9232                                       |
| H(10C)      | 4.5484                                       |
| H(11A)      | 3.0944                                       |
| H(11B)      | 1.9744                                       |
| H(11C)      | 2.8500                                       |
| H(12A)      | 5.8888                                       |
| H(12B)      | 5.4561                                       |
| H(12C)      | 5.2949                                       |

<sup>a</sup> Equation of the plane defined by C(1)-C(6):

$$0.0478x + 1.1172y + 6.5952z = 1.6293$$

TABLE 4.5; Principal geometrical characteristics (distances, Å;  
angles, °) of  $(\eta^6\text{-C}_6\text{H}_5\text{CO}_2\text{Me})\text{Cr}(\text{CO})_2(\text{CNBu}^t)$

| Conformation             | Staggered                  |
|--------------------------|----------------------------|
| Ring planarity           | Planar                     |
| Deviation of $\alpha$ -C | 0.079, towards the Cr-atom |
| av Ring C-C              | 1.405(7)                   |
| Cr-Arene                 | 1.697(1)                   |
| av Cr-C-ring             | 2.204(8)                   |
| av Cr-CO                 | 1.833(4)                   |
| Cr-CN                    | 1.940(5)                   |
| OC-Cr-CO                 | 86.2(2)                    |
| av OC-Cr-CN              | 90.5(2)                    |
| av Cr-C-O                | 178.1(3)                   |
| Cr-C-N                   | 177.3(4)                   |
| C-N-C                    | 166.8(4)                   |

#### 4.2.1 OC-Cr-CO and OC-Cr-CN angles

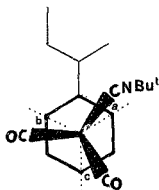
The molecule has the usual "piano-stool" arrangement of ligands. Within the ligand tripod, the OC-Cr-CO angle is  $86.2(2)^\circ$ , and the av. OC-Cr-CN angle  $90.5(2)^\circ$ . These values are intermediate between those for  $(\eta^5\text{-C}_6\text{H}_5\text{CO}_2\text{Me})\text{-Cr}(\text{CO})_2(\text{PPh}_3)$  [OC-Cr-CO,  $85.3(1)^\circ$ , and av. OC-Cr-P,  $90.1(1)^\circ$ ]<sup>11</sup> and  $(\eta^5\text{-C}_6\text{H}_5\text{CO}_2\text{Me})\text{Cr}(\text{CO})_3$  [av. OC-Cr-CO,  $88.2(1)^\circ$ ]<sup>12b</sup> as expected, since CNBu<sup>t</sup> is a poorer  $\pi$ -acceptor than CO, but a stronger  $\sigma$ -acceptor than  $\text{PPh}_3$ .<sup>11a</sup>

#### 4.2.2 Conformation

$(\eta^5\text{-C}_6\text{H}_5\text{CO}_2\text{Me})\text{Cr}(\text{CO})_2(\text{CNBu}^t)$  is an exception to the electronic conformation preference, since the molecule adopts a staggered conformation in the crystal. However, the relation of the ligand tripod to the arene ring is normal (Fig 3.4) (ie. when viewed down the ligand tripod onto the arene ring the -OMe group points to the left), but the CNBu<sup>t</sup> ligand which is parallel to the ring substituent has moved towards the CO<sub>2</sub>Me group. (The angle between Cr-CN and Cr-C(1) (bearing substituent) projected on the plane of the arene ring is  $37.7^\circ$ ). The "angles of eclipse" (Fig 4.3) are less than the ideal  $30^\circ$  for a symmetrical staggered conformation (av.  $21.3^\circ$ ), placing the conformation intermediate between staggered and the "off-anti-eclipsed" of the  $(\eta^5\text{-C}_6\text{H}_5\text{CO}_2\text{Me})\text{Cr}(\text{CO})_2\text{PF}_3$  structure (av.  $18.1^\circ$ ).<sup>13</sup> However, in the latter structure, the PF<sub>3</sub> ligand has moved away from the CO<sub>2</sub>Me substituent. The only other isonitrile derivative,  $(\eta^5\text{-C}_6\text{H}_5\text{CO}_2\text{Me})\text{Cr}(\text{CO})_2(\text{CNCOC}_6\text{H}_5)$ ,<sup>14</sup> also has a staggered structure, but the CNR ligand is anti-parallel to the CO<sub>2</sub>Me group (Fig 3.5).

#### 4.2.3 Cr-C bond lengths

The av. Cr-CO bond length, and the av. Cr-C ring and Cr-Arene distances of 1.833(4), 2.204(5) and 1.697(1) $\text{\AA}$  respectively, are intermediate between the values of 1.823(4), 2.198(4) and 1.695(1) $\text{\AA}$  and 1.842(3), 2.217(2) and 1.716(1) $\text{\AA}$  for  $(\eta^5\text{-C}_6\text{H}_5\text{CO}_2\text{Me})\text{Cr}(\text{CO})_2\text{PPh}_3$ <sup>11</sup> and  $(\eta^5\text{-C}_6\text{H}_5\text{CO}_2\text{Me})\text{Cr}(\text{CO})_3$ <sup>12b</sup>



**Figure 4.3** Conformation of the  $(\eta^5\text{-C}_6\text{H}_5\text{CO}_2\text{Me})\text{Cr}(\text{CO})_2(\text{CNBu}^{\text{T}})$  molecule, viewed down ligand tripod onto arene ring. The "angles of eclipse" at the ortho and para positions, are a, 22.3°, c, 22.8°, and b, 18.9°, respectively.

respectively, as expected. ( $\pi$ -acceptor strength  $\text{CO} > \text{CNR} > \text{PR}_3^{\text{a}}$ ). The longer Cr-CN bond length of 1.940(5)Å also reflects the poor  $\pi$ -acceptor property of the CNR ligand relative to CO. Note that the Cr-CO, Cr-C ring and Cr-arene distances are very similar to those for  $(\eta^5\text{-C}_6\text{H}_5\text{CO}_2\text{Me})\text{Cr}(\text{CO})_2(\text{PF}_3)$  (1.833(11), 2.201(10) and 1.898(2)Å respectively.)<sup>11</sup>

#### 4.2.4 Ring C-C bond lengths

The ring C-C bond lengths (av. 1.405(7)Å) are similar to those in the related structures.

#### 4.2.5 Ring planarity and bending of CO<sub>2</sub>Me-group

The arene ring is essentially planar, with the  $\alpha$ -C-atom of the arene substituent bending slightly towards the Cr-atom, as observed for other  $(\eta^5\text{-C}_6\text{H}_5\text{CO}_2\text{Me})\text{Cr}(\text{CO})_2\text{L}$  (L = CO, <sup>11b</sup> CS, <sup>11</sup> PF<sub>3</sub>) structures.

#### 4.2.6 Cr-C-O and Cr-C-N bond angles

As expected,<sup>9</sup> the Cr-C-O angles deviate slightly from linearity (av. 178.1(3)°). The Cr-C-N group is also slightly bent, with a Cr-C-N angle of 177.3(4)°.

#### 4.2.7 Conformation of the CNBu<sup>t</sup> ligand

In ( $\eta^6\text{-C}_6\text{H}_5\text{CO}_2\text{Me}$ )Cr(CO)<sub>2</sub>(CNBu<sup>t</sup>), the isonitrile ligand is bent, with a C-N-C angle of 166.8(4)°, similar to that of 168(1)° observed for ( $\eta^6\text{-C}_6\text{H}_5\text{CO}_2\text{Me}$ )Cr(CO)<sub>2</sub>(CNCO<sub>6</sub>H<sub>5</sub>)<sup>1,16</sup>. The CNBu<sup>t</sup> ligand bends outwards, away from the carbonyls, towards the CO<sub>2</sub>Me ring substituent. (see Fig. 8.2, ch. VIII).

#### 4.3 Unusual Structural Features of ( $\eta^6\text{-C}_6\text{H}_5\text{CO}_2\text{Me}$ )Cr(CO)<sub>2</sub>(CNBu<sup>t</sup>)

The structure of ( $\eta^6\text{-C}_6\text{H}_5\text{CO}_2\text{Me}$ )Cr(CO)<sub>2</sub>(CNBu<sup>t</sup>) has been discussed above in terms of its similarity to related ( $\eta^6\text{-C}_6\text{H}_5\text{CO}_2\text{Me}$ )Cr(CO)<sub>2</sub>L structures. However, the molecule possesses certain unusual features, which will be considered in more detail, and possible reasons for irregularities discussed.

##### 4.3.1 Staggered Conformation

On electronic grounds, an anti-eclipsed conformation would have been predicted, as is found for the complexes ( $\eta^6\text{-C}_6\text{H}_5\text{CO}_2\text{Me}$ )Cr(CO)<sub>2</sub>L (L = CO,<sup>10b</sup> CS,<sup>11</sup> CSe,<sup>12</sup> PPh<sub>3</sub><sup>11</sup>). The staggered conformation (Fig. 4.1) adopted by the ( $\eta^6\text{-C}_6\text{H}_5\text{CO}_2\text{Me}$ )Cr(CO)<sub>2</sub>(CNBu<sup>t</sup>) molecule is thus unexpected. However, from theoretical calculation, the energy barrier between the eclipsed and staggered conformation is not expected to be substantial.<sup>17,18</sup> It is unlikely that the movement from the eclipsed position originates from steric factors, since the PPh<sub>3</sub> ligand adopts the eclipsed geometry, and the steric bulk of the <sup>t</sup>BuNC group is expected to be less than that of the PPh<sub>3</sub> ligand.<sup>14</sup> Note, however, that the PPh<sub>3</sub> group eclipses the ortho position on the COMe side of the COOMe ring substituent, whereas the <sup>t</sup>BuNC ligand lies on the C=O side.

##### 4.3.2. Position of <sup>t</sup>BuNC vis-à-vis CO<sub>2</sub>Me

In ( $\eta^6\text{-C}_6\text{H}_5\text{CO}_2\text{Me}$ )Cr(CO)<sub>2</sub>(CNBu<sup>t</sup>), the CNBu<sup>t</sup> ligand is parallel to the CO<sub>2</sub>Me ring substituent (Fig. 4.1). In

contrast to the "off-anti-eclipsed" conformation of  $(\eta^6\text{-C}_6\text{H}_5\text{CO}_2\text{Me})\text{Cr}(\text{CO})_2(\text{PF}_3)$ , where the  $\text{PF}_3$  ligand has moved away from the  $\text{CO}_2\text{Me}$  group (angle between  $\text{Cr-PF}_3$  and  $\text{Cr-C}(\text{CO}_2\text{Me})$  projected on the plane of the arene ring is  $77.6^\circ$ ),<sup>14</sup> the  $\text{CNBu}^t$  ligand has moved towards the  $\text{CO}_2\text{Me}$  group (angle between  $\text{Cr-CNbu}^t$  and  $\text{Cr-C}(\text{CO}_2\text{Me})$  in projection is  $37.7^\circ$ ). In the other reported isonitrile derivative,  $(\eta^6\text{-C}_6\text{H}_5\text{CO}_2\text{Me})\text{Cr}(\text{CO})_2(\text{CNCOC}_6\text{H}_5)$ , the conformation is also staggered, but the  $\text{Cr}(\text{CO})_2$  tripod has a completely different orientation relative to the  $\text{C}_6\text{H}_5\text{CO}_2\text{Me}$  ring (Fig. 3.5), and the  $\text{CNCOC}_6\text{H}_5$  and  $\text{CO}_2\text{Me}$  groups are antiparallel.<sup>14</sup>

#### 4.3.3 Bending of the $\text{CNu}^t$ ligand

The  $\text{CNu}^t$  ligand bends out towards the  $\text{CO}_2\text{Me}$  ring substituent (see Fig. 8.2), with a  $\text{C-N}^t$  angle of  $166.8(4)^\circ$ . This aspect is discussed further in                      in relation to the anomalous IR data (ch. II) of the  $\text{Cr}(\text{CO})_2(\text{CNR})$  complexes.

#### 4.3.4 Intra- and Inter- molecular Interactions

It is possible that the molecular geometry observed (both the position of the  $\text{CNu}^t$  ligand relative to the ring, and the bending out of the  $\text{CNu}^t$  ligand towards the  $\text{CO}_2\text{Me}$  group) could be due to an interaction between O(2) and a H-atom of the  $\text{tBu}$  group. Although there are no exceptionally short non-bonding intermolecular distances, weak intramolecular (e.g.  $\text{O}(2)\dots\text{H}(8\text{A})$ ,  $2.55\text{\AA}$ ) and intermolecular (e.g.  $\text{O}(2)\dots\text{H}(10\text{C})$ ,  $2.75\text{\AA}$ ) interactions are possible. The unusual structural features observed may, however, be a consequence of purely packing considerations in the crystal.

### 4.4 Experimental

#### 4.4.1 Data collection

The complex  $(\eta^6\text{-C}_6\text{H}_5\text{CO}_2\text{Me})\text{Cr}(\text{CO})_2(\text{CNBu}^t)$  was prepared as described in ch. II. Red crystals were obtained by slow recrystallization from dichloromethane-hexane under nitrogen at  $15^\circ\text{C}$ . Despite the crystalline appearance in ordinary light, examination under polarized light characterized most



of the material as polycrystalline. Suitable single-crystal fragments of diffraction quality could be cut from the large specimens. Preliminary investigation was done by standard Weissenberg and precession photography. Refined cell constants were obtained during data collection on a Philips PW1100 four-circle diffractometer using graphite-monochromated MoK $\alpha$  radiation ( $\lambda = 0.7107 \text{ \AA}$ ) at room temperature (20°C). Lorentz and polarization corrections were applied, but no corrections for absorption were made as the linear absorption coefficient  $\mu$  was only  $3.50 \text{ cm}^{-1}$ . Crystal data and details of the structure analysis are summarized in Table 4.6.

#### 4.4.2 Structure Solution and Refinement

Structure analysis and refinements were carried out by using the program SHELX.<sup>44a</sup> Initial co-ordinates for the chromium atom were derived from a Patterson synthesis and difference Fourier syntheses yielded positions first for all 21 non-hydrogen atoms, and after least-squares refinement of these, also for the 17 hydrogen atoms. Positional parameters for all atoms and anisotropic temperature factors for non-hydrogen atoms were refined by full-matrix least-squares analyses. The hydrogen atoms were assigned a common isotropic temperature factor, which refined to the value of  $0.0784(27) \text{ \AA}^2$ . Least-squares refinement was considered complete when all parameter shifts were less than 0.5 $\sigma$ . At this stage the conventional R was 0.0418. Unit weights were used, and scattering factors for Cr<sup>3+</sup> were taken from "International Tables for X-ray Crystallography."<sup>45b</sup> Anomalous dispersion corrections<sup>46c</sup> for chromium were made. Fractional atomic co-ordinates, and anisotropic thermal parameters for the non-hydrogen atoms are listed in Tables 4.7 and 4.8 respectively. A listing of the Structure Factors is to be found in Appendix D.

TABLE 4.8: Crystal data and details of structural analysis for  
 $(\pi^6\text{C}_6\text{H}_5\text{CO}_2\text{Me})\text{Cr}(\text{CO})_2(\text{CNBu}^+)$

|                                |   |
|--------------------------------|---|
| Formula                        | $\text{CrC}_{15}\text{H}_{17}\text{NO}_4$ |
| Mr                             | 327.30                                    |
| Crystal dimensions (mm)        | 0.16 x 0.16 x 0.14                        |
| Space Group                    | $F\bar{1}$ (No 2)                         |
| a(Å)                           | 12.812(6)                                 |
| b(Å)                           | 9.314(5)                                  |
| c(Å)                           | 6.807(3)                                  |
| $\alpha$ (°)                   | 97.28(3)                                  |
| $\beta$ (°)                    | 87.94(3)                                  |
| $\gamma$ (°)                   | 106.02(3)                                 |
| U(Å <sup>3</sup> )             | 774.47                                    |
| Z                              | 2   |
| Dc(gcm <sup>-3</sup> )         | 1.44                                      |
| F(000)                         | 169.99                                    |
| $\mu$ (cm <sup>-1</sup> )      | 3.50                                      |
| $\lambda$ (Å)                  | MoK $\alpha$ (0.7107)                     |
| Scan mode                      | $\omega/2\theta$                          |
| Range (°)                      | 35 $\theta$ 523                           |
| Scan width (°)                 | 1.20                                      |
| Scan speed (°s <sup>-1</sup> ) | 0.04                                      |
| Range of hkl                   | $\pm h, \pm k, + l$                       |
| Measured intensities           | 2147                                      |
| Unique reflections             | 2115                                      |
| Internal consistency R-index   | 0.3358                                    |
| Omitted reflections            | -   |
| R (R = Rw)                     | 0.0418                                    |

TABLE 4.7: Fractional Atomic Co-ordinates for  $(\eta^6\text{-C}_6\text{H}_5\text{CO}_2\text{Me})\text{Cr}(\text{CO})_2^-$   
(CNBu<sup>t</sup>)

| Atom   | x/a        | y/b        | z/c        |
|--------|------------|------------|------------|
| Cr     | 0.3668(0)  | 0.2001(1)  | 0.4679(1)  |
| C(1)   | 0.2524(3)  | 0.1541(5)  | 0.2213(6)  |
| C(2)   | 0.2814(4)  | 0.0211(5)  | 0.2408(6)  |
| C(3)   | 0.3914(4)  | 0.0227(6)  | 0.2384(7)  |
| C(4)   | 0.4723(4)  | 0.1571(6)  | 0.2202(7)  |
| C(5)   | 0.4434(4)  | 0.2895(6)  | 0.1933(7)  |
| C(6)   | 0.3353(4)  | 0.2873(5)  | 0.1949(6)  |
| C(7)   | 0.1380(4)  | 0.1618(5)  | 0.2306(6)  |
| C(8)   | -0.0456(4) | 0.0259(7)  | 0.2639(9)  |
| C(9)   | 0.1778(3)  | 0.5196(5)  | 0.7383(6)  |
| C(10)  | 0.0615(4)  | 0.4223(7)  | 0.7540(10) |
| C(11)  | 0.1906(5)  | 0.6187(7)  | 0.5746(8)  |
| C(12)  | 0.2156(5)  | 0.6098(6)  | 0.9378(7)  |
| CO(1)  | 0.3224(3)  | 0.0703(4)  | 0.6535(5)  |
| CO(2)  | 0.4873(3)  | 0.2861(4)  | 0.6244(5)  |
| OC(1)  | 0.2965(2)  | -0.0132(3) | 0.7704(4)  |
| OC(2)  | 0.5619(2)  | 0.3369(3)  | 0.7267(4)  |
| O(1)   | 0.0678(2)  | 0.0274(4)  | 0.2513(5)  |
| O(2)   | 0.1105(3)  | 0.2741(4)  | 0.2218(5)  |
| CN     | 0.2926(3)  | 0.3380(5)  | 0.6081(6)  |
| NC     | 0.2450(3)  | 0.4180(4)  | 0.6863(6)  |
| H(2)   | 0.224 (3)  | -0.066 (5) | 0.270 (6)  |
| H(3)   | 0.408 (3)  | -0.071 (4) | 0.265 (5)  |
| H(4)   | 0.549 (3)  | 0.157 (4)  | 0.224 (6)  |
| H(5)   | 0.500 (3)  | 0.383 (4)  | 0.174 (6)  |
| H(6)   | 0.315 (3)  | 0.376 (4)  | 0.175 (5)  |
| H(8A)  | -0.065 (3) | 0.566 (4)  | 0.154 (6)  |
| H(8B)  | -0.060 (3) | 0.071 (4)  | 0.385 (6)  |
| H(8C)  | -0.088 (3) | -0.085 (5) | 0.224 (6)  |
| H(10A) | 0.019 (3)  | 0.495 (4)  | 0.777 (6)  |
| H(10B) | 0.040 (3)  | 0.372 (5)  | 0.627 (6)  |
| H(10C) | 0.054 (3)  | 0.358 (4)  | 0.876 (6)  |
| H(11A) | 0.144 (3)  | 0.687 (5)  | 0.599 (6)  |
| H(11B) | 0.165 (3)  | 0.557 (4)  | 0.451 (6)  |
| H(11C) | 0.263 (3)  | 0.676 (5)  | 0.563 (6)  |
| H(12A) | 0.205 (3)  | 0.544 (4)  | 1.046 (6)  |
| H(12B) | 0.177 (3)  | 0.685 (5)  | 0.959 (6)  |
| H(12C) | 0.289 (3)  | 0.663 (4)  | 0.936 (6)  |

TABLE 4.8: Anisotropic Thermal Parameters ( $\text{\AA}^2$ ) for the non-hydrogen<sup>a</sup> atoms of  $(\eta^5\text{C}_6\text{H}_5\text{CO}_2\text{Me})\text{Cr}(\text{CO})_2(\text{CNBu}^t)$

| Atom  | U11       | U22       | U33       | U23        | U13        | U12       |
|-------|-----------|-----------|-----------|------------|------------|-----------|
| Cr    | 0.0442(3) | 0.0421(3) | 0.0471(3) | -0.0027(2) | -0.0010(2) | 0.0203(2) |
| C(1)  | 0.059 (3) | 0.050 (3) | 0.037 (2) | -0.004 (2) | -0.002 (2) | 0.022 (2) |
| C(2)  | 0.070 (3) | 0.049 (3) | 0.045 (2) | -0.007 (2) | -0.004 (2) | 0.023 (2) |
| C(3)  | 0.083 (4) | 0.062 (3) | 0.057 (3) | -0.013 (2) | -0.002 (2) | 0.042 (3) |
| C(4)  | 0.063 (3) | 0.094 (4) | 0.060 (3) | 0.000 (3)  | 0.014 (2)  | 0.040 (3) |
| C(5)  | 0.064 (3) | 0.070 (3) | 0.060 (3) | 0.011 (2)  | 0.013 (2)  | 0.025 (3) |
| C(6)  | 0.066 (3) | 0.061 (3) | 0.045 (2) | 0.010 (2)  | 0.003 (2)  | 0.026 (2) |
| C(7)  | 0.061 (3) | 0.055 (3) | 0.037 (2) | 0.004 (2)  | 0.008 (2)  | 0.017 (2) |
| C(8)  | 0.061 (3) | 0.088 (4) | 0.071 (4) | -0.006 (3) | -0.008 (3) | 0.016 (3) |
| C(9)  | 0.049 (2) | 0.050 (2) | 0.055 (3) | -0.009 (2) | -0.003 (2) | 0.027 (2) |
| C(10) | 0.055 (3) | 0.084 (4) | 0.086 (4) | -0.013 (3) | -0.001 (3) | 0.021 (3) |
| C(11) | 0.096 (4) | 0.073 (4) | 0.069 (3) | 0.002 (3)  | -0.007 (3) | 0.040 (3) |
| C(12) | 0.068 (3) | 0.071 (3) | 0.060 (3) | -0.015 (3) | -0.007 (3) | 0.027 (3) |
| CO(1) | 0.049 (2) | 0.048 (2) | 0.050 (2) | -0.009 (2) | -0.011 (2) | 0.018 (2) |
| CO(2) | 0.053 (2) | 0.049 (2) | 0.062 (2) | 0.001 (2)  | -0.001 (2) | 0.021 (2) |
| OG(1) | 0.088 (2) | 0.066 (2) | 0.062 (2) | 0.015 (1)  | -0.002 (1) | 0.016 (2) |
| OG(2) | 0.081 (2) | 0.065 (2) | 0.065 (2) | -0.003 (2) | -0.026 (2) | 0.011 (1) |
| O(1)  | 0.056 (2) | 0.065 (2) | 0.066 (2) | 0.001 (2)  | -0.004 (2) | 0.016 (2) |
| O(2)  | 0.067 (2) | 0.060 (2) | 0.093 (3) | 0.004 (2)  | -0.015 (2) | 0.030 (2) |
| CN    | 0.046 (2) | 0.053 (3) | 0.049 (2) | 0.001 (2)  | -0.005 (2) | 0.018 (2) |
| NC    | 0.060 (2) | 0.063 (2) | 0.063 (2) | -0.010 (2) | -0.002 (2) | 0.036 (2) |

<sup>a</sup> The hydrogen atoms were assigned a common isotropic temperature factor, which refined to the value of  $0.0784(27)\text{\AA}^2$ .

V. CATALYTIC SYNTHESIS AND CHARACTERIZATION OF ISONITRILE  
DERIVATIVES OF  $(\eta^5\text{-C}_5\text{H}_5)_2\text{Mn}(\text{CO})_3$

5.1 Introduction

Direct displacement of CO in  $(\eta^5\text{-C}_5\text{H}_5)_2\text{Mn}(\text{CO})_3$  by donor ligands L to give  $(\eta^5\text{-C}_5\text{H}_5)_2\text{Mn}(\text{CO})_2\text{L}$  is extremely difficult to achieve by thermal means.<sup>17</sup> Consequently the synthetic routes presently available to synthesize  $(\eta^5\text{-C}_5\text{H}_5)_2\text{Mn}(\text{CO})_2\text{L}$  complexes employ photochemical<sup>18</sup> or  $\text{Me}_3\text{NO}$  induced<sup>19</sup> techniques.

With isonitrile ligands (L = RNC), preparation of  $(\eta^5\text{-C}_5\text{H}_5)_2\text{Mn}(\text{CO})_2(\text{CNR})$  derivatives has involved photochemical methods. Irradiation of  $(\eta^5\text{-C}_5\text{H}_5)_2\text{Mn}(\text{CO})_3$  in the presence of THF (tetrahydrofuran) or KCN yields  $(\eta^5\text{-C}_5\text{H}_5)_2\text{Mn}(\text{CO})_2(\text{THF})$ <sup>18</sup> or  $\text{K}^+[(\eta^5\text{-C}_5\text{H}_5)_2\text{Mn}(\text{CO})_2\text{CN}]^-$ <sup>20a</sup>, which on reaction with RNC<sup>18,21</sup> or  $\text{RX}$  (X = I, Cl, Br)<sup>18b,c,22,23</sup> yields the desired product  $(\eta^5\text{-C}_5\text{H}_5)_2\text{Mn}(\text{CO})_2(\text{CNR})$ .  $(\eta^5\text{-C}_5\text{H}_5)_2\text{Mn}(\text{CO})_2(\text{CNBu}^t)$  has also been obtained from the photolysis of  $(\eta^5\text{-C}_5\text{H}_5)_2\text{Mn}(\text{CO})_2[\text{CPh}_2]$  and  $^t\text{BuNC}$  in THF solution.<sup>21</sup> To date, isolation of the apparently unstable  $(\eta^5\text{-C}_5\text{H}_5)_2\text{Mn}(\text{CO})_2(\text{CNR})$  derivatives has not been achieved.<sup>16</sup> Tri-substituted derivatives,  $(\eta^5\text{-C}_5\text{H}_5)_2\text{Mn}(\text{CNR})_3$ , have also been reported, and have been synthesized either by irradiation of  $(\eta^5\text{-C}_5\text{H}_5)_2\text{Mn}(\text{CO})_3$  and RNC in THF,<sup>22</sup> or from  $[\text{Mn}(\text{CNC}_6\text{H}_5)_3]\text{I}$  and  $\text{Na}[\text{C}_5\text{H}_5]$ .<sup>24</sup>

The complex,  $(\eta^5\text{-C}_5\text{H}_4\text{Me})\text{Mn}(\text{CO})_2(\text{CNBu}^t)$  has been catalytically synthesized by electrochemical techniques.<sup>25</sup> However, this reaction involves the displacement of acetonitrile (and not CO) from  $(\eta^5\text{-C}_5\text{H}_4\text{Me})\text{Mn}(\text{CO})_2(\text{NCMe})$  by  $\text{Bu}^t\text{NC}$ , and consequently still necessitates the use of photochemical, or  $\text{Me}_3\text{NO}$ -induced techniques in the synthesis of the acetonitrile derivative. To date no thermal displacement reactions of CO or  $(\eta^5\text{-C}_5\text{H}_5)_2\text{Mn}(\text{CO})_3$  by isonitriles have been reported.

Since PdO has been found to be an effective catalyst for the direct displacement of CO by RNC on several metal carbonyl complexes,<sup>26,26</sup> the thermal reaction between  $(\eta^5\text{-C}_5\text{H}_5)_2\text{Mn}(\text{CO})_3$  and a variety of RNC ligands, with PdO as catalyst, was investigated.

## 5.2 Results and discussion

### 5.2.1 PdO catalysed reaction of $(\eta^5\text{-C}_5\text{H}_5)\text{Mn}(\text{CO})_3$ with isonitriles

PdO was found to be an effective, though not highly active catalyst for the reaction of  $(\eta^5\text{-C}_5\text{H}_5)\text{Mn}(\text{CO})_3$  with isonitrile ligands (RNC), allowing for the synthesis, under moderate thermal reaction conditions, of a series of  $(\eta^5\text{-C}_5\text{H}_5)\text{Mn}(\text{CO})_2(\text{CNR})$  substituted complexes. Product yields varied from poor (MeNC) to excellent ( $\text{C}_6\text{H}_{11}\text{NC}$ ) (Table 5.1). By contrast, the thermal uncatalysed reaction did not proceed under the identical experimental conditions.

Since the catalyst mixture  $[(\eta^5\text{-C}_5\text{H}_5)\text{Fe}(\text{CO})_2]_2/\text{PdO}$  was found to catalyse related substitution reactions between isonitriles and metal carbonyl complexes,<sup>44</sup> and was applied successfully to the reaction between  $(\eta^5\text{-Arene})\text{Cr}(\text{CO})_3$  and RNC (see ch II), the catalytic potential of an iron dimer-PdO mixture was investigated for the reaction of  $(\eta^5\text{-C}_5\text{H}_5)\text{Mn}(\text{CO})_3$  with  $\text{tBuNC}$ . However, it was found that the reaction rates observed either for the use of a catalyst mixture (iron dimer/PdO) or for PdO alone (equal amounts of Pd in both reactions) are the same.

The PdO-catalysed synthetic route can be extended to related systems. For example, the reaction between  $(\eta^5\text{-C}_5\text{H}_5)\text{V}(\text{CO})_4$  and  $\text{tBuNC}$  in toluene in the presence of PdO (110°C, 4 h) yielded a yellow product identified as  $(\eta^5\text{-C}_5\text{H}_5)\text{V}(\text{CO})_3(\text{CNBu}^t)$  [IR(hexane),  $\nu(\text{NC})$ : 2100(w),  $\nu(\text{CO})$ : 1970(s), 1904 (sh,sp), 1892 (vs)  $\text{cm}^{-1}$ ] by comparison with the IR spectra of  $(\eta^5\text{-C}_5\text{H}_5)\text{V}(\text{CO})_3(\text{PR}_3)$  complexes.<sup>57</sup> The thermal reaction in the absence of PdO (110°C, 4 h) gave only recovered starting material,  $(\eta^5\text{-C}_5\text{H}_5)\text{V}(\text{CO})_4$ .

### 5.2.2 Characterization of $(\eta^5\text{-C}_5\text{H}_5)\text{Mn}(\text{CO})_2(\text{CNR})$ products

The isonitrile complexes  $(\eta^5\text{-C}_5\text{H}_5)\text{Mn}(\text{CO})_2(\text{CNR})$  have been fully characterized by IR and NMR spectroscopy. (Table 5.2).

#### (a) Infra Red

The IR spectra of  $(\eta^5\text{-C}_5\text{H}_5)\text{Mn}(\text{CO})_2(\text{CNR})$  complexes are expected to show two  $\nu(\text{CO})$  and one  $\nu(\text{NC})$  stretching vibration.

This has been observed previously for  $RNC = MeNC^{13}$  and  $CNCOPh^{13b,c}$ , and was also observed for the complexes with  $RNC = C_6H_5CH_2NC$ ,  $\sigma,6-Me_2C_6H_3NC$ , and  $MeNC$  prepared in this study. However, for  $RNC = Bu^tNC$  and  $C_6H_{11}NC$ , two  $\nu(NC)$  (and two  $\nu(CO)$ ) vibrations were observed in both the solid state and solution. This phenomenon of observing more IR active  $\nu(NC)$  bands than expected has also been detected in a series of  $(\eta^5\text{Arene})Cr(CO)_2(CNBu^t)$  complexes (see ch II), and will be discussed in ch VIII.

(b) Proton Nuclear Magnetic Resonance

The  $^1H$  NMR spectra of the  $(\eta^5\text{C}_5\text{H}_5)\text{Mn(CO)}_2(\text{CNR})$  complexes (Table 5.2) are as expected, and show no unusual features.

(c) Mass spectrum of  $(\eta^5\text{C}_5\text{H}_5)\text{Mn(CO)}_2(\text{CNBu}^t)$

The fragmentation pattern of the complex  $(\eta^5\text{C}_5\text{H}_5)\text{Mn(CO)}_2(\text{CNBu}^t)$  is shown in Fig. 5.1, together with peak intensities. Loss of the CO ligands precedes loss of the  $CNBu^t$ , and the  $Bu^t$  fragment is lost before the CN linkage.<sup>17</sup> The cyclopentadienyl ring is lost last. Such a fragmentation pattern is typical of half-sandwich metal carbonyl complexes, and has been observed for other  $(\eta^5\text{C}_5\text{H}_5)\text{Mn(CO)}_2(\text{CNR})$  complexes.<sup>18</sup>

5.3 Experimental-preparation of  $(\eta^5\text{C}_5\text{H}_5)\text{Mn(CO)}_2(\text{CNR})$ , (R =  $Bu^t$ ,  $C_6H_5CH_2$ ,  $C_6H_{11}$ ,  $C_6H_3Me_2-2,6,Me$ )

$(\eta^5\text{C}_5\text{H}_5)\text{Mn(CO)}_3$  (2 mmol) and PdO (30 mg) were added to toluene (10 ml) and the solution heated to reflux (110°C). The appropriate RNC (5 mmol) was then added to the reaction vessel, and the reaction monitored by TLC (Silica; eluent: hexane, or hexane/ $CH_2Cl_2$  (10%)). The reaction was allowed to proceed for 6 h (except in the case R = Me, where the reaction time was 24 h), after which heating was stopped and the product isolated by column chromatography. (Silica, 2cm x 40 cm column). Gradient elution, starting with hexane (to remove unreacted starting material) and gradually increasing the proportion of  $CH_2Cl_2$  to 50% in a  $CH_2Cl_2$ /hexane mixture, was employed. Recrystallization from  $CH_2Cl_2$ /hexane gave the desired products as yellow solids (Table 5.1).

TABLE 5.1: Analytical data for the  $(\eta^5\text{-C}_5\text{H}_5)\text{Mn}(\text{CO})_2(\text{CNR})$  complexes

| Complex   | Isolated yield(%) <sup>a</sup> | M.p.(°C) | Elemental Analysis<br>(Found Calcd.)(%) |          |          |
|---|--------------------------------|----------|---|----------|----------|
|   |                                |          | C                                       | H        | N        |
| $(\eta^5\text{-C}_5\text{H}_5)\text{Mn}(\text{CO})_2(\text{CNBu}^t)$                                | 60                             | 95-96    | 55.6(56.0)                              | 5.4(5.5) | 5.4(5.4) |
| $(\eta^5\text{-C}_5\text{H}_5)\text{Mn}(\text{CO})_2(\text{CNCH}_2\text{C}_6\text{H}_5)$            | 70                             | 51-52    | 61.4(61.4)                              | 4.2(4.1) | 4.8(4.8) |
| $(\eta^5\text{-C}_5\text{H}_5)\text{Mn}(\text{CO})_2(\text{CNC}_6\text{H}_{11})$                    | 95                             | 68-69    | 58.7(58.9)                              | 5.7(5.7) | 4.9(4.9) |
| $(\eta^5\text{-C}_5\text{H}_5)\text{Mn}(\text{CO})_2(\text{CNC}_6\text{H}_3\text{Me}_2\text{-2,6})$ | 15                             | 79-80    | 61.1(62.5)                              | 4.6(4.6) | 4.3(4.6) |
| $(\eta^5\text{-C}_5\text{H}_5)\text{Mn}(\text{CO})_2(\text{CNMe})$                                  | 5 <sup>b</sup>                 | 90-93    | 49.1(49.8)                              | 3.9(3.7) | 5.9(6.5) |

<sup>a</sup> After 6 h .

<sup>b</sup> After 24 h.



TABLE 5.2: Spectroscopic data for the  $(\eta^5\text{-C}_5\text{H}_5)_2\text{Mn}(\text{CO})_2(\text{CNR})_2$  complexes

| Complex  | IR ( $\text{cm}^{-1}$ ) <sup>a</sup> |                         | $\text{C}_5\text{H}_5$ | <sup>1</sup> H NMR (ppm) <sup>b</sup> |                        | $\text{C}_n$ |
|--|--------------------------------------|-------------------------|------------------------|---------------------------------------|------------------------|--------------|
|  | $\nu(\text{NC})$                     | $\nu(\text{CO})$        |                        | $\text{C}_6\text{H}_n$                | $\text{C}_6\text{H}_n$ |              |
| $(\eta^5\text{-C}_5\text{H}_5)_2\text{Mn}(\text{CO})_2(\text{CNBu}^t)$                       | 2114, 2078                           | 1952, 1907 <sup>c</sup> | 4.25                   | -                                     | 0.94                   |              |
| $(\eta^5\text{-C}_5\text{H}_5)_2\text{Mn}(\text{CO})_2(\text{CNCH}_2\text{C}_6\text{H}_5)$   | 2112                                 | 1957, 1911              | 4.23                   | 7.01, 6.99                            | 3.92                   |              |
| $(\eta^5\text{-C}_5\text{H}_5)_2\text{Mn}(\text{CO})_2(\text{CNC}_6\text{H}_{11})$           | 2104, 2070(sh)                       | 1954, 1907              | 4.27                   | 1.29, 1.02                            | -                      |              |
| $(\eta^5\text{-C}_5\text{H}_5)_2\text{Mn}(\text{CO})_2(\text{CNC}_6\text{H}_4\text{Me}-2,6)$ | 2080                                 | 1954, 1916              | 4.27                   | 6.71                                  | 2.14                   |              |
| $(\eta^5\text{-C}_5\text{H}_5)_2\text{Mn}(\text{CO})_2(\text{CNMe})$                         | 2130                                 | 1958, 1907              | 4.22                   | -                                     | 2.12                   |              |

<sup>a</sup> Recorded in hexane

<sup>b</sup> Recorded in  $\text{C}_6\text{D}_6$  relative to TMS.

<sup>c</sup> XBr,  $\nu(\text{NC})$  2118,  $\nu(\text{CO})$  1971, 1926  $\text{cm}^{-1}$

<sup>d</sup> sh = shoulder

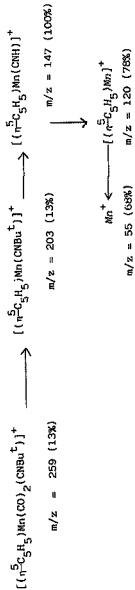


Figure 5.1 Fragmentation pattern for  $(\eta^5\text{-C}_5\text{H}_5)\text{Mn}(\text{CO})_2(\text{CNBu}^t)$

VI. THE MODIFICATION OF  $(\eta^5\text{-C}_5\text{H}_5)\text{Mn}(\text{CO})_3$  BY LIGANDS L

6.1 Introduction

Considerable interest has been focussed on the half-sandwich metal carbonyl complex,  $(\eta^5\text{-C}_5\text{H}_5)\text{Mn}(\text{CO})_3$ , owing to the exceptional stabilizing capacity of  $(\eta^5\text{-C}_5\text{H}_5)\text{Mn}(\text{CO})_2$  moiety.<sup>17</sup> This has been exploited in the capture and display of ligands L. Complexes of the type  $(\eta^5\text{-C}_5\text{H}_5)\text{Mn}(\text{CO})_2\text{L}$  have been detected, isolated and unequivocally characterized, by techniques including X-ray crystallography, for a wide range of exotic and unstable ligands L.

Some twenty  $(\eta^5\text{-C}_5\text{H}_5)\text{Mn}(\text{CO})_2\text{L}$  complexes have been studied by X-ray crystallography.<sup>11-14</sup> In most cases, the  $(\eta^5\text{-C}_5\text{H}_5)\text{Mn}(\text{CO})_2$  moiety has been used to anchor and display the ligand L, often a carbene, L itself being of prime concern in the structural study, and the geometry around the Mn-atom itself of secondary interest.

However, the substitution in  $(\eta^5\text{-C}_5\text{H}_5)\text{Mn}(\text{CO})_3$  of a CO for a ligand L, can result in structural modifications in the resulting  $(\eta^5\text{-C}_5\text{H}_5)\text{Mn}(\text{CO})_2\text{L}$  complex, compared to the parent carbonyl,  $(\eta^5\text{-C}_5\text{H}_5)\text{Mn}(\text{CO})_3$ . The structure of  $(\eta^5\text{-C}_5\text{H}_5)\text{Mn}(\text{CO})_3$  will be discussed in detail, and the structural effect of ligand substitution examined by considering the  $(\eta^5\text{-C}_5\text{H}_5)\text{Mn}(\text{CO})_2\text{L}$  complexes for which X-ray crystal and molecular structures have been reported. Structural trends, and notable exceptions, will be rationalized in terms of electronic and steric factors.

6.2 The Structure of  $(\eta^5\text{-C}_5\text{H}_5)\text{Mn}(\text{CO})_3$

The crystal and molecular structure of  $(\eta^5\text{-C}_5\text{H}_5)\text{Mn}(\text{CO})_3$  was first determined by Berndt and Marsh in 1963.<sup>18a</sup> (R value of 9%), and in 1981 redetermined by Fitzpatrick, Le Page, Sedman and Butler<sup>18b</sup>. (R value of 2.66%), improving the accuracy of bond parameter data.

6.2.1 Ligand geometry and conformation

The molecule has the typical "piano-stool" geometry, with the OC-Mn-CO angles being equal within experimental error (av. 92.02(9)<sup>18b</sup>).

### 6.2.2 Conformation

The ( $C_5H_5$ ) ring-(CO)<sub>3</sub> tripod conformation is shown in Fig. 6.1. Two ring C-atoms (C3 and C5) are eclipsed by two carbonyls (C12 and C13 respectively), while the third CO ligand (C11) eclipses the C1-C2 bond of the ring. The deviations from the fully eclipsed structure destroy possible mirror (m) symmetry of the ( $\eta^5-C_5H_5$ )Mn(CO)<sub>3</sub> molecule.<sup>a,b</sup>

### 6.2.3 Mn-C-ring and Mn-CO bond lengths

The av. values for the Mn-C-ring and Mn-CO bond lengths are 2.124(2) and 1.780(2)Å respectively. The distance between the Mn atom and the centre of gravity of the cyclopentadiene ring, Mn-Cp, is 1.765Å.<sup>a,b</sup>

### 6.2.4 Ring planarity and C-C bond lengths

The ( $C_5H_5$ ) ring is essentially planar. A notable feature of the ( $C_5H_5$ ) ring is the non-equivalence of the C-C bonds (see Fig 6.2). This breakdown of the 5-fold ring symmetry in the crystal is indicative of some degree of C-C bond localization. There does not appear to be a correlation between the ring C-C bond lengths and the ring-tripod ligand arrangement, as found for ( $\eta^5-C_6H_6$ )Cr(CO)<sub>3</sub> (see section 3.2.4.)

### 6.2.5 Mn-C-O bond angles

The av. Mn-C-O bond angle is 178.9(2)°.<sup>a,b</sup> Near linearity of M-C-O bonds is predicted for M(CO)<sub>n</sub> (n = 2,3) groups.<sup>a</sup> (see section 3.2.6)

### 6.2.6 Packing considerations

The compound crystallizes in the monoclinic centrosymmetric space group P2<sub>1</sub>/a, with Z = 4. In general the packing is rather loose,<sup>a</sup> with the shortest non-hydrogen intermolecular contact involving the cyclopentadienyl ring being 3.407Å.<sup>a,b</sup>

However, the orientation of the ring with respect to the carbonyl groups is probably determined largely by crystal packing forces, since the intrinsic electronic barrier to rotation of the ring about the molecular axis

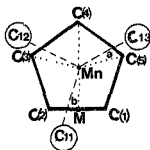


Figure 6.1 Conformation of  $(\eta^5\text{-C}_5\text{H}_5)\text{Mn}(\text{CO})_3$ , looking down onto the  $(\text{C}_5\text{H}_5)$  ring. (CO C-atoms are circled; M is the midpoint of the C(1)-C(2) bond.) Angles of eclipse, a and b are 7.25 and 5.93° respectively.<sup>a,b</sup>

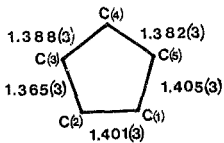


Figure 6.2 Ring C-C bond lengths (Å) in  $(\eta^5\text{-C}_5\text{H}_5)\text{Mn}(\text{CO})_3$ .<sup>a,b</sup>

in  $(\eta^5\text{-C}_5\text{H}_5)\text{Mn}(\text{CO})_3$  is estimated to be very small (ca. 0.008  $\text{kJ mol}^{-1}$ ).<sup>11</sup> Potential energy calculations<sup>12</sup> have shown that the barrier to ring rotation in the solid phase of 7.24  $\text{kJ mol}^{-1}$  is due to non-bonded intermolecular C...H and O...H interactions. (eg. O...H distances of 2.48 to 3.08 Å).<sup>13a</sup>

Crystal packing forces could also be responsible for minor deviations from ideal geometry observed.

### 6.3 X-ray Crystallographic Studies of $(\eta^5\text{-C}_5\text{H}_5)\text{Mn}(\text{CO})_2\text{L}$ complexes

The  $(\eta^5\text{-C}_5\text{H}_5)\text{Mn}(\text{CO})_2\text{L}$  complexes for which X-ray crystal and molecular structures have been reported in the literature are listed in Table 6.1. The principal geometric characteristics of the  $(\eta^5\text{-C}_5\text{H}_5)\text{Mn}(\text{CO})_2\text{L}$  structures are given in Table 6.2. Trends and special features will be discussed.

#### 6.3.1. OC-Mn-CO and OC-Mn-L angles

Although the  $(\eta^5\text{-C}_5\text{H}_5)\text{Mn}(\text{CO})_2\text{L}$  complexes all adopt the "piano-stool" arrangement of ligands, in general the av. OC-Mn-L angle is greater than the OC-Mn-CO angle. The reverse is expected if L is a better  $\pi$ -acceptor than CO.<sup>14</sup> However, in most cases L is a vinylidene, carbene or  $\eta^2$  olefinic ligand.

Since  $\text{PR}_3$  is a poorer  $\pi$ -acceptor than CO,<sup>15a</sup> the smaller av. CO-Mn-P (91.6(3)°) than OC-Mn-CO (92.4(4)°) angle seems anomalous. However, the CO-Mn-P angles are 92.7(3) and 90.5(3)°.<sup>12</sup> The difference could be due to steric repulsions between the bulky  $\text{PPh}_3$  group (Tolman cone angle 145°)<sup>13</sup> or crystal packing forces. Hence caution must be exercised in interpreting small bond parameter deviations in terms of electronic effects.

#### 6.3.2 Molecular Conformation

In  $(\eta^5\text{-C}_5\text{H}_5)\text{Mn}(\text{CO})_3$ , one CO ligand eclipses a C-C bond of the  $(\text{C}_5\text{H}_5)$  ring, while the other two carbonyls eclipse ring C-atoms. For  $(\eta^5\text{-C}_5\text{H}_5)\text{Mn}(\text{CO})_2\text{L}$ , the ligand L may eclipse a C-C bond or a C-atom of the  $(\text{C}_5\text{H}_5)$  ring. In the cases L =  $\text{SO}_2$ ,<sup>11</sup>  $\text{PPh}_3$ ,<sup>12</sup>  $\text{N}_2\text{C}(\text{CO}_2\text{Me})_2$ ,<sup>16</sup>  $\eta^2\text{-C}_5\text{H}_6$ ,<sup>17</sup> L eclipses a ring C-atom, but for all the

other structures of Table 6.1 (excluding  $(\eta^5\text{-C}_5\text{H}_5)\text{Mn}(\text{CO})_2$  [ $\text{PPh}_2(\text{OC}(\text{Me})(\text{CHC}(\text{O})\text{Me}))$ ], where the  $(\text{C}_5\text{H}_5)$  ring is disordered<sup>43</sup>), L eclipses a ring C-C bond. Hence it appears that in general with vinylidene, carbene and  $\eta^2$ -olefinic ligands L, L eclipses a ring C-C bond, and with ligands such as  $\text{L} = \text{PPh}_3$ , L eclipses a ring C-atom. Note also that in  $(\eta^5\text{-C}_5\text{H}_5)\text{Mn}(\text{CO})(\text{PPh}_3)_2$ ,<sup>44</sup> both  $\text{PPh}_3$  ligands, and the CO, near-eclipse ring C-atoms. This phenomenon could possibly have an electronic basis. MO calculation of  $(\eta^5\text{-C}_5\text{H}_5)\text{Mn}(\text{CO})_2\text{L}$  complexes for different ligand types L, might provide information on the electronically most favourable conformation. However, crystal packing forces probably also play a role in determining molecular conformation, especially as the barrier to rotation in complexes of the type  $(\eta^5\text{-C}_5\text{H}_5)\text{Mn}(\text{CO})_2\text{L}$  is predicted to be small.<sup>45</sup>

### 6.3.3. Mn-C ring and Mn-CO bond lengths

For the  $(\eta^5\text{-C}_5\text{H}_5)\text{Mn}(\text{CO})_2\text{L}$  structures, the Mn-C-ring bond distances are generally in the range 2.12 to 2.18 Å, cf. av. Mn-C-ring of 2.124(2) Å for  $(\eta^5\text{-C}_5\text{H}_5)\text{Mn}(\text{CO})_3$ .<sup>46b</sup> A notable exception is  $\text{L} = \text{SO}_2$ <sup>41</sup> (av. Mn-C-ring 2.090(2) Å). Possibly this could reflect a weaker bonding of the  $\text{SO}_2$  ligand to Mn, compensated for by increased Mn-Ring bonding. A weaker bonding of the  $\text{SO}_2$  ligand could possibly account for the reported instability of the  $(\eta^5\text{-C}_5\text{H}_5)\text{Mn}(\text{CO})_2(\text{SO}_2)$  complex,<sup>41</sup> which has also been ascribed to steric crowding of the  $\text{SO}_2$  and CO ligands.<sup>41</sup>

The Mn-CO bond lengths are generally 1.74 to 1.80 Å, comparable to the av. Mn-CO bond length of 1.780(2) Å for the parent complex,  $(\eta^5\text{-C}_5\text{H}_5)\text{Mn}(\text{CO})_3$ .<sup>46b</sup> For ligands such as  $\text{PPh}_3$ , which is a weaker  $\pi$ -acceptor than CO,<sup>46a</sup> a decrease in Mn-CO bond length relative to  $(\eta^5\text{-C}_5\text{H}_5)\text{Mn}(\text{CO})_3$  would be expected. This is indeed observed (av. Mn-CO bond lengths of 1.75(2) Å and 1.780(2) Å respectively for  $(\eta^5\text{-C}_5\text{H}_5)\text{Mn}(\text{CO})_2(\text{PPh}_3)$ <sup>42</sup> and  $(\eta^5\text{-C}_5\text{H}_5)\text{Mn}(\text{CO})_3$ <sup>46b</sup>). Further, the Mn-CO bond length in  $(\eta^5\text{-C}_5\text{H}_5)\text{Mn}(\text{CO})(\text{PPh}_3)_2$  is 1.748(9) Å.<sup>44</sup>

### 6.3.4 Ring C-C bond lengths

The ring C-C bond lengths for the  $(\eta^5\text{-C}_5\text{H}_5)\text{Mn}(\text{CO})_2\text{L}$

TABLE 6.1: X-ray Crystal Structures of  $(\eta^5\text{-C}_5\text{H}_5)\text{Mn}(\text{CO})_2\text{L}$  complexes

| Complex   | Space Group Z                      | Reference        |
|---|------------------------------------|------------------|
| $(\eta^5\text{-C}_5\text{H}_5)\text{Mn}(\text{CO})_3$   | $P2_1/a$ , 4                       | 59               |
| $(\eta^5\text{-C}_5\text{H}_5)\text{Mn}(\text{CO})_2(\text{SO})_2$  | $P2_1/c$ , 4                       | 51               |
| $(\eta^5\text{-C}_5\text{H}_5)\text{Mn}(\text{CO})_2(\text{PPh}_3)$   | $P\bar{1}$ , 2                     | 52               |
| $(\eta^5\text{-C}_5\text{H}_5)\text{Mn}(\text{CO})_2[\text{PPh}_2\{\text{OC}(\text{Me})\{\text{CHC}(\text{O})\text{Me}\}}]$         | $P\bar{1}$ , 2                     | 53               |
| $(\eta^5\text{-C}_5\text{H}_5)\text{Mn}(\text{CO})_2[\text{PhP}\{\text{OC}(\text{CH}_2)\text{CHC}(\text{Me})\text{O}\}]^{\text{a}}$ | $P2_1/c$ , 4                       | 54               |
| $(\eta^5\text{-C}_5\text{H}_5)\text{Mn}(\text{CO})_2[\text{C}(\text{O})\text{Ph}]^+[\text{NMe}_4]^+$                                | $\text{Ib}2a$ , 16 <sup>b</sup>    | 55               |
| $(\eta^5\text{-C}_5\text{H}_5)\text{Mn}(\text{CO})_2[\text{N}_2\text{C}(\text{CO}_2\text{Me})_2]$                                   | $P2_1/n$ , 4                       | 56               |
| $(\eta^5\text{-C}_5\text{H}_5)\text{Mn}(\text{CO})_2[\text{SC}(\text{C}_6\text{H}_5(\text{Me}_2)_2)^{-2,6}]$                        | $P2_1/n$ , 4                       | 57               |
| $(\eta^5\text{-C}_5\text{H}_5)\text{Mn}(\text{CO})_2[\text{C}_2\text{C}(\text{C}_6\text{H}_{11})_2]$                                | $P2_1/c$ , 4                       | 58               |
| $(\eta^5\text{-C}_5\text{H}_5)\text{Mn}(\text{CO})_2(\text{CCMe}_2)$  | $\text{Pr}ma$ , 4 <sup>c</sup>     | 59               |
| $(\eta^5\text{-C}_5\text{H}_5)\text{Mn}(\text{CO})_2(\text{CCHPh})$   | $\text{Pccn}$ , 8                  | 70               |
| $(\eta^5\text{-C}_5\text{H}_5)\text{Mn}(\text{CO})_2(\text{CMe}_2)$   | $\text{Cmc}2_1$ , 8 <sup>c,d</sup> | 71               |
| $(\eta^5\text{-C}_5\text{H}_5)\text{Mn}(\text{CO})_2(\text{CPh}_2)$   | <sup>e</sup>                       | 37 <sup>f</sup>  |
| $(\eta^5\text{-C}_5\text{H}_5)\text{Mn}(\text{CO})_2(\text{CFPh})$  | $P2_1/c$ , 4                       | 72               |
| $(\eta^5\text{-C}_5\text{H}_5)\text{Mn}(\text{CO})_2[\text{C}(\text{OEt})\text{Ph}]$  | $P2_1/c$ , 4                       | 73               |
| $(\eta^5\text{-C}_5\text{H}_5)\text{Mn}(\text{CO})_2[\text{C}(\text{Ph})\{\text{C}(\text{O})\text{Ph}\}]^{\text{g}}$                | $P2_1/n$ , 4                       | 74               |
| $(\eta^5\text{-C}_5\text{H}_5)\text{Mn}(\text{CO})_2[\text{C}(\text{OMe})\{\text{C}_6\text{H}_5\{\text{CHMe}_2\}(\text{Me})-2,5\}]$ | $P2_1$ , 2                         | 75               |
| $(\eta^5\text{-C}_5\text{H}_5)\text{Mn}(\text{CO})_2[\text{C}(\text{CO}_2\text{Me})\text{CHPPH}_3]$                                 | $P2_1/a$ , 4                       | 76               |
| $[(\eta^5\text{-C}_5\text{H}_5)\text{Mn}(\text{CO})_2(\text{CPh})]_2\text{O}$   | $P2_1/c$ , 4                       | 77               |
| $(\eta^5\text{-C}_5\text{H}_5)\text{Mn}(\text{CO})_2[\eta^2\text{C}(\text{O})\text{CPh}_2]$   | $P2_1/c$ , 4                       | 78               |
| $(\eta^5\text{-C}_5\text{H}_5)\text{Mn}(\text{CO})_2[\eta^2\text{CH}_2\text{CHC}(\text{O})\text{Me}]$                               | $P2_12_12_1$ , 4                   | 79               |
| $(\eta^5\text{-C}_5\text{H}_5)\text{Mn}(\text{CO})_2[\eta^2\text{CH}_2\text{CPhCO}_2\text{Me}]$                                     | $P2_1/a$ , 8 <sup>b</sup>          | 80               |
| $(\eta^5\text{-C}_5\text{H}_5)\text{Mn}(\text{CO})_2[\eta^2\text{CHPhCHP}(\text{O})\{\text{OEt}\}_2]$                               | $P\bar{1}$ , 4 <sup>b</sup>        | 81               |
| $(\eta^5\text{-C}_5\text{H}_5)\text{Mn}(\text{CO})_2(\eta^2\text{C}_6\text{H}_5)$   | $P2_1/c$ , 4                       | 82               |
| $(\eta^5\text{-C}_5\text{H}_5)\text{Mn}(\text{CO})_2(\eta^2\text{C}_6\text{H}_5)$   | $P2_1/n$ , 2 <sup>c</sup>          | 83a              |
|   | $\text{Pr}ma$ , 4 <sup>c</sup>     | 83b <sup>h</sup> |
| $[(\eta^5\text{-C}_5\text{H}_5)\text{Mn}(\text{CO})_2]_2(\text{C}_5\text{H}_5)$   | $P2_1/c$ , 4                       | 84               |

- a Dienediolate group disordered  
b 2 crystallographically independent molecules in the asymmetric unit  
c Molecule possesses crystallographic m symmetry  
d 2 crystallographically independent half-molecules in the asymmetric unit  
e Unpublished structure  
f Ref. 41 therein  
g No co-ordinates, or bond data pertaining to Table 6.2. available  
h Redetermined structure



TABLE 6.4 Principal geometric characteristics (bond lengths (Å), bond angles (°) of  $(\eta^5\text{-C}_5\text{H}_5)_2\text{Ni}(\text{CO})_2$  complexes

|  | 1                      |                       | 2                      |                       | 3                     |                      | 4                      |                       | 5                      |                       |                       |                      |
|--|------------------------|-----------------------|------------------------|-----------------------|-----------------------|----------------------|------------------------|-----------------------|------------------------|-----------------------|-----------------------|----------------------|
|  | Mn-C-ring <sup>a</sup> | Mn-CO                 | C-C(ring) <sup>a</sup> | Mn-C-O                | OC-Mn-CO              | OC-Mn-L              | Mn-C-ring <sup>a</sup> | Mn-CO                 | C-C(ring) <sup>a</sup> | Mn-C-O                | OC-Mn-CO              | OC-Mn-L              |
| CO <sup>b</sup>  | 2.124(2)               | 1.780(2) <sup>a</sup> | 1.388(3)               | 178.9(2) <sup>a</sup> | 92.02(9) <sup>a</sup> | -                    | 2.124(2)               | 1.780(2) <sup>a</sup> | 1.388(3)               | 178.9(2) <sup>a</sup> | 92.02(9) <sup>a</sup> | -                    |
| SO <sub>2</sub>  | 2.09 (2)               | 1.75 (2) <sup>a</sup> | 1.36 (3)               | 178 (1) <sup>a</sup>  | 90.6 (6)              | 92.9(5) <sup>a</sup> | 2.09 (2)               | 1.75 (2) <sup>a</sup> | 1.36 (3)               | 178 (1) <sup>a</sup>  | 90.6 (6)              | 92.9(5) <sup>a</sup> |
| PhPh <sub>3</sub>  | 2.15 (1)               | 1.75 (2) <sup>a</sup> | 1.42 (2)               | 178 (1) <sup>a</sup>  | 92.4 (4)              | 91.6(3) <sup>a</sup> | 2.15 (1)               | 1.75 (2) <sup>a</sup> | 1.42 (2)               | 178 (1) <sup>a</sup>  | 92.4 (4)              | 91.6(3) <sup>a</sup> |
| PhPh <sub>2</sub> (OCMe)(CHC(O)Me)   | 2.18 (1) <sup>c</sup>  | 1.77 (1) <sup>a</sup> | 1.54 c,d               | 177.2 a,d             | 92.8 <sup>d</sup>     | 94.3 a,d             | 2.18 (1) <sup>c</sup>  | 1.77 (1) <sup>a</sup> | 1.54 c,d               | 177.2 a,d             | 92.8 <sup>d</sup>     | 94.3 a,d             |
| PhPh(OC(CH <sub>2</sub> )(CHC(Me)O)  |                        | 1.77 <sup>a</sup>     | e                      | e                     | e                     | e                    |                        | 1.77 <sup>a</sup>     | e                      | e                     | e                     | e                    |
| (C(O)Ph) <sub>2</sub>  | 2.17 (4)               | 1.78 (3) <sup>a</sup> | 1.39 (8)               | 174(3) <sup>a</sup>   | 90 (1) <sup>a</sup>   | 88 (1) <sup>a</sup>  | 2.17 (4)               | 1.78 (3) <sup>a</sup> | 1.39 (8)               | 174(3) <sup>a</sup>   | 90 (1) <sup>a</sup>   | 88 (1) <sup>a</sup>  |
| N <sub>2</sub> (CO) <sub>2</sub> (Me) <sub>2</sub>                                     | 2.138(7)               | 1.797(7) <sup>a</sup> | 1.39 (1)               | 179.6 a,d             | 90.3(3)               | 94.8(3) <sup>a</sup> | 2.138(7)               | 1.797(7) <sup>a</sup> | 1.39 (1)               | 179.6 a,d             | 90.3(3)               | 94.8(3) <sup>a</sup> |
| SO <sub>2</sub> (C <sub>6</sub> H <sub>5</sub> ) <sub>2</sub> (Me) <sub>2</sub> f,-2,6 | 2.143(4)               | 1.777(3) <sup>a</sup> | 1.385 <sup>d</sup>     | 180.7 a,d             | 89.1(1)               | 94.1(1) <sup>a</sup> | 2.143(4)               | 1.777(3) <sup>a</sup> | 1.385 <sup>d</sup>     | 180.7 a,d             | 89.1(1)               | 94.1(1) <sup>a</sup> |
| C <sub>2</sub> Cl <sub>2</sub> (H <sub>11</sub> ) <sub>2</sub>                         | 2.12 (1)               | 1.767(7) <sup>a</sup> | 1.35 (2)               | 179.1(6) <sup>a</sup> | 87.9(3)               | 90.9(3) <sup>a</sup> | 2.12 (1)               | 1.767(7) <sup>a</sup> | 1.35 (2)               | 179.1(6) <sup>a</sup> | 87.9(3)               | 90.9(3) <sup>a</sup> |
| COHMe <sub>2</sub>   | 2.13 (2)               | 1.74 (2)              | 1.38 (2) <sup>f</sup>  | 178 (1)               | 87.7(7)               | 91.5(8)              | 2.13 (2)               | 1.74 (2)              | 1.38 (2) <sup>f</sup>  | 178 (1)               | 87.7(7)               | 91.5(8)              |
| COHPh  | 2.16 (2)               | 1.80 (3) <sup>a</sup> | 1.43 (3)               | 178 (2) <sup>a</sup>  | 89 (1)                | 92 (1) <sup>a</sup>  | 2.16 (2)               | 1.80 (3) <sup>a</sup> | 1.43 (3)               | 178 (2) <sup>a</sup>  | 89 (1)                | 92 (1) <sup>a</sup>  |
| OMe <sub>2</sub>   | 2.187(7)               | 1.793(5) <sup>a</sup> | 1.417(9)               | 179.3 a,d             | 88.8(2) <sup>e</sup>  | 90.6(3) <sup>a</sup> | 2.187(7)               | 1.793(5) <sup>a</sup> | 1.417(9)               | 179.3 a,d             | 88.8(2) <sup>e</sup>  | 90.6(3) <sup>a</sup> |
| CFPh   | 2.148(7)               | 1.780(6) <sup>a</sup> | 1.396 <sup>d</sup>     | 180.0 a,d             | 90.8(3)               | 91.9(3) <sup>a</sup> | 2.148(7)               | 1.780(6) <sup>a</sup> | 1.396 <sup>d</sup>     | 180.0 a,d             | 90.8(3)               | 91.9(3) <sup>a</sup> |
| ClOEtPh  | 2.17 (1)               | 1.80 (2) <sup>a</sup> | .42 (2)                | 176 (1) <sup>a</sup>  | 91.1(7)               | 34.1(7) <sup>a</sup> | 2.17 (1)               | 1.80 (2) <sup>a</sup> | .42 (2)                | 176 (1) <sup>a</sup>  | 91.1(7)               | 34.1(7) <sup>a</sup> |
| Cl(OMe)(C <sub>6</sub> H <sub>5</sub> (CHMe <sub>2</sub> )(Me)-2,5                     | 2.15 (2)               | 1.80 (2) <sup>a</sup> | 1.407 <sup>d</sup>     | 175.7 a,d             | 89.0(8)               | 92.4(8) <sup>a</sup> | 2.15 (2)               | 1.80 (2) <sup>a</sup> | 1.407 <sup>d</sup>     | 175.7 a,d             | 89.0(8)               | 92.4(8) <sup>a</sup> |
| Cl(CMe)(OMe)Ph <sub>3</sub>  | 2.158(5)               | 1.770(4) <sup>a</sup> | 1.418(5)               | 177.5(3) <sup>a</sup> | 91.7(2)               | 90.6(1) <sup>a</sup> | 2.158(5)               | 1.770(4) <sup>a</sup> | 1.418(5)               | 177.5(3) <sup>a</sup> | 91.7(2)               | 90.6(1) <sup>a</sup> |
| Cl(Ph)-h   | 2.16 (2)               | 1.78 (2) <sup>a</sup> | 1.411 <sup>d</sup>     | 178.6 a,d             | 89.2(9) <sup>a</sup>  | 95.4(9) <sup>a</sup> | 2.16 (2)               | 1.78 (2) <sup>a</sup> | 1.411 <sup>d</sup>     | 178.6 a,d             | 89.2(9) <sup>a</sup>  | 95.4(9) <sup>a</sup> |
| f-C(O)CFPh <sub>2</sub>  | e                      | 1.77 <sup>a</sup>     | 1.36                   | e                     | e                     | e,1                  | e                      | 1.77 <sup>a</sup>     | 1.36                   | e                     | e                     | e,1                  |

TABLE 6.2 (cont)

| L   | Mn-C ring <sup>a</sup> | Mn-CO                 | C-C(ring) <sup>a</sup> | Mn-C-O                | OC-Mn-OC             | OC-Mn-L                       |
|---|------------------------|-----------------------|------------------------|-----------------------|----------------------|-------------------------------|
| <sup>2</sup> <sub>n</sub> -CH <sub>2</sub> CHC(O)Me   | 2.137(8)               | 1.787(7) <sup>a</sup> | 1.39(1)                | 177.1(6) <sup>a</sup> | 88.5(4)              | 96.5(4) <sup>a,j</sup>        |
| <sup>2</sup> <sub>n</sub> CH <sub>2</sub> CHCO <sub>2</sub> Me  | 2.186                  | 1.766                 | 1.44(3)                | 177.2                 | 90.5                 | 81, d, k, 106 <sup>d, l</sup> |
| <sup>2</sup> <sub>n</sub> CH <sub>2</sub> CH <sub>2</sub> CH <sub>2</sub> CH <sub>2</sub> CH(O)OEt <sup>b</sup> | 2.121(8)               | 1.770(7) <sup>a</sup> | 1.35(1)                | 176.9(6) <sup>a</sup> | 87.6                 | 95.7(2) <sup>a, j</sup>       |
| <sup>2</sup> <sub>n</sub> C <sub>8</sub> H <sub>8</sub>   | 2.156(2)               | 1.787(2) <sup>a</sup> | 1.410                  | 178.7(2) <sup>a</sup> | 88.8(1)              | 93.4                          |
| <sup>2</sup> <sub>n</sub> C <sub>8</sub> H <sub>8</sub> <sup>m</sup>  | 2.131(3)               | 1.773(2)              | 1.364(5)               | 178.1(2)              | 91.4(5)              | 95.1(5) <sup>j</sup>          |
| <sup>2</sup> <sub>n</sub> C <sub>8</sub> H <sub>6</sub> <sup>n</sup>  | 2.143(9)               | 1.769(9) <sup>a</sup> | 1.40(1) <sup>a</sup>   | 177.2(7) <sup>a</sup> | 89.5(4) <sup>a</sup> | 84, d, k, 110 <sup>d, j</sup> |

- a Average value  
 b Ref 59b  
 c Disordered C<sub>2</sub>H<sub>2</sub> ring; bond lengths from highest occupancy (75%) atomic positions  
 d Bond data obtained from the Cambridge Crystallographic Data Base  
 e Bond data not available  
 f Ring C-C bonds not equal [C(2)-C(3): 1.34(2), C(3)-C(4): 1.45(2), C(4)-C(4): 1.28(2)<sup>a</sup>]<sup>\*\*</sup>  
 g OC-Mn-C (aromatic) angles not equal (values: 85.5(1) and 95.7(1)<sup>o</sup>)<sup>\*\*</sup>  
 h Two <sup>2</sup><sub>n</sub>C<sub>8</sub>H<sub>8</sub> coordinated <sup>2</sup><sub>n</sub>-olefinic C-atoms not equidistant from Mn-atom (1.96(2) and 2.17(2)<sup>a</sup>)<sup>\*\*</sup>  
 i OC-Mn-A, A = midpoint of <sup>2</sup><sub>n</sub> C-C double bond  
 k av. value of OC-Mn-C for CO and nearest <sup>2</sup><sub>n</sub>C-C-atom  
 l av. value of OC-Mn-C for C<sup>o</sup> and farther <sup>2</sup><sub>n</sub>C-C-atom  
 m Ref 63(b)  
 n [(<sup>2</sup><sub>n</sub>C<sub>8</sub>H<sub>6</sub>)Mn(CO)<sub>2</sub>]<sub>2</sub>(C<sub>5</sub>H<sub>5</sub>)<sub>2</sub>, av. values for the two Mn fragments quoted.

complexes are generally in the range 1.35 to 1.43 Å, cf. av. value of 1.388(3) Å for  $(\eta^5\text{-C}_5\text{H}_5)_2\text{Mn}(\text{CO})_3$ .<sup>11b</sup> With one exception, the C-C bond lengths within one structure are all equal within experimental error. The exception,  $(\eta^5\text{-C}_5\text{H}_5)\text{Mn}(\text{CO})_2(\text{CCMe}_2)$ ,<sup>11c</sup> has an alternating pattern of C-C bond lengths (Fig. 6.3), indicative of some degree of C-C bond localization. The pattern is not, however, similar to that observed for  $(\eta^5\text{-C}_5\text{H}_5)\text{Mn}(\text{CO})_3$ , which also has non-equivalent ring C-C bonds (see Fig. 6.2). It is interesting, and perhaps significant, to note that the shortest C-C bond (C4-C4') in  $(\eta^5\text{-C}_5\text{H}_5)\text{Mn}(\text{CO})_2(\text{CCMe}_2)$  corresponds to the C-C bond eclipsed by the vinylidene ligand. The non-equivalent ring C-C bond lengths could, however, be indicative of some unresolved disorder of the  $\text{C}_5$ -ring. A 25%  $\text{C}_5$ -ring disorder was observed for  $(\eta^5\text{-C}_5\text{H}_5)\text{Mn}(\text{CO})_2[\text{PPh}_2(\text{OC}(\text{Me})-\text{CHC}(\text{O})\text{Me})]$ .<sup>11d</sup>

#### 6.3.5 Mn-C-O bond angles

The Mn-C-O bond angles are in the range 174-179°, as expected.<sup>11</sup>

#### 6.3.6 Packing, and Steric Factors

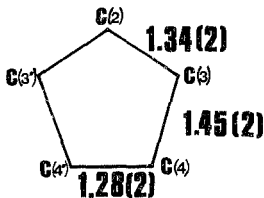
Crystal packing forces are probably responsible for (i) The overall conformation of the ligand tripod with respect to the cyclopentadienyl ring, although the electronic nature of the ligand L could govern whether L eclipses a ring C-atom or a ring C-C bond.

(ii) Angular deviations which destroy possible  $m$  molecular symmetry. For  $L = \text{CCMe}_2$ ,<sup>11c</sup>  $\text{CMe}_2$ ,<sup>11e</sup>  $\eta^2\text{-C}_7\text{H}_8$ ,<sup>11f</sup> crystallographic  $m$  molecular symmetry is observed.

(iii) Small distortions and deviations from ideal geometry.

Steric factors could account for anomalous bond angle and bond length data. For example, for  $(\eta^5\text{-C}_5\text{H}_5)\text{Mn}(\text{CO})_2[\text{C}(\text{CO}_2\text{Me})\text{CHPPH}_3]$ ,<sup>11g</sup> the OC-Mn-C carbene bond angles are 85.5(1) and 95.7(1)°, for CO(1) and CO(2) respectively cf. the ideal value of 90°, due to the bulky  $\text{CO}_2\text{Me}$  substituent directed towards the CO(2) ligand.

In the complex  $(\eta^5\text{-C}_5\text{H}_5)\text{Mn}(\text{CO})_2[\eta^2\text{-C}(\text{O})\text{CPh}_2]$ ,<sup>11h</sup>



**Figure 6.3** Ring C-C bond lengths ( $\text{\AA}$ )<sup>11</sup> in  $(\eta^5\text{C}_5\text{H}_5)\text{Mn}(\text{CO})_2(\text{CMe})$ . (Atoms C(3) and C(4) are related to C(3') and C(4') by a crystallographic mirror plane through C(2) and the midpoint of the C(4)-C(4') bond.)

the two co-ordinated  $\pi^2$ -olefinic C-atoms (C1 and C2) are not equidistant from the Mn-atom (2.17(2) and 1.96(2) $\text{\AA}$  respectively), possibly due to steric interactions between the phenyl rings on C1 and the carbonyl groups. Further, the Mn-CO bond lengths differ (1.73 and 1.81 $\text{\AA}$ ).

6.4 Conclusion

The overall geometry of the  $(\eta^5\text{C}_5\text{H}_5)\text{Mn}(\text{CO})_2\text{L}$  complexes is similar to that of  $(\eta^5\text{C}_5\text{H}_5)\text{Mn}(\text{CO})_3$ . Observed bond angle and bond length trends can be rationalized in electronic terms, and anomalies explained by the influence of steric factors and/or crystal packing forces.

VII. THE CRYSTAL AND MOLECULAR STRUCTURE OF  $(\eta^5\text{-C}_5\text{H}_5)\text{Mn}(\text{CO})_2(\text{CNBu}^t)$

7.1 Introduction

An X-ray crystal study of  $(\eta^2\text{-C}_6\text{H}_8)\text{Mn}(\text{CO})_2(\text{CNBu}^t)$ , was undertaken as part of an investigation into the anomalous IR spectra exhibited by certain complexes of this type. It was hoped that the X-ray study of  $(\eta^5\text{-C}_5\text{H}_5)\text{Mn}(\text{CO})_2(\text{CNBu}^t)$ , in conjunction with that of  $(\eta^5\text{-C}_5\text{H}_5\text{CO}_2\text{Me})\text{Cr}(\text{CO})_2(\text{CNBu}^t)$  (ch. IV), might provide a structural explanation of the anomalous IR data of these complexes. This aspect will be discussed in ch. VIII.

$(\eta^5\text{-C}_5\text{H}_5)\text{Mn}(\text{CO})_2(\text{CNBu}^t)$  crystallizes in the orthorhombic non-centrosymmetric space group  $Pna2_1$ , with four molecules in the unit cell. Fig. 7.2 shows a view of the unit cell, looking down the b-axis. The molecule is shown in Fig. 7.1, together with the numbering system used in the analysis.

Bond lengths and bond angles, and bond parameters involving hydrogen atoms are given in Tables 7.1, 7.2 and 7.3 respectively. Table 7.4 lists the deviations ( $\text{\AA}$ ) of the atoms from the mean plane through the cyclopentadienyl ring (C-atoms C(1)-C(5)).

7.2 Discussion of the Structure of  $(\eta^5\text{-C}_5\text{H}_5)\text{Mn}(\text{CO})_2(\text{CNBu}^t)$

The structure of  $(\eta^5\text{-C}_5\text{H}_5)\text{Mn}(\text{CO})_2(\text{CNBu}^t)$  will be discussed in terms of the structural features analysed for the related  $(\eta^5\text{-C}_5\text{H}_5)\text{Mn}(\text{CO})_2\text{L}$  complexes (Table 6.2). The principal geometric characteristics of  $(\eta^5\text{-C}_5\text{H}_5)\text{Mn}(\text{CO})_2(\text{CNBu}^t)$  are summarized in Table 7.5.

7.2.1 C-Mn-CO and OC-Mn-CN angles

The complex has the "piano-stool" arrangement of ligands, with the C-Mn-C angles all close to  $90^\circ$ . The CO-Mn-CO angle is slightly smaller than the CO-Mn-CN angles, as expected<sup>10</sup> since  $\text{CNBu}^t$  is a poorer  $\pi$ -acceptor than CO.<sup>11</sup> However, the difference (of  $1^\circ$ ) is too slight to be significant.

7.2.2 Molecular conformation

In  $(\eta^5\text{-C}_5\text{H}_5)\text{Mn}(\text{CO})_2(\text{CNBu}^t)$ , the  $\text{CNBu}^t$  ligand essentially eclipses a ring C-C bond (in projection, angle of eclipse C(4)-Mn-C(6) is  $13.7^\circ$ ), but the disorder in the C5-ring (vide

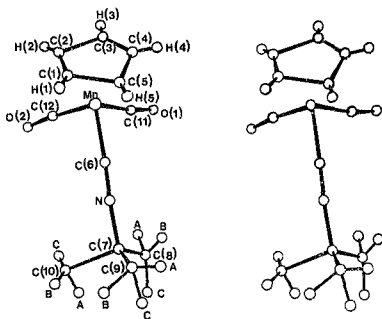


Figure 7.1. ORTEP<sup>a</sup> view of the  $(\eta^5\text{-C}_5\text{H}_5)\text{Mn}(\text{CO})_2(\text{CNBu}^t)$  molecule, showing the numbering system

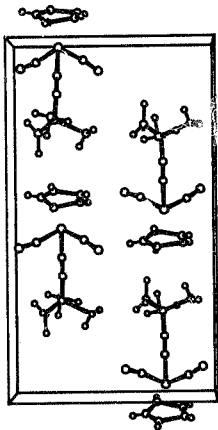


Figure 7.2: ORTEP's view of the unit cell of  $(n\text{-C}_5\text{H}_{12})\text{Mn}(\text{CO})_2(\text{CMBA})_2$ , looking down the b-axis

Figure 7.2: ORTEP's view of the unit cell of  $(\eta^5\text{-C}_5\text{H}_5)_2\text{Mn}(\text{CO})_2(\text{CNBu}^t)_2$ , looking down the b-axis

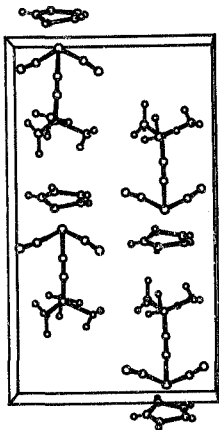




TABLE 7.1 Bond lengths (Å) for  $(n^5\text{C}_5\text{H}_5)\text{Mn}(\text{CO})_2(\text{CNBu}^t)$ 

|           |         |            |         |
|-----------|---------|------------|---------|
| Mn-C(1)   | 2.10(3) | C(1)-C(2)  | 1.55(5) |
| Mn-C(2)   | 2.09(2) | C(2)-C(3)  | 1.23(4) |
| Mn-C(3)   | 2.12(4) | C(3)-C(4)  | 1.39(5) |
| Mn-C(4)   | 2.17(2) | C(4)-C(5)  | 1.49(4) |
| Mn-C(5)   | 2.20(3) | C(5)-C(1)  | 1.27(5) |
| Mn-C(11)  | 1.82(3) | C(11)-O(1) | 1.13(4) |
| Mn-C(12)  | 1.72(4) | C(12)-O(2) | 1.20(5) |
| Mn-C(6)   | 1.85(2) | C(6)-N     | 1.17(2) |
| N-C(7)    | 1.48(2) | C(7)-C(9)  | 1.82(4) |
| C(7)-C(8) | 1.30(5) | C(7)-C(10) | 1.45(3) |

TABLE 7.2 Bond angles (°) for  $(n^5\text{C}_5\text{H}_5)\text{Mn}(\text{CO})_2(\text{CNBu}^t)$ 

|                |        |                 |        |
|----------------|--------|-----------------|--------|
| C(2)-Mn-C(1)   | 43(1)  | C(9)-C(7)-C(8)  | 107(2) |
| C(3)-Mn-C(1)   | 63(1)  | C(10)-C(7)-C(8) | 120(3) |
| C(3)-Mn-C(2)   | 34(1)  | C(10)-C(7)-C(9) | 110(2) |
| C(4)-Mn-C(1)   | 65(1)  | C(11)-Mn-C(1)   | 137(2) |
| C(4)-Mn-C(2)   | 64(1)  | C(11)-Mn-C(2)   | 98(1)  |
| C(4)-Mn-C(3)   | 38(1)  | C(11)-Mn-C(3)   | 96(2)  |
| C(5)-Mn-C(1)   | 34(1)  | C(11)-Mn-C(4)   | 122(1) |
| C(5)-Mn-C(2)   | 63(1)  | C(11)-Mn-C(5)   | 158(1) |
| C(5)-Mn-C(3)   | 61(1)  | C(12)-Mn-C(1)   | 90(2)  |
| C(5)-Mn-C(4)   | 40(1)  | C(12)-Mn-C(2)   | 113(2) |
| C(6)-Mn-C(1)   | 133(2) | C(12)-Mn-C(3)   | 147(2) |
| C(6)-Mn-C(2)   | 153(1) | C(12)-Mn-C(4)   | 147(1) |
| C(6)-Mn-C(3)   | 119(2) | C(12)-Mn-C(5)   | 107(1) |
| C(6)-Mn-C(4)   | 90(1)  | C(2)-C(1)-Mn    | 68(2)  |
| C(6)-Mn-C(5)   | 101(1) | C(5)-C(1)-Mn    | 77(2)  |
| C(2)-C(1)-C(5) | 105(3) | C(1)-C(2)-Mn    | 69(2)  |
| C(1)-C(2)-C(3) | 105(4) | C(3)-C(2)-Mn    | 75(2)  |
| C(2)-C(3)-C(4) | 118(4) | C(2)-C(3)-Mn    | 72(2)  |
| C(3)-C(4)-C(5) | 99(3)  | C(4)-C(3)-Mn    | 73(2)  |
| C(4)-C(5)-C(1) | 112(3) | C(3)-C(4)-Mn    | 69(2)  |
| C(8)-C(7)-N    | 108(3) | C(5)-C(4)-Mn    | 71(2)  |
| C(9)-C(7)-N    | 101(3) | C(4)-C(5)-Mn    | 59(2)  |
| C(10)-C(7)-N   | 109(2) | C(1)-C(5)-Mn    | 69(2)  |

TABLE 7.2 (cont.)

|               |        |                |       |
|---------------|--------|----------------|-------|
| O(1)-C(11)-Mn | 173(3) | C(11)-Mn-C(6)  | 91(2) |
| O(2)-C(12)-Mn | 173(3) | C(12)-Mn-C(6)  | 93(2) |
| N-C(6)-Mn     | 177(2) | C(12)-Mn-C(11) | 91(1) |
| C(7)-N-C(6)   | 172(2) |                |       |

TABLE 7.3 Bond parameters involving hydrogen atoms for  
( $n^5\text{-C}_5\text{H}_5$ )Mn(CO)<sub>2</sub>(CNBu<sup>t</sup>)

(a) Bond angles involving hydrogen atoms (°)

|                  |         |                     |         |
|------------------|---------|---------------------|---------|
| H(1)-C(1)-Mn     | 93(10)  | H(1)-C(1)-C(2)      | 95(11)  |
| H(2)-C(2)-Mn     | 110(10) | H(1)-C(1)-C(5)      | 151(13) |
| H(3)-C(3)-Mn     | 139(11) | H(2)-C(2)-C(1)      | 112(11) |
| H(4)-C(4)-Mn     | 136(7)  | H(2)-C(2)-C(3)      | 143(11) |
| H(5)-C(5)-Mn     | 137(7)  | H(3)-C(3)-C(2)      | 129(13) |
| H(8A)-C(8)-C(7)  | 102(17) | H(3)-C(3)-C(4)      | 110(12) |
| H(8B)-C(8)-C(7)  | 101(16) | H(4)-C(4)-C(3)      | 147(7)  |
| H(8C)-C(8)-C(7)  | 119(10) | H(4)-C(4)-C(5)      | 108(7)  |
| H(8A)-C(8)-H(8B) | 137(23) | H(5)-C(5)-C(4)      | 94(7)   |
| H(8B)-C(8)-H(8C) | 84(21)  | H(5)-C(5)-C(1)      | 151(7)  |
| H(8C)-C(8)-H(8A) | 115(18) | H(10A)-C(10)-C(7)   | 122(9)  |
| H(9A)-C(9)-C(7)  | 87(21)  | H(10B)-C(10)-C(7)   | 108(11) |
| H(9B)-C(9)-C(7)  | 106(13) | H(10C)-C(10)-C(7)   | 121(13) |
| H(9C)-C(9)-C(7)  | 94(9)   | H(10A)-C(10)-H(10B) | 78(13)  |
| H(9A)-C(9)-H(9B) | 107(25) | H(10B)-C(10)-H(10C) | 83(15)  |
| H(9B)-C(9)-H(9C) | 155(17) | H(10C)-C(10)-H(10A) | 117(15) |
| H(9C)-C(9)-H(9A) | 89(19)  |                     |         |

(b) Bond lengths involving hydrogen atoms (Å)

|            |        |              |        |
|------------|--------|--------------|--------|
| C(1)-H(1)  | 0.9(1) | C(8)-H(8C)   | 1.3(2) |
| C(2)-H(2)  | 0.7(1) | C(9)-H(9A)   | 0.9(3) |
| C(3)-H(3)  | 0.8(1) | C(9)-H(9B)   | 1.0(3) |
| C(4)-H(4)  | 1.0(1) | C(9)-H(9C)   | 1.1(2) |
| C(5)-H(5)  | 1.1(1) | C(10)-H(10A) | 1.2(2) |
| C(8)-H(8A) | 1.0(3) | C(10)-H(10B) | 1.0(2) |
| C(8)-H(8B) | 0.8(2) | C(10)-H(10C) | 0.9(2) |

TABLE 7.4 Deviations ( $\text{\AA}$ ) of atoms from the plane defined by the 5 C-atoms (C(1)-C(5)) of the cyclopentadienyl ring<sup>a</sup> of  $(\eta^5\text{-C}_5\text{H}_5)\text{Mn}(\text{CO})_2(\text{CNBu}^t)$

| Atom   | Deviation from Plane ( $\text{\AA}$ ) <sup>0</sup> |
|--------|--|
| Mn     | -1.7789  |
| N      | -3.5564  |
| O(1)   | -3.3044  |
| O(2)   | -3.4878  |
| C(1)   | -0.0340  |
| C(2)   | -0.0102  |
| C(3)   | 0.0451   |
| C(4)   | -0.0565  |
| C(5)   | 0.0557   |
| H(1)   | -0.3396  |
| H(2)   | -0.0876  |
| H(3)   | 0.2305   |
| H(4)   | 0.1922   |
| H(5)   | 0.4329   |
| C(6)   | -2.8395  |
| C(7)   | -4.6073  |
| C(8)   | -5.4712  |
| H(6A)  | -6.3209  |
| H(6B)  | -4.9481  |
| H(6C)  | -5.8411  |
| C(9)   | -5.4473  |
| H(9A)  | -5.9892  |
| H(9B)  | -5.7743  |
| H(9C)  | -4.9344  |
| C(10)  | -3.9937  |
| H(10A) | -3.9949  |
| H(10B) | -4.7604  |
| H(10C) | -3.6776  |
| C(11)  | -2.8159  |
| C(12)  | -2.7204  |

<sup>a</sup> Equation of the plane defined by atoms C(1)-C(5):  
 $(17.7778)x + (-2.2175)y + (-0.0794)z = 8.6923$

TABLE 7.5 Principal geometric characteristics (distances, Å,  
angles, °) of  $(\eta^5\text{C}_5\text{H}_5)\text{Mn}(\text{CO})_2(\text{CNBu}^t)$

|                            |         |
|----------------------------|---------|
| Mn-Cp <sup>a</sup>         | 1.78    |
| av. Mn-C ring              | 2.14(4) |
| av. Mn-CO                  | 1.77(4) |
| Mn-CN                      | 1.85(2) |
| av. C-C(ring) <sup>b</sup> | 1.39(4) |
| av. Mn-C-O                 | 173(3)  |
| Mn-C-N                     | 177(2)  |
| C-N-C                      | 172(2)  |
| CO-Mn-CO                   | 91(1)   |
| av. CO-Mn-CN               | 92(2)   |

<sup>a</sup> Co = centre of gravity of C5-ring

<sup>b</sup> Ring C-C bonds not equivalent (see Fig. 7.3)

*infra*) precludes a detailed analysis of the conformation of the  $\text{Mn}(\text{CO})_2\text{L}$  "tripod" relative to the  $(\text{C}_5\text{H}_5)$  ring, as has been done for the  $(\eta^5\text{-C}_5\text{H}_5)\text{Mn}(\text{CO})_3$  precursor<sup>33b</sup> (see section 6.2.2).

#### 7.2.3. Mn-C bond lengths

The av. Mn-C ring bond length is  $2.14(4)\text{\AA}$ , cf.  $2.124(2)\text{\AA}$  for  $(\eta^5\text{-C}_5\text{H}_5)\text{Mn}(\text{CO})_3$ <sup>33b</sup>. The Mn-Cp distance is  $1.779\text{\AA}$ , cf.  $1.766\text{\AA}$  for  $(\eta^5\text{-C}_5\text{H}_5)\text{Mn}(\text{CO})_3$ <sup>33b</sup>, and  $1.790\text{\AA}$ ,  $1.778(1)\text{\AA}$  and  $1.773(3)\text{\AA}$  for the complexes  $(\eta^5\text{-C}_5\text{H}_5)\text{Mn}(\text{CO})_2\text{L}$ ,  $\text{L} = (\text{C}(\text{CO}_2\text{Me})\text{-CHPh}_3)^{33a}$ ,  $(\eta^2\text{-CH}_2\text{CHC}(\text{O})\text{Me})^{33c}$  and  $(\eta^2\text{-C}_7\text{H}_8)^{33b}$  respectively.

The av. Mn-CO distance is  $1.77(4)\text{\AA}$  cf.  $1.780(2)\text{\AA}$  and  $1.75(2)\text{\AA}$  for  $(\eta^5\text{-C}_5\text{H}_5)\text{Mn}(\text{CO})_3$ <sup>33b</sup> and  $(\eta^5\text{-C}_5\text{H}_5)\text{Mn}(\text{CO})_2(\text{PPh}_3)^{33c}$  respectively. This trend is in the expected direction, since  $\text{CNBu}^t$  is a poorer  $\pi$ -acceptor than CO, but a better  $\sigma$ -acceptor than  $\text{PPh}_3$ <sup>33a</sup>. However, with the small range ( $3^\circ$ ), the Mn-CO bond distances are effectively equal within the limits of experimental error. Note that the Mn-CO bond lengths in  $(\eta^5\text{-C}_5\text{H}_5)\text{Mn}(\text{CO})_2(\text{CNBu}^t)$  are not equal within error limits ( $1.82(3)$  and  $1.72(4)\text{\AA}$  for Mn-C(11) and Mn-C(12) respectively.) A similar effect was observed for  $(\eta^5\text{-C}_5\text{H}_5)\text{Mn}(\text{CO})_2(\eta^2\text{-C}(\text{O})\text{CPh}_2)^{33c}$  (see section 6.3.6.) The Mn-CN bond length is  $1.85(2)\text{\AA}$ .

#### 7.2.4 Ring planarity and C-C bond lengths

As for  $(\eta^5\text{-C}_5\text{H}_5)\text{Mn}(\text{CO})_3$ <sup>33b</sup>, the C5-ring in  $(\eta^5\text{-C}_5\text{H}_5)\text{Mn}(\text{CO})_2(\text{CNBu}^t)$  is essentially planar (see Table 7.4). However, the ring C-C bond lengths are not equivalent (Fig. 7.3), indicative of some degree of disorder. A 25% disorder of the C5-ring was observed for  $(\eta^5\text{-C}_5\text{H}_5)\text{Mn}(\text{CO})_2[\text{PPh}_2\text{-OC}(\text{Me})(\text{CHC}(\text{O})\text{Me})]^{33c}$ . Unresolved C5-ring disorder could also account for the non-equivalent ring C-C bond lengths (Fig. 6.3.) in  $(\eta^5\text{-C}_5\text{H}_5)\text{Mn}(\text{CO})_2(\text{CCMe}_2)^{33c}$ . Non-equivalent ring C-C bond lengths could be a genuine electronic effect indicative of some degree of C-C bond localization, in accurately determined structures, eg.  $(\eta^5\text{-C}_5\text{H}_5)\text{Mn}(\text{CO})_3$ <sup>33b</sup>

#### 7.2.5 M-C-O and M-C-N bond angles

Both the Mn-C-O bond angles are  $173(3)^\circ$ . Near linearity (ca.  $175^\circ$ ) is expected.<sup>33</sup> Crystal packing forces

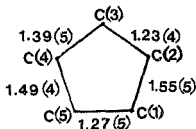


Figure 7.3 Ring C-C bond lengths (Å) in  $(\eta^5\text{-C}_5\text{H}_5)\text{Mn}(\text{CO})_2(\text{CNBu}^t)$

could also be responsible for deviations. The isocyanide ligand co-ordinates in a linear fashion, with the Mn-C-N bond angle  $177(4)^\circ$ .

#### 7.2.6 Conformation of the $\text{CNBu}^t$ ligand

The isocyanide ligand is slightly bent, with a C-N-C angle of  $172(2)^\circ$ . However, for terminal isocyanide ligands, a C-N-R angle  $>170^\circ$  is considered linear.<sup>11b</sup> Note that the  $\text{CNBu}^t$  ligand bends inwards away from the ring, in contrast to the  $\text{CNBu}^t$  ligand in  $(\eta^5\text{-C}_5\text{H}_5\text{CO}_2\text{Me})\text{Cr}(\text{CO})_2(\text{CNBu}^t)$  (ch. IV), which bends outwards towards the arene ring.

#### 7.2.7 Packing

As for  $(\eta^5\text{-C}_5\text{H}_5)\text{Mn}(\text{CO})_3$ ,<sup>11b,12</sup> the overall conformation, and in particular the orientation of the ligand tripod with respect to the  $(\text{C}_5\text{H}_5)$  ring, is probably determined largely by crystal packing forces. Short non-bonded intermolecular distances include C(11)...H(5): $2.96\text{\AA}$ , O(1)...H(5): $2.41\text{\AA}$ , O(1)...H(1): $2.61\text{\AA}$  and O(1)...H(10C): $2.86\text{\AA}$ .

Small distortion due to close intramolecular non-bonded contacts could also be due to packing requirements eg. C(12)...C(1): 2.72<sup>o</sup>Å and C(12)...H(1): 2.39<sup>o</sup>Å.

7.3

### Experimental

#### 7.3.1 Data collection

The complex ( $n^{\text{C}}_{15}\text{H}_5$ )Mn(CO)<sub>2</sub>(CNBu<sup>t</sup>) was prepared as described in ch. V. Crystals of ( $n^{\text{C}}_{15}\text{H}_5$ )Mn(CO)<sub>2</sub>(CNBu<sup>t</sup>) were obtained from a dichloromethane solution as pale yellow needles. Preliminary investigation by standard Weissenberg photography established the space group as either the centrosymmetric Pnma or the non-centrosymmetric Pna2<sub>1</sub>. Refined cell constants were obtained during data collection on a Phillips PW1100 four-circle diffractometer using graphite-monochromated MoK $\alpha$  radiation ( $\lambda = 0.7107\text{\AA}$ ) at room temperature (20°C). During data collection, the crystal deteriorated on long exposure to the X-ray beam, as was evidenced by the fall-off in intensity of certain standard reflections which were checked at intervals. The data were corrected for Lorentz and polarization effects, but absorption corrections were not made as the linear absorption coefficient was only 9.70 cm<sup>-1</sup>. Crystal data and details of the structure analysis are summarized in Table 7.6.

#### 7.3.2 Structure Solution and Refinement

Structure analysis and refinement were carried out using the program SHELX 82.<sup>68a</sup> Initial co-ordinates for the manganese atom were derived from a Patterson synthesis, the other fifteen non-hydrogen atoms being located from difference Fourier syntheses. The basic structure was solved using the centrosymmetric Pnma, but refinement was only possible after transforming to the non-centrosymmetric Pna2<sub>1</sub>. The fourteen hydrogen atoms were placed from subsequent difference Fourier syntheses. Positional parameters and anisotropic temperature factors for the non-hydrogen atoms were refined by full-matrix least squares analysis. The methyl hydrogens were assigned a common isotropic temperature factor, which refined to a value of 0.067(23)<sup>o</sup>Å.

The cyclopentadienyl ring showed disorder, and in the initial stages was refined as a rigid pentagon. All restraints were removed in the final cycles. Least-squares refinement was considered complete when all positional shifts were less than 0.5 $\sigma$ . At this stage the conventional R was 0.0996. Unit weights were used. Scattering factors for Mn were taken from "International Tables for X-ray Crystallography,"<sup>a,b</sup> and anomalous dispersion corrections for manganese were made.<sup>c</sup> Final atomic coordinates and anisotropic temperature factors for the non-hydrogen atoms are given in Tables 7.7 and 7.8 respectively. A listing of the Structure Factors is to be found in Appendix D.



TABLE 7.6 Crystal data and details of structural analysis for  
 $(\eta^5\text{-C}_5\text{H}_5)_2\text{Mn}(\text{CO})_2(\text{CNBu}^t)$

|                                      |   |
|--------------------------------------|---|
| Formula                              | MnC <sub>12</sub> H <sub>14</sub> NO <sub>2</sub> |
| Mr                                   | 259.18  |
| Crystal dimensions (mm)              | 0.60 x .05 x .09                                  |
| Space Group                          | Pna2 <sub>1</sub>                                 |
| a (Å)                                | 19.123(9)   |
| b (Å)                                | 6.020(3)  |
| c (Å)                                | 10.942(5)   |
| V (Å <sup>3</sup> )                  | 1259.65   |
| Z                                    | 4   |
| D <sub>c</sub> (g cm <sup>-3</sup> ) | 1.37  |
| F (000)                              | 535.97  |
| $\mu$ (cm <sup>-1</sup> )            | 9.70  |
| $\lambda$ (Å)                        | MoK $\alpha$ (0.7107)                             |
| Scan mode                            | $\omega/2\theta$                                  |
| Range ( $^\circ$ )                   | $3 \leq 2\theta \leq 25$                          |
| Scan width ( $^\circ$ )              | 1.00  |
| Scan speed ( $^\circ\text{s}^{-1}$ ) | 0.033   |
| Range of hkl                         | +h, +k, +l  |
| measured intensities                 | 1049  |
| Unique reflections                   | .876  |
| Internal consistency R-index         | 0.0000  |
| Omitted reflections                  | 112   |
| Observed reflection criterion        | F $\geq$ (F)                                      |
| R (R = Rw)                           | 0.0996  |

TABLE 7.7 Fractional atomic co-ordinates for  $(n^5\text{C}_5\text{H}_5)_2\text{Mn}(\text{CO})_2$ -  
(CNBu<sup>t</sup>)

| Atom   | x/a       | y/b        | z/c       |
|--------|-----------|------------|-----------|
| Mn     | 0.4714(1) | 0.6579(5)  | 0.7500(0) |
| N      | 0.341(1)  | 0.393(3)   | 0.745(4)  |
| O(1)   | 0.423(1)  | 0.748(6)   | 0.553(2)  |
| O(2)   | 0.416(2)  | 0.956(5)   | 0.935(3)  |
| C(1)   | 0.569(3)  | 0.625(6)   | 0.845(4)  |
| C(2)   | 0.530(1)  | 0.707(5)   | 0.712(2)  |
| C(3)   | 0.562(2)  | 0.550(7)   | 0.648(4)  |
| C(4)   | 0.534(1)  | 0.363(4)   | 0.706(3)  |
| C(5)   | 0.548(2)  | 0.425(5)   | 0.835(3)  |
| C(6)   | 0.394(1)  | 0.491(4)   | 0.748(5)  |
| C(7)   | 0.270(1)  | 0.299(3)   | 0.737(3)  |
| C(8)   | 0.235(2)  | 0.411(9)   | 0.655(3)  |
| C(9)   | 0.235(3)  | 0.377(5)   | 0.885(4)  |
| C(10)  | 0.275(1)  | 0.059(4)   | 0.728(3)  |
| C(11)  | 0.439(2)  | 0.841(5)   | 0.633(3)  |
| C(12)  | 0.443(2)  | 0.830(9)   | 0.864(3)  |
| H(1)   | 0.566(8)  | 0.761(28)  | 0.878(15) |
| H(2)   | 0.588(7)  | 0.825(24)  | 0.710(12) |
| H(3)   | 0.573(8)  | 0.521(27)  | 0.578(13) |
| H(4)   | 0.527(7)  | 0.197(24)  | 0.702(11) |
| H(5)   | 0.548(7)  | 0.247(23)  | 0.868(12) |
| H(8A)  | 0.185(18) | 0.350(48)  | 0.687(30) |
| H(8B)  | 0.264(12) | 0.417(43)  | 0.000(23) |
| H(8C)  | 0.240(11) | 0.620(40)  | 0.853(19) |
| H(9A)  | 0.192(18) | 0.345(53)  | 0.853(31) |
| H(9B)  | 0.238(12) | 0.536(44)  | 0.889(21) |
| H(9C)  | 0.238(11) | 0.201(38)  | 0.923(18) |
| H(10A) | 0.263(11) | -0.059(34) | 0.814(20) |
| H(10B) | 0.226(10) | -0.001(32) | 0.708(17) |
| H(10C) | 0.286(11) | -0.009(36) | 0.655(20) |

TABLE 7.8 Anisotropic thermal parameters ( $\text{\AA}^2$ ) for the non-hydrogen<sup>a</sup> atoms of  $(\eta^5\text{-C}_5\text{H}_5)\text{Mn}(\text{CO})_2(\text{CNBu}^t)$

| Atom               | $U_{11}$ | $U_{22}$ | $U_{33}$ | $U_{23}$ | $U_{13}$ | $U_{12}$  |
|--------------------|----------|----------|----------|----------|----------|-----------|
| Mn                 | 0.034(1) | 0.071(2) | 0.053(2) | 0.007(4) | 0.000(3) | -0.002(2) |
| N                  | 0.05(1)  | 0.08(1)  | 0.08(1)  | -0.02(2) | -0.02(2) | -0.01(1)  |
| O(1)               | 0.04(1)  | 0.17(3)  | 0.05(1)  | 0.02(2)  | 0.01(1)  | 0.00(2)   |
| O(2)               | 0.10(2)  | 0.09(2)  | 0.06(1)  | -0.03(1) | -0.01(1) | 0.04(2)   |
| C(1)               | 0.13(3)  | 0.05(2)  | 0.07(2)  | -0.03(2) | -0.08(2) | 0.02(2)   |
| C(2)               | 0.02(1)  | 0.05(2)  | 0.07(2)  | -0.00(2) | -0.00(1) | 0.01(1)   |
| C(3)               | 0.10(3)  | 0.09(3)  | 0.07(3)  | -0.04(3) | -0.01(2) | 0.04(2)   |
| C(4)               | 0.06(1)  | 0.02(1)  | 0.12(3)  | 0.03(1)  | 0.05(2)  | 0.01(1)   |
| C(5) <sup>b</sup>  | 0.058(8) |          |          |          |          |           |
| C(6) <sup>b</sup>  | 0.068(6) |          |          |          |          |           |
| C(7) <sup>b</sup>  | 0.047(6) |          |          |          |          |           |
| C(8)               | 0.05(1)  | 0.17(5)  | 0.05(2)  | -0.00(2) | -0.01(1) | 0.01(2)   |
| C(9)               | 0.19(6)  | 0.07(2)  | 0.09(3)  | -0.03(2) | 0.09(4)  | -0.09(3)  |
| C(10) <sup>b</sup> | 0.056(6) |          |          |          |          |           |
| C(11) <sup>b</sup> | 0.042(6) |          |          |          |          |           |
| C(12)              | 0.05(2)  | 0.19(4)  | 0.04(1)  | -0.01(2) | -0.02(1) | 0.02(2)   |

<sup>a</sup> The ring H-atoms (H1 to H5) have isotropic temperature factor of  $0.0001(38)\text{\AA}^2$ ; the methyl H-atoms (H8A-C, H9A-C, H10A-C) were assigned a common temperature factor which refined to  $0.087(23)\text{\AA}^2$ .

<sup>b</sup> Refined as an isotropic atom.

VIII. ANOMALOUS INFRA RED SPECTRA OF ( $\eta^6$ -ARENE)Cr(CO)<sub>2</sub>(CNR) AND ( $\eta^5$ -C<sub>5</sub>H<sub>5</sub>)Mn(CO)<sub>2</sub>(CNR) COMPLEXES

8.1 Introduction - Anomalous IR data

As mentioned previously, certain complexes of the type ( $\eta^6$ -Arene)Cr(CO)<sub>2</sub>(CNR) and ( $\eta^5$ -C<sub>5</sub>H<sub>5</sub>)Mn(CO)<sub>2</sub>(CNR) were found to give anomalous infra red (IR) spectra, both in solution and the solid state. (Chs. II and V respectively).

On the basis of group theory analysis, compounds of the above type are predicted to give infra red spectra with two  $\nu$ (CO) bands and one  $\nu$ (NC) absorption band. This is indeed observed for complexes ( $\eta^5$ -C<sub>5</sub>H<sub>5</sub>)Mn(CO)<sub>2</sub>(CNR) (R = CH<sub>2</sub>C<sub>6</sub>H<sub>5</sub>, C<sub>6</sub>H<sub>3</sub>Me<sub>2</sub>-2,6, Me). However, for R = Bu<sup>t</sup> and C<sub>6</sub>H<sub>11</sub>, two  $\nu$ (CO) and two  $\nu$ (NC) bands are observed in both the solid state and in hexane solution (see Table 5.2). Further, all the ( $\eta^6$ -C<sub>6</sub>H<sub>5</sub>X'Cr(CO)<sub>2</sub>(CNR) (R = Bu<sup>t</sup>, X = Me, H, C<sub>2</sub>, CO<sub>2</sub>Me; R = C<sub>6</sub>H<sub>3</sub>Me<sub>2</sub>-2,6, X = Me, H) complexes studied also gave two  $\nu$ (CO) and two  $\nu$ (NC) bands both in the solid state and in CH<sub>2</sub>Cl<sub>2</sub> or hexane solution (Table 2.1), with the exception of ( $\eta^6$ -C<sub>6</sub>H<sub>5</sub>CO<sub>2</sub>Me)Cr(CO)<sub>2</sub>(CNC<sub>6</sub>H<sub>3</sub>Me<sub>2</sub>-2,6), which in solution (hexane, CCl<sub>4</sub>, CH<sub>2</sub>Cl<sub>2</sub>, CHCl<sub>3</sub>) gives two  $\nu$ (CO) bands and only one  $\nu$ (NC) band, as expected, but in the solid state (KBr), gives three  $\nu$ (CO) bands and one  $\nu$ (NC) band (Figure 8.1(a); see section 8.5). A typical example of the anomalous IR data is shown in Figure 8.1(b), the solid state spectrum of ( $\eta^6$ -C<sub>6</sub>H<sub>5</sub>CO<sub>2</sub>Me)Cr(CO)<sub>2</sub>(CNBu<sup>t</sup>). [IR(KBr):  $\nu$ (NC): 2090, 2060(sh);  $\nu$ (CO): 1908, 1856,  $\nu$ (COOMe): 1700 cm<sup>-1</sup>.]

Anomalous IR data of this nature is also observed for the related complex ( $\eta^5$ -C<sub>5</sub>H<sub>5</sub>)Ru(CNBU<sup>t</sup>)<sub>2</sub>I.<sup>8,9</sup> This complex is expected to give two  $\nu$ (NC) IR absorptions, but three  $\nu$ (NC) bands are observed in the IR spectrum in both solution (CH<sub>2</sub>Cl<sub>2</sub>, benzene) and the solid state. [IR(KBr):  $\nu$ (NC): 2130, 2098, 2060 cm<sup>-1</sup>.]

In the cases of the related complexes, ( $\eta^5$ -C<sub>5</sub>H<sub>5</sub>)Fe(CO)-[P(OMe)<sub>3</sub>]X (X = C<sub>2</sub>, Br, I)<sup>8,9a</sup> and ( $\eta^5$ -C<sub>5</sub>H<sub>4</sub>Me)Fe(CO)[P(OMe)<sub>3</sub>]I,<sup>8,9b</sup> the  $\nu$ (CO) absorption band is resolved into two components in n-heptane solutions. The doubling of the number of  $\nu$ (CO)

bands in these complexes has been ascribed to rotational isomerization,<sup>11</sup> arising from either restricted rotation about the M-P bond with the formation of eclipsed and staggered isomers, or restricted conformational rotation within the P(OMe)<sub>3</sub> ligand.

Similar effects of observing more than the anticipated number of infra red bands have been reported. For example, the complexes trans-( $\eta^5\text{-C}_5\text{H}_5$ )Fe(CO)<sub>2</sub>[C(O)CH = CHR] (R = Me, Ph)<sup>12a</sup> give three  $\nu(\text{CO})$  bands in the IR spectra, (hexane solution) instead of the expected two, and the related complexes ( $\eta^5\text{-C}_5\text{H}_5$ )Pt R<sub>1</sub> R<sub>2</sub>[C(O)Me] (R<sub>1</sub> = R<sub>2</sub> = Me, Et; R<sub>1</sub> = Me, R<sub>2</sub> = Et)<sup>12b</sup> have two  $\nu(\text{C(O)R})$  bands in the IR spectra (hexane or CCl<sub>4</sub>), while only one  $\nu(\text{C(O)R})$  band is predicted. This splitting has been ascribed to conformational isomerization about the metal-acetyl bond.<sup>11</sup> In the former case the resolution of the bands due to the conformers is not complete, with only the high frequency band showing splitting.<sup>12a</sup> The possibility of more than two isomers co-existing in solution also cannot be excluded.<sup>12a</sup> No solid state IR data of these complexes has been reported, however.

In an attempt to formulate a rationalization of the anomalous IR data of the ( $\eta^5\text{-Arene}$ )Cr(CO)<sub>2</sub>(CNR) and ( $\eta^5\text{-C}_5\text{H}_5$ )Mn(CO)<sub>2</sub>(CNR) complexes, IR spectral and X-ray crystallographic structural studies of two representative compounds, ( $\eta^5\text{-C}_5\text{H}_5\text{CO}_2\text{Me}$ )Cr(CO)<sub>2</sub>(CNBu<sup>t</sup>) and ( $\eta^5\text{-C}_5\text{H}_5$ )Mn(CO)<sub>2</sub>(CNBu<sup>t</sup>), were undertaken. Since the anomalous IR data persist both in solution and in the solid state, this fact must be taken into account by any proposed explanation of the effect.

8.2 IR spectral studies of ( $\eta^5\text{-C}_5\text{H}_5\text{CO}_2\text{Me}$ )Cr(CO)<sub>2</sub>(CNBu<sup>t</sup>) and ( $\eta^5\text{-C}_5\text{H}_5$ )Mn(CO)<sub>2</sub>(CNBu<sup>t</sup>) in different solvents

IR spectral studies of the complexes ( $\eta^5\text{-C}_5\text{H}_5\text{CO}_2\text{Me}$ )Cr(CO)<sub>2</sub>(CNBu<sup>t</sup>) and ( $\eta^5\text{-C}_5\text{H}_5$ )Mn(CO)<sub>2</sub>(CNBu<sup>t</sup>) in solvents of different polarity (Table 8.1 and 8.2 respectively) revealed that the relative intensity of the lower frequency band increases with decreasing solvent polarity. This suggests the existence of conformers with different dipole moments. In the case of ( $\eta^5\text{-C}_5\text{H}_5\text{CO}_2\text{Me}$ )Cr(CO)<sub>2</sub>(CNBu<sup>t</sup>), this

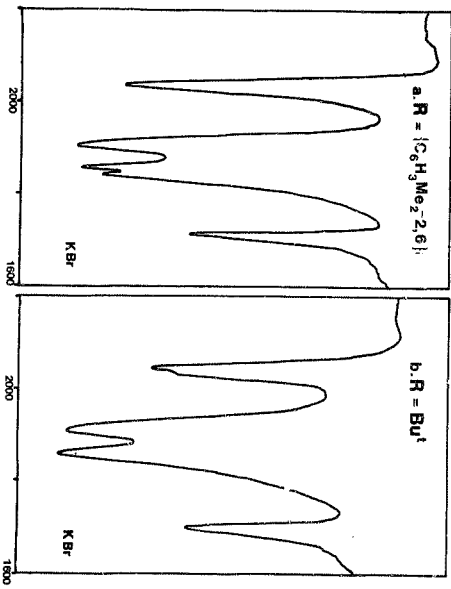


Figure B.1 Solid state IR spectra (KBr) of  $(\text{C}_6\text{H}_5\text{CO}_2\text{Me})_2\text{Cr}(\text{CO})_2$  (CMF: (a) R = C<sub>6</sub>H<sub>5</sub>Me<sub>2</sub>-2,6, (b) R = Bu<sup>t</sup>)

effect cannot be due to interaction of the RNC group with the arene-ring substituent, since  $(\eta^6\text{-C}_6\text{H}_6)\text{Cr}(\text{CO})_2(\text{CNBu}^t)$  also has two  $\nu(\text{NC})$  stretching frequencies. Further, unless there is fortuitous overlap of two sets of CO stretching frequencies, the two different conformers must have the CO ligands in very similar environments. To test this hypothesis and to determine the nature of the different conformers, crystal structure determinations of the complexes  $(\eta^6\text{-C}_6\text{H}_5\text{CO}_2\text{Me})\text{Cr}(\text{CO})_2(\text{CNBu}^t)$  and  $(\eta^5\text{-C}_5\text{H}_5)\text{Mn}(\text{CO})_2(\text{CNBu}^t)$ , were undertaken. The full crystal and molecular structures of these two complexes are reported in chs. IV and VII respectively. Structural features which could have bearing on the  $\nu(\text{NC})$  effect will be discussed.

8.3

Structural data of  $(\eta^6\text{-C}_6\text{H}_5\text{CO}_2\text{Me})\text{Cr}(\text{CO})_2(\text{CNBu}^t)$  and  $(\eta^5\text{-C}_5\text{H}_5)\text{Mn}(\text{CO})_2(\text{CNBu}^t)$  from X-ray Crystallographic Studies  
The  $(\eta^6\text{-C}_6\text{H}_5\text{CO}_2\text{Me})\text{Cr}(\text{CO})_2(\text{CNBu}^t)$  and  $(\eta^5\text{-C}_5\text{H}_5)\text{Mn}(\text{CO})_2(\text{CNBu}^t)$  molecules are illustrated in Figures 8.2 and 8.3 respectively. In both cases, the structural feature of note is the non-linear isonitrile ligand (C-N-C angle of  $166.8(4)^\circ$  and  $172(2)^\circ$  respectively). Further, in the case of  $(\eta^6\text{-C}_6\text{H}_5\text{CO}_2\text{Me})\text{Cr}(\text{CO})_2(\text{CNBu}^t)$ , the isonitrile ligand bends towards the ring (Figure 8.2), while for  $(\eta^5\text{-C}_5\text{H}_5)\text{Mn}(\text{CO})_2(\text{CNBu}^t)$ , the isonitrile bends away from the ring (Figure 8.3). In both isonitrile structures the C-N-C plane of the isonitrile ligand is close to perpendicular to the mean plane of the respective carbocycle rings ( $11^\circ$  for Cr,  $4^\circ$  for Mn; (Figure 8.4(c), (d)). It is thus possible that the observation of a non-linear RNC group could give rise to different conformers, two of which correspond to the structures shown in Figure 8.4(a) and (b). This could provide an explanation of the solution IR data. However, for both the Cr and Mn-structures, there is only one molecule in the asymmetric unit cell (Crystal data:  $P\bar{1}$ ,  $Z = 2$ , and  $Pna2_1$ ,  $Z = 4$ , respectively), of the conformations shown in Figure 8.4(a) and (b) respectively, and there is no evidence of disorder of the isonitrile ligand. Hence an alternative explanation is required to explain the solid state (KBr) IR data.

TABLE B.1: IR spectral study of  $[(\eta^5\text{-C}_6\text{H}_5\text{CO}_2\text{Me})\text{Cr}(\text{CO})_2(\text{CNBu}^t)]$  in different solvents<sup>a</sup>

| Solvent              | $\nu(\text{CO})/\text{cm}^{-1}$ | $\nu(\text{COOMe})/\text{cm}^{-1}$ | $\nu(\text{NC})/\text{cm}^{-1}$ |         | Intensity<br>Ratio A:B <sup>b</sup> |
|----------------------|---------------------------------|------------------------------------|---------------------------------|---------|-------------------------------------|
|                      |                                 |                                    | A                               | B       |                                     |
| chloroform           | 1924 vs 1872 s                  | 1708 m                             | 2112 ms                         | 2074 sh | 2.5                                 |
| dichloromethane      | 1920 vs 1868 s                  | 1710 m                             | 2100 ms                         | 2060 sh | 2.3                                 |
| toluene              | 1922 vs 1865 s                  | 1700 m                             | 2106 m                          | 2070 sh | -                                   |
| tetrahydrofuran      | 1924 vs 1879 s                  | 1718 m                             | 2104 m                          | 2076 sh | 1.5                                 |
| n-hexane             | 1960 vs 1880 s                  | 1697 m                             | 2100 m                          | 2076 sh | 1.9                                 |
| benzene              | 1940 vs 1898 s                  | 1720 m                             | 2100 mw                         | 2070 w  | 1.1                                 |
| carbon tetrachloride | 1930 vs 1884 s                  | 1699 m                             | 2112 m                          | 2070 ms | 0.8                                 |

<sup>a</sup> IR (KBr):  $\nu(\text{NC})$ , 2090, 2060(sh);  $\nu(\text{CO})$ , 1908, 1856;  $\nu(\text{COOMe})$ , 1700  $\text{cm}^{-1}$ .

<sup>b</sup> Estimated from peak areas ( $\pm 15\%$ )



TABLE 8.2: IR spectral study of  $(C_5H_5)Mn(CO)_2(CNSu^t)$  in different solvents<sup>a</sup>

| Solvents     | $\nu(CO)/cm^{-1}$ | $\nu(CN)/cm^{-1}$ |          | Ratio A:B <sup>b</sup> |
|--------------|-------------------|-------------------|----------|------------------------|
|              |                   | A                 | B        |                        |
| THF          | 1941, 1881        | 2106              | 2074(sh) | 2.9 : 1                |
| $CHCl_3$     | 1942, 1882        | 2114              | 2082(sh) | 2.2 : 1                |
| $CH_2Cl_2$   | 1940, 1881        | 2116              | 2082(sh) | 2.0 : 1                |
| $C_6H_5CH_3$ | 1943, 1883        | 2110              | 2080     | 1.7 : 1                |
| $C_6H_6$     | 1944, 1893        | 2108              | 2074     | 1.6 : 1                |
| $CCl_4$      | 1948, 1897        | 2104              | 2073     | 1.4 : 1                |
| $C_6H_{12}$  | 1952, 1905        | 2102              | 2070     | 1.2 : 1                |

<sup>a</sup> IR(KBr):  $\nu(NC)$ , 2118, 2072(sh);  $\nu(CO)$ , 1971, 1926  $cm^{-1}$

<sup>b</sup> Estimated from peak areas ( $\pm$  15%)

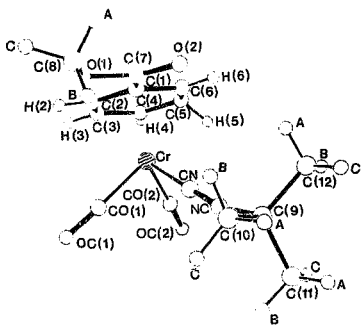


Figure 8.2 Sideways ORTEP <sup>33</sup> view of the  $(\eta^6\text{-C}_6\text{H}_5\text{CO}_2\text{Me})\text{Cr}(\text{CO})_2\text{-(CNBu)}_t$  molecule.

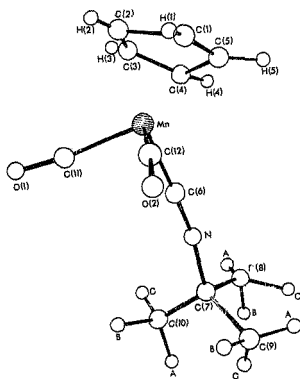
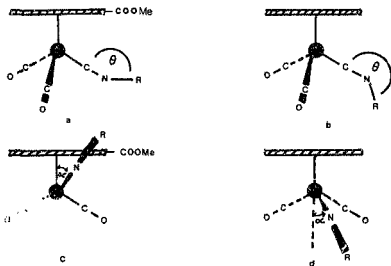


Figure 1. Sideways ORTEP<sup>33</sup> view of the  $(\eta^5\text{C}_5\text{H}_5)\text{Mn}(\text{CO})_2(\text{CNBu}^t)$  molecule



- (a)  $(\eta^6\text{-C}_6\text{H}_5\text{CO}_2\text{Me})\text{Cr}(\text{CO})_2(\text{CNBu}^t) - \theta = 166.8(4)^\circ$   
 (b)  $(\eta^5\text{-C}_5\text{H}_5)\text{Mn}(\text{CO})_2(\text{CNBu}^t) - \theta = 188(2)^\circ$   
 (c)  $(\eta^6\text{-C}_6\text{H}_5\text{CO}_2\text{Me})\text{Cr}(\text{CO})_2(\text{CNBu}^t) - \alpha = 11(1)^\circ$   
 (d)  $(\eta^5\text{-C}_5\text{H}_5)\text{Mn}(\text{CO})_2(\text{CNBu}^t) - \alpha = 4(2)^\circ$

**Figure 8.4** Diagram illustrating the conformation of the  $\text{CNBu}^t$  ligand in  $(\eta^6\text{-C}_6\text{H}_5\text{CO}_2\text{Me})\text{Cr}(\text{CO})_2(\text{CNBu}^t)$  ((a) and (c)) and  $(\eta^5\text{-C}_5\text{H}_5)\text{Mn}(\text{CO})_2(\text{CNBu}^t)$  ((b) and (d))

8.4 Structural data on  $(\eta^5\text{-C}_5\text{H}_5)\text{Ru}(\text{CNBu}^t)_2\text{I}$  from an X-ray Crystallographic study

As mentioned in section 8.1,  $(\eta^5\text{-C}_5\text{H}_5)\text{Ru}(\text{CNBu}^t)_2\text{I}$  gives three, instead of two  $\nu(\text{NC})$  absorptions in the IR spectrum both in solid state and in solution. The X-ray crystal and molecular structure of this complex has been reported.<sup>47</sup> The compound crystallizes in the triclinic space group  $\overline{P}1$  with  $Z = 4$ , i.e. there are two molecules in the asymmetric unit. These two crystallographically independent molecules do not have the same ligand conformation with respect to the cyclopentadienyl ring. This suggests a possible explanation of the solid-state IR data. The two conformations probably arise from packing forces in the crystal. Further, there is the possibility of intermolecular interactions between the two different molecules.

Of significance is the finding that each molecule contains two different types of RNC groups, viz. one near-linear ( $\text{C-N-C}, 175^\circ(\text{av.})$ ), and one with a larger  $\text{C-N-C}$  bend ( $162^\circ(\text{av.})$ ). In both molecules the bent isonitrile points away from the ring. This suggests the possibility of the existence of conformers (Figure 8.4(a) and (b)) to account for the solution IR data. Another possible explanation could be the lowering of the symmetry of the molecule by the bending of an isonitrile.

8.5 The solid state IR spectrum and crystal structure of  $(\eta^5\text{-C}_5\text{H}_5\text{CO}_2\text{Me})\text{Cr}(\text{CO})_2(\text{CNC}_6\text{H}_5\text{Me}_2-2,6)$

In hexane solution, the IR spectrum of the complex  $(\eta^5\text{-C}_5\text{H}_5\text{CO}_2\text{Me})\text{Cr}(\text{CO})_2(\text{CNC}_6\text{H}_5\text{Me}_2-2,6)$ , unlike that of the other  $(\eta^5\text{-Arene})\text{Cr}(\text{CO})_2(\text{CNR})$  derivatives studied, is as expected, viz. two  $\nu(\text{CO})$  bands and one  $\nu(\text{NC})$  band. However, in the solid state (KBr), three  $\nu(\text{CO})$  bands and one  $\nu(\text{NC})$  band is observed. (Figure 8.1(a): IR (KBr):  $\nu(\text{NC})$ : 2070;  $\nu(\text{CO})$ : 1904, 1855, 1840;  $\nu(\text{COOMe})$ : 1715  $\text{cm}^{-1}$ ).

If, as suggested in sections 8.2-8.3, the observation of two  $\nu(\text{NC})$  IR bands for  $(\eta^5\text{-C}_5\text{H}_5\text{CO}_2\text{Me})\text{Cr}(\text{CO})_2(\text{CNBu}^t)$ , arises due to the bent isonitrile ligand (conformers in solution, influence of crystal packing forces in solid state), the

observation of only one  $\nu(\text{NC})$  IR band (in both solution and solid state) for  $(\eta^5\text{C}_6\text{H}_5\text{CO}_2\text{Me})\text{Cr}(\text{CO})_2(\text{CNC}_6\text{H}_5\text{Me}_2-2,6)$  suggests the isonitrile ligand should be linear in this complex. Hence a crystal structure determination of the compound was undertaken. Also, the observation of splitting of one of the  $\nu(\text{CO})$  bands in the solid state IR spectrum only was considered likely to be accountable in terms of crystal packing.

Standard Weissenberg and precession photography gave the monoclinic space group  $P2_1/c$  (absences  $h0l$ ,  $l = 2n + 1$ , and  $0k0$ ,  $k = 2n + 1$ ), and the unit cell parameters were determined as  $a = 30.15(6)\text{\AA}$ ,  $b = 7.35(2)\text{\AA}$ ,  $c = 13.2(4)\text{\AA}$ ,  $\beta = 105^\circ$ ,  $V = 3560\text{\AA}^3$  with  $Z = 8$ . A full data set was collected, but attempts to solve the molecular structure, in  $P2_1/c$ , and other possible monoclinic space groups,\* using heavy atom, and direct methods, were not successful.

However, as the X-ray photographs obtained showed no evidence of centering, it appears as if the asymmetric unit contains at least two (possibly four) molecules, with the possibility of intermolecular interactions, eg. between a carbonyl on one molecule and a group on a crystallographically independent molecule. Therein probably lies the explanation of the anomalous solid state IR spectrum.

## 8.6 Possible explanations for the anomalous IR data

### 8.6.1 Conformers in solution

#### (a) RNC bending

As expected in sections 8.2-8.4, the observation of bent nitrile ligands in the three isonitrile derivatives studied crystallographically suggests the existence of conformers (eg. Figure 8.4(a) and (b)) could account for the anomalous IR solution data. The predominance of one or other conformer appears from the IR studies (section 8.2) to depend on the solvent polarity. It has been shown<sup>11</sup> for biphenylchromiumtricarbonyl that increased inductive electron withdrawal in chloroform than in benzene results from interaction of the strongly polar solvent with the electron-rich chromium centre.

\* The condition  $0k1$ ,  $k = 2n+1$  was also observed; hence it was thought that the compound might exhibit pseudo-orthorhombic symmetry.

(b) Tripodal rotation

Conformational isomers could also arise in solution due to the rotation of the  $L_3$  tripod around the metal-ring axis. For the complexes examined, the barrier to such a rotation is predicted to be very small.<sup>17</sup>

In's proposal receives a measure of support from recent low temperature  $C^{13}$  NMR studies on  $(\eta^6-C_6Et_6)Cr(CO)_2$  (CS),<sup>18a</sup> in which the low temperature isomer was found to possess the same symmetry as the solid state structure. It has been claimed that this demonstrates that rotation resulting in isomers co-existing in solution is due to tripodal rotation around the Cr-Arene bond, which is slowed down at low temperatures. However, this claim has been disputed by other workers,<sup>18b,c</sup> who interpret the results in terms of restricted ethyl group rotation about the arene ring.

8.6.2 Solid state effects

(a) Crystal lattice effects

In solid state infra red spectra, an absorption band splitting may occur when the band corresponds to a degenerate vibration of the isolated molecule because the site symmetry of the molecule in the crystal lattice may be lower than that of the isolated molecule.<sup>19,20</sup>

With non-degenerate vibrations, the coupling together of vibrations of adjacent molecules can give rise to various combinations leading to band multiplicity.<sup>21</sup> A simple factor-group analysis often fails to predict the number of observed IR bands. This is a consequence of the vibrational unit cell appropriate to the groups, being of different effective symmetry to the crystallographic unit cell.<sup>22</sup>

(b) Packing effects

The crystal lattice is governed by the principle of dense packing<sup>23</sup> i.e. the molecules pack together in such a way as to minimize the voids between adjacent molecules and so make the most economic use of space. As a result of the influence of crystal packing forces, interaction

between groups on adjacent molecules, or the same molecule may become possible owing to relatively short non-bonded distances. Hence the anomalous IR data could arise from short intermolecular or intramolecular non-bonded contacts (eg. O(2)...H(10C), 2.75Å, or O(2)...H(8A), 2.55Å respectively, in  $(\eta^6\text{C}_6\text{H}_5\text{CO}_2\text{Me})\text{Cr}(\text{CO})_2(\text{CNBu}^t)$ .)

8.6.3. Lowering of molecular symmetry by bent isonitrile

The anomalous IR data could also arise from a lowering of the molecular symmetry by the bent isonitrile ligand. (C-N-C in range 162-172°). It has been shown using Ab Initio MO Calculations\*\* that for RNC ligands, as the C-N-C angle decreases, the  $\pi$ -acceptor character of the RNC ligand increases markedly. Hence a bent isonitrile reflects an enhanced degree of back-bonding ( $M(3d) \rightarrow (CN) \pi^*$ )\*\* Hence the degree of bending found for a particular isonitrile ligand could reflect electronic rather than steric factors.

#### 8.7 Conclusion

From the foregoing analysis, the most likely localization of the anomalous IR data for the  $(\eta^6\text{-Arene})\text{Cr}(\text{CO})_2(\text{CNR})$  and  $(\eta^5\text{-C}_5\text{H}_5)\text{Mn}(\text{CO})_2(\text{CNR})$  complexes appears to be:-

(a) In solution, the existence of conformers with the RNC ligand bending towards (fig. 8.4(a)) or away from (Fig. 8.4(b)) the ring. The predominance of one or other conformer in a particular solvent depends on the solvent polarity. The results of the IR studies in solvents of varying polarities (section 8.2) favours conformers arising from RNC-bending (vide supra) rather than from tripod rotation.

(b) In solid state, a lowering of the molecular symmetry due to the bending of the RNC ligand (one conformer only present in the crystal\*) or intramolecular interactions between groups. Alternately, the phenomenon may be due to crystal lattice effects (see section 8.6.2.(a)).

\* It is possible that there could be more than one conformer in the polycrystalline sample of  $(\eta^6\text{C}_6\text{H}_5\text{CO}_2\text{Me})\text{Cr}(\text{CO})_2(\text{CNBu}^t)$ , but the  $(\eta^5\text{C}_5\text{H}_5)\text{Mn}(\text{CO})_2(\text{CNBu}^t)$  sample consisted of single crystals.



IX. THE GEOMETRY OF  $Fe(CO)_{5-n}(L)_n$  ( $n = 1, 2$ ) STRUCTURES, AND THE CRYSTAL AND MOLECULAR STRUCTURE OF  $Fe(CO)_3(CNMe)_2$

9.1 Introduction

For penta co-ordinate transition metal complexes of the type  $M(L)_5$ , two basic geometries are possible, viz. the  $D_{3h}$  trigonal bipyramidal (tb<sub>p</sub>), and the  $C_{4v}$  square pyramidal (spy). The energy difference between the two geometries is very small,<sup>1,2</sup> with the trigonal pyramidal arrangement of five valence electron pairs being slightly more stable for  $d^0$  and  $d^{10}$  transition metals, as well as for non-transition elements.<sup>3</sup>

However, according to Gillespie's<sup>4</sup> valence-shell electron-pair repulsion theory, for transition metal atoms with non-symmetrical d-configurations, the interaction of the valence-shell electron pairs with the non-bonding-d-shell as well as with each other, determines the overall geometry of the  $M(L)_5$  complex. This additional interaction may result in the square pyramidal geometry becoming more stable than the trigonal bipyramidal structure.

On the basis of Molecular Orbital (MO) calculations, Elian and Hoffmann<sup>5</sup> have shown that for  $d^8$  transition metals eg.  $Fe^0$ , complexes of the type  $M(L)_5$  are predicted to adopt a trigonal bipyramidal structure. Hence  $Fe(L)_5$  complexes would be expected to exhibit trigonal bipyramidal geometry.

The X-ray structure of iron pentacarbonyl,  $Fe(CO)_5$ , was first reported by Hanson<sup>6a</sup> in 1962, and redetermined the following year by Donohue and Caron.<sup>6b</sup> The geometry of the  $Fe(CO)_5$  molecule is trigonal bipyramidal, with no significant distortions according to the redetermined structure.<sup>6b</sup> The OC-Fe-CO angles are all close to the ideal values (ax OC-Fe-COax :  $176(2)^\circ$ , av. eq OC-Fe-COax  $90(1)^\circ$ , and eq OC-Fe-COeq :  $120(1)^\circ$ <sup>6b</sup>). Within the limits of experimental error, the Fe-Cax and Fe-Ceq bond lengths are equal (av. Fe-CO :  $1.79(2)\text{\AA}$ <sup>6b</sup>).

However, from a more recent (1969) electron diffraction study<sup>7</sup> of  $Fe(CO)_5$ , the Fe-COax bonds (av.  $1.806(5)\text{\AA}$ ) are significantly shorter than the Fe-COeq bonds (av.  $1.833(4)\text{\AA}$ ).

From an analysis of electronic effects in  $tbp d^8 M(L)_5$  complexes, Rossi and Hoffmann<sup>101</sup> have concluded that strong  $\sigma$ -donors will strengthen axial M-L bonds. A  $\pi$ -acceptor tends to counteract this  $\sigma$ -bonding effect, while a  $\pi$ -donor reinforces it. Hence for ligands that are good  $\pi$ -acceptors, the  $\sigma$ - and  $\pi$ -bonding effects oppose each other, although the  $\sigma$ -bonding effect seems to dominate, i.e. longer equatorial M-L bonds are found. This is indeed observed for  $Fe(CO)_5$  (*vide supra*), since carbonyls are good  $\pi$ -acceptors.<sup>102</sup>

Using valence-shell electron-pair repulsion theory, Gillespie<sup>98</sup> reached the conclusion that the oblate ellipsoidal electron clouds of  $d^8 tbp M(L)_5$  complexes favour axial bonds which are shorter than equatorial bonds. However, Gillespie pointed out that this difference in bond lengths is likely to be small.

When considering the overall geometry of  $M(L)_5$  complexes, steric and electrostatic effects<sup>101</sup> as well as electronic factors must be taken into account. For complexes of the type  $Fe(CO)_{5-n}(L)_n$  ( $n = 1-5$ ), where ligand(s) L has been substituted for one or more carbonyls, steric factors may have an important influence on structure, especially if L is a bulky ligand.

## 9.2 The Geometry of $Fe(CO)_4L$ Structures

### 9.2.1. Axial versus Equatorial Site Preference of L

Given that  $d^8$  complexes of the type  $M(L)_5$  are expected to display  $tbp$  geometry<sup>91,97</sup> for complexes of the type  $Fe(CO)_4L$ , the relative stability of the axial (ax) or equatorial (eq) location of a ligand L vis-à-vis CO is dependent on electronic factors, such as the  $\sigma$ - and  $\pi$ -bonding characteristics of the ligand L relative to CO, as well as on steric considerations.<sup>102</sup> A ligand L which has large steric requirements might be driven by steric forces towards an equatorial position, where the number of  $90^\circ$  interactions with adjacent ligands is smaller.<sup>103</sup>

Based on electronic considerations, Rossi and Hoffmann<sup>101</sup> have predicted that both good  $\sigma$ -donors and good  $\pi$ -donors

prefer axial sites. With a ligand that is both a good  $\sigma$ -donor and a good  $\pi$ -acceptor, however, the trends oppose, and the site occupied by the ligand depends on the relative strength of the  $\sigma$ - and  $\pi$ -bonding effects. Nevertheless, based on a simple  $\pi$ -bonding model, strong  $\pi$ -acceptors tend to occupy equatorial sites, so that back-bonding may be optimized.<sup>154</sup> This results from the greater availability of metal d-orbitals of correct symmetry to form  $\pi$ -bonds with ligands in equatorial versus axial sites.<sup>97</sup> Hence, for  $Fe(CO)_4L$  complexes, in the absence of overwhelming steric repulsion,<sup>97</sup> a ligand L that is a weaker  $\pi$ -acceptor and/or a stronger  $\sigma$ -donor than CO (eg. isonitriles,<sup>93</sup> phosphines,<sup>94, 103</sup> stibines,<sup>95</sup> arsines,<sup>104</sup> sulphides,<sup>105</sup> amines<sup>106</sup>) would be expected to occupy an axial position.

Table 9.1 lists complexes of the type  $Fe(CO)_4L$  (excluding those complexes with olefinic ligands and complexes with bidentate ligands such as  $Fe(CO)_4(AsC_6F_5)_2$ <sup>108</sup> [ $Fe(CO)_4(B_2H_{12})$ ]<sup>109</sup> in which the iron atom is essentially hexa co-ordinate) for which X-ray Crystal and Molecular structures have been determined. All these complexes exhibit  $tbp$  geometry ( $C_{3v}$  symmetry), with ligand L occupying an axial site, with the exception of  $L = PPh(PPh_2)_2$ ,<sup>110</sup> which occupies an equatorial position. This exception is probably due to the predominance of steric factors with the bulky phosphine ligand.

#### 9.2.2 Distortions to the $tbp$ geometry

Geometric data for the  $ax-L-Fe(CO)_4$   $tbp$  structures of Table 9.1 are summarized in Table 9.2. In the majority of cases, the  $tbp$  geometry is slightly distorted, with a bending of the equatorial CO ligands towards the axial L substituent<sup>111, 112</sup> (ie.  $axOC-Fe-CO_{eq}$  angles slightly greater than the ideal  $90^\circ$ , and  $L-Fe-CO_{eq}$  angles slightly less than  $90^\circ$ .)

A variety of possible reasons have been advanced to account for this phenomenon:-

- 1) Influence of crystal packing forces.<sup>98a</sup>

TABLE 9.1: X-Ray Crystal Structures of  $\text{Fe}(\text{CO})_4$  Complexes<sup>a</sup>

| Complex  | Space Group, Z | Geometry <sup>b</sup> | Position of I <sup>c</sup> | Reference |
|--|----------------|-----------------------|----------------------------|-----------|
| $[\text{HFe}(\text{CO})_4]^-$  | $P2_1/c, 4$    | thp                   | ax                         | 111       |
| $[\text{NiFe}(\text{CO})_4]^-$   | $P2_1/c, 4$    | thp                   | ax                         | 97        |
| $(\text{Me}_3\text{As})\text{Fe}(\text{CO})_4$   | $R3, 3, d$     | thp                   | ax                         | 112       |
| $(\text{Me}_2\text{Sb})\text{Fe}(\text{CO})_4$   | $R3, 3, d$     | thp                   | ax                         | 112       |
| $(\text{Ph}_3\text{Sb})\text{Fe}(\text{CO})_4$   | $P1, 2$        | thp                   | ax                         | 113       |
| $(\text{Ph}_3\text{P})\text{Fe}(\text{CO})_4$  | $P1, 2$        | thp                   | ax                         | 104       |
| $(\text{Bu}_3\text{P})\text{Fe}(\text{CO})_4$  | $P2_1^2/P1, 4$ | thp                   | ax                         | 114       |
| $(\text{Ph}_2\text{HP})\text{Fe}(\text{CO})_4$   | $P2_1/c, 4$    | thp                   | ax                         | 114       |
| $(\text{OC})_2\text{Fe}(\text{PMe}_2)_2\text{Fe}(\text{CO})_4$   | $P1, 1, e$     | thp f                 | ax                         | 114       |
| $[(\text{Me}_2\text{N})_3]_2\text{Fe}(\text{CO})_4$  | $P2_1/c, 4$    | thp                   | ax                         | 1         |
| $[\text{I}^-\text{PPh}_2\text{CH}_2\text{CH}_2\text{PPh}_2]_2\text{Fe}(\text{CO})_4$                   | $P2_1/c, 4$    | thp                   | ax                         | 115       |
| $[(\text{Me}_2\text{As})\text{C}(\text{CF}_3)_2\text{CPh}_2]_2\text{Fe}(\text{CO})_4$                  | $P2_1/c, 4$    | thp                   | ax                         | 120       |
| $[(\text{Me})\text{N}(\text{CH}_2\text{CH}_2\text{N}(\text{Me})\text{Fe})\text{Fe}(\text{CO})_4$       | $P2_1/c, 4$    | thp                   | ax                         | 110       |
| $[(\text{PPh}_2)_2\text{PPh}]_2\text{Fe}(\text{CO})_4$   | $P1, 2$        | thp                   | eq                         | 107       |
| $(\text{C}_5\text{H}_5\text{N})_2\text{Fe}(\text{CO})_4$   | $P2_1/n, 4$    | thp                   | ax                         | 107       |
| $[\text{DHCHN}(\text{CH}_2)_3]_2\text{Fe}(\text{CO})_4$  | $P2_1/c, 4$    | thp                   | ax                         | 107       |
| $[\text{CH}(\text{CH}_3)_3\text{N}]_2\text{Fe}(\text{CO})_4$   | $P2_1/n, 4$    | thp                   | ax                         | 121       |
| $[(\text{CO})_2\text{Me}]_2\text{C}_6\text{H}_5\text{N}(\text{CH}_2)_3\text{N}[\text{Fe}(\text{CO})_4$ | $P2_1/c, 4$    | thp                   | ax                         | 122       |
| $[\text{PhCH}(\text{CH}_3)_2\text{N}(\text{Me})]_2\text{Fe}(\text{CO})_4$                              | $P2_1/n, 4$    | thp                   | ax                         | 123       |
| $(\text{Ph}_2\text{C}_3\text{B})\text{Fe}(\text{CO})_4$  | $P1, 2$        | thp                   | ax                         | 124       |
| $[\text{CH}_2\text{S}(\text{CH}_2)_3]_2\text{Fe}(\text{CO})_4$   | $Pn2_1, a, 4$  | thp                   | ax                         | 106       |

TABLE 9.1 (Cont.)

| Complex                         | Space Group Z         | Geometry <sup>b</sup> | Position of L <sup>c</sup> | Reference |
|---------------------------------|-----------------------|-----------------------|----------------------------|-----------|
| $[(Me)N(CH_2)_2N(Me)C]Fe(CO)_4$ | C2/c, 8               | tbp                   | ax                         | 125       |
| $[O(C_6H_5)_2OC]Fe(CO)_4$       | P2 <sub>1</sub> /c, 4 | tbp                   | ax                         | 126       |
| $[(H_3C)_3Fe(CO)_4]^-$          | C2/c, 8               | tbp                   | ax                         | 127       |
| $[(C_6H_5)_3Fe(CO)_4]^-$        | P2 <sub>1</sub> , 2   | tbp                   | ax                         | 128       |

a L not an olefin or bidentate ligand

b tbp = trigonal bipyramidal

c ax = axial, eq = equatorial

d molecule possesses crystallographic 3-fold symmetry

e asymmetric unit corresponds to  $(Me)_2P(Fe(CO)_4)$  fragment

f co-ordination of Fe-atom

1  
98  
7

TABLE 9.2: Geometric data for  $\text{ex-L-Fe}(\text{CO})_4$  top structures  
(Bond angles in degrees, bond lengths in Å)

| L  | $\text{L-Fe-COax}$ | $\text{L-Fe-COeq}^a$ | $\text{exOC-Fe-OCeq}^b$ | $\text{eqOC-Fe-COeq}^c$ | $\text{Fe-C-O}^d$  | $\text{Fe-COax}$ | $\text{Fe-COeq}^e$ |
|--|--------------------|----------------------|-------------------------|-------------------------|--------------------|------------------|--------------------|
| H  | 175(5)             | 81(5)                | 99.1(7)                 | 117.6(8)                | 177.7(2)           | 1.72(2)          | 1.75(2)            |
| CN <sup>-</sup>  | 175.9(3)           | 87.4(3)              | 92.7(4)                 | 119.8(4)                | 176.9(9)           | 1.723(8)         | 1.769(8)           |
| Aske <sub>3</sub> <sup>b</sup>   | 180.0 <sup>c</sup> | 94.0 <sup>c</sup>    | 86.0 <sup>c</sup>       | 119.5 <sup>c</sup>      | 167 <sup>c,d</sup> | 2.4(3)           | 1.73 <sup>c</sup>  |
| SiMe <sub>3</sub>  | 180.0 <sup>c</sup> | 88.4 <sup>c</sup>    | 91.6 <sup>c</sup>       | 119.9 <sup>c</sup>      | 178 <sup>c,e</sup> | 1.81(9)          | 1.66 <sup>c</sup>  |
| SBPh <sub>3</sub>  | 178.1(4)           | 88.3(2)              | 91.7(2)                 | 119.9(2)                | 179(1)             | 1.765(4)         | 1.787(4)           |
| PPh <sub>3</sub>   | 178.3(1)           | 89.8(1)              | 91.2(2)                 | 119.9(2)                | 178.5(4)           | 1.795(4)         | 1.795(4)           |
| PBu <sub>3</sub>   | 175.7(1)           | 93.3(7)              | 87(1)                   | 119.7(2)                | 173.2(4)           | 1.754(4)         | 1.792(4)           |
| PfPh <sub>3</sub>  | 177.1(3)           | 89.2(2)              | 90.9(4)                 | 120.0(2)                | 177.7(2)           | 1.78(2)          | 1.793(9)           |
| PMe <sub>2</sub> <sup>e</sup>  | 175.4(6)           | 89.1(6)              | 91(1)                   | 120.0(9)                | 176(2)             | 1.73(2)          | 1.73(1)            |
| P(NMe <sub>2</sub> ) <sub>3</sub>  | 178.1(2)           | 92.1(2)              | 90.9(2)                 | 120.0(2)                | 177.9(5)           | 1.793(6)         | 1.787(5)           |
| [ $\eta^5\text{-C}_5\text{H}_5\text{CH}_2\text{CH}_2\text{PPh}_2$ ]      | 179.3(2)           | (2)                  | 91.5(3)                 | 120.0(3)                | 178.7(6)           | 1.771(6)         | 1.780(6)           |
| [Me <sub>2</sub> As]C(CF <sub>3</sub> ) <sub>2</sub> CPPh <sub>2</sub> ] | 178.8(9)           | (4)                  | 90.6(6)                 | 120.0(6)                | 179(2)             | 1.74(2)          | 1.74(1)            |
| [Me]NCH <sub>2</sub> CH <sub>2</sub> N(Me)P]                             | 175.4(2)           | 82.1(2)              | 91.0(3)                 | 120.0(3)                | 178.7(6)           | 1.803(6)         | 1.76(6)            |
| C <sub>5</sub> H <sub>5</sub> N  | 176.2(2)           | 89.5(2)              | 89.6(3)                 | 120.0(3)                | 178.3(6)           | 1.722(7)         | 1.805(7)           |
| [CHCHN(CH <sub>2</sub> ) <sub>2</sub> N]                                 | 175.8(2)           | 90.7(1)              | 89.4(2)                 | 120.0(2)                | 177.8(4)           | 1.774(4)         | 1.810(4)           |
| [CH(CH <sub>3</sub> ) <sub>3</sub> N]                                    | 175.6(2)           | 89.8(2)              | 90.3(3)                 | 120.0(3)                | 177.7(6)           | 1.765(7)         | 1.809(7)           |
| [CO <sub>2</sub> Me] <sub>2</sub> C(CH <sub>2</sub> Ph) <sub>2</sub> N]  | 178.7(1)           | 90.7(1)              | 89.3(2)                 | 120.0(2)                | 177.4(3)           | 1.773(4)         | 1.807(4)           |
| [PhCH(CH <sub>3</sub> ) <sub>2</sub> N(Me)]                              | 174.5(2)           | 91.1(2)              | 89.1(3)                 | 119.3(3)                | 176.5(6)           | 1.744(6)         | 1.790(6)           |
| (Ph <sub>2</sub> C <sub>3</sub> S)                                       | 172.2 <sup>c</sup> | 89.0 <sup>c</sup>    | 91.0 <sup>c</sup>       | 120.0 <sup>c</sup>      | 178.6 <sup>c</sup> | 1.758(4)         | 1.810(4)           |

TABLE 9.2 (Cont.)

| L   | L-Fe-00ax | L-Fe-00eq <sup>a</sup> | ax0C-Fe-00eq <sup>a</sup> | sq0C-Fe-00eq <sup>a</sup> | Fe-C-O <sup>b</sup> | Fe-00ax  | Fe-00eq <sup>a</sup> |
|---|-----------|------------------------|---------------------------|---------------------------|---------------------|----------|----------------------|
| $[\text{Et}_2\text{Si}(\text{CH}_2)_3]_3$                           | 179.4(3)  | 89.9(3)                | 91.7(4)                   | 120.0(5)                  | 175.2(8)            | 1.798(9) | 1.764(9)             |
| $[(\text{Me})_2\text{N}(\text{CH}_2)_2\text{N}(\text{Me})\text{C}]$ | 167.6(2)  | 90.8(2)                | 90.2(3)                   | 120.0 <sup>c</sup>        | 176.3(5)            | 1.767(6) | 1.789(8)             |
| $[\text{d}(\text{C}_6\text{H}_4)_2\text{O}]$                        | 179.28(6) | 88.85(7)               | 91.15(7)                  | 119.86(7)                 | 178.6(2)            | 1.795(2) | 1.799(2)             |
| $(\text{C}_2\text{H}_5)_2$  | 175.3(9)  | 83.9(8)                | 96.1(9)                   | 118.9(9)                  | 176(2)              | 1.74(2)  | 1.75(2)              |
| $(\text{SiO}_2)_2$  | 178(1)    | 86(1)                  | 94(1)                     | 119(1)                    | 177(3)              | 1.77(3)  | 1.75(3)              |

- a Average value
- b 3-fold symmetry crystallographically imposed on molecule
- c Bond data obtained from the Cambridge Crystallographic Data Base
- d Fe-C-O(eq): 162.8°, Fe-C-O(ax): 180.0°
- e Fe-C-O(eq): 176.8°, Fe-C-O(ax): 180.0°
- f av. Fe-C-O(eq): 171.9(4)°, Fe-C-O(ax): 177.2(4)°
- g  $(\text{OC})_4\text{Fe}(\text{PMe}_2)_2\text{Fe}(\text{CO})_4$

2) Steric factors

a) Intramolecular interactions, especially repulsions between phenyl groups on L with equatorial carbonyls.<sup>112, 114, 115</sup>

b) Short intermolecular contacts.<sup>112</sup>

3) Electronic factors

i) Rehybridization of orbitals of Fe resulting in a decrease in repulsions between electron pairs of Fe and L, and a concomitant enhancement of overlap of filled Fe-orbitals with acceptor-orbitals of the equatorial CO ligands. The new hybrid orbitals occupied by non-bonding electrons would be pointing away from the axial position of the tbp occupied by CO.<sup>129, 130</sup>

ii) An electron density donation from L  $d_{z^2}$  orbitals to eqCO  $2 \pi_y$  orbitals. A bending of eqCO ligands towards L would be expected to increase Fe-COeq orbital overlap.<sup>131</sup>

iii) Valence-shell electron-pair repulsions: An increase in the angle between multiple-bond character Fe-CO bonds, and the decrease in the angle between the single Fe-L bond and the Fe-COeq bonds would decrease repulsions between the bonding electrons and so stabilize the molecule<sup>132</sup> (applies to cases where the Fe-L bond is of single-bond character.)

9.2.3 Fe-CO bond length trends

In the parent complex,  $\text{Fe}(\text{CO})_5$ , the Fe-COax bonds (av. 1.806(5)Å) are significantly shorter than the Fe-COeq bonds (av. 1.833(4)Å).<sup>133</sup> The electronic rationale for this effect of shorter M-Lax bonds than M-Leq bonds in  $d^8$  tbp  $M(\text{L})_5$  complexes has been discussed in Section 9.1. However, for substituted complexes of the type  $\text{ax-LFe}(\text{CO})_4$ , the effect of L on the Fe-CO bond lengths must be considered. The nature of this effect depends on the electronic properties of the ligand L relative to CO. The two axial ligands compete for the two Fe  $d_x$  orbitals.<sup>117b, 122</sup> When L is a poorer  $\pi$ -acceptor than CO, metal back-bonding to



the axial CO will increase, resulting in a shorter Fe-COax bond.<sup>118,117b</sup> It has been shown from core electron-binding energies and valence-orbital ionization potentials<sup>133</sup> that for  $\underline{ax}$ -LFe(CO)<sub>4</sub> complexes, where L is a poorer  $\pi$ -acceptor than CO, the Fe  $dx^2-y^2$ ,  $dxy$  orbitals do not interact with the axial ligands, whereas the Fe  $dxz$ ,  $dyz$  orbitals are destabilized by ca. 0.3ev (relative to Fe(CO)<sub>5</sub>) because of the loss of the strongly back-bonding CO ligand.

The Fe-CO bond length data in Table 9.2 for  $\underline{ax}$ -LFe(CO)<sub>4</sub> complexes shows two trends:-

- 1) The Fe-C bond lengths in the substituted complexes are generally shorter than those in Fe(CO)<sub>5</sub> itself. This trend is rationalized in terms of the replacement of one CO group by a poorer  $\pi$ -acceptor ligand L increasing the amount of  $\pi$ -bonding to the remaining four CO groups and thus shortening the Fe-CO bond lengths.<sup>134</sup>
- 2) For the majority of  $\underline{ax}$ -LFe(CO)<sub>4</sub> complexes, the Fe-COax bond length is shorter than the Fe-COeq bond lengths. For ligands L which are poorer  $\pi$ -acceptors than CO, this is expected in terms of the axial trans-effect (vide supra).

In the case of  $\underline{eq}[(PPH_2)_2PhP]Fe(CO)_4$ , where no axial trans effect operates, the Fe-COeq and Fe-COax bond lengths are equal within experimental error (av. values of 178.0(6) and 178.8(6)<sup>c</sup> respectively<sup>134</sup>), but shorter than those found in Fe(CO)<sub>5</sub> (vide supra).

However, Cotton et al<sup>134</sup> have pointed out that caution must be exercised in interpreting Fe-CO bond length differences as significant, especially where the differences are small, as the data have generally not been corrected for thermal motion. For instance, a greater thermal motion in the axial carbonyl and correction for thermal motion, would lengthen the Fe-COax bond more than the Fe-COeq bonds.

#### 9.2.4 Fe-C-O bond angles

In these LFe(CO)<sub>4</sub> complexes, the carbonyl ligands

co-ordinate in an essentially linear manner, with Fe-C-O bond angles generally in the range 175 - 179°. (Table 9.2). Kettle<sup>9</sup> has shown that ca. 5° deviations from linearity are expected for  $M(CO)_n$  ( $n = 2-4$ ) groups, due to different occupation of the two anti-bonding  $\pi^*$  orbitals on a carbonyl ligand. This applies to other ligands electronically similar to CO, eg. CN. (In  $[(NC)Fe(CO)_4]^+$ , the Fe-C-N bond angle is found to be 178.0(7)°<sup>10</sup>). The reason for the different Fe-C-O angles within the  $Fe(CO)_4$  group must lie in crystal packing forces.<sup>11</sup>

The larger deviations from linearity of the  $sqFe-C-O$  bonds (av. Fe-C-O(eq): 171.9(4)°) than the  $axFe-C-O$  bond (Fe-C-O(ax): 177.2(4)°) in  $(tBu_3P)Fe(CO)_4$ <sup>11a</sup> could be due to steric repulsions between the eq CO ligands and the  $tBu$ -groups of the bulky phosphine ligand (Tolman cone angle<sup>11a</sup> for  $tBu_3P$ : 182°). A similar effect is observed with the bulky  $AsMe_3$  and  $SbMe_3$  ligands<sup>12</sup> (see footnotes d and e to Table 9.2). Deviations from ideal geometry could also be due to crystal packing forces.<sup>11a</sup>

### 9.3 The Geometry of $Fe(CO)_3(L)_2$ Structures

#### 9.3.1 Geometry - $tbp$ , distorted $tbp$ , $spy$

For penta co-ordinate complexes, there are two basic geometry types viz.  $tbp$  and  $spy$ . These two geometries may differ little in energy,<sup>13,14,15</sup> and the actual arrangement may lie somewhere between the two ideal configurations.<sup>13</sup> As mentioned previously, for  $d^6 M(L)_5$  complexes, a  $tbp$  geometry is predicted on electronic grounds.<sup>16,17</sup>

Table 9.3 lists complexes of the type  $Fe(CO)_3(L)_2$  (excluding those complexes where  $(L)_2$  = diene ligand, (eg. 1,2-bis(2'6'-di-isopropylphenyl)iminoethane<sup>18</sup>) which determines the substitution geometry) for which X-ray Crystal and Molecular structures have been determined. With the exception of the case where  $(L)_2$  is the bidentate phosphine ligand  $Ph_2PCH_2PPh_2$ <sup>19</sup>, all the complexes have the expected  $tbp$  geometry.

The exception, the complex  $Fe(CO)_3(Ph_2PCH_2PPh_2)$ <sup>19</sup> has a geometry intermediate between  $tbp$  and  $spy$ , and can be

viewed either as a distorted tbp with the P-atoms coordinating in axial and equatorial sites, or as a distorted spy in which both P-atoms occupy cis-basal sites. Regarding the structure as a severely distorted tbp, the axP-Fe-Pe<sub>q</sub> angle is 73.5(1)°, a significant deviation from the ideal 90°. This is a consequence of the steric strain inherent in the Ph<sub>2</sub>PCH<sub>2</sub>PPh<sub>2</sub> ligand itself. The distorted geometry is a consequence of the bidentate nature, and small bite size of the Ph<sub>2</sub>PCH<sub>2</sub>PPh<sub>2</sub> ligand.

The symmetrically substituted biphosphine complexes, diax-[(R<sub>3</sub>P)<sub>2</sub>Fe(CO)<sub>3</sub>] (R = OCH<sub>3</sub>,<sup>118</sup> NMe<sub>2</sub><sup>117</sup>), have essentially undistorted tbp geometry. However, the complex diax-{[(3,5-Me<sub>2</sub>C<sub>6</sub>H<sub>3</sub>O)<sub>3</sub>P]Fe(CO)<sub>3</sub>(CHO)}<sup>117</sup> has a slightly distorted tbp geometry, with av. OC-Fe-CHO angle of 86.3(2)° and av. OC-Fe-P angle of 93.3(1)°. This bending of the equatorial CO ligands towards the axial CHO group is probably a consequence of steric repulsions between the phenyl rings of the bulky phosphate ligand and the equatorial CO ligands. In ax-eq[Me<sub>3</sub>As(C<sub>6</sub>H<sub>4</sub>)AsMe<sub>3</sub>]Fe(CO)<sub>3</sub>,<sup>118</sup> the equatorial CO ligands bend towards the ax-As atom (axAs-Fe-COeq: 89°, axOC-Fe-COeq: 92°). This is probably due to electronic factors<sup>118</sup> (see Section 9.2.2.)

### 9.3.2 Ligand site preferences - ax-ax, ax-eq, eq-eq

On the basis of symmetry and overlap arguments, Rossi and Hoffmann<sup>101</sup> have shown that, for d<sup>8</sup> tbp M(L)<sub>5</sub> complexes, the stronger σ-donor ligand would preferentially occupy an axial site, while the stronger π-acceptor ligand would be found in an equatorial position. Hence a ligand L that is a stronger σ-donor, and/or weaker π-acceptor, would be expected on electronic grounds to occupy an axial site in tbp Fe(CO)<sub>3</sub>(L)<sub>2</sub> complexes.

In Table 9.3, the sites occupied by the ligands L and L' in the complexes Fe(CO)<sub>3</sub>LL' are given. For diphosphine derivatives (L = L' = P(OCH)<sub>3</sub>,<sup>118</sup> P(NMe)<sub>3</sub><sup>117</sup>), the phosphine ligands, which are weaker π-acceptors than CO,<sup>118</sup> occupy the two axial sites, with the more strongly π-accepting carbonyls in the equatorial positions, where

TABLE 9.3: X-Ray Crystal Structures of  $\text{Fe}(\text{CO})_3\text{L}'$  Structures

| Ligand L  | Ligand L'  | Geometry <sup>a</sup> | Site occupied by ligand <sup>b</sup> |    | Space Group, Z       | Reference |
|---|--|-----------------------|--------------------------------------|----|----------------------|-----------|
|   |  |                       | L                                    | L' |                      |           |
| $\text{P}(\text{OCH}_3)_3$                                  | $\text{P}(\text{OCH}_3)_3$   | tbp                   | ax                                   | ax | $\text{C}2/c, 4$     | 136       |
| $\text{P}(\text{NMe}_2)_3$                                  | $\text{P}(\text{NMe}_2)_3$   | tbp                   | ax                                   | ax | $\text{P}2_1/c, 4$   | 117       |
| $(3,5\text{-Me}_2\text{C}_6\text{H}_3\text{O})_3\text{P}$   | $(\text{CHO})^-$   | tbp                   | ax                                   | ax | $\text{C}2/c, 8$     | 137       |
| $\text{Me}_3\text{As}(\text{C}_6\text{H}_4)\text{AsMe}_3^c$ |  |                       | ax                                   | eq | $\text{Pnma}, 4^d$   | 138       |
| $\text{PPh}_3$  | $\text{cis-}[\text{CH}_3\text{CH}_2\text{OC}(\text{O})\text{C}]_2$   | tbp                   | ax                                   | eq | $\text{P}\bar{1}, 2$ | 139       |
| $\text{PPh}_3$  | $\text{trans-}[\text{CH}_3\text{CH}_2\text{OC}(\text{O})\text{C}]_2$ | tbp                   | eq                                   | eq | $\text{C}2/c, 8$     | 139       |
| $\text{PPh}_3$  | $\text{CH}_2\text{CHCO}_2\text{Me}$                                  | tbp                   | ax                                   | eq | $\text{P}\bar{1}, 2$ | 140       |
| $\text{Ph}_2\text{PCH}_2\text{PPh}_2^c$                     |  | tbp                   | ax                                   | eq | $\text{P}\bar{1}, 2$ | 134       |
|   |  | /spy <sup>e</sup>     | bs                                   | bs |                      |           |

<sup>a</sup> tbp = trigonal bipyramidal, spy = square pyramidal

<sup>b</sup> In tbp geometry, ax = axial, eq = equatorial  
In spy geometry, ap = apical, bs = basal

<sup>c</sup> Bidentate ligand

<sup>d</sup>  $(\text{Me}_3\text{As}(\text{C}_6\text{H}_4)\text{AsMe}_3)\text{Fe}(\text{CO})_3$  molecule possesses crystallographic mirror (m) symmetry

<sup>e</sup> Geometry intermediate between tbp and spy.

TABLE 9.4 Geometric data for  $\text{Fe}(\text{CO})_3\text{LL}'$  structures  $g$   
(Bond angles in degrees, bond lengths in Å)

| Complex   | $\text{Fe}-\text{O}_{\text{max}}$ | $\text{Fe}-\text{O}_{\text{eq}}$ | $\text{F}-\text{C}-\text{O}^a$ |
|---|-----------------------------------|----------------------------------|--------------------------------|
| $\text{diact}[(\text{CH}_3\text{O})_2\text{P}]_2\text{Fe}(\text{CO})_3$   | ~                                 | 1.761(6) <sup>a</sup>            | 179.4(4)                       |
| $\text{diact}[(\text{Me}_2\text{N})_2\text{P}]_2\text{Fe}(\text{CO})_3$   | ~                                 | 1.758(3) <sup>b</sup>            | 177.6(3)                       |
| $\text{diact}[(3,5-\text{Me}_2\text{C}_6\text{H}_3\text{O})_2\text{P}]_2\text{Fe}(\text{CO})_3$                                 | ~                                 | 1.760(5) <sup>a</sup>            | 177.1 <sup>b</sup>             |
| $\text{ax-eq}[(\text{Me}_3\text{As}(\text{C}_6\text{H}_4)_2)_2\text{Fe}(\text{CO})_3]$  | 1.81                              | 1.68                             | 174.0 <sup>b,c</sup>           |
| $\text{ax-eq}[(\text{Ph}_2\text{P})(\text{cis}-(\text{CH}_2\text{CH}_2\text{OC}(\text{O})\text{C}))_2\text{Fe}(\text{CO})_3]$   | 1.796(6)                          | 1.796(6) <sup>a</sup>            | 175.2(5)                       |
| $\text{eq-eq}[(\text{Ph}_2\text{P})(\text{trans}-(\text{CH}_2\text{CH}_2\text{OC}(\text{O})\text{C}))_2\text{Fe}(\text{CO})_3]$ | 1.803(5) <sup>a</sup>             | 1.766(5)                         | 176.0(5)                       |
| $\text{ax-eq}[(\text{Ph}_2\text{P})(\text{CH}_2\text{CH}(\text{O})\text{C}(\text{O})\text{C}))_2\text{Fe}(\text{CO})_3]$        | 1.794(2)                          | 1.787(2) <sup>a</sup>            | 176.6(2)                       |
| $\text{ax-eq}[(\text{Ph}_2\text{CH}_2)_2\text{Fe}(\text{CO})_3]$  | 1.74(1)                           | 1.77(1) <sup>a</sup>             | 177(1)                         |

<sup>a</sup> average value

<sup>b</sup> Bond data obtained from the Cambridge Crystallographic Data Base

<sup>c</sup>  $\text{Fe}-\text{C}-\text{O}(\text{eq})$ : 171.6°,  $\text{Fe}-\text{C}-\text{O}(\text{ax})$ : 178.9°

<sup>d</sup> Regarded as distorted top

backbonding to the metal atom can be optimized.<sup>116</sup> Diaxial substitution is also observed for the phosphite-formyl complex,  $[(3,5\text{-Me}_2\text{C}_6\text{H}_3\text{O})_3\text{P}(\text{CO})_3(\text{CHO})]^-$ .<sup>117</sup>

The bidentate arsine ligand,  $(\text{L})_2 = \text{Me}_3\text{As}(\text{C}_6\text{H}_4)\text{-AsMe}_3$ ,<sup>118</sup> co-ordinates to the Fe-atom in an ax-eq fashion. However, this co-ordination geometry is dictated by the steric restraints inherent in the bidentate ligand, reflected also in the axAs-Fe-Aseq angle of  $84^\circ$ . Hence only one As-atom is able to occupy the electronically favoured axial position. The subjugation of electronic factors to the spatial limitations of bidentate ligands is also demonstrated by the bidentate phosphine ligand,  $(\text{L})_2 = \text{Ph}_2\text{PCH}_2\text{PPh}_2$ ,<sup>119</sup> where P-atoms again co-ordinate ax-eq in a distorted tbp. The severe distortions to the geometry, with an axP-Fe-Peq angle of only  $73.5(1)^\circ$ , reflect the steric strain of this bidentate ligand.

The pair of related phosphine-olefin complexes,  $\text{L} = \text{PPh}_3$ ,  $\text{L}' = \text{cis}$  or  $\text{trans}$  isomer of  $\text{CH}_3\text{CH}_2\text{OCC}=\text{CCOCH}_2\text{CH}_3$ ,<sup>120</sup> provides an illustration of steric vs electronic control of the ligand site preference in tbp  $\text{Fe}(\text{CO})_3\text{LL}'$  complexes. In accordance with the electronic predictions of Rossi and Hoffmann,<sup>121</sup> the olefinic ligand should occupy an equatorial site with the carbon-carbon double bond approximately in the equatorial plane, as such a ligand arrangement provides for optimum  $\pi$ -backbonding interaction. This mode of co-ordination is indeed found for both the above isomeric olefin ligands.<sup>122</sup>

Further,  $\text{PR}_3$ , being a stronger  $\sigma$ -donor and weaker  $\pi$ -acceptor<sup>123,124</sup> than CO, should on electronic grounds<sup>125</sup> occupy an axial site. In the case of  $\text{Fe}(\text{CO})_3(\text{PPh}_3)(\text{cis-}[\text{CH}_3\text{CH}_2\text{OC}(\text{O})\text{C}]_2)$ , the phosphine ligand does indeed occupy the electronically favoured axial position.<sup>126</sup> However, in the case of the  $\text{Fe}(\text{CO})_3(\text{PPh}_3)(\text{trans-}[\text{CH}_3\text{CH}_2\text{OC}(\text{O})\text{C}]_2)$  complex, the phosphine co-ordinates in the electronically less favoured equatorial site.<sup>127</sup> This unexpected equatorial disposition of the phosphine ligand has been ascribed to the steric hinderance caused by the trans-substituents of the olefin at the axial sites of the trigonal bipyramid.<sup>128</sup> The bulky  $\text{PPh}_3$  ligand (Tolman cone

angle<sup>88</sup> for PPh<sub>3</sub>: 145°) thus prefers to co-ordinate at an electronically less favoured equatorial site. In this instance, steric effects dominate the electronic site preference in determining the final ligand arrangement. Further, in both the Fe(CO)<sub>3</sub>(PPh<sub>3</sub>)(olefin) complexes, the olefin substituents are directed towards the other side of the molecule away from the bulky PPh<sub>3</sub> ligand, in order to minimize steric repulsions in the compounds.<sup>137</sup>

In the complex Fe(CO)<sub>3</sub>(PPh<sub>3</sub>)(CH<sub>2</sub>=CHCO<sub>2</sub>Me),<sup>138</sup> the phosphine ligand occupies an axial site, while the olefin co-ordinates equatorially, as expected on electronic grounds.<sup>131, 139</sup> The co-ordination plane of the olefinic ligand is tilted by 11.2° from the equatorial plane of the iron atom, and the carbomethoxy group is directed away from the triphenyl phosphine ligand, a reflection of the influence of steric factors on structure.

### 9.3.3 Fe-CO bond length trends

Substitution of an axial CO by a poorer  $\pi$ -accepting ligand in Fe(CO)<sub>5</sub>, results in a shortening of the Fe-CO bonds in Fe(CO)<sub>4</sub>L relative to Fe(CO)<sub>5</sub>,<sup>146</sup> and a greater shortening of the axial Fe-CO bond trans to L than of the Fe-COeq bonds<sup>117b</sup> (axial trans effect). As would thus be anticipated, upon replacement of one CO ligand by a strongly  $\sigma$ -donating/weakly  $\pi$ -accepting ligand, such as PR<sub>3</sub>, additional CO replacement becomes more difficult.<sup>148</sup> However, this second substitution, once achieved, would be expected to result in a further shortening of the remaining Fe-COeq bonds.<sup>117b</sup> This is indeed observed for the diax complexes Fe(CO)<sub>3</sub>LL' (L = L' = P(OCH<sub>3</sub>)<sub>3</sub>,<sup>139</sup> P(NMe<sub>2</sub>)<sub>3</sub>,<sup>117</sup> L = P(OC<sub>6</sub>H<sub>3</sub>Me<sub>2</sub>-3,5)<sub>3</sub>, L' = CHO<sup>-137</sup>) (see Table 9.4).

Rosi and Hoffmann<sup>141</sup> have evaluated the relative strength of axial and equatorial bonds in d<sup>8</sup> tbp complexes. Their conclusions were that M-L  $\sigma$ -bonding results in stronger axial bonds,  $\pi$ -donation will weaken metal-ligand bonds, but greater weakening of the equatorial bonds is expected, while  $\pi$ -acceptor ligands strengthen metal-ligand bonding, especially when the ligand occupies an equatorial site. Hence if ligands are  $\pi$ -donors,  $\sigma$ - and  $\pi$ -bonding

effects co-operate, resulting in strong axial and weak equatorial bonds. However, for good  $\pi$ -acceptors, the  $\sigma$ - and  $\pi$ -bonding effects oppose each other, although the  $\sigma$ -effect seems to dominate, with longer equatorial bonds found. As expected, these conclusions parallel the site preference arguments.

Table 9.4 gives Fe-CO bond length data for the  $\text{Fe}(\text{CO})_3\text{LL}'$  complexes. For the complex  $\text{ax-eq}(\text{Me}_3\text{As}(\text{C}_6\text{H}_4)_2\text{AsMe}_3)\text{Fe}(\text{CO})_3$ ,<sup>118</sup> the short Fe-COeq bond of 1.66 Å reflects the increased back-bonding to the two remaining carbonyl ligands on equatorial substitution of a weakly  $\pi$ -accepting arsine ligand. A similar shortening of the sole remaining Fe-COeq bond (1.766(5) Å) is observed in the complex  $\text{eq-eq}(\text{Ph}_3\text{P})$ -[trans-( $\text{CH}_3\text{CH}_2\text{OC}(\text{O})\text{C}$ )<sub>2</sub>] $\text{Fe}(\text{CO})_3$ ,<sup>119</sup> where the weakly  $\pi$ -accepting phosphine ligand occupies an equatorial site. In the related complex,  $\text{ax-eq}(\text{Ph}_3\text{P})$ [cis-( $\text{CH}_3\text{CH}_2\text{OC}(\text{O})\text{C}$ )<sub>2</sub>]- $\text{Fe}(\text{CO})_3$ ,<sup>119</sup> the Fe-COax bond (1.795(5) Å) would be expected to be similar to that in the mono-substituted  $\text{ax}-(\text{Ph}_3\text{P})$ - $\text{Fe}(\text{CO})_4$ <sup>118</sup> (1.795(4) Å). The shorter Fe-COeq than Fe-COax bonds in both these olefinic complexes, reflects the stronger bonding of the equatorial carbonyls to Fe, owing to the equatorial substitution of an olefinic ligand, which is generally a poorer  $\pi$ -acceptor than CO.<sup>118</sup> The Fe-COax (1.784(2) Å) and Fe-COeq (1.780(2) and 1.783(2) Å) bond lengths in the related complex,  $\text{ax-eq}(\text{Ph}_3\text{P})\text{CH}_2\text{CHCO}_2\text{Me}\text{Fe}(\text{CO})_3$ ,<sup>116</sup> are, however, equal within experimental error.

#### 9.3.4 Fe-C-O bond angles

The Fe-C-O bond angles for the  $\text{Fe}(\text{CO})_3\text{L}_2$  complexes are given in Table 9.4. In accordance with Kettle's<sup>11</sup> predictions of near-linearity of M-C-O bonds for  $\text{M}(\text{CO})_3$  fragments, the Fe-C-O bond angles are in the range 175-179°. Variations of Fe-C-O angles within an  $\text{Fe}(\text{CO})_3$  group are ascribed to the influence of crystal packing forces!<sup>11</sup> Crystal packing forces could also account for minor deviations from ideal tpb geometry. Note that for  $\text{ax-eq}(\text{Me}_3\text{As}(\text{C}_6\text{H}_4)_2\text{AsMe}_3)$ - $\text{Fe}(\text{CO})_3$ <sup>118</sup> the axFe-C-O bond angle is essentially linear (178.9°), but the eqFe-C-O bond angle is only 171.6°. This deviation from linearity probably arises from steric



repulsion between the eq carbonyls and the bulky bidentate arsine ligand.

#### 9.4 The Crystal and Molecular Structure of $\text{Fe}(\text{CO})_2(\text{CNMe})_2$

##### 9.4.1 Anomalous Infra Red Data

On the basis of the electronic predictions of Rossi and Hoffmann,<sup>141</sup> the diisonitrile complex  $\text{Fe}(\text{CO})_3(\text{CNR})_2$  would be expected to have *tpb* geometry, with the isonitrile ligands, being stronger  $\sigma$ -donors, but weaker  $\pi$ -acceptors than CO,<sup>142</sup> occupying the axial sites. Such a *di-ax*-(RNC)<sub>2</sub>- $\text{Fe}(\text{CO})_3$  *tpb* geometry would have  $D_{3h}$  molecular symmetry.<sup>141</sup>

The infra red spectrum of this ligand arrangement is predicted from group theory analysis to give one  $\nu(\text{CN})$  and one  $\nu(\text{CO})$  stretching absorption.<sup>141</sup> However, complexes of the type  $\text{Fe}(\text{CO})_3(\text{CNR})_2$  (R = Me,<sup>141-2</sup>  $\text{C}_6\text{H}_{11}$ ,<sup>142</sup> Bu,<sup>141-2</sup>  $\text{CH}_2\text{Ph}$ ,<sup>142</sup> Ph,<sup>142</sup>  $\text{C}_6\text{H}_5\text{Me}_2$ -2,6,<sup>142</sup>  $\text{C}_6\text{H}_2\text{Me}_3$ -2,4,6,<sup>142</sup>  $\text{C}_2\text{H}_5$ <sup>141</sup>) typically give one  $\nu(\text{CN})$  and two  $\nu(\text{CO})$  absorptions in various solvents ( $\text{CHCl}_3$ ,<sup>141-2</sup> CS,<sup>141</sup>  $\text{CCl}_4$ <sup>141</sup>). For example, the compound  $\text{Fe}(\text{CO})_3(\text{CNMe})_2$  gave one  $\nu(\text{CN})$  and more than one  $\nu(\text{CO})$  absorptions in both solution and the solid state. [IR( $\text{CHCl}_3$  solution),<sup>142</sup>  $\nu(\text{CN})$ : 2160  $\text{cm}^{-1}$ ,  $\nu(\text{CO})$ : 2000, 1922  $\text{cm}^{-1}$ ; IR(KBr),  $\nu(\text{CN})$ : 2182(s)  $\text{cm}^{-1}$ ;  $\nu(\text{CO})$ : 2026(w), 1935(sh), 1919(s), 1897(s), 1878(sh)  $\text{cm}^{-1}$  (s = strong, w = weak, sh = shoulder)].

A similar phenomenon of anomalous IR data has been observed for the bisphosphite complex *di-ax*[( $\text{Me}_2\text{O}$ )<sub>3</sub>P]<sub>2</sub> $\text{Fe}(\text{CO})_3$ .<sup>143a</sup> Bisphosphine complexes of the type  $\text{Fe}(\text{CO})_3(\text{PR}_3)_2$  would also be predicted to give only one  $\nu(\text{CO})$  IR absorption. This is observed for  $\text{Fe}(\text{CO})_3(\text{PR}_3)_2$  (R = Ph,<sup>141, 143a</sup>  $\text{C}_2\text{H}_5$ <sup>142b</sup>) complexes. (Note that the diisonitrile complex  $\text{Fe}(\text{CO})_3(\text{CNC}_2\text{H}_5)_2$  (in *n*-hexadecane,  $\text{C}_{16}\text{H}_{34}$ <sup>143a</sup>) has been reported to give only one  $\nu(\text{CO})$  absorption also, in contrast to the results of other studies<sup>141-2</sup> (*vide supra*) on this and related complexes). However, the complex  $\text{Fe}(\text{CO})_3(\text{P}(\text{OMe})_3)_2$  gives three  $\nu(\text{CO})$  absorptions: the E' band splits into two bands, and there is also a third band assigned as  $A_1'$ ,<sup>143</sup> which is not expected to be infra red active in the  $D_{3h}$  symmetry.<sup>141</sup> A crystal structure determination of the  $\text{Fe}(\text{CO})_3(\text{P}(\text{OMe})_3)_2$  complex has been performed.<sup>144</sup> The geometry is *tpb* with the

phosphite ligands in axial sites. The anomalous IR data has been ascribed to a lowering of the symmetry of the molecule from  $D_{3h}$  due to internal asymmetry of the  $P(OMe)_3$  ligands.<sup>14</sup> The three P-O bonds of  $P(OMe)_3$  are not equivalent, probably due to an asymmetrical configuration of the three O-CH<sub>3</sub> groups. A feeble activation of the  $A_1$  band results from the vibration of one of the CO groups in  $Fe(CO)_3(P(OMe)_3)_2$  being different from that of the other two, owing to intersection of one CO with a phosphite ligand.<sup>14b</sup>

A crystal structure determination of the complex  $Fe(CO)_3(CNMe)_2$  was thus undertaken in order to determine whether the anomalous IR data (*vide supra*) could be ascribed to a deviation from idealized  $D_{3h}$  symmetry, due to possible non-linearity (the result of electronic or steric effects) of the C-N-C unit bound to Fe, which could allow the  $A_1$  band to gain a little intensity.<sup>14</sup>

The precedent for the above proposition was the X-ray molecular structure of the penta-isocyanide complex,  $Fe(CNBU^t)_5$ ,<sup>15</sup> which shows marked deviations from  $D_{3h}$  symmetry of idealized *trigonal bipyramidal* geometry, with substantial bending of the isocyanide ligands at the N-atoms (mean C-N-C angle  $134(2)^\circ$ ). This non-linearity of the isocyanide ligands has been attributed to extensive back-bonding of Fe(3d) electrons to the  $(\pi^*N)$  antibonding orbitals.<sup>15</sup> In addition, the small size of the methylisocyanide ligand ("fan-shaped" angle" for MeNC:  $52^\circ$  (width),  $52^\circ$  (thickness)) further limits the possibility that the anomalous IR data results from steric effects, eg. unexpected substitution geometry.<sup>15</sup>

#### 9.4.2. Discussion of the Structure

The geometry of the  $Fe(CO)_3(CNMe)_2$  molecule is illustrated in Figure 9.1, which also shows the numbering scheme used in the analysis.  $Fe(CO)_3(CNMe)_2$  crystallizes in the monoclinic space group  $P2_1/c$ , with  $Z = 4$ . A view of the unit cell, looking down the *b*-axis, is shown in Figure 9.2. Bond lengths and bond angles are given in Tables 9.5 and 9.6 respectively.

As predicted,<sup>14</sup> the geometry of the  $Fe(CO)_3(CNMe)_2$  complex is *trigonal bipyramidal*, with the methylisocyanide ligands in axial

positions. No distortions to the  $tpb$  geometry are apparent. The C-Fe-C angles are close to the ideal values (mean OC-Fe-CN:  $90.0(3)^\circ$ , mean OC-Fe-OO:  $120.0(4)^\circ$ , and NC-Fe-CN:  $177.1(3)^\circ$ ). Further, the CO and CNMe ligands are linearly co-ordinated to the central Fe atom. The slight deviations from linearity are in accordance with Kettle's<sup>19</sup> predictions for  $M(CR)_n$  ( $R = O, N, n = 2, 3$ ) units (mean Fe-C-O and Fe-C-N angles  $178.6(8)$  and  $177.5(6)^\circ$  respectively). The isonitrile ligands (mean C-N-C:  $177.2(9)^\circ$ ) are also linear.<sup>19b</sup>

Hence the anomalous IR data cannot be ascribed to a lowering of the idealized  $D_{3h}$  symmetry due to non-linearity of the isonitrile ligands. However, the  $D_{3h}$  symmetry could conceivably be lowered due to an internal asymmetry in the isonitrile ligands, similar to that observed for the phosphite ligands of  $di\text{ax}[\text{Fe}(\text{CO})_3(\text{P}(\text{OMe})_3)_2]$ .<sup>14, 15</sup> For the  $\text{CNCH}_3$  ligand, the uncertainty in the positions of the hydrogen atoms does not allow for a meaningful analysis of their relative orientations. Other explanations could account for the anomalous IR data. For example, Cotton and Parish<sup>14c</sup> have proposed that the second weak  $\nu(\text{CO})$  band could be a combination or overtone band which has gained intensity by Fermi resonance with the strong fundamental.

The Fe-CO bond lengths in  $di\text{ax}[\text{Fe}(\text{CO})_3(\text{CNMe})_2]$  (av.  $1.785(8)\text{\AA}$ ) are shorter than those in the parent carbonyl,  $\text{Fe}(\text{CO})_5$  (av. Fe-COax:  $1.806(5)\text{\AA}$  and av. Fe-COeq:  $1.833(4)\text{\AA}$ ), but slightly longer than the Fe-CO bonds in  $di\text{ax}[(\text{Me}_3\text{N})_3\text{P}]_2\text{Fe}(\text{CO})_3$ <sup>17</sup> and  $di\text{ax}[(\text{CH}_3\text{O})_3\text{P}]_2\text{Fe}(\text{CO})_3$ <sup>18</sup> (av. values of  $1.759(3)$  and  $1.761(6)\text{\AA}$  respectively). These trends are understandable in terms of the electronic nature of isonitrile ligands, which are better  $\pi$ -acceptors than phosphines, but poorer  $\pi$ -acceptors than CO.<sup>19a</sup>

The Fe-CNR bond length found in the only other structure of the type  $\text{Fe}(\text{CO})_{5-n}(\text{CNR})_n$  ( $n = 1-3$ ),  $\text{Fe}(\text{CNBu}^t)_5$ <sup>20</sup> (av.  $1.824(8)\text{\AA}$ ), is much shorter than the mean Fe-CNMe distance of  $1.867(8)\text{\AA}$  in  $\text{Fe}(\text{CO})_3(\text{CNMe})_2$ , consistent with the increased electron density on the Fe atom in the  $\text{Fe}(\text{CNBu}^t)_5$  complex. In the latter structure, however, the isonitrile ligands deviate markedly from linearity, indicative of extensive back-bonding.<sup>19</sup>

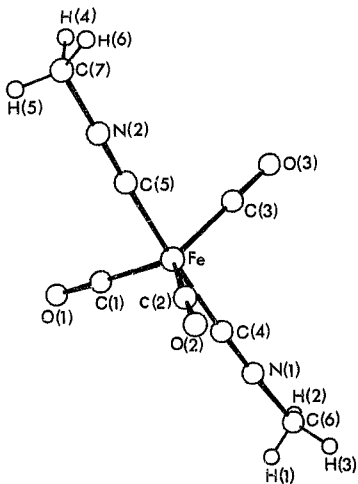


Figure 9.1: An ORTEP<sup>33</sup> view of the  $\text{Fe}(\text{CO})_3(\text{CNMe})_2$  molecule, showing the numbering system used.

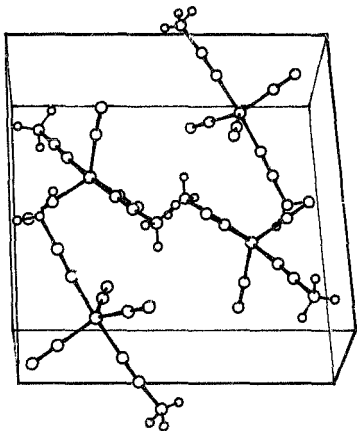


Figure 9.2: An ORTEP<sup>3</sup> view of the unit cell of  $\text{Fe}(\text{CO})_3(\text{CNMe})_2$ , looking down the  $b$ -axis.

TABLE 9.5: Bond lengths ( $\text{\AA}$ ) for  $\text{Fe}(\text{CO})_3(\text{CNMe})_2$

|           |           |           |           |
|-----------|-----------|-----------|-----------|
| Fe-C(1)   | 1.775(8)  | C(1)-O(1) | 1.150(9)  |
| Fe-C(2)   | 1.790(8)  | C(2)-O(2) | 1.138(8)  |
| Fe-C(3)   | 1.791(9)  | C(3)-O(3) | 1.144(9)  |
| Fe-C(4)   | 1.873(8)  | C(4)-N(1) | 1.148(8)  |
| Fe-C(5)   | 1.860(8)  | C(5)-N(2) | 1.150(8)  |
| N(1)-C(6) | 1.416(10) | N(2)-C(7) | 1.430(11) |
| C(6)-H(1) | 0.83(6)   | C(7)-H(4) | 0.98(11)  |
| C(6)-H(2) | 0.89(9)   | C(7)-H(5) | 0.93(13)  |
| C(6)-H(3) | 1.05(12)  | C(7)-H(6) | 1.04(12)  |

TABLE 9.6: Bond angles ( $^\circ$ ) for  $\text{Fe}(\text{CO})_3(\text{CNMe})_2$

|              |          |                |          |
|--------------|----------|----------------|----------|
| Fe-C(1)-O(1) | 178.4(8) | C(4)-N(1)-C(6) | 176.3(8) |
| Fe-C(2)-O(2) | 178.3(7) | C(5)-N(2)-C(7) | 178.1(9) |
| Fe-C(3)-O(3) | 179.2(8) | N(1)-C(6)-H(1) | 108(5)   |
| Fe-C(4)-N(1) | 178.0(6) | N(1)-C(6)-H(2) | 109(6)   |
| Fe-C(5)-N(2) | 176.9(6) | N(1)-C(6)-H(3) | 117(6)   |
| C(1)-Fe-C(4) | 90.7(3)  | N(2)-C(7)-H(4) | 103(6)   |
| C(2)-Fe-C(4) | 89.5(3)  | N(2)-C(7)-H(5) | 100(8)   |
| C(3)-Fe-C(4) | 89.1(3)  | N(2)-C(7)-H(6) | 118(7)   |
| C(1)-Fe-C(5) | 92.2(3)  | H(1)-C(6)-H(2) | 93(7)    |
| C(2)-Fe-C(5) | 89.2(3)  | H(1)-C(6)-H(3) | 93(8)    |
| C(3)-Fe-C(5) | 89.5(3)  | H(2)-C(6)-H(3) | 129(8)   |
| C(4)-Fe-C(5) | 177.1(3) | H(4)-C(7)-H(5) | 114(10)  |
| C(1)-Fe-C(2) | 119.6(4) | H(4)-C(7)-H(6) | 102(9)   |
| C(1)-Fe-C(3) | 118.2(4) | H(5)-C(7)-H(6) | 119(10)  |
| C(2)-Fe-C(3) | 122.2(4) |                |          |

## 9.5 EXPERIMENTAL

### 9.5.1 Data collection

The compound  $\text{Fe}(\text{CO})_3(\text{CNMe})_2$  was obtained from the  $\text{CoCl}_2 \cdot 2\text{H}_2\text{O}$  catalysed reaction between  $\text{Fe}(\text{CO})_5$  and  $\text{MeNC}$ .<sup>11a</sup> Since the compound was both air and light sensitive, yellow crystals were grown under nitrogen in the dark from a benzene-hexane solution at 20°C.

Preliminary investigations by standard Weissenberg and precession photography established the monoclinic space group  $\text{P}2_1/\text{c}$  from the absences  $h0l$ ,  $l = 2n + 1$ , and  $0k0$ ,  $k = 2n + 1$ . Refined cell constants were obtained during data collection on a Philips PW1100 four-circle diffractometer, using graphite monochromated  $\text{McK}\alpha$  radiation ( $\lambda = 0.7107\text{\AA}$ ) at room temperature (20°C). Lorentz and polarization corrections were applied, but corrections for absorption were omitted as the linear absorption coefficient is only  $16.32 \text{ cm}^{-1}$ . No special precautions were taken during data collection, and crystal deterioration was not observed. Crystal data and details of the structure analysis are summarized in Table 9.7.

### 9.5.2 Structure Solution and Refinement

Structure analysis and refinement were carried out using the program SHELXS2.<sup>11a</sup> Initial co-ordinates for the iron atom were derived from a Patterson synthesis and difference Fourier syntheses yielded positions, first for all 13 non-hydrogen atoms, and after least-squares refinement of these, also for the 6 hydrogen atoms. Positional parameters for all atoms, and anisotropic temperature factors for non-hydrogen atoms, were refined by full-matrix least-squares analyses. Least-squares refinement was considered complete when all parameter shifts were less than 0.5 $\sigma$ . At this stage, the conventional  $R = 0.0680$ . Unit weights were used. Scattering factors for  $\text{Fe}(\text{O})$  were taken from "International Tables for X-ray Crystallography,"<sup>11b</sup> and anomalous dispersion corrections<sup>11c</sup> for iron were made.

Fractional atomic co-ordinates of all atoms, and anisotropic thermal parameters for the non-hydrogen atoms, are given in Tables 9.8 and 9.9 respectively. A listing of the Structure Factors is to be found in Appendix D.



TABLE 9.7: Crystal data and details of structural analysis for  $\text{Fe}(\text{CO})_3(\text{CNMe})_2$

|   |  |
|---|--|
| Formula                                 | $\text{FeC}_7\text{H}_6\text{N}_2\text{O}_3$ |
| Mr                                      | 221.99                                       |
| Crystal dimensions (mm)                 | 0.19 x 0.19 x 0.14                           |
| Space Group                             | $P2_1/c$ (No. 14)                            |
| a ( $\text{\AA}$ )                      | 12.451(6)                                    |
| b ( $\text{\AA}$ )                      | 6.564(3)                                     |
| c ( $\text{\AA}$ )                      | 12.087(6)                                    |
| $\beta$ ( $^\circ$ )                    | 92.45(3)                                     |
| V ( $\text{\AA}^3$ )                    | 986.95                                       |
| Z                                       | 4  |
| F(000)                                  | 447.96                                       |
| D <sub>c</sub> ( $\text{gcm}^{-3}$ )    | 1.49   |
| $\mu$ ( $\text{cm}^{-1}$ )              | 16.32  |
| $\lambda$ ( $\text{\AA}$ )              | MoK $\alpha$ (0.7107)                        |
| Scan mode                               | $\omega/2\theta$                             |
| Range ( $^\circ$ )                      | 3 $\phi$ 523                                 |
| Scan width ( $^\circ$ )                 | 1.60   |
| Scan speed ( $^\circ \text{sec}^{-1}$ ) | 0.053  |
| Range of hkl                            | $\pm h, \pm k, \pm l$                        |
| Measured intensities                    | 1517   |
| Unique reflections                      | 1335   |
| Internal consistency R-index            | 0.0000                                       |
| R (R = R <sub>w</sub> )                 | 0.0680                                       |

TABLE 9.8(a): Fractional atomic co-ordinates for the non-hydrogen atoms of  $\text{Fe}(\text{CO})_3(\text{CNMe})_2$

| Atom | x/a       | y/b         | z/c        |
|------|-----------|-------------|------------|
| Fe   | 0.2457(1) | 0.3155(2)   | 0.5729(1)  |
| N(1) | 0.3692(5) | 0.0696(10)  | 0.4097(5)  |
| N(2) | 0.1393(5) | 0.5622(10)  | 0.7472(5)  |
| O(1) | 0.0518(5) | 0.3058(11)  | 0.4276(5)  |
| O(2) | 0.2863(6) | -0.0062(10) | 0.7371(5)  |
| O(3) | 0.3977(6) | 0.6515(10)  | 0.5450(6)  |
| C(1) | 0.1278(7) | 0.3069(12)  | 0.4852(6)  |
| C(2) | 0.2693(6) | 0.1199(11)  | 0.6743(6)  |
| C(3) | 0.3384(7) | 0.5203(13)  | 0.5550(7)  |
| C(4) | 0.3206(5) | 0.1514(11)  | 0.4710(5)  |
| C(5) | 0.1776(5) | 0.4692(11)  | 0.6785(6)  |
| C(6) | 0.4352(8) | -0.0411(19) | 0.3385(8)  |
| C(7) | 0.899(11) | 0.6818(20)  | 0.8298(10) |

TABLE 9.8(b): Fractional atomic co-ordinates and isotropic temperature factors for the hydrogen atoms of  $\text{Fe}(\text{CO})_3(\text{CNMe})_2$

| Atom | x/a       | y/b        | c/z       | $U(\text{\AA}^2)$ |
|------|-----------|------------|-----------|-------------------|
| H(1) | 0.399(5)  | -0.137(10) | 0.311(5)  | 0.05(2)           |
| H(2) | 0.438(7)  | 0.025(14)  | 0.274(8)  | 0.09(3)           |
| H(3) | 0.492(9)  | -0.139(20) | 0.376(9)  | 0.16(5)           |
| H(4) | 0.091(8)  | 0.820(18)  | 0.799(8)  | 0.12(4)           |
| H(5) | 0.022(10) | 0.621(21)  | 0.829(10) | 0.16(6)           |
| H(6) | 0.132(9)  | 0.702(19)  | 0.905(10) | 0.16(5)           |

TABLE 9.9: Anisotropic temperature factors ( $\text{\AA}^2$ ) for the non-hydrogen atoms of  $\text{Fe}(\text{CO})_3(\text{CNMe})_2$

| Atom | U11       | U22       | U33       | U23       | U13       | U12       |
|------|-----------|-----------|-----------|-----------|-----------|-----------|
| F(e) | 0.0457(6) | 0.0461(6) | 0.0469(6) | -0.006(5) | 0.0050(4) | 0.0026(5) |
| N(1) | 0.060(4)  | 0.066(4)  | 0.047(3)  | -0.006(3) | 0.005(3)  | 0.014(3)  |
| N(2) | 0.060(4)  | 0.062(4)  | 0.059(4)  | -0.008(3) | 0.009(3)  | 0.003(3)  |
| O(1) | 0.069(4)  | 0.117(6)  | 0.086(4)  | -0.021(4) | -0.027(3) | 0.024(4)  |
| O(2) | 0.069(4)  | 0.069(4)  | 0.082(4)  | 0.026(4)  | 0.025(4)  | 0.023(4)  |
| O(3) | 0.120(5)  | 0.073(4)  | 0.115(5)  | -0.003(4) | 0.039(4)  | -0.038(4) |
| C(1) | 0.069(5)  | 0.056(5)  | 0.056(4)  | -0.002(4) | 0.006(4)  | 0.008(4)  |
| C(2) | 0.065(5)  | 0.045(4)  | 0.055(4)  | 0.003(4)  | 0.015(4)  | 0.004(4)  |
| C(3) | 0.069(5)  | 0.056(5)  | 0.068(5)  | -0.004(4) | 0.016(4)  | -0.003(4) |
| C(4) | 0.044(4)  | 0.060(5)  | 0.040(4)  | 0.008(3)  | -0.006(3) | -0.004(3) |
| C(5) | 0.046(4)  | 0.051(4)  | 0.061(4)  | -0.001(4) | -0.003(3) | 0.001(3)  |
| C(6) | 0.071(6)  | 0.087(7)  | 0.050(5)  | -0.015(5) | 0.010(4)  | 0.018(6)  |
| C(7) | 0.098(8)  | 0.079(8)  | 0.085(7)  | -0.014(6) | 0.025(6)  | 0.028(7)  |

X. Derivatives of dirhenium decacarbonyl - a Survey of the Literature

10.1 Introduction

Since the preparation of dirhenium decacarbonyl,  $\text{Re}_2(\text{CO})_{10}$  by Hieber and Fuchs<sup>144</sup> in 1941, and that of dimanganese decacarbonyl,  $\text{Mn}_2(\text{CO})_{10}$ , by Brimm, Lynch and Seeny<sup>145</sup> in 1954, these two metal carbonyl dimers have been extensively investigated. Studies of these molecules have been carried out by IR spectroscopy<sup>146</sup> (in the solid, in solution, and in the gas phase<sup>146a</sup>), Raman spectroscopy,<sup>147</sup> single-crystal Raman spectroscopy,<sup>148</sup> high-pressure solid state Raman spectroscopy,<sup>149</sup> IR and Raman spectroscopy on  $^{13}\text{C}$  enriched samples,<sup>150</sup> polarized IR, and visible and near ultra violet (UV) spectroscopy,<sup>151</sup>  $^{17}\text{O}$  NMR spectroscopy ( $\text{Mn}_2(\text{CO})_{10}$ ),<sup>152</sup> electron spin resonance (ESR) spectroscopy,<sup>153</sup> mass spectroscopy (MS),<sup>154</sup> gas phase electron diffraction<sup>155-56</sup> and single-crystal X-ray diffraction at room temperature,<sup>157-58</sup> and at 74K ( $\text{Mn}_2(\text{CO})_{10}$ ).<sup>159</sup>

An enormous chemistry of  $\text{M}_2(\text{CO})_{10}$  (M = Re, Mn) has been reported.<sup>160</sup> Notwithstanding the substantial numbers of chemical reactions that have been carried out on the  $\text{M}_2(\text{CO})_{10}$  dimers, no significant attempt has been made in the literature to ascertain factors responsible for the stereochemistry of the products from the reaction of  $\text{M}_2(\text{CO})_{10}$  with ligand L.

A review of the reaction of  $\text{Re}_2(\text{CO})_{10}$  with ligands L, in which the products have the stoichiometry  $\text{Re}_2(\text{CO})_{10-n}(\text{L})_n$  (n = 1-10) and the rhenium-rhenium bond remains intact, has thus been undertaken. In particular, emphasis is placed on a description of the stereochemistry of the resulting  $\text{Re}_2(\text{CO})_{10-n}(\text{L})_n$  products.

The metal-metal bond in the  $\text{Re}_2(\text{CO})_{10}$  (or  $\text{Mn}_2(\text{CO})_{10}$ ) dimer may be cleaved by photolysis (eg. flash photolysis has been employed in kinetic studies of the homolysis of  $\text{M}_2(\text{CO})_{10}$  (M = Re, Mn), to give  $\text{M}(\text{CO})_5$  radicals<sup>161</sup>), or by chemical methods<sup>162</sup> such as the action of sodium metal, or of halogens. The latter methods have led to the synthesis

of a wide range of monometallic complexes, and for example, the area of rhenium pentacarbonyl chemistry has been the subject of extensive investigation in its own right. Reactions leading to monomeric rhenium species will however not be discussed here. (See Ref. 160 for a comprehensive review of this area of rhenium carbonyl chemistry.)

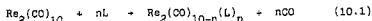
The review has been restricted to  $\text{Re}_2(\text{CO})_{10}$  derivatives. The metal-metal bond in  $\text{Re}_2(\text{CO})_{10}$  is stronger than that in  $\text{Mn}_2(\text{CO})_{10}$  ( $D(\text{Re-Re})$ : 128 kJ mol<sup>-1</sup>, cf.  $D(\text{Mn-Mn})$ : 67 kJ mol<sup>-1</sup>;<sup>161</sup> although controversy surrounds the exact values of  $D(\text{M-M})$  (see ch. XII), there is no dispute regarding the relative order, viz.  $D(\text{Re-Re}) > D(\text{Mn-Mn})$ , and hence the possibility of metal-metal bond cleavage during reaction with L is less probable. On occasion, reference to  $\text{Mn}_2(\text{CO})_{10-n}(\text{L})_n$  derivatives will, however, be made.

Further,  $\text{Re}_2(\text{CO})_{10}$  may also undergo reactions with itself, in the presence of ligand,<sup>162</sup> or with other metal carbonyl complexes, resulting in the formation of higher rhenium or mixed-metal clusters.<sup>163</sup> Such reactions, as well as those of the higher rhenium carbonyl clusters (some of which yield dimeric rhenium products,<sup>163</sup> often through decomposition reactions), as well as reactions of monomeric rhenium species which yield dimeric rhenium products,<sup>166</sup> will not be considered here.

Despite the tremendous growth in recent years in the use of single crystal X-ray diffraction methods in product characterization, relatively few X-ray crystal structures have been reported of dirhenium carbonyl complexes. This is due in part to the relatively few system studies reported in this area of rhenium carbonyl chemistry, owing to the synthetic difficulties often encountered (*vide infra*). In discussing the dirhenium carbonyl derivatives, emphasis will be placed on those complexes for which an X-ray crystal and molecular structure has been reported, and a discussion of the salient structural features of these complexes, as well as those of crystallographically studied dirhenium carbonyl complexes prepared by reaction of higher nuclear rhenium clusters,<sup>163</sup> or of rhenium monomers,<sup>163</sup> will be

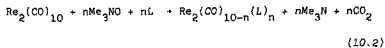
given in ch. XIII.

The reactions of interest are usually simple carbonyl substitution reactions, in which one or more carbonyl (CO) ligands are replaced by donor ligand(s) L, viz.



Such reactions generally involve photochemical techniques, although there are examples of thermal reactions of  $\text{Re}_2(\text{CO})_{10}$  with L, or of photochemically prepared  $\text{Re}_2(\text{CO})_{10-n}(\text{L})_n$  derivatives reacting with a ligand L.<sup>187-171</sup> Such examples are relatively few, possibly due to difficulty often encountered in effecting simple carbonyl substitution reactions under mild thermal conditions ( $\Delta H$  for CO dissociation,  $D(\text{Re}-\text{CO})$  is calculated to be 195 kJ mol<sup>-1</sup>).<sup>172</sup>

Trimethylamine-N-oxide induced reactions of  $\text{Re}_2(\text{CO})_{10}$  with L have been employed to circumvent this problem.<sup>187, 171-175</sup> In this method, CO is oxidized to  $\text{CO}_2$  under low temperature conditions, viz.

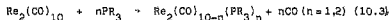


There have also been studies conducted in which CO ligands are converted into other ligand while attached to the metal. For instance, the anionic formyl complex  $\text{Li}^+(\text{Re}_2(\text{CO})_9\text{CHO})^-$  has been prepared by the reaction of  $\text{LiEt}_3\text{BH}$  with  $\text{Re}_2(\text{CO})_{10}$ ,<sup>174</sup> and the reaction of  $\text{Re}_2(\text{CO})_{10}$  with  $\text{LiR}$  in ether, and subsequent alkylation with  $[\text{R}'_2\text{O}][\text{BF}_4]/\text{H}_2\text{O}$  yields the carbene complex  $\text{Re}_2(\text{CO})_9\{\text{C}(\text{OR}')\text{R}\}$ .<sup>177, 214</sup>

The  $\text{Re}_2(\text{CO})_{10}/\text{L}$  systems that have been reported in the literature will be discussed under ligand type L.

#### 10.2 Reactions of $\text{Re}_2(\text{CO})_{10}$ with phosphines (and arsines)

The reaction of  $\text{Re}_2(\text{CO})_{10}$  with phosphine ligand (eqn. 10.3) has received considerable attention.



Uncertainty as to the mechanism of this reaction has resulted in extensive kinetic studies by several groups. Kinetic and mechanistic studies on this system will be

discussed in ch XV. The various synthetic methods employed to bring about reaction (10.3) are described below.

#### 10.2.1 Thermal reactions

The reaction between  $\text{Re}_2(\text{CO})_{10}$  and a large excess of phosphine,  $\text{PR}_3$  ( $\text{PR}_3 = \text{PPh}_3$ ,<sup>179-182</sup>,  $\text{PET}_2\text{Ph}$ ,<sup>183a</sup>  $\text{PMePh}_2$ ,<sup>183b</sup>  $\text{P(OPh)}_3$ ,<sup>183c</sup>  $\text{P}(\text{OC}_6\text{H}_4\text{Me-o})_3$ ,<sup>183d</sup>  $\text{P}(\text{OC}_6\text{H}_4\text{Cl-p})_3$ ,<sup>183e</sup>  $\text{P}(\text{C}_6\text{H}_4\text{Me-p})_3$ ,<sup>183f</sup>  $\text{P}(\text{C}_6\text{H}_{11})_3$ <sup>183g</sup>), in refluxing xylene gives  $\text{Re}_2(\text{CO})_8(\text{PR}_3)_2$ . Long reaction times (15 to 50 h) are required, and product yields are generally poor (<30%), although some workers have reported good yields (75%) for  $\text{PPh}_3$ .<sup>181</sup> In most cases, the reaction yields more than one product, eg. mer-trans- $\text{HRe}(\text{CO})_3(\text{PR}_3)_2$ <sup>180a,182,187</sup> ( $\text{PR}_3 = \text{Ph}_3$ ,  $\text{P}(\text{C}_6\text{H}_4\text{Me-p})_3$ ,<sup>183</sup>  $\text{P}(\text{C}_6\text{H}_{11})_3$ ,<sup>183g</sup>  $\text{P}(\text{OC}_6\text{H}_4\text{Me-o})_3$ <sup>183d</sup> (the latter originally incorrectly identified as the metalated complex  $[\text{Re}(\text{CO})_3(\text{PR}_3)(\text{PR}_3\text{-H})]$ <sup>184</sup>). In the case of  $\text{PR}_3 = \text{P}(\text{C}_6\text{H}_4\text{Me-o})_3$ <sup>183d</sup> only the metalated product  $\text{Re}(\text{CO})_4(\text{PR}_3\text{-H})$  was obtained. The reaction with  $\text{P}(\text{OEt})_3$ <sup>185</sup> yielded a mixture of seven products which were not characterized. With  $\text{PR}_3 = \text{P(OPh)}_3$ <sup>183c</sup> a trisubstituted product,  $\text{Re}_2(\text{CO})_7[\text{P(OPh)}_3]_3$  was also obtained. Chromatography is necessary to separate the products.<sup>182-184</sup>

The reaction between  $\text{Re}_2(\text{CO})_{10}$  and  $\text{PMe}_2\text{Ph}$ <sup>183b</sup> in refluxing petroleum ether (80-100°C, 96 h) yielded  $\text{Re}_2(\text{CO})_8(\text{PMe}_2\text{Ph})_2$  (46%), together with some  $\text{HRe}(\text{CO})_3(\text{PMe}_2\text{Ph})_2$ . If the reaction is conducted in n-hexane, and stopped after 5 h,  $\text{Re}_2(\text{CO})_9(\text{PMe}_2\text{Ph})$  is obtained.<sup>184</sup>

The monosubstituted  $\text{Re}_2(\text{CO})_9(\text{PPh}_3)$  has been obtained (38%) from  $\text{Re}_2(\text{CO})_8(\text{PPh}_3)_2$  by passing a stream of CO through a solution of  $\text{Re}_2(\text{CO})_8(\text{PPh}_3)_2$  at 130°C for 30 h.<sup>181</sup>  $\text{Re}_2(\text{CO})_9(\text{PPh}_3)$  has also been obtained as the major product from the 1:1 reaction of  $\text{Re}_2(\text{CO})_{10}$  with  $\text{PPh}_3$  in refluxing xylene.<sup>182b</sup>

Tetrasubstituted  $[\text{Re}(\text{CO})_3(\text{PPh}_3)_2]_2$  has been obtained from the reaction of  $\text{Re}_2(\text{CO})_{10}$  and  $\text{PPh}_3$  (1:5 ratio) in refluxing xylene.<sup>184b</sup> However, in solution this product appears to exist as the monomeric  $\text{HRe}(\text{CO})_3(\text{PPh}_3)_2$ .<sup>183b,188</sup> Heating  $\text{Re}_2(\text{CO})_{10}$  with the bidentate phosphine ligand,  $\text{Ph}_2\text{PCH}_2\text{CH}_2\text{PPh}_2$  (1:4 ratio), in a sealed evacuated tube (240°C, 2 h) gave the tetrasubstituted complex, cis-

$[\text{Re}(\text{CO})_3(\text{Ph}_2\text{PCH}_2\text{CH}_2\text{PPh}_2)_2]_2$  (20%).<sup>180b</sup>

### 10.2.2 Photochemical reactions

UV-irradiation of  $\text{Re}_2(\text{CO})_{10}$  and  $\text{PR}_3$  in petroleum ether ( $\text{PR}_3 = \text{PPh}_3$ ,  $\text{PEt}_2\text{Ph}$ <sup>180a</sup>) or cyclohexane ( $\text{PR}_3 = \text{PPh}_3$ <sup>180b</sup>) gave  $\text{Re}_2(\text{CO})_8(\text{PR}_3)_2$  in good yield (70-85%).

The photochemical reaction in cyclohexane between  $\text{Re}_2(\text{CO})_{10}$  and  $\text{PMePh}_2$ <sup>181</sup> (2:1 ratio) after 12 h of UV-irradiation, yielded  $\text{Re}_2(\text{CO})_9(\text{PMePh}_2)$  (4%),  $\text{Re}_2(\text{CO})_8(\text{PMePh}_2)_2$  (7%), two isomers of  $\text{Re}_2(\text{CO})_7(\text{PMePh}_2)_3$  (combined yield 10%) and a trace amount of  $\text{Re}_4(\text{CO})_{16}(\text{PMePh}_2)_6$ . When a 1:1 ratio between  $\text{Re}_2(\text{CO})_{10}$  and phosphine was used, only the two isomers of  $\text{Re}_2(\text{CO})_7(\text{PMePh}_2)_3$  (combined yield 22%) (and some  $\text{HRe}(\text{CO})_3(\text{PMePh}_2)_2$ ) was obtained.<sup>181</sup>

Irradiation of  $\text{Re}_2(\text{CO})_{10}$  and  $\text{PMe}_2\text{Ph}$ <sup>182</sup> (1:2 ratio) in petroleum ether (60-80°C) for 6 h gave  $\text{Re}_2(\text{CO})_8(\text{PMe}_2\text{Ph})_2$  (4%), and an isomer of  $\text{Re}_2(\text{CO})_7(\text{PMe}_2\text{Ph})_3$  (13%), as well as trace amounts of  $\text{HRe}(\text{CO})_3(\text{PMe}_2\text{Ph})_2$  and isomers of  $\text{Re}(\text{CO})_3(\text{PMe}_2\text{Ph})_2\text{Cl}$ . The same reaction in cyclohexane after 3 h yielded only  $\text{Re}_2(\text{CO})_7(\text{PMe}_2\text{Ph})_3$  (13%) and a trace of an isomer of  $\text{Re}(\text{CO})_3(\text{PMe}_2\text{Ph})_2\text{Cl}$ .<sup>182</sup> (The chlorine compounds arise from the addition of chlorinated solvents to the crude reaction mixtures). The products were separated by chromatography.

The bisphosphine complex  $\text{Re}_2(\text{CO})_8(\text{PPh}_2)_2$ <sup>183</sup> was obtained from the 10 h photochemical reaction between  $\text{Re}_2(\text{CO})_{10}$  and  $\text{PPh}_2$  (1:2 ratio) in benzene solution.

The photochemical reaction under vacuum of  $\text{Re}_2(\text{CO})_{10}$  with a 5-fold excess of  $\text{PPh}_3$ , at 60°C,<sup>184</sup> yielded three isomers of  $\text{Re}_2(\text{CO})_7(\text{PPh}_3)_3$ , assigned on the basis of <sup>13</sup>PNMR spectra as 1-ax,2,2-transdiag- $\text{Re}_2(\text{CO})_2-(\text{PPh}_3)_3$  (35%), 1-eq,2,2-axeq- $\text{Re}_2(\text{CO})_7(\text{PPh}_3)_3$  (15%), and 1-eq,2,2-transdiag- $\text{Re}_2(\text{CO})_7(\text{PPh}_3)_3$  (5%), as well as  $\text{Re}_2(\text{CO})_8(\text{PPh}_3)_2$  (40%), and a trace amount of a rhenium compound tentatively identified as  $\text{Re}_2(\text{CO})_6(\text{PPh}_3)_4$ .

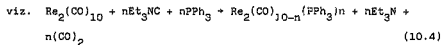
High temperature ultraviolet methods yielded  $\text{M}_2(\text{CO})_{10-n}(\text{PF}_3)_n$  (M = Mn, Re; n = 1-4) species as unresolved mixtures of isomers.<sup>185</sup>



There has been one report of a reaction of  $\text{Re}_2(\text{CO})_{10}$  with an arsine. A 6 h UV-irradiation of  $\text{Re}_2(\text{CO})_{10}$  and  $\text{AsMe}_2\text{Ph}$  (1:2 ratio<sup>173</sup>) in petroleum ether (40-60°C) yielded the bisarsine complex  $\text{Re}_2(\text{CO})_8(\text{AsMe}_2\text{Ph})_2$  (9%).

#### 10.2.3 Amine-oxide assisted reactions

An amine-oxide assisted reaction between  $\text{Re}_2(\text{CO})_{10}$  and  $\text{PPh}_3$  has been employed in the synthesis under mild conditions (20°C, 2 h) of  $\text{Re}_2(\text{CO})_9(\text{PPh}_3)$  and  $\text{Re}_2(\text{CO})_8(\text{PPh}_3)_2$ <sup>174</sup>

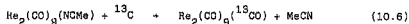
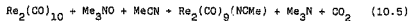


#### 10.2.4. Comment on product formulations

From the above it can be seen that synthetic studies of the seemingly simple thermal and photochemical routes yield a wide range of dimeric and monomeric rhenium-phosphine complexes. However, as product characterization has relied almost entirely on IR spectroscopy, product formulation, and assignment of geometric isomers, may in certain cases be subject to question, especially in the absence of any X-ray crystallographic studies of  $\text{Re}_2(\text{CO})_{10-n}(\text{PR}_3)_n$  complexes. Notwithstanding the uncertainty, the data suggest that in the majority of cases monosubstitution is axial, and disubstitution diaxial. This aspect will be discussed in ch XV.

#### 10.3 The reaction of $\text{Re}_2(\text{CO})_{10}$ with $^{13}\text{CO}$

The use of acetonitrile as a donor solvent in the reactions of  $\text{M}_2(\text{CO})_{10}$  (M = Re, Mn) and  $\text{Me}_3\text{NO}$  results in the complex  $\text{M}_2(\text{CO})_9(\text{NCMe})$ , from which the MeCN ligand can readily be displaced under mild thermal conditions. This method has been used in the synthesis of high purity  $^{13}\text{CO}$ -labelled  $\text{Re}_2(\text{CO})_9(^{13}\text{CO})$ <sup>175</sup> viz.



Sunlight irradiation of a hexane solution of

$Mn_2(CO)_{10}$  in contact with  $^{13}CO$ -rich (22.5%) carbon monoxide for several hours resulted in a threefold enrichment of the natural  $^{13}CO$  content of the  $Mn_2(CO)_{10}$  dimer.<sup>115b</sup> However, this method is unsatisfactory, as both  $Mn_2(CO)_{10}$  and  $Re_2(CO)_{10}$  exchange CO very slowly.<sup>115c</sup>

Indirect methods have also been employed in the preparation of  $^{13}C$ -enriched samples of  $M_2(CO)_{10}$ , for example, the reaction of a  $^{13}CO$ -enriched  $M(CO)_5X$  ( $M = Re, X = Cl; M = Mn, X = Br$ ) sample with  $NaM(CO)_5$ .<sup>115c</sup> (Both  $M(CO)_5X$  and  $NaM(CO)_5$  were themselves prepared from the  $M_2(CO)_{10}$  dimer, by cleavage with halogen X or sodium amalgam respectively). Isotopically labelled  $Re_2(CO)_{10}$  has also been prepared by reacting  $HRe_3(CO)_{14}$  with carbon monoxide (50%  $^{13}CO$ -enriched) under vacuum, to give  $HRe(CO)_5$  and  $Re_2(CO)_{10}$ .<sup>115a</sup>

Only the amine-oxide assisted reaction between  $Re_2(CO)_{10}$  and  $^{13}CO$  results in the production of high purity  $Re_2(CO)_9(^{13}CO)$ , suitable for synthetic purposes (as opposed to use in IR and Raman spectroscopic studies<sup>116</sup>). This reaction highlights the synthetic utility of the amine-oxide-induced route. This method has not been investigated (prior to this work) with ligands such as isonitriles and arsines, the reported reactions of  $Re_2(CO)_{10}$  with these ligands being entirely photochemical (see sections 10.4 and 10.2.(b) respectively).

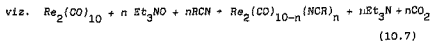
#### 10.4 Photochemical reaction of $Re_2(CO)_{10}$ with isonitriles

Methylisonitrile (MeNC) derivatives,  $M_2(CO)_{10-n}(CNMe)_n$  ( $M = Re, n = 1; M = Mn, n = 1,3,4$ ), have been prepared by the photochemical reaction of  $M_2(CO)_{10}$  with MeNC.<sup>117</sup> These complexes have been studied by Raman spectroscopy, and have been reported to be isostructural<sup>117b</sup> with the parent  $M_2(CO)_{10}$  compounds,<sup>118</sup> but the crystal and molecular structures have not been reported, presumably due to the disorder problems encountered.<sup>117b</sup>

#### 10.5 Amine-oxide assisted reaction of $Re_2(CO)_{10}$ with nitriles

The complexes  $Re_2(CO)_{10-n}(NCR)_n$  ( $n = 1,2; R = Me, Et, Pr^i$ ,  $Pr^t$ ) were prepared via the amine-oxide assisted reaction

of  $\text{Re}_2(\text{CO})_{10}$  with RCN.<sup>174</sup>



The complexes  $\text{Re}_2(\text{CO})_9(\text{NCMe})^{173}$  and  $\text{Re}_2(\text{CO})_8(\text{NCMe})_2^{175}$  have also been obtained from the amine-oxide assisted reaction of  $\text{Re}_2(\text{CO})_{10}$  in acetonitrile, in the absence of added donor ligand. (See also Section 10.10.1).

#### 10.6 Photochemical reactions of $\text{Re}_2(\text{CO})_{10}$ with olefins

The photochemical-induced reaction of  $\text{Re}_2(\text{CO})_{10}$  and olefins has been studied for several different olefins.<sup>149-71,153-5</sup>

The major disadvantage is that the photochemical reaction usually results in a complex mixture of products, which often requires sophisticated methods such as high-pressure liquid chromatography (HPLC<sup>156</sup>) for direct separation. In addition to the octacarbonyl- $\mu$ -olefinyl- $\mu$ -hydrido-dirhenium complexes (Fig. 10.1(a)), olefinic rhenium monomers, dirhenium complexes in which the Re-Re bond has been cleaved, with the olefin bridging the two Re atoms, or with the two metals joined through an olefinic residue, and even tri-rhenium olefinic complexes, are usually formed, in lesser or greater proportions. In some cases, monomeric and Re-Re bond cleaved dimeric products are formed exclusively from the reaction. Even in favourable cases, usually more than one octacarbonyl- $\mu$ -olefinyl- $\mu$ -hydrido-dirhenium complex is formed, due to cleavage, rearrangement or isomerization of the olefin ligand itself. In some instances, the simple substitution product, enneacarbonyl- $\eta$ -olefin-dirhenium (Fig. 10.1(b)), can also be isolated.<sup>153</sup>

##### 10.6.1. The photochemical reaction of $\text{Re}_2(\text{CO})_{10}$ with olefins in hexane solution

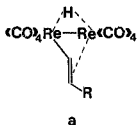
The photochemical reaction in hexane between  $\text{Re}_2(\text{CO})_{10}$  and a variety of acyclic and cyclic olefins with one to four C=C bonds has been studied.<sup>153</sup> Table 10.1 lists the olefin derivatives of dirhenium carbonyl dimer in which the rhenium-rhenium bond remains intact. The structures of these products are shown in Fig. 10.2.

With ethylene(I), styrol(II), 1,3-cyclopentadiene(III), 1,3-cyclohexadiene(IV), 1,3,5,7-cyclooctatetraen(V) and 6,6-dimethylfulven(VI), the main products were octacarbonyl- $\mu$ -olefinyl- $\mu$ -hydrido-dirhenium(I)' complexes (Fig. 10.2, I-V (A,B),(VIA)), isomerism of the olefin ligands being observed. With ethylene, octacarbonyl- $\mu$ - $\eta$ -1,3-butadienedirhenium(O) (Fig. 10.2(IC)) was also obtained. In the cases of ethylene, 1,3,5,7-cyclooctatetraen and 6,6-dimethylfulven, ennea-carbonyl- $\mu$ -olefin-dirhenium was also observed (Fig. 10.2(ID), (VC) and (VIB) respectively). For ethylene, additional vinyl-bridged trinuclear complexes resulted. The only dinuclear products obtained from the reactions of  $\text{Re}_2(\text{CO})_{10}$  with cyclohexane and with 1,3,5-cycloheptatriene, were metal-metal bond cleaved octacarbonyl- $\mu$ -olefinyl- $\mu$ -hydrido-dirhenium complexes. In the case of the latter olefin,  $\eta$ -cycloheptadienydirhenium tricarbonyl side products were also obtained.

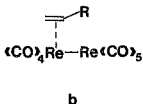
10.6.2. The photochemical reactions of  $\text{Re}_2(\text{CO})_{10}$  with 1,3-butadiene

In tetrahydrofuran (THF) solution photolysis of  $\text{Re}_2(\text{CO})_{10}$  and 1,3-butadiene or cyclooctatetraene,<sup>154</sup> yielded the olefinic complexes,  $(\text{CO})_4\text{Re}-\mu(\text{O};\eta^2\text{C}_4\text{H}_6)\text{Re}(\text{CO})_4$  (Fig. 10.3, (VIIA)) and  $(\text{CO})_4\text{Re}-\mu(\eta^2;\eta^2\text{C}_4\text{H}_6)\text{Re}(\text{CO})_4$  (Fig. 10.3(VIIB)). The latter complex has also been obtained from the photolysis of  $\text{Re}_2(\text{CO})_{10}$  with 1,3-butadiene in pentane solution.<sup>155</sup> The structure of this dimer (VIIB) has been determined by X-ray crystallography<sup>155</sup> (see ch XIII). In these reactions, trinuclear, and metal-metal bond-cleaved dinuclear rhenium compounds were also obtained.<sup>154-5</sup>

The photochemical reaction between  $\text{Re}_2(\text{CO})_{10}$  and 1,3-butadiene in hexane<sup>154</sup> has been reported to yield, in addition to Re-Re bond-cleaved dinuclear olefinic complexes, at a temperature of 240 K, the dimeric complex octacarbonyl- $\mu$ -[1,2- $\eta$ -1- $\eta$ -(1,3-butadien-1-yl)]- $\mu$ -hydrido-dirhenium (Fig. 10.3(VIID)). (VIID) rearranges in solution to octacarbonyl- $\mu$ - $\eta$ -1,3-butadienedirhenium(O),  $(\text{CO})_4\text{Re}-\mu(\eta^2;\eta^2\text{C}_4\text{H}_6)\text{Re}(\text{CO})_4$  (Fig. 10.3 (VIIB)), the product mentioned



(a) octacarbonyl- $\mu$ -olefinyl- $\mu$ -hydrido-dirhenium



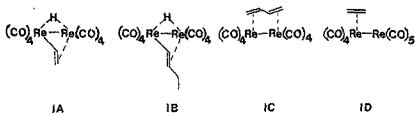
(b) enneacarbonyl- $\pi$ -olefin-dirhenium

Figure 10.1: Possible Re-Re bonded dimeric olefin derivatives of  $\text{Re}_2(\text{CO})_{10}$  (olefin =  $\text{C}=\text{C}-\text{R}$ )

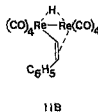
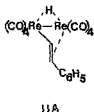
TABLE 10.1: Re-Re bonded dimeric products from the photochemical reaction of  $Re_2(CO)_{10}$  and olefins in hexane solution <sup>10</sup>

| Olefin                       | Re-Re bonded dimeric product(s)  |
|------------------------------|--|
| (I) ethylene                 | (IA) octacarbonyl- $\mu$ -hydrido- $\mu$ -(1-2-n-1-o-vinyl)-dirhenium<br>(IB) $\mu$ -[1-2-n-1-o-(1-buten-1-yl)]-octacarbonyl- $\mu$ -hydrido-dirhenium<br>(IC) $\mu$ -1-2:3-4-n-(1,3-butadiene)-octacarbonyl-dirhenium<br>(ID) enneacarbonyl-n-ethyl-en-dirhenium<br>(IA) octacarbonyl- $\mu$ -hydrido- $\mu$ -[1-2-n-2-o-(2-ethyl)]-dirhenium<br>(IB) octacarbonyl- $\mu$ -hydrido- $\mu$ -[1-2-n-2-o-(2-ethyl)]-dirhenium<br>(IIIA) octacarbonyl- $\mu$ -[1-2-n-1-o-(1,3-cyclopentadien-1-yl)]- $\mu$ -hydrido-dirhenium<br>(IIIB) octacarbonyl- $\mu$ -[1-2-n-2-o-(1,3-cyclopentadien-2-yl)]- $\mu$ -hydrido-dirhenium<br>(IIV) octacarbonyl- $\mu$ -[1-2-n-1-o-(1,3-cyclohexadien-1-yl)]- $\mu$ -hydrido-dirhenium<br>(IIV) octacarbonyl- $\mu$ -[1-2-n-2-o-(1,3-cyclohexadien-2-yl)]- $\mu$ -hydrido-dirhenium<br>(VA) octacarbonyl- $\mu$ -[1-2-n-1-o-(1,3,5,7-cyclooctatetraen-1-yl)]- $\mu$ -hydrido-dirhenium<br>(VB) $\mu$ -[7-8-n-7-o-(bicyclo-[4-2-0]octa-2,4,7-trien-7-yl)]octacarbonyl- $\mu$ -hydrido-dirhenium<br>(VC) enneacarbonyl- $\mu$ -2,1,3,5,7-cyclooctatetraen-dirhenium<br>(VIA) octacarbonyl- $\mu$ -[1-2-n-2-o-(6,6-dimethylfulven-2-yl $\dagger$ )]- $\mu$ -hydrido-dirhenium<br>(VIB) enneacarbonyl-1-2-n-(6,6-dimethylfulven)-dirhenium |
| (II) styrol                  | (IIB) octacarbonyl- $\mu$ -[1-2-n-2-o-(2-ethyl)]-dirhenium<br>(IIB) octacarbonyl- $\mu$ -[1-2-n-2-o-(2-ethyl)]-dirhenium   |
| (III) 1,3-cyclopentadiene    | (IIB) octacarbonyl- $\mu$ -[1-2-n-2-o-(2-ethyl)]-dirhenium   |
| (IV) 1,3-cyclohexadiene      | (IIB) octacarbonyl- $\mu$ -[1-2-n-2-o-(2-ethyl)]-dirhenium   |
| (V) 1,3,5,7-cyclooctatetraen | (IIB) octacarbonyl- $\mu$ -[1-2-n-2-o-(2-ethyl)]-dirhenium   |

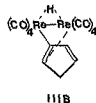
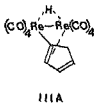
18



(I) ethylene ||



(II) styrol ||

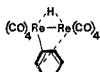


(III) 1,3-cyclopentadiene


Figure 10.2: Re-Re bonded dimeric products from the photochemical reaction of  $\text{Re}_2(\text{CO})_{10}$  with olefins in hexane solution



IV A



IV B

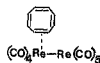
(IV) 1,3-cyclohexadiene 




VA

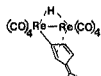


VB

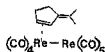


VC

(V) 1,3,5,7-cyclooctatetraen 



VIA



VIB

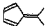
(VI) 6,6-dimethylfulven 

Figure 10.2: (contd.)



previously as obtained from the photochemical reaction of  $\text{Re}_2(\text{CO})_{10}$  and 1,3-butadiene in THF,<sup>119</sup> or in pentane solution,<sup>120</sup> and from that of  $\text{Re}_2(\text{CO})_{10}$  and ethylene in hexane solution (Fig. 10.2.(IC)<sup>121</sup>).

At a reaction temperature of 188K, however, the photochemical reaction between  $\text{Re}_2(\text{CO})_{10}$  and 1,3-butadiene in hexane<sup>122</sup> yielded, apart from the above Re-Re bond cleaved dimeric side products, in addition to the product (VIIJ),  $(\text{CO})_3\text{Re}(\eta\text{-}1,3\text{-butadiene})\text{Re}(\text{CO})_5$  (Fig. 10.3(VIIC)) in comparable amounts.

#### 10.6.3 The photochemical reaction of $\text{Re}_2(\text{CO})_{10}$ with 1,3,5-cycloheptatriene

Photolysis of  $\text{Re}_2(\text{CO})_{10}$  and excess 1,3,5-cycloheptatriene in petroleum ether (60-80°C)<sup>122</sup> yielded two Re-Re bonded dimeric products (Fig. 10.4),  $(\text{C}_7\text{H}_8)_2\text{Re}_2(\text{CO})_7$  (VIIIA) and  $(\text{C}_7\text{H}_8)_2\text{Re}_2(\text{CO})_8$  (VIIIB) (the structures of which have been deduced from FT <sup>1</sup>H NMR spectra), as well as monomeric and tetra-nuclear rhenium sideproducts. This is in contrast to the photochemical reaction of  $\text{Re}_2(\text{CO})_{10}$  with this olefin in hexane solution,<sup>123</sup> which gave only Re-Re bond-cleaved dimeric and  $\eta\text{-cycloheptadienyl}$  rhenium tricarbonyl monomeric products.

#### 10.6.4 The photochemical reactions of $\text{Re}_2(\text{CO})_{10}$ with 1-alkenes and 2-alkenes and further reactions of the products

Photolysis of a hexane<sup>124</sup> or toluene<sup>125-1</sup> solution of  $\text{Re}_2(\text{CO})_{10}$  in the presence of excess 1-alkene ((A) propylene,<sup>125-2</sup> (B) 1-butene<sup>125-1</sup> or (C) 1-hexene<sup>125-1</sup>) resulted in the formation of  $(\mu\text{-H})\text{Re}_2(\text{CO})_8(\mu\text{-}\eta^2\text{CH}=\text{CHR})$  (Fig. 10.5: R = Me (IXA1), Et (IXB1) or  $\text{Bu}^n$  (IXC) in high yields.<sup>125-2</sup> Mention has been made<sup>121</sup> of an X-ray crystal structure investigation of  $(\mu\text{-H})\text{Re}_2(\text{CO})_8(\mu\text{-}\eta^2\text{CH}=\text{CHMe})$  (IXA), revealing an Re-Re bond length of ca. 3.20Å, but the full structure has not been reported to date.

The photolysis in toluene of  $\text{Re}_2(\text{CO})_{10}$  with (A) or (B) also yields, in addition to the trans-isomers (IXA) or (IXB1), the cis-isomers (IXA2) or (IXB2).<sup>126</sup> In the case of

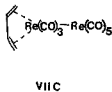
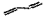


Figure 10.3: Re-Re bonded dimeric products from the photochemical reactions of  $\text{Re}_2(\text{CO})_{10}$  with 1,3-butadiene 

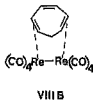
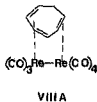

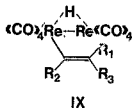


Figure 10.4: Re-Re bonded dimeric products from the photochemical reaction of  $\text{Re}_2(\text{CO})_{10}$  with 1,3,5-cycloheptatriene 



- (IXA1)  $R_1 = R_2 = H; R_3 = Me$   
 (IXA2)  $R_2 = R_3 = H; R_1 = Me$   
 (IXB1)  $R_1 = R_2 = H; R_3 = Et$   
 (IXB2)  $R_2 = R_3 = H; R_1 = Et$   
 (IXC)  $R_1 = R_2 = H; R_3 = Bu^{\eta}$   
 (IXD)  $R_1 = R_2 = R_3 = H$   
 (IXE)  $R_1 = R_3 = H; R_2 = Et$   
 (IXF)  $R_1 = H; R_2 = R_3 = Me$   
 (IXG)  $R_1 = R_2 = H; R_3 = O-Bu^{\eta}$   
 (IXH)  $R_1 = R_2 = H; R_3 = Ph$

Figure 10.5: Products from photolysis reactions of  $Re_2(CO)_{10}$  with 1-alkenes (A-E) and 2-alkenes (F)

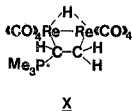


Figure 10.6: Dipolar addition product,  $(\mu-H)(\mu-CH=CH_2)Re_2(CO)_8(PMe_3)$

(B), a further isomer, (IXE),<sup>176</sup> is also obtained. The cis-products, (IXA2) and (IXB2), isomerize spontaneously to the trans-products, (IXA1) and (IXB1).<sup>176</sup>

Photolysis of  $\text{Re}_2(\text{CO})_{10}$  with ethylene<sup>173-1</sup> yields, in addition to (IXD),  $(\mu\text{-H})\text{Re}_2(\text{CO})_8(\mu\text{-}(\eta^2\text{-CH=CH}_2))$ , (IXB) and (IXE),  $(\mu\text{-H})\text{Re}_2(\text{CO})_8(\mu\text{-}(\eta^2\text{-EtC}=\text{CH}_2))$ , formed from subsequent photochemical reactions of (IXD).

A related study of internal olefins,<sup>173-1</sup> the photolysis of  $\text{Re}_2(\text{CO})_{10}$  with cis-2-butene resulted in the production, in low yield, of  $(\mu\text{-H})\text{Re}_2(\text{CO})_8(\mu\text{-}(\eta^2\text{-MeC}=\text{CHMe}))$ , (IXF). Extended photolysis resulted in isomerization of (IXF) to (IXB). This later complex (IXB) was the only organometallic product to be obtained from the photolysis of  $\text{Re}_2(\text{CO})_{10}$  with trans-2-butene,<sup>173-1</sup> and probably resulted from the observed<sup>173-1</sup> slow isomerization of trans-2-butene to 1-butene during reaction.

Compounds (IXA-C) all react with ethylene at 25°C,<sup>171</sup> to give (IXD). Similarly, (IXD) undergoes alkene-exchange with 1-hexene<sup>171</sup> to give (IXC). Treatment of a heptane solution of (IXC) with excess vinyl-n-butyl ether,<sup>173</sup> gives (IXG),  $(\mu\text{-H})(\mu\text{-trans-CH=CHO-Bu}^n)\text{Re}_2(\text{CO})_8$ . Dissolution of (IXD) in neat styrene<sup>176</sup> yields (IXH),  $(\mu\text{-H})(\mu\text{-trans CH}=\text{CHPh})\text{Re}_2(\text{CO})_8$  in quantitative yield (5-6 h). Compounds (IXA-F) react with excess olefin at room temperature to give the alkenyl-exchanged  $(\mu\text{-hydrido})(\mu\text{-alkenyl})\text{dirhenium-octa-carbonyl}$  complex.<sup>173</sup>

Compounds (IXA)-(IXH) all react with excess py<sup>173-1</sup> in the dark to yield free olefin and  $1,2\text{-eq,eq-Re}_2(\text{CO})_8(\text{py})_2$ . Room temperature reactions of (IXA)-(IXF) with  $\text{CO}$ <sup>173-1</sup> result in the formation of  $\text{Re}_2(\text{CO})_{10}$ , with liberation of olefin. However, the photolysis of (IXB1) in the presence of py<sup>171</sup> yields  $(\mu\text{-H})\text{Re}_2(\text{CO})_7(\mu\text{-}(\eta^2\text{CH}=\text{CH Et}))\text{py}$  as the major product.

A toluene solution of (IXD) reacts with  $\text{H}_2$  (1 atm.)<sup>176</sup> over 3 days to initially generate  $\text{H}_2\text{Re}_2(\text{CO})_8$ , which is subsequently slowly converted to  $\text{H}_3\text{Re}_3(\text{CO})_{12}$ . The reaction of (IXB1) with  $\text{H}_2$  is similar.

Dissolution of (IXD) in neat acetonitrile (MeCN)<sup>176</sup> results in complete conversion to 1,2-eq,eq-Re<sub>2</sub>(CO)<sub>8</sub>(NMe)<sub>2</sub> (5 h, room temperature). The major product of the reaction in toluene solution of (IXD) with H<sub>2</sub>S<sup>176</sup> (1 atm, 6 h), is Re<sub>2</sub>(CO)<sub>8</sub>(SH)<sub>2</sub>. (IXB1) reacts with excess acrylonitrile<sup>176</sup> in toluene solution to yield Re<sub>2</sub>(CO)<sub>8</sub>(NCH=CH<sub>2</sub>)<sub>2</sub>.

Compounds (IXA)-(IXH) all react with excess PPh<sub>3</sub><sup>176</sup> in hexane at 25°C to give free olefin and 1,2-ax,eq-Re<sub>2</sub>(CO)<sub>8</sub>(PPh<sub>3</sub>)<sub>2</sub>, which isomerizes to 1,2-diax-Re<sub>2</sub>(CO)<sub>8</sub>(PPh<sub>3</sub>)<sub>2</sub>. The reaction of (IXD) with PBu<sub>3</sub><sup>n</sup> follows the same pattern.<sup>176</sup> However, the reaction of (IXD) with P(OR)<sub>3</sub> (R = Me, Ph) yields 1,2-eq,eq-Re<sub>2</sub>(CO)<sub>8</sub>(P(OR)<sub>3</sub>)<sub>2</sub>, which is stable to isomerization.<sup>176</sup> Treatment of (IXD) with excess PMe<sub>3</sub><sup>176</sup> in hexane or toluene solution rapidly generates the dipolar addition product (μ-H)(μ-CH=CH<sub>2</sub>)Re<sub>2</sub>(CO)<sub>8</sub>(PMe<sub>3</sub>)<sub>2</sub> (X) (Fig. 10.6). This product (X) slowly decomposes in toluene solution to give 1,2-eq,eq-Re<sub>2</sub>(CO)<sub>8</sub>(PMe<sub>3</sub>)<sub>2</sub>, which is stable to isomerization.<sup>176</sup> Reaction of (IXA1) with excess PMe<sub>3</sub> in hexane at room temperature gives only 1,2-eq,eq-Re<sub>2</sub>(CO)<sub>8</sub>(PMe<sub>3</sub>)<sub>2</sub> in near-quantitative yield (2-3 h). These bisphosphine dirhenium octacarbonyl products are of importance, as they are rare examples of equatorially substituted phosphine derivatives of Re<sub>2</sub>(CO)<sub>10</sub>. The geometry of phosphine substitution in Re<sub>2</sub>(CO)<sub>10-n</sub>(PR<sub>3</sub>)<sub>n</sub> (n = 1-4) complexes will be discussed in ch. XV.

Similarly, (IXC) reacts with a variety of bidentate phosphino-ligands L-L (L-L = bis(diphenylphosphino)methane (dppm),<sup>176,188</sup> bis(dimethylphosphino)methane(dmpm),<sup>188</sup> bis(diethylphosphino)ethane(dmpe)<sup>188</sup> and bis(diphenylphosphino)ethane (dppe)<sup>188</sup>) to give the bridging ligand substituted dirhenium octacarbonyl compounds, 1,2-eq,eq-Re<sub>2</sub>(CO)<sub>8</sub>(μ-L-L), in high yields (90%).

The major products of the photochemical reaction of 1,2-eq,eq-Re<sub>2</sub>(CO)<sub>8</sub>(μ-L-L) (L-L = dppm, dmpm) with H<sub>2</sub>O or MeOH are (μ-H)(μ-OH)Re<sub>2</sub>(CO)<sub>8</sub>(μ-L-L) and (μ-OR)<sub>2</sub>Re<sub>2</sub>(CO)<sub>8</sub>(μ-L-L) (R = H or Me).<sup>188</sup> The structure of (μ-H)(μ-OH)Re<sub>2</sub>(CO)<sub>8</sub>(μ-dppm) has been determined by X-ray crystallography<sup>188</sup> (see ch. XIII).

Reactions of  $(\mu-H)(\mu-OR)Re_2(CO)_6(\mu-L-L)$  and  $(\mu-OR)_2Re_2(CO)_6(\mu-L-L)$  with dry  $HCl$  lead to the formation of  $(\mu-H)(\mu-Cl)Re_2(CO)_6(\mu-L-L)$  and  $(\mu-Cl)_2Re_2(CO)_6(\mu-L-L)$  respectively.<sup>118</sup>

Treatment of a solution of (IXB1) with an excess of 3,3-dimethylcyclopropene<sup>119</sup> at room temperature leads to the formation (2 days, 80%) of dirhenium-octacarbonyl-( $\mu$ -carbene) complex,  $Re_2(CO)_8(\mu-(\eta^1, \eta^3-CH_2CH_2CMe_2))$  (XIA) (Fig. 10.7), the structure of which has been determined by X-ray crystallography (see ch. XIII). Reaction of (XIA) with CO (10 atm, room temperature) leads to metal-metal bond cleavage and formation of  $Re_2(CO)_9(\mu-(\eta^1, \eta^3-CH_2CH_2CMe_2))$  (XIB), which is unusual in that it contains a  $\mu$ -carbene system not supported by a metal-metal bond.<sup>119</sup> On irradiation of (XIB) (2 h, room temperature), the  $\eta^1, \eta^2$ -butadienyl hydride,  $(\mu-H)Re_2(CO)_8(\mu-CH=CH_2CMe_2)$  (XIC) results.<sup>119</sup>

Treatment of (IXA1)<sup>118</sup> or (IXB1)<sup>119</sup> with excess phenylacetylene at room temperature gives the  $\mu$ -hydride- $\mu$ -alkynyl-octacarbonyl-dirhenium complex,  $(\mu-H)Re_2(CO)_8(\mu^2-C\equiv CPh)$  (XIIA) (Fig. 10.8) as the major product (85%, 5-10 h). Similarly, reaction of (IXA1) with (*p*-methoxyphenyl) acetylene yields  $(\mu-H)Re_2(CO)_8(\mu-p-C\equiv CC_6H_4OMe)$  (XIIB) (Fig. 10.8). Treatment of a hexane solution of (XIIA) with excess  $py$ <sup>120</sup> yields a single isomer of  $(\mu-H)(\mu-C\equiv CPh)Re_2(CO)_7(py)$ , in near quantitative yield (1-2 h, room temperature). This mono-substituted compound reacts slowly with excess  $py$ <sup>120</sup> to yield a single isomer of a disubstituted species,  $(\mu-H)(\mu-C\equiv CPh)Re_2(CO)_6(py)_2$ . (XIIB) also undergoes CO substitution by  $py$ ,<sup>120</sup> yielding  $(\mu-H)(\mu-p-C\equiv CC_6H_4OMe)Re_2(CO)_7(py)$ .

Treatment of a  $CH_2Cl_2$  or hexane solution of (XIIA) with excess  $PPh_3$ <sup>121</sup> results in essentially quantitative production of the disubstituted complex,  $(\mu-H)(\mu-C\equiv CPh)Re_2(CO)_6(PPh_3)_2$  (2 h). During monitoring of the reaction (in  $CD_2Cl_2$ ) by  $^1H$  NMR spectroscopy, the monosubstituted complex,  $(\mu-H)(\mu-C\equiv CPh)Re_2(CO)_7(PPh_3)$ , was observed as the initial product. The reaction of (XIIA) with  $PBu_3$ <sup>121</sup> is analogous.<sup>120</sup> However, treatment of a hexane solution of (XIIA) with excess  $PMe_3$  results in the immediate formation of a dimeric addition product,  $(\mu-H)(\mu-C\equiv CPh)Re_2(CO)_6(PMe_3)_2$  (Fig. 10.9 (XIIIA) or (XIIIB)).

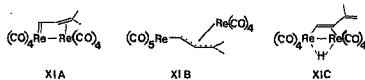


Figure 10.7: Dirhenium carbonyl ( $\mu$ -carbene) derivatives



(A) R = Ph

(B) R:  $C_6H_4OMe-p$

Figure 10.8: Products of reaction of  $(\mu-H)(\mu-trans-CH=CHMe)Re_2-(CO)_8$  with acetylene



Figure 10.9: Possible dipolar addition products,  $(\mu-H)(\mu-CsPh)Re_2-(CO)_8(PMe_3)$

10.7 Photochemical reaction of  $\text{Re}_2(\text{CO})_{10}$  with  $\text{R}_2\text{SiH}_2$

The first report of a dirhenium carbonyl derivative with a bridging  $\text{SiR}_2$  ligand was the formation of the complex  $\text{Re}_2(\text{CO})_8\text{H}_2(\mu\text{-SiPh}_2)$  in the photochemical reaction of  $\text{Re}_2(\text{CO})_{10}$  and  $\text{Ph}_2\text{SiH}_2$  in benzene solution.<sup>113a</sup> The X-ray crystal structure of this complex has been determined.<sup>113b</sup> The crystal structures of the related derivatives,  $\text{Re}_2(\text{CO})_7\text{H}_2(\mu\text{-SiEt}_2)_2$ <sup>113c</sup> and  $\text{Re}_2(\text{CO})_6\text{H}_4(\mu\text{-SiEt}_2)_2$ <sup>113d</sup> have also since been reported. No details of the synthesis of these compounds were given, but presumably the method was similar to that for the synthesis of  $\text{Re}_2(\text{CO})_8\text{H}_2(\mu\text{-SiPh}_2)$ <sup>113a</sup> (vide supra). The molecular structures of these three complexes will be considered in ch. XIII.

The room temperature reaction of  $\text{Re}_2(\text{CO})_8\text{H}_2(\mu\text{-SiPh}_2)$  with silicic acid in chloroform solution resulted in the formation of the dihydride derivative,  $\text{Re}_2(\text{CO})_8(\mu\text{-H})_2$ <sup>113e</sup> the structure of which has been determined by X-ray crystallography (see ch. XIII).

10.8 The photochemical reaction of  $\text{Re}_2(\text{CO})_{10}$  with  $\text{H}_2$

UV-irradiation of  $\text{Re}_2(\text{CO})_{10}$  with  $\text{H}_2$  in THF gives  $\text{Re}_2(\text{CO})_8(\mu\text{-H})_2$ , together with monomeric and trimeric rhenium products.<sup>114</sup>

This complex has also been obtained from UV-irradiation of  $\text{Re}_3(\text{CO})_{12}\text{H}_3$ <sup>115</sup> from the thermal reaction of  $\text{Re}_2(\text{CO})_8\text{H}_2(\mu\text{-SiPh}_2)$  with  $\text{SiO}_2 \cdot n\text{H}_2\text{O}$ <sup>116</sup> (vide supra), and from the thermal reaction of  $(\mu\text{-H})(\mu\text{-CHCH}_2)\text{Re}_2(\text{CO})_8$  with  $\text{H}_2$ <sup>117</sup> (see section 10.6.4).

10.9 Photochemical reaction of  $\text{Re}_2(\text{CO})_{10}$  with water

$\text{Re}_2(\text{CO})_{10}$  is stable towards water even under drastic conditions;<sup>118</sup> it is also not attacked by dilute acids or bases.<sup>119</sup> A "base reaction" can only be achieved with methanolic potassium hydroxide, whereupon a dinuclear complex  $\text{K}[\text{Re}_2(\text{CO})_8\text{O}_2\text{H}]$  is formed.<sup>120</sup>

The photolysis of  $\text{Re}_2(\text{CO})_{10}$  in wet THF leads to the formation of  $\text{eq-Re}_2(\text{CO})_9(\text{OH}_2)$ .<sup>121</sup> This product has been shown<sup>122</sup> to be formed via primary photochemical homolysis of the Re-Re bond, followed by thermal substitution of the  $\text{Re}(\text{CO})_5$  radical by  $\text{H}_2\text{O}$ , and then recombination with  $\text{Re}(\text{CO})_5$ .



to give  $\text{Re}_2(\text{CO})_9(\text{OH}_2)$ .

Under 366nm irradiation,  $\text{Re}_2(\text{CO})_9(\text{OH}_2)$  decomposes via the proposed unstable intermediate  $\text{Re}_2(\text{CO})_8(\text{OH}_2)_2$ , which loses  $\text{H}_2\text{O}$  and undergoes oxidative addition to an O-H bond to form  $(\mu\text{-H})\text{Re}_2(\text{CO})_8(\mu\text{-OH})$ , which decomposes to  $\text{HRe}(\text{CO})_5$  and  $\text{Re}_4(\text{CO})_{12}(\text{OH})_4$ , the observed decomposition products.<sup>173</sup>

In THF solution, the co-ordinated water in  $\text{eq-Re}_2(\text{CO})_9(\text{OH}_2)$  is readily displaced by stronger nucleophilic ligands, e.g. CO, MeCN,  $\text{PPh}_3$ , to give  $\text{Re}_2(\text{CO})_{10}$ ,  $\text{eq-Re}_2(\text{CO})_9(\text{NOMe})$  and  $\text{ax-Re}_2(\text{CO})_9\text{PPh}_3$  respectively.<sup>174</sup> Hence  $\text{eq-Re}_2(\text{CO})_9(\text{OH}_2)$  can be regarded as a lightly stabilized form of the co-ordinately unsaturated  $\text{Re}_2(\text{CO})_9$ .<sup>175</sup> However, in non-coordinating solvents (e.g. toluene), only rhenium cluster compounds are obtained.<sup>175</sup> The role of the THF is probably to stabilize the  $\text{Re}_2(\text{CO})_9$  intermediate.

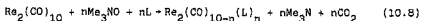
Under photolytic conditions,  $\text{Re}_2(\text{CO})_{10}$  reacts with  $\text{H}_2\text{O}$  in aqueous ether, yielding initially  $\text{Re}_3(\text{CO})_{12}\text{H}_3$  and  $\text{Re}_4(\text{CO})_{12}(\text{OH})_4$ , and after extended irradiation, exclusively  $\text{Re}_4(\text{CO})_{12}(\text{OH})_4$ .<sup>177</sup>

Irradiation of  $\text{Re}_2(\text{CO})_8$  (1,10-phenanthroline) (indirectly prepared<sup>178</sup>) in wet THF yields  $\text{Re}_2(\text{CO})_{10}$  and  $\text{Re}_2(\text{CO})_8$  (1,10-phenanthroline)<sub>2</sub>.<sup>178</sup> However, only  $\text{Re}_4(\text{CO})_{14}(\text{OH})_4$  and some  $\text{eq-Re}_2(\text{CO})_9(\text{NOMe})$  are formed from the reaction of  $\text{dieq-Re}_2(\text{CO})_8(\text{NOMe})_2$  with  $\text{H}_2\text{O}$  in refluxing THF.<sup>175</sup> The unstable  $\text{Re}_2(\text{CO})_8(\text{OH}_2)_2$  may be formed as an intermediate in the reaction of  $(\mu\text{-H})(\mu\text{-CHCH}_2)\text{Re}_2(\text{CO})_8$  with  $\text{H}_2\text{O}$  (wet THF), which eventually yields  $\text{Re}_4(\text{CO})_{12}(\text{OH})_4$ .<sup>179</sup>

#### 10.10 N-donor ligand derivatives of $\text{Re}_2(\text{CO})_{10}$

##### 10.10.1 Trimethylamine-N-oxide-induced reactions of $\text{Re}_2(\text{CO})_{10}$ with N-donor ligands

The thermal reactions of  $\text{Re}_2(\text{CO})_{10}$  with trimethylamine-N-oxide,  $\text{Me}_3\text{NO}$ , in the presence of N-donor ligands L lead to substituted derivatives,  $\text{Re}_2(\text{CO})_{10-n}(\text{L})_n$  ( $n = 1, 2$ ), according to eqn. (10.8).



The reaction is usually performed in acetonitrile

(MeCN) solvent, and in the absence of added donor ligand L, acetonitrile derivatives,  $\text{eq-Re}_2(\text{CO})_9(\text{NCMe})^{173}$  and  $\text{dieq-Re}_2(\text{CO})_8(\text{NCMe})_2^{173}$  are formed (see also section 10.5).

In the presence of N-donor ligand L, the reaction results in the formation of substituted derivatives  $\text{Re}_2(\text{CO})_{10-n}(\text{L})_n$  ( $n = 1, 2$ ). This method has been employed in the synthesis of the complexes  $\text{eq-Re}_2(\text{CO})_9\text{L}$  ( $\text{L} = \text{py},^{173}$  2-Mepy,<sup>173</sup> MeN<sub>2</sub>,<sup>167</sup> EtNH<sub>2</sub><sup>167</sup>) and  $\text{dieq-Re}_2(\text{CO})_8(\text{py})_2$ .<sup>173</sup> These derivatives have been shown to undergo photolysis reactions<sup>167</sup> resulting in the formation of new dirhenium carbonyl complexes (vide infra).

10.10.2 Photolytic reactions of  $\text{Re}_2(\text{CO})_{10-n}\text{L}$  ( $n = 1, 2$ , L = N-donor ligand)

Photolysis of solutions of mono- and di-substituted N-donor ligand derivatives of dirhenium carbonyl results in the formation of new di- and tri-substituted dimers. The photolysis reaction in THF solution of  $\text{eq-Re}_2(\text{CO})_9(\text{NCMe})$  and of  $\text{eq-Re}_2(\text{CO})_9(\text{py})$  or 1,2-dieq- $\text{Re}_2(\text{CO})_8(\text{py})_2$ , yields the products 1,2-dieq- $\text{Re}_2(\text{CO})_8(\text{NCMe})_2$  and 1,1-( $\mu\text{-H}$ ) $\text{Re}_2(\text{CO})_7(\text{py})(\text{NC}_5\text{H}_4)$  respectively.<sup>167</sup> Photolysis of  $\text{eq-Re}_2(\text{CO})_9(\text{RNH}_2)$  ( $\text{R} = \text{Me}, \text{Et}$ ) in heptane yields 1,1- $\text{Re}_2(\text{CO})_8(\text{RNH}_2)_2$ .<sup>167</sup> In these reactions, other photolysis products usually include  $\text{Re}_2(\text{CO})_{10}$ , monomeric rhenium carbonyl derivatives, and rhenium carbonyl cluster compounds.<sup>167</sup>

10.10.3 Preparation of  $(\mu\text{-H})\text{Re}_2(\text{CO})_8(\mu\text{-NC}_5\text{H}_4)$ , and subsequent reactions with donor ligands

The compound  $(\mu\text{-H})\text{Re}_2(\text{CO})_8(\mu\text{-NC}_5\text{H}_4)$  is formed by heating 1,2-dieq- $\text{Re}_2(\text{CO})_8(\text{py})_2$  in refluxing benzene.<sup>167</sup> This complex has been characterized by X-ray crystallography<sup>168</sup> (see ch. XIII), and itself undergoes further CO-substitution reactions with other donor ligand.<sup>167-9</sup>

(a) Thermal reactions with ligand L

In benzene solution,  $(\mu\text{-H})\text{Re}_2(\text{CO})_8(\mu\text{-NC}_5\text{H}_4)$  reacts slowly with py to give 1,1-( $\mu\text{-H}$ ) $\text{Re}_2(\text{CO})_7(\text{py})(\text{NC}_5\text{H}_4)$ ,<sup>167</sup> and with  $\text{PPh}_3$  to yield  $(\mu\text{-H})\text{Re}_2(\text{CO})_7(\mu\text{-NC}_5\text{H}_4)(\text{PPh}_3)$  and  $(\mu\text{-H})\text{Re}(\text{CO})_6(\mu\text{-NC}_5\text{H}_4)(\text{PPh}_3)_2$ .<sup>168</sup> Refluxing  $(\mu\text{-H})\text{Re}_2(\text{CO})_8(\mu\text{-NC}_5\text{H}_4)$  in acetonitrile solution gave  $(\mu\text{-H})\text{Re}_2(\text{CO})_7(\mu\text{-NC}_5\text{H}_4)(\text{NCMe})$ .<sup>168</sup>

the structure of which has been determined by X-ray crystallography<sup>166</sup> (see ch. XIII). All these thermal substitution reactions required very long reaction times (10-20 h).

(b) Reaction with  $\text{Me}_3\text{NO}$  in the presence of ligand L

When a solution of  $(\mu\text{-H})\text{Re}_2(\text{CO})_8(\mu\text{-NC}_5\text{H}_4)$  was treated with  $\text{Me}_3\text{NO}$ , in the presence of donor ligand L (L = py,  $\text{PPh}_3$ )<sup>166</sup> mono- and disubstitution of CO resulted. Initially formed was the complex  $(\mu\text{-H})\text{Re}_2(\text{CO})_7(\mu\text{-NC}_5\text{H}_4)(\text{L})$ , which over a 24 h period slowly converted to  $(\mu\text{-H})\text{Re}_2(\text{CO})_6(\mu\text{-NC}_5\text{H}_4)(\text{L})_2$ .<sup>166</sup> With L = 1-octene,<sup>166</sup> however, only the mono-substituted complex  $(\mu\text{-H})\text{Re}_2(\text{CO})_7(\mu\text{-NC}_5\text{H}_4)(\eta^2\text{-1-octene})$  resulted, which did not undergo further reaction to the di-substituted product at room temperature.

(c) Photochemical reactions with ligand L

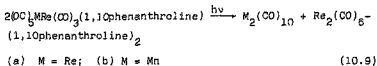
Photolysis of toluene solutions of  $(\mu\text{-H})\text{Re}_2(\text{CO})_8(\mu\text{-NC}_5\text{H}_4)$  and L (L = py,  $\text{PPh}_3$ )<sup>166</sup> resulted in the formation of mono-substituted  $(\mu\text{-H})\text{Re}_2(\text{CO})_7(\mu\text{-NC}_5\text{H}_4)(\text{L})$ , which over a period of 10-15 h was converted to di-substituted  $(\mu\text{-H})\text{Re}_2(\text{CO})_6(\mu\text{-NC}_5\text{H}_4)(\text{L})_2$ . After a further 10-15 h photolysis, tri-substituted  $(\mu\text{-H})\text{Re}_2(\text{CO})_5(\mu\text{-NC}_5\text{H}_4)(\text{L})_3$  could be obtained. However, with L =  $\text{P(OPh)}_3$ , 1-octene,<sup>166</sup> only mono-substituted products,  $(\mu\text{-H})\text{Re}_2(\text{CO})_7(\mu\text{-NC}_5\text{H}_4)(\text{L})$ , could be isolated even after prolonged periods of photolysis.

10.10.4 Preparation of bis-N-donor-ligand derivatives of  $\text{Re}_2(\text{CO})_{10}$

Although  $\text{Mn}_2(\text{CO})_8$  (1,10-phenanthroline) is synthesised by the photolysis reaction of  $\text{Mn}_2(\text{CO})_{10}$  and 1,10-phenanthroline,<sup>167-169</sup> the synthesis of the rhenium analogue,  $\text{Re}_2(\text{CO})_8(\text{L}_2)$  ( $[\text{L}_2] = 1,10\text{-phenanthroline}, 2,2'\text{-biquinoline}, 2,2'\text{-bipy}$  and 4,7-diphenyl-1,10-phenanthroline), was achieved by airless addition (in the dark) of a THF solution of  $\text{NaRe}(\text{CO})_5$  to a deoxygenated  $\text{CfRe}(\text{CO})_3(\text{L}_2)$  solution.<sup>168</sup> The displacement of  $\text{Cf}^-$  by  $\text{Re}(\text{CO})_5^-$  occurs rapidly at 298 K to yield a highly coloured solution of  $\text{Re}_2(\text{CO})_8(\text{L}_2)$ , and  $\text{NaCf}$  precipitate.

Irradiation of  $\text{Re}_2(\text{CO})_8(1,10\text{-phenanthroline})$  in wet THF yields  $\text{Re}_2(\text{CO})_{10}$  and  $\text{Re}_2(\text{CO})_8(1,10\text{-phenanthroline})_2$ .<sup>170</sup>

(eqn. 10.9(a)). This latter complex has also been obtained from the photolysis of  $(CO)_9MnRe(CO)_3(1,10\text{-phenanthroline})$  in  $THF^{11a}$  (eqn. 10.9(b)).



10.11 Dirhenium carbonyl carbene complexes

Reaction of  $Re_2(CO)_{10}$  with  $LiR$  in ether, (to give  $Re_2(CO)_9[C(OLi)R]^{117a}$ , and subsequent alkylation with  $[R'_3O][3F_4]/H_2O$  yields the carbene complex  $eq-Re_2(CO)_9[C(OR')R]$  ( $R = Me,^{117a} Ph,^{117b} C_6H_4Me-p,^{117b} R' = Me; R = SiPh_3, R' = Me^{117a} Et^{117a}$ ). Similarly, the reaction of  $Re_2(CO)_{10}$  with  $LiSiPh_3$  in THF, followed by treatment with  $MeFSO_3$  gives  $eq-Re_2(CO)_9[C(OMe)SiPh_3]$  or  $eq-Re_2(CO)_9[C(OC_4H_8OMe)SiPh_3]$ , depending on the reaction conditions.<sup>117a</sup> In addition, the reaction of  $Re_2(CO)_{10}$  with excess  $LiSiPh_3$  and subsequent alkylation with  $[Et_3O][BF_4]/H_2O$  yields not only  $eq-Re_2(CO)_9[C(OEt)SiPh_3]$ ,<sup>117a-c</sup> but 1,2-ax,  $eq-Re_2(CO)_8[C(OEt)SiPh_3]^{117b,c}$  and dirhenium products characterized by X-ray crystallography<sup>117c</sup> (see ch. XIII) as  $(CO)_4Re[\mu-C(SiPh_3)-CO(OEt)]Fe(CO)_3[C(OEt)SiPh_3]$  and  $Re_2(CO)_8[\mu-C(SiPh_3)CO](\mu-H)$ . The structures of  $eq-Re_2(CO)_9[C(OR')SiPh_3]$  ( $R = Me,^{117a} Et,^{117a,117b}$ ) and 1,2-ax,  $eq-Re_2(CO)_8[C(OEt)SiPh_3]^{117b}$  have also been determined crystallographically (see ch. XII). Further treatment of the carbene complex  $eq-Re_2(CO)_9[C(OMe)R]$  ( $R = Ph, C_6H_4Me-p$ ) with  $LiR$  / ether, followed by  $[Me_3O][BF_4]/H_2O$ , yields the  $\mu$ -methylidene complex  $Re_2(CO)_8[\mu-C(OMe)R]_2^{117b}$ . The molecular structure of one such complex,  $Re_2(CO)_8[\mu-C(OMe)C_6H_4Me-p]_2$ , has been determined by X-ray crystallography<sup>117b</sup> (see ch. XIII).

The isomeric carbene complex,  $ax-Re_2(CO)_9[C(OR')SiPh_3]$  ( $R' = Me, Et$ ), can be obtained by reaction of  $eq-Re_2(CO)_9[C(OR')SiPh_3]$  with  $AxX_2$  ( $X = Cl, Br$ ) to give  $[ax-Re_2(CO)_9(CSiPh_3)]^+[AX_2]^-$ , which is then treated with alcohol,  $R'OH,^{117a}$  The isomers,  $ax-or-eq-Re_2(CO)_9[C(OMe)SiPh_3]$ , react with dialkylamine,  $HNR_2$  ( $R' = Me, Et$ ) in pentane to

form  $ax-$  or  $eq-[Re_2(CO)_9C(NR_2)SiPh_3]$  respectively.<sup>178a</sup> Treatment of the  $ax-$  or  $eq-$  isomers of  $Re_2(CO)_9[C(OEt)-SiPh_3]$  with  $Li(C_6H_5)_2Me$  and subsequent alkylation with  $[Et_3O][BF_4]$  yields the two isomers of  $1,2-ax,eq-Re_2(CO)_9-[C(OEt)SiPh_3][C(OEt)C_6H_4Me]^{178b}$  (see Fig. 10.10 (XIVA) and (XIVB)).

The reaction of the cationic silyl carbyne complexes of dirhenium carbonyl,  $[ax-Re_2(CO)_9(CSiPh_3)]^+[A^+X_4]^-$  ( $X = Cl, Br$ ) with alcohols,  $R''OH$  ( $R'' = Me, Et, Pr^i, Bu^t$ ), has also been reported to yield alkoxy-carbene complexes,  $ax-Re_2(CO)_9[C(OR'')SiPh_3]$  and  $eq-Re_2(CO)_9[C(OR'')H]$ .<sup>211</sup> Halogen-silylcarbene complexes,  $ax-Re_2(CO)_9[C(X)SiPh_3]$  ( $X = Cl, Br$ ), can be isolated as intermediates.<sup>211</sup> Reaction of  $[ax-Re_2(CO)_9(CSiPh_3)]^+[A^+Br_4]^-$  with dimethylamine,  $H_2NMe_2$ , gives  $ax-Re_2(CO)_9[C(NMe)SiPh_3]$ , and  $eq-Re_2(CO)_9[C(NMe)H]$ .<sup>211</sup> The latter compound can also be obtained by treating  $eq-Re_2(CO)_9[C(OMe)H]$  with  $H_2NMe_2$ .<sup>211</sup> The X-ray crystal structure of  $eq-Re_2(CO)_9[C(OMe)H]$  has been reported<sup>211</sup> (see ch. XIII).

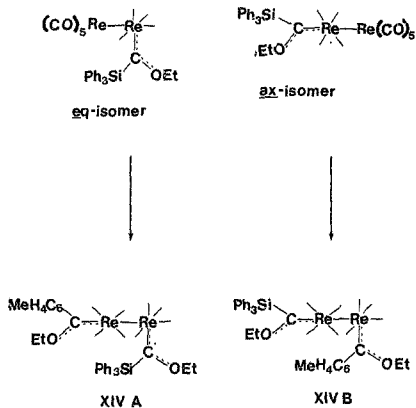
10.12 Thermal reaction of  $Re_2(CO)_{10}$  with acetylenes

The reaction of  $Re_2(CO)_{10}$  with  $PhCCPh$  at  $190^\circ C$  gives  $[Re_2(CO)_7(PhCCPh)_2]$ ,  $[Re_2(CO)_6(PhCCPh)_3]$ , and  $[Re_2(CO)_4(PhCCPh)_4]$ .<sup>212</sup> This latter complex reacts instantaneously with excess of isocyanide  $RNC$  ( $R = Bu^t, Bu^i, p-MeOC_6H_4$  or  $p-MeC_6H_4SO_2CH_2$ ) to give  $[Re_2(CO)_4(PhCCPh)_3(CNR)_2]$ .<sup>212</sup> An X-ray crystal structure analysis of one such isocyanide derivative,  $[Re_2(CO)_4(PhCCPh)_3(CNCH_2SO_2C_6H_4Me-p)_2]$ , has been performed<sup>212</sup> (see ch. XIII).

Complexes of the type  $\mu$ -hydrido- $\mu$ -alkynyl-dirhenium-octacarbonyl are obtained from the reaction of  $\mu$ -hydrido- $\mu$ -olefinyl dirhenium octacarbonyl with acetylenes<sup>168</sup> (see section 10.6.4).

10.13 Formation of  $[cis-Re_2(CO)_9(CHO)]^-$  from  $Re_2(CO)_{10}$

The anionic formyl complex of dirhenium carbonyl,  $Li^+[cis-Re_2(CO)_9(CHO)]^-$  was prepared by the reaction of  $LiEt_3BH$  with  $Re_2(CO)_{10}$  in THF solution.<sup>176</sup> Analogous products were obtained for  $Mn_2(CO)_{10}$  and for the mixed-metal decacarbonyl dimer,  $ReMn(CO)_{10}$ .<sup>176</sup>



**Figure 10.10:** The two isomers of 1,2-ax,eq-Re<sub>2</sub>(CO)<sub>9</sub>[C(OEt)SiPh<sub>3</sub>]-[C(OEt)C<sub>6</sub>H<sub>4</sub>Me], (XIVA) and (XIVB)

Treatment of the eq- or ax- isomers of Re<sub>2</sub>(CO)<sub>9</sub>-[C(OEt)SiPh<sub>3</sub>] with Li(C<sub>6</sub>H<sub>4</sub>Me) and subsequent alkylation with [Et<sub>3</sub>O][BF<sub>4</sub>] yields the two isomers of 1,2-ax,eq-Re<sub>2</sub>(CO)<sub>9</sub>[C(OEt)SiPh<sub>3</sub>][C(OEt)C<sub>6</sub>H<sub>4</sub>Me], (XIVA) and (XIVB) respectively.

In the transformylation reaction<sup>211</sup> of  $\text{Et}_4\text{N}^+[\text{trans-}[(\text{PhO})_3\text{P}](\text{CO})_3\text{FeCHO}]^-$  with  $\text{Re}_2(\text{CO})_{10}$  in THF,  $\text{Et}_4\text{N}^+[\text{cis-}\text{Re}_2(\text{CO})_9(\text{CHO})]^-$  was formed (82% yield as determined by  $^1\text{H}$  NMR integration) together with a co-product,  $(\text{CO})_4\text{Fe} - [\text{P}(\text{OPh})_3]$ .

$\text{Et}_4\text{N}^+[\text{cis-}\text{Re}_2(\text{CO})_9(\text{CHO})]^-$  was also synthesized (32% yield) by the reaction of  $\text{K}^+\text{HB}(\text{O-Pr}^i)_3^-$  with  $\text{Re}_2(\text{CO})_{10}$  in THF at  $0^\circ\text{C}$ , followed by aqueous basic workup and cation exchange with  $\text{Et}_4\text{N}^+\text{Br}^-$ .<sup>213</sup>

10.14 Formation of  $\text{Et}_4\text{N}^+[\text{cis-}\text{Re}_2(\text{CO})_9\text{H}]^-$  from  $\text{Re}_2(\text{CO})_{10}$

The reaction of  $\text{K}^+\text{HB}(\text{O-Pr}^i)_3^-$  with  $\text{Re}_2(\text{CO})_{10}$  under fluorescent laboratory lighting ( $45-50^\circ\text{C}$ , 3 h), followed by aqueous basic workup and cation exchange with  $\text{Et}_4\text{N}^+\text{Br}^-$  gave the hydrido anion  $\text{Et}_4\text{N}^+[\text{cis-}\text{Re}_2(\text{CO})_9\text{H}]^-$ .<sup>213</sup> This metal hydride can also be obtained from the photolysis of a THF solution of  $\text{Et}_4\text{N}^+[\text{cis-}\text{Re}_2(\text{CO})_9(\text{CHO})]^-$ .<sup>213</sup>

$\text{Et}_4\text{N}^+[\text{HRe}_2(\text{CO})_9]^-$  has also been detected, though not isolated, in the TEABH reduction of  $\text{Re}_2(\text{CO})_{10}$  in MeCN<sup>212</sup> (see section 10.15).

10.15 Quaternary Ammonium Borohydride reductions of  $\text{Re}_2(\text{CO})_{10}$

Quaternary ammonium borohydrides, used in single phase or phase transfer reactions, are highly effective reagents for preparing metal carbonyl anions from metal carbonyls.<sup>214</sup>

The tetraethylammonium borohydride (TEABH) reduction of  $\text{Re}_2(\text{CO})_{10}$  in MeCN ( $80^\circ\text{C}$ , 1 h) yielded the hydrido anion  $\text{Et}_4\text{N}^+[\text{HRe}_2(\text{CO})_9]^-$ .<sup>214</sup> On stirring the crude product from this reaction with  $\text{CH}_2\text{Cl}_2$  (room temperature, 1½ h), the chloro anion,  $\text{Et}_4\text{N}^+[\text{Re}_2(\text{CO})_9\text{Cl}]^-$  (39%) was formed.<sup>214</sup> This product was also obtained in high yield (89%) from the TEABH reduction of  $\text{Re}_2(\text{CO})_{10}$  in  $\text{CH}_2\text{Cl}_2$  (room temperature, 2 h).<sup>214</sup>

10.16 Conclusion

From the foregoing review of reactions of  $\text{Re}_2(\text{CO})_{10}$  with ligand(s) L to give dimeric products  $\text{Re}_2(\text{CO})_{10-n}(\text{L})_n$  ( $n = 1-4$ ) in which the Re-Re bond remains intact, several points become apparent.

- (i) The use of synthetic methods involving the direct reaction of the  $\text{Re}_2(\text{CO})_{10}$  dimer give products  $\text{Re}_2(\text{CO})_{10-n}(\text{L})_n$ ,

where  $n \leq 4$ , (except for the acetylene complex  $[\text{Re}_2(\text{CO})_4(\text{PhCCPh})_4]$  and the isonitrile derivatives,  $[\text{Re}_2(\text{CO})_4(\text{PhCCPh})_3(\text{CNR})_2]$  (see section 10.12). In the majority of reactions, only mono- and di-substituted products,  $\text{Re}_2(\text{CO})_{10-n}(\text{L})_n$  ( $n = 1-2$ ), result. In a few instances tri- and tetra-substituted complexes,  $\text{Re}_2(\text{CO})_{10-n}(\text{L})_n$  ( $n = 3,4$ ), have been prepared, but generally forcing reaction conditions are required. This limitation must be synthetic, and not steric in origin, since the decaphosphite dirhenium complex,  $\text{Re}_2[\text{P}(\text{OMe})_3]_{10}$ , has been prepared by indirect methods.<sup>215</sup> [Tolman cone angle<sup>85</sup> for  $\text{P}(\text{OMe})_3$ :  $107^\circ$ ].

(ii) Apart from routine characterization, there has been very little comment on the position of ligand attack in  $\text{Re}_2(\text{CO})_{10}$ , and the resultant stereochemistry of the  $\text{Re}_2(\text{CO})_{10-n}(\text{L})_n$  ( $n = 1-4$ ) complexes. Even where X-ray crystal structures of the product have been undertaken, little attempt has been made to rationalize the observed structure in terms of electronic and steric factors. The structures of  $\text{Re}_2(\text{CO})_{10-n}(\text{L})_n$  ( $n = 1-4$ ) complexes which have been determined by X-ray crystallographic techniques will be discussed in ch. XIII, and an attempt made to rationalize structural trends apparent, as well as any exceptions, in terms of underlying electronic and steric factors.

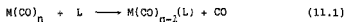
(iii) There have been no comprehensive systematic studies (chemical, structural, mechanistic) on  $\text{Re}_2(\text{CO})_{10}/\text{L}$  systems, apart from the kinetic-mechanistic studies on the  $\text{Re}_2(\text{CO})_{10}/\text{PR}_3$  system, which will be discussed in ch XV. Such a study was thus undertaken on the  $\text{Re}_2(\text{CO})_{10}/\text{RNC}$  system, which has received very little prior attention (see section 10.4). The results of this chemical and structural study will be presented in chs. XI and XIV respectively.



XI. CATALYTIC SYNTHESIS AND CHARACTERIZATION OF ISONITRILE  
DERIVATIVES OF Rhenium DECACARBONYL

11.1 Introduction

Facile synthetic routes are continually being sought to substituted metal carbonyl complexes. Until recently, photochemical or (vigorous) thermal techniques have been employed to achieve substitution of CO by a ligand L, as shown in eqn. (11.1).



With compounds containing a metal-metal bond, bond cleavage may occur, resulting in unwanted by-products, separation problems, and reduced yields.

The only report to date of the reaction between  $Re_2(CO)_{10}$  and isonitriles has been a mention of the synthesis (and a Raman study) of the complex  $Re_2(CO)_9(CNMe)$ ,<sup>192b</sup> which was synthesized by photochemical methods.<sup>192a</sup> However, the analogous reaction of  $Mn_2(CO)_{10}$  with isonitrile ligands (RNC) has received more attention. The derivatives  $Mn_2(CO)_{10-n}(CNR)_n$  (R = Me<sup>192, 214</sup> or Bu<sup>t</sup>,<sup>214</sup> n = 1-4) have been synthesized by thermal<sup>214</sup> (refluxing toluene) and/or photochemical methods.<sup>214, 192</sup> Indirect methods have also been employed in the synthesis of these complexes. For instance, a series of complexes,  $Mn_2(CO)_{10-n}(CNR)_n$  (n = 1,2,4,5; R = Me, Ph, p-C<sub>6</sub>H<sub>4</sub>), was prepared by nucleophilic attack of  $Mn(CO)_5^-$  on  $Mn(CO)_5^+(CNR)_nX$  (X = Cl, Br, CN).<sup>217</sup> The complex  $Mn_2(CO)_{10-n}(CNRPh)_n$  (n = 1,2) has been obtained in low yield from the reaction of  $RMn(CO)_5$  (R = Me, Ph) with PhNC in THF.<sup>218</sup> In a systematic study by Behrens et al.,<sup>219</sup> the complexes  $Mn_2(CO)_9(CNR)$  (R = Et, Si-Me<sub>3</sub>, GeMe<sub>3</sub>, SnMe<sub>3</sub>, PPh<sub>2</sub>, COMe) were prepared by reaction of  $Na[Mn_2(CO)_9CN]$  with Et<sub>3</sub>OBf or RCl.

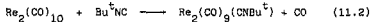
Recently, Albers and Coville<sup>220</sup> have reported that Pd/C or Pd/CaCO<sub>3</sub> catalyses the reaction between  $Mn_2(CO)_{10}$  and isonitriles, to give  $Mn_2(CO)_{10-n}(CNR)_n$  (n = 1-3, R = Bu<sup>t</sup>, C<sub>6</sub>H<sub>5</sub>CH<sub>2</sub>, C<sub>6</sub>H<sub>11</sub>, Me; n = 1-4, R = C<sub>6</sub>H<sub>3</sub>Me<sub>2</sub>-2,6). As a logical extension of this study, an investigation of the

transition metal catalysed thermal reaction between  $\text{Re}_2(\text{CO})_{10}$  and isonitrile ligands was undertaken.

What studies there have been of the properties of  $\text{M}_2(\text{CO})_{10-n}(\text{CNR})_n$  ( $\text{M} = \text{Mn}, n = 1-4; \text{M} = \text{Re}, n = 1, \text{R} = \text{Me}$ ) have employed Raman, IR and  $^1\text{H NMR}$  spectroscopy. No X-ray crystal structures of  $\text{M}_2(\text{CO})_{10-n}(\text{CNR})_n$  compounds have been reported prior to this work. Hence a systematic study was undertaken of the  $\text{Re}_2(\text{CO})_{10}/\text{RNC}$  system, in order to obtain chemical, mechanistic and structural information. Techniques employed in this investigation include IR, Raman,  $^1\text{H NMR}$  and mass spectroscopy, and single crystal X-ray diffraction (ch. XIV).

#### 11.2 Catalyst Testing

In sunlight, the thermal reaction (11.2) in benzene at  $55^\circ\text{C}$  between  $\text{Re}_2(\text{CO})_{10}$  and  $\text{Bu}^t\text{NC}$  (1:1 ratio)



yields predominately  $\text{Re}_2(\text{CO})_9(\text{CNBu}^t)$  (210 min). However, in the dark (complete exclusion of all light) or in artificial laboratory light (no sunlight), no reaction occurs between  $\text{Re}_2(\text{CO})_{10}$  and  $\text{Bu}^t\text{NC}$  at  $55^\circ\text{C}$  (210 min). If after several hours of no reaction in the dark, the reaction vessel was exposed to sunlight, the reaction to  $\text{Re}_2(\text{CO})_9(\text{CNBu}^t)$  proceeded at the above rate. Hence the thermal reaction between  $\text{Re}_2(\text{CO})_{10}$  and  $\text{Bu}^t\text{NC}$  is dependent on sunlight. No attempts have been made to elucidate the mechanism of this thermal uninitiated reaction, but sunlight-initiated fission of the Re-Re or of a Re-CO bond could be implicated.

Reaction (11.2) between  $\text{Re}_2(\text{CO})_{10}$  and  $\text{Bu}^t\text{NC}$  (1:1 ratio) in benzene at  $55^\circ\text{C}$  was used to screen potential catalysts (Table 11.1). Where catalysis was observed, the reaction time was taken as the complete conversion of  $\text{Re}_2(\text{CO})_{10}$  to  $\text{Re}_2(\text{CO})_9(\text{CNBu}^t)$  (as detected by TLC). Pd-metal, PdO and supported Pd-species were found to be exceptionally active catalysts, with reaction times ranging from less than 1 min for PdO and Pd/ $\text{CaCO}_3$ , to ca. 1 h for Pd-metal, and 2 h for Pd/C (5% Pd). (The supports,  $\text{CaCO}_3$  and activated carbon, were found to be inactive). The corresponding Pt-species

were much less active (e.g. Pt/A $\ell_2$ O $_3$  (5% Pt): 70 min. of. Pd/A $\ell_2$ O $_3$  (5% Pd): 5 min), or inactive (no catalysis with PtO $_2$ , Pt/C (5 or 10% Pt)). Other activated carbon-supported species (5% Rh, Ru, Re) were also inactive, as were the transition metal salts investigated (e.g. CoC $\ell_2$ ·2H $_2$ O, which is known to catalyze the reaction between Fe(CO) $_5$  and isonitriles<sup>11,12</sup>).

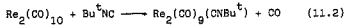
The iron carbonyl dimer, [( $\eta^5$ -C $_5$ H $_5$ )Fe(CO) $_2$ ] $_2$ , was tested for its catalytic ability, since this dimer has been found to be an active catalyst for related carbonyl substitution reactions, when used alone<sup>11,12</sup> or in combination with a co-catalyst such as PdO.<sup>13</sup> However, it was found that with [( $\eta^5$ -C $_5$ H $_5$ )Fe(CO) $_2$ ] $_2$  (4 mg) and PdO (4 mg), the reaction time was 1 min, the same as that for PdO (4 mg) alone, while that for [( $\eta^5$ -C $_5$ H $_5$ )Fe(CO) $_2$ ] $_2$  (4 mg) alone was 40 min. Hence in the case of this reaction, PdO would seem to be the active catalyst.

When catalysis was observed with a given species, the reaction proceeded at the same rate irrespective of whether the catalytic reaction was conducted in sunlight, in artificial light only, or in the dark. If, in the instance of the blank reaction in the dark, after several hours during which no reaction was observed, catalyst was added to the solution of Re $_2$ (CO) $_{10}$  and Bu $^t$ NC, the reaction to Re $_2$ (CO) $_9$ (CNBu $^t$ ) proceeded at the normal rate for that catalyst. Hence the catalyzed reaction is not dependent on sunlight, as in the blank reaction.

It was thought that a reducing agent such as LiAlH $_4$  might catalyze reaction (11.2). However, when a few mgs of LiAlH $_4$  were added to a solution of Re $_2$ (CO) $_{10}$  and Bu $^t$ NC in the dark, no reaction was observed (55°C, 2 h). It was thought traces of oxygen in the solution could be responsible for this lack of reaction. Further, erratic results initially obtained with some Pt-species (e.g. Pt/C, PtO $_2$ ) suggested that Pt might play a role in removing traces of oxygen from the solution. Hence the combination of Pt/C and LiAlH $_4$  was investigated as a potential catalyst for reaction (11.2).

It was found that if a small amount of LiAlH $_4$  was added to a reaction mixture of Re $_2$ (CO) $_{10}$  (0.2 mmol), Bu $^t$ NC (0.22 mmol)

TABLE 11.1: Effect of potential catalysts on the reaction



| Potential catalyst <sup>a</sup>  | Reaction time (min) |
|--|---------------------|
| -  | 210 <sup>b</sup>    |
| PdO  | <1                  |
| PtO <sub>2</sub>   | nc <sup>c</sup>     |
| Pd(O)  | 50                  |
| Pd-impregnated polymer (~40 mesh)  | 105                 |
| Pd/C (10%)   | 105                 |
| Pd/C (5%)  | 120                 |
| Pt/C (10%)   | nc <sup>c</sup>     |
| Pt/C (5%)  | nc <sup>c</sup>     |
| Rh/C (5%)  | nc <sup>c</sup>     |
| Ru/C (5%)  | nc <sup>c</sup>     |
| Re/C (5%)  | nc <sup>c</sup>     |
| Pd/CaCO <sub>3</sub> (10%)   | <1                  |
| Pd/BaCO <sub>3</sub> (5%)  | 6                   |
| Pd/BaSO <sub>4</sub> (5%)  | 130                 |
| Pd/Al <sub>2</sub> O <sub>3</sub> (5%)   | 5                   |
| Pt/Al <sub>2</sub> O <sub>3</sub> (5%)   | 70                  |
| Activated carbon, "Bergwerksverband"   | nc <sup>c</sup>     |
| CaCO <sub>3</sub>  | nc <sup>c</sup>     |
| Platinous Bromide  | nc <sup>c</sup>     |
| Potassium tetrachloroplatinate(II)   | nc <sup>c</sup>     |
| CoCl <sub>2</sub> ·2H <sub>2</sub> O   | nc <sup>c</sup>     |
| IrCl <sub>3</sub> ·nH <sub>2</sub> O   | nc <sup>c</sup>     |
| Zn(O)  | nc <sup>c</sup>     |
| [( <sup>55</sup> C <sub>5</sub> H <sub>5</sub> )Fe(CO) <sub>2</sub> ] <sub>2</sub> | 40                  |

<sup>a</sup> Sources of chemicals used in this study given in Appendix A

<sup>b</sup> In sunlight; no reaction in the dark

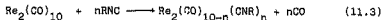
<sup>c</sup> No catalysis

and Pt/C (5% Pt; 1mg) in benzene, which had been heated at 55°C for 4 h in the dark (with no reaction being observed), reaction to  $\text{Re}_2(\text{CO})_9(\text{CNBu}^t)$  was complete in less than 15 mins (the time depending on the amount of  $\text{LiAlH}_4$  added). On addition of a further equivalent of  $\text{Bu}^t\text{NC}$ , the reaction to  $\text{Re}_2(\text{CO})_8(\text{CNBu}^t)_2$  was complete in less than 5 mins. However, if Pt/C and  $\text{LiAlH}_4$  were added together to a solution of  $\text{Re}_2(\text{CO})_{10}$  and  $\text{Bu}^t\text{NC}$  (in the dark) with no pre-heating, no reaction was observed (for several hours). If more  $\text{LiAlH}_4$  was then added after a few hours, a sluggish reaction was observed which proceeded very slowly over a period of several hours. If a solution of  $\text{Re}_2(\text{CO})_{10}$ ,  $\text{Bu}^t\text{NC}$  and Pt/C was heated at 55°C for 4 h (in the dark), oxygen bubbled through the solution, and  $\text{LiAlH}_4$  then added, no reaction was observed (for several hours). If more  $\text{LiAlH}_4$  was added after 2 h, a sluggish reaction was observed (cf. above). (The addition of oxygen has no effect on the reaction rate of the thermal uncatalysed reaction (in sunlight)). Hence the role of Pt/C in the Pt/C -  $\text{LiAlH}_4$  catalytic system appears to be the removal from the solution of traces of  $\text{O}_2$ , which if present presumably prevent the catalysis of the reaction by  $\text{LiAlH}_4$  by oxidizing the active catalytic species. No attempts have been made to further elucidate the mechanism by which the  $\text{LiAlH}_4$ -catalysed reaction operates. Other reducing agents such as zinc-metal do not catalyse reaction (11.2), hence the  $\text{LiAlH}_4$ -catalysed reaction could involve a mechanism involving the formation of hydride species.

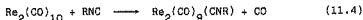
On the basis of the results of the catalyst testing study (Table 11.1), PdO was selected as the catalyst to be used in the synthesis of  $\text{Re}_2(\text{CO})_{10-n}(\text{CNR})_n$  derivatives (vide infra).

11.3 PdO-catalysed reaction of  $\text{Re}_2(\text{CO})_{10}$  with isocyanides

Using PdO as catalyst, a series of isocyanide derivatives,  $\text{Re}_2(\text{CO})_{10-n}(\text{CNR})_n$  ( $n = 1-3$ ,  $R = \text{Bu}^t$ ,  $\text{C}_6\text{H}_5\text{CH}_2$ ,  $\text{C}_6\text{H}_{11}$ ;  $n = 1-4$ ,  $R = 2,6\text{-Me}_2\text{C}_6\text{H}_3$ , Me), were prepared (reaction (11.3)) in generally high isolated yields, under moderate reaction conditions (Table 11.2).



The power of this catalytic method is seen when comparing the reaction times at 55°C for the uncatalysed and the PdO-catalysed reaction (11.4)



There is a substantial improvement in all cases (Table 11.3).

Owing to the facile nature of the PdO-catalysed synthesis of  $\text{Re}_2(\text{CO})_{10-n}(\text{CNR})_n$  ( $n = 1, 2$ ), some  $\text{Re}_2(\text{CO})_{10(n+1)}(\text{CNR})_{n+1}$  is also generally formed, accounting for the less than quantitative yield obtained. The products are readily purified by column chromatography.

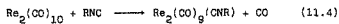
For  $\text{Re}_2(\text{CO})_{10-n}(\text{CNR})_n$  ( $n = 1, 2$ ) derivatives, reaction times are of the order of 1 to 5 min, but the synthesis of  $\text{Re}_2(\text{CO})_7(\text{CNR})_3$  requires longer times (ca. 45 min). Tetra-substitution to give  $\text{Re}_2(\text{CO})_6(\text{CNR})_4$  could only be achieved in poor yields (20-40%) for  $\text{R} = \text{Me}$  and 2,6- $\text{Me}_2\text{C}_6\text{H}_3$ ; the other isonitriles gave no tetra-substituted product after 3 h reaction. This could reflect the better  $\pi$ -acceptor ability of aromatic (2,6- $\text{Me}_2\text{C}_6\text{H}_3\text{NC}$ ) than of aliphatic isonitrile ligands.<sup>11b</sup> In the case of  $\text{MeNC}$ , this could be due to the small size of the  $\text{MeNC}$  ligand<sup>11b</sup> and its electronic similarity to  $\text{CO}$ .<sup>11b</sup> Higher substitution could not be achieved for any of the isonitriles even after 24 h, except possibly for  $\text{RNC} = \text{CNC}_6\text{H}_3\text{Me}_2-2,6$ . In this case a maroon solid was obtained with a complex <sup>1</sup>H NMR spectrum and IR ( $\text{CHCl}_3$ ): 2085(sh), 2060(s), 1995(sh), 1975(m), 1895(sh), 1890(m)  $\text{cm}^{-1}$ , but the elemental analysis of this compound did not correspond to that calculated for  $\text{Re}_2(\text{CO})_5(\text{CNC}_6\text{H}_3\text{Me}_2-2,6)_5$ , and its identity was not pursued. Hence the limit for this catalytic synthetic method, involving direct substitution of  $\text{RNC}$  on  $\text{Re}_2(\text{CO})_{10}$ , is reached at the tetra-substituted step.

The reasons for this are thought to be electronic rather than steric, since  $\text{Re}_2[\text{P}(\text{OMe})_3]_{10}$  (Tolman cone angle<sup>11</sup> for  $\text{P}(\text{OMe})_3$ : 107°) is known<sup>11c</sup> (prepared by indirect methods). An X-ray crystal structure determination of the tetra-substituted  $\text{Re}_2(\text{CO})_6(\text{CNC}_6\text{H}_3\text{Me}_2-2,6)_4$  (ch. XIV) has shown that there are two cis-equatorial isonitrile ligands on each Re-atom. Since isonitriles are weaker  $\pi$ -acceptors than

TABLE 11.2: Reaction conditions and product yields for the PdO catalysed syntheses of the complexes  $\text{Re}_2(\text{CO})_{10-n}(\text{CNR})_n$

| <u>R</u>  | <u>n</u> | <u>T(°C)</u> | <u>t(min)</u> | <u>Isolated yield (%)</u> |
|---|----------|--------------|---------------|---------------------------|
| Bu <sup>t</sup>                                   | 1        | 55           | 1             | 98                        |
|   | 2        | 55           | 5             | 80                        |
|   | 3        | 55           | 45            | 80                        |
| C <sub>6</sub> H <sub>5</sub> CH <sub>2</sub>     | 1        | 55           | 1             | 75                        |
|   | 2        | 80           | 5             | 75                        |
|   | 3        | 80           | 45            | 85                        |
| C <sub>6</sub> H <sub>11</sub>                    | 1        | 55           | 1             | 70                        |
|   | 2        | 110          | 15            | 70                        |
|   | 3        | 110          | 60            | 75                        |
| 2,6-Me <sub>2</sub> C <sub>6</sub> H <sub>3</sub> | 1        | 55           | 5             | 70                        |
|   | 2        | 80           | 20            | 70                        |
|   | 3        | 110          | 40            | 98                        |
|   | 4        | 110          | 150           | 40                        |
| Me  | 1        | 55           | 10            | 80                        |
|   | 2        | 110          | 15            | 80                        |
|   | 3        | 110          | 30            | 80                        |
|   | 4        | 110          | 150           | 20                        |

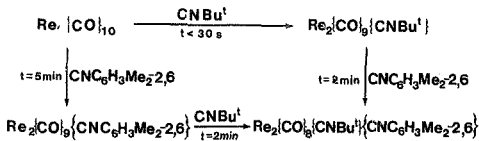
**TABLE 11.3:** Reaction times at 55°C for the uncatalysed and PdO-catalysed reaction



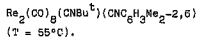
| R   | Reaction Time (min)      |               |
|---|--------------------------|---------------|
|   | Uncatalysed <sup>a</sup> | PdO catalysed |
| Bu <sup>t</sup>                                   | 210                      | <1            |
| C <sub>6</sub> H <sub>5</sub> CH <sub>2</sub>     | 360 <sup>b</sup>         | <1            |
| C <sub>6</sub> H <sub>11</sub>                    | 180                      | <1            |
| 2,6-Me <sub>2</sub> C <sub>6</sub> H <sub>3</sub> | 360 <sup>b</sup>         | 5             |
| Me  | 120                      | 10            |

<sup>a</sup> Under laboratory light conditions

<sup>b</sup> Reaction incomplete



**Figure 11.1:** Synthetic routes to the mixed-isocyanide derivative,





carbonyls,<sup>13</sup> the CO-group trans to an isonitrile ligand is less labile than that trans to another carbonyl ligand.<sup>13,14</sup> A fifth isonitrile ligand would have to go trans to another isonitrile, or trans to the Re-Re bond, both electronically unfavourable situations.<sup>13,15</sup> However, it is possible to prepare such complexes by means of indirect methods, e.g.  $Mn_2(CO)_5(CNR)_5$  (R = Me, Ph, p-C<sub>6</sub>H<sub>4</sub>) has been prepared by nucleophilic attack of  $Mn(CO)_5^-$  on  $Mn(CNR)_5^+$  (X = Cl, Br, CN).<sup>17</sup>

Since the catalytic reaction of  $Re_2(CO)_{10}$  with RNC proceeds in a quantitative and stepwise manner, the degree of isonitrile substitution can be controlled by the number of equivalents of RNC added. Hence it is possible to prepare mixed isonitrile derivatives by adding one equivalent of RNC, and on complete conversion of  $Re_2(CO)_{10}$  to  $Re_2(CO)_9(CNR)$ , a second equivalent of a different isonitrile, R'NC, to give the mixed-isonitrile derivative,  $Re_2(CO)_9(CNR)(CNR')$ , e.g.  $Re_2(CO)_9(CNBU^t)(CNC_6H_3Me_2-2,6)$ . The order in which the RNC and R'NC ligands are added in the mixed reaction is not of consequence, the same product being obtained in either case (see Fig. 11.1).

Satisfactory elemental analyses have been obtained for all the  $Re_2(CO)_{10-n}(CNR)_n$  (n = 1-4) complexes. (Table 11.4). These complexes have been characterized by IR (Table 11.5) and <sup>1</sup>H NMR (Table 11.6) spectroscopy (vide infra), and an X-ray crystallographic study of a series of representative complexes has been undertaken (ch. XIV).

#### 11.4 Characterization of the dirhenium carbonyl isonitrile derivatives

##### 11.4.1. Infra Red Spectroscopy

IR data for the  $Re_2(CO)_{10-n}(CNR)_n$  (n = 1-4) complexes are given in Table 11.5. These compounds have complex IR spectra.

In the case of the mono-substituted  $M_2(CO)_9(L)$  (M = Re, Mn) complex,  $ax-M_2(CO)_9(L)$  (point group C<sub>4v</sub>) is predicted to have 5 ν(CO) IR bands, while  $eq-M_2(CO)_9(L)$  (point group C<sub>s</sub>) should have 9 ν(CO) IR bands. However, many

TABLE 11.4: Analytical data for the  $\text{Re}_2(\text{CO})_{10-n}(\text{CNR})_n$  ( $n = 1-4$ ) complexes

| Complex  | Colour | mp (°C) | Elemental analysis (%) <sup>a</sup> |            |          |
|--|--------|---------|-------------------------------------|------------|----------|
|  |        |         | C                                   | H          | N        |
| $\text{Re}_2(\text{CO})_9(\text{CNRbu}^t)_1$   | white  | 104-106 | 23.6(23.8)                          | 1.2(1.3)   | 1.9(2.0) |
| $\text{Re}_2(\text{CO})_9(\text{CNC}_6\text{H}_5)_1$                                     | yellow | 66-67   | 27.9(27.5)                          | 0.98(0.95) | 2.0(1.9) |
| $\text{Re}_2(\text{CO})_9(\text{CNC}_6\text{H}_{11})_1$                                  | white  | 60-61   | 26.4(26.2)                          | 1.4(1.5)   | 2.0(1.9) |
| $\text{Re}_2(\text{CO})_9(\text{CNC}_6\text{H}_5)_2\text{Me}_2$ -(2,6)                   | cream  | 108-110 | 28.4(28.6)                          | 1.2(1.2)   | 1.9(1.9) |
| $\text{Re}_2(\text{CO})_9(\text{CNRMe})_1$   | yellow | 104-106 | 20.1(19.9)                          | 1.1(1.1)   | 1.1(1.1) |
| $\text{Re}_2(\text{CO})_8(\text{CNRbu}^t)_2$   | white  | 94-97   | 28.6(28.3)                          | 2.3(2.3)   | 2.1(2.1) |
| $\text{Re}_2(\text{CO})_8(\text{CNC}_6\text{H}_5)_2\text{H}_5$ 2                         | yel.   | 73-75   | 34.9(34.4)                          | 1.7(1.7)   | 3.5(3.4) |
| $\text{Re}_2(\text{CO})_8(\text{CNC}_6\text{H}_{11})_2$                                  | yel.   | 42-44   | 32.6(32.4)                          | 2.7(2.7)   | 3.4(3.4) |
| $\text{Re}_2(\text{CO})_8(\text{CNC}_6\text{H}_5)_2\text{Me}_2$ -(2,6) 2                 | yellow | 173-174 | 36.2(36.4)                          | 1.9(2.1)   | 3.3(3.3) |
| $\text{Re}_2(\text{CO})_8(\text{CNRMe})_2$   | yellow | 121-124 | 21.6(21.2)                          | 0.92(0.89) | 4.3(4.1) |
| $\text{Re}_2(\text{CO})_8(\text{CNRbu}^t)_1(\text{CNC}_6\text{H}_5)_3\text{Me}_2$ -(2,6) | yellow | 106-108 | 32.4(32.6)                          | 2.2(2.2)   | 3.5(3.5) |
| $\text{Re}_2(\text{CO})_7(\text{CNRbu}^t)_3$   | white  | 150-152 | 33.5(32.3)                          | 3.5(3.3)   | 5.2(5.1) |
| $\text{Re}_2(\text{CO})_7(\text{CNC}_6\text{H}_5)_3$                                     | yellow | 115-116 | 40.3(40.5)                          | 2.3(2.3)   | 4.6(4.6) |
| $\text{Re}_2(\text{CO})_7(\text{CNC}_6\text{H}_5)_2\text{C}_6\text{H}_5$ 3               | yellow | 44-46   | 36.4(37.5)                          | 3.7(3.7)   | 4.7(4.7) |
| $\text{Re}_2(\text{CO})_7(\text{CNC}_6\text{H}_{11})_3$                                  | yellow | 164-166 | 33.0(42.3)                          | 4.1(4.4)   | 2.8(3.1) |
| $\text{Re}_2(\text{CO})_7(\text{CNC}_6\text{H}_5)_2\text{Me}_2$ -(2,6) 3                 | yellow | 143-144 | 22.5(22.6)                          | 1.2(1.3)   | 5.9(6.0) |
| $\text{Re}_2(\text{CO})_7(\text{CNRMe})_3$   | yellow | 201-202 | 42.2(42.4)                          | 3.4(3.4)   | 5.3(5.3) |
| $\text{Re}_2(\text{CO})_6(\text{CNC}_6\text{H}_5)_3\text{Me}_2$ -(2,6) 4                 | yellow | 201-204 | 24.3(23.9)                          | 1.5(1.7)   | 7.8(8.0) |
| $\text{Re}_2(\text{CO})_6(\text{CNRMe})_4$   | yellow |         |                                     |            |          |

<sup>a</sup> Found, calculated in parentheses

TABLE II.5: Infra Red data of the complexes  $\text{Re}_2(\text{CO})_{10}\text{L}_n$  ( $\text{CNR}$ )<sub>n</sub> ( $n = 1-4$ )

| Complex   | $\nu(\text{CNC})(\text{cm}^{-1})^c$ | $\nu(\text{CO})(\text{cm}^{-1})^c$ |
|---|-------------------------------------|------------------------------------|
| $\text{Re}_2(\text{CO})_8(\text{CNBu}^t)_2^a$                   | 2173(m)                             | 2101(m)                            |
| $\text{Re}_2(\text{CO})_8(\text{CNCH}_2\text{C}_6\text{H}_5)^a$ | 2180(m)                             | 2100(m)                            |
| $\text{Re}_2(\text{CO})_8(\text{CNCH}_2\text{C}_6\text{H}_5)^b$ | 2180(m)                             | 2102(m)                            |
| $\text{Re}_2(\text{CO})_8(\text{CNCH}_2\text{C}_6\text{H}_5)^c$ | 2180(m)                             | 2090(m)                            |
| $\text{Re}_2(\text{CO})_8(\text{CNCH}_2\text{C}_6\text{H}_5)^d$ | 2180(m)                             | 2048(m)                            |
| $\text{Re}_2(\text{CO})_8(\text{CNMe})^a$                       | 2197(m)                             | 2105(m)                            |
| $\text{Re}_2(\text{CO})_8(\text{CNMe})^b$                       | 2197(m)                             | 2105(m)                            |
| $\text{Re}_2(\text{CO})_8(\text{CNMe})^c$                       | 2197(m)                             | 2076(w)                            |
| $\text{Re}_2(\text{CO})_8(\text{CNMe})^d$                       | 2197(m)                             | 2053(m)                            |
| $\text{Re}_2(\text{CO})_8(\text{CNBu}^t)_2$                     | 2154(m)                             | 2090(w)                            |
| $\text{Re}_2(\text{CO})_8(\text{CNCH}_2\text{C}_6\text{H}_5)^a$ | 2164(m)                             | 2066(w)                            |
| $\text{Re}_2(\text{CO})_8(\text{CNCH}_2\text{C}_6\text{H}_5)^b$ | 2164(m)                             | 2031(m)                            |
| $\text{Re}_2(\text{CO})_8(\text{CNCH}_2\text{C}_6\text{H}_5)^c$ | 2166(m)                             | 2028(s)                            |
| $\text{Re}_2(\text{CO})_8(\text{CNCH}_2\text{C}_6\text{H}_5)^d$ | 2166(m)                             | 2027(s)                            |
| $\text{Re}_2(\text{CO})_8(\text{CNCH}_2\text{C}_6\text{H}_5)^e$ | 2166(m)                             | 1984(vs)                           |
| $\text{Re}_2(\text{CO})_8(\text{CNMe})^a$                       | 2190(m)                             | 2055(m)                            |
| $\text{Re}_2(\text{CO})_8(\text{CNMe})^b$                       | 2190(m)                             | 2027(s)                            |
| $\text{Re}_2(\text{CO})_8(\text{CNMe})^c$                       | 2190(m)                             | 1980(vs)                           |
| $\text{Re}_2(\text{CO})_8(\text{CNMe})^d$                       | 2190(m)                             | 1947(sh)                           |
| $\text{Re}_2(\text{CO})_8(\text{CNMe})^e$                       | 2190(m)                             | 1922(m)                            |
| $\text{Re}_2(\text{CO})_7(\text{CNBu}^t)_2$                     | 2154(m)                             | 2072(w)                            |
| $\text{Re}_2(\text{CO})_7(\text{CNCH}_2\text{C}_6\text{H}_5)^a$ | 2154(m)                             | 2032(m)                            |
| $\text{Re}_2(\text{CO})_7(\text{CNCH}_2\text{C}_6\text{H}_5)^b$ | 2154(m)                             | 2030(s)                            |
| $\text{Re}_2(\text{CO})_7(\text{CNCH}_2\text{C}_6\text{H}_5)^c$ | 2154(m)                             | 1982(vs)                           |
| $\text{Re}_2(\text{CO})_7(\text{CNCH}_2\text{C}_6\text{H}_5)^d$ | 2154(m)                             | 1980(vs)                           |
| $\text{Re}_2(\text{CO})_7(\text{CNCH}_2\text{C}_6\text{H}_5)^e$ | 2154(m)                             | 1967(vs)                           |
| $\text{Re}_2(\text{CO})_7(\text{CNCH}_2\text{C}_6\text{H}_5)^f$ | 2156(m)                             | 2030(w)                            |
| $\text{Re}_2(\text{CO})_7(\text{CNCH}_2\text{C}_6\text{H}_5)^g$ | 2156(m)                             | 1987(vs)                           |
| $\text{Re}_2(\text{CO})_7(\text{CNCH}_2\text{C}_6\text{H}_5)^h$ | 2156(m)                             | 1963(vs)                           |
| $\text{Re}_2(\text{CO})_7(\text{CNCH}_2\text{C}_6\text{H}_5)^i$ | 2156(m)                             | 1962(vs)                           |
| $\text{Re}_2(\text{CO})_7(\text{CNCH}_2\text{C}_6\text{H}_5)^j$ | 2156(m)                             | 1960(vs)                           |
| $\text{Re}_2(\text{CO})_7(\text{CNMe})^a$                       | 2122(m)                             | 2032(m)                            |
| $\text{Re}_2(\text{CO})_7(\text{CNMe})^b$                       | 2122(m)                             | 1990(vs)                           |
| $\text{Re}_2(\text{CO})_7(\text{CNMe})^c$                       | 2122(m)                             | 1968(vs)                           |
| $\text{Re}_2(\text{CO})_7(\text{CNMe})^d$                       | 2180(m)                             | 2033(m)                            |
| $\text{Re}_2(\text{CO})_7(\text{CNMe})^e$                       | 2180(m)                             | 1990(vs)                           |
| $\text{Re}_2(\text{CO})_7(\text{CNMe})^f$                       | 2180(m)                             | 1968(vs)                           |
| $\text{Re}_2(\text{CO})_7(\text{CNMe})^g$                       | 2180(m)                             | 1929(sh)                           |
| $\text{Re}_2(\text{CO})_7(\text{CNMe})^h$                       | 2180(m)                             | 1929(sh)                           |
| $\text{Re}_2(\text{CO})_7(\text{CNMe})^i$                       | 2180(m)                             | 1919(sh)                           |
| $\text{Re}_2(\text{CO})_7(\text{CNMe})^j$                       | 2180(m)                             | 1896(m)                            |
| $\text{Re}_2(\text{CO})_6(\text{CNMe})_4$                       | 2168(m)                             | 2040(w)                            |
|   |                                     | 2032(sh)                           |
|   |                                     | 1980(vs)                           |
|   |                                     | 1959(vs)                           |
|   |                                     | 1919(sh)                           |
|   |                                     | 1896(m)                            |
|   |                                     | 1971(vs)                           |
|   |                                     | 1928(m)                            |
|   |                                     | 1890(m)                            |

a Recorded in hexane

b Recorded in chloroform

c sh = shoulder, w = weak, m = medium, s = strong, vs = very strong

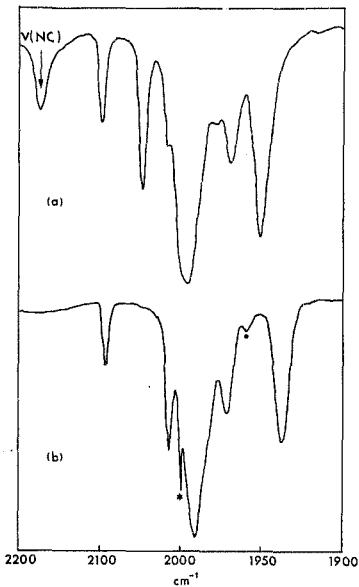


Figure 11.2: IR spectra (recorded in hexane, at X5 expansion) of  
(a)  $\text{eq-Re}_2(\text{CO})_9(\text{CNBu}^t)$ , and (b)  $\text{ax-Mn}_2(\text{CO})_9(\text{PMe}_2\text{Ph})$

- \* 'peak' due to monochromator change at  $2000\text{cm}^{-1}$
- weak band due to the presence of the  $^{13}\text{C}$ -isotope

$eq-M_2(CO)_9(L)$  complexes reported in the literature<sup>112</sup> have fewer  $\nu(CO)$  IR bands - usually 6, owing to band overlap. Axial complexes such as  $ax-Mn_2(CO)_9(PR_3)_2$ ,<sup>112-13</sup> do have 5  $\nu(CO)$  IR bands, but there is also a weak band due to the presence of the  $^{13}C$  isotope (e.g.  $ax-Mn_2(CO)_9(PhMe_2Ph)$ , IR(hexane),  $\nu(CO)$ : 2094(m), 2015(s), 1981(vs), 1971(ms), 1959(w) - ( $^{13}C$  peak), 1937(s)  $cm^{-1}$ ). Hence the two isomers may both have IR spectra with the same number (6) of  $\nu(CO)$  bands, the difference being in the relative intensities of the bands. The  $Re_2(CO)_9-(CNR)$  complexes are found to have one  $\nu(CN)$  and 6 or 7  $\nu(CO)$  bands, not inconsistent with an  $eq-Re_2(CO)_9(CNR)$  geometry. The complex  $Re_2(CO)_9(CNBut)$  has been shown by X-ray crystallography to have the  $ButNC$  ligand in the equatorial position (ch. XIV). Fig. 11.2 shows the IR spectra ( $\nu(CO)$  region) of (a)  $eq-Re_2(CO)_9(CNBut)$  and (b)  $ax-Mn_2(CO)_9(PMe_2Ph)$ <sup>112</sup> (substitution geometry established by X-ray crystallography<sup>114</sup>). The intensity patterns ( $\nu(CO)$  bands) are superficially similar ((a) m,m-s,sh,vs,m-s,s; (b) m,s,vs,m-s,w,s). However, with the knowledge of which pattern corresponds to which structure, these two spectra, backed up as they are by X-ray crystal structures, could be used as reference spectra for the assignment of substitution geometry for  $M_2(CO)_9(L)$  complexes.

For di-substituted  $M_2(CO)_8(L)_2$  complexes, there are three possible geometry-types, viz. diax, ax,eq and dieq. Diaxial is ruled out for  $Re_2(CO)_8(CNR)_2$  derivatives, because for this geometry (point group  $D_{4d}$ ) 2  $\nu(CO)$  IR bands are predicted, as is indeed observed for  $diax-Mn_2(CO)_8(PR_3)_2$  complexes.<sup>115</sup> The  $Re_2(CO)_8(CNR)_2$  complexes have complex IR spectra with 4 or 5  $\nu(CO)$  bands. For ax,eq, and for dieq geometry, the two ligands may be on the same ( $(CO)_3M-M(CO)_3-(L)_2$ ) or different ( $(L)(CO)_4Re-Re(CO)_4(L)$ ) metal atoms. However, 8  $\nu(CO)$  IR bands are expected for all four cases (assuming staggered conformations). Fewer bands (usually 6) are generally exhibited by  $ax,eq-M_2(CO)_8(L)_2$  complexes,<sup>112</sup> owing to band overlap. It is thus impossible to determine the substitution geometry from the IR spectrum, without a prior knowledge of the intensity patterns characteristic of

all the possible isomers. Further, the possibility of the product being a mixture of different geometric isomers (vide infra) cannot be excluded on the basis of IR data alone, although  $^1\text{H}$  NMR is useful in this regard (see section 11.4.2).

X-ray crystallographic studies (ch. XIV) have shown the substitution of both  $\text{Re}_2(\text{CO})_8(\text{CNC}_6\text{H}_4\text{Me}_2-2,6)_2$  and  $\text{Mn}_2(\text{CO})_8(\text{CNBu}^t)_2$  to be diequatorial. However, in the former complex, the two isonitrile ligands are on different rhenium atoms, i.e. 1,2-cis-dieq-Re<sub>2</sub>(CO)<sub>8</sub>(CNC<sub>6</sub>H<sub>4</sub>Me<sub>2</sub>-2,6)<sub>2</sub> [FTIR(hexane),  $\nu(\text{NC})$ : 2150(m), 2122(sh);  $\nu(\text{CO})$ : 2053(m), 2028(s), 1985(vs), 1952(m), 1943(s)  $\text{cm}^{-1}$ ], while the latter complex has both isonitrile ligands on the same manganese atom, i.e. 1,1-cis-dieq-Mn<sub>2</sub>(CO)<sub>8</sub>(CNBu<sup>t</sup>)<sub>2</sub> [FTIR(hexane),  $\nu(\text{NC})$ : 2174(w), 2154(w);  $\nu(\text{CO})$ : 2055(m), 1999(vs), 1972(vs), 1963(w), 1952(m), 1935(m)  $\text{cm}^{-1}$ ]. The 1,2-dieq-Mn<sub>2</sub>(CO)<sub>8</sub>(CNBu<sup>t</sup>)<sub>2</sub> isomer is however also known [FTIR(hexane),  $\nu(\text{NC})$ : 2144(w);  $\nu(\text{CO})$ : 2049(w), 2006(s), 1977(vs), 1943(sh), 1939(w)  $\text{cm}^{-1}$ ];<sup>222</sup> (see section 11.4.2.) and 1,1-cis-dieq-Re<sub>2</sub>(CO)<sub>8</sub>(CNBu<sup>t</sup>)<sub>2</sub> has been prepared indirectly [FTIR(hexane),  $\nu(\text{NC})$ : 2183(m), 2157(w);  $\nu(\text{CO})$ : 2065(m), 2032(s), 1987(vs), 1952(m), 1935(s)  $\text{cm}^{-1}$ ].<sup>223</sup>

It is interesting to note that the IR spectrum of a polycrystalline sample of  $\text{Mn}_2(\text{CO})_8(\text{CNBu}^t)_2$  [IR(hexane),  $\nu(\text{NC})$ : 2172(w), 2152(m);  $\nu(\text{CO})$ : 2057(m), 1996(m), 1976(vs), 1949(w), 1936(m)  $\text{cm}^{-1}$ ];<sup>222</sup> is clearly a superposition of the above two spectrum types, indicative of the presence of both isomers, viz. 1,2-dieq-Mn<sub>2</sub>(CO)<sub>8</sub>(CNBu<sup>t</sup>)<sub>2</sub> and 1,1-cis-dieq-Mn<sub>2</sub>(CO)<sub>8</sub>(CNBu<sup>t</sup>)<sub>2</sub>, the former predominating. The other  $\text{Mn}_2(\text{CO})_8(\text{CNR})_2$  complexes reported have similar spectra.<sup>224</sup> The  $^1\text{H}$  NMR spectra of these  $\text{Mn}_2(\text{CO})_8(\text{CNR})_2$  complexes also provide evidence for the presence of two isomers, in contrast to the  $\text{Re}_2(\text{CO})_8(\text{CNR})_2$  complexes (see section 11.4.2).

The FTIR spectra (hexane) of single-crystal samples of 1,2-dieq-Re<sub>2</sub>(CO)<sub>8</sub>(CNC<sub>6</sub>H<sub>4</sub>Me<sub>2</sub>-2,6)<sub>2</sub> and 1,1-cis-dieq-Mn<sub>2</sub>(CO)<sub>8</sub>(CNBu<sup>t</sup>)<sub>2</sub> are shown ( $\nu(\text{CO})$  region) in Fig. 11.3(a) and (b) respectively. In both cases there are 6  $\nu(\text{CO})$  bands, but the relative intensities of the bands differ significantly. Hence IR spectra could be used to assign the substitution

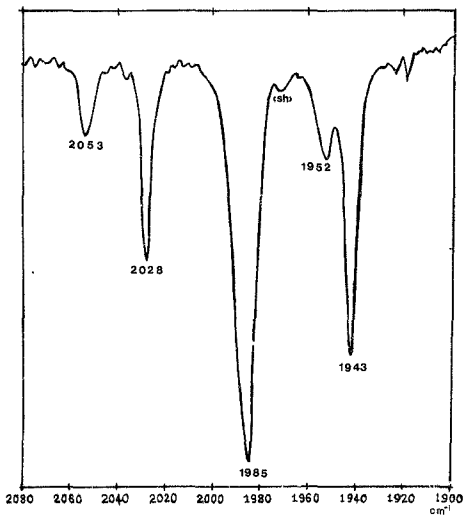


Figure 11.3(a): FTIR spectrum of  $1,2\text{-dieq-Re}_2(\text{CO})_8(\text{CNC}_6\text{H}_3\text{Me}_2\text{-}2,6)_2$   
(recorded in hexane)

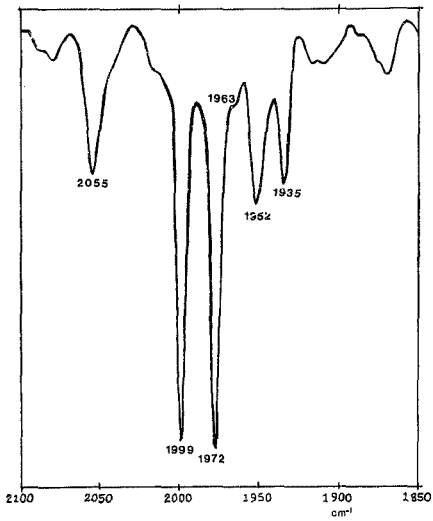


Figure 11.3(b): FTIR spectrum of  $1,1\text{-cis-dieq-Mn}_2(\text{CO})_8(\text{CNEu}^v)_2$   
(recorded in hexane)



geometry of such complexes. (This aspect of establishing a correlation between IR spectral data and substitution geometry for  $M_2(CO)_8(L)_2$  complexes will be further elaborated in ch. XV). All the  $Re_2(CO)_8(CNR)_2$  complexes prepared have IR spectra similar to that of 1,2-dieq- $Re_2(CO)_8(CNC_6H_3Me_2-2,6)_2$ . The  $Re_2(CO)_8(CNR)_2$  complexes all have one  $\nu(NC)$  IR band, with the exception of  $Re_2(CO)_8(CNC_6H_3Me_2-2,6)_2$ , which has two. As expected, the *trans*-isonitrile derivative,  $Re_2(CO)_8(CNBU^t)(CNC_6H_3Me_2-2,6)$ , has two  $\nu(NC)$  absorptions.

For  $M_2(CO)_7(CNR)_3$  complexes, 7  $\nu(CO)$  IR bands are predicted for the most likely geometries with all three RNC ligands equatorially substituted (axial substitution is electronically disfavoured,<sup>13</sup> and no *ax*- $M_2(CO)_{10-n}(CNR)_n$  ( $n = 1, 2$ ) isomers are known). The  $Re_2(CO)_7(CNR)_3$  complexes have 4 to 6  $\nu(CO)$ , and 1 or 2  $\nu(NC)$  bands in their IR spectra. The structure of  $Re_2(CO)_7(CNMe)_3$  has been determined by X-ray crystallography (ch. XIV), and was found to be a 1-eq,1,2-cis-dieq-isomer. Different conformations are possible in solution, but probably not isolable. The conformation observed in the crystal could be largely determined by crystal packing forces (see ch. XIV).

The IR spectrum of an all-equatorially substituted  $M_2(CO)_6(CNR)_4$  compound is expected to have 6  $\nu(CO)$  bands for both the staggered and eclipsed forms. The  $Re_2(CO)_6(CNR)_4$  ( $R = C_6H_3Me_2-2,6$ ; Me) complexes have 3 or 4  $\nu(CO)$  bands, and 1 ( $R = Me$ ) or 2 ( $R = C_6H_3Me_2-2,6$ )  $\nu(NC)$  bands. The complex  $Re_2(CO)_6(CNC_6H_3Me_2-2,6)_4$  has been shown crystallographically (ch. XIV) to have a staggered geometry, with two isonitrile ligands occupying *cis*-equatorial positions on each rhenium atom. [FTIR (benzene),  $\nu(NC)$ : 2109(m), 2089(m);  $\nu(CO)$ : 1978(vs), 1942(m), 1929(w), 1899(m)  $cm^{-1}$ ]. The analogous  $Mn_2(CO)_6(CNC_6H_3Me_2-2,6)_4$ , however, has 1  $\nu(NC)$  and 6  $\nu(CO)$  bands.<sup>12c</sup>

From the above discussion it is apparent that the number of  $\nu(CO)$  bands observed in an IR spectrum of a metal carbonyl complex of the type  $M_2(CO)_{10-n}(L)_n$  ( $n = 1-4$ ) is often less than the number predicted by the application of Group Theory,

due to possible band overlap. Further, Group Theory often predicts the same number of bands for alternate geometries. Hence IR data alone is not sufficient for an unambiguous assignment of substitution geometry. However, used in conjunction with X-ray crystallography for selected complexes, it is possible to establish a correlation between IR spectral data (intensity patterns) and substitution geometry, as was illustrated in the case of the two possible isomers of  $\text{dieq-M}_2(\text{CO})_8(\text{CNR})_2$  ( $M = \text{Re, Mn}$ ). This correlation is extended to other isomers of  $\text{M}_2(\text{CO})_8(\text{L})_2$  in ch. XV. (Section 15B).

#### 11.4.2 Proton Nuclear Magnetic Resonance Spectroscopy

The  $^1\text{H}$  NMR spectra of the  $\text{Re}_2(\text{CO})_{10-n}(\text{CNR})_n$  ( $n = 1-4$ ) complexes are given in Table 11.6. The monosubstituted  $\text{Re}_2(\text{CO})_9(\text{CNR})$ , disubstituted  $\text{Re}_2(\text{CO})_8(\text{CNR})_2$  (with the exception of  $R = \text{Me}$ , *vide infra*) and tetra-substituted  $\text{Re}_2(\text{CO})_6(\text{CNR})_4$  complexes give the expected  $^1\text{H}$  NMR spectra (single  $\delta(\text{CH}_x)$  ( $x = 2,3$ ) resonances). The simple spectrum observed for  $\text{Re}_2(\text{CO})_6(\text{CNC}_6\text{H}_3\text{Me}_2-2,4)_4$  is in contrast to the complex spectrum reported for the analogous  $\text{Mn}_2(\text{CO})_6(\text{CNC}_6\text{H}_3\text{Me}_2-2,6)_4$ .<sup>220</sup> The signal for the  $\text{CH}_2$  or  $\text{CH}_3$  protons of the trisubstituted  $\text{Re}_2(\text{CO})_7(\text{CNR})_3$  complexes consists of two resonances in a 1:2 ratio. This was also observed for the  $\text{Mn}_2(\text{CO})_7(\text{CNR})_3$  complexes.<sup>221</sup> The three isocyanides are expected to arrange themselves in equatorial positions around the dimer in a 2:1 ratio, as indicated in Fig. 11.5. Such a structure (C) is found in the solid state for  $\text{Re}_2(\text{CO})_7(\text{CNCMe})_3$  (ch. XIV).

The  $^1\text{H}$  NMR spectra for the  $\text{Re}_2(\text{CO})_{10-n}(\text{CNR})_n$  ( $n = 1-4$ ) complexes show a trend of the  $\text{CH}_x$  ( $x = 2,3$ ) resonance to lower field with increasing  $\nu$  (Fig. 11.4). The trend to lower field is expected (consequence of increased electron lensity on the metal<sup>192b</sup>), but the remarkable feature is the linear shift with similar slopes for all the isocyanides studied. This provides strong evidence for the dimer being treated as a single unit and not as two poorly interacting halves.

An interesting observation in the case of  $\text{Re}_2(\text{CO})_{10-n}$ -

$(\text{CNCH}_2\text{C}_6\text{H}_5)_n$  ( $n = 1-3$ ) is that the  $\text{C}_6\text{H}_5$ -signal, which is a complex multiplet for mono- and di-substituted derivatives, becomes a sharp singlet for  $\text{Re}_2(\text{CO})_7(\text{CNCH}_2\text{C}_6\text{H}_5)_3$ . For the  $\text{Re}_2(\text{CO})_{10-n}(\text{CNC}_6\text{H}_3\text{Me}_2-2,6)_n$  ( $n = 1-4$ ) derivatives, there are only two  $\text{C}_6\text{H}_3$ -resonances when  $n = 4$ , as opposed to the three for  $n = 1, 2, 3$ .

In the case of the disubstituted derivatives,  $\text{Re}_2(\text{CO})_8(\text{CNR})_2$ , the  $^1\text{H}$  NMR spectra are as expected for  $\text{R} = \text{Bu}^t, \text{C}_6\text{H}_5\text{CH}_2, \text{C}_6\text{H}_{11}, 2,6\text{-Me}_2\text{C}_6\text{H}_3$  (i.e. a single resonance for  $\text{CH}_x$  ( $x = 2, 3$ ), but for  $\text{R} = \text{Me}$ , the  $\text{CH}_3$ -group has two resonances in a ca. 1:5 ratio. This phenomenon is observed for the  $\text{CH}_2$  or  $\text{CH}_3$  protons of all the related  $\text{Mn}_2(\text{CO})_8(\text{CNR})_2$  ( $\text{R} = \text{Bu}^t, \text{C}_6\text{H}_5\text{CH}_2, \text{C}_6\text{H}_{11}, 2,6\text{-Me}_2\text{C}_6\text{H}_3$  and Me) complexes.<sup>228</sup> This suggests that two isomers are present in solution. For  $\text{Mn}_2(\text{CO})_8(\text{CNBu}^t)_2$ , these isomers have been shown to be 1,1-cis-dieq- $\text{Mn}_2(\text{CO})_8(\text{CNBu}^t)$  (Fig. 11.6(A)) and 1,2-dieq- $\text{Mn}_2(\text{CO})_8(\text{CNBu}^t)_2$  (Fig. 11.6(B)), with the latter predominating (see section 11.5.2). There also appear to be two isomers in solution for the mixed isonitrile derivative,  $\text{Re}_2(\text{CO})_8(\text{CNBu}^t)(\text{CNC}_6\text{H}_3\text{Me}_2-2,6)$ .

#### 11.4.3 Raman Spectroscopy<sup>228</sup>

Raman studies were undertaken<sup>228</sup> on the  $\text{Re}_2(\text{CO})_{10-n}(\text{CNR})_n$  ( $n = 1-3, \text{R} = \text{Bu}^t, \text{C}_6\text{H}_5\text{CH}_2; n = 1-4, \text{R} = 2,6\text{-Me}_2\text{C}_6\text{H}_3, \text{Me}$ ) complexes. For  $\text{Re}_2(\text{CO})_{10-n}(\text{CNR})_n$ , as the value of  $n$  increases, the peak frequencies in the CO-stretching region decrease regularly, while the peak frequencies in the M-C-O bending region increase. However, this usual behaviour of the CO-stretching and M-C-O bending modes is not followed by that of the main peak at ca.  $120 \text{ cm}^{-1}$ , assigned to the C-Re-C bending mode. As a function of  $n$ , this peak frequency increases ( $n = 0-2$ ), reaches a maximum at  $n = 2$ , then decreases ( $n = 3, 4; \text{R} = \text{Bu}^t, \text{C}_6\text{H}_5\text{CH}_2, 2,6\text{-Me}_2\text{C}_6\text{H}_3$ ). This effect can be explained by a decrement of the force constant of the Re-C bond, then by an increment of the force constant, due to the increasing steric hindrance effect induced by multiple substitution of bulky isonitrile groups [e.g. "fan-shaped" angles<sup>229</sup> (widthness, thickness) for

TABLE 11.6:  $^1\text{H}$  NMR data of the complexes  $\text{Re}_2(\text{CO})_{10-n}(\text{CNR})_n$   
( $n = 1-4$ )

| R  | n | $\delta/\text{ppm}^{\text{a}}$                    |                               |   |
|--|---|---|-------------------------------|---|
|  |   | $\text{C}_6\text{H}_n$                            | $\text{CH}_3$                 | or $\text{CH}_2$  |
| Bu <sup>t</sup>  | 1 | -   | 0.75                          |   |
|  | 2 | -   | 0.87                          |   |
|  | 3 |   | 1.02, 0.98 <sup>b</sup>       |   |
| $\text{C}_6\text{H}_5\text{CH}_2$  | 1 | 6.74-6.99 <sup>c</sup>                            |                               | 3.77  |
|  | 2 | 6.82-7.00 <sup>c</sup>                            |                               | 3.87  |
|  | 3 | 6.95  |                               | 4.05, 4.00 <sup>b</sup>   |
| $\text{C}_6\text{H}_{11}$  | 1 | 1.26-1.05 <sup>c</sup> , 0.97-0.82 <sup>c</sup>   | -                             |   |
|  | 2 | 1.26, 1.09 <sup>c</sup> , 0.90, 0.85 <sup>c</sup> | -                             |   |
|  | 3 | 1.40 <sup>c</sup> , 0.93, 0.89 <sup>c</sup>       | -                             |   |
| 2,6-Me <sub>2</sub> C <sub>6</sub> H <sub>3</sub>  | 1 | 6.69, 6.63, 6.58                                  | 2.00                          |   |
|  | 2 | 6.68, 6.63, 6.58                                  | 2.10                          |   |
|  | 3 | 6.67, 6.64, 6.59                                  | 2.23, 2.18 <sup>b</sup>       |   |
|  | 4 | 6.64, 6.60  | 2.34                          |   |
| Me   | 1 | -   | 1.94                          |   |
|  | 2 | -   | 2.16, 2.10 <sup>d</sup>       |   |
|  | 3 | -   | 2.31, 2.25 <sup>b</sup>       |   |
|  | 4 | -   | 2.45                          |   |
| $\text{Re}_2(\text{CO})_8(\text{CNBu}^{\text{t}})-$<br>( $\text{CNC}_6\text{H}_3\text{Me}_2-2,6$ ) |   | 6.69, 6.64, 6.60 <sup>c</sup>                     | 0.86; 2.14, 2.10 <sup>d</sup> | (Bu <sup>t</sup> )(C <sub>6</sub> H <sub>3</sub> -<br>Me <sub>2</sub> -2,6) |

<sup>a</sup> Recorded in  $\text{C}_6\text{D}_6$ , relative to TMS

<sup>b</sup> Ratio 1:2

<sup>c</sup> Multiplet

<sup>d</sup> Ratio 1:5

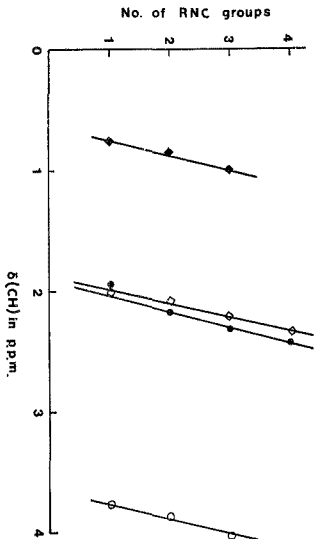
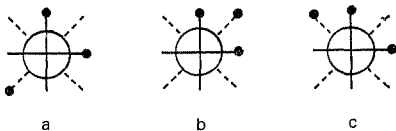
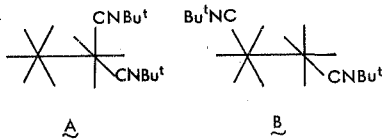


Figure 11.4: plot of  $\delta(\text{CH})$  ( $x = 2, 3$ ) vs  $n(\text{RNC})$  for the  $\text{Re}_2(\text{CO})_{10-n}$  (CNR) $_n$  ( $n = 1-4$ ) complexes  
 ( $\blacklozenge = \text{Bu}^t\text{NC}$ ,  $\blacklozenge = 2,6\text{-Me}_2\text{C}_6\text{H}_3\text{NC}$ ,  $\bullet = \text{MeNC}$  and  $\circ = \text{C}_6\text{H}_5\text{CH}_2\text{NC}$ )



**Figure 11.5:** Newman projection of possible cis-equatorial conformational isomers of  $M_2(CO)_7(CNR)_3$  ( $M = Re, Mn$ ), as viewed down the M-M bond ( $\bullet = RNC$ )



**Figure 11.6:** Isomers of  $Mn_2(CO)_8(CNBu^t)_2$   
 (A) 1,1-cis-dieq, and (B) 1,2-dieq

Bu<sup>t</sup>NC and 2,6-Me<sub>2</sub>-C<sub>6</sub>H<sub>3</sub> respectively: 70°, 68°; 106°, 53°] and the capacity of the isocyanitriles to bend.

In the UV spectra<sup>224</sup> of the Re<sub>2</sub>(CO)<sub>10-n</sub>(CNR)<sub>n</sub> complexes, the  $\sigma \rightarrow \sigma^*$  band of the Re-Re bond undergoes a red shift as a function of increasing n, indicative of an increase in electron density on the metal atoms, a result of replacing CO ligands with the poorer  $\pi$ -acceptor RNC ligands.<sup>21</sup> However, the intensity of this band remains relatively constant, indicating that increasing degree of isocyanitrile substitution does not cause any significant deformations of the complex in solution. This has been supported by X-ray data (see ch.XIV).

#### 11.4.4 Mass Spectroscopy

##### (a) Mass spectrum of Re<sub>2</sub>(CO)<sub>9</sub>(CNBu<sup>t</sup>)

The mass spectral data for Re<sub>2</sub>(CO)<sub>9</sub>(CNBu<sup>t</sup>) is given in Table 11.7. Since there are two naturally occurring isotopes of rhenium, <sup>185</sup>Re and <sup>187</sup>Re, with natural abundances of 37.5% and 62.5% respectively, for monomeric fragments, two peaks occur in the mass spectrum, with the ratio ca. 1:1.67, corresponding to the two isotopes. For dimeric fragments, three peaks occur, corresponding to the possible isotope combinations (<sup>185</sup>Re)<sub>2</sub>, (<sup>185</sup>Re <sup>187</sup>Re), (<sup>187</sup>Re)<sub>2</sub>, in the ratio ca. 1:3.36: 2.79. Where peak overlap occurs for two different fragments, the ideal isotope ratio will be disturbed.

Figs. 11.7(a) and 11.7(b) respectively show the dimeric (where Re<sub>2</sub> unit remains intact) and monomeric (Re fragment) fragmentation paths for Re<sub>2</sub>(CO)<sub>9</sub>(CNBu<sup>t</sup>). Obviously cross-over from the dimeric to the monomeric paths is possible at any stage. The fragmentation pattern is as expected. (Note that the Bu<sup>t</sup> group is lost before the CN fragment, which is the last to be lost. This behaviour is typical for the CNBu<sup>t</sup> ligand, and reflects the stability of the Me<sub>3</sub>C<sup>+</sup> ion.<sup>27</sup>) No one path appears to predominate. It is not possible to deduce from the MS data whether the Bu<sup>t</sup>NC substitution is axial or equatorial.

TABLE 11.7: Mass spectral data for  $\text{Re}_2(\text{CO})_9(\text{CNBu}^t)$

| $m/z$ <sup>a,b</sup> | Relative intensities(%) | Fragment                                    |
|----------------------|-------------------------|---|
| 165,187              | 1, 2                    | $\text{Re}^+$                               |
| 211, 213             | <1, 1                   | $\text{Re}(\text{CN})^+$                    |
| 212, 214             | <1, <1                  | $\text{Re}(\text{CNH})^+$                   |
| 213, 215             | 1, <1                   | $\text{Re}(\text{CO})^+$                    |
| 241, 243             | 1, <1                   | $\text{Re}(\text{CO})_2^+$                  |
| 268, 270             | 1, 2                    | $\text{Re}(\text{CNBu}^t)^+$                |
| 269, 271             | 2, 3                    | $\text{Re}(\text{CO})_3^+$                  |
| 296, 298             | 8, 13                   | $\text{Re}(\text{CO})(\text{CNBu}^t)^+$     |
| 297, 299             | <1, 3                   | $\text{Re}(\text{CO})_4^+$                  |
| 324, 326             | 61, 100                 | $\text{Re}(\text{CO})_2(\text{CNBu}^t)^+$   |
| 325, 327             | 4, 6                    | $\text{Re}(\text{CO})_5^+$                  |
| 352, 354             | 2, 4                    | $\text{Re}(\text{CO})_3(\text{CNBu}^t)^+$   |
| 370, 372, 374        | 4, 13, 11               | $\text{Re}_2^+$                             |
| 380, 382             | 11, 18                  | $\text{Re}(\text{CO})_4(\text{CNBu}^t)^+$   |
| 396, 398, 400        | 10, 29, 25              | $\text{Re}_2(\text{CN})^+$                  |
| 397, 399, 401        | 5, 16, 12               | $\text{Re}_2(\text{CNH})^+$                 |
| 398, 400, 402        | 29, 25, 2               | $\text{Re}_2(\text{CO})^+$                  |
| 426, 428, 430        | 8, 20, 16               | $\text{Re}_2(\text{CO})_2^+$                |
| 453, 455, 457        | 18, 21, 16              | $\text{Re}_2(\text{CNBu}^t)^+$              |
| 454, 456, 458        | 8, 23, 20               | $\text{Re}_2(\text{CO})_3^+$                |
| 481, 483, 485        | 3, 13, 11               | $\text{Re}_2(\text{CO})(\text{CNBu}^t)^+$   |
| 482, 484, 486        | 11, 29, 23              | $\text{Re}_2(\text{CO})_4^+$                |
| 509, 511, 513        | 5, 16, 15               | $\text{Re}_2(\text{CO})_2(\text{CNBu}^t)^+$ |
| 510, 512, 514        | 13, 36, 11              | $\text{Re}_2(\text{CO})_5^+$                |
| 537, 539, 541        | 3, 15, 15               | $\text{Re}_2(\text{CO})_3(\text{CNBu}^t)^+$ |
| 538, 540, 542        | 13, 34, 11              | $\text{Re}_2(\text{CO})_6^+$                |
| 565, 567, 569        | 3, 13, 13               | $\text{Re}_2(\text{CO})_4(\text{CNBu}^t)^+$ |
| 566, 568, 570        | 16, 47, 41              | $\text{Re}_2(\text{CO})_7^+$                |
| 593, 595, 597        | 28, 84, 70              | $\text{Re}_2(\text{CO})_5(\text{CNBu}^t)^+$ |
| 594, 596, 598        | 11, 17, 8               | $\text{Re}_2(\text{CO})_8^+$                |
| 621, 623, 625        | 3, 8, 6                 | $\text{Re}_3(\text{CO})_6(\text{CNBu}^t)^+$ |



TABLE 11.7: Mass spectral data for  $\text{Re}_2(\text{CO})_9(\text{CNBu}^t)$  (Contd)

| <u>m/z</u>  | <u>Relative intensities(%)</u> | <u>Fragment</u>                             |
|-------------|--------------------------------|---|
| 622,624,626 | 2, 3, 1                        | $\text{Re}_2(\text{CO})_9^+$                |
| 649,651,653 | 2, 6, 4                        | $\text{Re}_2(\text{CO})_7(\text{CNBu}^t)^+$ |
| 677,679,681 | 1, 2, 2                        | $\text{Re}_2(\text{CO})_8(\text{CNBu}^t)^+$ |
| 705,707,709 | 11, 36, 31                     | $\text{Re}_2(\text{CO})_9(\text{CNBu}^t)^+$ |

<sup>a</sup> Fragments with m/z <185 are not reported.

<sup>b</sup> For monomeric fragments,  $^{185}\text{Re}$ ,  $^{187}\text{Re}$ , and for dimeric fragments  $(^{185}\text{Re})_2$ ,  $(^{185}\text{Re} \ ^{187}\text{Re})$ ,  $(^{187}\text{Re})_2$

FIGURE 11.7(a): Dimeric fragmentation pattern for  $\text{Re}_2(\text{CO})_9(\text{CNBu}^t)$

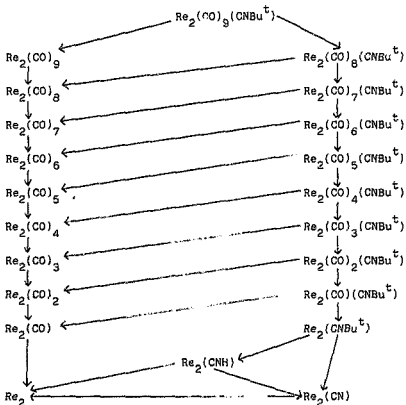
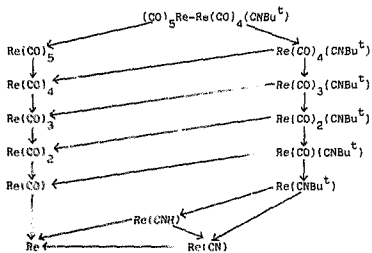


FIGURE 11.7(b): Monomeric fragmentation pattern for  $\text{Re}_2(\text{CO})_9(\text{CNBu}^t)$



(b) Mass spectrum of  $Mn_2(CO)_8(CNBu^t)_2$

Mass spectra were recorded of (I) a polycrystalline sample of  $Mn_2(CO)_8(CNBu^t)_2$ , containing both isomers,  $[Mn(CO)_4(CNBu^t)]_2$  and  $(CO)_5Mn-Mn(CO)_3(CNBu^t)_2$  (see section 11.4.2.), and of (II) single crystals of one isomer,  $(CO)_5Mn-Mn(CO)_3(CNBu^t)_2$ , used in the X-ray diffraction study (Ch. XIV). The mass spectral data for (I) and (II) are given in Table 1.8.

The possible fragmentation paths for  $Mn_2(CO)_8(CNBu^t)_2$  are shown in Fig. 11.8(a) (dimeric fragmentation path, i.e.  $Mn_2$  unit remains intact), and Fig. 11.8(b) (monomeric fragmentation path, i.e. Mn fragment), together with the metastable peaks. The possible cross-overs between the dimeric and monomeric fragmentation paths (eg.  $Mn_2(CNBu^t)$  ( $193$ )  $m/z = 99$ ,  $Mn(CNBu^t)$  ( $138$ )) have not been shown. In the case of (II), the monomeric path commencing with the half-dimer fragment  $Mn(CO)_4(CNBu^t)$  ( $m/z = 250$ ) would be expected to be absent.

Examination of Table 11.8 reveals that the most dramatic relative intensity changes in going from spectrum (I) to spectrum (II) occur for  $m/z = 250$  (I): 76%, cf. (II): 3%) and  $m/z = 305$  (I): 25%, cf. (II): 100%). The diminution of the  $m/z = 250$  peak for (II) is as expected, indicating the absence of the  $Mn(CO)_4(CNBu^t)^+$  fragment. This peak still occurs due to the  $Mn_2(CO)_5^+$  fragment. The effect is less pronounced for peaks lower down in the direct fragmentation path (e.g.  $m/z = 194$ ), because these fragments may be reached by cross-over from other monomeric and dimeric paths, and peak overlap of monomeric and dimeric fragments frequently occurs for this system. The enhancement of the  $m/z = 305$  peak for (II) is also expected, since this peak represents the  $Mn(CO)_3(CNBu^t)_2$  fragment, the precursor in the only monomeric fragmentation route now available.

The mass spectra data further bear out the conclusion from the IR and  $^1H$  NMR spectra (*vide supra*), in conjunction with the X-ray diffraction study (ch. XIV) on the nature of the isonitrila substitution in the two isomers of

TABLE 11.8: Mass spectral data for  $Mn_2(CO)_8(CNBU)_2$

| $m/z$ | Relative intensity(%)      |                                    | Fragment(s)                            |
|-------|----------------------------|------------------------------------|--|
|       | (I) $Mn_2(CO)_8(CNBU)_2^b$ | (II) $(CO)_2Mn-Mn(CO)_3(CNBU)_2^c$ |  |
| 55    | 100                        | 25                                 | $Mn^+$                                 |
| 57    | 31                         | 54                                 | $Bu^+$                                 |
| 81    | 10                         | 43                                 | $Mn(CN)^+$                             |
| 82    | 95                         | 42                                 | $Mn(CNH)^+$                            |
| 83    | 10                         | 22                                 | $M(CO)^+; CNBU^+$                      |
| 110   | 37                         | 6                                  | $Mn_2^+$                               |
| 111   | 8                          | 6                                  | $Mn(CO)_2^+$                           |
| 136   | 33                         | 32                                 | $Mn_2(CN)^+$                           |
| 137   | 20                         | 9                                  | $Mn_2(CO)^+$                           |
| 138   | 100                        | 67                                 | $Mn_2(CO)^+; Mn(CNBU)^+$               |
| 139   | 6                          | 6                                  | $Mn(CO)_3^+$                           |
| 166   | 36                         | 32                                 | $Mn_2(CO)_2^+; Mn(CO)(CNBU)^+$         |
| 167   | 3                          | 7                                  | $Mn(CO)_4^+$                           |
| 193   | 54                         | 3                                  | $Mn_2(CNBU)^+$                         |
| 194   | 49                         | 13                                 | $Mn_2(CO)_3^+; Mn(CO)_2(CNBU)^+$       |
| 195   | 4                          | 1                                  | $Mn(CO)_5^+$                           |
| 221   | 34                         | 96                                 | $Mn_2(CO)(CNBU)^+; Mn(CNBU)^+$         |
| 222   | 10                         | 13                                 | $Mn_2(CO)_4^+; Mn(CO)_3(CNBU)^+$       |
| 249   | 55                         | 20                                 | $Mn_2(CO)_2(CNBU)^+; Mn(CO)_2(CNBU)^+$ |
| 250   | 76                         | 3                                  | $Mn_2(CO)_5^+; Mn(CO)_4(CNBU)^+^d$     |

1  
175  
1

TABLE 11.8: Mass spectral data for Mn<sub>2</sub>(CO)<sub>8</sub>(CNBu<sup>t</sup>)<sub>2</sub> (Contd.)

| m/z | Relative Intensity(%)  |  | Fragments   |
|-----|--|--|---|
|     | (I) Mn <sub>2</sub> (CO) <sub>8</sub> (CNBu <sup>t</sup> ) <sub>2</sub> <sup>b</sup> | (II) (CO) <sub>5</sub> Mn-Mn(CO) <sub>3</sub> (CNBu <sup>t</sup> ) <sub>2</sub> <sup>c</sup> |   |
| 276 | 1  | 7  | Mn <sub>2</sub> (CNBu <sup>t</sup> ) <sub>2</sub> <sup>+</sup>  |
| 277 | 76   | 16   | Mn <sub>2</sub> (CO) <sub>3</sub> (CNBu <sup>t</sup> ) <sup>+</sup> ; Mn(CO) <sub>2</sub> (CNBu <sup>t</sup> ) <sub>2</sub> <sup>+</sup>              |
| 278 | 1  | 1  | Mn <sub>2</sub> (CO) <sub>6</sub> <sup>+</sup>  |
| 304 | 1  | 12   | Mn <sub>2</sub> (CO) <sub>4</sub> (CNBu <sup>t</sup> ) <sub>2</sub> <sup>+</sup>  |
| 305 | 25   | 100  | Mn <sub>2</sub> (CO) <sub>4</sub> (CNBu <sup>t</sup> ) <sub>2</sub> <sup>+</sup> ; Mn(CO) <sub>3</sub> (CNBu <sup>t</sup> ) <sub>2</sub> <sup>+</sup> |
| 306 | 6  | 13   | Mn <sub>2</sub> (CO) <sub>7</sub> <sup>+</sup>  |
| 332 | <1   | 35   | Mn <sub>2</sub> (CO) <sub>2</sub> (CNBu <sup>t</sup> ) <sub>2</sub> <sup>+</sup>  |
| 333 | 4  | 24   | Mn <sub>2</sub> (CO) <sub>5</sub> (CNBu <sup>t</sup> ) <sub>2</sub> <sup>+</sup>  |
| 334 | <1   | 2  | Mn <sub>2</sub> (CO) <sub>8</sub> <sup>+</sup>  |
| 360 | <1   | 13   | Mn <sub>2</sub> (CO) <sub>3</sub> (CNBu <sup>t</sup> ) <sub>2</sub> <sup>+</sup>  |
| 361 | <1   | 3  | Mn <sub>2</sub> (CO) <sub>6</sub> (CNBu <sup>t</sup> ) <sub>2</sub> <sup>+</sup>  |
| 388 | <1   | 7  | Mn <sub>2</sub> (CO) <sub>4</sub> (CNBu <sup>t</sup> ) <sub>2</sub> <sup>+</sup>  |
| 389 | <1   | 6  | Mn <sub>2</sub> (CO) <sub>7</sub> (CNBu <sup>t</sup> ) <sub>2</sub> <sup>+</sup>  |
| 416 | <1   | <1   | Mn <sub>2</sub> (CO) <sub>5</sub> (CNBu <sup>t</sup> ) <sub>2</sub> <sup>+</sup>  |
| 417 | <1   | <1   | Mn <sub>2</sub> (CO) <sub>8</sub> (CNBu <sup>t</sup> ) <sub>2</sub> <sup>+</sup>  |
| 444 | 18   | <1   | Mn <sub>2</sub> (CO) <sub>6</sub> (CNBu <sup>t</sup> ) <sub>2</sub> <sup>+</sup>  |
| 472 | <1   | <1   | Mn <sub>2</sub> (CO) <sub>7</sub> (CNBu <sup>t</sup> ) <sub>2</sub> <sup>+</sup>  |
| 500 | <1   | 6  | Mn <sub>2</sub> (CO) <sub>8</sub> (CNBu <sup>t</sup> ) <sub>2</sub> <sup>+</sup>  |

<sup>a</sup> Fragments with m/z <55 are not reported. <sup>b</sup> (I) Polycrystalline sample of Mn<sub>2</sub>(CO)<sub>8</sub>(CNBu<sup>t</sup>)<sub>2</sub> containing a mixture of isomers ([Mn(CO)<sub>4</sub>(CNBu<sup>t</sup>)<sub>2</sub>]<sub>2</sub> and [(CO)<sub>5</sub>Mn-Mn(CO)<sub>3</sub>(CNBu<sup>t</sup>)<sub>2</sub>]) <sup>c</sup> (II) Single crystals of isomer [(CO)<sub>5</sub>Mn-Mn(CO)<sub>3</sub>(CNBu<sup>t</sup>)<sub>2</sub>]<sub>2</sub> <sup>d</sup> Not applicable for (CO)<sub>5</sub>Mn-Mn(CO)<sub>3</sub>(CNBu<sup>t</sup>)<sub>2</sub> (III) (see text)

Figure 11.8(a): Dimeric fragmentation pattern for  $\text{Mn}_2(\text{CO})_8(\text{CNBu}^t)_2$

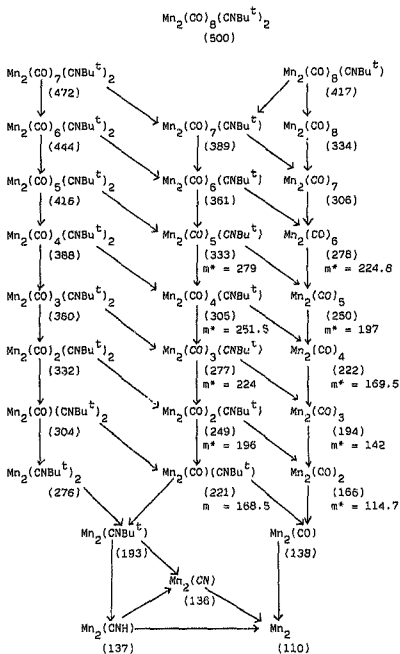
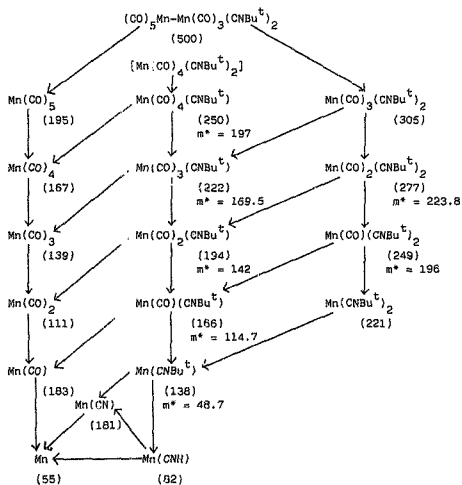


Figure 11.8(b): Monomeric fragmentation pattern for  $Mn_2(CO)_8(CNBut)_2$





$\text{Mn}_2(\text{CO})_8(\text{CNBu}^t)_2$  and suggest a method for detecting isomers and of assigning the substitution geometry of  $\text{M}_2(\text{CO})_8(\text{CNR})_2$  complexes.

(c) Mass spectrum of  $\text{Re}_2(\text{CO})_8(\text{CNC}_6\text{H}_3\text{Me}_2-2,6)_2$

The mass spectral data for  $\text{Re}_2(\text{CO})_8(\text{CNC}_6\text{H}_3\text{Me}_2-2,6)_2$  is given in Table 11.9. The isotopes  $^{185}\text{Re}$  and  $^{187}\text{Re}$  give rise to two peaks for monomeric fragments, and three peaks for dimeric fragments (see section 11.4.4(a))

A single crystal sample of  $[\text{Re}(\text{CO})_4(\text{CNC}_6\text{H}_3\text{Me}_2-2,6)]_2$  (used in the X-ray diffraction study (ch. XIV)) was used. Figs. 11.9(a) and (b) show the dimeric ( $\text{Re}_2$  unit remains intact) and monomeric ( $\text{Re}$  fragment) fragmentation paths respectively. Cross-over from dimeric to monomeric paths is of course possible.

As expected, the peaks corresponding to the monomeric fragments  $\text{Re}(\text{CO})_{3-n}(\text{CNC}_6\text{H}_3\text{Me}_2-2,6)_2$  ( $n = 0-3$ ) with two isonitrile ligands on one  $\text{Re}$ -atom, are not present in the spectrum. (The peak corresponding to the fragment  $\text{Re}(\text{CO})_5^+$  ( $m/z$ : 325, 327) is likewise absent).

At low temperatures (135°C), the fragmentation pattern of  $[\text{Re}(\text{CO})_4(\text{CNC}_6\text{H}_3\text{Me}_2-2,6)]_2$  is dominated by the monomeric fragmentation path(s). However, as the temperature is increased, (probe heated to 175°C), the intensity of the peaks of the monomeric precursor fragment,  $[\text{Re}(\text{CO})_4(\text{CNC}_6\text{H}_3\text{Me}_2-2,6)]^+$  ( $m/z$ : 428, 430) and of  $[\text{Re}(\text{CO})_3(\text{CNC}_6\text{H}_3\text{Me}_2-2,6)]^+$  ( $m/z$ : 400, 402), decrease drastically, while peaks corresponding to  $\text{Re}_2$ -fragments previously absent appear, or increase in intensity if previously weakly present. Hence it would appear that for  $[\text{Re}(\text{CO})_4(\text{CNC}_6\text{H}_3\text{Me}_2-2,6)]_2$  the monomeric fragmentation path predominates at low temperatures, and the dimeric fragmentation path (i.e. ligand loss before metal-metal bond cleavage) is favoured at elevated temperatures.

It is interesting to note that the peaks corresponding to the dirhenium carbonyl fragments,  $\text{Re}_2(\text{CO})_{8-n}$  ( $n = 0-4$ ) are entirely absent from the spectrum of  $[\text{Re}(\text{CO})_4(\text{CNC}_6\text{H}_3\text{Me}_2-2,6)]_2$ . This indicates that for this complex, dimeric

TABLE 11.9: Mass spectral data for the complex  $[\text{Re}(\text{CO})_4(\text{CNC}_6\text{H}_3\text{Me}_2-2,6)]_2$

| $m/z^a$     | Relative Intensity(%) <sup>b</sup> | Fragment  |
|-------------|------------------------------------|---|
| 185,187     | <1                                 | $\text{Re}^+$   |
| 211,213     | 3, 5                               | $\text{Re}(\text{CN})^+$  |
| 213,215     | 5, 5                               | $\text{Re}(\text{CO})^+$  |
| 241,243     | 11,24                              | $\text{Re}(\text{CO})_2^+$  |
| 269,271     | 19,24                              | $\text{Re}(\text{CO})_3^+$  |
| 297,299     | 15,27                              | $\text{Re}(\text{CO})_4^+$  |
| 316,318     | <1                                 | $\text{Re}(\text{CNC}_6\text{H}_3\text{Me}_2-2,6)^+$                  |
| 344,346     | 7,13                               | $\text{Re}(\text{CO})(\text{CNC}_6\text{H}_3\text{Me}_2-2,6)^+$       |
| 372,374     | 14,11                              | $\text{Re}(\text{CO})_2(\text{CNC}_6\text{H}_3\text{Me}_2-2,6)^+$     |
| 370,372,374 | 10,14,11                           | $\text{Re}_2^+$   |
| 396,398,400 | 6, 9,53                            | $\text{Re}_2(\text{CN})^+$  |
| 398,400,402 | 9,53,82                            | $\text{Re}_2(\text{CO})^+$  |
| 400,402     | 53,82 <sup>c</sup>                 | $\text{Re}(\text{CO})_3(\text{CNC}_6\text{H}_3\text{Me}_2-2,6)^+$     |
| 428,430     | 60,100 <sup>c</sup>                | $\text{Re}(\text{CO})_4(\text{CNC}_6\text{H}_3\text{Me}_2-2,6)^+$     |
| 426,428,430 | 6,60,100                           | $\text{Re}_2(\text{CO})_2^+$  |
| 454,456,458 | <1                                 | $\text{Re}_2(\text{CO})_3^+$  |
| 482,484,486 | - <sup>d</sup>                     | $\text{Re}_2(\text{CO})_4^+$  |
| 501,503,505 | 15,17,16                           | $\text{Re}_2(\text{CNC}_6\text{H}_3\text{Me}_2-2,6)^+$                |
| 510,512,514 | - <sup>d</sup>                     | $\text{Re}(\text{CO})_5$  |
| 529,531,533 | 22,32,28                           | $\text{Re}_2(\text{CO})(\text{CNC}_6\text{H}_3\text{Me}_2-2,6)^+$     |
| 538,540,542 | - <sup>d</sup>                     | $\text{Re}_2(\text{CO})_6^+$  |
| 557,559,561 | 11,18,14                           | $\text{Re}_2(\text{CO})_2(\text{CNC}_6\text{H}_3\text{Me}_2-2,6)^+$   |
| 566,568,670 | - <sup>d</sup>                     | $\text{Re}_2(\text{CO})_7^+$  |
| 585,587,589 | 5,10, 8                            | $\text{Re}_2(\text{CO})_3(\text{CNC}_6\text{H}_3\text{Me}_2-2,6)^+$   |
| 594,596,598 | - <sup>d</sup>                     | $\text{Re}_2(\text{CO})_8^+$  |
| 613,615,617 | 11,33,27                           | $\text{Re}_2(\text{CO})_4(\text{CNC}_6\text{H}_3\text{Me}_2-2,6)^+$   |
| 637,634,636 | - <sup>d,e</sup>                   | $\text{Re}_2(\text{CNC}_6\text{H}_3\text{Me}_2-2,6)_2^+$              |
| 641,643,645 | <1 <sup>f</sup>                    | $\text{Re}_2(\text{CO})_5(\text{CNC}_6\text{H}_3\text{Me}_2-2,6)^+$   |
| 660,662,664 | - <sup>d,e</sup>                   | $\text{Re}_2(\text{CO})(\text{CNC}_6\text{H}_3\text{Me}_2-2,6)_2^+$   |
| 669,671,673 | - <sup>d,e</sup>                   | $\text{Re}_2(\text{CO})_6(\text{CNC}_6\text{H}_3\text{Me}_2-2,6)^+$   |
| 688,690,692 | <1 <sup>f</sup>                    | $\text{Re}_2(\text{CO})_2(\text{CNC}_6\text{H}_3\text{Me}_2-2,6)_2^+$ |
| 697,699,701 | 2, 6, 5                            | $\text{Re}_2(\text{CO})_7(\text{CNC}_6\text{H}_3\text{Me}_2-2,6)^+$   |

TABLE 11.9: Mass spectral data for the complex  $[\text{Re}(\text{CO})_4(\text{CNC}_5\text{H}_3\text{Me}_2-2,6)]_2$  (Contd)

| $m/z^a$       | Relative intensity(%) <sup>b</sup> | Fragment  |
|---------------|------------------------------------|---|
| 716, 718, 720 | - d, e                             | $\text{Re}_2(\text{CO})_3(\text{CNC}_6\text{H}_3\text{Me}_2-2,6)_2^+$ |
| 725, 727, 729 | - d, e                             | $\text{Re}_2(\text{CO})_6(\text{CNC}_6\text{H}_3\text{Me}_2-2,6)_2^+$ |
| 744, 746, 748 | - d, e                             | $\text{Re}_2(\text{CO})_4(\text{CNC}_6\text{H}_3\text{Me}_2-2,6)_2^+$ |
| 772, 774, 776 | - d, e                             | $\text{Re}_2(\text{CO})_5(\text{CNC}_6\text{H}_3\text{Me}_2-2,6)_2^+$ |
| 800, 802, 804 | - d, e                             | $\text{Re}_2(\text{CO})_6(\text{CNC}_6\text{H}_3\text{Me}_2-2,6)_2^+$ |
| 828, 830, 832 | - d, e                             | $\text{Re}_2(\text{CO})_7(\text{CNC}_6\text{H}_3\text{Me}_2-2,6)_2^+$ |
| 856, 858, 860 | - d, e                             | $\text{Re}_2(\text{CO})_8(\text{CNC}_6\text{H}_3\text{Me}_2-2,6)_2^+$ |

<sup>a</sup> Fragments of  $m/z < 180$  are not reported

<sup>b</sup> At an ion chamber temperature of 135°C; probe then heated to 175°C (see c, e, f)

<sup>c</sup> Intensity decreases as temperature is increased

<sup>d</sup> Peak absent

<sup>e</sup> Peak appears as temperature is increased

<sup>f</sup> Intensity increases as temperature is increased

Figure 11.9(a): Dimeric fragmentation pattern for  $[\text{Re}(\text{CO})_4(\text{CNC}_6\text{H}_3\text{Me}_2-2,6)]_2$

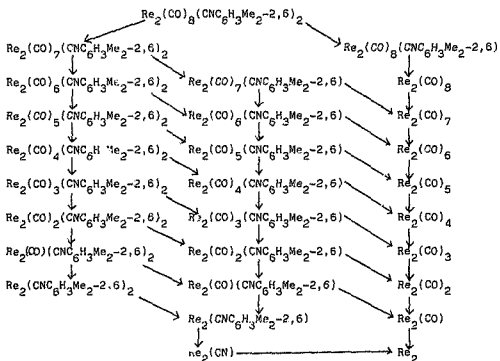
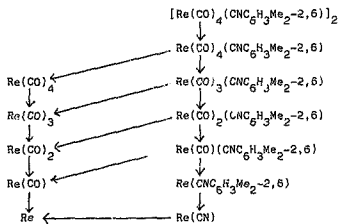


Figure 11.9(b): Monomeric fragmentation path for  $[\text{Re}(\text{CO})_4(\text{CNC}_6\text{H}_3\text{Me}_2-2,6)]_2$



fragmentation routes involving loss of both isonitrile ligands before the loss of at least five carbonyls is strongly disfavoured.

11.5 Mechanism of the reaction of  $M_2(CO)_{10}$  ( $M = Re, Mn$ ) with isonitriles

11.5.1 Mechanism of the PdO-catalysed reaction between  $Re_2(CO)_9$  and  $Bu^tNC$  to give  $Re_2(CO)_9(CNBu^t)$  -  $^{13}CO$  labelling study

The reaction of  $Mn_2(CO)_{10}$  and  $Bu^tNC$  (thermal, at  $80^\circ C$ , or in the presence of Pd/C (5% Pd) catalyst, at  $25^\circ C$ ) to give the monosubstituted  $Mn_2(CO)_9(CNBu^t)$ , has been demonstrated to proceed without Mn-Mn bond scission.<sup>27</sup> In the experiment,  $Mn_2(CO)_{10}$  and isotopically labelled  $Mn_2(^{13}CO)_{10}$  (1:1 ratio) was used, and the product analysed by mass spectroscopy. The product consisted of  $Mn_2(CO)_9(CNBu^t)$  and  $Mn_2(^{13}CO)_9(CNBu^t)$  (1:1 ratio), with less than 1% mixed-isotope (ie. Mn-Mn bond cleavage) product.

To investigate the mechanism of the PdO-catalysed reaction between  $Re_2(CO)_{10}$  and RNC, the PdO-catalysed reaction of  $Re_2(CO)_{10}$  and  $Re_2(^{13}CO)_{10}$  with  $Bu^tNC$  (1:1:2 ratio) at  $50^\circ C$  was performed. The reaction to  $Re_2(CO)_9(CNBu^t)$  was complete in less than 1 min. This product was analysed by mass spectroscopy, in order to determine whether any mixing of the labelled carbonyls, indicative of Re-Re bond cleavage, had occurred. The results clearly indicated that Re-Re bond cleavage had not occurred. For instance, parent ion peaks (equal intensities) appeared at  $m/e$  values of 707 and 716, corresponding to  $^{187}Re^{185}Re(CO)_9(CNBu^t)^+$  and  $^{187}Re^{185}Re(^{13}CO)_9(CNBu^t)^+$  respectively, but there were no peaks at 711 or 712 for  $^{187}Re^{185}Re(CO)_4(^{13}CO)_4(CNBu^t)^+$  or  $^{187}Re^{185}Re(CO)_4(^{13}CO)_5(CNBu^t)^+$ , the expected bond-cleavage products. Hence the PdO-catalysed reaction of  $Re_2(CO)_{10}$  with  $Bu^tNC$ , like that of  $Mn_2(CO)_{10}$ , proceeds without metal-metal bond cleavage.

11.5.2 Kinetic studies of the reaction of  $M_2(CO)_{10}$  ( $M = Mn, Re$ ) with  $Bu^tNC$ <sup>28</sup>

The reaction of  $Mn_2(CO)_{10}$  with  $Bu^tNC$  has been studied kinetically. The PdO-catalysed reaction of  $Mn_2(CO)_{10}$  with 2-equivalents of  $Bu^tNC$  in benzene at  $50^\circ C$  (2 h) yields crude

$\text{Mn}_2(\text{CO})_8(\text{CNBu}^t)_2$ . Recrystallization from hexane ( $-5^\circ\text{C}$ ) yielded a first crop of material which consisted only of 1,1-dieq- $\text{Mn}_2(\text{CO})_8(\text{CNBu}^t)_2$ , isomer A (Fig. 11.6). Repeated recrystallization ( $-5^\circ\text{C}$ , hexane) yielded 1,2-dieq- $\text{Mn}_2(\text{CO})_8(\text{CNBu}^t)_2$ , isomer B (Fig. 11.6) (fifth crop).

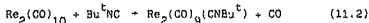
Kinetic studies have shown that isomer B is initially formed, and is converted to isomer A on heating. Kinetic investigation of the isomerization reaction B-A have shown that at  $50^\circ\text{C}$ , equilibrium is established with the ratio of A:B either 1:3 (benzene) or 1:1 (hexane).

However, with  $\text{Re}_2(\text{CO})_8(\text{CNBu}^t)_2$ , only isomer B is formed at  $25^\circ\text{C}$ , and the attempted thermal interconversion of B-A was unsuccessful even at  $125^\circ\text{C}$ . For the  $\text{Re}_2(\text{CO})_8(\text{CNR})_2$  complexes prepared (see section 11.4.1) since isomer A was only observed (in the  $^1\text{H}$  NMR spectrum) for  $\text{Re}_2(\text{CO})_8(\text{CNMe})_2$  (see section 11.4.2.), the small size of the MeNC ligand ("fan-shaped" angle:  $52^\circ$  (width) and  $52^\circ$  (thickness)) and its electronic similarity to  $\text{CO}^{123b}$  may facilitate the interconversion of isomer B to isomer A. The results suggest that for  $\text{Re}_2(\text{CO})_8(\text{CNR})_2$ , isomer A is separated from isomer B by a high energy barrier. This is supported by the inability to convert isomer A,  $(\text{CO})_5\text{Re}-\text{Re}(\text{CO})_3(\text{CNBu}^t)_2$  (prepared indirectly from the reaction of  $\text{NaRe}(\text{CO})_5$  with  $\text{Re}(\text{CO})_3(\text{CNBu}^t)_2\text{I}^{123}$ ), to isomer B,  $[\text{Re}(\text{CO})_4(\text{CNBu}^t)]_2$ .<sup>123</sup>

## 11.6 Experimental

### 11.6.1 Catalyst testing

To screen potential catalysts, use was made of reaction (11.2)



$\text{Re}_2(\text{CO})_{10}$  (0.20 mmol) and potential catalyst (4 mg; see Table 11.1) were stirred in benzene (4 ml) at  $55^\circ\text{C}$ .  $\text{Bu}^t\text{NC}$  (0.22 mmol) was then added to the solution, and the progress of the reaction was monitored by TLC (Silica; eluent: hexane: benzene (20%)). Reaction times for the substitution reaction (11.2) corresponded to the complete conversion of  $\text{Re}_2(\text{CO})_{10}$  to  $\text{Re}_2(\text{CO})_8(\text{CNBu}^t)$ , as detected by TLC.

11.6.2 PdO-catalysed synthesis of  $Re_2(CO)_{10-n}(CNR)_n$

( $n = 1-3$ ,  $R = Bu^t, C_6H_5CH_2, C_6H_{11}$ ;  $n = 1-4$ ,

$R = 2,6-Me_2C_6H_3, Me$ )

$Re_2(CO)_{10}$  (1.0 mmol) and the catalyst, PdO (20 mg) were stirred in toluene (10 ml). RNC (n mmol) was then added to the solution and the reaction was monitored by TLC (Silica; eluent: hexane: benzene (20% or 30%)). The reaction was terminated when complete conversion of  $Re_2(CO)_{10}$  to  $Re_2(CO)_{10-n}(CNR)_n$  had occurred, or when no further reaction could be detected (by TLC). Column chromatography (Silica; 20cm x 1cm column; eluent: hexane: benzene (20%)) gave the required products in the indicated yields (Table 11.2). Recrystallization under nitrogen from solutions of dichloromethane-hexane, or benzene-hexane, gave the products as white or yellow crystalline solids. In the case of the  $C_6H_{11}NC$  derivatives ( $n = 1-3$ ), yellow oils were obtained, which on standing solidified over a period of several months.

11.6.3. PdO-catalysed synthesis of  $Re_2(CO)_8(CNBU^t)(CNC_6H_3Me_2-2,6)$

$Re_2(CO)_{10}$  (1.0 mmol) and PdO (20 mg) were stirred in benzene (10 ml) at 55°C. RNC (1 mmol,  $R = Bu^t$  or  $2,6-Me_2-C_6H_3$ ) was then added to the solution, and the reaction monitored by TLC (Silica; eluent: hexane: benzene (30%)). After conversion of the  $Re_2(CO)_{10}$  to  $Re_2(CO)_9(CNR)$  was judged (by TLC) to be complete, R'NC (1 mmol,  $R' = 2,6-Me_2-C_6H_3$  or  $Bu^t$ ) was added. The reaction was terminated once all the  $Re_2(CO)_9(CNR)$  had been converted to  $Re_2(CO)_8(CNR)-(CNR')$ . The product,  $Re_2(CO)_8(CNBU^t)(CNC_6H_3Me_2-2,6)$ , was isolated using the same procedure as that for the  $Re_2(CO)_{10-n}(CNR)_n$  derivatives (*vide supra*), and recrystallized from dichloromethane-hexane solution to give a yellow crystalline solid. (70% isolated yield).

11.6.4. PdO-catalysed reaction of  $Re_2(CO)_{10}$  and  $Re_2(^{13}CO)_{10}$  with  $Bu^tNC$  (1:1:2 ratio)

$Re_2(CO)_{10}$  (0.015 mmol) and  $Re_2(^{13}CO)_{10}$  (0.015 mmol), with catalyst PdO (10 mg), were stirred in benzene at 50°C.



(The reaction vessel was foil-wrapped to exclude all light).  $\text{Bu}^t\text{NC}$  (0.031 mmol) was then added to the solution and the reaction monitored by TLC (Silica; eluent: hexane:benzene (10%)). The reaction to  $\text{Re}_2(\text{CO})_9(\text{CNBu}^t)$  was complete in less than 1 min, and the heating was stopped after 5 min. The product was isolated by plate thin layer chromatography [Silica gel TLC plate (Whatman Chemical Separation Inc., K6F silica gel, 20 x 20 cm, layer thickness 250 $\mu$ ); eluent: hexane: benzene (10%)], extracted with dichloromethane, and recrystallized from dichloromethane-pentane solution, to give a white material,  $\text{Re}_2(\text{CO})_9(\text{CNBu}^t)$  (90% isolated yield).

XII. THE MODIFICATION OF  $\text{Re}_2(\text{CO})_{10}$  BY LIGANDS L

12.1 Introduction

Dirhenium decacarbonyl,  $\text{Re}_2(\text{CO})_{10}$ , together with its analogue, dimanganese decacarbonyl,  $\text{Mn}_2(\text{CO})_{10}$ , is an example of a simple metal carbonyl dimer, with a single metal-metal bond, and no bridging ligands. Owing to their relative chemical simplicity, these complexes have been used as model compounds in theoretical calculations,<sup>1,2</sup> and extensively studied by spectroscopic and diffraction methods.<sup>1,3-15</sup>

Substituted derivatives of the type  $\text{Re}_2(\text{CO})_{10-n}(\text{L})_n$  ( $n = 1-4$ ), have been less extensively investigated, possibly due to synthetic difficulties encountered in such carbonyl substitution reactions (ch. X). Substitution of one or more carbonyls for ligand(s) L result in extensive structural changes, relative to the parent carbonyl,  $\text{Re}_2(\text{CO})_{10}$ . In the extreme case, under suitable chemical conditions, the reaction between  $\text{Re}_2(\text{CO})_{10}$  and ligand L may result in the cleavage of the Re-Re bond, and the formation of mononuclear products of the type  $\text{Re}(\text{CO})_{5-n}(\text{L})_n$ .<sup>1,6</sup> Reaction between  $\text{Re}_2(\text{CO})_{10}$  and L may also yield dinuclear products in which the Re-Re bond has been cleaved,<sup>1,7-9</sup> the two halves of the dimer being held together by bridging ligand(s) L. In cases where the Re-Re bond remains intact (or acquires some multiple bond character) in the  $\text{Re}_2(\text{CO})_{10-n}(\text{L})_n$  dimer, the structural changes in the product can be rationalized in terms of the steric and electronic properties of the ligand L. An understanding of the structural features of  $\text{Re}_2(\text{CO})_{10}$  is fundamental to an analysis of the structural modifications of the molecule by ligands L.

12.2 The Structure of  $\text{Re}_2(\text{CO})_{10}$

The (partial) X-ray crystal structures of the isomorphous  $\text{Re}_2(\text{CO})_{10}$  and  $\text{Mn}_2(\text{CO})_{10}$  were first determined by Dahl, Ishishi and Rundle in 1957,<sup>1,10</sup> and a refined structure of  $\text{Mn}_2(\text{CO})_{10}$  was published by Dahl and Rundle in 1963.<sup>1,11</sup>

Both structures were redetermined by Churchill, Amoh and Wasserman in 1981,<sup>158</sup> the main changes being in the M-M bond length distances. An X-ray crystal structure study at 74K of  $Mn_2(CO)_{10}$  has also been published by Martin, Rees and Mitschler in 1982.<sup>159</sup> Prior to the full X-ray crystal structure of  $Re_2(CO)_{10}$  by Churchill *et al* in 1981, the only full structural determination of this molecule was an electron diffraction study in the gas phase by Gapotchenko *et al* in 1972.<sup>154</sup> Similar studies have been reported for  $Mn_2(CO)_{10}$ , by Gapotchenko *et al* (1968)<sup>155b</sup> and Almennigen *et al* (1969).<sup>155a</sup>

$Re_2(CO)_{10}$  crystallizes in the monoclinic space group,  $I2/a$ , with 4 molecules in the unit cell, the two halves of the dimer being related by a crystallographic 2-fold axis. The molecular symmetry is  $D_{4d}$ , each Re-atom being octahedrally coordinated to 5 CO groups and the other Re atom, with the equatorial carbonyls on the two halves of the dimer in a staggered configuration. The main structural features of the molecule are discussed below, in terms of the underlying electronic and/or steric factors determining the observed geometry.

#### 12.2.1 The Re-Re bond length

The  $Re_2(CO)_{10}$  molecule is diamagnetic, and obeys the 18-Electron Rule.<sup>160</sup> The rhenium atoms are connected by a single bond, the Re-Re bond length<sup>158</sup> in the crystal being  $3.0413(11)\text{\AA}$ . In  $Mn_2(CO)_{10}$ , the Mn-Mn bond length<sup>159</sup> is  $2.9038(6)\text{\AA}$ .

Bond length is generally taken as a reflection of bond strength. Measurements of bond strengths (where reported) are often subject to large experimental uncertainties. The earliest thermochemical measurement of the Mn-Mn bond enthalpy for  $Mn_2(CO)_{10}$  gave a  $\Delta H$  value of  $142\text{kJ mol}^{-1}$ .<sup>161</sup> Subsequent calorimetric measurements<sup>162</sup> for  $Mn_2(CO)_{10}$  and  $Re_2(CO)_{10}$  have given values for  $D(\text{Mn-Mn})$  and  $D(\text{Re-Re})$  of 67 and  $128\text{ kJ mol}^{-1}$  respectively.

Estimates of metal-metal bond energies of  $M_2(CO)_{10}$  ( $M = \text{Re}, \text{Mn}$ ), have been made using indirect methods.

Several groups have carried out mass spectral studies<sup>15a</sup> of  $Mn_2(CO)_{10}$  and  $Re_2(CO)_{10}$ . From appearance and ionization potentials, the average metal-metal bond dissociation energy may be calculated for the process

$M_2(CO)_{10} \rightarrow 2M(CO)_5$  ( $M = Mn, Re$ ). A range of  $D(M-M)$  values have been reported. ( $D(Mn-Mn)$ : 79.0,<sup>15a</sup> 87.9,<sup>15b</sup> 92.5,<sup>15c</sup> 104.1<sup>15d</sup> kJ mol<sup>-1</sup>;  $D(Re-Re)$ : 213.9,<sup>15c</sup> 186.9<sup>15d</sup> kJ mol<sup>-1</sup>).

A correlation between metal-metal stretching force constants and metal-metal dissociation energies (derived from electron impact measurements), has been found for  $M_2(CO)_{10}$  ( $M = Mn, Re$ ).<sup>147b</sup> From Raman spectra, metal-metal bond stretching force constants have been calculated using the method of normal co-ordinate analysis.<sup>147</sup> ( $f(Mn-Mn)$ : 0.59 mdyn/Å,<sup>147b</sup>  $f(Re-Re)$ : 0.82 mdyn/Å;<sup>147a-b</sup> another study<sup>147c</sup> gave values of 1.4 and 1.6 mdyn/Å respectively).

From kinetic studies of the decomposition of  $M_2(CO)_{10}$  ( $M = Mn, Re$ ), the energy of activation  $\Delta H^\ddagger$  for M-M bond homolysis has been calculated. (For  $M_2(CO)_{10}$ ,<sup>23a, 161a</sup>  $\Delta H^\ddagger = 151$  kJ mol<sup>-1</sup>, and for  $Re_2(CO)_{10}$ ,<sup>111</sup>  $\Delta H^\ddagger = 162$  kJ mol<sup>-1</sup>). However, the estimates of the Mn-Mn bond strength have subsequently been felt<sup>23a</sup> to be too low, in the light of the recent result<sup>177</sup> that the thermal reaction between  $Mn_2(CO)_{10}$  and  $PR_3$  to give  $Mn_2(CO)_9(PR_3)$  proceeds without Mn-Mn bond scission (see Section 15C).

Metal-metal bond energies have been calculated from bond length ( $d$ ) - Enthalpy ( $E$ ) relationship of the form  $E = Ad^{-v}$  ( $A$  a constant).<sup>112</sup> Using bond lengths of 3.04 Å and 2.92 Å for Re-Re and Mn-Mn respectively,  $E(M-M)$  was calculated as 80 and 35 kJ mol<sup>-1</sup> respectively for  $Re_2(CO)_{10}$  and  $Mn_2(CO)_{10}$ . However, it should be noted that the M-M bond lengths used are those from the electron diffraction gas phase study of  $Re_2(CO)_{10}$ ,<sup>136</sup> and from the early X-ray crystal study of  $Mn_2(CO)_{10}$ . These values, especially for  $Mn_2(CO)_{10}$ , differ significantly from the refined values of the redetermined structures,<sup>133</sup> and, as acknowledged by

the authors, the use of incorrect bond length data could affect the accuracy of the results. Using  $\Delta H$  (disrupt) values of 2029 and 1068  $\text{kJ mol}^{-1}$  for  $\text{Re}_2(\text{CO})_{10}$  and  $\text{Mn}_2(\text{CO})_{10}$  respectively, where  $\Delta H$  (disrupt) represents the enthalpy change for the process  $\text{M}_2(\text{CO})_{10} \longrightarrow 2\text{M} + 10 \text{CO}$ , the average enthalpy contribution assignable to the bonding of each carbonyl ligand to the metal ( $D(\text{M-CO})$ ) was calculated from the relationship

$\Delta H(\text{disrupt}) = E(\text{M-M}) + 10 D(\text{M-CO})$ , and found to be 195 and 103  $\text{kJ mol}^{-1}$  for  $\text{Re}_2(\text{CO})_{10}$  and  $\text{Mn}_2(\text{CO})_{10}$  respectively. Hence the percentage  $\Delta H$  (disrupt) due to M-M bonding (i.e.  $100 (E(\text{M-M}))/\Delta H$  (disrupt)) was calculated as 4% and 3% respectively for  $\text{Re}_2(\text{CO})_{10}$  and  $\text{Mn}_2(\text{CO})_{10}$ , i.e. less than 5% of the total disruption enthalpy is due to metal-metal bond cleavage.

As is apparent from the foregoing analysis, controversy surrounds the exact values of  $D(\text{Re-Re})$  and  $D(\text{Mn-Mn})$  in  $\text{Re}_2(\text{CO})_{10}$  and  $\text{Mn}_2(\text{CO})_{10}$ . However, there is no doubt as to the relative order of the M-M bond strengths, viz.  $D(\text{Re-Re}) > D(\text{Mn-Mn})$ .

On the basis of their MO calculations, Brown *et al*<sup>235</sup> have suggested that the term "unsupported" metal-metal bond applied to dirhenium decacarbonyl and dimanganese decacarbonyl requires modification, since an important contribution to the metal-metal bond energy in these dimers arises by interaction of metal orbitals with ligand orbitals on the opposite metal. However, this conclusion has been questioned<sup>155</sup> as other theoreticians<sup>234</sup> find no evidence of this cross-interaction from the results of their MO calculations. This effect is nevertheless evoked by some authors in explaining certain structural effects (*vide infra*).

#### 12.2.2 The Re-CO bond lengths

From the X-ray crystal structure of  $\text{Re}_2(\text{CO})_{10}$ <sup>138</sup> the Re-COax bond length is 1.929(7)Å, compared to an average value for Re-COeq of 1.987(15)Å. The shorter M-COax than M-COeq bond length, also observed in the X-ray crystal

structure of  $Mn_2(CO)_{10}$ ,<sup>150-9</sup> is ascribed to competition for  $d\pi$ -electron density between mutually trans pairs of equatorial CO ligands. Low temperature electron density studies of  $Mn_2(CO)_{10}$ <sup>153</sup> have shown a greater electron deficiency in the axial than the equatorial carbonyls, again indicative of a stronger bonding to the metal of the axial than the equatorial carbonyl ligands.

As a result of the above electronic effect, CO has a larger trans influence than  $M(CO)_5$ .<sup>153</sup> Consequently, in reactions of  $M_2(CO)_{10}$  with ligand L, equatorial substitution is expected, unless steric factors dominate with bulky ligands, eg. phosphines, to give products of the type  $ax-M_2(CO)_9L$  eg.  $ax-Mn_2(CO)_9(PMe_2Ph)$ .<sup>224</sup>

#### 12.2.3 Molecular Conformation

In the crystal, the  $Re_2(CO)_{10}$  molecule adopts a staggered configuration, of molecular symmetry  $D_{4d}$ , with OC-Re-Re-CO torsional angles close to the ideal  $45^\circ$ .<sup>153</sup> Repulsive interactions between equatorial CO groups might be expected to be less in the staggered than in the eclipsed conformation.<sup>153</sup>

The results of an electron diffraction study of  $Re_2(CO)_{10}$  in the gas phase<sup>154</sup> were interpreted in terms of an eclipsed configuration, of molecular symmetry  $D_{4h}$ . However, the validity of this anomalous result has been questioned,<sup>154b</sup> and force field calculations have shown that the difference in values of the eq-eq' interaction constants influenced by the change in molecular geometry from the staggered  $D_{4d}$ , to the eclipsed  $D_{4h}$  conformation, is small.<sup>154b</sup> Further, electron diffraction studies of  $Mn_2(CO)_{10}$  in the gas phase<sup>155</sup> have indicated a staggered conformation, of molecular symmetry  $D_{4d}$ , with the barrier to internal rotation estimated at ca.  $8.4 \text{ KJ mol}^{-1}$  or more.<sup>155b</sup> The agreement between experimental and theoretical curves for  $Mn_2(CO)_{10}$  does not differ substantially for models with  $D_{4h}$  and  $D_{4d}$  symmetry, suggestive of an error of interpretation in the case of the  $Re_2(CO)_{10}$  study.<sup>154b</sup>

In high pressure solid state Raman spectroscopic studies,<sup>148</sup> at ca. 8 Kbar for  $\text{Re}_2(\text{CO})_{10}$ , and ca. 5 Kbar for  $\text{Mn}_2(\text{CO})_{10}$ , changes were observed in the spectra indicative of a phase change and a repacking of the molecules, consistent with a transition from the staggered D<sub>4d</sub> conformation to the eclipsed D<sub>4h</sub> form. For  $\text{Re}_2(\text{CO})_{10}$ , observation of spectral shifts at the phase transition provides evidence that in becoming eclipsed, the back-bonding from Re to axial-CO is sharply increased.

#### 12.2.4 OC-Re-CO bond angles

A feature of the structure of  $\text{Re}_2(\text{CO})_{10}$  (and  $\text{Mn}_2(\text{CO})_{10}$ ) is the obtuse axOC-M-COeq, and the acute eqOC-M-COeq bond angles. This is also reflected in M-M-COeq angles of less than 90°, and is apparent in both the gas phase ( $\text{Mn}_2(\text{CO})_{10}$ )<sup>152a</sup> and the crystalline state.<sup>152-b</sup>

This bending in of the M-COeq bonds towards the M-M bond has been variously ascribed to electronic and/or steric factors:-

##### (a) Steric

- (i) C...C repulsions between equatorial carbonyls of the two halves of the dimer.<sup>157b</sup>
- (ii) Repulsive interactions between axial and equatorial carbonyls in one half of the molecule.<sup>157b,159</sup>  
(In terms of non-bonding interactions, C...C repulsions of type (ii) are stronger than those of type (i).)<sup>157b</sup>
- (iii) Influence of neighbouring molecules which increases O...O distances.<sup>157b</sup> (i.e., crystal packing effects). However, this could not account for the gas phase observations (for  $\text{Mn}_2(\text{CO})_{10}$ ).<sup>153a</sup>

##### (b) Electronic

- (i) Bonding interactions between a metal atom and the equatorial carbonyl on the opposite metal atom, i.e., a back-bonding interaction of the 'type M (filled d orbitals) → CO(π\* orbital)', where M, CO are not bonded directly.<sup>215,217</sup>
- (ii) Rehybridization which decreases repulsions between the non-bonding d-electrons on the two metals, by mixing of p-character into the non-bonding orbitals dxz and dyz.<sup>159-21</sup>

- (iii) An increase in the angle between the multiple-bonded M-CO bonds and a decrease in the angle between the single M-M bond and the equatorial bonds would decrease repulsions between the bonding electrons.<sup>129</sup>
- (iv) Molecular orbital energy level diagrams (Elian and Hoffmann, 1975<sup>130</sup>) have shown that for 5-coordinate metal carbonyl fragments, the energetically most favorable geometry corresponds to an eqC-M-Cax angle of slightly greater than 90°, at which point  $\pi$ -interaction is maximized and anti-bonding interaction minimized.

This latter explanation receives further experimental support from the X-ray crystal structure of  $\text{HMn}(\text{CO})_5$ ,<sup>129</sup> which also showed a bending of the equatorial carbonyls towards the axial H-atom. Here the acute  $\text{axO}'\text{-Mn-COeq}$  angles cannot be ascribed to metal-carbonyl cross interaction (i). Further, it has been shown by a combination of <sup>13</sup>C enrichment and IR spectroscopy,<sup>131</sup> that  $\text{axOC-Mn-COeq}$  bond angle in  $\text{Mn}(\text{CO})_5$  (molecular symmetry  $\text{C}_{4v}$ ) is 96(3)°. Explanations such as (i), (ii) would also not be applicable here. Clearly, if this effect were (partly) steric in origin, repulsive interactions of the type (i) would also be eliminated.

#### 12.2.5 Re-C-O bond angles

In  $\text{Re}_2(\text{CO})_{10}$ , (and  $\text{Mn}_2(\text{CO})_{10}$ ) the carbonyl ligands are close to linear, with M-C-O bond angles in the range 176 - 180°.<sup>132</sup>

Non-linearity of M-C-O fragments in  $\text{M}(\text{CO})_n$  ( $n = 2-4$ ) groups has been examined,<sup>133</sup> and is a consequence of bonding and not solely a result of crystal packing forces. The M-C-O fragments are bent (ca. 5° deviation from linearity) due to different occupation of the two antibonding  $\pi^*$  orbitals on a carbonyl ligand. (Hence linearity is expected for  $\text{M}(\text{CN})_n$  only).

The reason for the different M-C-O angles within one  $\text{M}(\text{CO})_n$  group (often equal within experimental error) must lie in crystal packing forces<sup>133</sup> (eg. for  $\text{Re}_2(\text{CO})_{10}$ , repulsive non-bonded O...O interactions between neighbouring



molecules which increases O...O distances<sup>157b</sup>), or in the influence of other groups within the molecule which may lower the symmetry of the  $M_n$  group.<sup>159</sup>

#### 12.2.6 Packing

$Re_2(CO)_{10}$  crystallizes in the monoclinic space group  $I2/a$ . The Re-Re distances in the dimeric molecules are required by crystallographic symmetry to be parallel to one another.<sup>157b</sup> Hence repulsive non-bonding interactions between O-atoms of carbonyls on neighbouring molecules could be in part responsible for small deviations observed from the molecular  $D_{4d}$  symmetry.<sup>158</sup>

Johnson<sup>245</sup> has proposed a model for the rationalization of the structures of simple binary carbonyls by considering the  $M_n$  unit as surrounded by a close-packed array of CO groups, with the M-atoms occupying the interstices. Thus anomalous bond lengths and distortions could be due to packing forces.

#### 12.3 Ringing the changes: the effect of ligand substitution on molecular geometry

In derivatives of the type  $Re_2(CO)_{10-n}(L)_n$  ( $n = 1-10$ ), where a metal-metal bond is retained in the dimer, the substitution of carbonyl group(s) for ligand(s) L may nevertheless drastically affect the structure of the molecule relative to the parent carbonyl,  $Re_2(CO)_{10}$ . Such changes can be rationalized in terms of the steric and electronic properties of the ligand L relative to CO.

##### 12.3.1 The Re-Re bond length

The Re-Re bond length is sensitive to changes in the metal co-ordination sphere. However, such variations should be interpreted with caution, as the metal-metal bond length is governed by an often complex set of factors, which may give rise to opposing trends.

##### Factors affecting the Re-Re bond length

###### (a) Bond Order

Problems arise as it is by no means always apparent whether a metal-metal bond exists, or what the bond order

is. In general, the possibility of a metal-metal bond is considered when the metal-metal distance is of the same order as in the bulk metal,<sup>241</sup> but variability of metal-metal distances due to other factors (*vide infra*) precludes a conclusion based solely on bond length. The metal-metal bond defines a relatively flat energy minimum as a function of interatomic distance.<sup>241</sup> Experimental data, such as metal-metal distances and magnetic properties, provide information, but not an unequivocal delineation.

Spiro<sup>242</sup> has proposed that quantitative Raman intensity data for metal-metal stretching modes be used to establish a scale of metal-metal force constants, reflecting relative metal-metal bond strengths, with the view to the eventual establishment of a quantitative scale of metal-metal bond orders. The relation between force constants and bond strengths is a general, though not necessary one.<sup>242</sup> For  $M_2(CO)_D$  ( $M = Re, Mn$ ), a correlation between M-M stretching force constants derived from Raman spectra, and metal-metal dissociation energies obtained from mass-spectrometric studies, is found<sup>147b</sup> (see section 12.2.1).

Recently Bocyens<sup>243</sup> has proposed a general relationship between bonds that differ in order only. This method assumes that bond order derives essentially from changes in the repulsive part of covalent interactions, specifically from a modification of the internuclear repulsion due to electronic screening. Since the electron density in the region between atomic cores is sensitive to the nature of the ligands attached to the bonded atoms, in a series of compounds, metal-metal bond orders are expected over the whole range from 1 to 4, including non-integral bond orders, which in practice are often obtained.

In Organometallic chemistry, the metal-metal bond order has been based largely on Tolman's "18-Electron" or "Effective Atomic Number" (EAN) Rule.<sup>244</sup> In metal complexes, there is a tendency to achieve an 18-electron configuration, often by metal-metal bonding. Metal-metal bonding may be a compromise in the absence of other bonding partners.<sup>241</sup>

However, this is not always unambiguous, as the number of electrons donated by a ligand can vary according to the mode of bonding of the ligand. Ambiguity arises as to the presence of a metal-metal bond where the compound can be formulated on electronic structure according to the 18-electron rule without a metal-metal bond, especially where the metal-metal distance is shorter than that in related compounds containing a metal-metal bond. However, structural constraints such as crystal lattice effects or bridging ligands, may force the metal atoms closer together. Often in the literature a shorter than "normal" Re-Re single bond is taken as indicative of some degree of multiple bonding.<sup>111, 114</sup>

Although it is true in general that when two atoms are directly bonded to each other, the shorter the inter-nuclear distance, the stronger the bond and the lower the bond order,<sup>172</sup> metal-metal bond distances do not provide reliable estimates of the metal-metal bond order, especially when bridging ligands are present,<sup>115</sup> as metal-metal bond order is dependent on other geometric, steric and/or electronic factors (vide infra). Cotton<sup>244</sup> has pointed out that with multiple metal-metal bonds, bond length is no indication of bond order, especially in the cases of triple and quadruple bonds.

At best, in a series of closely related complexes, a higher metal-metal bond order, or a stronger metal-metal bond, might be reflected in a shorter metal-metal bond length, where other structural differences are not significant. Hence X-ray analysis data alone cannot provide unequivocal information on the nature of the metal-metal bond, but electron density studies could prove useful in this regard.

(b) Electronic nature of ligands

The  $\sigma$ - or  $\pi$ -donor/acceptor properties of the ligand L in  $\text{Re}_2(\text{CO})_{10-n}\text{L}_n$ , relative to CO, affect the bonding of the ligand L to the Re-atoms, and hence the Re-Re bond length. With ligands such as isonitriles, phosphines, hydrides, which are weaker  $\pi$ -acceptors than CO,<sup>113, 114</sup> an increase in the Re-Re bond length can be expected,<sup>112b, 112c</sup> since more

However, this is not always unambiguous, as the number of electrons donated by a ligand can vary according to the mode of bonding of the ligand. Ambiguity arises as to the presence of a metal-metal bond where the compound can be formulated on electronic structure according to the 18-electron rule without a metal-metal bond, especially where the metal-metal distance is shorter than that in related compounds containing a metal-metal bond. However, structural constraints such as crystal lattice effects or bridging ligands, may force the metal atoms closer together. Often in the literature a shorter than "normal" Re-Re single bond is taken as indicative of some degree of multiple bonding.<sup>112, 113</sup>

Although it is true in general that when two atoms are directly bonded to each other, the shorter the internuclear distance, the stronger the bond and the lower the bond order,<sup>112</sup> metal-metal bond distances do not provide reliable estimates of the metal-metal bond order, especially when bridging ligands are present,<sup>113</sup> as metal-metal bond order is dependent on other geometric, steric and/or electronic factors (vide infra). Cotton<sup>746</sup> has pointed out that with multiple metal-metal bonds, bond length is no indication of bond order, especially in the cases of triple and quadruple bonds.

At best, in a series of closely related complexes, a higher metal-metal bond order, or a stronger metal-metal bond, might be reflected in a shorter metal-metal bond length, where other structural differences are not significant. Hence X-ray analysis data alone cannot provide unequivocal information on the nature of the metal-metal bond, but electron density studies could prove useful in this regard.

(b) Electronic nature of ligands

The  $\sigma$ - or  $\pi$ -donor/acceptor properties of the ligand L in  $\text{Re}_2(\text{CO})_{10-n}\text{L}_n$ , relative to CO, affect the bonding of the ligand L to the Re-atoms, and hence the Re-Re bond length. With ligands such as isocyanides, phosphines, hydrides, which are weaker  $\pi$ -acceptors than CO,<sup>117, 118</sup> an increase in the Re-Re bond length can be expected,<sup>119b, 120</sup> since more

negative  $\pi$ -electron charge becomes localized on the metal, increasing the  $\pi$ -electron repulsions which weaken the metal-metal bond.

(c) Steric factors

Steric strain with bulky ligands may result in a lengthening of the Re-Re bond, to relieve interatomic non-bonded repulsions.

Where the molecule is forced into an eclipsed conformation by bridging ligands, repulsive interactions between eclipsed equatorial carbonyls might give rise to a longer Re-Re bond length. <sup>222b, 222</sup>

(d) Bridging ligands

In ligand-bridged  $\text{Re}_2(\text{CO})_{10-n}(\text{L})_n$  complexes, the metal-metal bond length is dependent on the particular ligand-bridged geometry, viz. the metal-to-bridging atom distance, and the M-B-M angle size <sup>223, 227</sup> (B = bridging ligand). In general, in bridged dimeric systems, the M-B-M angle is sharply acute (ca. 70-75°) where a M-M bond exists, and obtuse (ca. 90-100°) where no direct M-M bond exists. <sup>224</sup> An acute M-B-M angle with no metal-metal bond, however, could be due to repulsions between large bridging atoms, eg. halogens. <sup>221</sup> Stability of an  $\text{M}_2\text{B}_2$  bridged system is governed not only by the minimization of all non-bonded repulsions between atoms, but also by interorbital electron-pair interactions, which for a more electronegative bridging atom favours a wider bridging angle. <sup>225</sup>

With bridging ligands, two opposing factors may operate in determining the Re-Re bond length observed, viz. the "bite" of the bridging ligand, a ligand with a small bite size forcing the metal atoms closer together, and C...O repulsions between eclipsed carbonyl groups, which favour a longer Re-Re bond distance. <sup>226b, 222</sup> The number of bridging ligands also plays a role in determining the Re-Re bond length. In similar complexes, the one with more bridging groups usually has a shorter metal-metal bond. <sup>222</sup> However, this could in part be due to the reduced number of eclipsed CO groups in the more highly bridged species. <sup>222</sup>

### 12.3.2 The Re-CO bond lengths

The stronger bonding of Re-COax than Re-COeq observed in  $\text{Re}_2(\text{CO})_{10}$  (section 12.2.2), might be expected also in  $\text{Re}_2(\text{CO})_{10-n}(\text{L})_n$  derivatives. However, in substituted derivatives, bonding effects due to the electronic nature of the ligand L must also be considered, and these may alter or obscure the above effect.

Since  $\pi$ -acceptor ligands must compete for the two metal d $\pi$  orbitals,<sup>13</sup> the  $\pi$ -bonding between the metal atom and a CO trans to a ligand L, which is a weaker  $\pi$ -acceptor than CO, is greater than that to a CO cis to L.<sup>13</sup> Hence a shortening of the Re-CO (trans to L) relative to the  $\pi$  (cis to L) bond length is expected with poor  $\pi$ -acceptor ligands L.<sup>13</sup> This is also the origin of the cis-labilization effects observed with poor  $\pi$ -acceptors L, resulting in initial cis-eq substitution for  $\text{Re}_2(\text{CO})_8(\text{L})_2$  complexes.<sup>13</sup> Final substitution geometry is thus expected to cis-dieq- $\text{Re}_2(\text{CO})_8(\text{L})_2$ , unless steric factors predominate, as in the case of bulky phosphine ligands, to give di-ax- $\text{Re}_2(\text{CO})_8(\text{L})_2$  complexes (vide infra).

Isonitrile (RNC) ligands are better  $\sigma$ -donors, but weaker  $\pi$ -acceptors than CO,<sup>14</sup> but stronger  $\pi$ -acceptors than phosphines ( $\text{PR}_3$ ).<sup>14</sup> With isonitrile ligands, one would expect to observe the above effects. Phosphines however, have a larger cone angle<sup>15</sup> than isonitriles,<sup>14</sup> and steric effects may dominate. In the reaction of  $\text{Mn}_2(\text{CO})_{10}$  with  $\text{PR}_3$ , to give di-ax- $\text{Mn}_2(\text{CO})_8(\text{PR}_3)_2$ , the cis-labilization effect accounts for the observation that the rate constant for the second substitution is larger than that for the first.<sup>16</sup> According to the proposed mechanism, the first step is mono-substitution to give ax- $\text{Mn}_2(\text{CO})_9\text{L}$  (steric factors governing axial substitution), then loss of a CO cis to the  $\text{PR}_3$  group on the same Mn-atom, follows by exchange of CO via a bridging mechanism, and  $\text{PR}_3$  substitution on the other Mn-atom, steric consideration necessitating di-axial substitution.

### 12.3.3 Molecular Conformation

On steric ground, staggered molecular conformation is favoured, as this minimizes repulsive interactions.<sup>111</sup> However, bridging ligands necessitate an eclipsed configuration, where O...O repulsions between eclipsed equatorial carbonyls may result in distortions from the ideal molecular geometry.<sup>111b</sup>

### 12.3.4 OC-Re-CO bond angles

As discussed above (section 12.2.4.) the bending in towards the Re-Re bond of the equatorial carbonyls in  $Re_2$  would be due to steric and/or electronic factors.

Steric in origin (due to attempts to minimize  $Re$ , interactions), a more pronounced effect might be expected with bulky ligands more sterically demanding than relatively small CO ligand (Tolman cone angle estimated at ca. 95°).<sup>112</sup> If the origin of this effect is predominately electronic in nature, however, for ligands electronically similar to CO, eg. the isoelectronic  $RNC$ ,<sup>113</sup> similar trends might be expected to be observed as with  $Re_2(CO)_{10}$ , especially if the ligand itself, although bulkier than CO, is not very sterically demanding, a situation which might impose severe steric constraints on the structure of the  $Re_2(CO)_{10-n}(L)_n$  derivative.

### 12.3.5 Re-C-O bond angles

The analysis of non-linearity of M-C-O fragments in  $M(CO)_n$  ( $n = 2-4$ ) groups<sup>114</sup> applies to other  $MR_n$  groups also, eg.  $R = CN, NO$ . Hence near-linear co-ordination of those ligands ( $M-C-N$  ca. 175°) is predicted.

### 12.3.6 Packing

The packing of the molecules in the crystal is determined by the molecular geometry, crystallographic symmetry demands, and the principle of dense packing.<sup>115</sup> The molecules pack in such a way as to make the most efficient use of space i.e. maximum closeness, without causing repulsive intermolecular interactions. Hence structural changes in the molecule may result in differences in

crystallographic space group and packing order. Further, interactions between groups on neighbouring molecules may cause anomalous structural features. Deviations from ideal geometry could reflect packing requirements in the crystal lattice.<sup>233</sup>



XIII X-RAY CRYSTALLOGRAPHIC STUDIES OF DIRHENIUM CARBONYL  
DERIVATIVES - A SURVEY OF THE LITERATURE

13.1 Introduction

As discussed in the previous chapter, the basic structure of the dirhenium decacarbonyl dimer may be changed (to a lesser or greater extent) by the substitution of one or more carbonyl groups for ligand(s) L. These structural effects can be rationalized in terms of the steric and/or electronic properties of ligand L relative to CO.

Despite the tremendous growth in recent years of the use of single crystal X-ray diffraction methods in product characterization, relatively few X-ray structures have been reported of dirhenium decacarbonyl derivatives. This could be due in part to synthetic difficulties often encountered in the preparation of such substituted derivatives of  $\text{Re}_2(\text{CO})_{10}$  (ch. X).

This review briefly describes the derivatives of dirhenium decacarbonyl for which an X-ray crystal and molecular structure has been reported in the Literature. Only those complexes with a direct Re-Re bond will be considered. The majority of these complexes were synthesized from the direct reaction of  $\text{Re}_2(\text{CO})_{10}$  with ligand L (ch. X), but some were prepared from the reaction of higher rhenium clusters, eg.  $[\text{Re}_3(\text{H})_3(\text{CO})_{12}]$ .<sup>145</sup> The purpose of this review is to assess the effect of ligand substitution on molecular conformation and bond parameters, for a wide variety of ligands L.

Dirhenium carbonyl complexes which contain bridging bidentate ligands and/or bridging halogen atoms, but no direct Re-Re bond, will not be included in this review.

For example, dirhenium complexes of the type

$(\mu\text{-X})_2\text{Re}_2(\text{CO})_6(\text{L})_2$  (eg. X = Br, L = THF<sup>249a</sup>; X = Br, (L)<sub>2</sub> =  $\mu\text{-S}_2\text{Ph}_2$ ,<sup>129b</sup>  $\mu\text{-S}_2\text{Me}_2$ ,<sup>140</sup>  $\mu\text{-Se}_2\text{Ph}_2$ ,<sup>249d</sup>  $\mu\text{-P}_2\text{Ph}_4$ ,<sup>149c</sup> X = Cl, (L)<sub>2</sub> =  $\mu\text{-Ph}_2\text{AsCH}_2\text{AsPh}_2$ <sup>150b</sup>), prepared indirectly from monomeric rhenium halocarbonyl compounds,<sup>249a, 250a</sup> (Re...Re distances range from 3.81 to 3.97 Å).<sup>249, 250</sup>

Further, dirhenium complexes formed from reactions of

$\text{Re}_2(\text{CO})_{10}$  (or derivatives thereof) with ligand L, but which lack a direct Re-Re bond, will also not be included in this review (eg.  $(\text{CO})_4\text{Re}-\mu-(\text{C}_8\text{H}_8)-\text{Re}(\text{CO})_5$ ,<sup>155</sup> formed from the photolysis of  $\text{Re}_2(\text{CO})_{10}$  with cyclooctatetraene;  $(\mu\text{-Br})\text{-Re}_2(\text{CO})_8[\mu\text{-CPh}]$ ,<sup>211</sup> formed from the reaction of  $\text{Re}_2(\text{CO})_9\text{-[C(OMe)Ph]}$  with  $\text{Al}_2\text{Br}_6$ ). The so-called "metal-ring" compounds, eg.  $[\text{Re}_2(\text{CO})_8\{\text{Sn(II)Re}(\text{CO})_4(\text{PPh}_3)\}]$ ,<sup>152</sup> (formed from reaction of  $\text{Re}_2(\text{CO})_8(\text{PPh}_3)_2$  with  $\text{SnI}_2$ ), with a non-bonded Re-Re distance of 3.176(1)Å across the metal ring, are likewise excluded.

Those derivatives of  $\text{Re}_2(\text{CO})_{10}$ , in which the direct Re-Re bond has been retained, for which X-ray crystal and molecular structures have been reported in the Literature, are listed in Table 13.1. In all the rhenium-rhenium bonded structures listed in Table 13.1, the basic dimeric unit has been retained, although a change in the metal-metal bond order may have resulted. The Re-Re bond length distances for each structure are also given in Table 13.1. A brief description of the salient features of these complexes, in terms of the electronic and steric effects of the ligand(s) L, will be given.

### 13.2 Literature Structures

#### 13.2.1 Structures without bridging ligands

(a) Mono-substitution: eq- $\text{Re}_2(\text{CO})_9(\text{L})$ , {L = CH(OMe); C(OR)(SiPh<sub>3</sub>), R = Me, Et}

To date, the only mono-substituted derivatives of  $\text{Re}_2(\text{CO})_{10}$  reported are eq- $\text{Re}_2(\text{CO})_9[\text{CH(OMe)}]$ ,<sup>211</sup> (i), eq- $\text{Re}_2(\text{CO})_9[\text{C(OMe)(SiPh}_3)]$ ,<sup>213</sup> (ii) and eq- $\text{Re}_2(\text{CO})_9\text{-[Re}_2(\text{CO})_9(\text{C(OMe)(SiPh}_3)\text{)]}$ ,<sup>159,213</sup> (iii). All three molecules are equatorially substituted, as expected,<sup>159,213</sup> and adopt a staggered conformation, like the parent carbonyl,  $\text{Re}_2(\text{CO})_{10}$ ,<sup>154</sup> to minimize repulsive interactions between equatorial CO groups.<sup>120</sup>

The Re-Re bond lengths for compounds (i), (ii) and (iii), (see Table 13.1) are the same within error limits (ca. 3.05Å) and slightly longer (ca. 0.009Å) than that for  $\text{Re}_2(\text{CO})_{10}$  (3.0413(11)Å). Although significance cannot be

TABLE 13.1: X-ray crystal structures of dirhenium carbonyl derivatives, with a direct Re-Re bond

| Complex   | Space group, Z        | Re-Re bond length(Å) | Reference        |
|---|-----------------------|----------------------|------------------|
| Re <sub>2</sub> (CO) <sub>10</sub>  | I2/a, 4 <sup>a</sup>  | 3.0413(11)           | 188              |
| eg-Re <sub>2</sub> (CO) <sub>8</sub> (CH(OMe))  | Cc, 8 <sup>b</sup>    | 3.047, 3.051         | 211 <sup>c</sup> |
| eg-Re <sub>2</sub> (CO) <sub>8</sub> (C(OMe)(SiPh <sub>3</sub> ))   | P2 <sub>1</sub> /c, 4 | 3.052(1)             | 253              |
| eg-Re <sub>2</sub> (CO) <sub>8</sub> (C(OEt)(SiPh <sub>3</sub> ))   | Cc, 8 <sup>b</sup>    | 3.350(3), 3.052(4)   | 177a, 253        |
| 1,2-ax,eq-Re <sub>2</sub> (CO) <sub>8</sub> (C(OEt)(SiPh <sub>3</sub> )) <sub>2</sub>                                   | Pc, 2                 | 3.091(2)             | 195              |
| Re <sub>2</sub> (CO) <sub>8</sub> (μ-(η <sup>3</sup> -1,5-C <sub>4</sub> H <sub>6</sub> ))                              | P2 <sub>1</sub> /n, 4 | 3.114(1)             | 195              |
| Re <sub>2</sub> (CO) <sub>8</sub> (μ-(η <sup>3</sup> -1,5-C <sub>4</sub> H <sub>6</sub> )) <sub>2</sub>                 | P2 <sub>1</sub> /c, 4 | 3.058(1)             | 199              |
| Re <sub>2</sub> (CO) <sub>8</sub> (μ-NC <sub>5</sub> H <sub>4</sub> (μ-H))  | P1, 4 <sup>b</sup>    | 3.2088(4), 3.1956(5) | 168              |
| Re <sub>2</sub> (CO) <sub>7</sub> (OMe) <sub>2</sub> (μ-NC <sub>5</sub> H <sub>4</sub> (μ-H))                           | Pbca, 8 <sup>d</sup>  | 3.2324(5)            | 168              |
| Re <sub>2</sub> (CO) <sub>8</sub> (μ-SiPh <sub>2</sub> ) <sub>2</sub>   |                       | 3.001(1)             | 202-3            |
| Re <sub>2</sub> (CO) <sub>8</sub> (H) <sub>2</sub> (μ-SiPh <sub>2</sub> )   | I <sup>h</sup> , n, 8 | 3.121(2)             | 200              |
| Re <sub>2</sub> (CO) <sub>7</sub> (H) <sub>2</sub> (μ-SiEt <sub>2</sub> ) <sub>2</sub>                                  | P1, 2                 | 3.052(1)             | 202              |
| Re <sub>2</sub> (CO) <sub>6</sub> (H) <sub>4</sub> (μ-SiEt <sub>2</sub> ) <sub>2</sub>                                  | P1, 1 <sup>e</sup>    | 3.084(1)             | 201              |
| Re <sub>2</sub> (CO) <sub>8</sub> (μ-C(OMe)(C <sub>6</sub> H <sub>4</sub> Me-o)) <sub>2</sub>                           | C2/c, 4 <sup>a</sup>  | 2.81(3)              | 177b             |
| (CO) <sub>4</sub> Re <sub>2</sub> (C(SiPh <sub>3</sub> )(CO(OEt)))Re(CO) <sub>3</sub> -<br>[C(OEt)(SiPh <sub>3</sub> )] | P2 <sub>1</sub> /c, 4 | 2.937(1)             | 178c             |
| Re <sub>2</sub> (CO) <sub>8</sub> (μ-C(SiPh <sub>3</sub> ))(CO)(μ-H)  | P2 <sub>1</sub> /c, 4 | 3.036(2)             | 178c             |
| Re <sub>2</sub> (CO) <sub>8</sub> (μ-H) <sub>2</sub>  | P2 <sub>1</sub> /c, 4 | 2.90 <sup>f</sup>    | 20 <sup>g</sup>  |
| Re <sub>2</sub> (CO) <sub>6</sub> (μ-H) <sub>2</sub> (μ-Ph <sub>2</sub> C <sup>10</sup> (Ph) <sub>2</sub> )             | Pbca, 8               | 2.893(2)             | 244a, b          |
| Re <sub>2</sub> (CO) <sub>6</sub> (μ-H)(μ-NCMe)(μ-Ph <sub>2</sub> PCH <sub>2</sub> Ph <sub>2</sub> )                    | P2 <sub>1</sub> /n, 4 | 3.035(3)             | 244a, c          |

**TABLE 13.1:** X-ray crystal structures of dirhenium carbonyl derivatives, with a direct Re-Re bond  
(Contd)

| <u>Complex</u>   | <u>Space group, Z</u> | <u>Re-Re bond length(A)</u> | <u>Reference</u> |
|--|-----------------------|-----------------------------|------------------|
| $\text{Re}_2(\text{CO})_6(\mu\text{-H})(\mu\text{-OH})[\mu\text{-Ph}_2\text{PCH}_2\text{PPh}_2]$       | $\bar{P}1, 2$         | 3.030(1)                    | 198              |
| $\text{Re}_2(\text{CO})_4(\text{PhCCPh})_3(\text{CNCH}_2\text{SO}_2\text{C}_6\text{H}_4\text{Me-p})_2$ | $\bar{P}1, 2$         | 2.786(1)                    | 212              |
| $\text{Re}_2(\text{CO})_4(\text{PhCCPh})_4$  | d                     | 2.78 <sup>f</sup>           | 212              |

<sup>a</sup> Molecule possesses crystallographic  $C_2$  symmetry

<sup>b</sup> Two crystallographically independent molecules in the asymmetric unit

<sup>c</sup> Data obtained from the Cambridge Crystallographic Data Base

<sup>d</sup> Unpublished structure; data not quoted in reference

<sup>e</sup> Molecule possesses crystallographic  $\bar{1}$  symmetry

<sup>f</sup> Unrefined bond length value

attached to such a small difference, the slight increase could reflect the weaker  $\pi$ -acceptor ability of the carbene ligands relative to CO.<sup>23</sup>

Of note are the acute Re-Re-CO angles, and the obtuse Re-Re-C (carbene) angles observed for all three complexes (see Table 13.2). The bending in of the carbonyl ligands, reflected by the acute Re-Re-CO angles, is in accord with electronic predictions<sup>8</sup> (see section 12.2.4). The reversal of this trend for the carbene ligands could be due to steric interaction between the phenyl rings and eq-carbonyls for (i) and (ii), or, since steric crowding would not be expected to be severe with the [C(OMe)H] ligand in (i), a result of the electronic nature of the carbene ligand and its bonding to the Re-centre.

(b) Di-substitution: 1,2-ax,eq-Re<sub>2</sub>(CO)<sub>8</sub>[C(OEt)(SiPh<sub>3</sub>)<sub>2</sub>]

The only di-substituted derivative of Re<sub>2</sub>(CO)<sub>10</sub> without a bridging ligand reported to date is 1,2-ax,eq-Re<sub>2</sub>(CO)<sub>8</sub>[C(OEt)(SiPh<sub>3</sub>)<sub>2</sub>].<sup>23</sup> This complex, like that of the eq-Re<sub>2</sub>(CO)<sub>9</sub> (carbene) complexes (i), (ii) and (iii) (*vide supra*) is staggered. One [C(OEt)(SiPh<sub>3</sub>)<sub>2</sub>] ligand occupies an equatorial position of Re(1), while the second carbene occupies the axial site on Re(2). The overall electronic stabilization of the complex governs this 1,2-ax,eq-substitution geometry.<sup>23</sup> In an axial position, the carbene ligand is a stronger  $\pi$ -donor than in an equatorial position. The resultant increased electron density on the Re-atom is reflected in the lengthening of the Re-Re bond length in 1,2-ax,eq-Re<sub>2</sub>(CO)<sub>8</sub>[C(OEt)(SiPh<sub>3</sub>)<sub>2</sub>] (3.091(2)Å) relative to that in eq-Re<sub>2</sub>(CO)<sub>9</sub> (carbene) (see Table 13.1), eg. av. 3.051(3)Å for eq-Re<sub>2</sub>(CO)<sub>9</sub>[C(OEt)(SiPh<sub>3</sub>)<sub>2</sub>].

The effect of acute Re-Re-CO and obtuse Re-Re-CO (carbene) angles observed for eq-Re<sub>2</sub>(CO)<sub>9</sub> (carbene) complexes (i)-(ii), (Table 13.2), is also found for 1,2-ax,eq-Re<sub>2</sub>(CO)<sub>8</sub>[C(OEt)(SiPh<sub>3</sub>)<sub>2</sub>],<sup>23</sup> viz. av. Re(1)-Re(2)-CO: 83°; av. Re(2)-Re(1)-CO: 86° and Re(2)-Re(1)-C(eq carbene): 96.9(8)° (Re(1)-Re(2)-C(ax carbene): 178.7(9)°).

TABLE 13.2: Average values of the Re-Re-C bond angles(°) for the eq-Re<sub>2</sub>(CO)<sub>9</sub>(carbene) structures (i)-(iii)

| Complex                | (i) eq-Re <sub>2</sub> (CO) <sub>9</sub> [CH(OMe)] <sup>a</sup> | (ii) eq-Re <sub>2</sub> (CO) <sub>9</sub> [C(OMe)(SiPh <sub>3</sub> )] <sup>b</sup> | (iii) eq-Re <sub>2</sub> (CO) <sub>9</sub> [C(OEt)(SiPh <sub>3</sub> )] <sup>b</sup> |
|------------------------|---|---|--|
| av. Re(2)-Re(1)-CO     | 82.8, 83.9 <sup>c</sup>   | 84  | 83, 84 <sup>c</sup>  |
| av. Re(1)-Re(2)-CO     | 86.5, 84.2 <sup>c</sup>   | 87  | 85, 85 <sup>c</sup>  |
| Re(2)-Re(1)-C(carbene) | 94.5, 97.9 <sup>c</sup>   | 98.1(8)   | 94(1), 98(1) <sup>c</sup>  |

<sup>a</sup> Data obtained from the Cambridge Crystallographic Data Base

<sup>b</sup> Ref. 253

<sup>c</sup> Two crystallographically independent molecules in the asymmetric unit

13.2.2 Structures with bridging ligands

(a) A bridging olefin -  $\text{Re}_2(\text{CO})_8\{\mu-(\eta^2, \eta^2\text{C}_4\text{H}_6)\}$

In  $\text{Re}_2(\text{CO})_8\{\mu-(\eta^2, \eta^2\text{C}_4\text{H}_6)\}$ ,<sup>153</sup> the  $\text{Re}_2(\text{CO})_8$  fragment, in which the carbonyl groups are eclipsed (as necessitated by the bridging olefin), is co-ordinated to the bridging 1,3-butadiene ligand in the trans-configuration. With the alkyl ligand acting as a 2-electron donor to each Re-atom, the compound obeys the 18-Electron Rule,<sup>154</sup> the Re-Re single bond being 3.114(1)Å.<sup>153</sup> Re-COax and Re-CO(trans to alkyl ligand) bond lengths are approximately the same, and ca. 0.1Å shorter than the Re-CO(trans to CO) bonds, in accordance with electronic expectations.<sup>155-157</sup> Further, Re-Re-COeq bond angles are less than or equal to 90°, i.e. the carbonyl ligands bend in towards the Re-Re bond, as noted for  $\text{Re}_2(\text{CO})_{10}$ .<sup>158, 159</sup> As expected,<sup>15</sup> the carbonyl ligands are slightly bent, with Re-C-O bond angles in the range 173 - 179°, averaging 177°.

(b) A bridging carbene -  $\text{Re}_2(\text{CO})_8\{\mu-\eta^1, \eta^3\text{CH}\cdot\text{CH}\cdot\text{CMe}_2\}$

In  $\text{Re}_2(\text{CO})_8\{\mu-\eta^1, \eta^3\text{CH}\cdot\text{CH}\cdot\text{CMe}_2\}$ ,<sup>160</sup> the two  $\text{Re}(\text{CO})_4$  fragments, which are eclipsed with respect to each other, are bridged by a  $\mu$ -allylidene ligand formed by ring opening of the cyclopropene. The  $\mu-(\text{CH}\cdot\text{CH}\cdot\text{CMe}_2)$  moiety is  $\eta^1$ -bonded to Re(1) and  $\eta^3$ -bonded to Re(2), resulting in the carbene ligand bridging the dirhenium unit in a highly asymmetric fashion. In accordance with the 18-Electron Rule,<sup>154</sup> a formal Re-Re single bond is required by the total of 34 valence electrons around the dirhenium unit. The Re-Re bond length of 3.058(1)Å is comparable to that of other Re-Re single bonded complexes (Table 13.1).

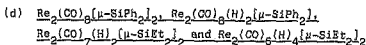
(c)  $\text{Re}_2(\text{CO})_8\{\mu-\text{NC}_5\text{H}_4\}\{\mu-\text{H}\}$  and  $\text{Re}_2(\text{CO})_7(\text{ONMe}_3)-$   
 $\{\mu-\text{NC}_5\text{H}_4\}\{\mu-\text{H}\}$

The complex  $\text{Re}_2(\text{CO})_8\{\mu-\text{NC}_5\text{H}_4\}\{\mu-\text{H}\}$ , and its derivative,  $\text{Re}_2(\text{CO})_7(\text{ONMe}_3)\{\mu-\text{NC}_5\text{H}_4\}\{\mu-\text{H}\}$ , are closely related structurally. In the case of  $\text{Re}_2(\text{CO})_8\{\mu-\text{NC}_5\text{H}_4\}\{\mu-\text{H}\}$ ,<sup>161</sup> the two crystallographically independent molecules (PI, Z = 4) are structurally very similar, with small differences attributable to crystal packing forces. An eclipsed conformation is

necessitated by the bridging pyridyl ligand, which is opposite to a symmetrical hydride bridge. (Re-H-Re bond angles of 120(6) and 116(5)°). Each Re-atom has a distorted octahedral co-ordination geometry, with C-Re-Re-C torsion angles of less than 6°. The Re-Re-COeq bond angles are less than or equal to 90°, i.e. the carbonyls bend in towards the Re-Re bond. The av. Re-CO (trans to CO) (1.99(1) and 2.00(2)Å) are greater than the av. Re-CO (not trans to CO) (1.94(3) and 1.95(2)Å) bond lengths, as predicted on electronic grounds.<sup>142</sup> Of the latter Re-CO bonds, the longest is that trans to C(pyridyl). Re-C-O bond angles are in the 175 - 179° range.

Closely related to the structure of  $\text{Re}_2(\text{CO})_8(\mu\text{-NC}_5\text{H}_4)(\mu\text{-H})$  is that of the  $\text{Re}_2(\text{CO})_7(\text{ONMe}_3)(\mu\text{-NC}_5\text{H}_4)(\mu\text{-H})$  molecule,<sup>143</sup> in which one of the equatorial carbonyl ligands trans to another CO-group, has been substituted with the  $\text{-ONMe}_3$  group. The eclipsed structure is maintained, but there are larger distortions from octahedral symmetry, with C-Re-Re-C torsion angles of ca. 10°, due to the bulkier (relative to CO)  $\text{Me}_3\text{NO}$ -group. The Re-H-Re angle is slightly larger at 131(17)°. Re-Re-C angles range from 83-110°. It is noteworthy that the Re-Re-O bond angle is acute (83.7(2)°). The remaining pair of trans carbonyls have the longest Re-CO bonds, with the shorter Re-CO bond being trans to the  $\text{ONMe}_3$  ligand. Again the Re-C-O bond angles range from 175 - 179°.

The Re-Re bond length of 3.2324(5)Å in  $\text{Re}_2(\text{CO})_7(\text{ONMe}_3)(\mu\text{-NC}_5\text{H}_4)(\mu\text{-H})$  is longer than that for  $\text{Re}_2(\text{CO})_8(\mu\text{-NC}_5\text{H}_4)(\mu\text{-H})$  (3.2088(4) and 3.1954(5)Å). This is ascribed to the larger steric requirements of the  $\text{Me}_3\text{NO}$  ligand.<sup>143</sup> Both the Re-Re bonds are single (in accordance with the 18-Electron Rule).



The above four complexes form a series of chemically and structurally related compounds. In all four molecules, an eclipsed conformation is necessitated by the bridging silane ligand(s), although molecular symmetry differs ( $\text{Re}_2(\text{CO})_8[\mu\text{-SiPh}_2]_2$ ,<sup>144,145</sup>  $\text{D}_2\text{h}$ ;  $\text{Re}_2(\text{CO})_8(\text{H})_2[\mu\text{-SiPh}_2]_2$ ,<sup>146</sup>  $\text{C}_2\text{v}$

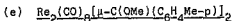


$\text{Re}_2(\text{CO})_7(\text{H})_2[\mu\text{-SiEt}_2]_2$ ,<sup>211</sup> Cs;  $\text{Re}_2(\text{CO})_6(\text{H})_4[\mu\text{-SiEt}_2]_2$ ,<sup>211</sup>  $\text{C}_2\text{h}$  (molecule possesses crystallographic  $\bar{1}$  symmetry). The non-bridging hydrogen atoms were not located directly, their positions being inferred from vacancies in the (distorted) octahedral metal co-ordination sphere; spectroscopic evidence indicated that the hydride ligands are terminally bonded to the rhenium atoms with no attractive interactions with the silicon atoms.<sup>212</sup>

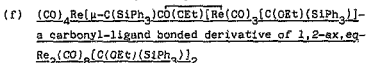
In all four structures,<sup>202-3</sup> the Re-Si bond length is approximately constant, with acute Re-Si-Re bond angles in the range 74 - 76°. There are, however, significant variations in the Re-Re single bond length, which has values of 3.001(1), 3.052(1), 3.084(1) and 3.121(2) Å for the complexes  $\text{Re}_2(\text{CO})_8[\mu\text{-SiPh}_2]_2$ ,<sup>202</sup>  $\text{Re}_2(\text{CO})_7(\text{H})_2[\mu\text{-SiEt}_2]_2$ ,<sup>202</sup>  $\text{Re}_2(\text{CO})_6(\text{H})_4[\mu\text{-SiEt}_2]_2$ <sup>211</sup> and  $\text{Re}_2(\text{CO})_8(\text{H})_2[\mu\text{-SiPh}_2]_2$ ,<sup>211</sup> respectively. Considering the first three cases, this increase in Re-Re bond length is due to the progressive replacement of a carbonyl by hydride ligands, which are weaker  $\pi$ -acceptors than CO.<sup>212</sup> This electronic effect is strong enough to counteract any possible Re-Re bond shortening due to reduced non-bonded repulsions with fewer eclipsed carbonyl groups (the above four complexes have 4, 2, 3 and 4 eclipsed CO pairs respectively). In the case of  $\text{Re}_2(\text{CO})_8(\text{H})_2[\mu\text{-SiPh}_2]_2$ , with only one silane bridge, the longer bond is ascribed to 0...0 repulsions between the two extra pairs of eclipsed carbonyls,<sup>202</sup> compared to  $\text{Re}_2(\text{CO})_7(\text{H})_2[\mu\text{-SiEt}_2]_2$ , which also has two hydride ligands.

Full details of the structure of  $\text{Re}_2(\text{CO})_8[\mu\text{-SiPh}_2]_2$ <sup>202-3</sup> have not been reported. For the other three structures, the av. Re-Re-CO bond angle is ca. 90° ( $\text{Re}_2(\text{CO})_8(\text{H})_2[\mu\text{-SiPh}_2]_2$ , 89.6(9)°;  $\text{Re}_2(\text{CO})_7(\text{H})_2[\mu\text{-SiEt}_2]_2$ , 90.4(5)°, and  $\text{Re}_2(\text{CO})_6(\text{H})_4[\mu\text{-SiEt}_2]_2$ , 90.2(3)°). In the case of  $\text{Re}_2(\text{CO})_8(\text{H})_2[\mu\text{-SiPh}_2]_2$ ,<sup>202</sup> the Re-COax bond lengths are shorter than the Re-COeq bond lengths. This is also true for  $\text{Re}_2(\text{CO})_6(\text{H})_4[\mu\text{-SiEt}_2]_2$ ,<sup>211</sup> but the differences are too slight to be significant. Further, for  $\text{Re}_2(\text{CO})_8(\text{H})_2[\mu\text{-SiPh}_2]_2$ , the bond Re-CO (trans to H) is longer than that trans to another CO. There are no significant

differences between the Re-CO bond lengths in  $\text{Re}_2(\text{CO})_7(\text{H})_2-[\mu\text{-SiEt}_2]_2$ .<sup>212</sup> In all these three structures, the Re-C-O bond angles are in the range 170 - 179°, as expected.<sup>21</sup>

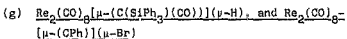


The structure of  $\text{Re}_2(\text{CO})_8[\mu\text{-C}(\text{OMe})(\text{C}_6\text{H}_4\text{Me-p})]_2$  resembles that of  $\text{Re}_2(\text{CO})_8[\mu\text{-SiPh}_2]_2$  (*vide supra*). The  $\text{Re}_2(\text{CO})_8[\mu\text{-C}(\text{OMe})(\text{C}_6\text{H}_4\text{Me-p})]_2$ <sup>177b</sup> molecule adopts an eclipsed structure, necessitated by the bridging ligands, and has crystallographic  $\text{C}_2$  symmetry. The Re-C-Re bridging angle is an acute 77(1)°, and the Re-Re bond short at 2.71(3)Å. The shortness of the Re-Re bond (Table 13.1) would seem to indicate some degree of multiple bonding, but more than a single Re-Re bond is not required by the 18-Electron Rule.



The molecule  $(\text{CO})_4\text{Re}[\mu\text{-C}(\text{SiPh}_3)\text{CO}(\text{OEt})\text{Re}(\text{CO})_3[\text{C}(\text{OEt})(\text{SiPh}_3)]]$ <sup>178c</sup> can be viewed as a derivative of 1,2-ax,eq- $\text{Re}_2(\text{CO})_8[\text{C}(\text{OEt})(\text{SiPh}_3)]_2$  (see section 13.2.1(b), in which the equatorially co-ordinated  $[\text{C}(\text{OEt})(\text{SiPh}_3)]_2$  ligand on Re(2) has become bridging, and a CO-group has formally inserted into the C-OEt bond, with the oxygen of the CO being bonded to Re(1) (Re(1)-O: 2.217(13)Å), Re(1) bearing the second axially substituted  $[\text{C}(\text{OEt})(\text{SiPh}_3)]$  ligand. (See Fig. 13.1).

The Re-Re bond is short at 2.937(1)Å. In terms of the 18-Electron Rule, a non-integral Re-Re bond order of 1½ is found. The bridging Re-C-Re angle is an acute 81.7(6)°. The C-C-(OEt)-O is essentially planar. The geometry of this complex is determined by the unusual double-bridging ligand.



The geometry of the  $\text{Re}_2(\text{CO})_8[\mu\text{-C}(\text{SiPh}_3)(\text{CO})](\mu\text{-H})$ <sup>178c</sup> molecule resembles that of  $\text{Re}_2(\text{CO})_8[\mu\text{-CPh}](\mu\text{-Br})$ .<sup>211</sup> For both molecules, the four carbonyls of the  $\text{Re}_2(\text{CO})_8$ -unit are eclipsed, as necessitated by the bridging carbene ligand, which is opposite to a bridging hydride (located indirectly) or bromide atom respectively. However, in the case of

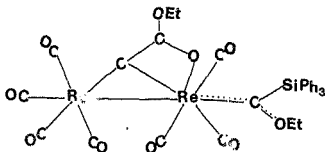


Figure 13.1: Schematic representation of the structure of  $(\text{CO})_4\text{Re}[\mu\text{-C}(\text{SiPh}_3)\text{C}(\text{OEt})]\text{Re}[\text{C}(\text{OEt})(\text{SiPh}_3)]$

$\text{Re}_2(\text{CO})_8[\mu\text{-C}(\text{Ph})](\mu\text{-Br})$ , the 18-Electron count can be satisfied without a rhenium-rhenium bond. (The rhenium-rhenium distance is not quoted for this complex<sup>211</sup>). For the related  $\text{Re}_2(\text{CO})_8[\mu\text{-C}(\text{SiPh}_3)(\text{CO})](\mu\text{-H})$ , application of the 18-Electron Rule gives a non-integral Re-Re bond order of  $1\frac{1}{2}$ . Some degree of multiple bonding is supported by the relatively short Re-Re bond length of 3.036(2)Å. (Table 13.1). A Re-Re bond order of  $1\frac{1}{2}$  is also found for the complex  $(\text{CO})_4\text{Re}[\mu\text{-C}(\text{SiPh}_3)\text{C}(\text{OEt})]\text{Re}(\text{CO})_3[\text{C}(\text{OEt})(\text{SiPh}_3)]$  with a Re-Re bond length of 2.937(1)Å (vide supra).

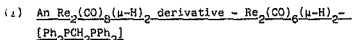
(h)  $\text{Re}_2(\text{CO})_8(\mu\text{-H})_2$  - an Re-Re double bond?

The  $\text{Re}_2(\text{CO})_8(\mu\text{-H})_2$  molecule,<sup>212</sup> with two hydride bridges (not located directly), adopts an eclipsed configuration, of molecular symmetry  $D_{2h}$ , and no significant differences from idealized octahedral metal co-ordination geometry.

The Re-Re bond length is short at 2.90Å. In accordance with the formal application of the 18-Electron Rule,<sup>212</sup> each

hydrogen donates half an electron to each Re-atom, requiring a double Re-Re bond. However, it has been suggested that the bonding in this complex can be described in alternate manners in terms of which a double Re-Re bond is not needed to balance the electron-counting.<sup>23</sup>

In such cases, molecular orbital calculations may be needed to evaluate the possible bonding modes, and electron density studies might provide useful information. However, owing to the relatively short Re-Re bond length, some degree of multiple bonding is usually ascribed to  $\text{Re}_2(\text{CO})_8(\mu\text{-H})_2$ . This is probably backed up by the formal application of the 18-Electron Rule, giving an Re-Re bond order of 2.



$\text{Re}_2(\text{CO})_6(\mu\text{-H})_2[\text{Ph}_2\text{PCH}_2\text{PPh}_2]^{23a,b}$  can be regarded as a derivative of  $\text{Re}_2(\text{CO})_8(\mu\text{-H})_2$ , with two of the CO ligands trans to CO replaced by the bis-phosphine ligand. The two hydrides (located indirectly from the distribution of carbonyls) bridge the Re-Re bond, and lie on either side of the  $\text{Re}_2\text{P}_2$ -plane.

For the 18-Electron Rule to hold, a double Re-Re bond is required. This supports the formal application of the 18-Electron Rule to  $\text{Re}_2(\text{CO})_8(\mu\text{-H})_2$ , to give a double Re-Re bond also. The bond length for  $\text{Re}_2(\text{CO})_8(\mu\text{-H})_2$ - $[\text{Ph}_2\text{PCH}_2\text{PPh}_2]$  and  $\text{Re}_2(\text{CO})_8(\mu\text{-H})_2$  are similar, and relatively short (2.893(2)<sup>23a,b</sup> and 2.90 Å<sup>23c</sup>, respectively.)

The structure of  $\text{Re}_2(\text{CO})_6(\mu\text{-H})_2[\text{Ph}_2\text{PCH}_2\text{PPh}_2]$  is eclipsed. Four of the carbonyls bend away from the Re-Re bond, with the av. Re-Re-CO angle of 134.6(10)°, cf ca. 90° for octahedral co-ordination of Re without bridging hydrides; this observed configuration has been confirmed by potential energy calculations. The deviation from octahedral co-ordination are probably due to steric restrictions imposed by the bulky bis-phosphine ligand. The mean cone angle<sup>23a</sup> for half  $\text{Ph}_2\text{PCH}_2\text{PPh}_2$  chelate: 121°.

The two phosphine atoms exhibit distorted tetrahedral co-ordination geometry. The two phenyl rings are

approximately parallel, with interplanar distances of  $3.4\text{\AA}$ , indicative of graphite packing. Hence packing forces could be responsible for distortions from idealized geometry. The carbonyl ligands are near-linear, with Re-C-O angles ranging from  $175 - 180^\circ$ .

(j)  $\text{Re}_2(\text{CO})_6(\mu\text{-H})(\mu\text{-NCHMe})(\text{Ph}_2\text{PCH}_2\text{PPh}_2)$  - derivative of  $\text{Re}_2(\text{CO})_6(\mu\text{-H})_2(\text{Ph}_2\text{PCH}_2\text{PPh}_2)$

$\text{Re}_2(\text{CO})_6(\mu\text{-H})(\mu\text{-NCHMe})(\text{Ph}_2\text{PCH}_2\text{PPh}_2)$  is derived from  $\text{Re}_2(\text{CO})_6(\mu\text{-H})_2(\text{Ph}_2\text{PCH}_2\text{PPh}_2)$  by insertion of MeCN into an Re-H bond.<sup>24a,c</sup> The NCHMe ligand symmetrically bridges the metal-metal bond, as does the hydride (from analysis of the carbonyl distribution) with the carbonyl groups eclipsed, as in  $\text{Re}_2(\text{CO})_6(\mu\text{-H})(\text{Ph}_2\text{PCH}_2\text{PPh}_2)$ .

The complex  $\text{Re}_2(\text{CO})_6(\mu\text{-H})(\mu\text{-NCHMe})(\text{Ph}_2\text{PCH}_2\text{PPh}_2)$  is electron precise, and in accordance with the 18-Electron Rule, the Re-Re bond is single. This is reflected in the Re-Re bond length of  $3.035(3)\text{\AA}$ , compared to that of  $2.893(2)\text{\AA}$  for  $\text{Re}_2(\text{CO})_6(\mu\text{-H})_2(\text{Ph}_2\text{PCH}_2\text{PPh}_2)$ , for which a double Re-Re bond is required in terms of the 18-Electron Rule.

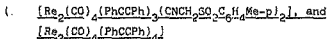
(k)  $\text{Re}_2(\text{CO})_6(\mu\text{-H})(\mu\text{-OH})(\mu\text{-Ph}_2\text{PCH}_2\text{PPh}_2)$  - a formal derivative of  $\text{Re}_2(\text{CO})_6(\mu\text{-H})_2(\mu\text{-Ph}_2\text{PCH}_2\text{PPh}_2)$

$\text{Re}_2(\text{CO})_6(\mu\text{-H})(\mu\text{-OH})(\mu\text{-Ph}_2\text{PCH}_2\text{PPh}_2)$ <sup>19a</sup> may be regarded as a formal derivative of  $\text{Re}_2(\text{CO})_6(\mu\text{-H})_2(\mu\text{-Ph}_2\text{PCH}_2\text{PPh}_2)$ ,<sup>24a,b</sup> with one bridging hydride replaced by a bridging hydroxide ligand. For both complexes, an Re-Re double bond is required in terms of the 18-Electron Rule. In the case of  $\text{Re}_2(\text{CO})_6(\mu\text{-H})_2(\mu\text{-Ph}_2\text{PCH}_2\text{PPh}_2)$ , the Re-Re bond is short at  $2.893(2)\text{\AA}$ , but for  $\text{Re}_2(\text{CO})_6(\mu\text{-H})(\mu\text{-OH})(\mu\text{-Ph}_2\text{PCH}_2\text{PPh}_2)$ , the Re-Re bond is surprisingly long at  $3.030(1)\text{\AA}$  (cf. Re-Re single bond value of  $3.035(3)\text{\AA}$  for the related  $\text{Re}_2(\text{CO})_6(\mu\text{-H})(\mu\text{-NCHMe})(\text{Ph}_2\text{PCH}_2\text{PPh}_2)$  (vide supra)).

Like  $\text{Re}_2(\text{CO})_6(\mu\text{-H})_2(\mu\text{-Ph}_2\text{PCH}_2\text{PPh}_2)$ ,  $\text{Re}_2(\text{CO})_6(\mu\text{-H})(\mu\text{-OH})(\mu\text{-Ph}_2\text{PCH}_2\text{PPh}_2)$ <sup>19a</sup> has a distorted octahedral co-ordination geometry about each rhenium atom. The hydride and hydroxo bridges are both slightly asymmetric, and lie opposite each other on either side of the  $\text{Re}_2\text{P}_2$ -plane.

The Re-O-Re angle is 88.6(2)°. The structure is eclipsed. The Re-Re-P and Re-Re-CO(trans to P) angles are ca. 90°, but the remaining four carbonyls bend away from the Re-Re bond, with the av. Re-Re-CO angle of 135.3(2)°. Similar deviations are observed for the related  $\text{Re}_2(\text{CO})_6(\mu\text{-H})_2[\mu\text{-Ph}_2\text{PCH}_2\text{PPh}_2]$  (section 13.2.2(i)), and probably reflect steric repulsions between the carbonyls and the bulky phosphine ligand (Polman cone angle<sup>11a</sup> for half of  $\text{P}_1_2\text{PCH}_2\text{PPh}_2$ : 121°). The phenyl rings are approximately parallel, as for  $\text{Re}_2(\text{CO})_6(\mu\text{-H})_2[\mu\text{-Ph}_2\text{PCH}_2\text{PPh}_2]$ .

In  $\text{Re}_2(\text{CO})_6(\mu\text{-H})(\mu\text{-OH})(\mu\text{-Ph}_2\text{PCH}_2\text{PPh}_2)$ ,<sup>11b</sup> the av. Re-CO bond length (1.921Å) is significantly shorter than in  $\text{Re}_2(\text{CO})_{10}$  (1.975Å).<sup>11c</sup> This may reflect stronger Re-CO bonding due to increased electron density on the metal atoms, since phosphine is a poor  $\pi$ -acceptor compared to a CO.<sup>12a</sup> Further, the Re-CO(trans to P) bond lengths are longer than those trans to H or OH ligands, which do not have  $\pi$ -acceptor character<sup>11c</sup> (av. 1.950Å and 1.907Å respectively). This difference is due to competition for  $\pi$ -electron density<sup>11c</sup> between the carbonyl and trans-phosphine ligand. The carbonyl ligands are near-linear, with Re-C-O angles ranging from 175 - 180°.



The mixed acetylene-isonitrile derivative,  $[\text{Re}(\text{CO})_4(\text{PhCCPh})_3(\text{CNCH}_2\text{SO}_2\text{C}_6\text{H}_4\text{Me-p})_2]$ ,<sup>11c</sup> has an interesting structure. The three acetylene molecules are linked in a chain, with the end carbon atoms of the chain each  $\sigma$ -bonded to one rhenium atom, and with the two neighbouring carbon atoms, forming an allyl ligand to the other rhenium atom. The two isonitrile ligands are terminally bonded to one Re-atom only, occupying positions *cis* to each other. The RNC ligands are slightly bent with av. C-N-C angle of 167.6(7)°, a C-N-R angle greater than 170° being considered linear for terminal RNC ligands.<sup>11b</sup> Slight deviations from linearity could be due to steric crowding. Both the isonitrile and carbonyl ligands co-ordinate in a near-linear fashion, with av. values of 174.6(7) and 176.5(9)° for Re-C-N and Re-C-O angles respectively.

Although the Re-Re bond length of 2.786(1)Å is relatively short, the Re-Re bond is only a single bond if the 18-Electron Rule is applied, with (PhCCPh)<sub>3</sub> acting as an 8-electron donor. The relatively short Re-Re bond length could be largely due to the steric restrictions imposed by the 6-atom carbon chain linked to the two metal atoms.

A partial crystal structure of the related complex, [Re<sub>2</sub>(CO)<sub>4</sub>(PhCCPh)<sub>4</sub>],<sup>21,22</sup> has been determined, but disorder problems prevented refinement. The chain of three acetylene molecules is bonded as in [Re<sub>2</sub>(CO)<sub>4</sub>(PhCCPh)<sub>3</sub>-(CNCH<sub>2</sub>SO<sub>2</sub>C<sub>6</sub>H<sub>4</sub>Me-p)<sub>2</sub>], with the fourth acetylene molecule separately bonded to one Re-atom only, taking the place of the two RNC ligands.

The Re-Re bond length is ca. 2.78Å, once again relatively short, but similar to the above single Re-Re bond length of 2.786(1)Å. However, in the case of [Re<sub>2</sub>(CO)<sub>4</sub>-(PhCCPh)<sub>4</sub>], the Re-Re bond is probably a double bond, since with the fourth PhCCPh ligand (replacing the two RNC ligands) co-ordinated to only one Re-atom acting as a 2-electron donor, the 18-Electron Rule requires a double Re-Re bond, and it is difficult to envisage how the lone PhCCPh ligand can act as more than a two-electron donor when co-ordinated to only one metal atom. This example demonstrates that metal-metal bond length is not a reliable indication of metal-metal bond order, especially where geometric constraints may be important.

### 13.3 Assessment

From the foregoing structural study of dirhenium decacarbonyl derivatives, it is possible to draw some general conclusions regarding the modification of Re<sub>2</sub>(CO)<sub>10</sub> by ligands L. These are outlined below.

#### 13.3.1 The Re-Re bond length

The Re-Re bond length alone provides little information on the nature of the metal-metal bonding. All factors must be considered.

- (a) Bond Order: Bond order is usually assigned on the basis of the 18-Electron Rule. Where ambiguities arise, the answer is uncertain. A more reliable method is needed for such cases.
- (b) Electronic nature of ligands: In a closely related series, a ligand L which is a weaker  $\pi$ -acceptor than CO, may significantly increase the Re-Re bond length.
- (c) Steric factor: Repulsive interactions between eclipsed carbonyl groups may increase the Re-Re bond length.
- (d) Bridging ligands: A bridging ligand with a small bite may result in a seemingly anomalous short Re-Re bond length.

#### 13.3.2 The Re-CO bond lengths

The Re-COax bonds are shorter than Re-COeq bonds; eq-Re<sub>2</sub>(CO)<sub>9</sub>L substitution results, unless steric factors dominate. The Re-CO bond trans to L, a poorer  $\pi$ -acceptor than CO, is shorter than that trans to another CO; cis-dieq-Re<sub>2</sub>(CO)<sub>8</sub>(L)<sub>2</sub> substitution results, in the absence of steric constraints.

#### 13.3.3 Molecular conformation

Molecules without bridging ligands adopt a staggered conformation. Bridging ligands necessitate an eclipsed conformation.

#### 13.3.4 OC-Re-CO bond angles

Generally, Re-Re-CO bond angles are less than or equal to 90° i.e. the carbonyls bend in towards the Re-Re bond. Where this is not the case, severe steric restraints are imposed on the structure by bulky ligands, resulting in pronounced distortions from the ideal geometry.

#### 13.3.5 Re-C-O bond angles

The Re-C-O bond angles are always in the range 170 - 179°. The same is true for Re-C-N bond angles of isonitrile ligands.

#### 13.3.6 Packing

Small deviations in structure (from ideal geometry) probably stem from interaction with neighbouring molecules i.e. crystal packing.



XIV. X-RAY CRYSTALLOGRAPHIC STUDIES OF ISONITRILE DERIVATES OF  
 $M_2(CO)_{10}$  ( $M = Re, Mn$ )

14.1 Introduction

Although the structures of the parent carbonyls,  $Re_2(CO)_{10}$  and  $Mn_2(CO)_{10}$ , have been determined,<sup>158</sup> and studies made of the bonding in these complexes,<sup>159</sup> no X-ray crystal structures have been reported of isonitrile substituted derivatives,  $Mn_2(CO)_{10-n}(CNR)_n$  ( $M = Re, Mn$ ). As part of a systematic study of the structural and chemical properties of isonitrile derivatives of dirhenium carbonyl,  $Re_2(CO)_{10-n}(CNR)_n$  ( $n = 1-4$ ), an X-ray crystallographic study of a series of representative complexes was undertaken.

Specifically, his X-ray Crystallographic study was undertaken with the aim, firstly, of establishing the stereochemistry of the mono- to tetra-isonitrile-substituted dirhenium carbonyl derivatives, and secondly, of obtaining bond length and bond angle data relating to the structural effect (if any) of increasing degree of isonitrile substitution. In particular, any weakening of the metal-metal bond would be expected to be reflected in an increase in the M-M bond length. Since isonitriles are weaker  $\pi$ -acceptors than carbonyls,<sup>61</sup> substitution of isonitriles for carbonyls in  $M_2(CO)_{10}$  would result in increased localization of  $\pi$ -electron charge on the metal, increasing  $\pi$ -electron repulsions and thereby weakening the M-M bond.<sup>152b</sup>

Obviously, the structure of the parent carbonyl,  $Re_2(CO)_{10}$ , is of interest in the context of this study, and this structure has been reported in the literature,<sup>158</sup> together with the structure of the isomorphous  $Mn_2(CO)_{10}$ . (Monoclinic space group  $I2/a$ ,  $Z = 4$ ). The molecules adopt a staggered conformation, with point group symmetry  $D_{4d}$ . A feature of both structures is the shorter M-COax bond length, compared to the M-COeq bond lengths. This is ascribed to the competition for  $d\pi$ -electrons between pairs of mutually trans CO ligands.<sup>158</sup>

Consequently, on electronic grounds, substitution would be predicted to be equatorial rather than axial. However,

with bulky ligands such as phosphines, steric factors may dominate, resulting in axial substitution, as has been shown by the X-ray crystal structure of  $ax-[Mn_2(CO)_9(PMe_2Ph)]^{22}$  (Tolman cone angle for  $PMe_2Ph$ :  $122^\circ^{23}$ ;  $141.7^\circ^{24}$ ). Hence, for monosubstituted derivatives of  $M_2(CO)_9$  ( $M = Re, Mn$ ), there are two possibilities (Fig. 14.1), viz. (IA) equatorial, or (IB) axial substitution.

With disubstituted complexes, there are more possibilities. With bulky phosphine ligands, diaxial substitution may be found, as has been shown by X-ray crystal structures of diax- $[Mn_2(CO)_8(PMePh_2)_2]^{25}$  (Tolman cone angle for  $PMePh_2$ :  $136^\circ^{26}$ ), diax- $[Mn_2(CO)_8(PEt_3)_2]$  (Tolman cone angle for  $PEt_3$ :  $132^\circ^{27}$ ;  $166.4^\circ^{28}$ ) and diax- $[Re_2(CO)_8(PMe_2Ph)_2]$  (see ch 15E) (Tolman cone angle for  $PMe_2Ph$ :  $122^\circ^{23}$ ;  $141.7^\circ^{24}$ ). However, for di-isocyanide derivatives, diaxial substitution is not expected, because for this geometry of point group  $D_{4d}$ , only two  $\nu(CO)$  bands are predicted in the IR spectrum (as is indeed observed for the above biphosphine derivatives, see ch XV), but the IR spectra of the di-isocyanide derivatives are much more complex (see ch XI). Axial-equatorial substitution is also a possibility, and has been observed for some  $Re_2(CO)_8(PR_3)_2$  complexes (see ch XV), but is considered unlikely for the smaller isocyanide ligands, in view of the electronic factors favouring equatorial substitution (vide supra). Further, trans-substitution is electronically disfavoured.<sup>13</sup> Even considering only cis-diequatorial substitution, there are still two possibilities (Fig 14.2), viz. (IIa) with the two RNC ligands on the same metal atom, or on different metal atoms (conformers (IIb) and (IIc)).

Several structures are also possible for the trisubstituted case, considering only cis-equatorial substitution (vide supra). (Fig. 14.3, IIIa-c). Considering the case of tetrasubstitution, there are again several cis-equatorially substituted possibilities, assuming two RNC ligands on each metal atom (Fig 14.4, IVa-c). Although repulsive interactions between equatorial CO groups are expected to be less in the staggered than eclipsed conformation,<sup>13</sup>

here the eclipsed conformation (IVc) is considered as well, since from steric considerations of the RNC ligands, this might be expected to be the most favourable structure.

The crystal and molecular structures were determined of the complexes  $\text{Re}_2(\text{CO})_9(\text{CNBu}^t)$  (I),  $\text{Re}_2(\text{CO})_8(\text{CNC}_6\text{H}_3\text{Me}_2-2,6)_2$  (II),  $\text{Re}_2(\text{CO})_7(\text{CNMe})_2$  (III) and  $\text{Re}_2(\text{CO})_6(\text{CNC}_6\text{H}_3\text{Me}_2-2,6)_4$  (IV). The X-ray structure of the di-isocyanide dimanganese carbonyl derivative,  $\text{Mn}_2(\text{CO})_8(\text{CNBu}^t)_2$  (V), was also determined, in order to establish whether certain differences observed in the IR and  $^1\text{H}$  NMR spectra of  $\text{Re}_2(\text{CO})_8(\text{CNR})_2$  and of  $\text{Mn}_2(\text{CO})_8(\text{CNR})_2$  complexes (see sections 11.4.1 and 11.4.2) could be correlated with structural differences on the molecular level. The structure of  $\text{Mn}_2(\text{CO})_6(\text{CNC}_6\text{H}_3\text{Me}_2-2,6)_4$  (VI) was also investigated by X-ray Crystallography, with the aims of obtaining bond parameter data for a tetra-isocyanide dimanganese derivative, and establishing whether differences observed in the IR and  $^1\text{H}$  NMR spectra of  $\text{Re}_2(\text{CO})_6(\text{CNC}_6\text{H}_3\text{Me}_2-2,6)_4$  and  $\text{Mn}_2(\text{CO})_6(\text{CNC}_6\text{H}_3\text{Me}_2-2,6)_4$  (see sections 11.4.1 and 11.4.2) could have a structural basis.

#### 14.2 X-ray Crystallographic Studies

##### 14.2.1 Structure of $\text{Re}_2(\text{CO})_9(\text{CNBu}^t)$ (I)

The molecular structure of  $\text{Re}_2(\text{CO})_9(\text{CNBu}^t)$  and the numbering system used in the crystal structure determination is shown in Fig. 14.5. Bond lengths and bond angles are given in Tables 14.1 and 14.2 respectively. The compound crystallizes in the orthorhombic space group Pbcu, with  $Z = 8$ . A view of the unit cell, looking down the  $b$ -axis is shown in Fig. 14.6.

Substitution was found to be equatorial (Fig. 14.1(Ia)), as predicted (*vide supra*). This equatorial substitution of CO by  $\text{CNBu}^t$  is in keeping with previous arguments on the final position of the incoming ligand in an octahedral environment.<sup>102</sup>

The two halves of the molecule are staggered with respect to each other, as in the parent carbonyl,  $\text{Re}_2(\text{CO})_{10}$ .<sup>103</sup> This staggered geometry presumably arises from steric considerations (i.e. reduced interaction of equatorial CO

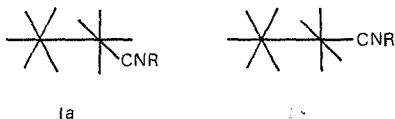


Figure 14.1: The two possible structures of  $\text{Re}_2(\text{CO})_9(\text{CNR})$ :  
(Ia) equatorial substitution, (Ib) axial substitution

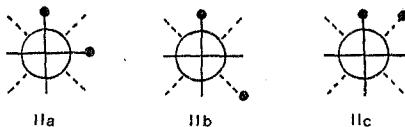
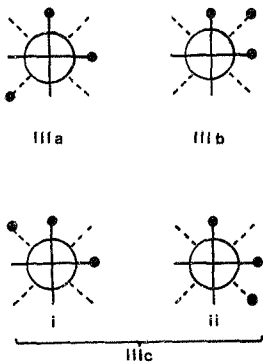
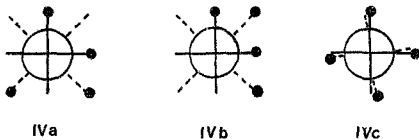


Figure 14.2: Newman projections of possible structures of  
 $\text{M}_2(\text{CO})_8(\text{CNR})_2$  ( $\text{M} = \text{Re}, \text{Mn}$ ), as viewed down the  
M-M axis ( $\bullet = \text{RNC}$ )



**Figure 14.3:** Newman projections of possible conformations of  $\text{Fe}_2(\text{CO})_7(\text{CNR})_3$ , as viewed down the Re-Re axis (● = RNC)



**Figure 14.4:** Newman projections of possible conformations of  $\text{M}_2(\text{CO})_6(\text{CNR})_4$  (M = Re, Mn), as viewed down the M-M axis (● = RNC)

groups on the two Re atoms),<sup>15</sup> and has been observed in all previously reported structures of  $\text{Re}_2(\text{CO})_{10-n}(\text{L})_n$  ( $n = 1, 2$ ) derivatives not containing bridging ligands (see ch. XIII).

The axial Re-CO bond distance (av.  $1.902(19)\text{\AA}$ ) is shorter than the average equatorial Re-CO bond distance (av.  $1.983(20)\text{\AA}$ ), excluding Re-C(1) in which the CO group is trans to the  $\text{Bu}^t\text{NC}$  group ( $1.916(18)\text{\AA}$ ). This effect of a shorter Re-C(ox) bond length relative to the Re-COeq bond length has been observed in the structure of  $\text{Re}_2(\text{CO})_{10}$ ,<sup>15</sup> and is ascribed to competition for d $\pi$ -electron density between mutually trans pairs of equatorial carbonyls. The shorter Re-C(1) bond length (cf. av. Re-COeq) could also reflect the greater  $\pi$ -acceptor ability of the CO group relative to the  $\text{Bu}^t\text{NC}$  group.<sup>15</sup>

#### 14.2.2. Structure of $\text{Re}_2(\text{CO})_8(\text{CNC}_6\text{H}_5\text{Me}_2-2,6)_2$ (II)

The compound (II) was found to crystallize in the centrosymmetric triclinic space group  $\text{P}\bar{1}$ , with  $Z = 2$ . The molecular structure of  $\text{Re}_2(\text{CO})_8(\text{CNC}_6\text{H}_5\text{Me}_2-2,6)_2$  and the numbering system used in the crystal structure determination is shown in Fig. 14.7. Bond lengths and bond angles are given in Tables 14.3 and 14.4 respectively.

Viewed down the Re-Re bond, the conformation is staggered, as expected.<sup>15</sup> In the crystal, the molecule adopts the conformation (IIb) (Fig. 14.2), with the two isonitrile ligands on different Re-atoms. This conformation might be expected to be sterically most favourable, since the bulky 2,6- $\text{Me}_2\text{C}_6\text{H}_3\text{NC}$  ligands ("fan-shaped" angles<sup>15</sup>:  $108^\circ$  (widthness) and  $53^\circ$  (thickness)) are as far away from each other as possible, but in the crystal the conformation adopted is probably also determined by crystal packing considerations (*vide infra*).

The phenyl rings are essentially planar. The mean planes of the C6-rings are  $73.1^\circ$  to each other. This is probably determined mainly by crystal packing forces. As can be seen from the packing diagram (Fig. 14.8), viewed down the  $b$ -axis, the molecules pack in rows, with the

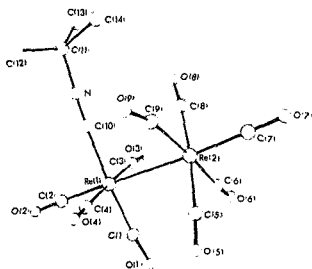


Figure 14.5: ORTEP<sup>44</sup> view of the  $\text{Re}_2(\text{CO})_9(\text{CNBu}^t)$  molecule (I), showing the numbering system used

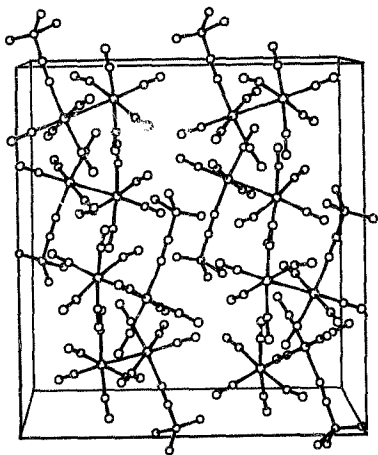


Figure 14.6: ORTEP<sup>35</sup> view of the unit cell of  $\text{Re}_2(\text{CO})_9(\text{CNBU}^t)(\text{I})$ , looking down the  $b$ -axis



TABLE 14.1: Bond lengths (Å) for  $\text{Re}_2(\text{CO})_9(\text{CNBu}^t)(1)$

|             |           |             |           |
|-------------|-----------|-------------|-----------|
| Re(1)-Re(2) | 3.048(1)  |             |           |
| Re(1)-C(1)  | 1.916(18) | C(1)-O(1)   | 1.149(18) |
| Re(1)-C(2)  | 1.916(18) | C(2)-O(2)   | 1.142(17) |
| Re(1)-C(3)  | 2.089(20) | C(3)-O(3)   | 1.077(18) |
| Re(1)-C(4)  | 1.974(21) | C(4)-O(4)   | 1.144(19) |
| Re(1)-C(10) | 2.064(15) | C(10)-N     | 1.130(15) |
| Re(2)-C(5)  | 1.913(20) | C(5)-O(5)   | 1.139(20) |
| Re(2)-C(6)  | 1.999(22) | C(6)-O(6)   | 1.151(20) |
| Re(2)-C(7)  | 1.887(21) | C(7)-O(7)   | 1.158(20) |
| Re(2)-C(8)  | 1.928(18) | C(8)-O(8)   | 1.169(18) |
| Re(2)-C(9)  | 1.965(20) | C(9)-O(9)   | 1.133(18) |
| N-C(11)     | 1.481(20) | C(11)-C(12) | 1.503(39) |
| C(11)-C(14) | 1.667(48) | C(11)-C(13) | 1.486(33) |

TABLE 14.2: Bond angles (°) for  $\text{Re}_2(\text{CO})_9(\text{CNBu}^t)(\text{I})$

|                   |           |                   |           |
|-------------------|-----------|-------------------|-----------|
| C(10)-N-C(11)     | 175.7(18) |                   |           |
| Re(1)-C(1)-O(1)   | 178.1(15) | Re(2)-C(5)-O(5)   | 176.5(18) |
| Re(1)-C(2)-O(2)   | 175.8(15) | Re(2)-C(6)-O(6)   | 174.6(18) |
| Re(1)-C(3)-O(3)   | 175.3(16) | Re(2)-C(7)-O(7)   | 178.2(18) |
| Re(1)-C(4)-O(4)   | 177.1(16) | Re(2)-C(8)-O(8)   | 175.8(16) |
| Re(1)-C(10)-N     | 175.5(13) | Re(2)-C(9)-O(9)   | 175.7(17) |
| C(1)-Re(1)-Re(2)  | 87.4(5)   | C(5)-Re(2)-Re(1)  | 88.2(5)   |
| C(1)-Re(1)-C(2)   | 93.1(7)   | C(5)-Re(2)-C(6)   | 87.8(8)   |
| C(1)-Re(1)-C(3)   | 90.1(7)   | C(5)-Re(2)-C(7)   | 93.2(8)   |
| C(1)-Re(1)-C(4)   | 39.7(7)   | C(5)-Re(2)-C(8)   | 172.6(7)  |
| C(1)-Re(1)-C(10)  | 174.9(6)  | C(5)-Re(2)-C(9)   | 92.8(8)   |
| C(2)-Re(1)-Re(2)  | 177.4(5)  | C(6)-Re(2)-Re(1)  | 88.8(6)   |
| C(2)-Re(1)-C(3)   | 93.5(7)   | C(6)-Re(2)-C(7)   | 94.4(8)   |
| C(2)-Re(1)-C(4)   | 91.3(7)   | C(6)-Re(2)-C(8)   | 93.1(8)   |
| C(2)-Re(1)-C(10)  | 92.1(6)   | C(6)-Re(2)-C(9)   | 172.2(8)  |
| C(3)-Re(1)-Re(2)  | 89.0(5)   | C(7)-Re(2)-Re(1)  | 176.5(6)  |
| C(3)-Re(1)-C(4)   | 175.2(7)  | C(7)-Re(2)-C(8)   | 94.1(8)   |
| C(3)-Re(1)-C(10)  | 89.7(6)   | C(7)-Re(2)-C(9)   | 93.4(8)   |
| C(4)-Re(1)-Re(2)  | 86.2(5)   | C(8)-Re(2)-Re(1)  | 84.4(5)   |
| C(4)-Re(1)-C(10)  | 90.1(7)   | C(8)-Re(2)-C(9)   | 85.4(7)   |
| C(10)-Re(1)-Re(2) | 87.5(4)   | C(9)-Re(2)-Re(1)  | 83.4(5)   |
| N-C(11)-C(12)     | 111.2(22) | C(12)-C(11)-C(13) | 126.6(26) |
| N-C(11)-C(13)     | 110.1(19) | C(12)-C(11)-C(14) | 96.1(23)  |
| N-C(11)-C(14)     | 104.9(21) | C(13)-C(11)-C(14) | 104.6(23) |

orientation of the rings alternating along a row, and with the rings lining up in a coplanar manner (less than 2° deviation) with those of the row above.

#### 14.2.3. Structure of $Mn_2(CO)_8(CNBU^t)_2$ (V)

The molecular structure of  $Mn_2(CO)_8(CNBU^t)_2$  and the numbering system used in the crystal structure determination is shown in Fig. 14.9. Bond lengths and bond angles are given in Tables 14.5 and 14.6 respectively. The compound crystallizes in the monoclinic space group  $P2_1/n$ , with  $Z = 4$ . Fig. 14.10 shows the unit cell, viewed down the b-axis.

In contrast to  $Re_2(CO)_8(CNC_6H_5Me_2-2,6)_2$  (vide supra), the conformation of the  $Mn_2(CO)_8(CNBU^t)_2$  molecule is (IIa) (Fig. 14.2), with both isonitrile ligands in cis-equatorial positions on the same Mn-atom. Electronically, this might be expected to be the most favourable geometry, since the isonitrile ligand is a stronger  $\sigma$ -donor, but weaker  $\pi$ -acceptor than carbonyl,<sup>11</sup> resulting in a cis-labilization effect<sup>12</sup> (but see section 14.4).

From <sup>1</sup>H NMR data (section 11.4.2.), in the case of the di-isonitrile derivatives of dimanganese carbonyl, two isomers, (IIa) and (IIb) (or (IIc)) (Fig. 14.2) appear to exist in solution, the isomer (IIa) (which is the minor component-ratio of (IIa):(IIb) is 1:5) having been preferentially crystallized out of solution (pentane, -5°C) in the case of  $Mn_2(CO)_8(CNBU^t)_2$ . However, with the di-isonitrile derivatives of dirhenium carbonyl, (with the exception of MeNC) the <sup>1</sup>H NMR spectra give no evidence of another isomer in addition to (IIb). The formation of isomers for  $Mn_2(CO)_8(CNBU^t)_2$  will be further discussed in section 14.4.

#### 14.2.4 Structure of $Re_2(CO)_7(CNMe)_3$ (III)

Complex (III) crystallizes in the monoclinic space group  $P2_1/n$ , with  $Z = 4$ . Unfortunately the structure displayed disorder (vide infra). Fig. 14.11 shows the molecular structure, and the numbering system used in the crystal structure analysis. Bond lengths and bond angles

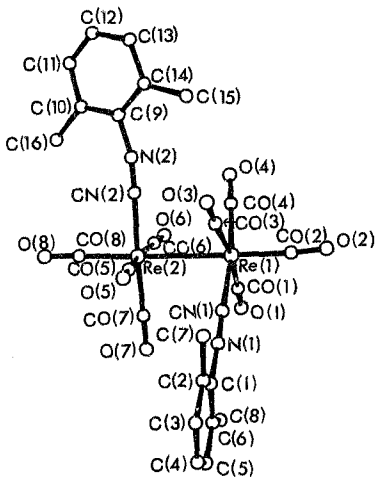


Figure 14.7: ORTEP<sup>a</sup> view of the  $\text{Re}_2(\text{CO})_8(\text{CNC}_6\text{H}_3\text{Me}_2-2,6)_2$  molecule (II), showing the numbering system used.

Figure 14.8: ORTEP<sup>+</sup> view of the unit cell of  $\text{Re}_2(\text{CO})_8(\text{CNC}_5\text{H}_4\text{Me}_2-2,6)_2$  (III), looking down the  $\bar{b}$ -axis

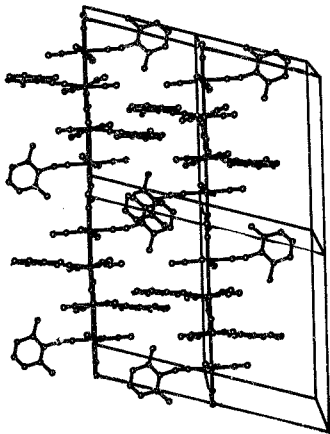


TABLE 14.3: Bond lengths (Å) for  $\text{Re}_2(\text{CO})_8(\text{CNC}_6\text{H}_3\text{Me}_2-2,6)_2(\text{II})$

|             |          |             |          |
|-------------|----------|-------------|----------|
| Re(1)-Re(2) | 3.047(0) |             |          |
| Re(1)-CO(1) | 1.982(6) | CO(1)-O(1)  | 1.131(6) |
| Re(1)-CO(2) | 1.916(6) | CO(2)-O(2)  | 1.151(6) |
| Re(1)-CO(3) | 1.976(6) | CO(3)-O(3)  | 1.138(6) |
| Re(1)-CO(4) | 1.980(7) | CO(4)-O(4)  | 1.125(7) |
| Re(2)-CO(5) | 1.951(6) | CO(5)-O(5)  | 1.141(6) |
| Re(2)-CO(6) | 1.995(7) | CO(6)-O(6)  | 1.117(6) |
| Re(2)-CO(7) | 1.969(6) | CO(7)-O(7)  | 1.126(6) |
| Re(2)-CO(8) | 1.931(6) | CO(8)-O(8)  | 1.143(6) |
| Re(1)-CN(1) | 2.041(6) | CN(1)-N(1)  | 1.157(6) |
| Re(2)-CN(2) | 2.059(6) | CN(2)-N(2)  | 1.138(6) |
| N(1)-C(1)   | 1.444(7) | N(2)-C(9)   | 1.413(7) |
| C(1)-C(2)   | 1.373(8) | C(9)-C(10)  | 1.407(7) |
| C(2)-C(3)   | 1.465(9) | C(10)-C(11) | 1.427(8) |
| C(3)-C(4)   | 1.418(9) | C(11)-C(12) | 1.340(9) |
| C(4)-C(5)   | 1.318(9) | C(12)-C(13) | 1.403(8) |
| C(5)-C(6)   | 1.441(8) | C(13)-C(14) | 1.467(8) |
| C(6)-C(1)   | 1.417(8) | C(14)-C(9)  | 1.406(7) |
| C(2)-C(7)   | 1.526(8) | C(10)-C(16) | 1.487(9) |
| C(6)-C(8)   | 1.495(8) | C(14)-C(15) | 1.533(8) |

TABLE 14.4: Bond angles(°) for  $\text{Re}_2(\text{CO})_8(\text{CNC}_6\text{H}_5\text{Me}_2-2,6)_2(\text{II})$ 

|                   |          |                   |          |
|-------------------|----------|-------------------|----------|
| Re(1)-CO(1)-O(1)  | 177.8(6) | Re(2)-CO(5)-O(5)  | 178.8(5) |
| Re(1)-CO(2)-O(2)  | 175.7(5) | Re(2)-CO(5)-O(6)  | 177.6(5) |
| Re(1)-CO(3)-O(3)  | 177.8(5) | Re(2)-CO(7)-O(7)  | 179.8(2) |
| Re(1)-CO(4)-O(4)  | 177.8(5) | Re(2)-CO(8)-O(8)  | 178.2(5) |
| Re(1)-CN(1)-N(1)  | 178.0(5) | Re(2)-CN(2)-N(2)  | 176.8(5) |
| CN(1)-N(1)-C(1)   | 175.9(5) | CN(2)-N(2)-C(9)   | 166.1(5) |
| CO(1)-Re(1)-Re(2) | 88.0(2)  | CO(5)-Re(2)-Re(1) | 86.4(1)  |
| CO(1)-Re(1)-CO(2) | 94.0(2)  | CO(5)-Re(2)-CO(6) | 172.0(2) |
| CO(1)-Re(1)-CO(3) | 171.1(2) | CO(5)-Re(2)-CO(7) | 91.3(2)  |
| CO(1)-Re(1)-CO(4) | 91.0(2)  | CO(5)-Re(2)-CO(8) | 92.3(2)  |
| CO(1)-Re(1)-CN(1) | 88.1(2)  | CO(5)-Re(2)-CN(2) | 91.0(2)  |
| CO(2)-Re(1)-Re(2) | 178.0(2) | CO(6)-Re(2)-Re(1) | 85.7(1)  |
| CO(2)-Re(1)-CO(3) | 94.2(2)  | CO(6)-Re(2)-CO(7) | 89.4(2)  |
| CO(2)-Re(1)-CO(4) | 94.4(2)  | CO(6)-Re(2)-CO(8) | 95.6(2)  |
| CO(2)-Re(1)-CN(1) | 93.8(2)  | CO(6)-Re(2)-CN(2) | 88.0(2)  |
| CO(3)-Re(1)-Re(2) | 83.8(1)  | CO(7)-Re(2)-Re(1) | 87.9(1)  |
| CO(3)-Re(1)-CO(4) | 91.8(2)  | CO(7)-Re(2)-CO(8) | 94.0(2)  |
| CO(3)-Re(1)-CN(1) | 87.9(2)  | CO(7)-Re(2)-CN(2) | 176.7(2) |
| CO(4)-Re(1)-Re(2) | 85.3(2)  | CO(8)-Re(2)-Re(1) | 177.8(2) |
| CO(4)-Re(1)-CN(1) | 171.8(2) | CO(8)-Re(2)-CN(2) | 89.3(2)  |
| CN(1)-Re(1)-Re(2) | 86.5(1)  | CN(2)-Re(2)-Re(1) | 89.9(1)  |
| C(6)-C(1)-C(2)    | 125.7(6) | C(14)-C(9)-C(10)  | 124.9(6) |
| C(1)-C(2)-C(3)    | 117.1(6) | C(9)-C(10)-C(11)  | 115.3(6) |
| C(2)-C(3)-C(4)    | 115.5(7) | C(10)-C(11)-C(12) | 121.7(6) |
| C(3)-C(4)-C(5)    | 126.7(8) | C(11)-C(12)-C(13) | 124.4(7) |
| C(4)-C(5)-C(6)    | 119.3(7) | C(12)-C(13)-C(14) | 116.5(6) |
| C(5)-C(6)-C(1)    | 115.6(6) | C(13)-C(14)-C(9)  | 117.1(8) |
| N(1)-C(1)-C(2)    | 115.7(5) | N(2)-C(9)-C(10)   | 117.3(5) |
| N(1)-C(1)-C(6)    | 118.6(5) | N(2)-C(9)-C(14)   | 117.8(5) |
| C(1)-C(2)-C(7)    | 124.5(6) | C(9)-C(10)-C(16)  | 122.2(6) |
| C(3)-C(2)-C(7)    | 118.4(6) | C(11)-C(10)-C(16) | 122.5(6) |
| C(1)-C(6)-C(8)    | 119.5(6) | C(9)-C(14)-C(15)  | 121.7(5) |
| C(5)-C(6)-C(8)    | 124.8(6) | C(13)-C(14)-C(15) | 121.2(5) |

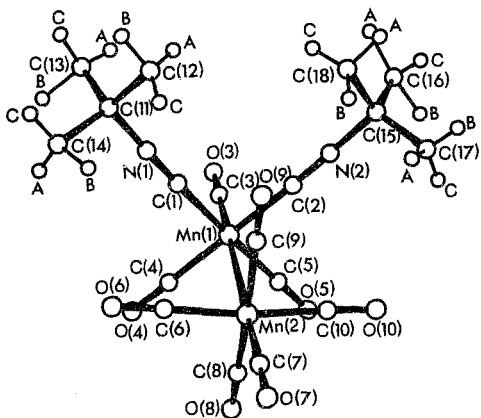


Figure 14.9: ORTEP<sup>3</sup> view of the  $\text{Mn}_2(\text{CO})_8(\text{CNBu}^+)_2$  molecule (V), showing the numbering system used.



Figure 14.10: ORTEP's view of the unit cell of  $Mn_2(CO)_8(CMBAu)_2(V)$ , looking down the  $b$ -axis

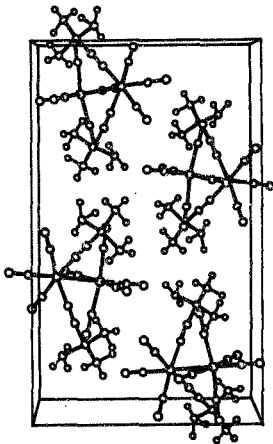


TABLE 14.5: Bond lengths ( $\text{\AA}$ ) for  $\text{Mn}_2(\text{CO})_8(\text{CNBu}^t)_2^{(16)}$ 

|              |           |              |           |
|--------------|-----------|--------------|-----------|
| Mn(1)-Mn(2)  | 2.924(1)  |              |           |
| Mn(1)-C(1)   | 1.947(4)  | C(1)-N(1)    | 1.150(5)  |
| Mn(1)-C(2)   | 1.941(4)  | C(2)-N(2)    | 1.158(5)  |
| Mn(1)-C(3)   | 1.779(5)  | C(3)-O(3)    | 1.149(6)  |
| Mn(1)-C(4)   | 1.833(5)  | C(4)-O(4)    | 1.143(6)  |
| Mn(1)-C(5)   | 1.814(4)  | C(5)-O(5)    | 1.152(6)  |
| Mn(2)-C(6)   | 1.837(5)  | C(6)-O(6)    | 1.140(6)  |
| Mn(2)-C(7)   | 1.788(5)  | C(7)-O(7)    | 1.144(7)  |
| Mn(2)-C(8)   | 1.837(5)  | C(8)-O(8)    | 1.150(7)  |
| Mn(2)-C(9)   | 1.845(5)  | C(9)-O(9)    | 1.132(6)  |
| Mn(2)-C(10)  | 1.843(5)  | C(10)-C(10)  | 1.138(6)  |
| N(1)-C(11)   | 1.448(8)  | N(2)-C(15)   | 1.464(6)  |
| C(11)-C(12)  | 1.529(10) | C(15)-C(16)  | 1.547(11) |
| C(11)-C(13)  | 1.529(11) | C(15)-C(17)  | 1.479(11) |
| C(11)-C(14)  | 1.534(10) | C(15)-C(18)  | 1.513(10) |
| C(12)-H(12A) | 0.90(10)  | C(16)-H(16A) | 1.22(14)  |
| C(12)-H(12B) | 1.02(6)   | C(16)-H(16B) | 1.17(9)   |
| C(12)-H(12C) | 0.98(9)   | C(16)-H(16C) | 0.75(6)   |
| C(13)-H(13A) | 0.84(7)   | C(17)-H(17A) | 0.97(7)   |
| C(13)-H(13B) | 1.13(10)  | C(17)-H(17B) | 0.85(7)   |
| C(13)-H(13C) | 1.04(8)   | C(17)-H(17C) | 0.98(8)   |
| C(14)-H(14A) | 0.92(8)   | C(18)-H(18A) | 1.03(8)   |
| C(14)-H(14B) | 1.05(6)   | C(18)-H(18B) | 0.91(8)   |
| C(14)-H(14C) | 0.96(6)   | C(18)-H(18C) | 1.01(8)   |

TABLE 14.6: Bond angles ( $^{\circ}$ ) for  $Mn_2(CO)_8(CNBU^t)_2(V)$ 

|                     |          |                     |          |
|---------------------|----------|---------------------|----------|
| Mn(1)-C(1)-N(1)     | 177.7(4) | Mn(2)-C(6)-O(6)     | 177.6(4) |
| Mn(1)-C(2)-N(2)     | 177.5(4) | Mn(2)-C(7)-O(7)     | 178.6(5) |
| Mn(1)-C(3)-O(3)     | 177.6(4) | Mn(2)-C(8)-O(8)     | 178.9(5) |
| Mn(1)-C(4)-O(4)     | 178.0(4) | Mn(2)-C(9)-O(9)     | 176.9(4) |
| Mn(1)-C(5)-O(5)     | 177.6(4) | Mn(2)-C(10)-O(10)   | 178.1(4) |
| C(1)-N(1)-C(11)     | 178.1(4) | C(2)-N(2)-C(15)     | 175.3(4) |
| C(12)-C(11)-C(13)   | 112.2(6) | C(16)-C(15)-C(17)   | 112.9(7) |
| C(12)-C(11)-C(14)   | 111.5(6) | C(16)-C(15)-C(18)   | 110.0(6) |
| C(13)-C(11)-C(14)   | 110.2(6) | C(17)-C(15)-C(18)   | 114.6(7) |
| C(12)-C(11)-N(1)    | 107.6(4) | C(16)-C(15)-N(2)    | 104.7(5) |
| C(13)-C(11)-N(1)    | 107.7(5) | C(17)-C(15)-N(2)    | 106.7(5) |
| C(14)-C(11)-N(1)    | 107.4(5) | C(18)-C(15)-N(2)    | 107.2(4) |
| C(1)-Mn(1)-Mn(2)    | 90.7(1)  | C(6)-Mn(2)-Mn(1)    | 84.0(2)  |
| C(1)-Mn(1)-C(2)     | 86.1(2)  | C(6)-Mn(2)-C(7)     | 95.6(2)  |
| C(1)-Mn(1)-C(3)     | 93.0(2)  | C(6)-Mn(2)-C(8)     | 90.3(3)  |
| C(1)-Mn(1)-C(4)     | 91.0(2)  | C(8)-Mn(2)-C(9)     | 89.0(2)  |
| C(1)-Mn(1)-C(5)     | 175.3(2) | C(6)-Mn(2)-C(10)    | 168.8(2) |
| C(2)-Mn(1)-Mn(2)    | 89.2(1)  | C(7)-Mn(2)-Mn(1)    | 177.1(2) |
| C(2)-Mn(1)-C(3)     | 93.3(2)  | C(7)-Mn(2)-C(8)     | 98.1(2)  |
| C(2)-Mn(1)-C(4)     | 174.1(2) | C(7)-Mn(2)-C(9)     | 94.9(2)  |
| C(2)-Mn(1)-C(5)     | 91.4(2)  | C(7)-Mn(2)-C(10)    | 95.6(2)  |
| C(3)-Mn(1)-Mn(2)    | 175.6(2) | C(8)-Mn(2)-Mn(1)    | 84.8(2)  |
| C(3)-Mn(1)-C(4)     | 91.9(2)  | C(8)-Mn(2)-C(9)     | 167.0(2) |
| C(3)-Mn(1)-C(5)     | 91.0(2)  | C(8)-Mn(2)-C(10)    | 88.4(2)  |
| C(4)-Mn(1)-Mn(2)    | 85.7(1)  | C(9)-Mn(2)-Mn(1)    | 82.2(1)  |
| C(4)-Mn(1)-C(5)     | 91.1(2)  | C(9)-Mn(2)-C(10)    | 89.8(2)  |
| C(5)-Mn(1)-Mn(2)    | 85.4(1)  | C(10)-Mn(2)-Mn(1)   | 84.8(1)  |
| H(12A)-C(12)-H(12B) | 103(7)   | H(16A)-C(16)-H(16B) | 163(8)   |
| H(12A)-C(12)-H(12C) | 133(8)   | H(16A)-C(16)-H(16C) | 83(8)    |
| H(12B)-C(12)-H(12C) | 110(6)   | H(16B)-C(16)-H(16C) | 93(7)    |
| H(13A)-C(13)-H(13B) | 146(7)   | H(17A)-C(17)-H(17B) | 96(6)    |
| H(13A)-C(13)-H(13C) | 106(6)   | H(17A)-C(17)-H(17C) | 123(6)   |
| H(13B)-C(13)-H(13C) | 100(7)   | H(17B)-C(17)-H(17C) | 111(6)   |
| H(14A)-C(14)-H(14B) | 110(6)   | H(18A)-C(18)-H(18B) | 104(7)   |
| H(14A)-C(14)-H(14C) | 115(6)   | H(18A)-C(18)-H(18C) | 109(6)   |

TABLE 14.6: Bond angles ( $^{\circ}$ ) for  $Mn_2(CO)_8(ONBu^t)_2(V)$  (Contd)

|                     |        |                     |        |
|---------------------|--------|---------------------|--------|
| H(14B)-C(14)-H(14C) | 116(5) | H(18B)-C(18)-H(18C) | 134(7) |
| H(12A)-C(12)-C(11)  | 101(6) | H(16A)-C(16)-C(15)  | 98(7)  |
| H(12B)-C(12)-C(11)  | 105(3) | H(16B)-C(16)-C(15)  | 99(5)  |
| H(12C)-C(12)-C(11)  | 102(5) | H(16C)-C(16)-C(15)  | 105(5) |
| H(13A)-C(13)-C(11)  | 105(5) | H(17A)-C(17)-C(15)  | 100(4) |
| H(13B)-C(13)-C(11)  | 97(5)  | H(17B)-C(17)-C(15)  | 113(4) |
| H(13C)-C(13)-C(11)  | 99(4)  | H(17C)-C(17)-C(15)  | 112(5) |
| H(14A)-C(14)-C(11)  | 112(5) | H(18A)-C(18)-C(15)  | 108(4) |
| H(14B)-C(14)-C(11)  | 95(4)  | H(18B)-C(18)-C(15)  | 91(5)  |
| H(14C)-C(14)-C(11)  | 107(4) | H(18C)-C(18)-C(15)  | 109(5) |

are given in Tables 14.7 and 14.8 respectively. The unit cell, viewed down the  $b$ -axis, is shown in Fig. 14.12.

The complex  $\text{Re}_2(\text{CO})_7(\text{CNCMe})_3$  might be expected on steric grounds to adopt conformation (IIIa) (Fig. 14.3), but the structure found in the crystal is (IIIc) (Fig. 14.3). Again the structure is staggered, with two methyl isonitrile ligands occupying *cis*-equatorial positions on Re(2), but the third MeNC ligand on Re(1) is disordered with respect to the carbonyl trans to it, with 50% occupancy of both sites, which are equivalent with respect to the two isonitrile ligands on Re(2) (Fig. 14.3 ((i) and (ii)). Disorder of this type has been observed previously with MeNC ligands,<sup>12b</sup> and is thought to be due to the relatively small size of the MeNC ligand ("fan-shaped" angle<sup>12a</sup> for MeNC: 52° (width) and 52° (thickness), cf. cone-angle<sup>12a</sup> for CO ca 95°, an estimate which may be too large), and its electronic similarity to CO.<sup>12b</sup> The distance C(11A)...C(11B) between the methyl atom C(11A) and the methyl atom C(11B) of a neighbouring molecule (translated by {0 0 1}) is within bonding distance (1.57(4)Å). However, the atoms C(11A) and C(11B) constitute the disordered methyl isonitrile group, with site occupancy factors of 0.5.

#### 14.2.5 Structure of $\text{Re}_2(\text{CO})_6(\text{CNC}_6\text{H}_5\text{Me}_2-2,6)_4$ (IV)

Compound (IV) crystallizes in the orthorhombic space group Pccn with  $Z = 4$ , an asymmetric unit being an  $\text{Re}(\text{CO})_3$ - $(\text{CNC}_6\text{H}_5\text{Me}_2-2,6)_2$ -fragment, the two halves of the molecule being related by a crystallographic 2-fold axis, generating the equivalent position  $(x-1, y-1, z)$ . The molecular structure and the numbering system used in the crystal structure analysis, is shown in Fig. 14.13. Bond lengths and bond angles are given in Tables 14.9 and 14.10 respectively.

From steric considerations of the RCN ligand, the  $\text{Re}_2(\text{CO})_6(\text{CNC}_6\text{H}_5\text{Me}_2-2,6)_4$  molecule might have been expected to adopt the eclipsed conformation (IVc) (Fig. 14.4). Of the possible staggered conformations, (IVa) and (IVb) (Fig. 14.4), (IVb) would be less favourable on steric grounds. The molecular geometry found in the crystal is that of (IVa), with *cis*-equatorial substitution of a pair

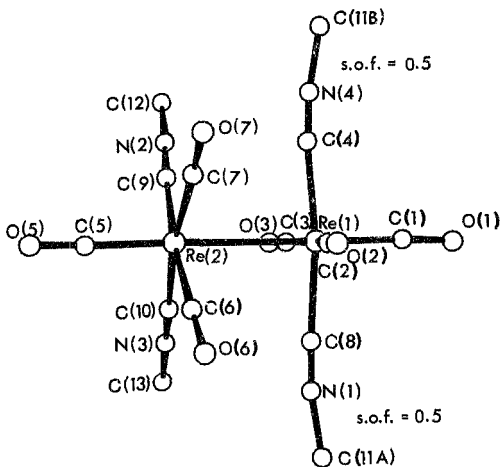


Figure 14.11: ORTEP<sup>++</sup> view of the  $\text{Re}_2(\text{CO})_7(\text{CNMe})_3$  molecule (III), showing the numbering system used. (Site occupancy factor (s.o.f.) of 0.5 for N(1), N(4), and C(11A), C(11B))

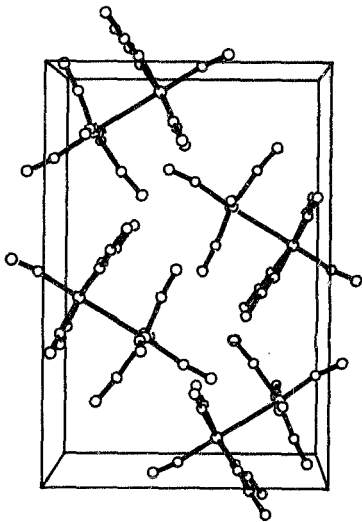


Figure 14.12: ORTEP<sup>33</sup> view of the unit cell of  $\text{Re}_2(\text{CO})_7(\text{CNMe})_3(\text{III})$ , looking down the  $b$ -axis

TABLE 14.7: Bond lengths ( $\text{\AA}$ ) for  $\text{Re}_2(\text{CO})_7(\text{CNMe})_3(\text{III})$

|             |           |            |           |
|-------------|-----------|------------|-----------|
| Re(1)-Re(2) | 3.049(1)  |            |           |
| Re(1)-C(1)  | 1.908(16) | C(1)-O(1)  | 1.160(17) |
| Re(1)-C(2)  | 1.916(16) | C(2)-O(2)  | 1.174(17) |
| Re(1)-C(3)  | 1.937(18) | C(3)-O(3)  | 1.126(19) |
| Re(2)-C(5)  | 1.870(16) | C(5)-O(5)  | 1.156(17) |
| Re(2)-C(6)  | 1.921(16) | C(6)-O(6)  | 1.175(17) |
| Re(2)-C(7)  | 1.936(17) | C(7)-O(7)  | 1.139(18) |
| Re(2)-C(9)  | 2.044(13) | C(9)-N(2)  | 1.140(15) |
| Re(2)-C(10) | 2.095(15) | C(10)-N(3) | 1.137(16) |
| Re(1)-C(8)  | 2.121(17) | C(8)-N(1)  | 1.066(19) |
| Re(1)-C(4)  | 2.127(17) | C(4)-N(4)  | 1.045(19) |
| N(1)-C(11A) | 1.420(30) | N(2)-C(12) | 1.455(20) |
| N(4)-C(11B) | 1.414(29) | N(3)-C(13) | 1.431(20) |



TABLE 14.8: Bond angles ( $^{\circ}$ ) for  $\text{Re}_2(\text{CO})_7(\text{CNMe})_3(\text{III})$ 

|                  |           |                   |           |
|------------------|-----------|-------------------|-----------|
| Re(1)-C(1)-O(1)  | 175.4(15) | Re(2)-C(5)-O(5)   | 172.0(16) |
| Re(1)-C(2)-O(2)  | 179.4(13) | Re(2)-C(6)-O(6)   | 178.1(14) |
| Re(1)-C(3)-O(3)  | 179.7(10) | Re(2)-C(7)-O(7)   | 178.0(15) |
| Re(1)-C(4)-N(4)  | 173.0(16) | Re(2)-C(9)-N(2)   | 176.7(12) |
| Re(1)-C(8)-N(1)  | 175.1(15) | Re(2)-C(10)-N(3)  | 179.0(14) |
| C(4)-N(4)-C(11B) | 172.2(22) | C(9)-N(2)-C(12)   | 175.9(15) |
| C(8)-N(1)-C(11A) | 170.4(22) | C(10)-N(3)-C(13)  | 177.1(14) |
| C(1)-Re(1)-Re(2) | 179.2(5)  | C(5)-Re(2)-Re(1)  | 178.4(5)  |
| C(1)-Re(1)-C(2)  | 96.2(6)   | C(5)-Re(2)-C(6)   | 93.6(7)   |
| C(1)-Re(1)-C(3)  | 96.5(6)   | C(5)-Re(2)-C(7)   | 96.3(7)   |
| C(1)-Re(1)-C(4)  | 93.9(6)   | C(5)-Re(2)-C(9)   | 92.8(6)   |
| C(1)-Re(1)-C(8)  | 94.2(6)   | C(5)-Re(2)-C(10)  | 92.2(6)   |
| C(2)-Re(1)-Re(2) | 83.7(4)   | C(6)-Re(2)-Re(1)  | 86.4(4)   |
| C(2)-Re(1)-C(3)  | 167.2(6)  | C(6)-Re(2)-C(7)   | 89.8(6)   |
| C(2)-Re(1)-C(4)  | 89.6(6)   | C(6)-Re(2)-C(9)   | 173.4(5)  |
| C(2)-Re(1)-C(8)  | 88.2(6)   | C(6)-Re(2)-C(10)  | 91.2(6)   |
| C(3)-Re(1)-Re(2) | 83.6(4)   | C(7)-Re(2)-Re(1)  | 85.3(4)   |
| C(3)-Re(1)-C(4)  | 90.5(7)   | C(7)-Re(2)-C(9)   | 91.2(6)   |
| C(3)-Re(1)-C(8)  | 89.9(7)   | C(7)-Re(2)-C(10)  | 171.4(6)  |
| C(4)-Re(1)-Re(2) | 85.2(4)   | C(9)-Re(2)-Re(1)  | 87.2(3)   |
| C(4)-Re(1)-C(8)  | 171.7(6)  | C(9)-Re(2)-C(10)  | 86.7(5)   |
| C(8)-Re(1)-Re(2) | 86.6(4)   | C(10)-Re(2)-Re(1) | 86.3(4)   |

of isonitrile ligands on each Re-atom.

The relative arrangements of the xylyl (xylyl = 2,6-Me<sub>2</sub>C<sub>6</sub>H<sub>3</sub>) isonitrile ligands, adopted (vide supra), as well as the relative orientation of the xylyl rings, probably reflects both steric requirements and crystal packing forces. The C6 rings are essentially planar. The xylyl rings are all close to being coplanar, the angles between the mean planes through rings A and B (A' and B'), A and B' (A' and B), A and A', and B and B' being 6.6, 5.7, 4.8, and 2.4° respectively. Fig. 14.14 shows the packing of the molecules in the unit cell, viewed down the b-axis. The xylyl rings of one molecule fit neatly into the gaps between the xylyl rings of adjacent molecules.

#### 14.2.6 Structure of Mn<sub>2</sub>(CO)<sub>8</sub>(CNC<sub>6</sub>H<sub>3</sub>Me<sub>2</sub>-2,6)<sub>4</sub>(VI)

The complex Mn<sub>2</sub>(CO)<sub>8</sub>(CNC<sub>6</sub>H<sub>3</sub>Me<sub>2</sub>-2,6)<sub>4</sub>(VI) is isomorphous with the rhenium analogue, Re<sub>2</sub>(CO)<sub>8</sub>(CNC<sub>6</sub>H<sub>3</sub>Me<sub>2</sub>-2,6)<sub>4</sub>(IV) (Space group Pccn, Z = 4), which is not surprising in view of the similarity of the two complexes.

The molecular structure and the numbering system used in the crystal structure analysis is shown in Fig. 14.15. Bond lengths and bond angles are given in Tables 14.11 and 14.12 respectively.

Fig. 14.16 shows the packing of the molecules in the unit cell, viewed down the b-axis. The xylyl rings are close to being coplanar, with angles between the mean planes through rings A and B (A' and B'), A and B' (A' and B), A and A', and B and B', of 7.9, 7.4, 3.0 and 2.6° respectively. Slight structural differences between (VI) and (IV) are due to the shorter Mn-Mn and Mn-C bond distances relative to the Re-Re and Re-C bond lengths.

Since the structure of (VI) is the same as that of (IV) in the crystal, this cannot provide an explanation of the spectral (IR, <sup>1</sup>H NMR) differences between the two compounds in solution.

#### 14.3 Structural Trends

One of the main aims in undertaking the crystal structure determinations was to obtain bond parameter data and to

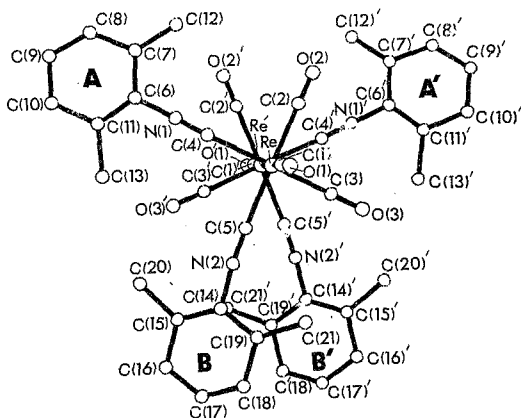


Figure 14.13: ORTEP<sup>32</sup> view of the  $\text{Re}_2(\text{CO})_6(\text{CNC}_6\text{H}_3\text{Me}_2-2,6)_4$  molecule (IV), showing the numbering system used (Re related to  $\text{Re}'$  by a 2-fold axis, generating the equivalent position  $(x-i, y-i, z)$ , and similarly for the other atoms).

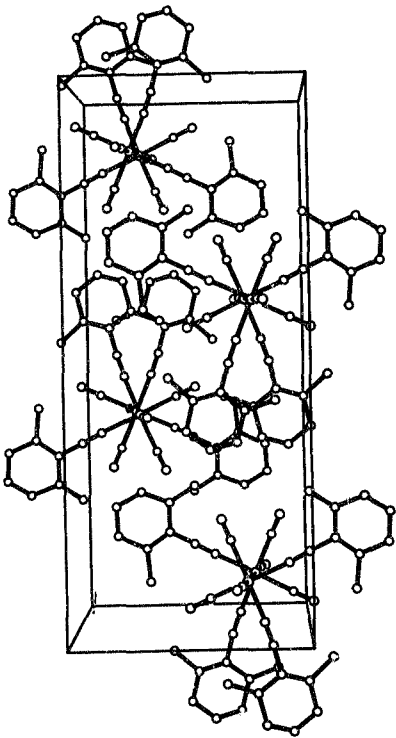


Figure 14.4: ORTEP's view of the unit cell of  $\text{Re}_2(\text{CO})_6(\text{CNC}_6\text{H}_5)_2$  looking down the  $b$ -axis

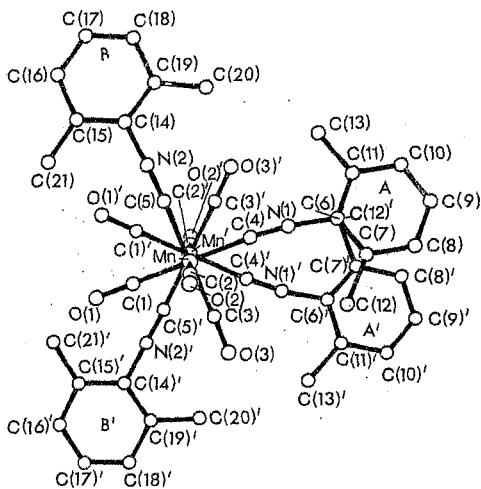
TABLE 14.9: Bond lengths (Å) for  $\text{Re}_2(\text{CO})_6(\text{CNC}_6\text{H}_3\text{Me}_2-2,6)_4(\text{IV})$

|                                   |           |             |            |
|-----------------------------------|-----------|-------------|------------|
| Re(x,y,z)-Re(½-x,½-y,z): 3.081(2) |           |             |            |
| Re-C(1)                           | 1.968(20) | C(1)-O(1)   | 1.088(21)  |
| Re-C(2)                           | 1.980(20) | C(2)-O(2)   | 1.093(21)  |
| Re-C(3)                           | 1.924(21) | C(3)-O(3)   | 1.174(23)  |
| Re-C(4)                           | 2.031(22) | C(4)-N(1)   | 1.171(25)  |
| Re-C(5)                           | 2.027(18) | C(5)-N(2)   | 1.161(22)  |
| N(1)-C(6)                         | 1.407(24) | N(2)-C(14)  | 1.413(22)  |
| C(6)-C(7)                         | 1.391(26) | C(14)-C(15) | 1.438(29)  |
| C(7)-C(8)                         | 1.448(32) | C(15)-C(16) | 1.472(30)  |
| C(8)-C(9)                         | 1.413(35) | C(16)-C(17) | 1.395(34)  |
| C(9)-C(10)                        | 1.396(31) | C(17)-C(18) | 1.263(37)  |
| C(10)-C(11)                       | 1.428(32) | C(18)-C(19) | 1.1472(35) |
| C(11)-C(6)                        | 1.381(27) | C(19)-C(14) | 1.396(19)  |
| C(7)-C(12)                        | 1.524(33) | C(15)-C(20) | 1.573(32)  |
| C(11)-C(13)                       | 1.545(28) | C(19)-C(21) | 1.485(34)  |

TABLE 14.10: Bond angles ( $^{\circ}$ ) for  $\text{Re}_2(\text{CO})_6(\text{CNC}_6\text{H}_5\text{Me}_2-2,6)_4(\text{IV})$

|                         |           |                         |           |
|-------------------------|-----------|-------------------------|-----------|
| Re-C(1)-O(1)            | 172.8(19) | C(1)-Re-C(2)            | 92.5(7)   |
| Re-C(2)-O(2)            | 174.0(19) | C(1)-Re-C(3)            | 95.5(8)   |
| Re-C(3)-O(3)            | 175.7(20) | C(1)-Re-C(4)            | 93.8(8)   |
| Re-C(4)-N(1)            | 178.1(18) | C(1)-Re-C(5)            | 92.6(7)   |
| Re-C(5)-N(2)            | 174.2(18) | C(2)-Re-C(3)            | 90.2(8)   |
| C(4)-N(1)-C(6)          | 177.0(20) | C(2)-Re-C(4)            | 89.3(8)   |
| C(5)-N(2)-C(14)         | 176.6(22) | C(3)-Re-C(5)            | 87.2(8)   |
| C(2)-Re-Re <sup>a</sup> | 86.6(8)   | C(4)-Re-C(5)            | 92.6(7)   |
| C(3)-Re-Re <sup>a</sup> | 83.5(8)   | C(2)-Re-C(5)            | 174.5(7)  |
| C(4)-Re-Re <sup>a</sup> | 87.3(8)   | C(3)-Re-C(4)            | 170.7(8)  |
| C(5)-Re-Re <sup>a</sup> | 88.4(8)   | C(1)-Re-Re <sup>a</sup> | 178.5(8)  |
| C(11)-C(8)-C(7)         | 124.8(18) | C(19)-C(14)-C(15)       | 126.3(19) |
| C(6)-C(7)-C(8)          | 115.1(20) | C(14)-C(15)-C(16)       | 114.6(19) |
| C(7)-C(8)-C(9)          | 120.7(23) | C(15)-C(16)-C(17)       | 116.3(23) |
| C(8)-C(9)-C(10)         | 121.6(25) | C(16)-C(17)-C(18)       | 127.6(28) |
| C(9)-C(10)-C(11)        | 117.6(23) | C(17)-C(18)-C(19)       | 121.5(27) |
| C(10)-C(11)-C(6)        | 119.9(18) | C(18)-C(19)-C(14)       | 113.4(21) |
| C(12)-C(7)-C(6)         | 120.9(20) | C(20)-C(15)-C(14)       | 124.4(19) |
| C(12)-C(7)-C(8)         | 123.9(20) | C(20)-C(15)-C(16)       | 120.8(20) |
| C(13)-C(11)-C(6)        | 120.6(19) | C(21)-C(19)-C(14)       | 121.8(21) |
| C(13)-C(11)-C(10)       | 119.5(19) | C(21)-C(19)-C(18)       | 124.5(23) |
| N(1)-C(6)-C(7)          | 117.7(18) | N(2)-C(14)-C(15)        | 118.5(19) |
| N(1)-C(6)-C(11)         | 117.5(17) | N(2)-C(14)-C(19)        | 115.1(19) |

<sup>a</sup> Re' is related to Re by a 2-fold axis, generating the equivalent position ( $\frac{1}{2}-x$ ,  $\frac{1}{2}-y$ ,  $z$ ).



**Figure 14.15:** ORTEP<sup>33</sup> view of the  $\text{Mn}_2(\text{CO})_6(\text{CNC}_6\text{H}_3\text{Me}_2-2,6)_4$  molecule (VI), showing the numbering system used ( $\text{Mn}'$  related to Mn by a 2-fold axis generating the equivalent position ( $x-i, y-i, z$ ), and similarly for other atoms).

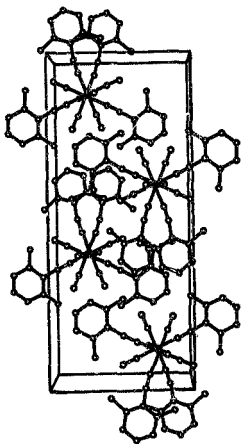


Figure 14.16: ORTEP<sup>a</sup> view of the unit cell of  $\text{Mn}_2(\text{CO})_6(\text{CMC})_3$  ( $\text{CMC} = \text{C}_6\text{H}_3\text{Me}_2$ ), looking down the  $b$ -axis



TABLE 14.11: Bond lengths (Å) for  $\text{Mn}_2(\text{CO})_6(\text{CNC}_5\text{H}_5\text{Me}_2-2,6)_4(\text{VI})$

|   |          |             |         |
|---|----------|-------------|---------|
| $\text{Mn}(x, y, z) - \text{Mn}(\frac{1}{2}-x, \frac{1}{2}-y, z)$ : | 2.946(6) |             |         |
| Mn-C(1)   | 1.80(2)  | C(1)-O(1)   | 1.15(2) |
| Mn-C(2)   | 1.72(2)  | C(2)-O(2)   | 1.20(2) |
| Mn-C(3)   | 1.81(2)  | C(3)-O(3)   | 1.16(2) |
| Mn-C(4)   | 1.90(2)  | C(4)-N(1)   | 1.15(2) |
| Mn-C(5)   | 1.90(2)  | C(5)-N(2)   | 1.17(2) |
| N(1)-C(6)   | 1.42(2)  | N(2)-C(14)  | 1.41(2) |
| C(6)-C(7)   | 1.35(2)  | C(14)-C(15) | 1.41(2) |
| C(7)-C(8)   | 1.43(3)  | C(15)-C(16) | 1.40(3) |
| C(8)-C(9)   | 1.38(3)  | C(16)-C(17) | 1.40(3) |
| C(9)-C(10)  | 1.37(3)  | C(17)-C(18) | 1.38(3) |
| C(10)-C(11)   | 1.43(3)  | C(18)-C(19) | 1.44(2) |
| C(11)-C(6)  | 1.39(3)  | C(19)-C(14) | 1.42(2) |
| C(7)-C(12)  | 1.54(3)  | C(15)-C(21) | 1.48(3) |
| C(11)-C(13)   | 1.53(3)  | C(19)-C(20) | 1.51(3) |

TABLE 14.12: Bond angles ( $^{\circ}$ ) for  $Mn_2(CO)_6(CNC_6H_3Me_2-2,6)_4(VI)$

|                         |        |                         |          |
|-------------------------|--------|-------------------------|----------|
| Mn-C(1)-O(1)            | 177(2) | O(1)-Mn-C(2)            | 92.4(10) |
| Mn-C(2)-O(2)            | 179(2) | C(1)-Mn-C(3)            | 91.2(8)  |
| Mn-C(3)-O(3)            | 173(2) | C(1)-Mn-C(5)            | 88.6(8)  |
| Mn-C(4)-N(1)            | 175(2) | C(2)-Mn-C(3)            | 92.7(8)  |
| Mn-C(5)-N(2)            | 17'(2) | C(2)-Mn-C(4)            | 92.5(9)  |
| C(4)-N(1)-C(6)          | 172(2) | C(2)-Mn-C(5)            | 96.0(8)  |
| C(5)-N(2)-C(14)         | 179(2) | C(3)-Mn-C(4)            | 88.3(8)  |
| C(1)-Mn-Mn <sup>a</sup> | 85(1)  | C(4)-Mn-C(5)            | 91.2(7)  |
| C(3)-Mn-Mn <sup>a</sup> | 81(1)  | C(1)-Mn-C(4)            | 175.1(9) |
| C(4)-Mn-Mn <sup>a</sup> | 90(1)  | C(3)-Mn-C(5)            | 171.4(8) |
| C(5)-Mn-Mn <sup>a</sup> | 90(1)  | C(2)-Mn-Mn <sup>a</sup> | 173(1)   |
| C(11)-C(6)-C(7)         | 123(2) | C(19)-C(14)-C(15)       | 125(2)   |
| C(6)-C(7)-C(8)          | 118(2) | C(14)-C(15)-C(16)       | 115(2)   |
| C(7)-C(8)-C(9)          | 119(2) | C(15)-C(16)-C(17)       | 122(2)   |
| C(8)-C(9)-C(10)         | 123(2) | C(16)-C(17)-C(18)       | 123(2)   |
| C(9)-C(10)-C(11)        | 118(2) | C(17)-C(18)-C(19)       | 118(2)   |
| C(10)-C(11)-C(6)        | 119(2) | C(18)-C(19)-C(14)       | 118(2)   |
| C(12)-C(7)-C(6)         | 121(2) | C(21)-C(15)-C(14)       | 121(2)   |
| C(12)-C(7)-C(8)         | 121(2) | C(21)-C(15)-C(16)       | 124(2)   |
| C(13)-C(11)-C(6)        | 122(2) | C(20)-C(19)-C(14)       | 122(2)   |
| C(13)-C(11)-C(10)       | 119(2) | C(20)-C(19)-C(18)       | 120(2)   |
| N(1)-C(6)-C(7)          | 119(2) | N(2)-C(14)-C(15)        | 120(2)   |
| N(1)-C(6)-C(11)         | 118(2) | N(2)-C(14)-C(19)        | 118(2)   |

<sup>a</sup> Mn' is related to Mn by a 2-fold axis, generating the equivalent position ( $\frac{1}{2}-x, \frac{1}{2}-y, z$ ).

see if any trends could be observed, relating to the structural effect (if any) of increasing isonitrile substitution.

#### 14.3.1 The M-M bond length

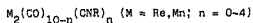
Specifically, the effect of increasing isonitrile substitution on the metal-metal bond was of interest. Since isonitriles are weaker  $\pi$ -acceptors than carbonyls,<sup>19a</sup> increasing isonitrile substitution would be expected to result in a weakening and hence a lengthening of the metal-metal bond.<sup>19b</sup> As can be seen from the Re-Re bond length data given for a series of  $\text{Re}_2(\text{CO})_{10-n}(\text{CNR})_n$  ( $n = 0-4$ ) complexes (Table 14.13a), there is a slight lengthening of the Re-Re bond with increasing  $n$ , but this only becomes significant at the  $n = 4$  level. This effect is more apparent for the  $\text{Mn}_2(\text{CO})_{10-n}(\text{CNR})_n$  ( $n = 0, 2, 4$ ) series (Table 14.13b), possibly due to the weaker Mn-Mn bond relative to the Re-Re bond (see section 12.2.1), or to steric effects (greater steric crowding with Mn). The inference is that the isonitrile ligands are not having as great an effect (in the ground state) of weakening the metal-metal bond as might have been anticipated.<sup>19b</sup>

A lengthening of the metal-metal bond on increasing isonitrile substitution could also be expected on purely steric grounds in order to reduce repulsions between bulky isonitrile groups. For instance, as no significant bond lengthening is observed for the series  $\text{Re}_2(\text{CO})_{10-n}(\text{CNR})_n$  ( $n = 0-3$ ), and the Re-Re-Ceq angles are acute i.e., no bending out of CNR (or CO) ligands (see section 14.3.4), there seems to be little steric effect observed, except possibly for  $\text{Re}_2(\text{CO})_6(\text{CNC}_6\text{H}_3\text{Me}_2-2,6)_4$  ("fan-shaped" angle<sup>20</sup> for  $\text{CNC}_6\text{H}_3\text{Me}_2-2,6$ :  $106^\circ$  (width) and  $53^\circ$  (thickness)), where a lengthening of the Re-Re bond is observed.

#### 14.3.2 The M-CO bond lengths

Studies of  $\text{M}_2(\text{CO})_{10}$  ( $\text{M} = \text{Re}, \text{Mn}$ )<sup>13a-d</sup> have shown that the M-CO<sub>ax</sub> bonds are shorter than the M-CO<sub>eq</sub> bonds (see Table 14.14), implying stronger bonding of axial carbonyls. However, when considering the substituted isonitrile

TABLE 14.13: Metal-metal bond length data for the complexes



(a)  $Re_2(CO)_{10-n}(CNR)_n \quad (n = 0-4)$

| Complex                          | Re-Re Bond length(Å)  |
|----------------------------------|-----------------------|
| $Re_2(CO)_{10}$                  | 3.041(1) <sup>a</sup> |
| $Re_2(CO)_9(CNBU^t)_1$           | 3.048(1)              |
| $Re_2(CO)_8(CNC_6H_3Me_2-2,6)_2$ | 3.047(1)              |
| $Re_2(CO)_7(CNMe)_3$             | 3.049(1)              |
| $Re_2(CO)_6(CNC_6H_3Me_2-2,6)_4$ | 3.081(2)              |

(b)  $Mn_2(CO)_{10-n}(CNR)_n \quad (n = 0, 2, 4)$

| Complex                          | Mn-Mn bond length(Å)  |
|----------------------------------|-----------------------|
| $Mn_2(CO)_{10}$                  | 2.904(1) <sup>a</sup> |
| $Mn_2(CO)_8(CNBU^t)_2$           | 2.924(1)              |
| $Mn_2(CO)_6(CNC_6H_3Me_2-2,6)_4$ | 2.946(6)              |

<sup>a</sup> Ref. 158

derivatives, the possible effect of the isonitrile ligand on the trans carbonyl could also be important.<sup>112</sup> Since the isonitrile ligand is a poorer  $\pi$ -acceptor than carbonyl,<sup>111</sup> it would be expected that the M-CO bond trans to an RNC ligand would be shorter than that trans to another CO.<sup>112</sup>

Although this effect is indeed observed for  $\text{Re}_2(\text{CO})_9(\text{CNBu}^t)$ , with Re-C(1) trans to  $\text{CNBu}^t$  (1.916(18) $\text{\AA}$ ) significantly shorter than the av. value of the other Re-COeq bonds (av. 1.983(20) $\text{\AA}$ ), this trend does not continue for the  $\text{Re}_2(\text{CO})_{10-n}(\text{CNR})_n$  ( $n = 2-4$ ) derivatives (see Table 14.14(a)). However, for the  $\text{Re}_2(\text{CO})_{10-n}(\text{CNR})_n$  ( $n = 1-3$ ) complexes, the av. Re-COax bond is significantly shorter than the av. Re-COeq (trans to CO or CN) bonds, as expected (vide supra). However, for  $\text{Re}_2(\text{CO})_6(\text{CNC}_6\text{H}_5)_2(\text{Me}_2\text{-}2,6)_4$ , the Re-COax bond (1.968(20) $\text{\AA}$ ) is longer than the av. Re-COeq (all trans to CN) bonds (av. 1.952(20) $\text{\AA}$ ), indicative of a strong trans effect of the isonitrile ligands.<sup>112</sup> The Re-CN bond lengths are relatively constant for the series  $\text{Re}_2(\text{CO})_{10-n}(\text{CNR})_n$  ( $n = 1-4$ ) (see Table 14.14(a)).

For the  $\text{Mn}_2(\text{CO})_{10-n}(\text{CNR})_n$  ( $n = 2,4$ ) complexes, the Mn-COax bond lengths are significantly shorter than the Mn-COeq (trans to CO or CN) bonds (Table 14.14(b)). This effect is more pronounced than in the parent  $\text{Mn}_2(\text{CO})_{10}$ .<sup>113</sup> In the case of  $\text{Mn}_2(\text{CO})_8(\text{CNBu}^t)_2$ , the Mn-CO (trans to CN) bonds (av. 1.814(5) $\text{\AA}$ ) are shorter than the Mn-CO (trans to CO) bonds (av. 1.841(5) $\text{\AA}$ ), as expected (vide supra).

#### 14.3.3 Molecular conformation

In all the structures discussed (I-VI), the molecule adopts a staggered conformation, like the parent carbonyls,  $\text{M}_2(\text{CO})_{10}$  ( $M = \text{Re}, \text{Mn}$ ),<sup>114</sup> with C-M-M-C torsional angles close to the ideal  $45^\circ$ . (Torsional angles of structures (I)-(VI) are listed in Appendix C). A staggered conformation is expected to minimize repulsions between equatorial ligands.<sup>115</sup>

The axC-M-M-Cax fragment is essentially linear, as evidenced by M-M-COax bond angles of ca.  $177^\circ$  (see Table 14.15).

TABLE 14.14: Average M-C bond length data for the complexes



(a)  $Re_2(CO)_{10-n}(CNR)_n$  (n = 0-4)

| Complex                           | av. Re-C bond length(Å) |             |             |                                     |
|-----------------------------------|-------------------------|-------------|-------------|-------------------------------------|
|                                   | Re-COax                 | Re-COeq     |             | Re-CN                               |
|                                   |                         | trans to CO | trans to CN |                                     |
| $Re_2(CO)_{10}$ <sup>a</sup>      | 1.929(7)                | 1.987(6)    | -           | -                                   |
| $Re_2(CO)_9(CNBU^t)$              | 1.902(19)               | 1.983(20)   | 1.916(18)   | 2.068(15)                           |
| $Re_2(CO)_8(CNC_6H_3Me_2-2,6)_2$  | 1.924(6)                | 1.976(6)    | 1.975(7)    | 2.050(6)                            |
| $Re_2(CO)_7(CNMe)_3$ <sup>b</sup> | 1.889(16)               | 1.927(16)   | 1.929(17)   | 2.070(14)<br>2.124(17) <sup>c</sup> |
| $Re_2(CO)_6(CNC_6H_3Me_2-2,6)_4$  | 1.968(20)               | -           | 1.952(20)   | 2.029(20)                           |

(b)  $Mn_2(CO)_{10-n}(CNR)_n$  (n = 0, 2, 4)

| Complex                          | av. Mn-C bond length(Å) |             |             |          |
|----------------------------------|-------------------------|-------------|-------------|----------|
|                                  | Mn-COax                 | Mn-COeq     |             | Mn-CN    |
|                                  |                         | trans to CO | trans to CN |          |
| $Mn_2(CO)_{10}$ <sup>a</sup>     | 1.811(3)                | 1.856(2)    | -           | -        |
| $Mn_2(CO)_8(CNBU^t)_2$           | 1.784(5)                | 1.841(5)    | 1.814(5)    | 1.944(4) |
| $Mn_2(CO)_6(CNC_6H_3Me_2-2,6)_4$ | 1.72(2)                 | -           | 1.81(2)     | 1.90(2)  |

<sup>a</sup> Ref. 158

<sup>b</sup> Disordered structure

<sup>c</sup> av. for disordered MeNC ligand

#### 14.3.4 C-M-C and M-M-Ceq bond angles

In structures (I)-(VI), all the C-M-C angles are close to 90°, but significantly, the axC-M-Ceq angles are all greater than 90°, while the eqC-M-Ceq angles are ca. 90°. (See Table 14.16). This is true whether the equatorial ligand is a carbonyl or isonitrile ligand. Hence the ligands are all bending slightly inwards towards the M-M bond. This is also reflected in the acute M-M-Ceq angles (ca. 86°) (see Table 14.15). Similar trends were observed for  $\mu_n(\text{CO})_{10}$  (M = Re, Mn).<sup>133,3</sup>

This is thought to be a genuine electronic effect, and has been rationalized by Elian and Hoffmann<sup>3</sup> on the basis of MO Theory. From a consideration of energy level diagrams, theoretical predictions indicate that the energetically most favourable geometry corresponds to an eqC-M-Cax angle of slightly greater than 90°, at which point  $\pi$ -interaction is maximized, and anti-bonding interaction minimized.

The consistency of the axC-M-Ceq (93-100°), eqC-M-Ceq (ca. 90°) and M-M-Ceq (85-88°) bond angles for the series  $\mu_n(\text{CO})_{10-n}(\text{CNR})_n$  (M = Re, n = 0-4; M = Mn, n = 0,2,4) (see Tables 14.15-16), indicate that this effect is genuine. Also significant is the observation that the M-M-CN angles are less than 90° for these structures (Table 14.15). Since isonitriles such as  $\text{CNC}_6\text{H}_5\text{Me}_2$ -2.6 ("fan-shaped" angles,<sup>33</sup> 106° (wideness) and 53° (thickness)) have greater steric bulk than CO (cone angle ca. 100°),<sup>33a</sup> this estimate, however, seems too large; this would indicate that any steric factors are less important than electronic factors in determining the direction of the bending of the equatorial ligands. Again no structural effect of increasing isonitrile substitution is apparent.

#### 14.3.5 M-C-O, M-C-N and C-N-C bond angles

In all the structures (I-VI), both the carbonyl and the isonitrile ligands co-ordinate in an essentially linear fashion, with M-C-O and M-C-N bond angles all in the range 170-179° (see Table 14.17). Near-linearity of

TABLE 14.15: Average M-M-C bond angle data ( $^{\circ}$ ) for the complexes

$M_2(CO)_{10-n}(CNR)_n$  ((a) M = Re, n = 0-4; (b) M = Mn,  
n = 0,2,4)

| Complex                          | M-M-COax  | M-M-COeq | M-M-CN  |
|----------------------------------|-----------|----------|---------|
| (a)                              |           |          |         |
| $Re_2(CO)_{10}^a$                | 176.3(2)  | 86.4(2)  | -       |
| $Re_2(CO)_9(CNBU)^t$             | 177.0(6)  | 86.8(5)  | 87.5(4) |
| $Re_2(CO)_8(CNC_6H_3Me_2-2,6)_2$ | 177.9(2)  | 86.2(1)  | 88.2(1) |
| $Re_2(CO)_7(CNMe)_3^b$           | 178.8(5)  | 84.8(4)  | 86.3(4) |
| $Re_2(CO)_6(CNC_6H_3Me_2-2,6)_4$ | 178.5(8)  | 85.1(8)  | 87.9(8) |
| (b)                              |           |          |         |
| $Mn_2(CO)_{10}^a$                | 177.03(9) | 86.38(7) | -       |
| $Mn_2(CO)_8(CNBU)^t_2$           | 176.4(2)  | 84.5(1)  | 90.0(1) |
| $Mn_2(CO)_6(CNC_6H_3Me_2-2,6)_4$ | 173(1)    | 83(1)    | 90(1)   |

<sup>a</sup> Ref. 158

<sup>b</sup> Disordered structure



TABLE 14.16: Average cis C-M-C bond angle data (°) for the complexes  $M_2(CO)_{10-n}(CHR)_n$  ((a)  $M = Re$ ,  $n = 0-4$ ; (b)  $M = Mn$ ,  $n = 0, 2, 4$ )

| Complex                              | axCO-M-COeq | axCO-M-CN | eqCO-M-COeq | eqCO-M-CN | CN-M-CN |
|--------------------------------------|-------------|-----------|-------------|-----------|---------|
| (a)                                  |             |           |             |           |         |
| $Re_2(CO)_{10}^a$                    | 93.7(3)     | -         | 89.8(2)     | -         | -       |
| $Re_2(CO)_9(CNBU^t)_1$               | 93.3(8)     | 92.1(6)   | 89.8(8)     | 89.9(7)   | -       |
| $Re_2(CO)_8(CNC_6^-H_3Me_{2-2,6})_2$ | 94.1(2)     | 91.1(2)   | 90.9(2)     | 88.8(2)   | -       |
| $Re_2(CO)_7(CNMe)_3^b$               | 95.7(7)     | 93.3(6)   | 89.8(6)     | 90.1(6)   | 86.7(5) |
| $Re_2(CO)_6(CNC_6^-H_3Me_{2-2,6})_4$ | 94.0(8)     | 93.2(8)   | 90.2(8)     | 88.3(8)   | 92.6(7) |
| (b)                                  |             |           |             |           |         |
| $Mn_2(CO)_{10}^a$                    | 93.65(11)   | -         | 89.79(10)   | -         | -       |
| $Mn_2(CO)_8(CNBU^t)_2$               | 94.5(2)     | 93.2(2)   | 89.7(2)     | 91.2(2)   | 86.1(2) |
| $Mn_2(CO)_6(CNC_6^-H_3Me_{2-2,6})_4$ | 92.6(9)     | 94.3(9)   | 91.2(8)     | 88.5(8)   | 91.2(7) |

<sup>a</sup> Ref. 158

<sup>b</sup> Disordered structure

M-C-R bonds for  $M(CR)_n$  ( $R = O, N, n > 1$ ) groups has been predicted on electronic grounds. <sup>19</sup>

The observation that deviations from linearity are not greater for the M-C-N bonds than for the M-C-O bonds (see Table 14.17), nor indeed do more highly substituted complexes show any greater distortions, is indicative of the apparent lack of any noticeable effect of the steric bulk<sup>20</sup> of the isonitrile ligands on the molecular geometry.

Further, the isonitrile ligands themselves show only small deviations from linearity, the C-N-C angles being generally in the range 170-180° (see Table 14.17). This slight deviation from linearity is normal for terminal isonitrile ligands (isonitriles with C-N-C angles > 180° are considered to be essentially linear<sup>21b</sup>). Individual isonitrile ligands which show slight deviations from linearity (eg. (II): CN(2)-N(2)-C(9): 166.1(5)°; (III): C(8)-N(1)-C(11A): 170.4(22)°) probably reflect the influence of crystal packing forces. A greater bending of the isonitrile ligands in the more highly substituted complexes is not observed.

#### 14.3.6 Packing

The role of crystal packing forces in determining structure should not be neglected. In the case of  $Re_2(CO)_6(CNC_6H_3Me_2-2,6)_2$  (II) (see section 14.2.2) and  $Re_2(CO)_6(CNC_6H_3Me_2-2,6)_4$  (IV) (see section 14.2.5) (and the isomorphous  $Mn_2(CO)_6(CNC_6H_3Me_2-2,6)_4$  (VI), section 14.2.6), the conformation adopted in the crystal, as well as the relative orientation of the xylyl rings, is probably determined largely by the influence of packing forces. (See packing diagram of (II), (IV) and (VI), Figs. 14.8, 14.14 and 14.16 respectively.) For the tri-substituted  $Re_2(CO)_7(CNMe)_3$ , the conformation adopted in the crystal, (IIIc) (Fig. 14.3), is probably favoured over the other possible conformations (IIIa) and (IIIb) (Fig. 14.3) due to packing considerations. In solution all isomers probably co-exist.

Packing forces could also be responsible for small

TABLE 14.17 Average bond data (°) for the M-C-O, M-C-N and C-N-C bond angles of the complexes  $M_2(CO)_{10-n}(CNR)_n$  ((a) M = Re, n = 0-4; (b) M = Mn, n = 0,2,4)

| Complex   | M-C-Oax    | M-C-Oeq    | M-C-N                  | C-N-C                  |
|---|------------|------------|------------------------|------------------------|
| (a)   |            |            |                        |                        |
| Re <sub>2</sub> (CO) <sub>10</sub> <sup>a</sup>   | 177.5(7)   | 178.0(5)   | -                      | -                      |
| Re <sub>2</sub> (CO) <sub>9</sub> (CNBu) <sup>b</sup>   | 177.0(17)  | 175.9(17)  | 175.5(13)              | 175.7(16)              |
| Re <sub>2</sub> (CO) <sub>8</sub> (CNC <sub>6</sub> H <sub>3</sub> Me <sub>2</sub> -2,6) <sub>2</sub> | 177.0(5)   | 178.3(5)   | 177.4(5)               | 171.0(5)               |
| Re <sub>2</sub> (CO) <sub>7</sub> (CNMe) <sub>3</sub> <sup>b</sup>                                    | 173.7(16)  | 178.8(13)  | 177.9(13)              | 176.5(15)              |
|   |            |            | 174.1(14) <sup>c</sup> | 171.3(22) <sup>c</sup> |
| Re <sub>2</sub> (CO) <sub>6</sub> (CNC <sub>6</sub> H <sub>3</sub> Me <sub>2</sub> -2,6) <sub>4</sub> | 172.8(19)  | 174.9(20)  | 176.3(18)              | 176.8(21)              |
| (b)   |            |            |                        |                        |
| Mn <sub>2</sub> (CO) <sub>10</sub> <sup>a</sup>   | 179.21(27) | 177.89(23) | -                      | -                      |
| Mn <sub>2</sub> (CO) <sub>8</sub> (CNBu) <sub>2</sub> <sup>b</sup>                                    | 178.1(5)   | 177.9(4)   | 177.6(4)               | 176.7(4)               |
| Mn <sub>2</sub> (CO) <sub>6</sub> (CNC <sub>6</sub> H <sub>3</sub> Me <sub>2</sub> -2,6) <sub>4</sub> | 179(2)     | 175(2)     | 176(2)                 | 176(2)                 |

<sup>a</sup> Ref. 158

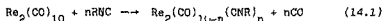
<sup>b</sup> Disordered structure

<sup>c</sup> av. for disordered MeNC ligand

deviations in geometry. For example, non-bonded O...O interactions could result in M-C-O bonds deviating from linearity by 5-10°. Hence deviations from ideal geometry might occur in order to achieve close-packing.<sup>24</sup>

14.4 Relating structure to chemical reactivity

Investigations of the reaction (14.1) of  $\text{Re}_2(\text{CO})_{10}$  with RNC to give products  $\text{Re}_2(\text{CO})_{10-n}(\text{CNR})_n$  ( $n = 1-4$ ) (see ch. XI).



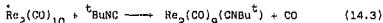
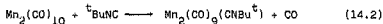
showed that

- (i) reaction proceeds more slowly as  $n$  increases, and
- (ii) direct substitution with  $n > 4$  could not be achieved (except perhaps for  $\text{R} = 2,6\text{-Me}_2\text{C}_6\text{H}_3$ ).

This can be explained in terms of

- (i) increasing electron density on the metal atom, and
- (ii) a fifth RNC ligand would have to occupy an electronically less favourable equatorial trans to RNC,<sup>142</sup> or axial<sup>159</sup> site.

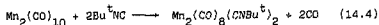
<sup>13</sup>CO labelling studies have shown that for the thermal (80°, 4h) and Pd/C (10%) catalysed (25°C, 10 min) reaction (14.2),<sup>277</sup> and the PdO-catalysed (55°C, 5 min) reaction (14.3) (see ch. XI),



no metal-metal bond cleavage occurs. However total scrambling was observed for the  $\text{Mn}_2(\text{CO})_{10-n}(\text{CNBu}^t)_n$  ( $n = 2,3$ ) products also formed in the thermal reaction (14.2).<sup>277</sup> Hence an alternate mechanism for the synthesis of the higher derivatives,  $\text{M}_2(\text{CO})_{10-n}(\text{CNR})_n$  ( $n \geq 1$ ), involving metal-metal bond cleavage cannot be ruled out on the basis of available data.

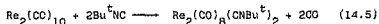
An interesting result is that of the different substitution geometries observed for the  $\text{M}_2(\text{CO})_8(\text{CNR})_2$  structures, viz. 1,2-cis-dieq- $\text{Re}_2(\text{CO})_8(\text{CNC}_6\text{H}_3\text{Me}_2-2,6)_2$  and 1,1-cis-dieq- $\text{Mn}_2(\text{CO})_8(\text{CNBu}^t)_2$ . This latter isomer might be expected to be the electronically favoured product in a direct substitution reaction not involving metal-metal bond cleavage, in accordance with the so-called cis-labilization

effect.<sup>111</sup> However, kinetic studies<sup>223</sup> on the PdO-catalysed reaction (14.4) at 25°C in benzene,



have shown the 1,2-isomer (Isomer(B), Fig. 11.5) is formed first. The 1,2-isomer (B) can be isomerized to the 1,1-isomer (A) (Fig. 11.5) on heating. (Ratio of B:A, 3:1 (benzene); 1:1 (hexane)). These results show that cis-labilization is not necessarily implicated in the reaction of  $\text{Mn}_2(\text{CO})_{10}$  with RNC ligands. Further, isomer (A) reacts faster than isomer (B) with RNC to give 1,1-cis-dieq, 2-eq- $\text{Mn}_2(\text{CO})_7(\text{CNBu}^t)_3$ , which is the opposite to the expected result in terms of the cis-labilization effect. The reaction of both the isomers (A) and (B) to give the tri-substituted product is faster than the isomerization of (B) to (A).

In the case of the analogous reaction (14.5) with  $\text{Re}_2(\text{CO})_{10}$ ,<sup>223</sup>



only isomer (B) is formed, and isomerization to isomer (A) cannot be achieved even on extended heating at 125°C. Hence there would appear to be a substantial barrier to the isomerization reaction (B) to (A) for  $\text{Re}_2(\text{CO})_8(\text{CNBu}^t)_2$ . This is supported by the inability to convert isomer (A) to (B),<sup>223</sup> isomer (A),  $(\text{CO})_5\text{Re}(\text{CO})_3(\text{CNBu}^t)_2$ , being prepared indirectly from the reaction of  $\text{NaRe}(\text{CO})_5$  with  $\text{Re}(\text{CO})_3(\text{CNBu}^t)_2$ .<sup>223</sup>

From the above kinetic results it is apparent that the differences in the  $\text{M}_2(\text{CO})_8(\text{CNR})_2$  (M = Re, Mn) structures determined reflect the kinetics of the reaction of  $\text{M}_2(\text{CO})_{10}$  with RNC ligands.

## 14.5

### Experimental

#### 14.5.1 Data collection

The synthesis of the complexes  $\text{Re}_2(\text{CO})_9(\text{CNBu}^t)(\text{I})$ ,  $\text{Re}_2(\text{CO})_8(\text{CNC}_6\text{H}_3\text{Me}_2-2,6)_2(\text{II})$ ,  $\text{Re}_2(\text{CO})_7(\text{CNMe})_3(\text{III})$  and  $\text{Re}_2(\text{CO})_6(\text{CNC}_6\text{H}_3\text{Me}_2-2,6)_4(\text{IV})$  is described in ch. XI, and of  $\text{Mn}_2(\text{CO})_8(\text{CNBu}^t)_2(\text{V})$  and  $\text{Mn}_2(\text{CO})_6(\text{CNC}_6\text{H}_3\text{Me}_2-2,6)_4(\text{VI})$  in Ref. 220. Crystals of the complexes were grown under

nitrogen at 20°C from solutions of dichloromethane-hexane (I,II,IV) or benzene-hexane (III), or from deoxygenated pentane solutions at -5°C (V,VI).

In each case, preliminary investigation was done using standard Weissenberg and precession photography. Refined cell constants were obtained during data collection on a Philips FW1100 four-circle diffractometer at 20°C, using either MoK $\alpha$  (I,II,III,V and VI) or CuK $\alpha$  (IV) graphite-monochromated radiation (see Appendix 8(d) for details). Lorentz and polarization corrections were applied in all cases. For the rhenium structures (I-IV), the data was corrected for absorption using the computer program DIFABS, an empirical method for correcting diffractometer data for absorption effects, written by N. Walker and D. Stuart,<sup>237a</sup> and adapted by G. Kruger.<sup>237b</sup>

Crystal data and details of the data collections and structural analyses are summarized in Tables 14.18 (I-IV) and 14.19 (V and VI). Definitions of the crystallographic R-indices used are given in Appendix B(f).

#### 14.5.2 Structure solution and refinement

The structures were solved and refined using the program SHELXS2.<sup>238a</sup> The metal atom(s) were placed by a Patterson synthesis, and the positions of the other non-hydrogen atoms, and hydrogen atoms, if located (V only), were found by difference Fourier syntheses. Refinement of positional parameters of all atoms, and anisotropic temperature factors for the non-carbon (II-IV,VI) or non-hydrogen (V) atoms, was done by full-matrix least-squares methods, and was considered complete when all parameter shifts were less than 0.5 $\sigma$ . Scattering factors for Re(O) and Mn(O) were taken from "International Tables for X-ray Crystallography",<sup>238b</sup> and anomalous dispersion corrections<sup>238c</sup> were made for the rhenium and manganese atoms. Final fractional atomic co-ordinates, together with isotropic temperature factors for the carbon (I-IV,VI) or hydrogen (V) atoms for structures (I)-(VI) are given in Tables 14.20 to 14.25 respectively, and anisotropic temperature factors for the non-carbon (I-IV,VI) or non-hydrogen (V) atoms in Tables 14.26 to 14.31

TABLE 14.18: Crystal data and details of structure analyses for the  $Re_2(CO)_{10-n}(CNR)_n$  ( $n = 1-4$ ) complexes (I-IV)

| Complex Formula         | (I)                      | (II)                  | (III)                                     | (IV)                 |
|-------------------------|--------------------------|-----------------------|---|----------------------|
| $Re_2(CO)_8(CNMe)_2$    | $Re_2(CO)_8(CNMe)_2$     | $Re_2(CO)_6(CNMe)_3$  | $Re_2(CO)_4(CNMe)_5$                      | $Re_2(CO)_6(CNMe)_2$ |
| $Re_2C_4H_8O_8$         | $Re_2C_{25}H_{10}O_2O_8$ | $Re_2C_{12}H_8N_2O_7$ | $Re_2C_6H_2N_2O_6$                        |                      |
| 707.62                  | 950.75                   | 691.63                | 1065.15                                   |                      |
| white, needles          | cream, needles           | yellow, crystals      | yellow, rectangular                       |                      |
| Crystal dimensions (mm) | 0.19x0.18x0.13           | 0.20x0.12x1.10        | 0.20x0.19x0.14                            | 0.60x0.40x0.40       |
| Space Group             | Pbcn (No. 61)            | P1 (No. 2)            | P2 <sub>1</sub> /n (No. 14 <sup>n</sup> ) | Pccn (No. 56)        |
| a(Å)                    | 17.160(7)                | 15.145(7)             | 10.874(5)                                 | 13.832(6)            |
| b(Å)                    | 18.300(7)                | 9.294(4)              | 16.175(7)                                 | 11.322(5)            |
| c(Å)                    | 12.370(5)                | 10.328(5)             | 17.711(5)                                 | 26.401(11)           |
| a(°)                    | 90                       | 92.70(3)              | 90  | 90                   |
| β(°)                    | 90                       | 74.47(2)              | 90.07(3)                                  | 90                   |
| γ(°)                    | 90                       | 98.85(3)              | 90  | 90                   |
| U(Å <sup>3</sup> )      | 3984.53                  | 1383.94               | 1883.92                                   | 4134.55              |
| Z                       | 8                        | 2                     | 4   | 4                    |
| F(000)                  | 2575.22                  | 807.80                | 1255.61                                   | 2055.61              |
| Dc(g cm <sup>-3</sup> ) | 2.42                     | 2.04                  | 2.44                                      | 1.71                 |
| μ(cm <sup>-1</sup> )    | 119.71                   | 84.10                 | 123.37                                    | 104.39               |
| λ(Å)                    | 0.7107(MoKα)             | 0.7107(MoKα)          | 0.7107(MoKα)                              | 1.5418(CuKα)         |
| Scan Mode               | ω/2θ                     | ω/2θ                  | ω/2θ                                      | ω/2θ                 |

TABLE 14.18: Crystal data and details of structure analyses for the  $\text{Re}_2(\text{CO})_{10-n}(\text{CNR})_n$  ( $n = 1-4$ ) complexes  
<sup>a</sup> (I-IV)

|   | (I)        | (II)       | (III)      | (IV)       |
|---|------------|------------|------------|------------|
| Range (°)                                     | 35°-26     | 35°-23     | 35°-26     | 35°-56     |
| Scan width (°)                                | 0.90       | 1.40       | 1.30       | 1.60       |
| Scan speed (°sec <sup>-1</sup> )              | 0.030      | 0.047      | 0.043      | 0.052      |
| Range of h <sub>k</sub> l                     | -h, +h, +l | ±h, ±k, ±l | ±h, ±k, ±l | +h, +k, +l |
| Measured intensities                          | 2520       | 3815       | 3828.      | 3470       |
| Unique reflections                            | 2168       | 3748       | 3631       | 3052       |
| Internal consistency R-index                  | 0.0000     | 0.0117     | 0.0700     | 0.0000     |
| Omitted reflections                           | 272        | 347        | 236        | 160        |
| Cut-off criterion                             | F < σF     | F < σF     | F < σF     | F < σF     |
| R   | 0.0505     | 0.0386     | 0.0596     | 0.1090     |
| R <sub>w</sub>                                | 0.0391     | 0.0334     | 0.0467     | 0.1112     |
| k (weight w <sub>hkl</sub> /σ <sup>2</sup> F) | 0.2600     | 0.3329     | 0.4835     | 3.1265     |

<sup>a</sup> Cell choice 2 ("International Tables for Crystallography Vol. A. Space Group Symmetry", T. Hahn (Ed.), D. Reidel Publishing Co., Dordrecht, Holland (1983), p 177).



TABLE 14.19: Crystal data and details of structure analyses for the  $Mn_2(CO)_{10-n}(CNR)_n$  ( $n = 2, 4$ ) complexes (V, VI)

|                                  | (V)                             | (VI)                             |
|----------------------------------|---------------------------------|----------------------------------|
| Complex                          | $Mn_2(CO)_8(CNtBu^t)_2$         | $Mn_2(CO)_6(CNC_6H_5Me_2-2,6)_4$ |
| Formula                          | $Mn_2C_{18}H_{18}N_2O_8$        | $Mn_2C_{42}H_{36}N_4O_6$         |
| Mr                               | 500.21                          | 802.63                           |
| Colour, shape                    | yellow, rectangular             | orange, rectangular              |
| Crystal dimensions (mm)          | 0.17x0.16x0.13                  | 0.16x0.16x0.14                   |
| Space Group                      | $P2_1/n$ (No. 14 <sup>b</sup> ) | Pccn (No. 56)                    |
| a(Å)                             | 20.535(8)                       | 13.895(6)                        |
| b(Å)                             | 12.291(5)                       | 11.131(4)                        |
| c(Å)                             | 9.289(4)                        | 26.125(10)                       |
| α(°)                             | 90                              | 90                               |
| β(°)                             | 90.38(3)                        | 90                               |
| γ(°)                             | 90                              | 90                               |
| U(Å <sup>3</sup> )               | 1344.45                         | 4040.63                          |
| Z                                | 4                               | 4                                |
| F(000)                           | 1519.94                         | 1555.97                          |
| Dc(gcm <sup>-3</sup> )           | 1.42                            | 1.32                             |
| μ(cm <sup>-1</sup> )             | 10.72                           | 6.25                             |
| λ(Å)                             | 0.7107(MoKα)                    | 0.7107(MoKα)                     |
| Scan mode                        | ω/2θ                            | ω/2θ                             |
| Range (°)                        | 3≤θ≤26                          | 3≤θ≤26                           |
| Scan width (°)                   | 0.60                            | 0.40                             |
| Scan speed (°sec <sup>-1</sup> ) | 0.020                           | 0.016                            |
| Range of h, k, l                 | +h, +k, +l                      | +h, +k, +l                       |
| Measured intensities             | 4178                            | 3184                             |
| Unique reflections               | 3798                            | 2690                             |
| Internal consistency R-index     | 0.0000                          | 0.0223                           |
| Omitted reflections              | -                               | 1111                             |
| Out-off criterion                | -                               | F<2σF                            |
| R = R <sub>w</sub> <sup>a</sup>  | 0.0563                          | 0.1320                           |

<sup>a</sup> Unit weights used

<sup>b</sup> Cell choice 2 ("International Tables for Crystallography Vol. A. Space Group Symmetry", T. Hahn (Ed.), D. Reidel Publishing Co., Dordrecht, Holland (1983), p 177).

respectively. Appendix D contains a listing of the Structure Factors.

14.5.3 Refinement problems with  $Mn_2(CO)_6(CNC_6H_5Mn_2-2,6)_4$  (VI)

Problem was experienced with the refinement of (VI). Initially a data set was collected under  $CuK\alpha$  radiation ( $\lambda = 1.5418\text{\AA}$ ). The structure was solved using this data set ( 2823 unique reflections), but refinement of the structure below an R-value of 0.19 could not be achieved. Data was re-collected, using  $MoK\alpha$  radiation ( $\lambda = 0.7107\text{\AA}$ ). With this new data set ( 2690 unique reflections), refinement of the structure could proceed. Refinement below an R-value of ca. 0.17 could only be achieved after omitting all reflections (1111) with  $F < 2\sigma F$ . The final R-value of the refined structure was 0.1320. At this stage, all parameter shifts were less than  $0.5\sigma$ , and there was no residual electron density. Inability to refine the structure further could be due to (i) a too small an effective data set (1579 unique reflections), (ii) a poor data set due to inferior quality crystals, or (iii) compound deterioration before data collection (crystal decomposition during data collection was not, however, observed).

TABLE 14.20: Final atomic co-ordinates, and isotropic temperature factors of the C-atoms, for  $\text{Re}_2(\text{CO})_9(\text{CNBu}^t)(\text{I})$

| Atom  | $x/a$      | $y/b$       | $z/c$       | $U(\text{\AA}^2)$ |
|-------|------------|-------------|-------------|-------------------|
| Re(1) | 0.3693(0)  | -0.1472(0)  | -0.2293(1)  |                   |
| Re(2) | 0.2234(0)  | -0.0982(0)  | -0.1789(1)  |                   |
| O(1)  | 0.2849(8)  | -0.2931(7)  | -0.3315(11) |                   |
| O(2)  | 0.5176(7)  | -0.2018(7)  | -0.4099(10) |                   |
| O(3)  | 0.2896(8)  | -0.091187   | -0.5146(10) |                   |
| O(4)  | 0.4277(9)  | -0.1994(9)  | -0.073F(12) |                   |
| O(5)  | 0.2237(8)  | -0.2496(8)  | -0.0697(11) |                   |
| O(6)  | 0.1240(7)  | -0.1643(8)  | -0.3690(11) |                   |
| O(7)  | 0.0842(8)  | -0.0405(8)  | -0.0524(11) |                   |
| O(8)  | 0.2476(6)  | 0.0439(7)   | -0.3101(11) |                   |
| O(9)  | 0.3443(7)  | -0.0385(7)  | -0.0154(9)  |                   |
| N     | 0.4350(7)  | 0.0138(7)   | -0.2579(11) |                   |
| C(1)  | 0.3191(9)  | -0.2397(10) | -0.3195(14) | 0.053(5)          |
| C(2)  | 0.4633(10) | -0.1787(9)  | -0.3690(15) | 0.052(5)          |
| C(3)  | 0.3197(10) | -0.1090(10) | -0.4428(17) | 0.057(5)          |
| C(4)  | 0.4082(10) | -0.1906(10) | -0.1575(17) | 0.060(5)          |
| C(5)  | 0.2223(11) | -0.1928(11) | -0.1073(16) | 0.067(5)          |
| C(6)  | 0.1599(12) | -0.1428(11) | -0.2962(17) | 0.079(6)          |
| C(7)  | 0.1368(11) | -0.0636(11) | -0.1000(16) | 0.071(6)          |
| C(8)  | 0.2375(10) | -0.0081(10) | -0.2573(15) | 0.051(5)          |
| C(9)  | 0.2992(11) | -0.0576(10) | -0.0760(16) | 0.065(6)          |
| C(10) | 0.4146(8)  | -0.0443(8)  | -0.2706(12) | 0.036(4)          |
| C(11) | 0.4627(11) | 0.0886(10)  | -0.2327(16) | 0.068(5)          |
| C(12) | 0.5457(24) | 0.0877(23)  | -0.1941(31) | 0.250(20)         |
| C(13) | 0.4272(21) | 0.1419(18)  | -0.3087(26) | 0.194(14)         |
| C(14) | 0.4231(27) | 0.1084(26)  | 0.1132(39)  | 0.276(23)         |

TABLE 14.21: Final atomic co-ordinates, and isotropic temperature factors of the C-atoms, for  $\text{Re}_2(\text{CO})_8(\text{CNC}_6\text{H}_3\text{Me}_2-2,6)_2(\text{II})$

| Atom  | $x/a$      | $y/b$       | $z/c$       | $U(\text{\AA}^2)$ |
|-------|------------|-------------|-------------|-------------------|
| Re(1) | 0.3591(0)  | -0.2532(0)  | -0.0150(0)  |                   |
| Re(2) | 0.1661(0)  | -0.1993(0)  | -0.0172(0)  |                   |
| N(1)  | 0.3659(5)  | -0.4271(9)  | -0.2913(8)  |                   |
| N(2)  | 0.0923(5)  | -0.2582(9)  | 0.2985(8)   |                   |
| O(1)  | 0.4388(5)  | 0.0250(9)   | -0.1890(9)  |                   |
| O(2)  | 0.5479(4)  | -0.3179(9)  | 0.0029(8)   |                   |
| O(3)  | 0.2543(5)  | -0.5381(8)  | 0.1347(7)   |                   |
| O(4)  | 0.3248(5)  | -0.0727(9)  | 0.2497(8)   |                   |
| O(5)  | 0.1273(5)  | -0.5267(8)  | -0.0846(9)  |                   |
| O(6)  | 0.2334(5)  | 0.1202(8)   | 0.0551(8)   |                   |
| O(7)  | 0.2449(5)  | -0.1250(8)  | -0.3191(7)  |                   |
| O(8)  | -0.0316(4) | -0.1566(8)  | -0.0144(8)  |                   |
| CN(1) | 0.3619(6)  | -0.3657(10) | -0.1902(10) | 0.048(2)          |
| CN(2) | 0.1201(6)  | -0.2407(10) | 0.1858(10)  | 0.051(2)          |
| CO(1) | 0.4097(7)  | -0.0743(12) | -0.1234(10) | 0.060(3)          |
| CO(2) | 0.4785(7)  | -0.2925(11) | -0.0091(10) | 0.060(3)          |
| CO(3) | 0.2917(7)  | -0.4323(12) | 0.0820(10)  | 0.054(3)          |
| CO(4) | 0.3391(7)  | -0.1372(12) | 0.1534(11)  | 0.064(3)          |
| CO(5) | 0.1420(6)  | -0.4063(12) | -0.0586(10) | 0.054(3)          |
| CO(6) | 0.2076(6)  | 0.0065(12)  | 0.0246(10)  | 0.056(3)          |
| CO(7) | 0.2163(6)  | -0.1522(11) | -0.2132(11) | 0.057(3)          |
| CO(8) | 0.0418(7)  | -0.1711(11) | -0.0135(10) | 0.059(3)          |
| C(1)  | 0.3652(6)  | -0.5109(11) | -0.4124(10) | 0.051(2)          |
| C(2)  | 0.3346(7)  | -0.6574(12) | -0.3946(11) | 0.069(3)          |
| C(3)  | 0.3335(8)  | -0.7459(14) | -0.5155(13) | 0.092(4)          |
| C(4)  | 0.3663(9)  | -0.6695(15) | -0.6388(13) | 0.097(4)          |
| C(5)  | 0.3979(7)  | -0.5295(13) | -0.6546(11) | 0.075(3)          |
| C(6)  | 0.3984(7)  | -0.4386(12) | -0.5377(11) | 0.072(3)          |
| C(7)  | 0.3029(7)  | -0.7330(13) | -0.2585(11) | 0.076(3)          |
| C(8)  | 0.4292(8)  | -0.2778(14) | -0.5409(12) | 0.088(4)          |
| C(9)  | 0.0401(6)  | -0.2632(11) | 0.4344(10)  | 0.060(3)          |

TABLE 14.21: Final atomic co-ordinates, and isotropic temperature factors of the C-atoms, for  $\text{Re}_2(\text{CO})_8(\text{CNC}_6\text{H}_3\text{N}_2-2,6)_2(\text{II})$   
(Contd)

| Atom  | $x/\text{\AA}$ | $y/\text{\AA}$ | $z/\text{\AA}$ | $U(\text{\AA}^2)$ |
|-------|----------------|----------------|----------------|-------------------|
| C(10) | -0.0419(7)     | -0.2003(12)    | 0.4567(11)     | 0.075(3)          |
| C(11) | -0.0917(8)     | -0.2064(14)    | 0.6053(12)     | 0.086(4)          |
| C(12) | -0.0836(8)     | -0.2734(14)    | 0.6959(12)     | 0.088(4)          |
| C(13) | 0.0169(8)      | -0.3395(14)    | 0.6665(12)     | 0.085(4)          |
| C(14) | 0.0737(7)      | -0.3304(12)    | 0.5268(11)     | 0.067(3)          |
| C(15) | 0.1829(7)      | -0.3993(13)    | 0.4828(11)     | 0.079(3)          |
| C(16) | -0.0732(8)     | -0.1300(14)    | 0.3639(13)     | 0.093(4)          |

TABLE 14.22: Final atomic co-ordinates, and isotropic temperature factors of the C-atoms, for  $\text{Re}_2(\text{CO})_7(\text{CNMe})_3(\text{III})$

| Atom                | x/a         | y/b        | z/c         | $U(\text{\AA}^2)$ |
|---------------------|-------------|------------|-------------|-------------------|
| Re(1)               | 0.3462(0)   | 0.3410(0)  | 0.2501(0)   |                   |
| Re(2)               | 0.1060(0)   | 0.4333(0)  | 0.2499(1)   |                   |
| O(1)                | 0.5907(10)  | 0.2467(10) | 0.2489(13)  |                   |
| O(2)                | 0.1745(11)  | 0.1869(7)  | 0.2470(13)  |                   |
| O(3)                | 0.4638(10)  | 0.5131(9)  | 0.2486(16)  |                   |
| O(5)                | -0.1363(10) | 0.5293(9)  | 0.2472(15)  |                   |
| O(6)                | 0.0208(13)  | 0.3164(9)  | 0.0446(12)  |                   |
| O(7)                | 0.0213(12)  | 0.3175(9)  | 0.4541(13)  |                   |
| N(2)                | 0.2315(10)  | 0.5527(8)  | 0.4556(11)  |                   |
| N(3)                | 0.2327(10)  | 0.5564(9)  | 0.0433(11)  |                   |
| N(1) <sup>a</sup>   | 0.3377(12)  | 0.3453(10) | -0.0470(13) | 0.014(2)          |
| N(4) <sup>a</sup>   | 0.3337(12)  | 0.3432(10) | 0.5454(13)  | 0.014(2)          |
| C(1)                | 0.4964(13)  | 0.2799(10) | 0.2527(14)  | 0.063(4)          |
| C(2)                | 0.2392(12)  | 0.2469(10) | 0.2478(14)  | 0.056(4)          |
| C(3)                | 0.4206(13)  | 0.4498(11) | 0.2488(15)  | 0.061(4)          |
| C(4)                | 0.3314(14)  | 0.3455(11) | 0.4479(16)  | 0.073(5)          |
| C(5)                | -0.0395(14) | 0.4999(11) | 0.2464(15)  | 0.066(4)          |
| C(6)                | 0.0511(13)  | 0.3627(10) | 0.1234(14)  | 0.059(4)          |
| C(7)                | 0.0541(13)  | 0.3612(11) | 0.3776(15)  | 0.063(4)          |
| C(8)                | 0.3349(14)  | 0.3437(11) | 0.0524(16)  | 0.076(5)          |
| C(9)                | 0.1844(10)  | 0.5138(8)  | 0.3808(11)  | 0.039(3)          |
| C(10)               | 0.1886(11)  | 0.5142(10) | 0.1155(13)  | 0.051(4)          |
| C(11A) <sup>a</sup> | 0.3489(23)  | 0.3337(19) | -0.1779(25) | 0.052(5)          |
| C(11B) <sup>a</sup> | 0.3455(23)  | 0.3299(19) | 0.8754(25)  | 0.052(5)          |
| C(12)               | 0.2914(15)  | 0.6073(12) | 0.5448(16)  | 0.078(5)          |
| C(13)               | 0.2931(15)  | 0.6101(12) | -0.0432(16) | 0.079(5)          |

<sup>a</sup> Disordered isonitrile: Atoms N(1), N(4), C(11A) and C(11B) have s.o.f. of 0.5; Atoms N(1) and N(4), and C(11A) and C(11B), assigned common isotropic temperature factors.

TABLE 14.23: Final atomic co-ordinates, and isotropic temperature factors of the C-atoms, for  $\text{Re}_2(\text{CO})_6(\text{CNC}_6\text{H}_3\text{Me}_2-2,6)_4(\text{IV})$

| Atom  | x/a         | y/b         | z/c        | $U(\text{\AA}^2)$ |
|-------|-------------|-------------|------------|-------------------|
| Re    | 0.1394(1)   | 0.2342(1)   | 0.6076(0)  |                   |
| N(1)  | 0.1248(11)  | 0.4887(16)  | 0.6599(6)  |                   |
| N(2)  | 0.1333(11)  | 0.3320(20)  | 0.4946(5)  |                   |
| O(1)  | -0.0774(11) | 0.1845(17)  | 0.6081(5)  |                   |
| O(2)  | 0.1684(12)  | 0.1326(19)  | 0.7143(5)  |                   |
| O(3)  | 0.1819(13)  | -0.0077(14) | 0.5577(5)  |                   |
| C(1)  | -0.0015(14) | 0.2098(15)  | 0.4582(6)  | 0.046(4)          |
| C(2)  | 0.1549(13)  | 0.1637(17)  | 0.6758(7)  | 0.059(5)          |
| C(3)  | 0.1697(15)  | 0.0845(19)  | 0.5770(8)  | 0.064(5)          |
| C(4)  | 0.1309(15)  | 0.3905(19)  | 0.6401(7)  | 0.063(5)          |
| C(5)  | 0.1371(13)  | 0.3024(18)  | 0.5366(7)  | 0.052(4)          |
| C(6)  | 0.1228(13)  | 0.6001(17)  | 0.6835(7)  | 0.056(5)          |
| C(7)  | 0.1173(15)  | 0.6030(20)  | 0.7361(3)  | 0.067(6)          |
| C(8)  | 0.1178(18)  | 0.7201(23)  | 0.7582(10) | 0.089(8)          |
| C(9)  | 0.1164(18)  | 0.8218(24)  | 0.7272(10) | 0.089(7)          |
| C(10) | 0.1227(16)  | 0.8138(23)  | 0.6745(9)  | 0.080(6)          |
| C(11) | 0.1246(14)  | 0.6984(19)  | 0.6526(7)  | 0.058(5)          |
| C(12) | 0.1171(18)  | 0.4894(26)  | 0.7670(10) | 0.099(8)          |
| C(13) | 0.1226(16)  | 0.6851(23)  | 0.5944(9)  | 0.077(6)          |
| C(14) | 0.1327(14)  | 0.3623(18)  | 0.4427(7)  | 0.060(5)          |
| C(15) | 0.1449(15)  | 0.4847(20)  | 0.4290(8)  | 0.070(6)          |
| C(16) | 0.1406(17)  | 0.5085(23)  | 0.3743(10) | 0.086(7)          |
| C(17) | 0.1342(17)  | 0.4100(24)  | 0.3427(10) | 0.086(7)          |
| C(18) | 0.1265(20)  | 0.3030(30)  | 0.3556(10) | 0.099(8)          |
| C(19) | 0.1260(15)  | 0.2674(19)  | 0.4092(9)  | 0.066(6)          |
| C(20) | 0.1540(18)  | 0.5888(23)  | 0.4682(10) | 0.092(8)          |
| C(21) | 0.1082(20)  | 0.1451(26)  | 0.4273(10) | 0.102(9)          |

TABLE 14.24(a): Final atomic co-ordinates of the non-H atoms for  
 $\text{Mn}_2(\text{CO})_9(\text{CNBu}^t)_2(\text{V})$

| Atom  | x/a        | y/b        | z/c        |
|-------|------------|------------|------------|
| Mn(1) | 0.1180(0)  | 0.3937(0)  | 0.4005(1)  |
| Mn(2) | 0.1375(0)  | 0.2059(1)  | 0.2125(1)  |
| N(1)  | 0.0292(2)  | 0.2591(3)  | 0.6014(4)  |
| N(2)  | 0.2298(2)  | 0.3125(3)  | 0.5985(4)  |
| O(3)  | 0.0998(2)  | 0.5944(3)  | 0.5652(4)  |
| O(4)  | 0.0071(2)  | 0.4510(3)  | 0.2073(4)  |
| O(5)  | 0.2092(2)  | 0.5108(3)  | 0.2090(4)  |
| O(6)  | -0.0061(2) | 0.1786(3)  | 0.2330(5)  |
| O(7)  | 0.1559(2)  | 0.0095(3)  | 0.0383(5)  |
| O(8)  | 0.1203(2)  | 0.3645(3)  | -0.0285(4) |
| O(9)  | 0.1521(2)  | 0.0868(3)  | 0.4897(4)  |
| O(10) | 0.2780(2)  | 0.2668(3)  | 0.2221(5)  |
| C(1)  | 0.0615(2)  | 0.3083(3)  | 0.5244(5)  |
| C(2)  | 0.1890(2)  | 0.3428(3)  | 0.5219(5)  |
| C(3)  | 0.1067(2)  | 0.5144(4)  | 0.5032(5)  |
| C(4)  | 0.0493(2)  | 0.4272(4)  | 0.2816(5)  |
| C(5)  | 0.1743(2)  | 0.4632(3)  | 0.2622(5)  |
| C(6)  | 0.0488(2)  | 0.1911(4)  | 0.2266(5)  |
| C(7)  | 0.1494(3)  | 0.0867(4)  | 0.1055(5)  |
| C(8)  | 0.1270(2)  | 0.3042(4)  | 0.0652(6)  |
| C(9)  | 0.1464(2)  | 0.1374(4)  | 0.3863(5)  |
| C(10) | 0.2242(2)  | 0.2444(4)  | 0.2208(5)  |
| C(11) | -0.0095(2) | 0.1954(4)  | 0.7001(5)  |
| C(12) | 0.0363(4)  | 0.1165(8)  | 0.7777(11) |
| C(13) | -0.0424(5) | 0.2743(8)  | 0.8040(11) |
| C(14) | -0.0610(4) | 0.1347(8)  | 0.6106(10) |
| C(15) | 0.2788(2)  | 0.2655(4)  | 0.6953(5)  |
| C(16) | 0.3024(6)  | 0.3614(8)  | 7980(11)   |
| C(17) | 0.3305(5)  | 0.2198(12) | 131(10)    |
| C(18) | 0.2444(3)  | 0.1827(6)  | 884(9)     |



TABLE 14.24(b): Final atomic co-ordinates and isotropic temperature factors of the Hydrogen atoms, for  $Mn_2(CO)_8(CNBU^t)_2(V)$

| Atom   | x/a       | y/b       | z/c       | $U(\text{\AA}^2)$ |
|--------|-----------|-----------|-----------|-------------------|
| H(12A) | 0.060(5)  | 0.163(8)  | 0.831(10) | 0.21(5)           |
| H(12B) | 0.008(3)  | 0.079(5)  | 0.852(6)  | 0.97(2)           |
| H(12C) | 0.047(4)  | 0.066(7)  | 0.701(10) | 0.20(4)           |
| H(13A) | -0.012(3) | 0.305(6)  | 0.849(7)  | 0.11(3)           |
| H(13B) | -0.086(5) | 0.286(8)  | 0.729(11) | 0.24(5)           |
| H(13C) | -0.062(4) | 0.219(6)  | 0.875(8)  | 0.17(3)           |
| H(14A) | -0.083(4) | 0.101(6)  | 0.550(8)  | 0.15(4)           |
| H(14B) | -0.027(3) | 0.088(5)  | 0.552(7)  | 0.13(3)           |
| H(14C) | -0.088(3) | 0.095(5)  | 0.677(6)  | 0.11(2)           |
| H(16A) | 0.275(7)  | 0.338(11) | 0.899(14) | 0.34(7)           |
| H(16B) | 0.334(4)  | 0.406(7)  | 0.702(10) | 0.2C(4)           |
| H(16C) | 0.332(3)  | 0.340(5)  | 0.828(7)  | 0.10(2)           |
| H(17A) | 0.311(3)  | 0.151(5)  | 0.577(8)  | 0.13(3)           |
| H(17B) | 0.362(3)  | 0.193(6)  | 0.651(7)  | 0.12(2)           |
| H(17C) | 0.346(4)  | 0.272(7)  | 0.532(8)  | 0.16(3)           |
| H(18A) | 0.278(4)  | 0.151(6)  | 0.861(8)  | 0.14(4)           |
| H(18B) | 0.244(4)  | 0.134(6)  | 0.715(9)  | 0.16(4)           |
| H(18C) | 0.209(4)  | 0.221(6)  | 0.843(8)  | 0.16(3)           |

TABLE 14.25: Final atomic co-ordinates, and isotropic temperature factors of the non-C atoms, for  $Mn_2(CO)_6(CNC_6H_3Me_2-2,6)_4$  (VI)

| Atom  | x/a       | y/b       | z/c       | U( $\text{\AA}^2$ ) |
|-------|-----------|-----------|-----------|---------------------|
| Mn    | 0.1443(2) | 0.2607(2) | 0.6082(1) |                     |
| N(1)  | 0.135(1)  | 0.163(1)  | 0.499(1)  |                     |
| N(2)  | 0.128(1)  | 0.012(1)  | 0.859(1)  |                     |
| O(1)  | 0.165(1)  | 0.362(1)  | 0.712(1)  |                     |
| O(2)  | -0.062(1) | 0.315(1)  | 0.608(1)  |                     |
| O(3)  | 0.183(1)  | 0.499(1)  | 0.562(1)  |                     |
| C(1)  | 0.159(1)  | 0.321(2)  | 0.672(1)  | 0.062(5)            |
| C(2)  | 0.021(1)  | 0.291(1)  | 0.608(1)  | 0.061(5)            |
| C(3)  | 0.174(1)  | 0.404(1)  | 0.580(1)  | 0.052(5)            |
| C(4)  | 0.140(1)  | 0.195(1)  | 0.541(1)  | 0.059(5)            |
| C(5)  | 0.134(1)  | 0.105(1)  | 0.338(1)  | 0.053(4)            |
| C(6)  | 0.132(1)  | 0.141(1)  | 0.446(1)  | 0.063(5)            |
| C(7)  | 0.120(1)  | 0.234(2)  | 0.413(1)  | 0.072(6)            |
| C(8)  | 0.121(1)  | 0.210(2)  | 0.360(1)  | 0.087(7)            |
| C(9)  | 0.131(2)  | 0.093(2)  | 0.343(1)  | 0.101(8)            |
| C(10) | 0.143(2)  | -0.002(2) | 0.376(1)  | 0.096(7)            |
| C(11) | 0.142(2)  | 0.023(2)  | 0.430(1)  | 0.081(6)            |
| C(12) | 0.109(2)  | 0.383(2)  | 0.434(1)  | 0.087(7)            |
| C(13) | 0.155(2)  | -0.082(2) | 0.467(1)  | 0.095(8)            |
| C(14) | 0.122(1)  | -0.100(2) | 0.683(1)  | 0.056(5)            |
| C(15) | 0.119(1)  | -0.103(2) | 0.737(1)  | 0.068(6)            |
| C(16) | 0.118(2)  | -0.218(2) | 0.758(1)  | 0.087(7)            |
| C(17) | 0.119(2)  | -0.322(2) | 0.728(1)  | 0.097(8)            |
| C(18) | 0.121(2)  | -0.319(2) | 0.675(1)  | 0.079(6)            |
| C(19) | 0.122(1)  | -0.203(1) | 0.855(1)  | 0.058(5)            |
| C(20) | 0.124(1)  | -0.193(2) | 0.855(1)  | 0.070(6)            |
| C(21) | 0.119(2)  | 0.010(2)  | 0.755(1)  | 0.095(7)            |

TABLE 14.26: Anisotropic temperature factors ( $\text{\AA}^2$ ) for the non-C atoms of  $\text{Re}_2(\text{CO})_9(\text{CNBu}^t)_1(\text{I})$

| Atom  | U11       | U22       | U33       | U23        | U13        | U12        |
|-------|-----------|-----------|-----------|------------|------------|------------|
| Re(1) | 0.0434(4) | 0.0352(3) | 0.0425(6) | -0.0001(4) | -0.0050(4) | 0.0002(3)  |
| Re(2) | 0.0429(4) | 0.0499(4) | 0.0461(6) | 0.0024(4)  | -0.0002(4) | -0.0021(4) |
| O(1)  | 0.103(11) | 0.063(9)  | 0.117(12) | 0.010(9)   | -0.007(10) | -0.019(8)  |
| O(2)  | 0.062(8)  | 0.074(9)  | 0.086(10) | -0.027(8)  | 0.016(8)   | 0.003(7)   |
| O(3)  | 0.110(11) | 0.084(10) | 0.065(11) | 0.018(8)   | -0.033(9)  | -0.019(9)  |
| O(4)  | 0.127(13) | 0.130(13) | 0.075(12) | 0.026(10)  | -0.037(10) | 0.043(11)  |
| O(5)  | 0.132(12) | 0.075(9)  | 0.094(11) | 0.034(9)   | -0.023(10) | -0.009(10) |
| O(6)  | 0.086(10) | 0.143(15) | 0.082(11) | -0.023(10) | -0.020(9)  | -0.022(10) |
| O(7)  | 0.082(9)  | 0.112(12) | 0.102(12) | -0.013(10) | 0.040(10)  | 0.001(9)   |
| O(8)  | 0.062(8)  | 0.069(9)  | 0.107(11) | 0.015(9)   | -0.019(8)  | 0.002(6)   |
| O(9)  | 0.084(10) | 0.124(12) | 0.044(9)  | -0.022(8)  | 0.000(8)   | -0.014(8)  |
| N     | 0.049(8)  | 0.041(8)  | 0.057(10) | -0.013(7)  | -0.003(8)  | 0.002(7)   |

TABLE 14.27: Anisotropic temperature factors ( $\text{\AA}^2$ ) for the non-C atoms of  $\text{Re}_2(\text{CO})_9(\text{CNC}_6\text{H}_5\text{Me}_2-2,6)_2(\text{II})$

| Atom  | U11       | U22       | U33       | U23        | U13        | U12       |
|-------|-----------|-----------|-----------|------------|------------|-----------|
| Re(1) | 0.0419(2) | 0.0475(3) | 0.0433(3) | 0.0020(2)  | -0.0106(2) | 0.0054(2) |
| Re(2) | 0.0444(2) | 0.0441(3) | 0.0471(3) | -0.0008(2) | -0.0117(2) | 0.0092(2) |
| N(1)  | 0.046(4)  | 0.061(6)  | 0.055(5)  | 0.011(5)   | -0.004(4)  | 0.010(4)  |
| N(2)  | 0.055(5)  | 0.072(6)  | 0.045(5)  | -0.000(5)  | -0.006(4)  | 0.005(4)  |
| O(1)  | 0.094(6)  | 0.074(6)  | 0.123(7)  | 0.041(6)   | -0.022(5)  | -0.012(5) |
| O(2)  | 0.080(4)  | 0.101(7)  | 0.104(6)  | -0.004(5)  | -0.027(4)  | 0.027(4)  |
| O(3)  | 0.083(5)  | 0.067(5)  | 0.082(6)  | 0.023(5)   | -0.007(4)  | 0.005(4)  |
| O(4)  | 0.100(6)  | 0.113(7)  | 0.077(6)  | -0.041(5)  | -0.032(5)  | 0.036(5)  |
| O(5)  | 0.099(6)  | 0.057(5)  | 0.131(8)  | -0.013(5)  | -0.043(5)  | 0.008(4)  |
| O(6)  | 0.085(5)  | 0.054(5)  | 0.099(6)  | -0.011(5)  | -0.016(4)  | 0.003(4)  |
| O(7)  | 0.104(6)  | 0.091(6)  | 0.050(5)  | 0.010(4)   | -0.012(4)  | 0.017(5)  |
| O(8)  | 0.049(4)  | 0.083(6)  | 0.143(7)  | -0.007(5)  | -0.044(4)  | 0.021(4)  |

TABLE 14.28: Anisotropic temperature factors ( $\text{\AA}^2$ ) for the non-C atoms of  $\text{Re}_2(\text{CO})_7(\text{CNMe})_3(\text{III})$ :

| Atom  | U11       | U22       | U33        | U23        | U13        | U12       |
|-------|-----------|-----------|------------|------------|------------|-----------|
| Re(1) | 0.0418(3) | 0.0408(4) | 0.0341(3)  | -0.0001(3) | 0.0001(2)  | 0.0053(2) |
| Re(2) | 0.0374(3) | 0.0392(3) | 0.0461(3)  | 0.0003(3)  | -0.0001(2) | 0.0007(2) |
| O(1)  | 0.079(8)  | 0.149(15) | 0.143(11)  | 0.011(11)  | 0.006(8)   | 0.069(9)  |
| O(2)  | 0.093(8)  | 0.049(9)  | 0.149(12)  | 0.000(8)   | -0.019(8)  | -0.004(7) |
| O(3)  | 0.071(8)  | 0.071(10) | 0.22(15)   | 0.009(11)  | -0.008(9)  | -0.014(7) |
| O(5)  | 0.070(7)  | 0.093(11) | 0.0203(15) | 0.001(12)  | -0.000(9)  | 0.023(8)  |
| O(6)  | 0.144(12) | 0.101(12) | 0.087(9)   | -0.022(8)  | -0.038(8)  | -0.021(9) |
| O(7)  | 0.117(10) | 0.096(12) | 0.114(10)  | 0.037(9)   | 0.046(8)   | -0.009(8) |
| N(2)  | 0.058(7)  | 0.065(10) | 0.052(7)   | 0.006(7)   | 0.010(5)   | -0.008(6) |
| N(3)  | 0.071(8)  | 0.075(11) | 0.052(7)   | 0.022(7)   | -0.009(6)  | -0.019(7) |

TABLE 14.29: Anisotropic temperature factors ( $\text{\AA}^2$ ) for the non-C atoms of  $\text{Re}_2(\text{CO})_6(\text{CNC}_6\text{H}_3\text{Me}_2-2,6)_4(\text{IV})$ :

| Atom | U11       | U22       | U33       | U23       | U13       | U12        |
|------|-----------|-----------|-----------|-----------|-----------|------------|
| Re   | 0.0560(6) | 0.0587(6) | 0.0289(5) | 0.0034(3) | 0.0020(3) | 0.0054(4)  |
| N(1) | 0.045(10) | 0.075(12) | 0.067(10) | -0.010(8) | 0.009(8)  | 0.006(8)   |
| N(2) | 0.061(11) | 0.161(18) | 0.025(7)  | 0.032(9)  | -0.007(7) | 0.012(11)  |
| O(1) | 0.043(10) | 0.131(14) | 0.095(12) | 0.014(9)  | 0.003(8)  | -0.004(9)  |
| O(2) | 0.107(14) | 0.197(19) | 0.034(7)  | 0.044(9)  | 0.001(8)  | -0.018(13) |
| O(3) | 0.125(15) | 0.074(10) | 0.076(10) | -0.008(8) | 0.012(9)  | 0.017(10)  |

TABLE 14.30: Anisotropic temperature factors ( $\text{\AA}^2$ ) for the non-H atoms of  $\text{Mn}_2(\text{CO})_8(\text{CNBu}^t)_2(\text{V})$

| Atom  | U11       | U22       | U33       | U23        | U13        | U12        |
|-------|-----------|-----------|-----------|------------|------------|------------|
| Mn(1) | 0.0412(3) | 0.0444(3) | 0.0614(4) | 0.0003(3)  | -0.0047(3) | -0.0014(2) |
| Mn(2) | 0.0530(3) | 0.0529(4) | 0.0584(4) | -0.0039(3) | -0.0000(3) | -0.0001(3) |
| N(1)  | 0.048(2)  | 0.063(2)  | 0.067(2)  | 0.003(2)   | 0.004(2)   | -0.004(2)  |
| N(2)  | 0.048(2)  | 0.067(2)  | 0.063(2)  | 0.008(2)   | -0.009(2)  | -0.001(2)  |
| O(3)  | 0.094(3)  | 0.072(2)  | 0.124(3)  | -0.043(2)  | -0.013(2)  | 0.011(2)   |
| O(4)  | 0.074(2)  | 0.100(3)  | 0.119(3)  | 0.010(2)   | -0.040(2)  | 0.017(2)   |
| O(5)  | 0.092(3)  | 0.084(3)  | 0.109(3)  | 0.020(2)   | 0.013(2)   | -0.035(2)  |
| O(6)  | 0.054(2)  | 0.104(3)  | 0.143(4)  | -0.006(3)  | -0.009(2)  | -0.015(2)  |
| O(7)  | 0.162(4)  | 0.082(3)  | 0.099(3)  | -0.041(3)  | 0.002(3)   | 0.018(3)   |
| O(8)  | 0.111(3)  | 0.100(3)  | 0.082(3)  | 0.025(2)   | -0.012(2)  | 0.003(2)   |
| O(9)  | 0.092(2)  | 0.069(2)  | 0.076(2)  | 0.011(2)   | -0.008(2)  | -0.006(2)  |
| O(10) | 0.053(2)  | 0.112(3)  | 0.135(4)  | 0.015(3)   | 0.012(2)   | -0.002(2)  |
| C(11) | 0.043(2)  | 0.054(2)  | 0.095(3)  | -0.007(2)  | -0.009(2)  | 0.004(2)   |
| C(2)  | 0.048(2)  | 0.048(2)  | 0.062(3)  | -0.005(2)  | 0.006(2)   | -0.009(2)  |
| C(3)  | 0.053(2)  | 0.063(3)  | 0.076(3)  | -0.007(3)  | -0.010(2)  | 0.001(2)   |
| C(4)  | 0.059(3)  | 0.056(3)  | 0.086(3)  | -0.001(2)  | -0.002(2)  | -0.000(2)  |
| C(5)  | 0.058(2)  | 0.047(2)  | 0.075(3)  | 0.004(2)   | -0.011(2)  | -0.005(2)  |
| C(6)  | 0.068(3)  | 0.061(3)  | 0.077(3)  | -0.006(2)  | -0.011(2)  | -0.007(2)  |
| C(7)  | 0.087(3)  | 0.075(3)  | 0.065(3)  | -0.002(3)  | -0.001(3)  | 0.005(3)   |
| C(8)  | 0.062(3)  | 0.082(3)  | 0.073(3)  | -0.002(3)  | -0.005(2)  | -0.002(3)  |
| C(9)  | 0.054(2)  | 0.059(3)  | 0.065(3)  | -0.007(2)  | -0.002(2)  | -0.008(2)  |
| C(10) | 0.063(3)  | 0.066(3)  | 0.063(3)  | 0.008(2)   | 0.006(2)   | 0.007(2)   |
| C(11) | 0.054(2)  | 0.064(3)  | 0.067(3)  | 0.001(2)   | 0.009(2)   | -0.010(2)  |
| C(12) | 0.107(5)  | 0.097(5)  | 0.110(6)  | 0.032(5)   | 0.002(5)   | -0.001(4)  |
| C(13) | 0.111(6)  | 0.117(6)  | 0.114(6)  | -0.023(5)  | 0.045(6)   | -0.012(5)  |
| C(14) | 0.091(5)  | 0.124(7)  | 0.116(6)  | -0.003(5)  | -0.003(5)  | -0.052(5)  |
| C(15) | 0.050(2)  | 0.083(3)  | 0.059(3)  | 0.012(2)   | 0.007(2)   | -0.004(2)  |
| C(16) | 0.152(8)  | 0.131(7)  | 0.115(7)  | 0.015(5)   | -0.084(7)  | -0.033(6)  |
| C(17) | 0.088(5)  | 0.201(12) | 0.109(6)  | 0.045(8)   | 0.012(5)   | 0.065(7)   |
| C(18) | 0.081(4)  | 0.120(6)  | 0.092(5)  | 0.045(5)   | -0.003(4)  | 0.006(4)   |

TABLE 14.31: Anisotropic temperature factors ( $\text{\AA}^2$ ) for the non-C atoms of  $\text{Mn}_2(\text{CO})_6(\text{CNC}_5\text{H}_3\text{Me}_2-2,6)_4(\text{VI})$

| Atom | U11       | U22       | U33       | U23        | U13        | U12        |
|------|-----------|-----------|-----------|------------|------------|------------|
| Mn   | 0.081(2)  | 0.033(1)  | 0.049(1)  | -0.001(1)  | -0.001(2)  | -0.008(1)  |
| N(1) | 0.096(13) | 0.051(9)  | 0.050(10) | 0.001(8)   | -0.005(11) | -0.025(9)  |
| N(2) | 0.105(13) | 0.040(7)  | 0.074(12) | 0.007(8)   | 0.012(11)  | -0.023(8)  |
| O(1) | 0.142(16) | 0.110(11) | 0.050(9)  | -0.028(9)  | -0.008(10) | -0.013(11) |
| O(2) | 0.074(10) | 0.080(9)  | 0.103(11) | -0.011(10) | 0.004(10)  | 0.011(7)   |
| O(3) | 0.132(12) | 0.034(6)  | 0.087(11) | 0.012(7)   | 0.001(10)  | -0.016(7)  |

XV. THE REACTION BETWEEN RHENIUM DECACARBONYL AND PHOSPHINE LIGANDS

15A. Introduction

This chapter deals with aspects of the reaction between  $\text{Re}_2(\text{CO})_{10}$  (and  $\text{Mn}_2(\text{CO})_{10}$ ) with phosphine ligands. The synthetic methods (Thermal, photochemical,  $\text{NMe}_3\text{O}$ -assisted), and the products obtained for the reaction between  $\text{Re}_2(\text{CO})_{10}$  and  $\text{PR}_3$ , have been reviewed in section 10.2. Section 15B discusses the characterization of the  $\text{Re}_2(\text{CO})_{10-n}(\text{PR}_3)_n$  ( $n = 1-4$ ) products obtained, and in particular, the use of IR spectroscopy in the assignment of substitution geometry. Kinetic and mechanistic studies reported for the reaction of  $\text{M}_2(\text{CO})_{10}$  ( $\text{M} = \text{Re}, \text{Mn}$ ) with  $\text{PR}_3$  are covered in Section 15C.

In Section 15D, the catalytic synthesis and characterization of a range of  $\text{Re}_2(\text{CO})_{10}(\text{PR}_3)_n$  ( $n = 1, 2$ ) complexes is presented. This work is an extension of the Pd-catalysed substitution of  $\text{Re}_2(\text{CO})_{10}$  by RNC ligands (ch. XI) to the bulkier  $\text{PR}_3$  ligands. The preparation of isomers of  $\text{Re}_2(\text{CO})_8(\text{PR}_3)_2$  by alternate synthetic routes is also presented. The  $\text{Re}_2(\text{CO})_8(\text{PR}_3)_2$  products are discussed in relation to complexes of this type reported in the Literature, and a rationalization of the formation of isomers is given.

Finally, the Crystal and Molecular X-ray structure of di-ax $[\text{Re}_2(\text{CO})_8(\text{PMe}_2\text{Ph})_2]$  is presented in Section 15E. This structure determination was undertaken to establish the molecular geometry, and to investigate the structural effect of replacing the isonitrile ligand (see ch. XIV) with the more sterically demanding phosphine ligand.

15B. Discussion of the IR spectral data of  $\text{Re}_2(\text{CO})_{10-n}(\text{PR}_3)_n$  ( $n = 1-4$ ) complexes

15B.1 Introduction

The reaction (both thermal and photochemical) between  $\text{Re}_2(\text{CO})_{10}$  and  $\text{PR}_3$  has been investigated by many groups (see section 10.2) and in most cases, the product(s) obtained was either ax- $\text{Re}_2(\text{CO})_9(\text{PR}_3)$ , and/or di-ax- $\text{Re}_2(\text{CO})_8$ -

$(PR_3)_2$ . In some reactions, sideproducts such as mer-trans- $HRe(CO)_3(PR_3)_2$  were also obtained. There have, however, also been reports of the synthesis of equatorially-substituted  $Re_2(CO)_{10-n}(PR_3)_n$  ( $n = 1,2$ ) products, as well as  $Re_2(CO)_7(PR_3)_2$  and  $Re_2(CO)_6(PR_3)_4$  products. It is thus apparent that potentially a wide range of complexes (both expected and unexpected) have been observed from the reaction between  $Re_2(CO)_{10}$  and  $PR_3$ .

Techniques which have been employed in the characterization of products from the reaction of  $Re_2(CO)_{10}$  with  $PR_3$ , include IR spectroscopy,  $^1H$  NMR and  $^{31}P$  NMR spectroscopy, mass spectroscopy, elemental analysis and chemical reactivity. In general, elemental analysis is used to establish the molecular formula of the compound (but this would not differentiate between, for instance,  $Re_2(CO)_{10-2n}(PR_3)_{2n}$  and  $HRe(CO)_{5-n}(PR_3)_n$  ( $n = 1,2$ )). In some cases mass spectroscopy has been used to obtain the parent ion, and establish that the species in fact a dimer. Cleavage reactions may give information relating to the substitution geometry, in particular the number of phosphine ligands on each metal atom.  $^1H$  NMR and, more recently,  $^{31}P$  NMR spectroscopy has been used to obtain information on the sites occupied by the phosphine ligands (from the number and position of the resonances). IR spectroscopy, however, is the most ubiquitous, and sometimes the only, means of product identification. The number and intensity of the  $\nu(CO)$  bands in the IR spectrum relates to the molecular geometry. However, IR spectroscopy is not highly reliable in this regard, as the number of  $\nu(CO)$  bands predicted from Group Theory Analysis often does not correspond to the number observed in practice, as band overlap may occur, resulting in fewer bands. Alternately, there may be more bands, due to a Raman band which gains some weak IR intensity, or to a lowering of the molecular symmetry from the ideal point group symmetry as a result of internal asymmetry of the molecule.

Although X-ray Crystallography remains the ultimate technique for molecular structure determination, no X-ray



studies of  $\text{Re}_2(\text{CO})_{10-n}(\text{PR}_3)_n$  ( $n = 1-4$ ) complexes have been reported in the literature to date. Several  $\text{Mn}_2(\text{CO})_{10-n}(\text{PR}_3)_n$  ( $n = 1,2$ ) X-ray structures have, however, been reported, and these will be used to establish a correlation between IR data and molecular geometry, to aid in the structural interpretation of the IR spectra of  $\text{Re}_2(\text{CO})_{10-n}(\text{PR}_3)_n$  ( $n = 1,2$ ) complexes.

Despite the limitations of the IR spectral methods as a tool for structure assignment, especially when used alone, it has been used extensively in the literature, but in view of the confusion which exists over the characterization of certain of the substituted products, the existing IR spectral data for  $\text{Re}_2(\text{CO})_{10-n}(\text{PR}_3)_n$  ( $n = 1-4$ ) complexes will be reviewed here, and an attempt made to relate IR spectra to substitution geometry. Where relevant, reference will also be made to certain  $\text{Mn}_2(\text{CO})_{10-n}(\text{PR}_3)_n$  ( $n = 1,2$ ) complexes which aid in the structural interpretation of the IR data.

#### 15B.2. $\text{Re}_2(\text{CO})_9(\text{PR}_3)$ complexes

Complexes of the type  $\text{M}_2(\text{CO})_9(\text{L})$  have two possible geometries, (Fig. 15.1), viz. *ax*(IA) or *eq*(IB). Although *eq*- $\text{M}_2(\text{CO})_9(\text{L})$  (IB) is the electronically favoured isomer (see ch. XII), with bulky phosphine ligand L, steric factors may dominate, resulting in *ax*- $\text{M}_2(\text{CO})_9(\text{PR}_3)$  ( $\text{M} = \text{Re}, \text{Mn}$ ), (IA).

According to Group Theory, *ax*- $\text{M}_2(\text{CO})_9(\text{L})$ , of molecular symmetry  $D_{4d}$ , should exhibit 5 IR active  $\nu(\text{CO})$  bands, while *eq*- $\text{M}_2(\text{CO})_9(\text{L})$ , of molecular symmetry  $C_{6v}$ , should have 9 bands. However, in practice, many *eq*- $\text{Mn}_2(\text{CO})_9(\text{L})$  complexes<sup>222</sup> have only 6  $\nu(\text{CO})$  bands in the IR spectrum, owing to band overlap.

Table 15.1 lists IR spectral data of some reported  $\text{M}_2(\text{CO})_9(\text{PR}_3)$  ( $\text{M} = \text{Mn}, \text{Re}$ ) derivatives. In general, the degree of substitution is based on elemental analysis, and in some cases, a mass spectrum, while  $^1\text{H}$  NMR and/or IR spectroscopy is used to determine the molecular geometry (i.e. (IA) or (IB)).

The IR spectrum of *ax*- $\text{Mn}_2(\text{CO})_9(\text{PMe}_2\text{Ph})$ ,<sup>222</sup> the

axial substitution (IA) of which has been confirmed by an X-ray crystallographic structure,<sup>22\*</sup> with 5  $\nu(\text{CO})$  bands, (Table 15.1) is typical of a wide range of  $\underline{\text{ax}}\text{-Mn}_2(\text{CO})_9(\text{PR}_3)$  and  $\underline{\text{ax}}\text{-Mn}_2(\text{CO})_9(\text{AsR}_3)$  complexes.<sup>23\*</sup> Since the structure of these complexes is reliably known, the IR spectral pattern can be taken as typical of complexes of the type (IA).

In the reaction of  $\text{HMn}(\text{CO})_5$  with  $\text{AsPh}_3$ <sup>24\*</sup> in the presence of  $\text{O}_2$  at  $-10^\circ\text{C}$ , both the isomers  $\underline{\text{ax}}\text{-Mn}_2(\text{CO})_9\text{-}(\text{AsPh}_3)$  and  $\underline{\text{eq}}\text{-Mn}_2(\text{CO})_9(\text{AsPh}_3)$  were reported as being produced. However, the compound identifications were based on elemental analyses only. The IR spectra of these complexes gave 5 and 7 bands respectively in the carbonyl region (see Table 15.1). Both complexes gave very similar  $^1\text{H}$  NMR spectra.

Reports of  $\text{Re}_2(\text{CO})_9(\text{PR}_3)$  products are less numerous than those of  $\text{Re}_2(\text{CO})_9(\text{PR}_3)_2$  complexes, as the thermal reaction between  $\text{Re}_2(\text{CO})_{10}$  and  $\text{PR}_3$  tends to give  $\text{Re}_2(\text{CO})_9\text{-}(\text{PR}_3)_2$ , even when only one equivalent of phosphine is used. There have been several reports of the synthesis of  $\underline{\text{ax}}\text{-Re}_2(\text{CO})_9(\text{PPh}_3)$ .<sup>12,13\*</sup> The IR spectrum, in various solvents, is given in Table 15.1. In toluene,<sup>12,13</sup> there are 5  $\nu(\text{CO})$  bands, as expected. However, in certain solvents, eg. cyclohexane,<sup>11b</sup> and decalin,<sup>11a</sup> there is an additional weak band at ca.  $1975\text{ cm}^{-1}$ , a shoulder to the very strong band at ca.  $1998\text{ cm}^{-1}$ . This band (B2) gains some intensity in the IR spectrum by the lowering of the local symmetry induced by the triphenylphosphine ligand.<sup>11a</sup> In  $\text{CHCl}_3$ ,<sup>11a</sup> the weak peak at ca.  $1960\text{ cm}^{-1}$  is absent, but this may be due to band weakness or overlap. The IR spectrum in  $\text{CHCl}_3$  of  $\underline{\text{ax}}\text{-Re}_2(\text{CO})_9(\text{PMePh}_2)$ <sup>18\*</sup> has a similar pattern (Table 15.1). However,  $\text{Re}_2(\text{CO})_9(\text{PMe}_2\text{Ph})$  (identified by elemental analysis) has a different IR spectrum and its geometry has been assigned as  $\underline{\text{eq}}\text{-Re}_2(\text{CO})_9(\text{PMe}_2\text{Ph})$ <sup>18\*</sup> on the basis of the 7  $\nu(\text{CO})$  bands in the IR spectrum (Table 15.1). There has also been a report of  $\underline{\text{eq}}\text{-Re}_2(\text{CO})_9(\text{PPh}_3)$ .<sup>12\*</sup> The only evidence for this, however, is an IR spectrum (Table 15.1). It is to be noted that the spectra of these

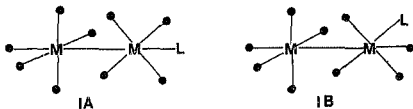
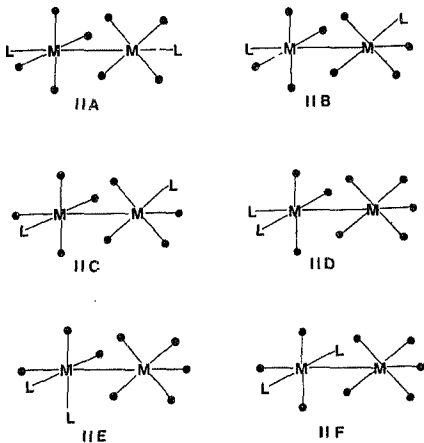


Figure 15.1: Possible isomers for  $M_2(CO)_9(L)$  complexes (\* = CO)  
(IA) ax and (IB) eq.

two reported *eq*-isomers do not correspond to that of *eq*- $Mn_2(CO)_9(AsPh_3)$ , or those of *eq*- $Mn_2(CO)_9(L)$  complexes<sup>22</sup> either (eg. *eq*- $Mn_2(CO)_9(py)$ , IR(hexane),  $\nu(CO)$ : 2091(w), 2017(s), 2006(s), 1980(vs), 1960(m), 1940(m)  $cm^{-1}$ ),<sup>22</sup> or those of the *eq*- $Re_2(CO)_9(CNR)$  complexes (ch. XI), and thus must be regarded with circumspection. The product  $Mn_2(CO)_9[P(OCH_2)_3CET]$  obtained from the reaction of  $Mn_2(CO)_{10}$  with  $P(OCH_2)_3CET$ , [IR(benzene),  $\nu(CO)$ : 2094(w), 2020(ms), 1995(vu), 1980(m), 1965(m), 1930(sh)  $cm^{-1}$ ] was concluded on the basis of  $^1H$  NMR data to be a mixture of *ax*- and *eq*-isomers!<sup>23</sup> In the complex IR spectrum of  $Mn_2(CO)_9(PF_3)[IR(hexane), \nu(CO): 2110(s), 2038(s), 2015(vs), 2002(m), 1992(2), 1980(m), 1960(w), 1954(m) cm^{-1}]$ , formed from the reaction of  $Mn_2(CO)_{10}$  with  $PF_3$ , assigned as *ax*- $Mn_2(CO)_9(PF_3)$ ,<sup>24</sup> there appear to be several unexplained peaks. The  $Re_2(CO)_9(PF_3)$  product is reported as being analogous.<sup>25</sup>

TABLE 15.1: IR spectral data of  $M_2(CO)_9(L)$  ( $M = Mn, Re, L = AsR_3, PR_3$ ) complexes

| Complex                    | Solvent     | $\nu(CO)/cm^{-1}$  | Ref  |
|----------------------------|-------------|--|------|
| ax- $Mn_2(CO)_9(PMe_2Ph)$  | benzene     | 2094(w), 2016(s), 1993(vs), 1969(sh), 1938(m)                    | 223  |
| ax- $Mn_2(CO)_9(AsPh_3)$   | hexane      | 2098(m), 2020(s), 2000(vs), 1977(s), 1943(s)                     | 258  |
| eq- $Mn_2(CO)_9(AsPh_3)$   | $CCl_4$     | 2102(w), 2085(w), 2028(vs), 2002(sh), 1995(s), 1940(sh), 1920(s) | 238  |
| ax- $Re_2(CO)_9(PPh_3)$    | toluene     | 2104(m), 2032(w), 1991(vs), 1960', 1960(w), 1934(m)              | 181a |
|                            | cyclohexane | 2107(2), 2034(w), 1998(vs), 1976(w,sh), 1968(m), 1941(m)         | 181a |
|                            | decalin     | 2106(w), 2034(w), 1998(vs), 1973(w,sh), 1967(m), 1941(m)         | 181b |
|                            | $CHCl_3$    | 2100(s), 2080(w), 2030(w), 2000(vs), 1940(s)                     | 182a |
| eq- $Re_2(CO)_9(PPh_3)$    | $CHCl_3$    | 1963(s), 1912(m), 1897(m), 1880(sh)                              | 182a |
| ax- $Re_2(CO)_9(PMePh_2)$  | $CHCl_3$    | 2060(w), 2000(m), 1972(sh), 1945(s,br), 1910(m)                  | 184  |
| eq- $Re_2(CO)_9(PMe_2Ph)$  | $CHCl_3$    | 2090(w), 2020(m), 2010(sh), 1995(sh), 1975(s)                    | 184  |
|                            |             | 1940(s), 1915(sh)  |      |
| ax- $Mn_2(CO)_9(AsMe_2Ph)$ | benzene     | 2092(m), 2020(s), 1991(vs), 1968(sh), 1936(m)                    | 223  |



**Figure 15.2:** Possible isomers for  $M_2(CO)_8(L)_2$  complexes (rotamers) not shown;  $\bullet = CO$   
 (IIA) diax, (IIB) 1,2-ax,eq, (IIC) 1,2-eq,eq,  
 (IID) 1,1-ax,eq, (IIE) 1,1-cis-dieq, and  
 (IIF) 1,1-trans-dieq.

TABLE 15.2: IR spectral data of  $M_2(CO)_8(L)_2$  ( $M = Mn, Re$ ;  $L = AsR_3, Ph_3$ ) complexes

| Complex  | Solvent    | $\nu(CO)/cm^{-1}$   | Ref      |
|--|------------|---|----------|
| $diox-M_2(CO)_8(Ph_3PPh)_2$                        | benzene    | 1983(w), 1954(vs)   | 223      |
| $1,2\text{-eq, eq-}Re_2(CO)_8(AsMe_2Ph)_2^a$       | benzene    | 2056(w), 1989(s), 1956(s), 1914(m)                              | 223      |
| $diox-Re_2(CO)_8(Ph_3)_2$                          | $CHCl_3$   | 2010(w), 1960(vs)   | 182a     |
| $1,2\text{-ax, eq-}Re_2(CO)_8(PMe_2Ph)_2^b$        | $CCl_4$    | 2100(w), 2060(mw), 2000(s), 1955(s, br), 1905(s)                | 183      |
| $1,2\text{-ax, eq-}Re_2(CO)_8(PMePh)_2^b$          | benzene    | 2090(w), 2058(m), 2000(s), 1955(s, br), 1925(s)                 | 184      |
| $1,2\text{-ax, eq-}Re_2(CO)_8(AsMe_2Ph)_2^b$       | $CCl_4$    | 2105(w), 2060(mw), 2005(s), 1945(s, br), 1905(s)                | 183      |
| $1,2\text{-ax, eq-}Re_2(CO)_8(PPh_3)_2$            | hexane     | 2068(mw), 2006(m), 1971(s), 1928(s), 1917(s)                    | 170      |
| $1,2\text{-ax, eq-}Re_2(CO)_8(Ph_3)_2$             | toluene    | 2069(mw), 2012(m), 1964(vs, br), 1934(m), 1921(m)               | 170      |
| $1,2\text{-eq, eq-}Re_2(CO)_8(PMe_2)_2$            | toluene    | 2063(w), 2005(m), 1959(s), 1925(w), 1910(m)                     | 170      |
| $1,2\text{-eq, eq-}Re_2(CO)_8[P(O)Me_3]_2$         | toluene    | 2077(w), 2024(mw), 1968(s), 1968(sh), 1946(w), 1918(mw)         | 170      |
| $1,2\text{-eq, eq-}Re_2(CO)_8[P(OPh)_3]_2$         | toluene    | 2081(w), 2032(m), 1994(s), 1976(sh), 1954(w), 1931(m)           | 170      |
| $1,2\text{-eq, eq-}Re_2(CO)_8[Ph_2CH_2PPh_2]$      | toluene    | 2073(m), 2030(m), 1980(s), 1956(w), 1940(w), 1915(m)            | 170, 198 |
| $1,2\text{-eq, eq-}Re_2(CO)_8[Me_2PCH_2PMe_2]$     | toluene    | 2067(m), 2012(s), 1980(sh), 1971(w), 1947(m), 1934(sh), 1914(s) | 198      |
| $1,2\text{-eq, eq-}Re_2(CO)_8[Ph_2PCH_2PPh_2]$     | toluene    | 2070(m), 2017(m), 1983(s), 1944(m), 1915(s)                     | 198      |
| $1,2\text{-eq, eq-}Re_2(CO)_8[Me_2PCH_2CH_2PMe_2]$ | toluene    | 2066(w), 2010(m), 1975(s), 1938(m), 1911(s)                     | 198      |
| $1,1-Mn_2(CO)_8(PHPh)_2^c$                         | $CH_2Cl_2$ | 2070(w), 2060(sh), 2022(sh), 1989(w), 1945(vs), 1914(s)         | 189      |
| $diox-Re_2(CO)_8(PHPh)_2^c$                        | $CH_2Cl_2$ | 1984(m), 1946(s)  | 189      |

<sup>a</sup> eclipsed conformation

<sup>b</sup> Incorrectly characterized in references as 1,2-eq, eq-isomer (see text)

<sup>c</sup> See text for a discussion of the substitution geometry

The vast majority of reported  $M_2(CO)_9(PR_3)$  ( $M = Re, Mn$ ) complexes are undoubtedly axially substituted, having the characteristic 5-band  $\nu(CO)$  IR spectrum exemplified by  $ax-Mn_2(CO)_9(PMe_2Ph)$ . Indeed, there does not appear to be any convincing evidence for the existence of  $eq-Re_2(CO)_9(PR_3)$  isomers. Further,  $Mn_2(CO)_9(AsMe_2Ph)^{223}$  is the  $ax$ -isomer (IA), with an IR spectrum (Table 15.1) analogous to that of  $ax-Mn_2(CO)_9(PMe_2Ph)^{221}$  although  $Mn_2(CO)_8(AsMe_2Ph)_2^{235}$  is equatorially substituted (vide infra).

### 15B.3 $Re_2(CO)_8(PR_3)_2$ complexes

The possible isomers for  $M_2(CO)_8(L)_2$  complexes are shown in Fig. 15.2. Not considering rotamers, there are six possible isomers, viz. (IIA)  $diax$ , (IIB)  $1,2-ax,eq$ , (IIC)  $1,2-eq,eq$ , (IID)  $1,1-ax,eq$ , (IIE)  $1,1-cis-dieq$ , and (IIF)  $1,1-trans-dieq - M_2(CO)_8(L)_2$ .

An X-ray crystallographic structure of  $Mn_2(CO)_8(PMePh_2)_2^{233}$  has shown the substitution geometry to be  $diax$  (IIA). From Group Theory,  $diax-M_2(CO)_8(L)_2$  (staggered conformation), of molecular symmetry  $D_{4d}$ , is predicted to give 2  $\nu(CO)$  bands in the IR spectrum. As the spectrum of  $diax-Mn_2(CO)_8(PMePh_2)_2$  (Table 15.2) shows, this is indeed found to be the case. This spectrum, typical of  $diax-M_2(CO)_8(L)_2$  substitution, is observed for a wide range of  $Mn_2(CO)_8(PR_3)_2$  complexes.<sup>223, 235</sup>

The related complex,  $Mn_2(CO)_8(AsMe_2Ph)_2$ , has been shown by an X-ray crystallographic structure<sup>235</sup> to have  $1,2-eq,eq$ -substitution. However, the conformation is eclipsed, not staggered as for the diequatorially substituted isonitrile derivatives of  $M_2(CO)_{10}$  ( $M = Mn, Re$ ) (ch. XIV), owing to steric congestion (see section 15.2). The IR spectrum is different having 4  $\nu(CO)$  bands (see Table 15.2). This is the number predicted by Group Theory for eclipsed  $1,2-dieq-M_2(CO)_8(L)_2$  (molecular symmetry  $C_{2h}$ ). Although the IR spectrum (in cyclohexane) of  $Mn_2(CO)_8(AsMe_3)_2$  is analogous,<sup>223</sup> that of  $Mn_2(CO)_8(AsEt_3)_2$ , which presumably has the same structure, has an additional weak band at  $1927\text{ cm}^{-1}$  [IR(cyclohexane),  $\nu(CO)$ : 2055(w), 1990(s), 1952(s),

1927(w), 1915(m)  $\text{cm}^{-1}$ ).<sup>211</sup>

There have been reports of diax- $\text{Mn}_2(\text{CO})_8(\text{AsR}_3)_2$  complexes,<sup>244a</sup> with the typical IR spectrum (eg. diax- $\text{Mn}_2(\text{CO})_8(\text{AsPh}_3)_2$ , IR( $\text{CS}_2$ ),  $\nu(\text{CO})$ : 1982(w), 1953(vs)  $\text{cm}^{-1}$ ).<sup>250a</sup> This indicates that the steric bulk (cone angle) of the  $\text{AsR}_3$  ligand determines the substitution geometry; the longer Mn-As than Mn-P bond facilitates eq-substitution, where the steric bulk of the  $\text{AsR}_3$  ligand is not too great.

A third type of arsine-complex,  $[\text{Mn}_2(\text{CO})_8(\mu\text{-AsR}_2)_2]$ , has been reported as the product of the so-called "Lambert's reaction" (ligand fragmentation at high temperature).<sup>244</sup> This product may be distinguished by elemental analysis, and IR spectral data (eg.  $[\text{Mn}_2(\text{CO})_8(\mu\text{-AsPh}_2)_2]$ , IR ( $\text{CS}_2$ ),  $\nu(\text{CO})$ : 2042(s), 1983(sh), 1978(s), 1965(m)  $\text{cm}^{-1}$ ),<sup>244a</sup> ie. 4  $\nu(\text{CO})$  peaks, as compared to 2 for diax-, and 4 or 5 (intensity pattern: w,s,s,(w),m) for dieq- $\text{Mn}_2(\text{CO})_8(\text{AsR}_3)_2$ .

The large majority of direct reactions (thermal, photochemical) between  $\text{Re}_2(\text{CO})_{10}$  and  $\text{PR}_3$  are reported to yield diax- $\text{Re}_2(\text{CO})_8(\text{PR}_3)_2$  ( $\text{PR}_3 = \text{PPh}_3$ <sup>144,2,145</sup>,  $\text{P}(\text{C}_6\text{H}_5)_2$ <sup>145</sup>,  $\text{P}(\text{O}i\text{Pr})_3$ <sup>145</sup>,  $\text{P}(\text{C}_6\text{H}_{11})_3$ <sup>145,24</sup>,  $\text{P}(\text{C}_6\text{H}_4\text{Me-}p)_3$ <sup>145</sup>,  $\text{P}(\text{OC}_6\text{H}_4\text{Me-}o)_3$ <sup>145</sup>,  $\text{P}(\text{OC}_6\text{H}_4\text{Cf-}p)_3$ <sup>145</sup>), as the sole or major product. These complexes all have one weak and one very strong band in the carbonyl region of the IR spectrum, characteristic of diax- $\text{M}_2(\text{CO})_8(\text{L})_2$  complexes (IIA). The IR spectrum of a typical example, the much-studied diax- $\text{Re}_2(\text{CO})_8(\text{PPh}_3)_2$ , is shown in Table 15.2.

There has been one report of diequatorially-substituted  $\text{Re}_2(\text{CO})_8(\text{PR}_3)_2$  complexes obtained from the direct reaction (thermal or photochemical) of  $\text{Re}_2(\text{CO})_{10}$  with  $\text{PR}_3$  ( $\text{PR}_3 = \text{PMe}_2\text{Ph}$ ,<sup>141</sup>  $\text{PMePh}_2$ <sup>141</sup>). The  $\text{Re}_2(\text{CO})_8(\text{PR}_3)_2$  products were characterized by elemental analyses, <sup>1</sup>H NMR and IR spectra, and cleavage reactions, and on the basis of IR spectral data (see Table 15.2), the geometry was assigned as 1,2-eq,eq- $\text{Re}_2(\text{CO})_8(\text{PR}_3)_2$  (IIC) (but see below). The IR spectrum of the related  $\text{Re}_2(\text{CO})_8(\text{AsMe}_2\text{Ph})_2$  complex<sup>141</sup> (Table 15.2) is analogous.

Reaction of  $(\mu\text{-H})(\mu\text{-olefin})\text{Re}_2(\text{CO})_8$  complexes with



PR<sub>3</sub> ligands<sup>17</sup> yields 1,2-eq,eq-Re<sub>2</sub>(CO)<sub>8</sub>(PR<sub>3</sub>)<sub>2</sub> (IIC) (R = P(OMe)<sub>3</sub>, PMe<sub>3</sub>, P(OPh)<sub>3</sub>) or 1,2-ax,eq-Re<sub>2</sub>(CO)<sub>8</sub>(PR<sub>3</sub>)<sub>2</sub> (IIB) (R = Bu<sup>n</sup>, Ph), depending on the size of the PR<sub>3</sub> ligand (Tolman cone angles<sup>18</sup>: P(OMe)<sub>3</sub>, 107°; PMe<sub>3</sub>, 113°; P(OPh)<sub>3</sub>, 121-128°; PBu<sub>3</sub><sup>n</sup>, 132°; PPh<sub>3</sub>, 145°). The latter products, 1,2-ax,eq-Re<sub>2</sub>(CO)<sub>8</sub>(PR<sub>3</sub>)<sub>2</sub>, isomerize spontaneously in toluene solution at room temperature to the well-known diax-Re<sub>2</sub>(CO)<sub>8</sub>(PR<sub>3</sub>)<sub>2</sub> isomers (IIA). The 1,2-eq,eq-Re<sub>2</sub>(CO)<sub>8</sub>(PR<sub>3</sub>)<sub>2</sub> products appear to be stable to isomerization. Bidentate phosphine ligands, (P)<sub>2</sub>, also gave 1,2-eq,eq-Re<sub>2</sub>(CO)<sub>8</sub>(P)<sub>2</sub> products ((P)<sub>2</sub> = Ph<sub>2</sub>PCH<sub>2</sub>PPh<sub>2</sub><sup>19,19'</sup>, Me<sub>2</sub>PCH<sub>2</sub>PMe<sub>2</sub><sup>19''</sup>, Ph<sub>2</sub>PCH<sub>2</sub>CH<sub>2</sub>PPh<sub>2</sub><sup>19'''</sup>, Me<sub>2</sub>PCH<sub>2</sub>CH<sub>2</sub>PMe<sub>2</sub><sup>19''''</sup>). Here the chelating nature of the (P)<sub>2</sub> ligand imposes a restriction on the product geometry; the Tolman cone angles for the (P)<sub>2</sub> ligands (half chelate)<sup>19a</sup> are in the range 105-125°. The 1,2-ax,eq-Re<sub>2</sub>(CO)<sub>8</sub>(PR<sub>3</sub>)<sub>2</sub> products were characterized by <sup>31</sup>P NMR spectroscopy, and the 1,2-eq,eq-Re<sub>2</sub>(CO)<sub>8</sub>(PR<sub>3</sub>)<sub>2</sub> products by <sup>1</sup>H NMR spectroscopy, and the similarity of the IR spectra of these products to the pattern observed for 1,2-eq,eq-Re<sub>2</sub>(CO)<sub>8</sub>(py)<sub>2</sub><sup>17b</sup> [IR (toluene), ν(CO): 2062(w), 2006(m), 1950(s,br), 1917(sh), 1905(m) cm<sup>-1</sup>]. IR spectral data for these Re<sub>2</sub>(CO)<sub>8</sub>(PR<sub>3</sub>)<sub>2</sub> and Re<sub>2</sub>(CO)<sub>8</sub>(P)<sub>2</sub> products are given in Table 15.2.

An examination of the IR data for the Re<sub>2</sub>(CO)<sub>8</sub>(PR<sub>3</sub>)<sub>2</sub> complexes in Table 15.2 shows that the 1,2-ax,eq-Re<sub>2</sub>(CO)<sub>8</sub>(PR<sub>3</sub>)<sub>2</sub> (R = Bu<sup>n</sup>, Ph) complexes have 5 ν(CO) bands, and the 1,2-eq,eq-Re<sub>2</sub>(CO)<sub>8</sub>(PR<sub>3</sub>)<sub>2</sub> (R = OMe, Me, OPh) complexes have 6 or 5 (R = Me) ν(CO) bands, but the intensity patterns are quite different. Note the strong similarity of the IR spectra of the 1,2-eq,eq-Re<sub>2</sub>(CO)<sub>8</sub>(PR<sub>3</sub>)<sub>2</sub> complexes to that of 1,2-eq,eq-Re<sub>2</sub>(CO)<sub>8</sub>(CNC<sub>6</sub>H<sub>3</sub>Me<sub>2</sub>-2,6)<sub>2</sub> [IR(hexane), ν(CO): 2053(w), 2028(m), 1985(s), 1952(w), 1943(ms) cm<sup>-1</sup>] (see ch. XI). Further, the 5 ν(CO) band pattern for the Re<sub>2</sub>(CO)<sub>8</sub>(L)<sub>2</sub> (L = PMe<sub>2</sub>Ph, PMePh<sub>2</sub>, AsMe<sub>2</sub>Ph) complexes resemble that for the above 1,2-ax,eq-isomers rather than that for the above 1,2-eq,eq-isomers. Hence these Re<sub>2</sub>(CO)<sub>8</sub>(L)<sub>2</sub> complexes may have been incorrectly assigned. <sup>1912</sup> as the 1,2-eq,eq-isomers (IIC), instead of the 1,2-ax,eq-isomers (IIB). This

seems likely in view of the size of the  $\text{PMe}_2\text{Ph}$  and  $\text{PMePh}_2$  ligands (Tolman cone angles<sup>13</sup> of 122° and 136° respectively).

However, there would appear to be a seeming anomaly, in that  $\text{Re}_2(\text{CO})_8(\text{PMePh}_2)_2^{13a}$  and  $\text{Re}_2(\text{CO})_8(\text{PMe}_2\text{Ph})_2^{13b}$  were prepared by the thermal reaction of  $\text{Re}_2(\text{CO})_{10}$  with  $\text{PMePh}_2$  or  $\text{PMe}_2\text{Ph}$  under forcing conditions (xylene, 140°C, 15 h, 30%, and petroleum ether, 80-100°C, 60 h (4%) or 96 h (46%), respectively), while 1,2-ax,eq- $\text{Re}_2(\text{CO})_8(\text{PR}_3)_2$  ( $\text{R} = \text{Bu}^n, \text{Ph}$ ) isomerizes spontaneously in toluene solution at 25°C to di-ax- $\text{Re}_2(\text{CO})_8(\text{PR}_3)_2$ , with a half-life of 10 h ( $\text{PPh}_3$ ) or 1-2 days ( $\text{PBu}_3^n$ ).

Further, traces of 1,2-ax,eq- $\text{Re}_2(\text{CO})_8(\text{PR}_3)_2$  isomers were observed, in addition to the major di-ax- $\text{Re}_2(\text{CO})_8(\text{PR}_3)_2$  products, in the Pd-catalysed (140°C) and the mild  $\text{Me}_3\text{NO}$ -assisted ( $\text{CH}_2\text{Cl}_2$ , 40°C) reactions of  $\text{Re}_2(\text{CO})_{10}$  with  $\text{PR}_3$  ( $\text{PR}_3 = \text{PMe}_2\text{Ph}, \text{PMePh}_2, \text{P}(\text{CH}_2\text{C}_6\text{H}_5)_3, \text{PMe}_3, \text{P}(\text{OMe})_3$ ) (see section 15D.1). However, in the PdO-catalysed reaction of  $\text{Re}_2(\text{CO})_{10}$  with  $\text{PPh}_3$ , no eq-isomers were observed. Hence the stability of the eq-isomers would appear to be governed by the size of the  $\text{PR}_3$  ligand. The role of the ligand size and synthetic route in determining product geometry will be discussed in section 15D.1.

Mixture of ax- and eq-isomers have been claimed to have been obtained for  $[\text{Mn}_2(\text{CO})_8\{\text{P}(\text{OCH}_2)_3\text{C}_6\text{H}_5\}_2]^{13c}$  and  $[\text{M}_2(\text{CO})_8(\text{PF}_3)_2] (\text{M} = \text{Mn}, \text{Re})^{13d}$  products. (The IR spectra are complex). With a small phosphine ligand such as  $\text{PF}_3$  (Tolman cone angle<sup>13</sup> of 164°), a mixture of isomers probably reflects steric versus electronic control of product geometry.

Of note is the complex  $\text{Mn}_2(\text{CO})_8(\text{PPhPh}_2)_2^{13e}$  which has a different IR spectrum (Table 15.2), and has been shown by <sup>55</sup>Mn NMR spectroscopy to have the structure  $(\text{CO})_5\text{Mn}-\text{Mn}(\text{CO})_3(\text{PPhPh}_2)_2$ , with both phosphine ligands on the same Mn-atom. Thus there are three possible geometries for the complex, viz. 1,1-ax,eq(IID), 1,1-cis-dieq(IIE) or 1,1-trans-dieq(IIF).

Oxidation of  $\text{Mn}_2(\text{CO})_8(\text{PPhPh}_2)_2$  with  $\text{NO}/\text{PF}_6^-$  gives  $[\text{Mn}(\text{CO})_5(\text{PPhPh}_2)]\text{PF}_6$  and also cis- $[\text{Mn}(\text{CO})_4(\text{PPhPh}_2)_2]\text{PF}_6^{13f}$ .

This would seem to exclude (IIF), the 1,1-trans-dieq-isomer, which is unlikely on electronic grounds, in view of the cis-labilization effect (see ch. XII).

An example of (IID), the 1,1-ax,eq-isomer, is  $Mn_2(CO)_8(C_4H_8)^{2+}$  [IR(hexane),  $\nu(CO)$ : 2083(m), 2028(s), 1994(vs), 1975(s), 1953(m)  $cm^{-1}$ ], and examples of the 1,1-cis-dieq-isomer, (IIE), are  $Mn_2(CO)_8(CNBU^t)_2$  [IR(hexane),  $\nu(CO)$ : 2055(m), 1999(vs), 1977(vs), 1963(w), 1952(m), 1935(m)  $cm^{-1}$ ] (see ch. XI),  $Mn_2(CO)_8(phen)^{2+}$  [IR(diethyl ether),  $\nu(CO)$ : 2051(s), 2018(vs), 1987(ms), 1954(w), 1908(w)  $cm^{-1}$ ],  $Re_2(CO)_8(phen)^{2+}$  [IR( $CH_2Cl_2$ ),  $\nu(CO)$ : 2073(m), 2012(s), 1992(m), 1959(m), 1915(m), 1899(m)  $cm^{-1}$ ] and  $Re_2(CO)_8(biquin)^{2+}$  [IR( $CH_2Cl_2$ ),  $\nu(CO)$ : 2076(m), 2020(s), 1986(m), 1958(m), 1915(m), 1889(m)  $cm^{-1}$ ]. On the basis of this IR data, the reported 1,1- $Re_2(CO)_8(CH_3NH_2)_2^{2+}$  [IR(THF),  $\nu(CO)$ : 2070(m), 1990(s), 1955(s,br), 1883(m), 1867(m)  $cm^{-1}$ ] appears to be the 1,1-ax,eq-isomer (IID). There is a greater resemblance of the IR spectrum of  $Mn_2(CO)_8(PHPh_2)_2$  to that of the (IID) isomer than to that of the (IIE) isomer.

The (IIE) isomer, 1,1-cis-dieq, is the most electronically favoured isomer, expected in the absence of steric constraints. The most sterically favoured of the 1,1-isomers would be expected to be (IIF). This 1,1-trans-dieq-isomer, although electronically disfavoured, cannot be excluded entirely, as cleavage and subsequent ligand rearrangement could account for the cis- $[Mn_2(CO)_4(PHPh_2)_2]$  product. No examples of isomer (IIF) are known, to allow for comparison of IR data. The 1,1-ax,eq-isomer (IID) seems likely, as, with small phosphines (Tolman cone angle<sup>68</sup> of  $PHPh_2$ : 128°), (IID) could be formed instead of (IIA), in accordance with the proposed mechanism of phosphine substitution, shown in Fig. 15.4 (see section 15D.1).

Note that the rhenium analogue,  $Re_2(CO)_8(PHPh_2)_2$ , has the typical di-ax spectrum (Table 15.2) of isomer (IIA). To date no complexes of the type  $(CO)_5Re-Re(CO)_3(PR_3)_2$  have been reported.

15B.4  $\text{Re}_2(\text{CO})_7(\text{PR}_3)_3$  complexes

There are six geometrical isomers of  $\text{M}_2(\text{CO})_7(\text{L})_3$  (Fig. 15.3), if each metal-atom M has at least one ligand L bound to it (as expected on steric grounds for bulky phosphine ligands), viz. (IIIA) 1-ax,2,2-trans-dieq, (IIIB) 1-eq,2,2-ax-eq, (IIIC) 1-eq,2,2-trans-dieq, (IIID) 1-ax,2,2-ax,eq, (IIIE) 1-ax,2,2-cis-dieq and (IIIF) 1-eq, 2,2-ci-dieq.

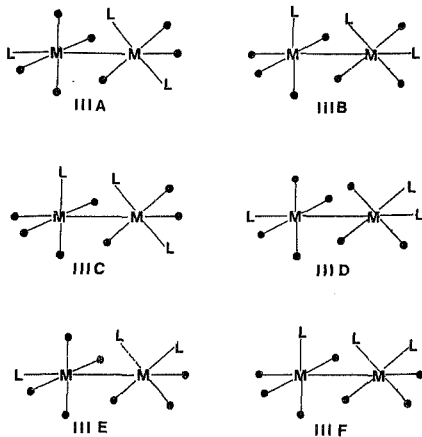
The most extensive investigation of  $\text{Re}_2(\text{CO})_7(\text{PR}_3)_3$  complexes was a study of the photochemical reaction of  $\text{Re}_2(\text{CO})_{10}$  with  $\text{PPh}_3$  under vacuum,<sup>114</sup> which yielded three isomers of  $\text{Re}_2(\text{CO})_7(\text{PPh}_3)_3$ , identified by  $^{31}\text{P}$  NMR as isomers (IIIA) (35%), (IIIB) (15%) and (IIIC) (5%). The IR spectra of these complexes are listed in Table 15.3.

Photochemical reactions of  $\text{Re}_2(\text{CO})_{10}$  with  $\text{PMe}_2\text{Ph}$ ,<sup>115</sup>  $\text{AsMe}_2\text{Ph}$ <sup>116</sup> and  $\text{PMePh}_2$ ,<sup>117</sup> yielded  $\text{Re}_2(\text{CO})_7(\text{PMe}_2\text{Ph})_2$  (IIIC),  $\text{Re}_2(\text{CO})_7(\text{AsMe}_2\text{Ph})_3$  (IIIC), and two isomers of  $\text{Re}_2(\text{CO})_7(\text{PMePh}_2)_3$ , (IIIA) and (IIIC), in essentially equal amounts (ca. 10%). These isomers were identified from IR spectra (see Table 15.3).

There has been one report of a (IIID) isomer. The  $\text{Re}_2(\text{CO})_7[\text{P}(\text{OPh})_3]_3$  product obtained from the thermal reaction of  $\text{Re}_2(\text{CO})_{10}$  with  $\text{P}(\text{OPh})_3$ <sup>118</sup> was assigned as (IIID) on the basis of the IR spectrum (Table 15.3). This isomer (IIID) might be expected to be the product of further reaction of *di*ax- $\text{Re}_2(\text{CO})_8(\text{PR}_3)_2$  with  $\text{PR}_3$ .

Mixtures of isomers (complex IR spectra) have been obtained for the products  $[\text{Mn}_2(\text{CO})_7(\text{P}(\text{OCH}_2)_3\text{CEt})_3]^{119}$  (identified by elemental analysis) and  $[\text{M}_2(\text{CO})_7(\text{PF}_3)_3]$  ( $\text{M} = \text{Mn}, \text{Re}$ )<sup>120</sup> ( $^1\text{H}$  NMR evidence), but these were not isolated.

No  $\text{Re}_2(\text{CO})_7(\text{PR}_3)_3$  (or  $\text{Mn}_2(\text{CO})_7(\text{PR}_3)_3$ ) isomers corresponding to (IIIE) and (IIIF) have been reported. Note that (IIIF) has the same structure as the  $\text{Re}_2(\text{CO})_7(\text{CNR})_3$  complexes (see ch. XIV).



**Figure 15.3:** Possible isomers for  $1,2,2\text{-M}_2(\text{CO})_7(\text{L})_3$  complexes.  
 (rotamers not shown;  $\bullet = \text{CO}$ )  
 (IIIA)1-ax,2,2-trans-dieq, (IIIB)1-eq,2,2-ax,eq  
 (IIIC)1-eq,2,2-trans-dieq, (IIID)1-ax,2,2-ax,eq  
 (IIIE)1-ax,2,2-cis-dieq and (IIIF)1-eq,2,2-cis-dieq

TABLE 15.3: IR spectral data of  $\text{Re}_2(\text{CO})_7(\text{PR}_3)_3$  complexes

| Complex   | Solvent                | $\nu(\text{CO})/\text{cm}^{-1}$                               | Ref |
|---|------------------------|---|-----|
| 1-ax,2,2-trans-dieq- $\text{Re}_2(\text{CO})_7(\text{PPh}_3)_3$           | $\text{CHCl}_3$        | 2050(w), 2022(w), 1959(s), 1920(s), 1897(s)                   | 186 |
| 1-eq,2,2-ax,eq- $\text{Re}_2(\text{CO})_7(\text{PPh}_3)_3$                | $\text{CHCl}_3$        | 2098(m), 2082(w), 2015(w), 2010(s), 1990(m), 1959(s), 1930(s) | 186 |
| 1-eq,2,2-trans-dieq- $\text{Re}_2(\text{CO})_7(\text{PPh}_3)_3$           | $\text{CHCl}_3$        | 2038(m), 2007(vs), 1957(s), 1927(sh), 1917(s), 1889(m)        | 186 |
| 1-eq,2,2-trans-dieq- $\text{Re}_2(\text{CO})_7(\text{PMe}_2\text{Ph})_3$  | $\text{CCl}_4$         | 2018(w), 1995(ms), 1940(s), 1918(sh), 1910(s), 1885(s)        | 183 |
| 1-eq,2,2-trans-dieq- $\text{Re}_2(\text{CO})_7(\text{AsMe}_2\text{Ph})_3$ | $\text{CHCl}_3$        | 2030(w), 1990(ms), 1945(s), 1920(sh), 1909(s), 1840(s)        | 183 |
| 1-ax,2,2-trans-dieq- $\text{Re}_2(\text{CO})_7(\text{PMePh}_2)_3$         | $\text{C}_6\text{H}_6$ | 2043(w), 1994(s), 1930(w), 1907(s), 1877(m)                   | 184 |
| 1-eq,2,2-trans-dieq- $\text{Re}_2(\text{CO})_7(\text{PMePh}_2)_3$         | $\text{C}_6\text{H}_6$ | 2021(w), 1995(s), 1990(s), 1938(s), 1910(s), 1885(m)          | 184 |
| 1-ax,2,2-ax,eq- $\text{Re}_2(\text{CO})_7[\text{P(OPh)}_3]_3$             | $\text{CHCl}_3$        | 2065(w), 2000(sh), 1980(s), 1962(s), 1912(m)                  | 185 |

### 15B.5 $\text{Re}_2(\text{CO})_6(\text{PR}_3)_4$ complexes

Very few reports exist for  $\text{Re}_2(\text{CO})_6(\text{PR}_3)_2$  complexes, and the evidence for these complexes is tenuous. An early claim to the preparation of  $\text{Re}_2(\text{CO})_6(\text{PPh}_3)_4$ <sup>180b</sup> from the thermal reaction of  $\text{Re}_2(\text{CO})_{10}$  with  $\text{PPh}_3$  was later proved incorrect when the product was identified as the monomeric hydride,  $\text{HRe}(\text{CO})_3(\text{PPh}_3)_2$ <sup>188</sup> with an IR spectrum (benzene,  $\nu(\text{CO}): 1930 \text{ cm}^{-1}$ ) typical of *mer-trans*- $\text{HRe}(\text{CO})_3(\text{PR}_3)_2$ <sup>182a</sup>. Another product prepared similarly and identified as *cis*- $[\text{Re}(\text{CO})_3(\text{Ph}_2\text{PCH}_2\text{CH}_2\text{PPh}_2)]_2$ <sup>188b</sup> is probably also  $\text{HRe}(\text{CO})_3(\text{Ph}_2\text{PCH}_2\text{CH}_2\text{PPh}_2)$ , as the IR spectrum (benzene,  $\nu(\text{CO}): 1910(\text{s}), 1850(\text{s}), 1800(\text{s}) \text{ cm}^{-1}$ ) resembles that of *fac*- $\text{HRe}(\text{CO})_3(\text{PR}_3)_2$  complexes.<sup>182a</sup>

The photochemical reaction of  $\text{Re}_2(\text{CO})_{10}$  with  $\text{PPh}_3$  under vacuum yielded, in addition to  $\text{Re}_2(\text{CO})_7(\text{PPh}_3)_3$  isomers, a trace product tentatively identified as  $\text{Re}_2(\text{CO})_6(\text{PPh}_3)_4$ <sup>186</sup> [ $\text{IR}(\text{CHCl}_3), \nu(\text{CO}): 1948(\text{s}) \text{ cm}^{-1}$ ]. Again the simplicity of the spectrum suggests the complex may be *mer-trans*- $\text{HRe}(\text{CO})_3(\text{PPh}_3)_2$ <sup>182a</sup>. However, MS data are consistent with the tetramer  $\text{Re}_2(\text{CO})_6(\text{PPh}_3)_4$ <sup>186</sup>. It has been suggested<sup>180b</sup> that these complexes exist as dimers in the solid state and as monomers in solution. The compound  $[\text{Re}(\text{CO})_3(\text{PPh}_3)_2]_2$  was reported to give several  $\nu(\text{CO})$  bands in Nujol, but only one in benzene solution<sup>180b</sup> (*vide supra*).

A mixture of isomers of  $[\text{Mn}_2(\text{CO})_6(\text{P}(\text{OCH}_2)_3\text{CET})_4]$ <sup>219</sup> has been reported, (identified by elemental analysis), and the IR spectrum is complex. Attempts to separate the isomers were not successful. A compound tentatively identified as  $\text{Mn}_2(\text{CO})_6(\text{PF}_3)_4$ <sup>190</sup> has been reported [ $\text{IR}(\text{hexane}), \nu(\text{CO}): 2078(\text{m}), 2034(\text{w}), 2012(\text{vs}), 1994(\text{m}), 1977(\text{w}), 1953(\text{vw}) \text{ cm}^{-1}$ ].

### 15B.6 Conclusions

From the foregoing analysis it is apparent that the vast majority of  $\text{Re}_2(\text{CO})_6(\text{PR}_3)_2$  complexes reported correspond to the *ax*-isomer. Only a few isolated examples of

$\text{eg-Re}_2(\text{CO})_9(\text{PR}_3)$  complexes have been reported, and the evidence (elemental analysis and/or IR spectra) for these is tenuous.

Regarding  $\text{Re}_2(\text{CO})_8(\text{PR}_3)_2$  complexes, at least four different isomers have been reported, viz. *diax*, *1,2-ax,eq*, *1,2-eq,eq* and *1,1* isomer, although the majority of products are *diax-Re}\_2(\text{CO})\_8(\text{PR}\_3)\_2. Combining the data for these complexes with that for the  $\text{M}_2(\text{CO})_8(\text{CNR})_2$  ( $\text{M} = \text{Re}, \text{Mn}$ ) complexes (see ch. XI), it is possible to relate IR data to structure for all the known isomers of  $\text{M}_2(\text{CO})_8(\text{L})_2$  (see Table 15.4).*

With the data for the  $\text{Re}_2(\text{CO})_7(\text{PR}_3)_3$  isomers, together with that for  $\text{Re}_2(\text{CO})_7(\text{CNR})_3$  (ch. XI), it is also possible to relate IR spectra to substitution geometry, although examples of tri-substituted derivatives are not numerous. Further, such complexes, backed up by X-ray crystal structure data, would be useful in establishing a reliable correlation between IR data and geometric isomers.

There is no reliable evidence for  $\text{Re}_2(\text{CO})_6(\text{PR}_3)_4$  complexes, and in cases where such products have been postulated, it has not been possible to assign the substitution geometry on the basis of IR data alone. The lack of  $\text{Re}_2(\text{CO})_6(\text{PR}_3)_4$  (or more highly substituted) products must reflect synthetic limitations of the direct method of  $\text{PR}_3$  substitution on  $\text{Re}_2(\text{CO})_{10}$ , and not steric constraints, since  $\text{Re}_2[\text{P}(\text{OMe})_3]_{10}$  (Tolman cone angle<sup>44</sup> for  $\text{P}(\text{OMe})_3$ :  $107^\circ$ ), has been prepared by indirect methods.<sup>45</sup>

#### 15C. A Survey of Kinetic and Mechanistic Studies

In consequence of the controversy surrounding the mechanism of substitution reactions of  $\text{M}_2(\text{CO})_{10}$  ( $\text{M} = \text{Mn}, \text{Re}$ ) with phosphines yielding  $\text{M}_2(\text{CO})_{10-n}(\text{PR}_3)_n$  ( $n = 1, 2$ ), the kinetics of this reaction have been studied by several groups over the past twenty years.

Two main schools of thought emerged: In 1966, Wawersik and Basolo<sup>44</sup> suggested that substitution of  $\text{Mn}_2(\text{CO})_{10}$  proceeds via rate-determining CO-dissociation, and that Mn-Mn bond



TABLE 15.4: Correlation between IR data and molecular geometry for  $M_2(CO)_2(L)_2$  complexes<sup>a</sup>

| Isomer <sup>b</sup>          | No. of $\nu(CO)$ IR bands |                       | Intensity pattern of $\nu(CO)$ IR bands <sup>c</sup> |  | Example                              |
|------------------------------|---------------------------|-----------------------|--|--|--------------------------------------|
|                              | Calculated <sup>c</sup>   | Observed <sup>d</sup> |  |  |                                      |
| (IIA) diax                   | 2                         | 2                     | w, vs  |  | $Re_2(CO)_8(Ph)_2$ , f, s, R         |
| (IIB) 1,2-ax, eq             | 8                         | 5                     | w, m, s, s, s  |  | $Re_2(CO)_8(PBu_3)_2$ , 177          |
| (IIC) 1,2-eq, eq (staggered) | 8                         | 5(6)                  | w, m, s, (sh), w, h, ms                              |  | $Re_2(CO)_8(CNC_6H_5-Me_2)_2$ , f, s |
| 1,2-eq, eq (eclipsed)        | 4                         | 4(5)                  | w, s, s, (w), m                                      |  | $Mn_2(CO)_8(AsMe_2Ph)_2$ , f, 223    |
| (IID) 1,1-ax, eq             | 8                         | 5                     | m, s, vs, s, m                                       |  | $Mn_2(CO)_8(C_4H_6)$ , 222           |
| (IIE) 1,1-cis-dieq           | 8                         | 6                     | m, vs, vs, w, m, m                                   |  | $Mn_2(CO)_8(C_4H_6)$ , f, h          |
| (IIF) 1,1-trans-dieq         | 8                         | -                     | no examples known                                    |  | -                                    |

<sup>a</sup> Staggered molecular geometry, unless otherwise stated.

<sup>b</sup> See Fig. 15.2

<sup>c</sup> Calculated from Group Theory Analysis; the Local Symmetry Approximation was assumed to hold.

<sup>d</sup> The number of bands could be affected by the solvent.

<sup>e</sup> On the basis of known examples (see section 15B.2).

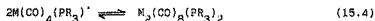
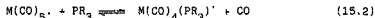
<sup>f</sup> Crystal structure reported

<sup>g</sup> This work

<sup>h</sup> This weak band is sometimes not visible in the IR spectrum.

cleavage does not occur even at 200°C. Hoggood and Poë<sup>233</sup> responded by proposing a mechanism involving homolytic fission of  $Mn_2(CO)_{10}$ , to give  $Mn(CO)_5$  radicals. Basolo's proposal recently received support from Sonnenberger and Atwood,<sup>262</sup> on the basis of their kinetic studies of the reaction of the mixed metal carbonyl,  $ReMn(CO)_{10}$ , with  $PR_3$ . The disagreement regarding the interpretation of kinetic results, resulted in a continuing dispute in the literature between Poë and Atwood<sup>261</sup>, the main protagonists. A summary of the main arguments and results follows.

Over a period of twenty years, Poë and co-workers have studied the kinetics of the reaction of  $M_2(CO)_{10}$  with  $PR_3$  in decalin at 140°C under  $N_2$  and  $O_2$  ( $M = Mn$ ,<sup>243a</sup>  $Tc$ ,<sup>244b</sup>  $Re$ <sup>245c</sup>). The results have been interpreted in terms of a substitution mechanism involving reversible homolytic fission of  $M_2(CO)_{10}$  to give  $M(CO)_5$  radicals (equation 15.1). Substitution of the 17-electron radical  $M(CO)_5$  (equation 15.2) is thought to be rapid, occurring through an associative (SN2) process). Recombination of radicals gives the  $M_2(CO)_{10-n}(PR_3)_n$  ( $n = 1, 2$ ) products (equations 15.3 and 15.4).



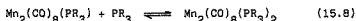
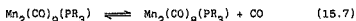
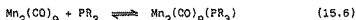
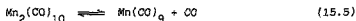
An associative substitution process is supported by substitution studies of  $Mn(CO)_5$ ,<sup>243a</sup> and  $Re(CO)_5$ ,<sup>244b</sup> radicals. Further, an associative process has been found for the substitution of  $PPh_3$  by  $P(OPh)_3$  in  $[Mn(CO)_5(PPh_3)]$ .<sup>245c</sup>

Brown and co-workers have studied the photochemical reaction of  $M_2(CO)_{10}$  ( $M = Re$ ,<sup>246a</sup>  $Mn$ <sup>246b</sup>) with  $PR_3$  in hexane. The radical chain mechanism proposed involves initial photolytic cleavage of the M-M bond, followed by rapid substitution of the  $M(CO)_5$  radicals, with subsequent recombination of the substituted radicals (equations 15.1 - 15.4). Studies of  $Mn(CO)_5$  radicals<sup>246c</sup> indicate that the substitution of the

17-electron metal carbonyl radicals occurs via an associative pathway. This proposed mechanism is essentially the same as that put forward by Poë for the thermal substitution reactions of  $M_2(CO)_{10}$  (vide supra).

From a study of the photochemistry of  $NM'(CO)_{10-n}^- (PPh_3)_n$  ( $M = M' = Re, Mn, n = 0; M = Mn, M' = Re, n = 0; M = M' = Mn, n = 1, 2$ ) compounds, Wright and Ginley<sup>118</sup> concluded that homolytic metal-metal bond cleavage occurring from an excited state derived from a  $\sigma \rightarrow \sigma^*$  one-electron transition associated with the metal-metal bond is consistent with the observed results.

Wawersik and Basolo<sup>247</sup> reported kinetic studies of  $Mn_2(CO)_{10}$  and  $Mn_2(CO)_9(PR_3)$  with  $PR_3$  in *p*-xylene (120°C), and interpreted the rate data as being consistent with a mechanism involving rate-determining CO-dissociation with no metal-metal bond cleavage (equations 15.5 to 15.8).



Cox and Davis<sup>122</sup> have rationalized the wide range of products obtained from the thermal reaction between  $Re_2(CO)_{10}$  and  $PPh_3$  in xylene (140°C) in terms of a dissociative mechanism. Apart from  $Re_2(CO)_{10-n}(PR_3)_n$  ( $n = 1-2$ ) products, complexes of the type  $HRe(CO)_{5-n}(PR_3)_n$  ( $n = 1, 2$ ) were obtained. However, no  $HRe(CO)_5$  was observed. This was taken as an indication that homolytic fission of the parent carbonyl  $Re_2(CO)_{10}$  is not an important process in the reaction, and that phosphine substitution precedes radical formation. It was suggested that the hydrides are formed by reaction of unstable radical intermediates,  $[Re(CO)_{5-n}(PR_3)_n]$  ( $n = 1, 2$ ), with the solvent. This type of reaction is known.

From a kinetic study of the substitution of  $MnRe(CO)_{10}$  by  $PR_3$  in decane (130°C), Sonnenberger and Atwood<sup>252</sup> have reported three observations claimed to be inconsistent with

a free radical mechanism:-

- (i) the predominance of the Re-substituted product,  $(CO)_5MnRe(CO)_4(PR_3)$ .
  - (ii) the failure of the Mn-substituted complex,  $(PR_3)-(CO)_4MnRe(CO)_5$ , to isomerize to  $(CO)_5MnRe(CO)_4(PR_3)$  when isolated in the pure state, and
  - (iii) the lack of isomerization to  $Mn_2$  and  $Re_2$  species.
- In terms of the proposed mechanism, CO-dissociation from  $MnRe(CO)_{10}$  to form  $MnRe(CO)_9$  is the rate-determining step. Since dissociation from Mn is expected to be 100 times faster than from Re (owing to the stronger Re-CO than Mn-CO bond<sup>172</sup>), the proposed mechanism involves CO-dissociation from the Mn-centre, and an intermediate with a CO-bridged dimer in which no metal-metal bond cleavage has occurred, followed by subsequent phosphine substitution on the Re-atom, to give the observed product,  $(CO)_5MnRe(CO)_4(PR_3)$ .

Further support for a dissociative mechanism, with no metal-metal bond cleavage, was provided by the report of Basolo and co-workers<sup>269</sup> that the scrambling reaction (equation 15.9) between  $Mn_2(CO)_{10}$  and  $Re_2(CO)_{10}$ , to give the mixed-metal carbonyl  $MnRe(CO)_{10}$ , does not occur in decalin (130°C) under an atmosphere of CO, and only very slowly in the absence of CO.



However, Poë and co-workers<sup>27</sup> have reported that the scrambling reaction (15.9) occurs in decalin (170°C) under CO, to reach a stable equilibrium.

Muettterties and co-workers,<sup>277</sup> using isotopic labelling and mass spectroscopic product analysis, have demonstrated that Mn-Mn bond scission in  $Mn_2(CO)_{10}$  phosphine thermal substitution reactions is not a significant process. Mixtures of  $Mn_2(CO)_{10}$  and  $Mn_2(^{13}CO)_{10}$  were reacted with  $PR_3$  in octane (120°C) under  $^{13}CO$  atmosphere. Mass spectral analysis of the product,  $Mn_2(CO)_9(PR_3)$ , showed no evidence of Mn-Mn bond scission. This is consistent with a dissociative mechanism

(equations 15.5-15.6). However, Mn-Mn bond scission was found to be a major process during the photochemically initiated ligand exchange reaction of  $Mn_2(CO)_{10}$  at 25°C. Recent laser photolysis studies<sup>21</sup> of  $Mn_2(CO)_{10}$  in matrices have indicated that the primary process is CO-dissociation from  $Mn_2(CO)_{10}$  to give  $Mn_2(CO)_9$  rather than Mn-Mn bond scission, for about 30% of the reacting  $Mn_2(CO)_{10}$ . The CO-bridged  $Mn_2(CO)_9$  reacts with  $PR_3$  ligands to give  $Mn_2(CO)_9(PR_3)$ .

Similar results have been obtained by Muetterties and Stolzenberg<sup>21</sup> for the reactions of  $Re_2(CO)_{10}$  with  $PR_3$ . Thus in the thermal reaction of  $^{185}Re_2(CO)_{10}$  and  $^{187}Re_2(CO)_{10}$  with  $PR_3$  in octane (150°C) under CO atmosphere, mass spectral analysis of the product,  $Re_2(CO)_9(PR_3)$ , showed no scrambling indicative of Re-Re bond cleavage, in support of a CO-dissociative mechanism. Similar results were obtained for the thermal reaction of  $Re_2(CO)_9(PR_3)$  with  $PR_3$  to give  $Re_2(CO)_9(PR_3)_2$ . However, the photochemically initiated reactions at 25°C led to complete scrambling within short reaction times, indicating that the primary mode of reaction for  $Re_2(CO)_{10}$  under photolysis conditions involves Re-Re bond scission as an elementary step.

Thus Muetterties and co-workers have demonstrated unambiguously and via non-kinetic arguments that the mechanism of the thermal reaction (140°C) of  $M_2(CO)_{10}$  ( $M = Mn, Re$ ) with  $PR_3$  under CO atmosphere to give  $M_2(CO)_9(PR_3)$ , does not involve metal-metal bond cleavage. The results are consistent with the CO-dissociative mechanism, proposed by Basolo, and supported by Atwood. However, Muetterties and co-workers have shown that for the photochemically initiated reaction, metal-metal bond cleavage is implicated as an initial step. This is in accord with the homolytic fission and radical chain mechanism proposed by Brown and co-workers, based on the results of kinetic studies of the photochemical reaction between  $M_2(CO)_{10}$  and  $PR_3$ . Hence the mechanism for the thermal reaction of  $M_2(CO)_{10}$  with  $PR_3$  under CO is represented by equations (15.5 to 15.8), while

that for the photochemical reaction between  $M_2(CO)_{10}$  and  $PR_3$  is represented by equations (15.1 to 15.4). Note that metal-metal bond scission has also been excluded for the thermal reaction of  $Re_2(CO)_9(PR_3)$  with  $PR_3$  to give  $Re_2(CO)_8(PR_3)_2$ .<sup>171</sup>

15D.1 Synthesis and characterization of  $Re_2(CO)_{10}(PR_3)_n$   
(n = 1,2) derivatives

As part of an extension of the Pd-catalysed reaction of  $Re_2(CO)_{10}$  with isonitriles (ch. XI) to other ligands, the reaction of  $Re_2(CO)_{10}$  with phosphine ligands was investigated. The thermal reaction between  $Re_2(CO)_{10}$  and phosphines was found to be extremely sluggish even at elevated temperatures, eg. after 10 h reflux at 140°C, the reaction between  $Re_2(CO)_{10}$  and 2 equivalents  $PMe_2Ph$  yielded 80% recovered  $Re_2(CO)_{10}$ , and small amounts of  $Re_2(CO)_9(PMe_2Ph)$  and  $Re_2(CO)_8(PMe_2Ph)_2$ , together with other trace products which were not characterized.

Use of Pd-catalysts, eg. Pd/C (10%), Pd/CaCO<sub>3</sub> (10%), or PdO, considerably improves the reaction, yielding mono- and di-substituted phosphine derivatives in poor to good yields after moderate reaction times (Table 15.5). PdO was found to be a more active catalyst than Pd/C (10%) (or Pd/CaCO<sub>3</sub> (10%)) for this reaction (although this probably reflects the greater Pd-content for the same mass of catalyst). In favourable cases, the di-phosphine complex can be obtained in good yield as the sole reaction product after relatively short reaction times, eg. 84%  $Re_2(CO)_8(PMe_2Ph)_2$  after 1 h (xylene, 140°C).

In the cases of  $PR_3 = PMePh_2$ ,  $PMe_2Ph$ , trace products were also isolated, and identified as  $\text{fac-HRe(CO)}_3(PMePh_2)_2$  [IR(CHCl<sub>3</sub>),  $\nu(CO)$ : 2000(s,sp), 1910(s), 1870(s)  $cm^{-1}$ ] and  $\text{fac-HRe(CO)}_3(PMe_2Ph)_2$  [IR(CHCl<sub>3</sub>),  $\nu(CO)$ : 2030(s,sp), 1946(s), 1883(s)  $cm^{-1}$ ] by comparison with the IR spectrum of  $\text{fac-HRe(CO)}_3(PPh_3)_2$ <sup>182a</sup> [IR(CHCl<sub>3</sub>),  $\nu(CO)$ : 2009(s), 1960(s), 1900(r)  $cm^{-1}$ ]. Such products could have been formed with other  $PR_3$  ligands also but in many cases product decomposition on silica plates was observed, and minor product

isolation not achieved.

Comparison of the IR data for the  $\text{Re}_2(\text{CO})_{10-n}(\text{PR}_3)_n$  ( $n = 1-2$ ) products (Table 15.6) with that of  $\underline{\text{ax}}\text{-Mn}_2(\text{CO})_9(\text{PMe}_2\text{Ph})$  [IR(benzene),  $\nu(\text{CO})$ : 2074(w), 2016(s), 1993(vs), 1969(sh), 1938(m)  $\text{cm}^{-1}$ ]<sup>223</sup> and  $\underline{\text{di}}\underline{\text{ax}}\text{-Mn}_2(\text{CO})_8(\text{PMePh}_2)_2$  [IR(benzene),  $\nu(\text{CO})$ : 1983(w), 1954(vs)  $\text{cm}^{-1}$ ]<sup>223</sup> for which axial substitution has been established by X-ray crystallographic structures,<sup>224, 225</sup> indicates that the products are  $\underline{\text{ax}}\text{-Re}_2(\text{CO})_9(\text{PR}_3)$  and  $\underline{\text{di}}\underline{\text{ax}}\text{-Re}_2(\text{CO})_8(\text{PR}_3)_2$ . An X-ray crystal and molecular structure of the  $\text{Re}_2(\text{CO})_8(\text{PMe}_2\text{Ph})_2$  complex (section 15E) confirmed the diaxial substitution.

These  $\text{Re}_2(\text{CO})_8(\text{PR}_3)_2$  products can be prepared independently by the  $\text{NMe}_3\text{O}$ -assisted reaction ( $\text{CH}_2\text{Cl}_2$ , 40°C) between  $\text{Re}_2(\text{CO})_{10}$  and  $\text{PR}_3$ , which yields as the major products  $\underline{\text{ax}}\text{-Re}_2(\text{CO})_9(\text{PR}_3)$  (ca. 40%) and  $\underline{\text{di}}\underline{\text{ax}}\text{-Re}_2(\text{CO})_8(\text{PR}_3)_2$  (ca. 30%), as well as a minor product, identified as  $\text{C}\ell\text{Re}(\text{CO})_3(\text{PR}_3)_2$  (ca. 10%). The IR spectra of the latter complexes (Table 15.7) show three strong bands in the carbonyl region. This pattern is characteristic of that of  $\underline{\text{fac}}\text{-XRe}(\text{CO})_3(\text{PR}_3)_2$  complexes (X = H, halogen) [eg.  $\text{HRe}(\text{CO})_3(\text{PPh}_3)_2$ , [IR( $\text{CHCl}_3$ ),  $\nu(\text{CO})$ : 2009(s), 1960(s), 1900(s)  $\text{cm}^{-1}$ ]<sup>192a</sup>]. This IR spectrum is quite distinct from that of  $\underline{\text{mer}}\text{-trans}\text{-HRe}(\text{CO})_3(\text{PPh}_3)_2$  [IR( $\text{CHCl}_3$ ),  $\nu(\text{CO})$ : 1935(s)  $\text{cm}^{-1}$ ]<sup>192a</sup>. The products are probably the chloride,  $\underline{\text{fac}}\text{-C}\ell\text{Re}(\text{CO})_3(\text{PR}_3)_2$ , since the reaction was conducted in  $\text{CH}_2\text{Cl}_2$  and the hydrogen in  $\text{HRe}(\text{CO})_3(\text{PR}_3)_2$  is readily replaced by chlorine.<sup>186b</sup> That the  $\underline{\text{fac}}$ -isomer, the kinetic product, is obtained, rather than the  $\underline{\text{mer}}\text{-trans}$ -isomer ( $\underline{\text{mer}}\text{-trans}\text{-H M}(\text{CO})_3(\text{PR}_3)_2$ , M = Re,<sup>186, 182, 183</sup> Mn<sup>223, 224</sup>) obtained by other workers from the thermal reaction of  $\text{M}_2(\text{CO})_{10}$  with  $\text{PR}_3$  (140°C), probably reflects the mild reaction conditions (40°C) of the  $\text{Me}_3\text{NO}$ -route, as  $\underline{\text{fac}}\text{-XRe}(\text{CO})_3(\text{PR}_3)_2$  isomers readily isomerize to the  $\underline{\text{mer}}\text{-trans}\text{-XRe}(\text{CO})_3(\text{PR}_3)_2$  isomers.<sup>219, 221</sup>

An attempt was made to prepare arsine derivatives of  $\text{Re}_2(\text{CO})_{10}$ , as the complex  $\text{Mn}_2(\text{CO})_8(\text{AsMe}_2\text{Ph})_2$  has been shown by an X-ray crystallographic structure to have 1,2-dia substitution.<sup>253</sup> The  $\text{Me}_3\text{NO}$ -assisted reaction

TABLE 15.5: Details of catalytic syntheses of  $\text{Re}_2(\text{CO})_{10-n}(\text{PR}_3)_n$  ( $n = 1,2$ ) complexes

| $\text{PR}_3$                                 | Catalyst  | Reaction time/h | Product   | Yield (%) |
|---|---|-----------------|---|-----------|
| $\text{PPh}_3$                                | $\text{Pd}/\text{Cl}(10\%)$                             | 9               | $\text{Re}_2(\text{CO})_9(\text{PPh}_3)$                                  | 20        |
|   |   |                 | $\text{Re}_2(\text{CO})_8(\text{PPh}_3)_2$                                | 20        |
|   |   |                 | $\text{Re}_2(\text{CO})_9(\text{PMePh}_2)$                                | 20        |
| $\text{PMePh}_2$                              | $\text{Pd}/\text{Cl}(10\%)$                             | 6               | $\text{Re}_2(\text{CO})_8(\text{PMePh}_2)_2$                              | 40        |
|   |   |                 | $\text{Re}_2(\text{CO})_8(\text{PMePh}_2)_2$                              | 60        |
|   |   |                 | $\text{HRe}(\text{CO})_3(\text{PMePh}_2)_2$                               | 3         |
|   |   |                 | $\text{Re}_2(\text{CO})_9(\text{PMe}_2\text{Ph})$                         | 2         |
| $\text{PMe}_2\text{Ph}$                       | $\text{Pd}/\text{C}$ or $\text{Pd}/\text{CaCO}_3(10\%)$ | 2               | $\text{Re}_2(\text{CO})_8(\text{PMe}_2\text{Ph})_2$                       | 82        |
|   |   |                 | $\text{HRe}(\text{CO})_3(\text{PMe}_2\text{Ph})_2$                        | 3         |
|   |   |                 | $\text{Re}_2(\text{CO})_8(\text{PMe}_2\text{Ph})_2$                       | 84        |
|   |   |                 | $\text{Re}_2(\text{CO})_{10}$   | 14        |
| $\text{P}(\text{CH}_2\text{C}_6\text{H}_5)_3$ | $\text{PdO}$  | 1               | $\text{Re}_2(\text{CO})_9(\text{P}(\text{CH}_2\text{C}_6\text{H}_5)_3)$   | 15        |
|   |   |                 | $\text{Re}_2(\text{CO})_8(\text{P}(\text{CH}_2\text{C}_6\text{H}_5)_3)_2$ | 12        |
|   |   |                 | $\text{Re}_2(\text{CO})_9(\text{PMe}_3)$                                  | 14        |
| $\text{PMe}_3$                                | $\text{PdO}$  | 2               | $\text{Re}_2(\text{CO})_8(\text{PMe}_3)_2$                                | 18        |
|   |   |                 | $\text{Re}_2(\text{CO})_9(\text{P}(\text{OMe})_3)$                        | 55        |
| $\text{P}(\text{OMe})_3$                      | $\text{Pd}/\text{Cl}(10\%)$                             | 4               | $\text{Re}_2(\text{CO})_8(\text{P}(\text{OMe})_3)_2$                      | 25        |



**TABLE 15.6:** IR spectral data for the  $\text{Re}_2(\text{CO})_{10-n}(\text{PR}_3)_n$  ( $n = 1, 2$ ) derivatives

| Complex   | $\nu(\text{CO})/\text{cm}^{-1}$ ( $\text{CHCl}_3$ solution) |
|---|---|
| $\text{Re}_2(\text{CO})_9(\text{PPh}_3)$                                  | 2114(w, sp), 2040(w, sp), 1998(vs), 1964(sh), 1940(m)       |
| $\text{Re}_2(\text{CO})_9(\text{PMePh}_2)$                                | 2111(w, sp), 1040(w, sp), 1995(vs), 1962(sh), 1938(m)       |
| $\text{Re}_2(\text{CO})_9(\text{PMe}_2\text{Ph})$                         | 2108(w, sp), 2038(m, sp), 1990(vs), 1960(sh), 1932(m)       |
| $\text{Re}_2(\text{CO})_9[\text{P}(\text{CH}_2\text{C}_6\text{H}_5)_3]$   | 2110(w, sp), 2034(w, sp), 1998(vs), 1962(sh), 1938(m)       |
| $\text{Re}_2(\text{CO})_9(\text{PMe}_3)$                                  | 2108(w, sp), 2040(m, sp), 1990(vs), 1956(sh), 1929(m)       |
| $\text{Re}_2(\text{CO})_9[\text{P}(\text{OMe})_3]$                        | 2108(w, sp), 2040(w, sp), 1994(vs), 1952(sh), 1930(m)       |
| $\text{Re}_2(\text{CO})_9(\text{AsMe}_2\text{Ph})$                        | 2112(w, sp), 2052(m, sp), 1998(vs), 1964(w), 1930(m)        |
| $\text{Re}_2(\text{CO})_8(\text{PPh}_3)_2$                                | 2000(sh), 1958(vs)  |
| $\text{Re}_2(\text{CO})_8(\text{PMePh}_2)_2$                              | 2015(w, ) 1954(vs)  |
| $\text{Re}_2(\text{CO})_8(\text{PMe}_2\text{Ph})_2$                       | 2010(w), 1949(vs)   |
| $\text{Re}_2(\text{CO})_8[\text{P}(\text{CH}_2\text{C}_6\text{H}_5)_3]_2$ | 2010(sh), 1954(vs)  |
| $\text{Re}_2(\text{CO})_8(\text{PMe}_3)_2$                                | 2000(sh), 1943(vs)  |
| $\text{Re}_2(\text{CO})_8[\text{P}(\text{OMe})_3]_2$                      | 2000(sh), 1970(vs)  |

**TABLE 15.7:** IR spectral data for the  $\text{Cr}(\text{Re}(\text{CO})_3(\text{PR}_3)_2)$  complexes

| Complex  | $\nu(\text{CO})/\text{cm}^{-1}$ ( $\text{CHCl}_3$ solution) |
|--|---|
| $\text{Cr}(\text{Re}(\text{CO})_3(\text{PMePh}_2)_2)$                              | 2030(s, sp), 1954(s), 1895(s)                               |
| $\text{Cr}(\text{Re}(\text{CO})_3(\text{PMe}_2\text{Ph})_2)$                       | 2044(s, sp), 1957(s), 1896(s)                               |
| $\text{Cr}(\text{Re}(\text{CO})_3[\text{P}(\text{CH}_2\text{C}_6\text{H}_5)_3]_2)$ | 2024(s, sp), 1940(s), 1900(s)                               |
| $\text{Cr}(\text{Re}(\text{CO})_3(\text{PMe}_3)_2)$                                | 2036(s, sp), 1950(s), 1894(s)                               |
| $\text{Cr}(\text{Re}(\text{CO})_3[\text{P}(\text{OMe})_3]_2)$                      | 2043(s, sp), 1970(s), 1910(s)                               |
| $\text{Cr}(\text{Re}(\text{CO})_3(\text{AsMe}_2\text{Ph})_2)$                      | 2050(s, sp), 1960(s), 1914(s)                               |

between  $\text{Re}_2(\text{CO})_{10}$  and  $\text{AsMe}_2\text{Ph}$  yielded only  $\text{Re}_2(\text{CO})_9(\text{AsMe}_2\text{Ph})$  (74%) and  $\text{fac-CtRe}(\text{CO})_3(\text{AsMe}_2\text{Ph})_2$  (15%). The IR spectrum of  $\text{Re}_2(\text{CO})_9(\text{AsMe}_2\text{Ph})$  [IR( $\text{CHCl}_3$ ),  $\nu(\text{CO})$ : 2112(w,sp), 2052(m,sp), 1998(vs), 1964(w), 1930(m)  $\text{cm}^{-1}$ ] indicates ax-substitution. This is also the case for  $\text{Mn}_2(\text{CO})_9(\text{AsMe}_2\text{Ph})^{12}$ ; [IR(benzene),  $\nu(\text{CO})$ : 2094(w), 2016(s), 1993(vs), 1969(sh), 1938(m)  $\text{cm}^{-1}$ ].

The  $\text{Me}_3\text{NO}$ -assisted reaction between  $\text{Re}_2(\text{CO})_{10}$  and  $\text{PR}_3$  in  $\text{CH}_2\text{Cl}_2$  (40°C) or  $\text{CHCl}_3$  (20°C,  $\text{PR}_3 = \text{PPh}_3$ )<sup>17</sup> yielded axially substituted  $\text{Re}_2(\text{CO})_{10-n}(\text{PR}_3)_n$  (n = 1,2) products. However, it was found that when the  $\text{Me}_3\text{NO}$ -assisted reaction between  $\text{Re}_2(\text{CO})_{10}$  and  $\text{PMe}_2\text{Ph}$  was conducted in acetonitrile, MeCN, (see section 15D.2.3) instead of  $\text{CH}_2\text{Cl}_2$ , a cream product was obtained (80°C, 2 h), with a complex IR spectrum [IR(hexane),  $\nu(\text{CO})$ : 2078(mw,sp), 2000(m,sp), 1974(sh), 1964(vs, br), 1932(s), 1916(s)  $\text{cm}^{-1}$ ]. This product analysed as  $\text{Re}_2(\text{CO})_8(\text{PMe}_2\text{Ph})_2$  [C: 33.5%, H: 2.7%, cf. Calc. for  $\text{Re}_2\text{C}_{22}\text{H}_{22}\text{O}_8\text{P}_2$ , C: 33.0%, H: 2.5%; Found for diax- $\text{Re}_2(\text{CO})_8(\text{PMe}_2\text{Ph})_2$ , C: 33.3%, H: 2.6%; mp: 142-44°C, cf. 108-109°C for diax- $[\text{Re}_2(\text{CO})_8(\text{PMe}_2\text{Ph})_2]$ . The similarity to the IR spectrum of 1,2-ax,eq- $\text{Re}_2(\text{CO})_8(\text{PPh}_3)_2$  [IR(toluene),  $\nu(\text{CO})$ : 2069(mw), 2012(m), 1964(vs,br), 1934(m), 1921(m)  $\text{cm}^{-1}$ ]<sup>18</sup> suggests that the product is the isomer, 1,2-ax,eq- $\text{Re}_2(\text{CO})_8(\text{PMe}_2\text{Ph})_2$ . Attempts to obtain crystals suitable for an X-ray crystallographic study of this complex to confirm the substitution geometry have to date not been successful.

The reaction which led to the formation of this product did not follow the usual procedure for the  $\text{Me}_3\text{NO}$ -route (see section 15D.2.2) in that the  $\text{Me}_3\text{NO}$  was added before the  $\text{PMe}_2\text{Ph}$ , and the reaction was conducted in MeCN, not  $\text{CH}_2\text{Cl}_2$ . Reaction, presumably to diag- $\text{Re}_2(\text{CO})_9(\text{NCMe})_2$  (diag- $\text{Re}_2(\text{CO})_8(\text{NCMe})_2$  has been prepared by the amine-oxide assisted route [IR(NCMe),  $\nu(\text{CO})$ : 2070(w), 2015(w), 1962(s), 1909(m)  $\text{cm}^{-1}$ ].<sup>19</sup> From the IR data of Table 15.4 for  $\text{M}_2(\text{CO})_8(\text{L})_2$  complexes, this spectrum would appear to be that of a 1,2-ax,eq-isomer (IIC), was instantaneous, as evidenced by the colourless solution becoming yellow. On

subsequent addition of the  $\text{PMe}_2\text{Ph}$  ligand, reaction occurred with displacement of the  $\text{NCMe}$  ligands, to give 1,2-ax,eq- $\text{Re}_2(\text{CO})_8(\text{PMe}_2\text{Ph})_2$ , steric consideration determining 1,2-ax,eq- rather than 1,2-eq,eq-substitution. (Tolman cone angle<sup>23</sup> of  $\text{PMe}_2\text{Ph}$ : 122°).

It is significant to note that sidebands are often observed in the IR spectra of di-ax- $\text{Re}_2(\text{CO})_8(\text{PR}_3)_2$  complexes. For di-ax- $\text{Mn}_2(\text{CO})_8(\text{PR}_3)_2$ , Lewis et al.<sup>27</sup> have ascribed these to Raman active bands which gain weak IR intensity. However, this cannot be the case, as these sidebands disappear on recrystallization, eg. single crystals of di-ax- $\text{Re}_2(\text{CO})_8(\text{PMe}_2\text{Ph})_2$ , used in the X-ray study [section 15E], exhibited no sidebands in the IR spectrum ( $\text{CHCl}_3$ ). An IR spectrum run on a crude sample of di-ax- $\text{Re}_2(\text{CO})_8(\text{PMe}_2\text{Ph})_2$  (toluene solution) had sidebands at 2070(w), 2020(m), 1930(sh) and 1920(sh)  $\text{cm}^{-1}$ , in addition to the very strong band at 1950  $\text{cm}^{-1}$ . On heating in toluene solution (80°C) for 4 h, these sidebands were observed to grow in intensity, and a shoulder to the main 1950  $\text{cm}^{-1}$  band developed at ca. 1965  $\text{cm}^{-1}$ . It will be observed that these sidebands correspond to the  $\nu(\text{CO})$  bands of the 1,2-ax,eq- $\text{Re}_2(\text{CO})_8(\text{PMe}_2\text{Ph})_2$  isomer (vide supra). As the di-ax- $\text{Re}_2(\text{CO})_8(\text{PMe}_2\text{Ph})_2$  and 1,2-ax,eq- $\text{Re}_2(\text{CO})_8(\text{PMe}_2\text{Ph})_2$  products run together on TLC, separation of the isomers could not have been effected.

The formation of some 1,2-ax,eq- $\text{Re}_2(\text{CO})_8(\text{PMe}_2\text{Ph})_2$  in the Pd-catalysed and  $\text{Me}_3\text{NO}$ -assisted ( $\text{CH}_2\text{Cl}_2$  solvent) reactions, as evidenced by the above "sidebands", and the partial isomerization described above (ie. growth of sidebands on heating), are consistent with a report of the formation of eq-substituted isomers,  $\text{Re}_2(\text{CO})_8(\text{PMe}_2\text{Ph})_2$  [ $\text{IR}(\text{CCl}_4)$ ,  $\nu(\text{CO})$ : 2100(w), 2060(mw), 2000(s), 1055(s,br), 1905(s)  $\text{cm}^{-1}$ ]<sup>28</sup> and  $\text{Re}_2(\text{CO})_8(\text{PMePh}_2)_2$  [ $\text{IR}(\text{benzene})$ ,  $\nu(\text{CO})$ : 2090(w), 2058(m), 2000(s), 1955(s,br), 1925(s)  $\text{cm}^{-1}$ ]<sup>14</sup>, in the thermal reaction of  $\text{Re}_2(\text{CO})_{10}$  with  $\text{PR}_3$  at elevated temperatures and for extended reaction times (eg.  $\text{PMe}_2\text{Ph}$ <sup>13</sup>: petroleum ether, 80-100°C, 50-95 h;  $\text{PMePh}_2$ <sup>14</sup>: xylene, 140°C, 15 h). These isomers were originally assigned as 1,2-eq,eq- $\text{Re}_2(\text{CO})_8(\text{PR}_3)_2$

but from the IR data appear to be 1,2-ax,eq-Re<sub>2</sub>(CO)<sub>8</sub>(PR<sub>3</sub>)<sub>2</sub> (see section 15B.3). Following the published procedure<sup>194</sup> (see section 15D.2.4), the thermal reaction of Re<sub>2</sub>(CO)<sub>10</sub> with excess PMePh<sub>2</sub> (xylene, 140°C, 15 h) yielded a yellow product, characterized by IR data [IR(xylene), ν(CO): 2095(w), 2060(m), 2000(s), 1950(s), 1922(m) cm<sup>-1</sup>] as 1,2-ax,eq-Re<sub>2</sub>(CO)<sub>8</sub>(PMePh<sub>2</sub>)<sub>2</sub> [Tolman cone angle<sup>88</sup> of PMePh<sub>2</sub>: 136°].

Note that for the large phosphine ligand, PPh<sub>3</sub> (Tolman cone angle<sup>88</sup> of 145°), there were no sidebands in the IR spectrum of the crude di-ax-Re<sub>2</sub>(CO)<sub>8</sub>(PPh<sub>3</sub>)<sub>2</sub> product from the Pd-catalysed reaction. Hence the size of the phosphine ligand, i.e. steric factors, would appear to determine whether eq-substituted isomers are stable.

According to the mechanism of phosphine substitution on Re<sub>2</sub>(CO)<sub>10</sub>, to give di-ax-Re<sub>2</sub>(CO)<sub>8</sub>(PR<sub>3</sub>)<sub>2</sub>,<sup>195</sup> Re<sub>2</sub>(CO)<sub>10</sub> undergoes monosubstitution to yield ax-Re<sub>2</sub>(CO)<sub>9</sub>(PR<sub>3</sub>)<sub>2</sub>, steric considerations presumably determining the final axial position of the PR<sub>3</sub> ligand. In consequence of the cis-labilization effect (see ch XII), a CO cis to the PR<sub>3</sub> ligand is more easily lost, but the second incoming PR<sub>3</sub> cannot take up the cis position on the same metal because of steric interactions. A vacancy is created on the second metal via a bridging carbonyl mechanism, and the PR<sub>3</sub> ligand occupies the axial site, giving di-ax-Re<sub>2</sub>(CO)<sub>8</sub>(PR<sub>3</sub>)<sub>2</sub>, steric factors again governing axial substitution (see Fig. 15.4).

However, equatorially-substituted Re<sub>2</sub>(CO)<sub>8</sub>(PR<sub>3</sub>)<sub>2</sub> isomers have been formed by several methods:-

- (1) Reaction of (μ-H)(μ-olefin)Re<sub>2</sub>(CO)<sub>8</sub> complexes with PR<sub>3</sub> ligands, resulting in the formation of 1,2-eg,eq-Re<sub>2</sub>(CO)<sub>8</sub>(PR<sub>3</sub>)<sub>2</sub> (R = Me, OMe, OPh) or 1,2-ax,eq-Re<sub>2</sub>(CO)<sub>8</sub>(PR<sub>3</sub>)<sub>2</sub> (R = Bu<sup>n</sup>, Ph),<sup>196</sup> depending on the size of the phosphine ligand [Tolman cone angles<sup>88</sup>: P(OMe)<sub>3</sub>, 107°; PMe<sub>3</sub>, 118°; P(OPh)<sub>3</sub>, 121-128°; PBu<sup>n</sup>, 132°; PPh<sub>3</sub>, 145°]. Bidentate phosphine ligands, (P)<sub>2</sub>, also gave 1,2-eg,eq-Re<sub>2</sub>(CO)<sub>8</sub>(P)<sub>2</sub> products ((P)<sub>2</sub> = Ph<sub>2</sub>PCH<sub>2</sub>PPh<sub>2</sub>,<sup>179,198</sup> Me<sub>2</sub>PCH<sub>2</sub>PMe<sub>2</sub>, Ph<sub>2</sub>PCH<sub>2</sub>CH<sub>2</sub>PPh<sub>2</sub>, Me<sub>2</sub>PCH<sub>2</sub>CH<sub>2</sub>PMe<sub>2</sub>).<sup>199</sup> [The Tolman cone angles (half chelates)<sup>88a</sup> for these (P)<sub>2</sub> ligands range from

**Author** Harris Gillian Wendy

**Name of thesis** Chemical And Structural Studies Of Substituted Transition Metal Carbonyl Complexes. 1984

***PUBLISHER:***

University of the Witwatersrand, Johannesburg

©2013

***LEGAL NOTICES:***

**Copyright Notice:** All materials on the University of the Witwatersrand, Johannesburg Library website are protected by South African copyright law and may not be distributed, transmitted, displayed, or otherwise published in any format, without the prior written permission of the copyright owner.

**Disclaimer and Terms of Use:** Provided that you maintain all copyright and other notices contained therein, you may download material (one machine readable copy and one print copy per page) for your personal and/or educational non-commercial use only.

The University of the Witwatersrand, Johannesburg, is not responsible for any errors or omissions and excludes any and all liability for any errors in or omissions from the information on the Library website.